2016

Heat and Mass Transfer in Baled Switchgrass for Storage and Bioconversion Applications

Drew F. Schiavone
University of Kentucky, schiavonedrew@gmail.com
Digital Object Identifier: http://dx.doi.org/10.13023/ETD.2016.136

STUDENT AGREEMENT:

I represent that my thesis or dissertation and abstract are my original work. Proper attribution has been given to all outside sources. I understand that I am solely responsible for obtaining any needed copyright permissions. I have obtained needed written permission statement(s) from the owner(s) of each third-party copyrighted matter to be included in my work, allowing electronic distribution (if such use is not permitted by the fair use doctrine) which will be submitted to UKnowledge as Additional File.

I hereby grant to The University of Kentucky and its agents the irrevocable, non-exclusive, and royalty-free license to archive and make accessible my work in whole or in part in all forms of media, now or hereafter known. I agree that the document mentioned above may be made available immediately for worldwide access unless an embargo applies.

I retain all other ownership rights to the copyright of my work. I also retain the right to use in future works (such as articles or books) all or part of my work. I understand that I am free to register the copyright to my work.

REVIEW, APPROVAL AND ACCEPTANCE

The document mentioned above has been reviewed and accepted by the student's advisor, on behalf of the advisory committee, and by the Director of Graduate Studies (DGS), on behalf of the program; we verify that this is the final, approved version of the student's thesis including all changes required by the advisory committee. The undersigned agree to abide by the statements above.

Drew F. Schiavone, Student

Dr. Michael Montross, Major Professor

Dr. Donald G. Colliver, Director of Graduate Studies

HEAT AND MASS TRANSFER IN BALED SWITCHGRASS FOR STORAGE AND BIOCONVERSION APPLICATIONS

DISSERTATION

A dissertation submitted in partial fulfillment of the requirements for the degree of Doctor of Philosophy in the College of Engineering at the University of Kentucky

By

Drew F. Schiavone

Lexington, Kentucky

Director: Dr. Michael Montross, Professor of Biosystems & Agricultural Engineering

Lexington, Kentucky

2016

ABSTRACT OF DISSERTATION

HEAT AND MASS TRANSFER IN BALED SWITCHGRASS
FOR STORAGE AND BIOCONVERSION APPLICATIONS

The temperature and moisture content of biomass feedstocks both play a critical role in minimizing storage and transportation costs, achieving effective bioconversion, and developing relevant postharvest quality models. Hence, this study characterizes the heat and mass transfer occurring within baled switchgrass through the development of a mathematical model describing the relevant thermal and physical properties of this specific substrate. This mathematical model accounts for the effect of internal heat generation and temperature-induced free convection within the material in order to improve prediction accuracy. Inclusion of these terms is considered novel in terms of similar biomass models.

Two disparate length scales, characterizing both the overall bale structure (global domain) and the individual stems (local domain), are considered with different physical processes occurring on each scale. Material and fluid properties were based on the results of hydraulic conductivity experiments, moisture measurements and thermal analyses that were performed using the constant head method, TDR-based sensors and dual thermal probes, respectively. The unique contributions made by each of these components are also discussed in terms of their particular application within various storage and bioconversion operations.

Model validation was performed with rectangular bales of switchgrass (102 x 46 x 36 cm^3) stored in an environmental chamber with and without partial insulation to control directional heat transfer. Bale temperatures generally exhibited the same trend as ambient air; although initial periods of microbial growth and heat generation were observed. Moisture content uniformly declined during storage, thereby contributing to minimal heat generation in the latter phases of storage.

The mathematical model agreed closely with experimental data for low moisture content levels in terms of describing the temperature and moisture distribution within the material. The inclusion of internal heat generation was found to be necessary for improving the prediction accuracy of the model; particularly in the initial stage of storage. However, the effects of natural convection exhibited minimal contribution to the heat transfer as conduction was observed as the predominate mechanism occurring throughout storage. The results of this study and the newly developed model are expected

to enable the maintenance of baled biomass quality during storage and/or high-solids bioconversion.

KEYWORDS: drying, heat and mass transfer, numerical modeling, storage, switchgrass, thermophysical properties

Drew Frank Schiavone

April 18, 2016

HEAT AND MASS TRANSFER IN BALED SWITCHGRASS FOR STORAGE AND BIOCONVERSION APPLICATIONS

By

Drew Frank Schiavone

Dr. Michael Montross
Director of Dissertation

Dr. Donald G. Colliver
Director of Graduate Studies

April 18, 2016

To my wife Jessica, and two beautiful daughters; I could not have done it without you.
Thanks for all the love and support along the way...
&
in memoria di mio padre

ACKNOWLEDGEMENTS

I would like to thank my advisor Dr. Michael Montross for his support and guidance throughout my research. I would also like to extend my gratitude to the remaining members of my graduate committee, Dr. Nokes, Dr. Sama and Dr. Sekulic, for their continued input and feedback. The help that I received from our undergraduate research assistants and my fellow graduate students was also instrumental in accomplishing much of this work. Specific thanks should be given to Aaron Turner, Josh Jackson, Nathan Bush, Will Adams and Zac Hammond for their mechanical and technical assistance which made this work possible.

Finally, I would like to thank my family for their encouragement through these challenging years. I am indebted to my parents for their continual support and sacrifice throughout my early academic career, as well as, the confidence afforded to me from my brother during my time spent at the University of Kentucky. I am extremely appreciative of my wonderful wife, Jessica, for her patience, perseverance, grace and hopeful disposition over these years. Her support has been critical in my academic success; while my daughters have brought joy and laughter to our family even in the difficult seasons. I could not have made it through this program without the support of everyone mentioned here and certainly not without Jesus Christ, my Lord and Savior, who is the foundation and perfection of my faith.

TABLE OF CONTENTS

LIST OF FIGURES

LIST OF TABLES

LIST OF EQUATIONS

CHAPTER 1:INTRODUCTION

1.1 Biomass Feedstocks

Increased environmental concerns in recent years have prompted a growing interest in the use of alternative and renewable energy sources such as biofuels; particularly in developed countries (Goldstein, 2006). In accordance with this rising trend, biomass has received considerable attention as a potential feedstock for many renewable energy production systems, thereby reducing the use of fossil fuels. However, the energy content per unit of dry biomass is less than the half of oil fuel, thus making bioenergy generally uneconomic compared to oil (Monti et al., 2009). Hence, biofuels generally remain uncompetitive compared with fossil fuels due to the low-yield conversions and overall diminished process efficiency, which is dependent on the application of appropriate storage and bioconversion operations.

Some perennial grasses, such as switchgrass, have prolific yield and low inputs making them attractive as biomass feedstocks (Shinners et al., 2010). In fact, 'Alamo' switchgrass *(Panicum virgatum* L.) is a warm-season perennial grass that has previously been identified as a model energy crop and biomass feedstock (Perlack et al., 2005). The low bulk density of herbaceous biomass such as switchgrass requires densification to achieve effective bioconversion; particularly in terms of lowering transportation and storage costs. Densification by baling increases the bulk density of biomass; increasing the net calorific content per unit volume. Baling also provides a more condensed format, improving the ease, and lowering the costs associated with handling, transport and storage. Thus, effective on-farm bioconversion processes may necessitate the baling of fermentable biomass.

Switchgrass typically has a low bulk density, ranging from 50 to175 kg m^{-3} (Shinners et al., 2009b) with large rectangular bales typically between 140 to 175 kg m^{-3} (Richard, 2010; Sokhansanj and Turhollow, 2004). This relatively low density makes it more expensive to transport compared to wood chips, house coal and anthracite (Chico-Santamarta et al., 2010). Further developments are needed in order to reach a target of 210 kg m^{-3} in order to fully load a semi-truck by weight.

1.2 Practical Applications

1.2.1 Bioconversion

Herbaceous biomass can be converted to liquid fuels and other chemical products through a variety of conversion processes including enzyme hydrolysis and fermentation technologies. However, the specifics involving the production of bioethanol from switchgrass are not discussed in this study as they are available elsewhere in the literature (Schmer et al., 2008). It will be noted here that current developments dealing with the bioconversion of agricultural feedstocks may involve the storage of baled biomass under anaerobic conditions within modified bunker silos. However, the over-accumulation of end-products inhibits bacterial growth and prevents ongoing biodegradation within solid-state fermentation. For this reason, biomass conversion in a high-solids environment has generally been unsuccessful.

In this case, the percolation of water through the densified material may capitalize on the rapid bacterial production by restoring favorable conditions for end-product formation; which is an innovation in high-solids biomass conversion. Liquid fuels and other byproducts may thereby be removed from the baled material by leaching and/or pumping fluids through the biomass. Although baling increases the net calorific content per unit volume, the densified bales do not shed fluids easily. This enhanced fluid retention may result in diminished biodegradation efficiencies and adverse storage conditions. Hence, solid-state fermentation of densified forage poses unique challenges not typically encountered with the digestion of traditional liquid wastes.

1.2.2 Storage

Feedstock storage may be a necessity in many operations due to narrow harvest windows and the year-round demand for biomass at conversion facilities (Mooney et al., 2012). Hence, a logistics infrastructure is needed that is capable of supplying high-value biomass throughout the year while producing cost-competitive biofuels for the market (Smith et al., 2013). Offsite storage management is expected to be critical in maintaining desirable composition characteristics and to ensure feedstock access under variable weather conditions.

Cellulosic biorefineries in the U.S. are expected to keep only a 72 h feedstock inventory with the remaining feedstock inventory at the edge of field or at satellite storage facilities (Hess et al., 2009). Thus, most storage is projected to occur outdoors and away from the conversion facility, either on-farm or at a satellite location (Larson et al., 2010; Sokhansanj et al., 2009). Large-scale biofuel production may also necessitate the storage of baled feedstocks for extended periods of time in order to avoid fluctuation in production by bridging periods between production seasons (Darr and Shah, 2012; Wiselogel et al., 1996). Thus, it would be expected for bioconversion facilities to store biomass up to one year which may require on-farm storage at the grower's expense (Hess et al., 2007).

Biofuel production operations require cost-effective storage solutions which maintain desirable quality characteristics, provide aerobically stable environments and have flexible delivery schedules depending on regional weather factors (Inman et al., 2010). Storage operations must also be able to handle material with a wide range of moisture contents throughout the harvest window; with direct harvest operations (single-pass baling) potentially introducing high-moisture feedstock into the supply chain (Mooney et al., 2012). Therefore, the estimates of dry matter loss, storage conditions and bale quality are necessary to provide a stable, consistent and high-quality source of raw herbaceous biomass to a biorefinery. An understanding of the conversion process, particularly in terms of the feedstock quality, is also necessary.

Ideal storage conditions require inexpensive and convenient bulk handling formats such as high-density bales. The prevention of undesirable deterioration is also critical; particularly in terms of ensuring minimal nutrient, material and/or dry matter loss. Accordingly, the estimates of quantitative and qualitative changes in bale composition during storage (i.e., dry matter loss) are necessary to determine the storage and bioconversion effectiveness. As such, optimal storage conditions of biomass have been researched for various bulk formats including rectangular bales of various sizes.

Although a growing number of studies involve the assessment and analysis of weathering and deterioration within baled forage, much of this research involves intensive field trials and instrumentation for particular feedstocks. Additionally, many of these studies involve simultaneous comparisons of two or more storage methods; with

experimental treatments involving the bulk format of the material, exposure to environmental conditions and application of chemical and/or biological pre-treatments. While much of this previous research has addressed dry matter loss and other quality changes during storage, the conclusions have often been limited to specific experimental conditions (i.e., moisture level, bulk density, and fixed environmental conditions).

The postharvest quality and nutrient retention of densified forages are both known to be influenced by specific environmental storage factors, as well as, the physical and rheological properties of the material. Thus, the development of models which simulate changes during storage and/or bioconversion may be necessary for the results to establish broader application. However, there is currently limited research pertaining to the comprehensive storage effects of dedicated feedstocks such as switchgrass; particularly with regards to the development of postharvest quality models.

A brief overview of storage management is considered in the following discourse of the current study in order to highlight and discuss the conditions necessary for providing a consistent and high-quality feedstock, particularly to a biorefinery. Although specific operations will guide the particular postharvest management practices, proper storage will ensure optimal feedstock quality.

1.3 Baling Format

After harvest, switchgrass can be packaged for storage and transportation in large round bales or large rectangular bales which both have a history of successful application in the feed and forage industries (Mitchell et al., 2008; Vogel et al., 2011). Round bales are common in many regions for both outdoor storage of hay (Bransby et al., 2005; Collins et al., 1997; Huhnke, 2003) and silage when wrapped (Rhein et al., 2005; Shinners et al., 2009b). Round bales are generally stored on their sides, but may be stacked with bottom bales set on their round faces and upper bales on their round sides (Taylor et al., 1995). Round bales may exhibit dry matter losses up to 50 %-wb when exposed to excessive moisture; primarily in the outer layer (Huhnke, 2003; Taylor et al., 1995). However, previous studies have indicated improved dry matter retention with round bales, particularly with ground preparation and protection of materials (Huhnke, 2003; Sanderson et al., 1997; Taylor et al., 1995; Wiselogel et al., 1996).

Conversely, rectangular bales either need to be removed from the field soon after baling or protected from precipitation events since the flat surface of the bale does not shed water easily with the potential for significant dry matter loss (Collins and Owens, 2003). In fact, round switchgrass bales stored outside are typically reported to have less storage losses than large rectangular bales as they are less prone to water penetration especially when net wrapped (Groothuis et al., 2011; Hess et al., 2009). The round baler method may also be utilized by smaller bioenergy producers due to the lower capital costs for equipment (Turhollow et al., 1998).

However, the field capacity of a round baler is typically lower since the baler must stop to wrap and release the bale. Large rectangular balers continuously bale without the need for stopping; while estimations indicate a lower cost per unit of harvested area (Lazarus and Selley, 2002). Rectangular bales also allow easier handling and loading for transport without road width restrictions (Groothuis et al., 2011). In fact, the time required to load bales onto semi-trailers is double for round bales compared with rectangular bales (Hess et al., 2009). Based on this information and the current developments for bioconversion applications, rectangular bales have been considered in the current study.

1.4 Storage Losses

Ideal storage management for any herbaceous biomass involves preservation of the material so that it enters and leaves storage in an unaltered state (Hess et al., 2007). Hence, the maintenance of low biological activity during storage is important for reducing microbial growth and subsequent storage loss. In practical application, however, the plant and microbial respiration both contribute to biomass heating, dry matter loss and compositional changes from the loss of structural (fiber) and non-structural (extractable) components; thereby diminishing the overall quality of the biomass. It may be noted here that bale temperatures in excess of 70 °C are typically generated by oxidative chemical reactions rather than heat from microbial and plant respiration (Festenstein, 1971).

In any regard, the spontaneous heating of baled biomass is known to be influenced by the moisture content (high moisture increases microbial growth); bale size (larger bales restrict moisture and heat dissipation to surroundings), bale density (low

density bales lose heat more rapidly); environmental factors (e.g., ambient temperature, relative humidity and air movement); storage structure (well ventilated bales experience less heating effects); and the use of preservatives (control microbial growth) (Buckmaster and Rotz, 1986; Nelson, 1968).

The moisture content at the time of baling is generally considered the most significant of these factors affecting spontaneous heating; with elevated moisture content allowing bales to reach and maintain higher temperatures (Barnes et al., 2007). High density bales also help to resist moisture accumulation, restrict air circulation and increase internal temperatures (Huhnke, 1990a; Russell et al., 1990). The time/temperature curves for various types of hay bales during storage are available in the literature (Hathaway et al., 1984; Miller et al., 1967; Nelson, 1968; Ream et al., 1983; Weeks et al., 1975).

1.5 Moisture Control

Feedstock value must also be maintained throughout storage with the application of appropriate moisture tolerant storage systems. As such, moisture migration within baled biomass can be controlled to some extent by managing the storage conditions in terms of the moisture inputs which include the initial moisture content of the feedstock, direct exposure to precipitation, and indirect exposure to ground moisture. Specific storage conditions which address these factors include bale coverage, ground preparations and stack configuration, among others.

Exposure to adverse weather conditions (i.e., precipitation, high relative humidity and temperature, wind, ultraviolet radiation) could also reduce the quantity and/or quality of switchgrass during storage. Such conditions could lead to significant dry matter losses that negatively affect biofuel production and increase the handling and transportation costs for a biorefinery (Sanderson et al., 1997). Although significant losses occur by molding, the leaching of soluble nutrients by water flow through the bale may be considered the principal cause of weather damage. In fact, water from rainfall or water absorbed from the ground can remove a significant amount of soluble carbohydrates which are important for biofuel production. In any regard, dry matter storage losses correspond to economic losses for energy conversion operations.

Therefore, appropriate storage operations must effectively prevent the introduction of moisture through the use of environmental barriers. However, the initial moisture content of the feedstock must also be considered since the use of impermeable barriers may retain excess moisture that can result in unstable storage conditions.

Although there is currently limited experience with large-scale switchgrass storage for bioenergy, considerable research has been conducted in regards to the various storage platforms for such baled forages. In fact, various storage methods and configurations were reviewed by Darr and Shah (2012) for baled feedstocks including open (uncovered), tarped and permanent structure (covered), and wrapped (anaerobic silage). The balance between cost and performance was discussed for each storage configuration with respect to dry matter loss.

On-farm storage strategies can broadly be categorized into aerobically-stable (dry) and anaerobically-stable (wet) storage (Smith et al., 2013). Dry storage relies upon the stability imparted by reducing biological water availability, thereby inactivating cellulose-degrading fungi and bacteria. However, materials must remain dry since these organisms can be revived upon rewetting. Alternatively, wet storage involves limited oxygen availability and microbial fermentation which produces organic acids while inhibiting cellulose-degrading microbial growth (Smith et al., 2013). The wet and dry storage methods both maintain dry matter, although each method has its associated weaknesses.

1.5.1 Indoor and Outdoor

While indoor bale storage would not be economical for biofuel production (Wiselogel et al., 1996); outside storage is generally easier to manage and provides a reduced risk of spontaneous combustion (Coblentz, 2009). However, the primary concerns in storing biomass outdoor for extended periods involve higher dry matter losses and changes in composition. Open, unprotected storage is generally considered the lowest cost and lowest performance storage option for dry biomass which relies heavily on the feedstock's ability to shed water.

An effective storage configuration must also provide an effective balance between moisture exclusion from the environment and moisture loss from the feedstock. While an

open stack design permits moisture release, it stands a higher risk for exposure to precipitation resulting in moisture gain. While no ground preparations may be required for outside storage configurations in the absence of standing water, moist precipitation regions require some protection. Therefore, outside storage options typically result in greater dry matter loss compared with other storage systems which may have adverse impacts on the conversion economics.

The potential moisture loss may also be reduced through the minimization of the exposed surface area which can be achieved through various storage configurations (Darr and Shah, 2012). In the current study, the environmental impacts were minimized by performing storage evaluations indoor within a controlled environment.

1.5.2 Coverage Types

Dry matter loss can be minimized during outside storage if the material is protected (i.e., polyethylene tarps) from environmental impacts. In fact, tarping is widely implemented in storage operations to prevent water infiltration at the top of bales, but improved ground preparations are necessary to divert the water away from the base of the bale. While tarping and proper drainage can work in concert to minimize moisture input, a covered configuration may also hinder the drying process by preventing the release of moisture to the surrounding air. Wrapping of dry feedstocks has also been proposed in order to prevent water infiltration without extensive ground preparations (Hess et al., 2009).

Enclosed structures are the most expensive storage platforms but ensure the greatest switchgrass value and lowest storage loss (Duffy, 2007). The storage of hay indoors generally results in reduced dry matter and nutritive losses (Collins et al., 1995). In fact, permanent structures are considered to have the best performance with roofs and pads that protect the feedstock from moisture infiltration. While tarped storage also excludes moisture, this storage practice lacks the ventilation, water vapor (moisture) loss, and ground surface protection afforded through a permanent structure. As mentioned previously, however, the implementation of covered storage facilities is unlikely to be economical for biofuel production.

Alternatively, bale wrapping excludes precipitation and moisture transfer in stored biomass while retaining the initial feedstock moisture. The wrapping of wet materials promotes anaerobic conditions (ensiling) while effectively trapping any excess moisture and preventing air penetration into the material (Shinners et al., 2009b). Proper application of anaerobic wet storage (ensiling) supports rapid fermentation with the available soluble carbohydrate and water content. Biological degradation is prevented by the subsequent pH reduction and low oxygen concentration until feedstock use (Philipp et al., 2007; Shinners et al., 2009b; Tabacco et al., 2009).

In fact, wrapped silage losses have been reported between 3 to 12 % (Huhnke et al., 1997; Shinners et al., 2009a); while higher in situ degradability has been reported in round bale grass silage (Petit and Tremblay, 1992). Huhnke (1988) also reported a significant difference in the dry matter loss for covered and exposed alfalfa bales stored for 8 months.

1.5.3 Ensilage

Wet storage methods have been proposed for a number of feedstocks including switchgrass (Collins and Owens, 2003; Digman et al., 2010b; Hess et al., 2009), particularly in regions with high relative humidity and increased chance of precipitation after harvest (Digman et al., 2010a). Ensiling feedstocks with less than 30 to 35 %-wb has previously indicated increased mold growth and microbial heating within the material; conditions that are exacerbated by the air limitation (Gordon et al., 1961). Conversely, ensiling at more than 70 %-wb has resulted in increased effluent and clostridia bacterium growth which is undesirable (Davies and Nicholson, 1999; Gordon et al., 1959; McDonald et al., 1991; Moore et al., 1960). Accordingly, the moisture content for switchgrass at time of pickup under wet storage methods are typically greater than 40 %-wb (Mitchell and Schmer, 2012); although the ideal moisture for many feedstocks have not been investigated.

The impact of baling density is also necessary for assessing the preservation of round bale silage. Previous studies have indicated that increasing density generally reduces storage costs by increasing the storage capacity and reducing nutrient losses (Muck and Holmes, 2000). Pretreatments on switchgrass stored under wet conditions

have also been investigated with results indicating inhibition of microbial activity while improving ethanol conversion efficiency (Digman et al., 2010a).

Advantages of wet storage methods include reduced harvest costs, lower dry matter losses during storage, improved switchgrass cell wall recovery during enzymatic hydrolysis and lower potential risk of fire during storage (Digman et al., 2010a; Muck and Shinners, 2001). However, the costs associated with transportation, handling and drying of wet, aerobically unstable feedstocks limit the practicality of wet storage (Atchison and Hettenhaus, 2003). In fact, the wet storage method was found to be more expensive than other collection and storage methods because of the high cost associated with storage equipment, ensiling facilities and transportation of wet material by truck (Collins and Owens, 2003; Kumar and Sokhansanj, 2007).

1.6 Moisture Transfer

The storage of unprotected herbaceous biomass generally involves moisture transfer between the crop and the environment (including drying and rewetting processes), until a suitable equilibrium moisture is attained. Initially after harvesting, the plant cells are alive and continue to respire until the moisture content of the crop reduces to 30 % on a dry basis (Gupta et al., 1990); while microbial respiration generally proceeds at moisture levels exceeding 16 %-wb (Mitchell and Schmer, 2012).Therefore, harvesting moist switchgrass generally requires field drying to reduce the moisture content to safe storage levels after baling.

Typical field drying processes after baling involve moisture migration from the interior of the bale to the surface, as well as, from the bale surface to the surrounding air. Although the directional transfer of moisture is dependent on the moisture content of the biomass and the humidity of surrounding air; bale weight generally decreases during storage due to the loss of moisture and/or dry matter content. No further moisture losses occur when bales reach moisture equilibrium with the environment. The moisture gained or lost during storage may be considered as sources (or sinks) that alter the moisture content on a bulk level or on a local level with variable moisture regions.

1.6.1 Moisture Sources (Wetting)

Moisture sources may include the initial moisture content of the feedstock, atmospheric moisture (i.e., precipitation, relative humidity) and other environmental moisture inputs (i.e., soil/ground water). Although the principal moisture sink is typically the atmospheric air, local moisture sinks may also arise in those regions within a bale that are in direct contact with barriers and/or experience significant temperature gradients. Bales that are slowly dried or those that become rewetted may experience considerable microbial growth and subsequent nutrient losses. Hence, environmental factors (i.e., temperature, relative humidity, solar radiation, wind speed, ground moisture), crop characteristics (stem diameter, leaf-to-stem ratio, bulk density, etc.) and storage structure all play an important role in the moisture dynamics during storage (Barnes et al., 2007).

As mentioned previously, adverse weather conditions (i.e., precipitation and infiltration) may delay the drying process (Haghighi et al., 1990; Moore & Peterson, 1995) as significant amounts of moisture are added to the biomass. In fact, rainfall may result in the rewetting of a partially dried bale while extending the losses caused by respiration. Likewise, low temperatures generally slow the drying process; thereby extending the conditions that contribute to dry matter losses (Coblentz, 2009). Leaching losses are also related to the amount of rainfall and the moisture content of the baled material (Gupta et al., 1990).

Water vapor may also condense in response to lower external air temperatures, higher humidity levels and the insulating properties of the feedstock which enable heat retention (Shinners, 2000). The difference between internal bale temperature and air temperature represents a temperature gradient that can potentially lower the water holding capacity of the air. A broad region of moisture accumulation may form in response to a temperature gradient that can extend into the bale.

Elevated temperatures within a bale will also promote upward movement of vapor-phase water due to buoyancy effects induced by temperature differences between cool dry air and warmer humid air. Elevated temperatures may also occur as a result of biological activity or exposure to various environmental heat sources (i.e., solar radiation, ground temperature). The difference between the relative humidity within the material and the relative humidity of the surrounding environment may cause water vapor to

diffuse through the material and exit the bale.

1.6.2 Moisture Distribution

The moisture distribution within stored bales is generally not uniform in location or time, but is rather a dynamic property that varies in response to environmental factors (i.e., precipitation, diurnal temperature changes) and internal heating from respiration (i.e., microbial, fungal). High moisture may result in inhomogeneous conditions as the moisture redistributes and concentrates in specific regions. As discussed earlier, these high moisture regions form in biomass in direct contact with vapor barriers and in regions exposed to precipitation. Water channeling may also occur between the layers that form large rectangular bales, resulting in heterogeneous spoilage (Hess et al., 2009) and local damage at the top or bottom of bales depending on specific storage circumstances (Darr and Shah, 2012; Shinners et al., 2007, 2010).

Furthermore, self-heating may create temperature gradients that concentrate excess moisture at the surface of the bale. Uneven moisture distribution also poses various challenges associated with the characterization and estimates of bulk moisture content. High moisture regions arising from moisture infiltration and/or migration also result in biologically unstable regions that may promote microbial and fungal growth, thereby, contributing to the biological degradation of the material.

1.6.3 Moisture Sinks (Drying)

Natural and artificial drying operations may help to counteract the microbial activity associated with high-moisture while promoting safe storage conditions. Therefore, drying operations are also of particular importance in storing and processing agricultural biomass; particularly considering the high energy demand required for artificial drying processes. In fact, the drying input (natural gas) of switchgrass has been reported at 872 MJ mg^{-1} to dry to 10 % moisture content (Bergman et al., 2015); thus requiring 27.09 m^3 of natural gas combusted at 80 % efficiency (FPL, 2004). This large energy consumption and the wide application base for drying necessitate an undertaking of fundamental research in this field.

Switchgrass can also be dried in the field from an initial moisture content ranging from 43 to 66 % at the time of cutting (Sanderson et al., 2006; Shinners et al., 2010) to 22 % or less before being baled and transported to a storage facility or biorefinery (Rinehart, 2006; Sanderson et al., 2006). As a rule-of-thumb, biomass baled below 18 % moisture will experience minimal dry matter losses; generally in the range of 5 to 10 %. However, the specific storage changes and bioconversion processes occurring within baled material are currently underdeveloped; due in part to the significant variations in thermal and physical properties. Hence, accurate and effective models could provide valuable insight into the effective storage of baled biomass and/or the optimization of bioconversion operations.

Analytical drying models have been proposed for porous materials in the literature, but most have a narrow range of applicability; particularly in regards to relevant material properties and drying conditions. Thus, the formulation of a mathematical model for densified agricultural materials may enable sufficient assessment of the moisture transfer. The model itself must be general enough to be applicable throughout the drying regimes expected in storage, while being simple enough to be readily solved.

1.6.4 Optimal Moisture

Stable storage conditions are generally achieved by minimizing the biological degradation through the regulation of moisture content. In fact, dry matter losses and microbial heating are widely described as functions of the baling moisture, as well as, the maturity, density and type of storage facility. The loss of dry matter content and nutrient value occur due to various factors including respiration, microbial activity and mechanical handling which may occur during storage (Buckmaster et al., 1989). Therefore, a challenge exists in determining the optimal time to bale biomass in order to preserve quality.

If the biomass is baled at too high a moisture content, the larger package results in increased drying time which may allow mold growth to begin before drying is completed. Hence, biomass is typically allowed to dry to a moisture content that is safe for storage prior to baling. This practice, however, may cause excessive harvest and/or

collection losses as the nutrient rich material may become brittle and break from the stem during subsequent handling; a condition referred to as ‘leaf shatter’. While field losses (i.e., mechanical handling, harvest efficiency, leaf-shattering, etc.) are comparatively low when the crop is baled at moisture content above 18 % wet basis (Savoie, et al., 1982), considerable respiration and leaching losses may occur during the field curing process (Barr et al., 1995). Prolonged exposure to sunlight also bleaches nutrients from the leaves and stems.

While the vegetative growth stage of switchgrass may contain 70 to 80 % water at the time of harvest, safe storage is typically achieved with large round and rectangular bales of switchgrass requiring moisture levels below 18 and 16%, respectively, at the time of baling in order to reduce storage losses (Mitchell and Schmer, 2012). Although the threshold for larger bales is assumed to be lower (Collins et al., 1987), field drying is generally required prior to baling in order to meet these safe moisture levels. In this discussion, the term ‘safe storage’ implies minimal heating, molding and/or nutrient degradation. These low moisture levels are assumed to be relatively stable while exhibiting minimal evidence of microbial respiration (Rotz and Muck, 1994).

Although higher moisture contents may improve field losses, significant losses arise when sufficient moisture is present for microbial activity. This results in significant dry matter loss, nutrient degradation and microbial heat generation as microorganisms convert starch to sugar in an exothermic reaction (Miller, 1947; Rotz and Muck, 1994). Consequently, the storage of biomass with high moisture content may result in significant health risks due to microbial activity (Jirjis, 2005) and deleterious changes in the forage nutritive value (Coblentz et al., 1996, 2000; Roberts, 1995), in addition to the dust and mycotoxins that are associated with excessive mold growth.

Dry matter loss specially derives from compositional changes of the cell walls, as well as, physical losses that impact bioconversion processes (Weiselogel et al., 1996). Excessive heat development may also cause spontaneous combustion at temperatures exceeding 170 °C as a result of prolonged plant respiration and mold growth which have been correlated to increased moisture at baling (Moore and Peterson, 1995; Roberts, 1995; Scudamore and Livesey, 1998). The risk of spontaneous combustion also represents subsequent material loss and worker hazard. Even when temperatures do not

reach combustible levels, they may cause protein 'binding' causing indigestibility by feed animals or diminished bioconversion efficiency.

1.7 Storage Composition

The loss of dry matter and fermentable carbohydrates both have negative economic impact on the overall bioconversion operation (Wiselogel et al., 1996). Hence, the changes in herbaceous feedstock quality during storage have been widely reviewed, with numerous studies indicating significant losses of extractives and fibers (Agblevor et al., 1994; Cusi, 1979; Jirjis and Theander, 1990; Kubler, 1987; Moser, 1980). The various factors resulting in dry matter storage losses can be divided into biological causes, microbial activity, spontaneous heating and physical causes as discussed in this review.

Major contributions to biomass loss may be attributed to weathering, as well as, microbial activity which expedite the production of detrimental compounds which hinder the biochemical conversion of feedstocks (Cusi, 1979; Jirjis and Theander, 1990; Moser, 1980). Extensive research has been conducted in minimizing these storage losses, including moisture reduction prior to storage, improved drainage and the application of appropriate forms of bale protection. Low relative humidity and low ambient temperatures also reduce dry matter loss and compositional degradation. Balers can also be modified to spray preservatives (i.e. propionic acid) to limit microbial growth (Collins and Owens, 2003); although this topic is considered outside the scope of the current research.

Nutrient changes can be minimized by baling at low moisture levels and storing indoors (Moser, 1980; Weeks et al., 1975). However, herbaceous biomass baled at moisture levels exceeding 20 % will typically experience significant mold development and the associated heat generation which both impact the nutrient retention of the material (Miller et al., 1967; Nehrir et al., 1978; Nelson, 1968; Rohweder et al., 1978).

1.7.1 Respiration

Bale spoilage can be primarily attributed to the biochemical and enzymatic reactions of microbial respiration (Greenlees et al., 2000) which occur when there is sufficient moisture in the environment (Johnson, et al., 1984; Nelson, 1972; Rohweder et

al., 1978). Respiration during bale storage includes that from the plant cell components; as well as, the microorganisms; although it may be difficult to separate the effect of plant and microbial respiration. Plant respiration is positively correlated with temperature; with plant cells and respiration becoming inhibited at temperatures of 40 to 45 °C; which is easily attainable in moist hay (Barnes et al., 2007; Moore & Peterson, 1995). However, microbial respiration is generally responsible for most of the spontaneous heating and dry matter losses occurring in moist hay (Barnes et al., 2007).

1.7.2 Temperature and Moisture Effects

As mentioned earlier, several factors are known to affect bale storage quality including various environmental factors (weathering), material properties (baling moisture, density), and type of storage structure/facility (coverage, duration, orientation, etc.) (Wiselogel et al., 1996). In accordance with these factors, temperature and moisture (exacerbated by adverse weather conditions) serve as the primary factors affecting the microbial and fungal populations within a densified biomass (Coblentz, 2009; Russell and Buxton, 1985). In fact, bacterial growth is generally considered as a function of moisture content (Huhnke, 1990b); while significant fungal growth typically occurs at temperatures above 20 °C and relative humidity of more than 70 % (Barnes et al., 2007; Moore and Peterson, 1995).

A general rule-of-thumb was suggested by Waldo and Jorgensen (1981) with a 1 % loss in dry matter assumed for each 1 % decrease in moisture content; while simple linear regression models have also been developed for describing the storage loss of baled hay as a function of moisture content (Martin, 1980; Ream, et al., 1983):

$$\mathrm{DML} = 77 \cdot \mathrm{M_i} - 10.71 \qquad [1.1]$$

where: DML = dry matter loss (% of initial) and M_i = moisture content at baling (decimal, wb).

1.7.3 Spatial Distribution of Losses

Several studies have also shown that most dry matter loss and deterioration occur in the outer layers of a stored bale, a process generally termed ‘weathering’ (Coble et al., 1985). In some cases, water-logged bales become difficult to handle; particularly without comprising the integrity of the twine that holds the bale together. Therefore, herbaceous biomass such as baled switchgrass should generally be stored below 15 %-wb to prevent degradation by filamentous fungi and bacteria (Rotz, 2003). This must be accomplished through the simultaneous implementation of techniques that reduce rain infiltration and allow better drainage to reduce storage losses (Coble and Egg, 1985). Likewise, improvements in the local storage conditions typically require the techniques that promote moisture loss from bales, although any water that is introduced into the material is generally difficult to remove.

1.7.4 Compositional Changes

Changes in the physical and chemical constituents of the feedstock can have adverse effects on the efficiency of storage applications and/or the profitability of bioconversion operations. In fact, the production of biochemical fuels is significantly impacted by the structural and non-structural cell-wall constituents (Wiselogel et al., 1996). Previous studies (Lacey and Magan, 1991) have demonstrated that forages and grain are colonized and decomposed by various bacteria, yeast and filamentous fungi during storage. However, the relationship between the microbial populations and environmental conditions were not investigated. The decomposition of biomass has been considered by some to be a process similar to composting (Summers et al., 2003) which proceeds at a rate that is inversely correlated with the carbon-to-nitrogen ratio (C:N) (Henriksen and Breland, 1999).

Switchgrass generally stores easily due to the lignocellulosic-rich composition which is more readily subjected to the loss of soluble constituents during storage (Dien et al., 2006). In fact, the cellulose and hemicellulose carbohydrates must be preserved in high yields since they are a source of valuable chemical and fuel products (Wiselogel et al., 1996). These cell wall polysaccharides typically remain unchanged during storage due to the lignin matrix that provides a physical barrier to most microbial enzymes (Jung

and Deetz, 1993).

Studies have generally indicated no changes in the cellulose content for bales of various crops including round orchardgrass, alfalfa hay and switchgrass (Coblentz, 2009; Wiselogel et al., 1996). On the other hand, somewhat significant decreases in the structural carbohydrates have been reported in the weathered fraction of tall fescue, alfalfa/orchard grass and switchgrass bales stored unprotected for 9 months (Agblevor et al., 1994). The loss of lignin may also be considered to be a form of pretreatment which provides access to the structural carbohydrates for hydrolysis (Wiselogel et al., 1996). It has also been reported that hemicellulose may be broken down more easily by enzymes present during ensiling (Dewar et al., 1963). The conversion of cell wall polysaccharides by fermentation could also result in significant downstream losses associated with the conversion of acids to other useful products (Shinners et al., 2010).

The water soluble portion (extractives) of biomass generally accounts for 15 % of the dry weight reported for switchgrass (Chen et al., 2010). The acid-detergent fiber (ADF) fraction primarily consists of cellulose and lignin; while the neutral-detergent fiber (NDF) fraction (consisting of cell wall polysaccharides such as cellulose, hemicellulose and lignin) typically undergoes minimal changes compared with the soluble extractives (Huhnke, 1990a; Taylor et al., 1994). Numerous studies have shown that greater temperatures result in higher ADIN fractions which have been correlated with low dry matter content at the time of baling (Buckmaster and Rotz, 1986; Collins et al., 1987).

Common predictors of feedstock quality include the detergent fiber analysis method (Goering and Van Soest, 1970), the dietary fiber analysis method in which cell wall polysaccharides are broken down by hydrolysis (Jung and Lamb, 2004) and the NIRS (Near Infrared Reflectance Spectroscopy) method which predicts chemical composition. Comparisons of these analyses are outside the scope of the current study, but have been discussed elsewhere for alfalfa, bromegrass, corn stover, reed canary grass and miscanthus; among others (Jung and Lamb, 2004; Wolfrum and Lorenz, 2009).

Changes in the extractives content (non-structural cell components) may also be important for bioconversion and biofuel production applications. Some of switchgrass extractives contain fermentable carbohydrates (e.g., sucrose, glucose, and fructose) that

may account for 18 to 27 %-db of the total extractive weight (Chen et al., 2010; Dehority, 1993; Wiselogel et al., 1996). Hence, any substantial degradation and/or loss of the extractables could constitute a loss of valuable substrate. This becomes a significant concern as extractives have been shown to dramatically decrease for stored bales of switchgrass during storage (Agblevor et al., 1994; Wiselogel et al., 1996). On the other hand, the removal of toxic extractives during storage could promote the microbial growth desired for bioconversion processes.

It follows that, a quantification of temperature and moisture content during storage is necessary to assess the storage impacts on feedstock preservation, particularly in relation to the specific storage format that is employed. The accurate assessment of temperature and moisture may allow for the utilization of the feedstock at its optimal value while identifying quantitative losses. The quantification and monitoring of temperature and moisture in storage will be necessary in the near term to predict storage stability and biorefinery demands. Appropriate storage practices may be further refined as optimal biomass specifications are identified.

1.8 Storage Studies

Previous studies have demonstrated that considerable dry matter losses occur during the storage of baled herbaceous feedstocks including switchgrass, particularly in the outer layers due to ‘weathering’ effects. The associated temperature variations and movement of moisture within these baled feedstocks have generally been investigated under the ambient environmental conditions of typical storage operations including field and barn storage. Sampling routines are generally limited to hourly weather data and daily measurements of the bale conditions. Although the various storage evaluations have been detailed in the available literature, there is currently a lack of intensive time series measurement for rectangular bales of switchgrass, especially under controlled storage conditions.

While literature continues to develop for the agronomic practices and dry matter losses of switchgrass (Khanchi et al., 2009; Monti et al., 2009; Sanderson et al, 1997; Shinners et al., 2010), the impact of specific storage conditions remains poorly understood; particularly in the consideration of the material as a biomass feedstock.

Optimal processing economics require the storage of biomass feedstocks for continuous delivery of raw material to biorefineries. Therefore, evaluation of stored switchgrass is necessary to establish effective storage operations that reduce energy losses and provide high quality feedstocks at minimum cost.

1.8.1 Field Storage

Several studies have evaluated the dry matter loss of dedicated herbaceous crops such as switchgrass, with typical aerobic storage losses ranging from 3 to 39 % (Shinners, 2000; Shinners et al., 2007, 2011); although degradation has been reported as high as 42 % by volume for round bales (Rider et al., 1979). Harrigan and Rotz (1994) reported that round bales of alfalfa experienced 6 and 16 % loss of the forage over 6 to 9 months for inside and outside storage, respectively. Losses were typically reported in the outer 10 cm of the bales while the soluble dry matter constituents were the predominate losses. Likewise, Johnson et al. (1991) reported losses of 8 to 15 % for round switchgrass bales stored on sod compared with 2 to 4 % for bales stored on crushed rock after 6 to 8 months. Agblevor et al. (1993) also reported significant degradation and weathering in stored switchgrass after 9 months. The weathered layers were observed to have lower extractives, cellulose and hemicellulose content compared with the unweathered center of each bale.

Wiselogel et al. (1996) investigated the storage conditions of large round bales of switchgrass stored unprotected, outside for 26 weeks. Although minimal microbial heating occurred, significant weathering was observed, particularly in those bales exposed to high rainfall. The weathering effects were apparent in terms of various compositional changes. In this case, the loss of non-structural (extractives) in the outer weathered layer (11 %), and to a lesser extent, the unweathered inner fraction (8 %) was observed to be the predominate effect. Sanderson et al. (1997) also assessed the storage of large, round bales of switchgrass baled at 11 to 19 %-wb under protected and unprotected conditions on both a grass sod and gravel pad for up to 12 months. In general, bale weight declined linearly with dry matter losses of 0–2 % and 5–13 % of the original bale weight for those bales stored inside and outside, respectively.

Savoie et al. (2006) alternatively reported a positive but diminishing rate of dry matter loss approaching an asymptotic maximum. Bales stored outside also had visibly weathered layers, while rotted areas were observed in those bales in direct contact with sod. While drainable surfaces are typically considered for protection against dry matter losses, some studies have found no statistical difference among treatments (Khanchi et al., 2009; Sanderson et al., 1997).

Han et al. (2004) determined the effects of moisture content and crop density on the dry matter retention, forage quality and nutritive value of round baled alfalfa in silage form and dry hay form on a well-drained grass sod for 8 months. Moisture significantly increased in the hay; and to a lesser extent in silage since the respiration processes were observed to produce some water. The silage exhibited lower peak bale temperatures, indicating the impact of moisture-induced heating and oxygen exclusion. Although the dry hay bales lost an average of 18 % of the initial dry matter, silage bale weights were relatively stable during storage. Post-storage NDF and ADL concentrations were also higher in the dry hay bales compared with silage indicating improved preservation of dry matter.

Monti et al. (2009) also investigated the storage of rectangular and round bales of switchgrass with soft and hard cores on wood pallets under a sheltered roof for 96 and 114 days. Bale weight generally decreased over time due to significant declines in the moisture content. Although dark, weathered layers were observed in the outer 1–2 cm of each bale, the preservation of dry matter indicated minimal respiration and fermentation throughout storage. Similar results were presented for alfalfa-orchardgrass hays stored for 11 months on pallets (Coblentz and Hoffman, 2009); thus, indicating the significant storage surface effects on dry matter loss.

Shinners et al. (2010) stored round bales of switchgrass in a completely enclosed shed and outdoors on crushed rock and grass sod for 9 to 11 months. Bales were formed with twine, net wrap or plastic film. In this case, the plastic film was found to effectively prevent exposure to precipitation and subsequent leaching of soluble components. Moisture in outdoor bales was spatially variable, with higher moisture in the base and below the major axis of each bale; particularly those wrapped in plastic as condensation was drained toward the base. Dry matter loss averaged between 3.8 to 14.9 percent for

outside bales depending on coverage type, with those wrapped in plastic film exhibiting the greatest dry matter retention. The uniformly low moisture content of indoor bales resulted in minimal dry matter losses of 3.0 %; while silage preservation at 39.9 %-wb resulted in an average 1.1 % dry matter loss. Similar losses were reported for reed canarygrass bales wrapped with plastic film, net wrap, plastic twine, and sisal twine (Shinners et al., 2006), round alfalfa bales (Shinners et al., 2009b), and low- and high-moisture, tarped corn stover (Shah et al., 2011).

In general, the storage losses for tarped rectangular bales of switchgrass are greater than for tarped round bales (Larson et al., 2010). Dry matter losses of 7 and 25 % have similarly been reported for tarped and untarped rectangular bales after 6 months in storage, respectively (Martinson et al., 2011). Mitchell and Schmer (2012) also investigated the effects of harvest moisture content on the forage quality of large round bales of orchardgrass stored outside on a well-drained sod surface for 10 weeks. Results indicated molding even at relatively low moisture concentrations; with significant molding and forage quality losses at levels above 15 %-wb. A reduction in mold growth was achieved by baling dry at 12.4 %-wb or wrapping round bales up to 33.7 %-wb.

Chico-Santamarta et al. (2011) assessed the microbial growth within baled canola straw stored in an open shed for up to 20 months. Results indicated significant changes in the moisture content, microbial populations and C:N of the biomass; while bale temperatures indicated no self-heating. In general, the number of bacterial and fungal CFU followed the same trend as the ambient relative humidity, while increased ratios of C:N were observed centrally within each bale due to natural variations in the straw. Mwithiga et al. (2012) evaluated the storage effects of motorized and manually-packed bales of buffel grass placed on wooden platforms in an open hay barn with and without tarp cover. A marked decrease in moisture content generally occurred in all treatments, except during the coldest season of their evaluation. Results indicated that the open barn with and without tarp cover could be used to store bales for a period of up to 5 months with minimum changes in NDF and ADF.

Mooney et al. (2012) stored large round and rectangular bales of switchgrass outdoors with and without tarp cover for up to 529 days on grass, gravel and pallet surfaces. Precipitation readily penetrated rectangular bales causing partial decomposition,

particularly in bales without cover. However, round bales with or without cover generally exhibited improved ‘weathering’ resistance. Based on these results, bale shape (large round and rectangular bales) and storage environment (indoors and outdoors) were found to affect dry matter losses to the greatest extent. Dry matter losses for rectangular bales generally exceeds those of round bales for outdoor storage, while this disparity is diminished with indoor bale storage (Coble and Egg, 1987; Cundiff and Marsh, 1995; Monti et al., 2009; Sanderson et al., 1997; Shinners et al., 2010).

Smith et al. (2013) investigated moisture movement within round bales of corn stover and energy sorghum stored outdoors in uncovered, tarp-covered and wrapped stacks; with bales placed on level unprepared dry ground, as well as, well-drained graded gravel pads. Distinct patterns of moisture migration were observed in a variety of on-farm storage configurations ranging from open (untarped) to closed (stack wrapped). The greatest amount of moisture heterogeneity were caused by environmental exposure, positional orientation and barrier contact. Unprotected bales accumulated some moisture while wrapped bales provided better protection than both the tarped and untarped bales. It may also be noted that, the average moisture content generally decreased throughout storage due to gradual drying effects. Dry matter losses of 25–45 % were reported after 9 months; indicating an increased level of biological activity occurring within the high-moisture conditions maintained in the material.

1.8.2 Lab-scale Storage

Although previous studies have evaluated the storage of various herbaceous feedstocks, uncontrollable factors such as weather often hinder the effectiveness and comparability of individual field trials. In fact, variation in the ambient storage conditions (i.e., temperature, relative humidity) may significantly affect storage operations and the respective feedstock quality. In addition to weather unpredictability, variations in the material properties (i.e., temperature, moisture content, density) give rise to significant challenges in conducting consistent storage trials. The complexity of controlling these common storage variables can often prohibit direct and accurate comparisons between trials, thereby, limiting the application of the relevant information obtained.

The use of small-scale systems allows more treatments to be examined while simplifying replication and minimizing cost. These advantages are not possible in large, field-scale studies where baled-feedstocks are stored in commercial-size stacks. Thus, lab-scale systems have been proposed to minimize the effects of weather and storage variability without necessitating expensive field trials (Baron et al., 1991; Goering and van Soest, 1970; Goering et al., 1973; Moore et al., 1985; Yu, 1977).

Many of these lab-scale systems involve the packing of reconstituted forages into glass jars (Albert et al., 1989; Festenstein et al., 1965; Lacey and Lord, 1977; Lacey and Magan., 1991; Moore et al., 1985) polystyrene and paper sacks (Woolford and Tetlow; 1984) or polyvinyl chloride tubes (Baron et al.; 1991). Baron et al. (1991) also described the insulation of small hay packages in a controlled, laboratory environment to resist heat loss, while providing proper aeration to maximize temperature response and allow for water dissipation.

Although these methods generally provide useful information, few allow for interaction between hay packages, such as occurs in typical on-farm storage. Furthermore, these packaged materials have not been statistically compared with those of identical herbage of the same moisture content and density as conventional bales. Fiber orientation and packing arrangement are also lost with these packing systems resulting in changes in the heat and mass transfer. Simple lab-scale baling systems have been developed and evaluated as a result. In fact, Coblentz (1993a, 1993b) developed a system for preparing lab-scale bales of alfalfa at variable densities with a hydraulic press.

Coblentz et al. (1994) later investigated the efficacy of incubating lab-scale bales in isolated, laboratory environments. These lab-scale bales generally demonstrated an ability to generate heat, undergo quality changes and provide distinguishable response from the dominating influence of conventional bales. However, lab-scale bales were unable to maintain internal bale temperatures to the same extent as conventional bales, indicating that lab-scale bales lack the substrate necessary to sustain similar heat production. Heat and moisture dissipation within lab-scale bales are also significantly altered from conventional bales due to the increased ratio of surface area to volume, thereby preventing simulation of practical storage operations. For these reasons, small

lab-scale bales are generally unable to simulate conventional bales in regard to heat generation, mold development or quality changes.

1.9 Motivations

In recent years, there have been numerous studies addressing temperature and moisture distributions within baled biomass; primarily during traditional storage evaluations. However, numerical analyses of these processes are virtually nonexistent even though this knowledge is expected to play a critical role in developing and effectively applying postharvest quality models. Hence, the motivation for the proposed work was based on the need for an accurate mathematical model enabling the prediction of temperature and moisture content during drying, storage and/or bioconversion of rectangular-baled biomass. As such, the direct objective of this work was to evaluate the temperature and moisture within baled biomass during storage, as well as, quantify the microbial heating that may occur during storage and/or high-solids bioconversion.

1.9.1 Necessity of Study

While the current study provides no direct comparison of storage conditions; it does provide a thorough assessment of heat and mass transfer within a porous media that represents the rectangular-baled structure of biomass. This research is, therefore, expected to describe the moisture and temperature profile of baled biomass while accounting for fluid flow and the rapid effect of chemical reactions within bales due to microbial activity. While the fluid and hydrologic properties are expected to have significant impact on the long-term storage quality and bioconversion of baled biomass, these parameters have yet to be investigated for many agricultural feedstocks; particularly in a densified or baled format. In fact, quality assessments of baled biomass through heat and mass transfer simulations necessitate an understanding of the relevant fluid properties within the material. Likewise, the thermo-physical properties of the material (i.e., thermal conductivity, thermal diffusivity and specific heat) must be quantified in order to simulate heat transfer. Thus, the current study aims to characterize the fluid behavior and thermal energy transfer that occur within baled feedstocks.

1.9.2 Current Applications

Based on these motivations, the current research specifically assessed the short-term storage quality of rectangular-baled switchgrass under controlled environmental conditions with respect to temperature, moisture content and dry matter loss. Hence, this study involved an investigation of the relationship between the initial moisture content, storage configuration, bale temperature, microbial heat generation and temporal environmental conditions such as temperature and relative humidity. The effects of these factors on the physical and rheological properties of the material, including dry matter retention and biomass quality, were assessed under controlled environmental conditions for up to 60 days.

1.9.3 Practical Applications

The results of this study are intended to provide a practical understanding of the proper storage management of baled feedstocks such as switchgrass while defining the dynamic relationships between temperature, moisture content and feedstock quality. Hence, this study aims to contribute to the development of optimal storage operations for baled switchgrass in terms of improved temperature and moisture management. In accordance with this objective, the current study involves the development of a heat and mass transfer model describing the dynamic temperature and moisture content profile within baled switchgrass. Thus, this study promotes the development of improved agricultural practices and research efforts addressing the optimization of the high-solids bioconversion of switchgrass into fuels and chemicals as influenced by relevant storage operations.

The numerical modeling of porous media has a diverse range of applications with the current study expected to provide the information necessary to minimize storage loss and/or optimize the bioconversion of rectangular bales. The development of such a model is expected to serve as a decision aid regarding specific changes that may occur during storage and/or bioconversion; while providing quantitative information regarding relevant conditions such as nutrient and temperature changes. This research also stands to provide effective evaluation of alternative methods for storing baled biomass over a wide range of conditions. Model results may specifically assist in determining beneficial storage

changes, as well as, addressing issues pertaining to the presence of deterioration and/or the likelihood of stored heat resulting in spontaneous combustion.

CHAPTER 2:OBJECTIVES

The overall objective of this research was to develop and enable a better understanding of the quality of baled biomass during on-farm storage and/or high-solids bioconversion. Accordingly, this study investigated the temperature and moisture profiles within baled switchgrass while accounting for microbial heat generation within the densified biomass. Hence, the motivation for this research was based on the need for an accurate understanding of the heat and mass transfer occurring within rectangular-baled biomass. As such, this research addresses the quality changes that occur in storage and should provide the information necessary to minimize losses while enabling the identification of optimal storage parameters.

This research is also expected to contribute to those efforts aimed at the production of liquid fuels from high-density biomass that may involve percolation of fluids through the porous material. Therefore, the results of the current study stand to provide the understanding necessary to improve upon the current design criteria for bioconversion operations. Accordingly, these results should help managers obtain good quality feedstocks and efficient processing as quickly as possible. The project was divided into the following specific objectives:

- Assessment of fluid properties of baled switchgrass
- Evaluation of TDR for moisture measurements in baled switchgrass
- Evaluation of the thermophysical properties of baled switchgrass
- Heat and mass transfer model and simulation of baled switchgrass

2.1 Fluid Properties

To characterize fluid flow through baled biomass by determining specific hydraulic processes occurring within the porous material; specifically an assessment of 1) the saturated moisture content; 2) the leaching behavior; 3) the saturated hydraulic conductivity; 4) the unsaturated hydraulic conductivity; and 5) sorptivity. It was hypothesized that increasing the baling density would reduce the flow rate of water through the material in terms of the saturated and unsaturated hydraulic conductivity as the porosity was minimized at higher densities.

2.2 Moisture Measurement

Time-domain-reflectometry (TDR) techniques were used to evaluate the ability to quickly and accurately determine moisture content within herbaceous biomass. Hence, this study involved the calibration and validation of a TDR sensor for monitoring water content in ground and baled switchgrass. The TDR technique was proposed as a fast, simple, compact, cost-effective and non-destructive method for moisture measurement in baled forages. It was hypothesized that the calibrated models for moisture content that were developed for lab-scale bales (38 x 46 x 94 cm^3) would be in good agreement with the gravimetrically-determined values of moisture content in larger bales (102 x 46 x 36 cm^3) of switchgrass.

2.3 Thermophysical Property Analysis

A dual thermal probe consisting of a thermal conductivity probe and separate thermal diffusivity probe were used to determine thermal properties of baled switchgrass. The development of models enabling accurate simulation of heat and mass transfer within baled biomass requires an assessment of the thermal properties such as thermal conductivity, thermal diffusivity and specific heat. Hence, these parameters were investigated with respect to the specific material properties including moisture content, temperature, bulk density and stem orientation. It was hypothesized that the thermal conductivity would be greater in the lateral orientation (parallel to the flake composition) than for the transverse orientation (direction of bale compression) with this particular anisotropic behavior attributed to an improved level of heat conduction through the continuous stem material and void spaces within the lateral orientation.

2.4 Heat and Mass Transfer Modeling

A heat and mass transfer model was developed to predict the temperature and moisture content within porous bales. The empirical model predicts the rate of heat generation and dry matter loss as functions of the physical and thermal properties of the material. The analytical model was primarily based on a thermal conductivity approach although heat development within the bale by other physical and microbial processes was also accounted for to achieve greater accuracy in prediction. Likewise, fluid dynamics

within the porous material were included to improve the effectiveness of the model. The numerical model was simulated in MATLAB and subsequently validated with experimental storage data to determine model accuracy. It was hypothesized that the simulated temperatures according to the heat and mass transfer model would be in good agreement with the temperatures measured within baled switchgrass during the storage evaluation.

CHAPTER 3:LITERATURE REVIEW

Switchgrass (*Panicum virgatum* L.) is recognized as a potential bioenergy crop for biofuel production which may decrease greenhouse gas emissions and support agricultural economies; while reducing the dependence on fossil fuels (Balat and Balat, 2009; Goldstein, 2006; Sanderson et al., 2007; Schmer et al., 2008; Varvel et al., 2008). The development of sustainable markets requires high quality, high density and high volumes of biomass. Baling applications have been targeted in recent years; particularly due to the mechanization of the production chain, low labor requirements, and the ease of storage and transportation (Román, 2014). The biomass supply chain and conversion process are currently major barriers for the commercialization of cellulosic biofuels. Proper management through predictive modeling is expected to help ensure the sustainability of these processes.

Baled biomass may also need to be stored at biorefineries for up to 12 months in order to ensure continuous availability of raw material during non-harvesting seasons (Wiselogel et al., 1996). Stable storage of baled biomass typically requires a moisture content less than 18% (wet basis) to avoid dry matter loss (Moore & Peterson, 1995; Ohm et al., 1971). In fact, heating and other significant quality changes (i.e., molding, dry matter loss, nutrient loss, toxic metabolic production, spontaneous combustion, etc.) may occur in bales stored in excess of 20 %-wb (Martin, 1980; Miller et al., 1967; Moser, 1980; Nehrir et al., 1978; Nelson, 1968); as elevated moisture levels support microbial activity (Nelson, 1972; Ohm et al., 1971; Román, 2014). Consequently, switchgrass baled at high moisture levels may require a rapid reduction of moisture content (natural or artificial drying) to reach safe storage levels. However, adverse weather conditions (i.e., precipitation, high humidity and low ambient temperatures) may extend the drying time while reducing product quality (Fonnesbeck et al., 1986; Muck and Shinners, 2001; Parker et al., 1992).

The physical and thermophysical characteristics describing baled switchgrass significantly affect the overall biomass quality, as well as, the heat and mass transfer mechanisms occurring within the porous media. In fact, the design of an effective washing process and the formulation of an appropriate heat and mass transfer model for baled biomass both require an assessment of the relevant fluid properties (i.e., hydraulic

conductivity). Rapid, accurate and reliable moisture measurements are also essential for ensuring the proper storage management, energy production and fair marketing of herbaceous biomass. However, previous research pertaining to the dynamic moisture measurement within baled feedstocks is currently unavailable. Likewise, the thermal properties (i.e., thermal conductivity, thermal diffusivity and specific heat) are necessary to evaluate particular storage and/or bioconversion conditions of baled biomass in terms of the relevant heat and mass transfer equations.

Storage and handling of baled biomass are important factors to biomass quality. Economic analysis, and biomass supply chain and logistics planning require estimation of storage losses as well as drying time needed for safe storage of biomass. A brief description of the physical processes involved in storing baled biomass is also discussed in this review to provide a basic understanding of proper storage management practices and to indicate the need for intensive measurements for the development of a heat and mass transfer model. A mathematical model of baled biomass can then be formulated once these various physical, thermophysical and storage conditions have been characterized. As such, the development of a heat and mass transfer model for baled biomass requires characterization of the porous structure (i.e., physical/thermophysical properties), evaluation of environmental storage conditions, and a knowledge of relevant heat and mass transfer mechanisms. Therefore, each of these topics is briefly discussed in the following review of previously conducted research.

3.1 Fluid Properties

The over-accumulation of end-products in solid-state fermentation inhibits bacterial growth and prevents further biodegradation of densified forages. However, the percolation of water through densified forage is expected to capitalize on the rapid bacterial production by restoring favorable conditions for end-product formation. Liquid fuels and other byproducts may thereby be removed from the baled material by flushing water through the biomass. While baling increases the net calorific content per unit volume, baled forages do not shed fluids easily, which may also result in adverse storage conditions. Therefore, these issues necessitate an investigation of the fluid properties within baled forage.

While hydraulic properties have a significant impact on bioprocess modeling and design, these parameters are still unknown for many agricultural feedstocks. In fact, the hydrologic processes within baled biomass have yet to be investigated although such quantification is expected to be beneficial for the determination of bale quality and/or the development of moisture profile analysis and simulation within bales. Likewise, the hydraulic properties of baled forages are expected to play a critical role in the design of an effective washing process. However, literature regarding the flow of moisture through densified biomass is rather limited. In fact, no such studies have seemingly been documented for baled biomass even though this knowledge is expected to play a critical role in developing and effectively applying postharvest quality models.

Hydraulic conductivity (K) is specifically considered in the current study in order to assess the flushing ability of the solid-state conversion of baled biomass. This proportionality constant is important in fluid flow studies since it defines the relationship between flux and the hydraulic gradient. In fact, hydraulic conductivity is a commonly used parameter in soil science since it describes the ease with which fluid moves through pore spaces. An analysis of the saturated hydraulic conductivity (K_{sat}) was expected to impact the mathematical modeling of baled biomass as it describes water movement through saturated media. The hydraulic conductivity is known to be a function of the density and viscosity of the fluid as well as the intrinsic properties of the porous material itself (i.e., porosity, width, continuity, shape and overall tortuosity). An assessment of the nonlinear relationship between the hydraulic conductivity and moisture content is also

necessary for many of the widely-used flow models. Hence, the unsaturated hydraulic conductivity (K_u) involves flow through unsaturated media as a nonlinear function of moisture content.

3.1.1 Saturated State

The saturated hydraulic conductivity (K_{sat}) of baled biomass is considered in the current study to help describe and assess the flushing ability for solid-state conversion. In fact, knowledge of the saturated hydraulic conductivity is required for many of the widely-used models of fluid transport in the saturated zone. Darcy's law is an empirical equation which describes the relationship between flow rate and head loss through porous media at saturation:

$$K_{\mathrm{sat}} = \frac{\mathrm{Q}}{\mathrm{A}}\frac{\mathrm{L}}{\mathrm{H}} \qquad [3.1.1]$$

where: K_{sat} = hydraulic conductivity of the porous medium (cm s^{-1}), Q = flow rate through the medium (cm^3 s^{-1}), A = cross-sectional area of the bale, perpendicular to the direction of flow (cm^2), and L/H = the potential gradient or head loss per unit length (cm cm^{-1}) as indicated in Figure 3.1.1.

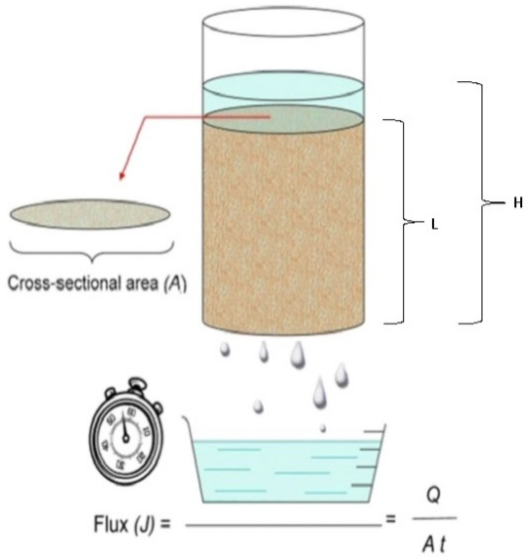

Figure 3.1.1 Diagram of the water flux (J) of a quantity of water (Q) moving through a cylindrical cross-sectional area (A) per unit time (t) (adapted from Soil Survey Technical Note, 2004).

This model assumes that the flow through the material is laminar, while turbulent flow associated with higher flow rates results in nonlinear behavior. In fact, turbulence, which is typically introduced at higher hydraulic gradients, results in the curvilinear downward decay of the saturated hydraulic conductivity. Although, saturated hydraulic conductivity is largely dependent on flow pores within the material, a challenge exists in relating the porosity and permeability has been noted in the literature (Hillel, 1998). However, one such relationship has been defined by Schmid and Luthin (1964) as follows:

$$K_{\text{sat}} = \frac{100 \cdot \kappa \rho_f g}{\mu} \qquad [3.1.2]$$

where: K_{sat} = hydraulic conductivity of the porous medium (cm s^{-1}), ρ_f = density of the fluid (kg m^{-3}), g = acceleration due to gravity (9.81 m s^{-2}), μ = the viscosity of the fluid (Pa s) and κ = the intrinsic permeability of the material (m^2). A study of the hydraulic conductivity of baled biomass must also consider relevant factors including bale density and/or porosity in accordance with this information.

3.1.2 Unsaturated State

Unsaturated hydraulic conductivity is also an important property which governs fluid flow in the unsaturated zone and essentially describes a nonlinear relationship with the volumetric water content (θ). Perkins (2011) described several methods of measuring the unsaturated hydraulic conductivity for various applications in soil science. There are also numerous techniques and instruments pertaining to the measurement of suction which essentially describes the free energy of water in porous materials based on the inherent ability to attract and retain water. In fact, a description of common techniques for measuring suction can be found throughout literature (Fredlund & Rahardjo 1993; Lee & Wray 1995; Likos & Lu 2004; Ridley & Wray 1996). However the challenge in acquiring accurate measurements is widely acknowledged due to the costly and time consuming procedures involved. Many of these techniques and instruments have limitations associated with measurement range, equilibration time, complexity and cost. Thus, a simple and economical method of measuring suction and capillary pressure

within baled biomass was selected based on the literature that has been reviewed in the current study.

The filter paper method is a commonly applied technique which indirectly calculates the suction by gravimetrically measuring the water content of a filter paper after it is brought into equilibrium with the porous material of interest. The suction is then inferred from the water content through a predetermined calibration curve for the filter paper. The filter paper technique was originally established by soil scientists and agronomists (Al-Khafaf and Hanks, 1974; Fawcett and Collis-George 1967; Gardner 1937; Hamblin 1981; McQueen and Miller 1968); and later employed in geotechnical engineering fields (Anne-Marie et al. 1994; Chandler et al. 1992; Chandler and Gutierez 1986; Fernando and Orlando, 2006; Greacen et al. 1989; Marinho 1994; McKeen 1980; Ridley and Burland, 1993). The advantages of this method are that it provides sufficient accuracy, maintains simplicity, and is relatively economical.

Suction can generally be described in distinct terms of matric and osmotic suction (Fredlund and Rahardjo 1993). Matric suction is governed by surface adsorptive forces, capillarity and texture; while osmotic suction is associated with dissolved salts found within the water. The sum of matric and osmotic suction is referred to as total suction with many filter paper curves having a bilinear trend with a single inflection point that generally occurs at a water content between 30 and 50 % (Bilcalho et al., 2011).

Most publications present calibration of filter paper according to a wetting path, in which the paper is air-dried initially (Chandler and Gutierez 1986; Chandler et al. 1992; Marinho 1994; Ridley and Burland, 1993). Likos and Lu (2002) also recommended batch-specific calibrations since filter paper calibration curves have been found to significantly vary from one batch to another. While Anne-Marie et al. (1994) developed two distinct curves corresponding to the total and matric suction, respectively; most filter paper calibrations employ single curves by using a combination of measurement techniques and/or procedures. In fact, the ASTM D 5298 (ASTM, 1992) is one of the most widely used calibration curves for filter paper that has been used to describe both the total suction and the matric suction with a single curve.

There are two primary techniques for conducting a filter paper test, although each has inherent limitations. The non-contact technique is known to introduce significant

suction errors which are induced by temperature and relative humidity gradients. Although the contact method may become inaccurate at the high matric suction range due to the dominance of vapor transport (Fredlund et al., 1995); relatively low suction occurs in highly porous materials as expected with baled biomass. Thus, the contact method was proposed for implementation in the current study using three previously reported calibration curves (ASTM D 5298; Chandler et al. 1992; Fernando and Orlando, 2006) that have been developed with Whatman 42 filter paper. In fact, the calibration of this particular filter paper has been widely reported with many of the associated calibration curves presented in a similar fashion to Figure 3.1.2.

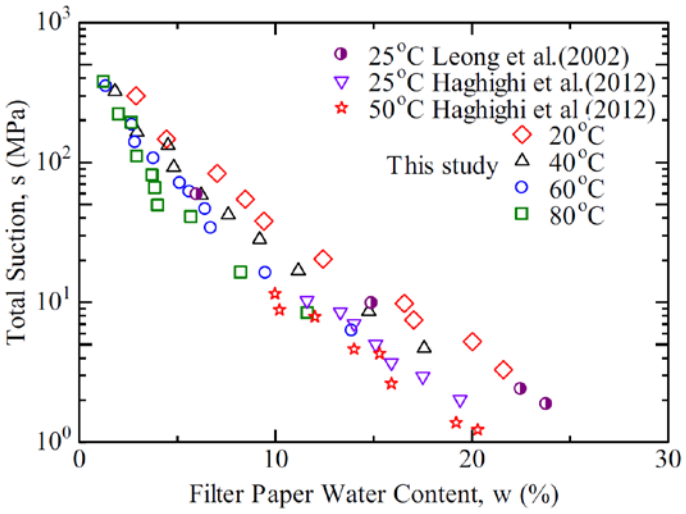

Figure 3.1.2 Calibration curves for Whatman 42 filter paper for water content ranging from 30 to 70 % (adapted from Zhu et al., 2016).

The Water Characteristic Curve (WCC) describes the relationship between suction and volumetric moisture content. Accordingly, the WCC describes the increase in inter-particle capillary forces with decreasing water in the pores. The van Genuchten method (van Genuchten, 1980) is commonly used in mathematically describing the WCC and was actually developed to provide an estimation of the relative hydraulic conductivity using the predictive models of Burdine (1953) and Mualem (1976). This method specifically describes the relationship of hydraulic conductivity and diffusivity as a function of the normalized water content. Thus, the van Genuchten equation fits suction data by the following expression:

$$\theta_e = \frac{\theta-\theta_s}{\theta_s-\theta_r} = \left[\frac{1}{1+(ah)^n}\right]^m \quad , \quad m=1-{}^1/_n \qquad [3.1.3]$$

where θ, θ_e, θ_s and θ_r = the actual, effective, saturation and residual moisture content (%), respectively; α (m^{-1}), n and m are unitless empirical parameters; and h is the pressure head (m). The constants used in this model are generally considered to have no direct description of physical attributes but are primarily used as fitting parameters. However, Guber et al. (2004) suggested that the physical meaning of the parameter, n, could be used in representing the impact of small aggregates in soil. Parameter values are also available for several types of compost materials (Wallach et al., 1992).

Disk infiltrometers are arguably the most common tools used in determining the infiltration of porous materials such as soil by controlling the water entry at prescribed suctions. The numerical simulations of cumulative infiltration versus time response from a disk infiltrometer have been presented in numerous studies (Fasinmirin and Olorunfemi, 2013; Gonzalez-Sosa et al., 2010; Moody et al., 2009; Ronayne et al., 2012; Zhao, 2013). Soil studies have indicated that the initial water content and dry density generally influence the infiltration characteristics of the material (Bhave and Sreeja, 2013).

The resulting relationship between hydraulic conductivity and suction is referred to as the *K*-function. This relationship describes the changes in the ability of water to flow through porous media as the available fluid pathways decrease. The flow through porous, unsaturated media is governed by widely-used flow models such as Richards' equation (Richards, 1931) which indicates the relevance of the *K*-function and WCC as follows.

$$\frac{\delta\theta}{\delta t} = \frac{\delta}{\delta z}\left[K(\theta)\left(\frac{\delta\psi}{\delta z}+1\right)\right] \qquad [3.1.4]$$

where z = the elevation (cm), θ = the water content (%); and ψ = the pressure head (m). These hydraulic parameters must be evaluated in lab and/or field settings through the experimentation procedures which are outlined in the preceding discussion.

3.1.3 Fluid Properties of Biomass

Hydraulic conductivity tests have previously been conducted with fibrous peat (Berry and Vickers, 1975; Delage and Lefebvre, 1984) which is a material that has similar physical characteristics to whole-plant silage. These tests were conducted in the vertical orientation (perpendicular to the fiber orientation) with results indicating a nearly linear relationship between the logarithm of the hydraulic conductivity and void ratio; as is common for many soils (Yao and Jofriet, 1992). Lau (1983) also evaluated the vertical hydraulic conductivity of alfalfa silage, with values reported on the order of 10^{-5} cm s^{-1} according to the results that were acquired from the falling head method. This study indicated that the variation of the vertical hydraulic conductivity was within 10 % of the mean under variable hydraulic heads (ranging from 0.6 to 1.2 m). These results indicate that Darcy's law was valid for whole-plant silage.

Custer et al. (1986) also evaluated the vertical hydraulic conductivity of chopped sorghum using the constant head method. The packing density, ρ_b (kg m^{-3}), was found to significantly impact the saturated hydraulic conductivity, K_{sat} (cm s^{-1}), according to the following expression:

$$K_{\mathrm{sat}} = 14.1 \exp(-0.00868\rho_{\mathrm{b}}) \qquad [3.1.5]$$

Custer et al. (1990) also measured the hydraulic conductivity of water flowing through chopped sweet sorghum at various packing densities, soaking times and hydraulic head levels using permeameters. Soaking time and hydraulic head were found to have minimal effect on the hydraulic conductivity, while packing density was found to have a significant effect. In fact, hydraulic conductivity was found to decrease by two orders of magnitude over the specified range of packing densities.

The hydraulic conductivity of whole plant com silage was evaluated by Tang and Jofriet (1991) at variable moisture contents (64.0 to 72.6 %) and void ratios (3.76 to 6.87). The hydraulic conductivities in horizontal and vertical (consolidation) direction were measured separately since the fiber orientation strongly influenced the results. In this case, the vertical and horizontal hydraulic conductivities were presented as functions of the porosity as follows:

$$K_v = 0.290\varepsilon^{71.4} \quad [3.1.6]$$

$$K_h = 1.510\varepsilon^{71.4} \quad [3.1.7]$$

where: ε = porosity (%) and K_v and K_h = vertical and horizontal hydraulic conductivities (m s^{-1}), respectively. However, the moisture content was found to have a negligible effect on the hydraulic conductivity in either directional orientation.

Yao and Jofriet (1992) found that the hydrostatic pressure within a silo was strongly influenced by the hydraulic conductivity of the alfalfa silage stored within the structure. Horizontal and vertical hydraulic conductivities of the alfalfa silage were evaluated at variable moisture contents (64 to 72 %) and void ratios (4.0 to 6.4). The results indicated that the logarithm of the hydraulic conductivity had an almost linear correlation with the void ratio, and to a lesser extent, the moisture content.

The hydraulic properties of carbonaceous fill material have also been investigated since these parameters influence the sizing of denitrification bioreactors. In fact, van Driel et al. (2006) reported an approximate value of 1.2 ± 1.0 cm s^{-1} for the horizontal hydraulic conductivity through a coarse wood fill layer, while Chun et al. (2009) reported a similar range for wood particles (2.7 to 4.9 cm s^{-1}). Christianson et al. (2010) also evaluated the saturated hydraulic conductivity for blends of woodchips, corn cobs and pea gravel at variable packing densities. The average value of the saturated hydraulic conductivity was reported as 9.5 cm s^{-1}, with the addition of pea gravel significantly increasing the hydraulic conductivity.

3.1.4 Practical Application

The current study aims to characterize the hydraulic properties and fluid flow within densified biomass feedstocks. This study specifically involves an evaluation of the saturated and unsaturated hydraulic conductivity of rectangular bales of ‘Alamo’ switchgrass (*Panicum virgatum* L.) and Miscanthus (*Miscanthus x giganteus*). The saturated moisture content, leaching behavior and sorptivity were also measured. These fluid characteristics were expected to significantly impact the long-term storage quality

of the feedstocks as well as the performance of the bioconversion process which may involve the percolation of water to remove end products.

In general, the hydraulic conductivity was expected to be similar in magnitude to that of consolidated silage (Yao and Jofriet, 1992) with statistical differences based on the density and forage type. The saturated hydraulic conductivity was expected to remain constant as laminar flow was assumed to predominate under the proposed experimental conditions. Likewise, the matric suction calibration equations developed by Chandler et al. (1992) were expected to sufficiently fit the experimental data; thereby providing a nonlinear model for unsaturated hydraulic conductivity as a function of density and moisture content.

Investigation of the washing and flushing ability within the high-solids environment is ultimately expected to enable a better understanding of the quality of baled biomass during on-farm storage and/or high-solids biomass conversion. Accordingly, these hydraulic parameters are expected to allow for the prediction of water retention from rainfall and/or water percolation during storage or bioconversion, respectively.

3.2 Moisture Measurement

Accurate and reliable moisture measurements are essential for ensuring the proper storage management, energy production and fair marketing of herbaceous biomass. Moisture content dictates the storage quality and dry matter loss of biomass; thereby contributing to biofuel loss. Moisture content also governs mold development which represents a loss in fuel value, increased risk of fire, and worker exposure to mold spores. Therefore, moisture content plays a vital role in achieving effective storage and bioconversion of agricultural feedstocks. Thus, accurate assessment of the moisture profile which governs dry matter loss and bale quality are required. Real time measurement of moisture content is also critical in obtaining a better understanding of storage quality and conversion requirements.

Gravimetric analysis (convection oven-drying) currently remains the most widely used method for determining moisture content in storage experiments (Chico-Santamarta et al., 2011; Opoku et al., 2004, 2006; Sanderson et al., 1997; Shinners et al., 2010; Wiselogel et al., 1996) primarily due to the improved accuracy relative to electronic-based sensors. While oven-drying provides accurate results, the labor-intensive and destructive nature of this technique is less than ideal. In fact, basic protocols have been described by Thaemert and Shewmaker (2004) for several methods of determining moisture content with ranking from the most to least accurate according to the standard error as follows: convection oven drying (±1%); microwave oven drying (-2 to +1%); near infrared reflectance spectroscopy, NIRS (±3%); and electronic/forage probe (±5%). Therefore, real-time measurement of the moisture content is not feasible due to the extensive drying times involved in gravimetric procedures.

Other methods such as forage moisture probes have been implemented in numerous studies due to the advantage of rapid sample analysis and the non-destructive nature of operation (Martinson et al., 2011; Savoie et al., 2011; Zahiroddini et al., 2004). However, electrical conductance and infrared techniques remain relatively labor and time-intensive; making representative sampling difficult. Furthermore, forage moisture probes are typically limited to a moisture range of 6 to 40 %, thereby restricting their application, particularly at high-moisture levels as is expected during heavy rainfall and/or water percolation in biomass feedstocks. Thus, neither the core-sampling nor

forage moisture probe method currently allow for automated and/or dynamic assessment of an overall moisture profile. Hence, there is a need for technology to provide accurate, reliable and timely moisture measurements within baled feedstocks particularly at elevated moisture levels.

Dielectric sensors have been employed extensively in the field of soil science for determining moisture content through the assessment of the dielectric constant of the material which is strongly influenced by the moisture content. In fact, dry soil typically has a dielectric constant between 3 to 5; while air and water are approximately 1 and 80, respectively. Consequently, the dielectric constant of the porous media may experience significant changes in response to any moisture changes that occur within the material. Hence, the dielectric constant can be correlated with the moisture content through media-specific calibration of measured data. In recent years, capacitance-based and time-domain-reflectometry (TDR) sensors have becomes the most common dielectric devices in use.

Capacitance-based sensors consist of two electrodes that are separated by a material that readily resists electrical current (referred to as the dielectric). In application, the soil becomes part of the dielectric when the electrodes are inserted into the soil media. A frequency (50 to 150 MHz) is applied to the electrodes by an oscillator, with the magnitude of the resonant frequency strongly influenced by the dielectric constant of the soil media. Consequently, the magnitude is inversely correlated with the moisture content of the soil media. A calibration equation can then be applied to the magnitude to estimate volumetric moisture content. However, capacitance-based sensors are greatly affected by the physical conditions (i.e., temperature fluctuations, texture of the media, etc.) in the immediate proximity of the sensor and may result in high variability as a result. This limitation, combined with the greater cost of sensors, results in diminished resolution of measurement within the material.

Alternatively, time domain reflectometry (TDR) offers a rapid, accurate and non-destructive (in situ) approach for measuring the moisture content. TDR has the particular advantage of providing intensive temporal and spatial measurements, making it a promising technology for measuring and managing the moisture content of agricultural feedstocks during storage, drying and/or the bioconversion. As such, TDR has been

considered in the current study as a prospective technology for measuring the moisture content of baled biomass. In this case, significant dependence on the temperature and bulk density of the material was expected among other factors. A method for real time monitoring of moisture content within biomass feedstocks was investigated accordingly in this study using a commercially available TDR sensor. To support the development of appropriate TDR-based calibrations for baled biomass, a brief discussion of the fundamentals of TDR is provided in the review that follows.

TDR measurements are easily automated with real-time analysis of measured waveforms; thereby, offering a practical tool for the assessment of various hydrologic processes. TDR offers a cost effective and accurate alternative for determining the moisture content and water retention properties within porous media that is based on the dielectric permittivity. TDR applications were originally reported for volumetric water measurements within granular soil samples using a coaxial transmission line (Topp et al., 1980). Empirical relationships were developed to describe the correlation between the apparent dielectric constant and the volumetric water content for conditions ranging from dry air to water saturation.

3.2.1 Time-Domain-Reflectometry Principles

TDR sensors essentially provide a linear voltage signal proportional to the moisture by measuring the dielectric constant (ε) using transmission line techniques. The bulk dielectric constant (ε_b) of soil is generally dominated by water ($\varepsilon = 80$), with the air ($\varepsilon = 1$) and mineral ($\varepsilon = 3$ to 5) constituents typically much smaller. The TDR method is relatively insensitive to the material composition due to the large disparity in the dielectric constants of the respective constituents. As a result, significant changes in the dielectric constant may develop with changes in the moisture content. The measured dielectric permittivity can be related to the water content using empirical and/or dielectric mixing models.

Dielectric constant measurements may be influenced by various factors including the physical properties of the material (i.e., bulk density, porosity, pore geometry) and sensor characteristics (i.e., measurement frequency). The water status (bound or free) and dipole moments induced by mineral constituents may also impact the dielectric

measurements (Jones and Or, 2003). Although the dielectric constant could increase with increasing temperature (Pepin et al., 1995), the temperature response may be influenced by the bulk electrical conductivity and/or relaxation time for free and bound water (Schwartz et al., 2009). As a result, the dielectric constant may be indirectly affected when the temperature influences the bulk electrical conductivity (Persson and Berndtsson, 1998; Sun and Young, 2001).

It may also be noted that the movement of water molecules is constrained near the solid surfaces due to interfacial forces that specifically hinder rotational movement. A subsequent reduction in the dielectric constant may be observed. Substantial amounts of water may also be bound in high porosity media, thereby reducing the measured bulk dielectric constant compared to media with low porosity. The dielectric constant has also been correlated with the amount of bound water with respect to distinct monolayers (Bockris et al., 1963; Or and Wraith, 1999; Thorp, 1959). Empirical expressions have also been derived for the dielectric constant in terms of the bound- and free-water (Friedman, 1998; Jones and Or, 2001).

3.2.2 Sensor Design

The dielectric measurement using time-domain-reflectometry involves the insertion of parallel steel rods (waveguides) into the porous media of interest and applying an electrical pulse via a voltage pulse generator. The imposed electrical pulse travels the length of the waveguides and is reflected back after reaching the terminal end. The dielectric constant of the material of interest influences the total travel time of the pulse, with longer pulse travel times correlated with larger dielectric constants. The water content is generally assumed uniform along the entire longitudinal axis of the probe for conventional designs. However, Chan and Knight (1999) have found that even distribution of water along the probe length doesn't necessarily provide the same mean value of the dielectric constant as localized concentrations may provide at one or more regions along the probe will influence it.

Various probe configurations have been proposed for media-specific applications including various geometric arrangements of the conducting rods (Campbell, 1990; Heimovaara, 1994). Although increasing the number of rods may provide a balanced

signal, the introduction of the additional rods may physically disrupt the material. As a compromise, the two-probe configuration offers minimal soil disturbance, while providing a relatively balanced signal (Jones and Or, 2030; Spaans and Baker, 1993; White and Zegelin, 1995).

Two- or three-rod configurations are often used as effective point (plane) measurements for water fronts moving through soil profiles, while seven-rod and parallel plate designs provide a larger sampling volume (Jones and Or, 2003). Although thin rod coatings have been successfully used in reducing signal attenuation, they typically reduce the sampling area (Ferre et al., 1998; Jones and Or, 2003). Insulation has also been shown effective with partial probe insertion (Plaut, 2013; Starr, 1999); although such rod coatings are typically less appealing as they significantly influence the permittivity and require extensive calibration (Mojid *et al*., 1998; Moret-Fernandez et al., 2009).

3.2.3 Time-Domain-Reflectometry Measurements

As mentioned previously, an electromagnetic (EM) pulse is applied to the waveguide (probe) of known length (L) and is reflected back after reaching the terminal end. The dielectric constant of the medium influences the propagation speed or total time for the pulse to travel to the terminal end of the waveguide and back. Thus, TDR determines the apparent dielectric constant by measuring the travel time, or the transmitting velocity, of a high frequency EM wave through the probe as represented by:

$$v = \frac{2L}{t} \qquad [3.2.1]$$

where: v = electromagnetic wave propagation velocity (m s^{-1}); L = probe length (m); and t = total travel time (s). Here, the actual travel time is based on the apparent probe length which is positively correlated with the water content and dielectric constant. The velocity of an EM wave is specifically according to:

$$v = \frac{c}{\sqrt{\mu_r \varepsilon_r}} \qquad [3.2.2]$$

where: c = electromagnetic wave velocity in free space (m s^{-1}); μ_r = relative dielectric constant; and ε_r = relative magnetic susceptibility which is typically equal to a value of 1. Accordingly, the bulk dielectric constant (ε_b) of the material surrounding the probe can then be evaluated based on the transmitting propagation velocity of the wave according to:

$$\varepsilon_b = \left(\frac{c}{v}\right)^2 = \left(\frac{ct}{2L}\right)^2 \qquad [3.2.3]$$

where: c = propagation speed of light in a vacuum ($3x10^8$ m s^{-1}), v = electromagnetic signal propagation speed (m s^{-1}), and t = travel time (s) for the pulse to traverse both directions (down and back: 2L).

3.2.4 Calibration

It follows, that calibration equations are necessary to relate the dielectric constant of the material to the moisture content (Noborio, 2001). In fact, probes need to be well correlated with regression models to improve prediction of moisture content. While, these calibration equations are generally provided by the probe manufacturer; site-specific calibrations may be needed in some soil and alternative media studies. Developing a calibration curve in this manner, involves comparison to the actual volumetric moisture content of a sample that is collected in close proximity to the sensor. Such empirical approaches are often used for mineral soils. In fact, this method was originally proposed by Topp et al. (1980) with the development of a third-order polynomial describing the relationship between the moisture content and bulk dielectric constant as follows:

$$\theta = -5.3x10^{-2} + 2.92x10^{-2}\varepsilon_b - 5.5x10^{-4}\varepsilon_b^2 + 4.3x10^{-6}\varepsilon_b^3 \qquad [3.2.4]$$

Although this expression covers a wide range of moisture contents, it fails to provide reasonable estimates for soils exceeding 50 %, which is common with samples having high organic matter and/or with alternative media (i.e., biomass, compost material).

Alternatively, the dielectric mixing approach expresses the composite (bulk) dielectric constant as a function of the dielectric constant and volume fraction of each

individual constituent (e.g. solid, water, air) within the media. This approach has been adopted in numerous soil studies (Birchak et al., 1974; Dobson et al., 1985; Friedman, 1998; Roth et al., 1990) with a general expression of a three-phase system given as:

$$\varepsilon_b = \left[\theta\varepsilon_w^\beta + (1-\eta)\varepsilon_s^\beta + (\eta-\theta)\varepsilon_a^\beta\right]^{1/\beta} \quad [3.2.5]$$

where: η = porosity; β = geometric indicator of the medium (β=1 for parallel, β=-1 for perpendicular, and β=0.5 for an isotropic two-phase mixed medium); 1-η, θ and η-θ are the volume fractions; and ε_s, ε_w and ε_a are the dielectric constants of the solid, water and air phases, respectively. Rearranging this equation and solving for the water content (θ) yields:

$$\theta = \frac{\varepsilon_b^\beta - (1-\eta)\varepsilon_s^\beta - \eta\varepsilon_a^\beta}{\varepsilon_w^\beta - \varepsilon_a^\beta} \quad [3.2.6]$$

Introducing common values of each constituent (β=0.5, ε_w=81, ε_s=4, and ε_a=1) into this dielectric mixing expression yields:

$$\theta = \frac{\sqrt{\varepsilon_b} - (2-\eta)}{8} \quad [3.2.7]$$

Thus, subsequent changes in the dielectric constant correspond to an electrical signal (mV) output from the sensor; which is affected by the physical and chemical properties of the material (i.e., bulk density, composition, electrical conductivity, temperature) (Moret-Fernandez et al., 2009; Wraith and Or, 1999). Coated probes can be used to minimize electrical conductivity effects (McIsaac, 2010; Robinson et al., 2003), while those materials consisting of high organic matter and bound water components often require intensive media-specific calibration (Jones et al., 2002; Jones and Or, 2003).

Some media with large porosities are also highly susceptible to bulk density variations. In fact, the bulk densities of some composting materials have been shown to have a noticeable effect on moisture content measurement (Cai et al., 2012). As such,

unified moisture content calibrations have been applied to composting sewage sludge with an error of 3.8 % over the specified range of densities (580 to 886 kg m^{-3}) (Chen et al., 2011; Yue et al., 2008). These studies have also shown that the bulk sludge temperatures may significantly affect the dielectric measurements with temperatures reported in excess of 55 °C during the compost process. Although independent measurements of the bulk density are generally expected to improve the calibration procedure, the impact of bound water poses a significant challenge which must be accounted for. This information indicates the level of care that must be taken in developing calibration equations which are imperative for providing accurate relationships of the dielectric constant and moisture content of a specific porous media.

3.2.5 Practical Application

The main advantages associated with TDR moisture sensors include the ability for continuous measurement through automation, measurement repeatability, superior accuracy (± 1 to 2 % VWC), improved sensitivity; and excellent spatial and temporal resolution (Jones et al., 2002). Other attractive characteristics of TDR include minimal sensor drift, non-destructive analysis, absence of radiation (associated with neutron probe techniques); and the ability to provide intensive temporal and spatial measurements which provide increased resolution (Jones et al., 2002).

Although TDR is effective in many porous materials, several factors are known to influence measurements, including temperature, water status and dipole moments. Air gaps and uneven pore distributions should be avoided since signals are undervalued when void spaces are present due to the low ε-value for air. Thus, porosity and bulk density variations may cause significant changes in ε due to the variation of porosity. As such, some commercially-available probes have been developed with integrated adjustments for density (Cormier et al. 2007). Measurement error may also increase as air gaps develop from repetitive probe insertion or within shrink–swell materials. Measurements may also depend on temperature; although several studies have shown that temperature-induced errors may be negligible compared to the intrinsic calibration errors (Persson et al., 2000).

On the other hand, significant temperature fluctuations during storage and/or bioconversion may significantly impact the moisture measurements (Schwartz et al., 2009). However, the lack of temperature-dependent data has limited the current application of TDR particularly in storage, bioconversion and composting operations. Additionally, waveform reflections can be totally attenuated in lossy materials. Hence, the disadvantages of this method include the development of media-specific calibrations, the high level of sensitivity to air gaps, and the relatively small zone of influence. Consequently, TDR devices must be carefully installed in the media in order to prevent air gaps between the sensor and material. Likewise, the effects of temperature should be considered in order to improve the accuracy of moisture content measurement by TDR. Independent measurement of bulk density is also expected to improve calibration accuracy.

The TDR technique is proposed in the current study as a fast, simple, compact, cost-effective and non-destructive method for moisture measurement in baled forage since moisture plays a key role in most storage studies. Hence, the current study investigates the ability to quickly and accurately determine moisture content within herbaceous biomass using TDR techniques which have been used extensively in measuring water content in soil science. This study specifically involves the calibration and validation of a commercially available TDR device for monitoring water content in ground and baled switchgrass. The purpose of this study was, therefore, to 1) determine if TDR could be used to monitor moisture content within a densified herbaceous feedstock; to 2) assess the specific impacts of temperature and bulk density on moisture measurements; and to 3) develop calibration equations for moisture content as a function of the dielectric constant of the material.

In general, the variation of output voltage was expected to be adequate for determining the moisture content within a densified feedstock. In fact, the development of a calibrated dielectric equation was expected to provide significantly similar values of moisture content compared with gravimetrically-determined values for chopped and baled switchgrass. Strong correlation was also expected between the voltage output and bulk density of the material. Hence, results were expected to demonstrate effective calibration of a commercially available TDR probe for ground and baled switchgrass;

particularly at high moisture and density levels. Moisture content was also expected to decrease over time as the biomass loses moisture to lower humidity surroundings during storage periods. A set of equations may need to be developed from pooled data with respect to the initial moisture content and air temperature in the case that a single prediction equation may be found unsuitable across all experimental conditions.

This study thereby represents a new approach for dynamic measurements of the moisture content in densified feedstocks. This study also stands to provide rapid, accurate and dynamic measurement of moisture content which could be utilized for process control at storage facilities and/or biorefineries. In fact, real time information on moisture content is important for ensuring optimal storage conditions and bioconversion operations. The ability to obtain high resolution measurements with automated and multiplexed TDR technology expected to provide a practical research and management tool. Other practical applications include process control for flushing of on-farm bioconversion operations; while ultimately aiming to provide optimal quality and efficient processing of feedstocks. Thus, a direct objective of this study was to develop and enable a better understanding of the quality of baled biomass during on-farm storage and/or high-solids bioconversion.

3.3 Thermal Analysis

The storage and conversion of baled switchgrass is of particular interest within on-farm solid-state conversion processes. In fact, effective bioconversion of biomass may involve a wide range of agricultural operations including drying, storage and pretreatment among others. Safe storage conditions may also involve artificial drying to lower the moisture content and the consequent risk of microbial degradation; thus improving feedstock quality and minimizing economic loss to farmers and processors. Accordingly, heat is transferred into the porous material with the rate of drying dependent on environmental conditions and material-specific properties.

The complex structure of lignocellulosic biomass such as switchgrass is composed of cellulose, hemicellulose and lignin which provides a natural resistance to enzymatic and microbial degradation; thus hindering hydrolysis and fermentation. Hence, the lignocellulosic nature of the feedstocks necessitates an initial pretreatment to promote the access and digestion of the components of interest. There are a number of pretreatment routes employed in biofuel production (Iroba and Tabil, 2013); with the application of heat associated with some of these processes. In fact, thermal aided pretreatment (heat transfer) and evaporative drying (heat and mass transfer) are commonly implemented in biofuel production applications (Singh and Heldman, 2009). In general, these unit operations involve a heat transfer response which is influenced by the thermophysical properties of the feedstock.

Most heat transfer processes associated with the storage and/or processing of biomass primarily involve heat conduction within the material while forced convection involves heat transfer between a moving fluid in direct contact with the surface of the material. The heat transfer within high water content materials such as biomass may specifically involves thermal gradients that are caused by natural temperature cycles and/or decomposition of the material. The transfer of heat into biomass may also be accompanied by simultaneous diffusion of water through the product to the surrounding air. In a porous absorbing media such as baled switchgrass, heat may develop through the process of moisture absorption (Henry, 1939). Although moisture diffusion through the bale may occur solely in response to a temperature gradient (Henry, 1939), this process likely represents simultaneous heat and mass transfer mechanisms within the material.

Consequently, many of the storage and/or bioconversion characteristics can be evaluated using specific heat and mass transfer principles; with changes in baled biomass determined through the development of relevant heat and mass transfer equations. Such studies entail an understanding of the biological material's response to the environmental conditions. Thus, certain thermal properties of the biomass are necessary in order to evaluate the storage and bioconversion conditions; as well as, to evaluate the drying rate of the feedstock and/or the temperature distribution under different environmental conditions. While the thermophysical properties govern the material's response to heat and mass transfer, there is currently a lack of basic thermophysical data for baled biomass.

Effective prediction of the thermal processes within biomass is critical for numerous practical applications; however, there is currently a lack of comprehensive experimental research on this topic. While extensive research has been conducted in measuring and estimating other relevant agricultural porous media, such as soil and grain, there are minimal studies reporting on the assessment of the thermophysical properties of baled biomass. Likewise, techniques allowing for the quantification of biomass properties, directly or indirectly, are currently deficient for most materials; thereby contributing to the constraints on our understanding of densified feedstocks. In fact, the application of engineering principles to biological systems, such as in the high-solids environment of baled switchgrass, is frequently hindered by the insufficient definition the basic physical properties of the material. Hence, an understanding of this dynamic system is dependent upon the ability to discern the properties which describe the fundamental relationships governing mass and energy balances.

Thermophysical properties of lignocellulosic biomass such as the thermal conductivity (k), thermal diffusivity (α) and specific heat (C_p) are necessary to evaluate optimal storage and bioprocessing conditions. In fact, an understanding and quantification of these thermophysical properties is important in many applications associated with modeling the transport of water and energy within biomass. Hence, these thermophysical properties may be considered invaluable in terms of designing effective biomass processing operations which involve the modeling of heat and mass transfer. In fact, a description of the thermal regime is necessary to evaluate the relevant energy

balances, which influence the rate of physical, chemical and biological reactions. Furthermore, the thermal properties of biological materials are known to be affected by other inherent physical properties of the material such as temperature, moisture content and bulk density (Wallapapan and Sweat, 1982). Hence, accurate, rapid and inexpensive measurements of these thermophysical parameters are needed; particularly in densified feedstocks.

3.3.1 Thermal Parameters

Heat transfer can be specifically quantified by the heat flow rate through the medium (thermal conductivity), as well as, the ease of heating the medium (specific heat). The ease at which the medium gains heat content (thermal diffusivity) is essentially a composite parameter of the thermal conductivity and specific heat (Andersland and Ladanyi, 1994). Accordingly, the thermal diffusivity of the medium is defined as the ratio between thermal conductivity and volumetric heat capacity. While there are several well-established methods for measuring each of these thermophysical properties (Dickerson, 1965; Mohsenin, 1980), but measuring the measurement of any two of these parameters allows for the assessment of the third parameter according to the following relationship:

$$\alpha = \frac{k}{C} = \frac{k}{\rho \cdot C_p} \qquad [3.3.1]$$

where: α = thermal diffusivity ($m^2\ s^{-1}$); k = thermal conductivity ($W\ m^{-1}\ °C^{-1}$); C = volumetric heat capacity ($kJ\ m^{-3}\ °C^{-1}$); C_p = mass heat capacity ($kJ\ kg^{-1}\ °C^{-1}$); and ρ = density ($kg\ m^{-3}$).

Thermal conduction involves heat transfer within a solid material or between two solid bodies in direct contact with each other. It follows that the thermal conductivity of a material represents the ability to transmit heat through conduction. A more specific definition of thermal conductivity is given as the amount of heat passing through a given area over time under the effect of a thermal gradient (Hanson et al., 2000). Steady state heat conduction is described by Fourier's law in which the thermal conductivity is expressed as the ratio of heat flux density to the temperature gradient within the material

(Fontana et al., 1998). For one-dimensional heat flow this relationship can be expressed by the following:

$$\frac{dQ}{dt} = -kA\frac{dT}{dx} \qquad [3.3.2]$$

where: Q = quantity of heat (J); t = unit of time (s); k = thermal conductivity (W m^{-1} K^{-1}); A = area (m^2); and dT/dx = temperature gradient in the x-direction (K m^{-1}).

Thermal conductivity is useful for the prediction and/or control of the heat flux in various heat transfer operations and thus, is necessary to ensure quality and efficient operations for biomass. Extensive tabulations of values for food products and agricultural materials are given in various sources (ASHRAE, 1989; Mohsenin, 1980; Okos, 1986). Specific heat is defined as the quantity of heat (on a unit-mass or unit-volume basis) that is required to raise a specified amount of the material by one degree in temperature (Duncan et al., 1966). This parameter can be expressed as:

$$\frac{dQ}{dt} = MC_p\frac{dT}{dx} \qquad [3.3.3]$$

where: Q = quantity of heat (J); t = unit of time (s); M = unit of mass (kg); C_p = specific heat at a constant pressure (kJ kg^{-1} °C^{-1}); and dT/dx = temperature gradient in the x-direction (K m^{-1}). However, this relationship does not apply if a phase change is encountered since heat transfer occurring during a phase change does not change the temperature. On the other hand, a relatively large temperature change may be correlated with a low heat capacity for a specified amount of heat application. Extensive tabulations of values are also given in various sources (Mohsenin, 1980; Okos, 1986).

It should also be noted that additional heat may be generated by the presence of some internal-heat source, in which case, an additional term for temperature change must be accounted for. Although this additional temperature change (ΔT_g) may be inherently included in terms of the experimental data, detailed knowledge and quantification of this term may not be directly available. In this case, however, the computed value of specific

heat would be expected to be less than the simple case which exhibits no internal-heat generation according to:

$$C_p = \frac{\Delta Q}{\Delta T + \Delta T_g} \quad [3.3.4]$$

Transient heat conduction occurs when heat is conducted into or out of the material; which leads to heat storage (heating) or heat loss (cooling); respectively. For a homogeneous solid with a constant thermal conductivity (k, W m^{-1} K^{-1}), specific heat (C_p, kJ kg^{-1} K^{-1}) and density (ρ, kg m^{-3}), the variation of temperature (T, K) within a three-dimensional object (Cartesian coordinates x, y and z) is described by Fourier's general law of heat conduction which can be expressed in terms of the following partial differential equation:

$$\frac{dT}{dt} = \frac{k}{\rho C_p}\left(\frac{\delta^2 T}{\delta x^2} + \frac{\delta^2 T}{\delta y^2} + \frac{\delta^2 T}{\delta z^2}\right) \quad [3.3.5]$$

In this form of the equation, thermal conductivity is assumed to be the same in all directions. As mentioned previously, thermal diffusivity may be considered to be a composite parameter that essentially indicates the rate of temperature change occurring in a material in response to a thermal gradient. In other words, this property describes the rate at which heat is propagated or diffused through the material. Substituting this relational definition of the thermal diffusivity from Equation 3.3.1 into Equation 3.3.5 results in the following form of the equation:

$$\frac{dT}{dt} = \alpha\left(\frac{\delta^2 T}{\delta x^2} + \frac{\delta^2 T}{\delta y^2} + \frac{\delta^2 T}{\delta z^2}\right) \quad [3.3.6]$$

In consideration of these thermophysical relationships, the thermal diffusivity of a material may be thought of as a parameter which is quantified as the ratio of the ability to conduct heat and the ability to store heat. As such, a material with high thermal diffusivity will experience a faster temperature increase compared to a low thermal diffusivity material (Andersland and Anderson, 1978). Although the thermal diffusivity

of a given material may be calculated indirectly based on the values of the other thermophysical properties, it may also be directly determined experimentally.

3.3.2 Thermal Variation

The thermal properties of a biological material are influenced by many factors including texture, ambient temperature, moisture content and bulk density of the material (Becker et al., 1992; Drouzas and Saravacos, 1988; Emami et al., 2007; Lawrence and William, 1984; Salomone et al., 1984). Hence, the thermal parameters are dependent on the structure and composition of the material which includes the packing arrangement, fiber orientation and porosity.

Readily measurable physical parameters (i.e., moisture content, apparent density) have previously been reported to have significant impacts on the thermal properties of wood, bark and cured tobacco (MacLean, 1941; Rowley, 1933; Samfield and Brock, 1958; Wangaard, 1940; Ward and Skarr, 1963). In fact, the effect of these parameters has been widely reported for different grains (Alam and Shove, 1973; Babbitt, 1945; Chandra and Muir, 1971; Chang, 1986; Dua and Ojha, 1969; Jasansky and Bilanski, 1973; Kazarian and Hall, 1965; Moysey et al., 1977; Sharma and Thompson, 1973; Sreenarayanan and Chattopadhyay, 1986; Timbers, 1975). Although the thermal conductivity of various grains are reported in many literature sources, many studies have been evaluated under constant moisture content and bulk density.

The thermal parameters are specifically impacted by the amount of water in the material due to the high heat capacity of water compared to that of the air and solid material. Moisture has been reported to have a profound influence on the specific heat of cellulosic materials (Hearmon, 1957; Hearmon and Burcham, 1955; Samfield and Brock, 1958; Weld, 1948); while thermal diffusivity generally decreases at higher water contents (Butts, 1990). Pore spaces that are filled predominantly with air generally have low values of thermal conductivity and heat capacity. At low moisture levels, the contact area between the solid particles may also be limited. However, as water content increases, a thin film forms around the solids which promote continuous contact surfaces and increased values of thermal conductivity and heat capacity as a result. A portion of the air that is present within the pore space may also be displaced at higher moisture levels.

Thus, the thermal conductivity of a porous material generally has a positive correlation with the moisture content.

Temperature may also impact the thermal transfer within biological materials such as grain. Thermal conductivity generally increases with increasing temperature due to the improved particle contact bonds and the associated increase in moisture migration (Farouki, 1981). For many porous materials, the thermal conductivity is positively correlated with the temperature of the material. Several temperature-dependent equations of specific heat were also proposed by Sweat (1986). Although the specific heat may vary to some extent with temperature, these minimal changes are typically considered negligible in many engineering applications (Costa, 2006).

Thermal conductivity is positively correlated with the density of the material; thus, requiring a knowledge of the bulk density to evaluate most agricultural products. The thermal diffusivity and rate of heat transfer generally have positive correlations with thermal conductivity when the density and specific heat are held constant. Conversely, increases in density and the amount of heat stored for a constant thermal conductivity will decrease the rate of heat transfer. Thermal conductivity and thermal diffusivity generally have positive correlations with the density of the material at high moisture contents. However, the density of the material typically has minimal impact at lower moisture contents. Specific heat has also been shown to have a positive correlation with moisture content and an inverse correlation with bulk density (Jiang et al., 1986). A multiple regression model describing the specific heat of tobacco was also reported by Brock and Samfield (1958) as a function of temperature, moisture content and bulk density.

The determination of these thermal properties may also be complicated by the anisotropism of the material. Furthermore, the degradation of lignocellulosic biomass may significantly alter these thermophysical characteristics; particularly with exposure to high temperatures. The thermal properties may also be affected by the moisture content and bulk density of the material which may undergo significant changes during drying, storage and/or bioconversion applications. A composite agricultural material may also have thermal properties that exhibit spatial variation which makes it necessary to experimentally determine values of the thermal properties.

Although the fundamental thermophysical properties discussed in this study (thermal conductivity, thermal diffusivity and specific heat) are difficult to estimate due to the porous nature of baled biomass (variable amounts of water, density and/or material composition); these properties may be determined by various techniques and/or instrumentation. Hence, this section of the review is dedicated to describing some of the more commonly used techniques for measuring these thermal properties. Accordingly, the fundamental modes of operation are discussed for relevant procedures along with a brief indication of applicability and/or limitations of the respective measurement technique.

3.3.3 Indirect Measurement Techniques

The thermal properties of many environmental and agricultural materials have been evaluated by indirect and analytical methods. The thermophysical properties of soil were calculated by DeVries (1975) based on the volume fractions of each constituent (solid, liquid and air). The resulting equations were used to estimate the thermal conductivity and heat capacity of various soils. However, the DeVries method requires an accurate assessment of the empirical constants which may significantly vary with the water content of the soil, making the calculations rather difficult in practice.

The specific heat of an agricultural material can be estimated based on its composition. In this case, the heat capacity is specifically evaluated by summing the contribution of each component that forms the composite material. Thus, the specific heat of a material that is predominately composed of water will be considerably close to the specific heat value of water. While the method of summing the individual components is rather simple, it does require the identification and quantification of each component. The heat capacity of various agricultural, environmental and food materials have been presented in many sources (Andersland and Ladanyi, 1994; Carslaw and Jaeger, 1959; DeVries, 1963). The summation method for calculating the heat capacity of a composite material may follow the general form:

$$\rho C \cong \rho_w C_w \theta + \rho_b C_m \qquad [3.3.7]$$

where: ρ = overall mass density (kg m^{-3}); C = overall volumetric heat capacity (kJ m^{-3} $°C^{-1}$); ρ_w = mass density of water (kg m^{-3}); C_w = volumetric heat capacity of water (kJ m^{-3} $°C^{-1}$); θ = volumetric water content (m^3 m^{-3}); ρ_b = bulk density of soil minerals (kg m^{-3}); C_m = volumetric heat capacity of soil minerals (kJ m^{-3} $°C^{-1}$).

Several equations have also been developed for evaluating the specific heat of various agricultural and food materials based on Siebel's observation (1918) in relation to the moisture content:

$$C_p = 0.837 + 3.348M \quad [3.3.8]$$

where: M = moisture content (%-wb) and C_p = specific heat (kJ kg^{-1} K^{-1}).

Likewise, the thermal conductivity of agricultural materials and food products can be estimated from their water content when data are not available. In fact, Anderson (1950) and Spells (1960) both presented the thermal conductivity of biological materials as functions of the weight fraction of water according to the following respective models:

$$k = k_w X_w + k_s(1 - X_w) \quad [3.3.9]$$

$$k = 0.056 + 0.57X_w \quad [3.3.10]$$

where: k = thermal conductivity of the wet hay/air mixture (W m^{-1} $°C^{-1}$); X_w = the weight fraction of water (%-wb); and the subscripts w and s represent the properties of the water and dry hay/air mixture, respectively. The latter expression was considered valid in biological materials containing greater than 50 % water. However, the use of this equation in the current study would require knowledge of the thermal conductivity of a dry bale of switchgrass; with the bale/air mixture considered as one solid and water as the secondary material.

Although thermal diffusivity can be measured according to several different methods, the indirect method is the most widely used. The indirect method involves the calculation of thermal diffusivity using the experimental values of the other thermophysical properties of the material (Singh and Heldman, 2009; Yang et al., 2002).

A number of equations have been developed to estimate thermal diffusivity on the basis of composition. In fact, the following model was proposed by Martens (1980); and later employed by Choi and Okos (1986); for various food materials:

$$\alpha = \frac{k}{\rho C_p} = \frac{0.551}{1120 \times 3.64 \times 10^3} = 1.352 \times 10^{-7} \quad [3.3.11]$$

where: α = thermal diffusivity ($m^2\ s^{-1}$); k = thermal conductivity ($W\ m^{-1}\ K^{-1}$); ρ = density ($kg\ m^{-3}$); and Cp = specific heat ($kJ\ kg^{-1}\ K^{-1}$). However, such equations are rather general in nature and do not reflect the effects of other factors such as temperature which may be significant. Additionally, these properties are largely unknown and/or unreported for agricultural feedstocks such as switchgrass. Thus, measurement of at least some of the fundamental thermal properties must be undertaken to provide a basis of understanding with this material.

3.3.4 Direct Measurement Techniques

3.3.4.1 Specific Heat

Specific heat measurement and calorimetric procedures are concerned with the amount of heat that is required to change the temperature of a material. Several calorimetric procedures exist for measuring specific heat (Sturtevant, 1949; Weld, 1948; White, 1928); although most methods require relatively long equilibration times. While calorimetric methods have the disadvantage of slow temperature stabilization, alternative methods have been proposed which require much shorter testing times. In fact, the transient-heat flow procedure is relatively quick, while some types of this analysis allow for the simultaneous determination of other thermophysical properties (Ward, 1960; Ward and Skaar, 1963).

Among the previously used methods for measuring specific heat, the method of mixtures has become the most common technique for biological materials (Dutta et al., 1988; Hwang and Hayakawa, 1979); in which a known sample mass is heated and placed into a well-insulated calorimeter to prevent heat loss. The heat dissolution is eliminated in this method since there is no contact between the calorimetric fluid and the material. The

temperature of the fluid/sample mixture is then assessed at equilibrium. The specific heat of the sample can be calculated if the known heat capacity of the fluid and the calorimetric container. Assuming there is no heat transfer to the surroundings, the heat that is lost by the material is considered to be equal to the heat that is gained by the fluid and calorimeter. The resulting equation can be solved for the specific heat of the sample as follows:

$$C_{ps} = \frac{(m_c c_{pc} + m_f C_{pf})(T_{eq} + T_f)}{m_s(T_s - T_{av})} \quad [3.3.12]$$

where: C_p = specific heat (kJ kg^{-1} °C^{-1}); m = mass (kg); T = temperature (°C); T_{eq} = equilibrium temperature (°C); and the subscripts are for the container (c), fluid (f) and solid (s); respectively.

The method of indirect mixtures has previously been used for measuring the specific heat of various food materials such as cornish pastry (Rodriguez et al. 1995), potato (Rice et al. 1988) and sugarbeet roots (Tabil et al. 2003). However, the heat loss from the calorimeter to the surroundings is a major source of error in the method of mixtures. Adiabatic calorimetry may be used to reduce the heat loss errors by maintaining the ambient temperature, as well as, the temperature of the calorimeter. This can be accomplished by placing the calorimeter in a water bath that is continuously adjusted to the temperature of the calorimeter (Rodriguez et al., 1995). Water absorption into porous, hygroscopic materials may also result in erroneous estimates of the specific heat according to the method of mixtures unless a correction factor is introduced to account for differential heat of wetting.

Due to these limitations, the differential scanning calorimeter (DSC), is generally considered to be the most accurate and rapid method for determining specific heat. A previous literature review reported on specific heat measurements for various agricultural materials while providing specific analyses on the key factors affecting the DSC method (Tang et al., 1991). DSC procedures have also been described for measuring borage seeds with the development of a model correlating specific heat, temperature and moisture content (Yang et al., 1997). The DSC method has also been used to evaluate the specific

heat of chickpea flour, isolated starch and isolated protein (Emami et al., 2007); while Izadifar and Baik (2007) measured the specific heat of rhizomes using DSC for various applications including drying and ethanol extraction.

3.3.4.2 Thermal Conductivity and Diffusivity

Steady-state and transient-state heat transfer are the two categorical methods for measuring thermal conductivity which have been described in the available literature for various agricultural and food materials (Mohsenin, 1980; Nesvadba, 1982; Reidy and Rippen, 1971). The specific techniques and procedures associated with each method differ in terms of the time and sample size required for testing. In general, the steady-state approaches are more complex, time consuming, and challenging in regards to the experimental methodology required. Therefore, only a brief discussion of steady-state methods is presented here, highlighting the basic principles of operation and the corresponding limitations with respect to the current study. A more thorough discussion of transient methods is also provided with information pertaining to application in the current study.

3.3.4.3 Steady-State

Steady-state techniques involve measurements performed under complete material equilibrium, with a simple and constant signal analysis. Early investigators used one-dimension, steady-state heat flow methods such as the hot plate technique which has been widely used in measuring the apparent thermal conductivity (thermal transmission) of insulating materials which can involve conductive, convective and radiative heat transfer components (Babbitt, 1945; Moote, 1953; Oxley, 1944).

More recent developments of the steady-state method involve: 1) the scale of the apparatus with thicker insulations; 2) the minimization of lateral heat flow and edge heat losses (e.g., additional guards); 3) improved instrumentation accuracy (e.g. multi-ranging digital voltmeters); 4) advanced and automated data acquisition and analysis; and 5) improved temperature control systems.

A known unidirectional heat flux is generated through a material in the hot plate method, whereby, the material may be considered as a slab of infinite width bounded by

parallel planes as shown in Figure 3.3.1. In this case, an isothermal heat source is applied on one parallel plane, while the material is insulated on the other. As a result, heat flows through the material towards the isothermal cold plate with the temperatures maintained by fluid circulation and/or electrical heating. Highly conductive material must be used for the plates while ensuring they are as flat as possible to promote uniform temperatures across them. The surfaces of the plates should also be highly emissive; particularly with low density materials which may have significant radiative heat transfer components. Lateral heat exchange must also be prevented by maintaining close temperature limits between the guard and metering area, while ensuring uniform contact resistance between the plates and the sample material across the entire interface.

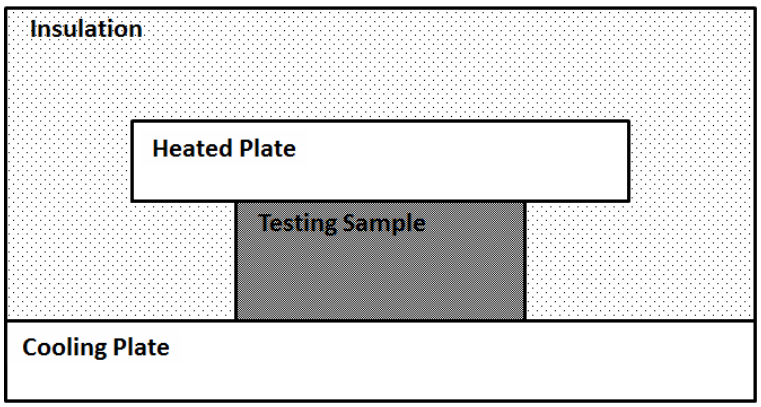

Figure 3.3.1. Diagram of guarded hot plate.

Edge heat losses may be further reduced with insulation, thereby, simulating a semi-infinite slab. Temperatures should be monitored in both plates until reaching constant values. These constant temperature values can then be used to calculate the thermal conductivity based on the sample thickness and the heat input. Accordingly, the ASTM hot-plate method has been used with various biological materials including burley tobacco (Duncan et al., 1966); with the calculation of thermal conductivity in steady-state given by the basic equation:

$$k = \frac{qd}{T_h - T_c} \qquad [3.3.13]$$

where: k = thermal conductivity coefficient (W m^{-1} °C^{-1}); q = quantity of heat through a unit area (W m^{-2}); d = distance between two sides of the sample or the length of the path of heat flow (m); and T_h and T_c = temperature (°C) on the warmer and cooler side of the sample; respectively. In this case, the quantity of heat that is transferred may be expressed as:

$$q = \frac{Q}{A} \qquad [3.3.14]$$

where: q = quantity of transferred heat (W m^{-2}); Q = quantity of heat (W); and A = area (m^2).

While the steady-state method may be considered mathematically simple and relatively accurate even with smaller sample sizes, this method requires a lengthy testing period to reach equilibrium. Significant moisture migration may occur from the warmer to the cooler surfaces during the extended equilibration time needed for the steady-state method; particularly with high moisture materials. In fact, moisture migration may introduce significant measurement errors associated with heat transfer (Dutta et al., 1988; Kazarian & Hall, 1965; Mohsenin, 1980); although the effect of moisture migration has been neglected in previous studies (Duncan et al., 1966). These undesirable features may be minimized through close control of the ambient conditions and by using a narrow temperature difference across the material.

Other sources of uncertainty may be attributed to erroneous temperature measurements through the material, excessive material thickness and significant edge heat losses. While thicker samples may be required to obtain an adequate representation of the overall material composition, the larger sample sizes may result in significant error as a result of temperature and moisture gradients. In fact, lower moisture regions may develop in the top portion of the sample due to the downward movement of water through the material (Tollner and Verma, 1987). This moisture redistribution may cause significant deviation from assumed temperature profiles. Lateral and downward heat flow may be minimized by edge and auxiliary guards, respectively.

Another source of uncertainty in measuring dense materials is associated with the presence of air at the interface since the thermal conductivity of air is relatively low. As

such, the presence of air films at the interface may significantly impact the uniform heat flux distribution and the apparent thermal resistance. Hence, it is recommended that good contact be established between the plates and the flat surfaces of the material (Salmon, 2001); thereby, limiting the assessment of fibrous materials. Thus, herbaceous materials such as baled switchgrass must have a high enough density to minimize the natural convection heat transfer within the material. Due to these reasons, the hot plate method is typically not recommended by the ASTM standards for moist biological materials.

3.3.4.4 Transient State

Many of these concerns are eliminated through the use of transient methods which include hot wire, single and dual heated probes which have previously been reviewed by several authors (Hooper and Lepper, 1950; Ingersioll et al., 1954; Nix et al., 1967). The prolonged measurement time (4-24 h) of steady-state methods could become a significant concern as the characteristics of lignocellulosic biomass are known to undergo deteriorative changes when exposed to elevated temperatures for extended periods. In addition, moisture transfer and natural convection within the material further complicate the use of the steady-state method. Hence, the transient line source method is generally considered to be better suited than the steady-state method (Lobo and Cohen 1990).

As such, the heated probe method has become commonly accepted for evaluating the thermal conductivity and thermal diffusivity of various biological materials, which limits the loss and migration of moisture. Line source probes involve measurements of the heat dissipation from a line heat source of known power. Transient methods, such as line source probes, require measurements of the temperature at specified locations within the material over time. The single probe method provides an assessment of the thermal conductivity, while the dual probe method further provides an assessment of the thermal diffusivity and heat capacity.

Transient heat flow methods were used by Hooper and Lepper (1950) to determine thermal conductivity using a simple line heat-source (a heated wire) which has become a common method for the evaluation for many biological materials (Bilanski and Fisher, 1976; Chang et al., 1980; Suter et al., 1975). The accuracy of the transient method is generally reported between ± 2 to 10 % for various biological materials (Sweat, 1976;

Wallapapan and Sweat, 1982). Hence, the transient method is generally considered to be an efficient and effective method for evaluating the thermal conductivity and thermal diffusivity of moist materials (Butts, 1990). Accordingly, transient methods for determining thermal conductivity in solid and porous materials have been developed extensively for use in soils (Blackwell 1956; De Vries and Peck 1958). Hence, the heated probe method is considered to provide rapid and practical measurements for various biological materials. Therefore, the current study investigates the use of transient methods for measuring the thermal properties of baled biomass.

3.3.4.5 Single Probe Technique

The line source method is a widely implemented transient-state method that uses a bare wire or probe as a heating source. Hooper and Lepper (1950) are credited with developing the original thermal conductivity probe; while the first application to find widespread use was reported by Jackson and Taylor (1986) for soil applications. The thermal probe has also become a common transient method for many agricultural materials (Mohsenin, 1980). In fact, the line heat source method has been considered a more accurate technique for assessing the thermal conductivity of moist biological materials (Dutta et al., 1988; Yang et al., 2002). The line heat source method has also been applied with apples (Ramaswamy and Tung, 1981), liquids (Asher et al., 1986), sugarbeet roots (Tabil et al., 2003) and other various food samples (Sweat and Haugh, 1974); typically as functions of the temperature.

The line source method is based on the theory of an infinitely long and infinitesimally thin line source of heat located along the axis of a homogeneous, cylindrical medium of infinite length (Lobo and Cohen, 1990). In particular, this technique aims to measure the rate that heat is conducted away from the probe. Hence, this method involves the solution of the Fourier heat conduction equation in terms of a semi-infinite line heat source (large length-to-diameter ratio). In practical applications, a high-thermal conductive probe is electrically heated while the subsequent temperature rise within the homogeneous and isotropic media is measured by thermocouple. Thus, the probe consists of both a heating and temperature sensing element. The heat source is supplied with a constant rate of heat that is typically monitored by the application of a

known voltage through a calibrated resistor. In principle, the heat generation rate in the hot wire is given by:

$$Q = I^2R \qquad [3.3.15]$$

where: Q = heat generation rate (W); I = electric current (A); and R = electric resistance (Ω).

A measurable temperature difference may be attained with sufficient power input to the wire over a specified time. Accordingly, a sufficient temperature rise was attained in wheat with a current of 560 mA (Kazarian and Hall, 1965), 800 mA was sufficient for sorghum (Sharma and Thompson, 1973), and 528 mA was effectively used with wheat samples (Chandra and Muir, 1971); while Jasansky and Bilanski (1973) reported no significant difference for sorghum over a wide range of currents.

This constant heat flux emanating from a small, cylindrical, heat-source typically results in a small rate of temperature rise along the probe which is monitored by a thermocouple. Thus, the temperature change in the wire is measured as heat flows out radially from the wire into the sample as depicted in Figure 3.3.2. The amount of heat that is transferred into the surrounding material can be deduced by comparing the temperature increase to the amount of heat applied to the probe. The temperature of the probe is directly related to the heating time according to the theoretical solution for a line heat source (Bristow et al., 1994; Campbell et al., 1991; DeVries and Peck, 1958; Reece, 1996).

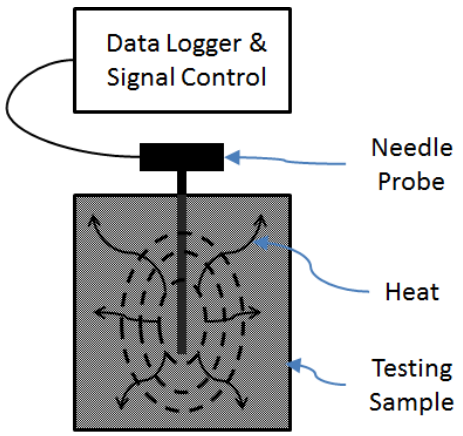

Figure 3.3.2. Radial heat flow from a line heat source in a porous medium.

An analysis of the temperature response and heat dissipation allows for the determination of the relevant thermal properties for a known voltage applied to the probe. The time response of the temperature change is specifically a function of the thermal conductivity of the material (Yang, et al., 2002). Therefore, the thermal conductivity can be determined on the basis of Fourier's Law, considering the measured and known uniaxial heat flux, the specimen thickness, and the contact surface temperatures (Nusier and Abu-Hamdeh, 2003; Reid, 2005; Salmon, 2001). The temperature rise at a point close to the line heat source can be expressed by the solution of the transient heat conduction equation as follows (Hooper and Lepper, 1950):

$$T_2 - T_1 = \frac{Q}{4\pi k} \ln\left(\frac{t_2}{t_1}\right) \qquad [3.3.16]$$

where: T = temperature (K); t = time (s), Q = line source strength (W m^{-1}); k = thermal conductivity of the sample (W m^{-1} K^{-1}); and the subscripts 1 and 2 are the initial and final conditions; respectively.

This equation describing the temperature rise at a line heat source can be rearranged in terms of the thermal conductivity as follows:

$$k = \frac{Q}{4\pi(T_2 - T_1)} \ln\left(\frac{t_2}{t_1}\right) \qquad [3.3.17]$$

where: k = thermal conductivity (W m^{-1} K^{-1}); Q = line source strength (W m^{-1}); T = temperature (K); t = time (s); and the subscripts 1 and 2 are the initial and final conditions; respectively.

Probe length and diameter are important in avoiding errors caused by axial heat flow. Blackwell (1956) used a numerical example to demonstrate an analytical analysis of the axial heat flow error with the use of probe methods for determining thermal conductivity. Errors attributable to axial heat flow would result in a higher measured thermal conductivity. However, this numerical evaluation does not consider thermal conductivity measurement error caused by heat conduction from the heated probe through the connecting wires of the heating element and the thermocouple. Thus,

transient techniques typically require careful calibration in order to account for the thermal resistance at interfaces, as well as, heat conduction through the connecting elements.

3.3.4.6 Dual Probe Technique

The dual-probe heat-pulse method allows for simultaneous determinination of the thermal conductivity, thermal diffusivity and specific heat. This methodology has emerged in recent years as a potentially useful measurement technique due to recent theoretical developments and the availability of instrumentation with the required accuracy and versatility. As discussed here, these recent technological developments provide the potential to determine the thermal properties of porous materials accurately and reliably.

The utility of a single probe apparatus was further developed by Nix et al. (1967, 1969) with the introduction of an additional temperature sensor placed a known distance from the conductivity probe. This development allowed for the simultaneous determination of the thermal diffusivity which has been applied to grain dust (Chang et al., 1980), granular starch (Marousis et al., 1991), organic waste (Iwabuchi et al., 1999), peanut pods, hulls and kernels (Suter et al., 1975), rapeseed (Moysey et al., 1977), rice bran (Sreenarayanan and Chattopadhyay, 1986), soil studies (Bristow et al., 1993, 1994; Campbell et al., 1991; Kluitenberg et al., 1993; Larson, 1988) and tomato juice concentrates (Choi and Okos, 1983) among others.

The ability to measure both of these terms is indeed valuable because thermal conductivity is simply the product of the two parameters. As such, the specific heat was also determined for each of these materials based on the measured values of thermal conductivity, thermal diffusivity and bulk density (Baik and Mittal, 2003; Marousis et al., 1991; Moysey et al., 1977; Suter et al., 1975).

The dual-probe heat-pulse method implements analytical solutions of the conduction heat transfer equation to provide the simultaneous determination of thermal conductivity and thermal diffusivity. The instrumentation consists of two closely-spaced, parallel probes; with one serving as a heating element and the other allowing for the

observation of the temperature at a nearby location. The temperature at this secondary sensor location is recorded as a function of time during the application of the heat pulse.

The resulting plot of wire temperature versus the logarithm of time can then be used to determine the thermal conductivity, with the slope of the straight line representing the thermal conductivity of the material as follows (Slusarchuk and Foulger, 1973):

$$S = \frac{T_2 - T_1}{\ln(t_2/t_1)} \qquad [3.3.18]$$

where: S = slope (K); T = temperature (K); t = time (s); and the subscripts 1 and 2 are the initial and final conditions; respectively.

In this case, the thermal conductivity can be evaluated according to the procedures proposed by Sharma and Thompson (1973) and Chang (1986) who both used the maximum slope (Wang and Hayakawa, 1993) in the line heat source equation as follows:

$$k = \frac{Q}{4\pi S} = \frac{I^2 R}{4\pi S} \qquad [3.3.19]$$

where: k = thermal conductivity (W m^{-1} K^{-1}); Q = line source strength (W m^{-1}); I = current (A); R = heating wire resistance (Ω m^{-1}); and S = slope (K) determined from the data points. This method essentially provides a measure of the thermal diffusivity; which will be discussed in further detail in the proceeding section of this report.

In practice, the medium to be measured has a finite size, while the line heat-source may be considered to have a finite length and mass. No axial heat flow is presumed to occur with this method due to the length of the heat source and relatively short testing duration. However, a time correction factor (t_0) may be subtracted from the observed time in order to compensate for the finite diameter of the line heat-source. Modifying the equation to account for this correction term yields (Hooper and Lepper, 1950):

$$k = \frac{Q}{4\pi(T_2 - T_1)} \ln\left(\frac{t_2 - t_0}{t_1 - t_0}\right) \qquad [3.3.20]$$

Note that this time correction factor can be determined by trial and error from experimental data, which ensures a straight line for the temperature versus logarithm of time.

The transient method is based on one-dimensional linear heat transfer conditions and allows for the thermal diffusivity to be determined from the measured temperature data over a specified time at a known distance from the line heat source. This technique assumes that: 1) the probe is sufficiently long for one-dimensional radial heat flow with negligible probe diameter; 2) the probe has an infinite thermal conductivity compared to the thermal conductivity of the medium; 3) the heat generation in the probe remains constant after initiation; and 4) the medium extends infinitely in the radial direction. These assumptions have generally been considered adequate in terms of accurately measuring thermophysical properties (Fontana et al., 2001). Based on these assumptions, the temperature at any given radius can be expressed as (Carslaw and Jaeger, 1959):

$$T = \frac{Q}{4\pi k} E_i\left(-\frac{r^2}{4\alpha t}\right) \qquad [3.3.21]$$

where: T = temperature (K); Q = power input (W m^{-1}); k = thermal conductivity (W m^{-1} K^{-1}); E_i = exponential integral; r = radial distance from line heat source (m); α = thermal diffusivity (m^2 s^{-1}); and t= time (s). Nix et al. (1967) also expressed the thermal diffusivity according to the following expression:

$$\Delta T = \frac{I^2 R}{2\pi k}\left(-\frac{C_e}{2} - \ln\beta + \frac{\beta^2}{2\cdot 1!} - \frac{\beta^4}{4\cdot 2!} + \cdots\right) \qquad [3.3.22]$$

where: ΔT = temperature rise of secondary probe (°C); C_e = Euler's constant (0.577215); $\beta = r/2\sqrt{\alpha t}$ (dimensionless); r = radial distance between probes; and t = heating time (s).

These approaches are based on the Fourier heat conduction equation in terms of the temperature distribution when energy is introduced into a system via an infinite line source with heat transfer occurring by conduction. The heat conduction in a

homogeneous and isotropic sample can be expressed by the following governing equation (in cylindrical coordinates) assuming negligible end effects and hot wire mass:

$$\frac{\delta T}{\delta t} = \alpha\left(\frac{\delta^2 T}{\delta r^2} + \frac{1}{r}\frac{\delta T}{\delta r}\right) \quad [3.3.23]$$

where: T = sample temperature in the cylinder (°C), t = time (s), r = radial distance from the heat source (m); and α = thermal diffusivity ($m^2\ s^{-1}$). Heat capacity can also be estimated based on the maximum temperature rise at a known distance from the heat source using the dual probe method (Campbell et al. 1991). As such, the heat capacity is inversely proportional to the magnitude of the maximum temperature change according to the following expression:

$$C = \rho c = \frac{Q}{e\pi r_m^2 \Delta T_m} \ln\left(\frac{t_2}{t_1}\right) \quad [3.3.24]$$

where: ρ = mass density ($kg\ m^{-3}$); c = mass heat capacity ($kJ\ kg^{-1}\ K^{-1}$); Q = power supplied to probe ($W\ m^{-1}$); C = volumetric heat capacity ($kJ\ m^{-3}\ K^{-1}$); e = base of the system of natural logarithms; r_m = fixed distance from heating probe, probe spacing (m); and ΔT_m = maximum temperature rise (K).

Hence, the thermal diffusivity and heat capacity can be directly calculated using the dual probe method. Furthermore, the thermal conductivity can be calculated using both of these values and the density of the material.

3.3.5 Method Selection for Current Study

Kluitenberg et al. (1993, 1995) addressed in detail several drawbacks associated with dual-probe measurement methods which may lead to deviation from the actual values of these thermal parameters. In particular, the dual probe method is sensitive to the probe spacing with significant variation attributed to errors in measuring the radial distance between the probes, variations in the local air-pathways, and inherent biological variations of the material. Reliable average values of the thermophysical properties may be obtained with additional thermocouples, replications and/or probes. Contact resistance

errors (Steinmanis, 1982) and moisture migration errors (Philip and deVries, 1957) may also result in poor agreement with true values (Bristow et al. (1994). This may be attributed to the dependence on the probe-to-medium contact, in which case, an air gap around the probe may lead to significant errors. Deviations from ideal boundary conditions generally require high accuracy in measuring the temperature with carefully calibrated correction factors (Mohsenin, 1980).

Moreover, high temperature measurements are especially prone to error due to the greater thermally induced moisture movement within the sample, which may be caused by increased temperature gradients as well as from the probe line heat source. Localized drying around the probe may also have a significant effect particularly at higher temperatures, where the heat transport is governed by the latent heat. Although a small diameter probe may provide a better approximation of a line heat source, the drying conditions near the interface could pose significant issues, particularly with large power inputs. As a result, lower thermal conductivity measurements are common with probe methods. Woodside (1958, 1959) suggested larger probe diameters with lower power inputs could compensate for the lower thermal conductivity measurements. The problems associated with contact resistance and moisture migration are minimized when all pore space is filled by a liquid. Using a saturated medium reduces the number of factors that are sources of error. Thus, concerns about contact resistance and moisture migration are minimized, and the validity of the infinite line-source solution permits for measurement with this technique.

The transient method has the advantage of providing rapid results without the need for the direct measurement of heat flux. In fact, most transient techniques are quick and portable with probes generally imposing only minimal disturbance in the medium. Probe methods also provide the ability to take repeated measurements while requiring relatively small sample sizes. The benefit of dual probe techniques, relative to the single probe approach, is the ability to measure all of the main thermophysical properties including thermal conductivity, thermal diffusivity and heat capacity. Thus, the dual-probe method shows great promise for the evaluation of the thermophysical properties of porous, biological materials such as baled switchgrass.

3.3.6 Thermal Properties of Biomass

The reliability and accuracy of the heated probe method has been demonstrated with various soils, grains and forages throughout the available literature. In fact, the heated probe method was found to be the most effective method for soils (Mitchell and Kao, 1978) with subsequent adaptations for field use (Goodrich 1986; Slusarchuk and Foulger 1973). The heated probe method has previously been used in determining the thermal conductivity of various soils including loam (Sepaskhah and Boersma,1979) and sand (Bush et al., 1979); while the deVries theory (DeVries, 1963) has been successfully applied to mineral soils (Skaggs and Smith, 1968). Tollner and Verma (1984, 1987) also presented an analytical procedure for determining the thermophysical properties of organic potting mixes (pine bark-sand) based on a steady-state approach involving a line heat source. However, significant errors resulted due to the diffusion of water vapor when testing required extended periods of time.

Successful application of the transient method has also been reported for various sands (Butts, 1990), mineral soils (Abu-Hamdeh and Reeder, 2000; Campbell et al., 1991) and clays (Bristow et al., 1994, Hiraiwa and Kasubuchi, 2000). The dual probe method has also been used to evaluate the fundamental thermophysical properties of high moisture materials including bentonite slurries, industrial sludges, peat soils and solid wastes (Hanson, 2000). Thermal conductivity generally varies with the organic matter content, salt concentration, texture of the material and water content. In fact, the thermal conductivity is widely reported to be positively correlated with the moisture content and bulk density of the material. Results of these studies have also indicated that the thermal conductivity of organic soils is typically lower than soils with sand and silt due to the large void ratios which prevent effective heat transfer (Hanson, 2000). Fibrous material also has higher thermal conductivity than sedimentary material due to the structural framework of the material. Organic soils typically have higher values of heat capacity compared to sands and silts due to the inherently high water concentration within the organic components.

The thermophysical properties of various organic materials such as grain have also been determined using a variety of methods. Early research in this field involved the solution of the one-dimensional, steady-state heat transfer equation for various grains

held in cylindrical test chambers (Babbitt, 1945; Bakke and Stiles, 1935; Dua and Ojha, 1969; Moote, 1953; Ojha et al., 1967). Specific heat has also been determined for a variety of grains primarily using the ice calorimetry method (Babbitt, 1945; Disney, 1954; Haswell, 1954; Moote, 1953; Pfalzner, 1951). Likewise, Sharma and Thompson (1973) evaluated the thermal conductivity and specific heat of grain sorghum using the line heat source theory and method of mixtures, respectively. The specific heat and thermal conductivity were expressed as functions of the moisture content as follows:

$$C = 0.3337 + 0.0077 \cdot M \qquad [3.3.25]$$

$$K = 0.0564 + 0.000858 \cdot M \qquad [3.3.26]$$

where: C = specific heat (Btu lb^{-1} $°F^{-1}$); K = thermal conductivity (Btu hr^{-1} ft^{-1} $°F^{-1}$) and M = moisture content (%-wb).

The thermal diffusivity of rapeseed was also measured over variable temperatures and moisture contents, while calculating the corresponding values of thermal conductivity (Timbers, 1975) and specific heat (Moysey et al., 1977). The line heat source method has also been used to evaluate the bulk thermal conductivities of wheat, corn and grain sorghum at variable densities (Brooker et al., 1992; Chang, 1986). The thermal conductivity has been expressed as a linear function of density in the general form:

$$k = C_1 + C_2\rho \qquad [3.3.27]$$

where: k = thermal conductivity (W m^{-1} K^{-1}), ρ = bulk density (kg m^{-3}); and C_1 and C_2 = coefficients which were determined by linear regression analysis.

The line heat source method was also used to evaluate the thermal conductivities of barley, lentils and peas which were subsequently related to temperature and moisture content (Alagusundaram et al., 1991) according to the general linear equation:

$$k = a + b \cdot T + c \cdot M \qquad [3.3.28]$$

where: k = thermal conductivity (W m^{-1} K^{-1}); a, b, c = empirical constants; T = temperature (K); and M = moisture content (%-wb).

The fundamental thermophysical properties of borage seeds were also determined at various moisture contents and temperatures (Yang et al., 2002) using the transient line heat source technique and differential scanning calorimetry, respectively. The maximum slope method was used to analyze the line source heating data with the specific heat and thermal conductivity expressed as:

$$C_p = 0.58 + 7.36(10^{-3})T - 4.11(10^{-5})T^2 + 3.04(10^{-2})M + 1.81(10^{-4})M^2 + 6.40(10^{-4})T \cdot M - 1.49(10^{-5})T \cdot M^2 \quad [3.3.29]$$

$$k = 0.097 + 1.285(10^{-4})T + 1.868(10^{-3})M + 1.951(10^{-4})T \cdot M \quad [3.3.30]$$

where: C_p = specific heat (kJ kg^{-1} K^{-1}); k = thermal conductivity (W m^{-1} K^{-1}); T = temperature (K) and M = moisture content (%-wb).

The specific heat model previously developed by Yang et al. (1997) was found to fit the specific heat data well; which further confirmed the practicality of the model for seed and grain applications. The fundamental thermophysical properties of strip tobacco were also evaluated as functions of the moisture content (Locklair et al., 1957), with the specific correlation between thermal conductivity, moisture content and bulk density later given as (Samfield and Brock, 1958):

$$k = 0.020 + 0.001M + 5.126(10^{-5})\rho \quad [3.3.31]$$

where: k = thermal conductivity (W m^{-1} °C^{-1}), M = moisture content (%-wb); and ρ = bulk density (kg m^{-3}).

The thermal conductivity of shredded flue-cured tobacco (Sykes and Johnson, 1973) and fibrous sheets of processed tobacco (Kobari et al., 1985) were likewise measured using the line heat source method. In general, results have indicated that the effective thermal conductivity is linearly related to the moisture content, but is

significantly higher in the direction parallel to the fiber orientation. Ott (1964) also determined the thermal diffusivity of baled alfalfa hay assuming one-dimensional heat transfer within an infinite plate; with results indicating that thermal diffusivity decreased with increasing bale density according to the following regression equation:

$$\alpha = 0.6014 - 0.001295 \cdot \rho \qquad [3.3.32]$$

where: α = thermal diffusivity ($m^2\ s^{-1}$) and ρ = density ($kg\ m^{-3}$). However, lower densities within the specified range exhibited deviations due to the presence of air in the material which governed the variability. Furthermore, the specific heat increased at high moisture contents and decreased at high densities due to the transitions from bound water to free water. The resulting regression model for specific heat was given as:

$$C = 2.10 - 0.281(10^{-2})\rho + 0.466(10^{-1})M \qquad [3.3.33]$$

where: C = specific heat ($kJ\ kg^{-1}\ K^{-1}$); ρ = density ($kg\ m^{-3}$) and M = moisture content (%-wb). The thermal conductivity of burley and flue cured tobacco lamina were also determined by Duncan et al. (1966) and Childs et al. (1983), respectively.

The thermal diffusivity of a single alfalfa stem was also measured at constant moisture content and density (Ford and Bilanski, 1969); while the specific heat and thermal conductivity of alfalfa silage was investigated using the steady-state method at variable moisture content and density (Scermely, 1975). Results indicated a linear correlation between thermal conductivity and the moisture content and bulk density of the silage.

Studies have also reported strong correlations between the moisture content and specific heat of ground alfalfa (Bern, 1964; Mohsenin, 1980) according to:

$$C_p = 0.22 - 0.0142\ M \qquad [3.3.34]$$

where: C_p = specific heat ($cal\ g^{-1}\ m^{-1}\ °C^{-1}$); and M = moisture content (%-wb) which is valid between 4 and 20 %-wb. However, the implementation of such an equation in the

current application of baled switchgrass would necessitate an assumption that the bale/air mixture is a single solid with water representing the secondary material. This assumption could be valid in those cases exhibiting minimal natural convective currents due to elevated densities, but would need to be modified for forced ventilation models.

Muck et al. (1983) also predicted the specific heat of alfalfa haylage using a weighted average of the specific heat of water and that of the dry matter. Measured values of the thermal conductivity (parallel plate method) and thermal diffusivity (Dickerson's method) have also been used to indirectly determine the specific heat of haylage (Jiang et al., 1986). Although the results indicated a significant moisture content and bulk density effect on thermal conductivity, less significant correlations were observed for thermal diffusivity. The following correlations were reported for each fundamental thermophysical property in terms of the moisture content and bulk density as follows:

$$C_p = 2.2573 - 3.237(10)^{-3}\rho_w + 1.197(10)^{-4}\rho_w M \quad [3.3.35]$$

$$\alpha = 1.829(10)^{-2} - 9.22(10)^{-5}\rho_w + 0.6(10)^{-7}\rho_w^2 - 1.08(10)^{-6}M^2 \quad [3.3.36]$$

$$k = 2.236(10)^{-1} - 3.074(10)^{-4}\rho_w - 1.061(10)^{-3}M + 8.16(10)^{-6}\rho_w M \quad [3.3.37]$$

where: C_p = specific heat (kJ kg^{-1} °C^{-1}); α = thermal diffusivity (m^2 s^{-1}); k = thermal conductivity (W m^{-1} °C^{-1}); ρ_w = wet density (kg m^{-3}); and M = moisture (%-wb). However, haylage has a different material composition compared with that of baled biomass feedstocks.

The thermal conductivity and thermal diffusivity of burley tobacco bales were measured simultaneously by Casada and Walton (1989a, 1989b) using a dual thermal probe. Although biological variation of the material and probe fabrication uncertainties resulted in some variation in the thermophysical assessment, these thermophysical properties were expressed as functions of the moisture content and bulk density. In fact, thermal conductivity increased linearly with moisture content while specific heat

decreased. The thermal conductivity was also reported to be linearly correlated with bulk density; although to a greater extent within the parallel orientation. In this case, the effective thermal conductivity was significantly higher in the parallel orientation due to the heat conduction through continuous solid leaf material, while the perpendicular orientation involved heat conduction through successive air spaces. Likewise, the center of the baled yielded the highest values of thermal conductivity since the oriented leaves resulted in higher density at the center of the bale. However, the effects of temperature were generally considered negligible in this study.

The thermal diffusivity of alfalfa was measured by Moore and Bilanski (1992) at a range of moisture contents (30 to 80 %-wb) and densities (200 to 500 kg m^{-3}) while estimating the thermal conductivity. A multiple regression model was fitted to the data which was found to be consistent with previously reported thermal properties of alfalfa. The thermophysical properties of baled timothy hay have also been evaluated using the dual thermal probe method at variable temperatures, moisture contents and bulk densities; while specific heat was measured using the method of indirect mixtures (Opoku, 2004, 2006). Multiple regression models were developed to predict thermal conductivity and diffusivity using the initial hay temperature, moisture content and bulk density. The measured specific heats were higher than the calculated values, but generally increased with temperature and moisture content while decreasing with bulk density.

Thermal conductivity of timothy hay was also measured by Iroba (2013) based on the line source method with the results indicating significant temperature, moisture and density effects. Thermal conductivity was positively correlated with each of the independent parameters; while thermal diffusivity exhibited a nonlinear relationship between these material properties. The specific heat capacity was also estimated from the measured values to produce the following regression equation as a function of moisture content:

$$C_p = 0.1929M - 0.5266 \qquad [3.3.38]$$

where: C_p = specific heat (kJ kg^{-1} °C^{-1}) and M = moisture content (%-wb). The specific heat values increased with temperature and moisture content; but decreased with bulk density.

The results obtained to date support the validity of the transient, line-source theory while substantiating further use of the dual-probe method in porous, biological materials. As noted in this review, previous studies have also indicated that the temperature and moisture content significantly affect thermal conductivity measurements. In fact, increases in the moisture content generally produce greater values of thermal conductivity and specific heat. While thermal conductivity generally increases linearly with temperature, moisture content and bulk density; the thermal diffusivity typically has a nonlinear relationship with these parameters.

3.3.7 Practical Applications

The thermophysical properties of many agricultural and lignocellulosic materials remain unavailable in the current literature. In fact, there is currently no data available for baled biomass feedstocks. The empirical relationships that describe these thermal properties as functions of the inherent physical characteristics of the material must also be developed for baled switchgrass to enable prediction of the heat or moisture transfer within bales. Therefore, a major objective of this study involved the determination of the relevant thermophysical properties of baled switchgrass as functions of temperature, moisture content, bulk density and physical orientation of the material. This involves measurement of the thermal conductivity and thermal diffusivity using a transient, dual-probe, line heat-source method with the maximum slope approach. The specific heat as calculated from the thermal conductivity and thermal diffusivity values was also validated.

The thermal conductivity is expected to increase with increasing moisture content, bulk density and temperature to a lesser extent. On the other hand, relatively small, nonlinear variation in the thermal diffusivity is expected with changes in the moisture content and bulk density. Convective heat transfer is also expected to be minimal with high bulk densities; although this inverse trend, and the effect of moisture migration, will both be accounted for in the ‘effective’ thermal conductivity term. Heat flow is also

expected to vary according to the directional orientation through the bale since different mechanisms of heat transfer will arise due to the stem orientation within the bales. Local density variation within the bales may also affect the measurement of the thermophysical properties.

These thermal properties are essential in developing accurate analytical and empirical models of the heat and mass transfer in densified biomass; designing optimal drying, storing and bioconversion operations; and improving production efficiency, thereby, increasing economic return for farmers and processors. Accurate characterization of the physical properties of lignocellulosic biomass must be pursued to improve the engineering analysis and design of storage and/or processing facilities.

3.4 Heat and Mass Transfer

Baled feedstocks may be stored on-farm or at bioconversion facilities for extended periods of time (up to one year) in order to bridge periods between production seasons. These prolonged storage periods necessitate a high degree of control over the associated storage conditions. In general, baled biomass is considered a complex domain involving unique physical, chemical and/or biological systems. Even in covered storage, fluctuations in the ambient air temperature and/or relative humidity may prompt specific changes in the physical characteristics (i.e., porosity, moisture absorption, etc.) and the biochemical reactions (i.e., microbial activity, overall bale quality, etc.) of baled biomass during storage, transportation and/or bioconversion. The temperature and moisture within the biomass may consequently vary throughout storage to a significant extent.

Accordingly, the temperature and moisture content are known to be influenced by specific environmental conditions (i.e., air temperature, relative humidity, solar radiation, air flow, etc.), the properties associated with the hygroscopic material itself (i.e., bulk composition and thermophysical properties of the material, natural convection characteristics), and the microbial activity which may lead to localized heating within the bulk material. Convective heat and moisture transfer may be dominant due to forced and/or natural air flow; while heat conduction may also cause temperature fluctuations which affect the material's ability to adsorb/desorb moisture. In turn, the moisture content of the biomass may strongly influence the degradation of the material; with optimal feedstock and/or biofuel quality achieved through the removal of moisture.

While the low moisture content required for the safe storage is difficult to attain through traditional field operations; artificial drying presents several problems associated with moisture heterogeneity, over-drying, and non-uniform air distribution within bales (Arinze et al., 1994). The thermal efficiency associated with forced-air techniques may be improved with partial air recirculation, airflow inversion and by heat reduction (Descôteaux and Savoie, 2003), but the energy demands are typically uneconomical (Hill, 1976; Muck and Shinners, 2001). Hence, a compromise must be made between the high energy requirements for moisture removal and the increased susceptibility to quality losses that arise through exposure to adverse weather conditions (Hill, 1976; Parker et al., 1992; Wirleitner, 2010).

The importance of heat and mass transfer within capillary porous materials has been extensively studied due to its wide array of practical applications. In fact, various agricultural products (e.g., wood and grain) have been modeled as porous hygroscopic materials with model developments generally based on mechanistic approaches. In these studies, the transfer phenomena are either derived from non-equilibrium thermodynamic principles or from macroscopic descriptions of Fourier's and Fick's laws (Liu, 1990). A model is essentially an abstract, simplified mathematical construct (or system) which represents the relevant features of a physical phenomenon (Bender, 1978). It should also be recognized that the application of such a theory must be consistent with the axioms and theorems that have been used in its formulation and interpretation.

Although many studies have investigated the deterioration and weathering of forage bales, few studies have researched the heat and moisture transfer within baled biomass. The development of a comprehensive heat and mass transfer model is expected to play a critical role in developing postharvest quality models for baled biomass. Boundary conditions are also expected to influence the heat, mass and momentum transfer within baled biomass. Changes in temperature can be modeled as heat transfer due to conduction, convection or a combination of both mechanisms; while the total moisture flux (including thermally-induced mass transfer) may be accounted for by some form of the diffusion theory. It may also be noted that convective boundary conditions may increase the temperature gradient across a porous material; thereby, contributing to the development of natural convection currents and the associated heat transfer which is of particular interest in the current study for baled switchgrass.

The current study is specifically concerned with describing the moisture and temperature transfer within baled switchgrass; while accounting for natural convection, fluid flow and the rapid effect of microbial heating within the bale. However, various environmental factors (e.g., rainfall and solar radiation) will be neglected as the present model represents a controlled environmental system in the absence of these environmental factors. Therefore, the development of a relevant heat and mass transfer model for baled switchgrass is suggested in the current study in order to promote efficient storage and/or bioconversion, establish optimal storage conditions and bale quality, as well as, to predict changes in the temperature and moisture content of baled switchgrass.

The underlying theories and fundamental mechanisms governing the drying and/or wetting of porous materials is discussed in this review, followed by an outline of modeling theory for porous media with particular reference to diffusion theory. Currently available models found in literature are also presented for various agricultural and biological applications. The topics discussed in this review are considered fundamental in obtaining suitable 'constitutive' equations for heat and mass transfer simulations within baled biomass.

3.4.1 Temperature and Moisture Migration

Switchgrass (*Panicum virgatum*) has been identified as a lignocellulosic crop representing great potential as a substrate for the sustainable production of cellulosic ethanol (Tilman et al., 2009). Safe storage of switchgrass dictates that the moisture content should generally remain below 18 % under typical storage conditions (Mitchell and Schmer, 2012). However, seasonal variations in the ambient temperature may result in the migration or redistribution of moisture within the biomass that jeopardizes storage stability. In fact, a localized increase in moisture content may result in an environment conducive to microbial and fungal growth under certain conditions. Temperature and moisture are accordingly the most important factors governing the storage quality of biomass. Agricultural forages such as switchgrass generally contain liquid water within the vascular bundles (interstitial) and the cells themselves (bound), as well as, water vapor in the intercellular spaces. The amount of water initially contained within switchgrass may vary depending on specific environmental factors, as well as, the plant variety, maturity, quality and storage format among other factors.

Pore-scale diffusion characteristics are also discussed briefly in this review since a basic understanding of pore-scale mechanics is necessary for describing relevant macroscale phenomena. In accordance with this topic, capillary tube geometry may be considered an idealization of the actual pore-scale media represented as a set of parallel, straight tubes; while tortuosity accounts for the complexity of those capillary paths. Hence, tortuosity compensates for the ideal approximation by increasing the length of the parallel, straight pores; which is particularly significant in media with a homogeneous pore size (Epstein, 1989; Grathwohl, 1998). Likewise, constrictivity addresses the

narrowing of the effective pore size which may significantly reduce the associated flow rate through the media. However, the heterogeneity of agricultural material often prevents an analytical description of the complete distribution of particles, aggregates and pore spaces. Hence, an implementation of such elaborate spatial models (e.g., the geometry of every pore) is typically unfeasible.

For these reasons, descriptions of the average/bulk properties are often used to characterize a porous material (e.g., substrate bulk density accounts for the porosity); while chemical and/or biological processes are often averaged and expressed as empirical functions. It may be similarly be assumed that there is only one temperature for the entire porous medium; thereby implying that separate phases are in thermal equilibrium. Although a model based on such relevant assumptions (material geometry, functional representation of diffusivity, etc.) can provide a general representation of a porous media, a more realistic representation of the porous matrix is important in accurately modeling anisotropic media. Although previous studies have typically involved homogeneous and isotropic porous structures, non-homogeneous and anisotropic effects have received some attention in recent years.

A fundamental knowledge of the temperature transfer and moisture migration occurring within biomass is necessary for the design and management of an effective storage operation with respect to the variable material properties and environmental conditions. While moisture transfer has been the subject of numerous agricultural studies, most of this research considers bulk/batch drying involving the average effect on a relatively large quantity of material. Therefore, moisture movement occurring within distinct units of the agricultural material must be considered in order to provide a thorough understanding of the thermophysical properties. Moisture transport within porous bodies and biological materials have been described by many theories including the moisture transport through intercellular spaces and the interaction between the biomass and the surrounding air (Fortes and Okos, 1980). However, the moisture movement between a crop and its environment is generally reported by three interrelated processes including diffusion, evaporation and condensation (Hill, 1976; Moore & Peterson, 1995). Brief descriptions of these physical processes are presented here to

provide a basic understanding of the wetting, drying and associated temperature transfer phenomena occurring within porous media.

3.4.1.1 Diffusion Theory

Diffusion describes the process by which a fluid migrates from high moisture regions to low moisture regions through the capillaries, vessels and cellular walls within a porous media due to an imposed concentration gradient. Grathwohl (1998) has also described diffusion as a mass transport process arising from Brownian motion (random thermal molecular motion). This diffusion of moisture through a porous medium depends on the amount of water present and the matric potential describing the water-holding force within capillaries and surfaces of the material (Parr et al., 1981; Miller, 1989). More specifically, longitudinal diffusion occurs as water is transported through the fibers; while transverse diffusion results in the progressive crossing of several cavities.

Suggested mechanisms of moisture transfer include: 1) liquid transport by capillary forces (i.e., moisture gradients, molar transport, molecular diffusion); 2) vapor transport by temperature and moisture gradients (i.e., thermal and mass diffusion); and 3) liquid and vapor transport by pressure differences (Parry, 1985).

Liquid diffusion formed the basis of early drying theories (Lewis, 1921; Sherwood, 1929); although this term may be somewhat misleading since the traditional definition refers to those processes occurring on a molecular level (e.g., mixing of gases). While ‘true’ liquid diffusion may indeed occur within a porous solid due to the existence of concentration gradients of a liquid mixture, the flow of liquid through a porous medium is actually the result of complicated phenomena involving the surface tension of the liquid and vapor properties of the solid structure. Vapor diffusion may also occur as a result of a vapor pressure gradient within the porous solid. This mechanism has been used in the formulation of several theories limited to the latter stages of drying (Harmathy, 1969; King, 1968). In contrast, capillary liquid movement is driven by surface tension forces which represent an important role in those regions of a porous solid containing continuous liquid paths. This mode of moisture transfer has been used in developing several drying theories in combination with other mechanisms (Ceaglske and Hougen, 1937; Philip and DeVries, 1957; Van Arsdel, 1947). Liquid and/or vapor movement may

also occur in those situations involving large pressure gradients induced through the porous solid (Chen and Pei, 1989; Whitaker, 1986). The movement of liquid by gravitational effects is, however, negligible in porous bodies due to the large surface tension effects which overcome the gravitational forces. This concept may be further substantiated by relatively small values of the dimensionless Bond number which is defined as:

$$\mathrm{Bo} = \frac{\Delta\rho L^2 g}{\sigma} \qquad [3.4.1]$$

where: $\Delta\rho$ = difference in density (kg m^{-3}); L = characteristic length (m); g = gravitational acceleration (m s^{-2}); and σ = surface tension (N m^{-1}).

In general, the diffusion of moisture is controlled by both the internal biomass resistance and the external resistance due to the boundary layer. Diffusion of the freely available fluid within the intercellular spaces of the porous medium may specifically be hindered by tortuous paths and small cross-sectional pore channels (Grathwohl, 1998). A diffusion coefficient can be used to characterize this internal resistance to moisture diffusion. Such terms are generally dependent on the temperature and moisture content (Avramidis and Siau, 1987).

While diffusion coefficients are generally difficult to measure, predictive equations have previously been formulated (Grathwohl, 1998). When the axial movement of moisture through a fibrous media becomes inhibited, radial movement becomes the major pathway for further moisture movement. However, the waxy epidermal layer on plant stems severely restrains diffusion in the radial direction (Moore & Peterson, 1995). Hence, removal of this epidermal layer can greatly increase moisture loss from grasses (Haghighi, 1990). The rate of diffusion into the free atmosphere is also restricted by the moisture concentration gradient, air resistance and stomata resistance in leaves (Hill, 1976).

3.4.1.2 Drying Theory

Drying is a heat and mass transfer phenomenon involving the migration of water to the surface and subsequently evaporates depending on the current environmental

conditions. Physical drying processes are now discussed in terms of a moist, porous, semi-infinite slab stored within a controlled environment (fixed air temperature, humidity and pressure) as shown in Figure 3.4.1.

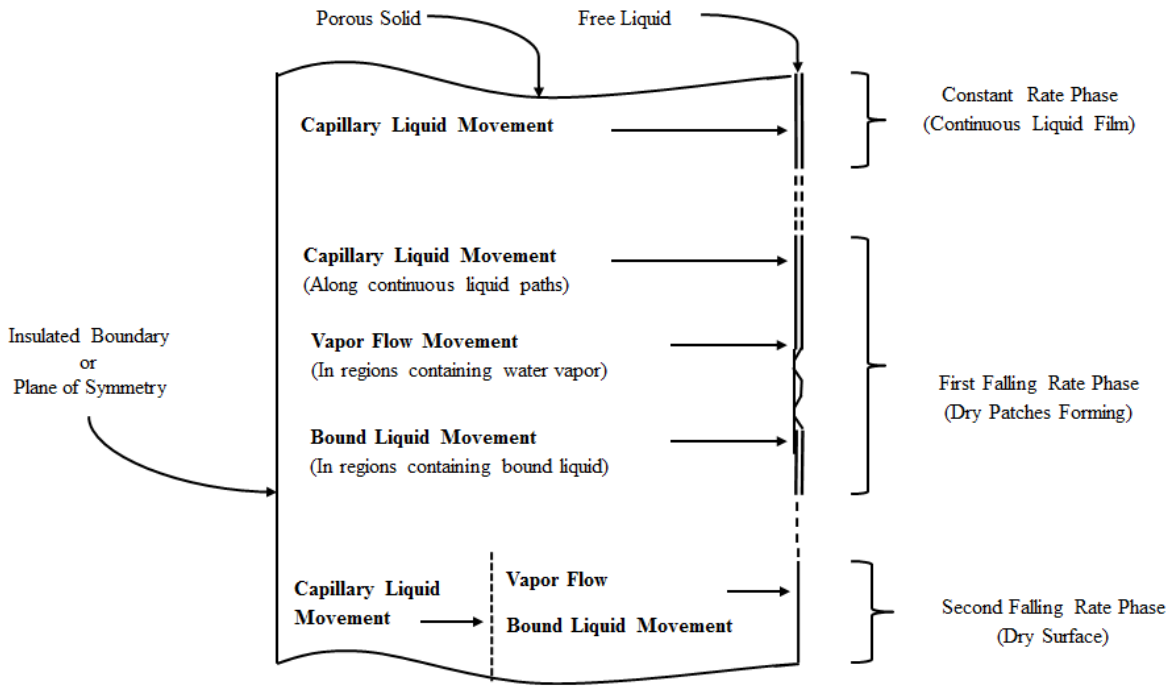

Figure 3.4.1. Moisture movement during a drying process.

The water contained within the solid may be classified as either free water (exerted vapor pressure is equivalent to the pressure to that of saturated liquid at the same temperature) that exists within the void spaces; or bound water (vapor pressure is lower than the pressure at saturated conditions) that is contained in very fine capillaries. A sufficiently high initial moisture content may saturate the surface of the material; giving rise to a constant rate phase of drying. In this phase, liquid evaporation is essentially constant and equal to the evaporation from a free liquid surface. With materials of high moisture content, the vapor pressure in the air over the solid is equivalent to the pressure of saturated liquid at the same temperature. Continuous paths of liquid may exist with capillary forces serving at the dominant mechanism of moisture movement in the 'wet' region of the porous medium (where free water exists). However, this intercellular moisture is quickly removed during this initial phase as characterized by a rapid, almost-constant drying rate.

The drying air within a sufficiently deep bed may become saturated in accordance with the amount of water vapor that air can hold at a given temperature (Moore & Peterson, 1995). Hence, drying air may emerge from the porous material near the wet-bulb temperature; with the vapor pressure difference between the surface and ambient air dependent on the internal air temperature and the ambient relative humidity of the environment (Moore & Peterson, 1995). For individual particles, however, a constant rate of drying will only be experienced in those cases involving a sufficiently high moisture content which provides the surface layer of free water. In this case, the rate is only dependent on the external conditions according to the following expression (Bakker-Arkema et al., 1976):

$$\frac{dM}{dt} = \left(\frac{h}{h_{fg}}\right)(T - T_{wb}) \qquad [3.4.2]$$

where: h = (volumetric) heat transfer coefficient (kJ m^{-3} °C^{-1} s^{-1}); h_{fg} = heat of vaporization of free water (kJ kg^{-1}); T = free stream temperature (K); and T_{wb} = wet-bulb air temperature (K).

As drying continues, a critical point is reached in which the water cannot be conducted quickly enough to maintain a moist surface; resulting in the formation of dry patches. In fact, the continuous paths of free liquid disappear during this sorption region; with all remaining water existing within the cells. This remaining water is slowly moved from the cells and into the intercellular space with an increased resistance to diffusion that may be attributed to the cell walls and membranes. This reduced flux of water corresponds to a slower drying rate (Hill, 1976) that can be considered to be directly proportional to the area of the surface that remains normally wetted.

The drying rate is also dependent on the axial and radial fluid transfer rate along the length of the stem and towards the surface of the material, respectively. This so-called ‘first falling rate’ period of drying continues until all wet patches disappear from the surface, indicating that the ‘hygroscopic limit’ has been attained (Chen and Johnson, 1969). At this point, capillary theory dictates that the vapor-pressure lowering effect becomes significant for capillary-porous bodies (Luikov, 1975); thus, marking the initiation of the ‘second falling rate’ phase. Moisture transfer in this region occurs

primarily as a result of vapor diffusion (water vapor diffuses from regions of ‘high’ to ‘low’ vapor pressures) and the movement of ‘bound’ liquid.

After reaching the plant surface, the moisture evaporates and moves away from the porous medium by the principles of moisture diffusion. In accordance with this theory, the moisture moves from the relatively high vapor pressure at the surface to the low vapor pressure of the ambient air. Hence, the rate of drying increases with greater vapor pressure deficits between the plant surface and ambient atmosphere. Sufficient energy is needed for liquid water evaporation. In this case, the energy must be equivalent to the latent heat of vaporization in order to overcome the bonds that are between separate liquid water molecules. This energy may develop with a decrease in the material and sorbed-moisture temperature, from heat generated by material respiration, and/or from any heat that is conducted into the material. However, the enthalpy associated with temperature change is typically neglected under the assumption that the air is near dynamic equilibrium with the liquid phase and there is a negligible temperature difference. Conversely, the vapor pressure gradient may reverse when the ambient relative humidity is high (i.e., during rainfall or at night); thereby, condensing moisture onto the plant surface and/or driving moisture back into the plant (releasing the same amount of heat into the liquid phase).

The uptake of moisture by cotton bales has been described in terms of gaseous diffusion through the pores of a solid body; although neglecting the role of temperature gradients (Henry, 1939). The effect of temperature gradient on water movement within soil was later evaluated by Gurr et al. (1952) using soluble tracers to distinguish liquid and vapor transport. Results indicated that vapor moves to lower temperatures while liquid moves oppositely as allowed by conducting water films. The driving force for diffusion is generally attributed to moisture content gradients (Droin et al., 1988; Jia et al., 2010; Vergnaud, 1991).

3.4.1.3 Sorption Theory

Local equilibrium between the biomass and the surrounding air requires cooler and warmer regions of the biomass to gain and lose moisture, respectively. Accordingly, a localized temperature increase will cause greater partial pressure of water vapor within

the interstitial air. Thus, water vapor will diffuse from warmer to cooler regions of the biomass due to the resulting vapor pressure gradient that is parallel to the temperature gradient (Stewart, 1975). If the biomass was non-hygroscopic, most of the moisture could migrate from warmer to cooler regions while leaving behind a dry region (Eckert and Faghri, 1980). However, the hygroscopic nature of agricultural materials typically results in the development of a moisture content gradient directionally opposing the temperature gradient. Therefore, a net diffusion flux of water vapor at any location can be defined as the sum of the opposing temperature and moisture gradient fluxes. Natural convection currents may also develop in response to air density gradients. The moisture migration process may be considered a diffusive and convective transport process through the intercellular spaces of the biomass; with the biomass moisture acting as a water source and/or sink.

Another important consideration involved in this study is the equilibrium moisture content (EMC) which represents the limiting moisture content that the material approaches when stored in a controlled environment of fixed temperature and relative humidity. Hence, the EMC occurs when biomass has reached a water content equilibrium with its environment, thereby inhibiting any further moisture exchange. Any moisture content above the maximum sorptional moisture content indicates the presence of free water; while any moisture content below this value indicates that only bound water exists in the solid structure. Equilibrium between the vapor pressure of the surrounding air and the pressure of the biomass water at the saturation temperature are specifically reached in this process. It follows that the EMC is of great importance in developing mathematical models describing the heat and mass transfer within hygroscopic agricultural materials.

A relationship between the relative humidity of the air and the moisture content of the solid at specified temperature may be provided by a sorption isotherm. Many well-known empirical and semi-empirical relationships currently exist in fitting isotherm curves to the EMC data; including those based on the kinetic theory of gas adsorption by a solid such as the BET model which assumes multilayer adsorption (Brunauer et al., 1938). Various modifications have also been proposed and developed for the BET equation including extensions for capillary adsorption (Brunauer et al., 1940). While the details of these theories are considered outside the scope of the current review, distinction

should be made between sorption (wetting) and desorption (drying) isotherms; with a number of proposed theories explaining this hysteresis effect (Ngoddy and Bakker-Arkema, 1970). While most agricultural applications involve the transfer of moisture from the material to the flowing air (desorption), this process may be reversed in those circumstances involving the flow of moisture from air to a relatively dry crop (adsorption). It may also be noted that the EMC in the desorption process may be somewhat higher than the equilibrium moisture content in the adsorption process due to a hysteresis effect.

3.4.1.4 Influential Factors

A number of internal (crop characteristics) and external (environmental conditions) parameters influence the moisture equilibrium and drying behavior of agricultural materials as outlined in the following discussion. Internal parameters include specific material properties such as density, permeability, porosity and thermophysical properties among others; while external parameters include air temperature, relative humidity and air velocity. It should be noted, however, that the high level of correlation between these material properties and the environmental factors often present a challenge in analyzing the effect of the individual parameters on the drying rate (Borreani & Tabacco, 1998).

Inherent properties of agricultural materials which impact the drying behavior include the initial moisture content, plant variety and other physical characteristics (Moore & Peterson, 1995; Wright et al. 2001). In fact, the initial moisture content of timothy hay was shown to be negatively correlated with the drying rate (Savoie & Mailhot, 1986); while dry matter loss was shown to exhibit positive correlations with both the moisture content and the density of alfalfa bales (Shinners et al., 1996). The drying of some hay crops may also be affected by the number of stomates and/or the leaf-to-stalk ratio that is unique to each plant variety. It may also be noted here, that the mechanical crimping, crushing or conditioning performed during harvest operations may improve the direct movement of water from the interior portions of the stems by overcoming the fluid resistance imposed by the cuticle layer.

The drying of agricultural materials also depends on the packaging and handling

of the biomass since the density and thickness of the material significantly impacts the associated drying rate (Smith, 1990). For instance, the convective air currents become more inhibited at higher densities. Previous studies have also shown that soft-core bales experience greater axial airflow compared to uniform-density bales; thereby, achieving a more even distribution of air while reducing drying times (Román, 2014). A bulk material may also be classified as either hygroscopic or non-hygroscopic depending on its ability to 'bind' water. The various factors contributing to the internal moisture diffusion within a complex porous media may be lumped into an effective diffusivity term (Coumans, 1987, 2000; Gigler et al., 2000; Keey, 1991; Lievense et. al, 1990).

External environmental factors (i.e., air temperature, relative humidity, wind velocity, solar radiation) also impact the drying rate of biomass, as well as, affecting the rate of internal moisture movement (Keey et al., 2000; Walker, 1993). Solar radiation has previously been reported to have the greatest impact on thin-layer drying rates during field drying (Bartzanas et al., 2010; Haghighi, 1990; Smith, 1990); although the vapor pressure deficit (VPD) is also considered an important parameter affecting the drying rate of biomass (Haghighi, 1990; Moore & Peterson, 1995). The VPD is essentially the measure of the drying power of air obtained by the difference of actual and total vapor pressure at a given air temperature (Wright et al., 2000). The gradient in vapor pressure is controlled by the biomass temperature and surrounding relative humidity.

Solar radiation and vapor pressure deficit have both been reported to have a positive correlation with the drying rate (Savoie and Mailhot, 1986). On the other hand, the effects of wind speed (Savoie & Mailhot, 1986; Smith, 1990; Smith et al., 1988; Wright et al., 2000) and soil moisture content (Womac et al., 2005) have generally been shown to have weaker correlations with the drying rate of biomass. Nevertheless, the resistance to moisture diffusion is typically inversely proportional to the wind speed. Lower relative humidities may also result in higher drying rates due to the reduction of surface moisture content and increased moisture gradient.

3.4.1.5 Coupled Heat and Mass Transfer

As shown in this review, the drying or wetting of a hygroscopic material involves two distinct transport processes occurring simultaneously. The first component includes

heat transfer from an external medium to the surface of the agricultural material, as well as, heat transfer within the material. The other component involves mass transfer in terms of moisture diffusion inside the material to the surface, as well as, the external transport of moisture to the surrounding environment. Thus, drying may be considered a simultaneous heat and mass transfer problem that can be expressed in terms of a system of coupled nonlinear partial differential equations. An understanding of these simultaneous heat and mass transfer processes within a porous agricultural material will help to improve storage and quality parameters. The modeling of these transfer processes requires a sufficient knowledge of the different drying regimes encountered, the principal modes of mass transport that occur, and the type of porous structure to be dried. Once these have been identified, a mathematical model of the overall process may be formulated.

Heat transfer within agricultural materials generally occurs by conduction from imposed temperature gradients; while convection from moisture migration generally occurs to a lesser extent (Valentas et al., 1997). The heat generated by the biomass and the latent heat of evaporation may also be considered significant in terms of the heat transfer equations (Mason, 2006). These heat sources may be transferred by convection and conduction in both the liquid and gas phases. Although radiative heat gain and/or loss may be significant in outdoor field operations (Robinzon et al., 2000), this mechanism is expected to be insignificant with material stored indoors.

The natural (buoyancy-driven) convection phenomena may also be induced by the internal heat generation from exothermic reactions such as, heat generation from respiration and microbial activity. Many relevant theories and applications have been summarized by Nield and Bejan (2006); with the existing analyses typically focused on horizontal porous layers and enclosures with uniform heating and/or cooling at the boundaries (Bergholz, 1980; Rudraiah et al., 1980).

Likewise, moisture transport can occur by several different mechanisms such as capillary flow (suction pressure differences), liquid diffusion (concentration gradients) and vapor diffusion (partial pressure gradients) (Valentas et al., 1997). Many drying applications of agricultural materials occur within the falling rate period; while

predominately involving liquid diffusion. This moisture diffusion is affected by the temperature, concentration difference, and product structure (Erbay and Icier, 2009).

Mass transfer to the surrounding atmosphere also occurs by convection processes. In this case, a difference in partial vapor pressure exists between the boundary layer of the material and the surrounding air. Although liquid water movement poses unique modeling challenges due to the inhibition of capillary and surface tension forces; various methods have been proposed for the diffusive transport of moisture through porous media (Mason, 2006; van Genuchten, 1980). In fact, the diffusion through a porous medium was recently modeled by the Buckingham-Darcy equation as defined by (Wu, 2003):

$$J_w = -K_u \frac{\delta h}{\delta x} \qquad [3.4.3]$$

where: J_w = water flux (m s^{-1}); K_u = unsaturated hydraulic conductivity (m s^{-1}); and h = matric potential (m) which are functions of the volumetric water content.

The equilibrium between the liquid and gaseous water phases have also been described with respect to water mass transfer kinetics (Petric and Selimbašić, 2008); while Fick's law is considered a fundamental diffusion model that assumes diminished flux with increased capillary length according to the diffusion coefficient. Fick's second law has also been used in modeling diffusion within various composting materials, particularly with the derivation of an effective diffusion coefficient that accounts for specific properties of the porous medium as follows (Cussler, 1997):

$$D_e = \frac{D\varepsilon\delta}{\tau} \qquad [3.4.4]$$

where: D_e = effective diffusivity (m^2 s^{-1}); D = diffusivity (m^2 s^{-1}); ε, δ and τ = porosity, constrictivity, and tortuosity, respectively (Grathwohl, 1998).

3.4.1.6 Microbial Activity and Solid State Fermentation

Although great efforts are being made to biologically convert biomass substrates into liquid fuels, there is still a need to understand how the material biologically decomposes. In many composting models, the substrate is regarded as one homogeneous

compound acted upon by a microbial community. However, cellulose (glucose polymer) and hemicellulose (pentose sugar heteropolymer) substrates are easier to decompose due to their simple structures; while lignin (aromatic network polymer) is particularly recalcitrant to microbial degradation (Adney et al., 2008; Chandra et al., 2007; Gajalakshmi & Abbasi, 2008; Wyman et al., 2005).

As a result, substrate models have previously been partitioned into distinct components (carbohydrates, sugars/starches, proteins/lipids, hemicelluloses, cellulose and lignin) based on their degradability by microbial populations; although challenges exist in obtaining the kinetic parameters for these sophisticated composting systems (Adney et al., 2008; Kaiser, 1996; Sole-Mauri et al., 2007). In natural systems, degradation occurs via a complex ecology of heterotrophic bacterial and fungal microorganisms that generate heat and other gaseous products. While previous studies have shown a link between microbial community structure and biomass degradation over time (Steger et al., 2005; Yu et al., 2007); the available literature is still limited (Fontenelle et al., 2011a, 2011b; Reddy et al., 2011).

The amount of moisture in a substrate is critical because decomposition involves enzymatic action, biomass growth, and nutrient and gas transport (Bellon-Maurel et al., 2003; Gervais & Molin, 2003). The mass transfer of nutrients, gases and enzymes occur at the microscale (i.e., microbial growth mechanism) and the macroscale (i.e., bulk flow of air, conduction, convection and diffusion) (Raghavarao et al., 2003); with variations in water transport occurring as a result of water evaporation (mass transfer) and water production from metabolism. The moisture migration process may be considered to be inherently unsteady due to the time varying nature of the ambient (boundary) conditions.

It may also be noted that the microbial growth can be severely diminished at low moisture contents (< 30 %) as some microorganisms may not have enough water to sustain growth (Gervais & Molin, 2003); while oxygen transfer may be prohibited at high moisture contents (> 70 %) as the void spaces within are filled with water (Tiquia et al., 2002). Moisture migration may be considered a dynamic process in most practical applications since the transport processes generally diminish water vapor gradients while sorption relationships maintain gradients.

Temperatures also influence microbial activity, the rate of substrate degradation, and the extent of heat and mass transfer processes (Cen and Xia, 1999; Mitchell et al., 2000; Pandey, 2003; Perez-Guerra et al., 2003). In fact, temperature variations, and the associated formation of temperature gradients, may occur within the porous media due to the non-uniform, localized heat accumulation arising from the metabolic activity. Although axial convection and evaporation may serve as the main heat transfer mechanisms occurring within aerated packed beds; traditional methods of conduction and convection may only provide limited heat transfer within packed beds due to the poor thermal conductivity of many substrates (Mitchell et al., 2000). Likewise, the rate of heat transfer may be hampered by local and global heat transfer rates and/or the rate at which heat is transferred between phases (e.g., transfer from the particle surface to the gas phase) (Raimbault, 1998). Many heat transfer models have assumed thermal equilibrium between phases (VanderGheynst et al., 1997); while the waste metabolic heat produced through microbial activity can be indicated by a number of different factors (Petric and Selimbašić, 2008; Saucedo-castaneda et al., 1990).

Forced aeration through a porous media may cause evaporative cooling effects while supplying oxygen and supporting microbial growth at the inter- and intra-particular levels (Raghavarao et al., 2003). A drying zone with constant depth may be established under constant inlet conditions. This drying zone will progress through the bed with constant velocity until emerging from the bed with the overall drying rate starting to fall. However, high aeration rates can lead to significant drying of the porous matrix due to rapid water evaporation and a subsequent reduction in microbial activity (Haug, 1993). The flow of saturated air may prevent drying while helping to sustain humidity requirements and evenly dissipate the metabolic heat. Microbial growth can also be hindered when the void spaces are filled primarily with water as opposed to air. On the other hand, the lower diffusion efficiency of natural aeration implies a limitation of mass transfer processes while either slowing the microbial growth or generating additional heat (Raghavarao et al., 2003).

3.4.1.7 Application in Current Study

To efficiently design and operate effective storage and/or bioconversion operations, a heat and mass transfer model must be formulated that is general enough to be applicable for storage applications and throughout the relevant drying regimes, while being simple enough to be readily solved. Although simple analytical models of the drying process have been proposed; these models are typically applicable over only a narrow range of drying conditions. The temperature and moisture dependent transport properties of biological materials further indicate the necessary coupling of non-linear heat and mass transfer problems which preclude analytical solutions.

In formulating a relevant theory for baled switchgrass, the physical makeup of the medium becomes important as it affects specific heat and mass transfer mechanisms. In this case, baled biomass may be considered to be a porous structure composed of individual stems; each of which is also a porous structure, but on a much smaller scale. Typically, the stems themselves contain the moisture to be removed; whereas, no liquid exists in between the closely packed stems throughout the bale. Thus, two disparate length scales, one characterizing the overall bale structure and the other the individual stems, emerge in this problem with different physical processes occurring on each scale.

3.4.2 Modeling Theory

Heat and mass transfer models are broadly categorized by two primary strategies; the inductive (based on measured data) and deductive (based on theory) strategies. The inductive approach generally employs a flexible modeling system (i.e., linear regression) for evaluating the relationship between model inputs and outputs. Such an empirical approach is useful when the underlying mechanisms are poorly understood; thereby necessitating the calculation of empirical approximations for each specific application (Hamelers, 2004). In contrast, the deductive (mechanistic) approach involves model development through a fundamental theoretical basis. While deductive models typically yield better extrapolations and representations of the governing processes (Ljung and Glad, 1994), few deductive models have been developed for agricultural applications due to their relative complexity (Hamelers, 2004).

Intermediate strategies have also been employed based on deterministic equations,

lumped parameters and stochastic models (Mason, 2006; Seki, 2000). The heat and mass transfer within baled switchgrass may be modeled according to such an intermediate strategy while exploiting both the theoretical information and experimental data. Therefore, the upscaling of pore-scale balance laws (conservation laws) are considered in the current study in terms of the fluid flow models (Darcy's), diffusion-type models (thin-layer models) and empirical-based models presented in this review. These constitutive equations will subsequently be used in developing models for temperature and moisture transport within variably saturated bales of switchgrass. An understanding of a coupled heat and mass transfer system, and a knowledge of the associated pore scale effects, are evidently essential for the investigation of porous biomass.

3.4.2.1 Fluid Dynamic Modeling

Darcy's Law (saturated fluid flow), Richards' equation (unsaturated fluid flow) and Phillip and DeVries model (enhanced diffusion) are now discussed in regards to fluid flow modeling within porous media. The relationship between pressure drop and flow rate across a saturated porous medium was first established by Darcy (1856) with the average fluid flux considered to be proportional to the hydraulic head gradient. Thus, Darcy's law is considered to be an empirical relationship between the pressure gradient, bulk viscous resistance, and gravitational force. Recent studies have focused on this relationship in a wide range of porous media applications (Poulsen and Moldrup, 2007; Stombaugh and Nokes, 1996; Van Ginkel et al., 2002).

Extensions to the Darcy model have also been developed for applications with sufficiently small flow velocities or in cases with high permeability. The Brinkman (1947) and the Forchheimer (1901) extensions to Darcy's law account for viscous stresses at boundary walls (no-slip) and the non-linear drag effects, respectively. The necessity of the simultaneous inclusion of all or some of these extensions has been discussed in more detail in the available literature (Lai and Kulacki, 1991).

Richards (1931) also coupled Darcy's law with a liquid mass balance which has become a standard modeling approach for fluid flow within porous media (e.g., soils and compost piles). Richards' equation was specifically implemented by replacing the flux term in a postulated form of the mass conservation or continuity equation with Darcy's

law; thus relying on the assumption that Darcy's law is valid for unsaturated media. Hence, Richard's equation assumes constant air pressure and an incompressible water phase.

Limitations of this model involve the exclusion of the liquid-gas phase change, the assumption of negligible humidity and temperature gradients, the hysteretic pressure head-saturation curve, and the empirically-derived relationship between pressure and saturation. Several notable extensions and functional modifications have also been proposed in describing the dynamic and hysteretic pressure-saturation relationship (Joekar-Niasar et al., 2007, 2008; Joekar-Niasar and Hassanizadeh, 2012).

Philip and DeVries (1957) formulated a moisture transfer model with consideration given to vapor movement (diffusion) and liquid movement (capillary action). Both terms were expressed as functions of the temperature and moisture content gradients. Vapor diffusion was specifically modeled using a Fick's enhancement factor accounting for the tortuosity and volume fraction of air. A mass-flow factor was also expressed in terms of the pore-scale gradients. However, the assumption of liquid continuity within pore and capillary space poses a significant limitation, particularly in latter stages of drying. DeVries (1958) later generalized this approach by separately considering the liquid and vapor phases with an extended model for coupled heat and mass transfer in porous media based on the diffusive heat flux. While the heat transport equation maintained similarity to the classical Fourier's law, advective heat transport was also included in the fluid phases. These models have been widely applied to diffusion and evaporation problems, despite the empirically-based enhancements and continuity assumptions (Cass et al., 1984).

The convective currents and thermal instabilities of superposed porous and fluid layers have also been investigated with regards to Darcy's Law (Derjani et al., 1986; Masuoka, 1974; Nield, 1983). Neale & Nader (1974) also postulated that the tangential components of the fluid velocity and Darcian velocity of a porous medium may be considered equal. The resulting no slip-flow condition at the interface was assumed to negate the application of Darcy's law as adjacent velocity gradients were induced. Use of the Brinkman-extended Darcy equation was subsequently proposed to account for the macroscopic viscous stress within a porous medium. The proportionality of the slip

velocity and shear rate was also proposed by Beavers and Joseph (1967) for those cases involving fluid flow through a porous media in accordance with Darcy's law. Beckermann and Viskanta (1988) later coupled the momentum equation for the fluid region (Navier-Stokes) and the porous medium (Darcy's law) through a set of matching conditions at the interface between the porous material and fluid.

3.4.2.2 Diffusion Modeling

An energy balance is typically placed within a thermodynamic framework; with the resulting equations solved in a deterministic manner using either a lumped parameter approach or a distributed parameter design. The kinetic parameters associated with a lumped parameter model have been estimated for the bulk materials (Higgins & Walker, 2001; Petric and Selimbašić, 2008; Sole- Mauri et al., 2007; Vlyssides et al., 2009); while the kinetic parameters of distributive models are typically estimated for various regions within the bulk material (Fanaei & Vaziri, 2009; von Meien & Mitchell, 2002). For this reason, lumped parameter models are typically described by ordinary differential equations (ODEs) whereas partial differential equations (PDEs) are used in distributed parameter models.

In general, the important components of a heat balance include heat transport (by conduction, convection or radiation), heat production/accumulation, and/or the latent/sensible heat inputs/outputs. The inclusion of these various components in a model depend of the specific application and the associated assumptions made. The full energy equation can be expressed in both Cartesian and cylindrical coordinates as follows:

$$\rho C_p \left(\frac{\delta T}{\delta t} + v_x \frac{\delta T}{\delta x} + v_y \frac{\delta T}{\delta y} + v_z \frac{\delta T}{\delta z}\right) = k\left[\frac{\delta^2 T}{\delta x^2} + \frac{\delta^2 T}{\delta y^2} + \frac{\delta^2 T}{\delta z^2}\right] + \frac{\delta Q}{\delta t} \qquad [3.4.5]$$

$$\rho C_p \left(\frac{\delta T}{\delta t} + v_r \frac{\delta T}{\delta r} + \frac{v_\theta}{r}\frac{\delta T}{\delta \theta} + v_z \frac{\delta T}{\delta z}\right) = k\left[\frac{1}{r}\frac{\delta}{\delta r}\left(r\frac{\delta T}{\delta r}\right) + \frac{1}{r^2}\frac{\delta^2 T}{\delta \theta^2} + \frac{\delta^2 T}{\delta z^2}\right] + \frac{\delta Q}{\delta t} \qquad [3.4.6]$$

which describes temporal changes in temperature with the inclusion of a heat generation term.

In general, the inherent properties of a sufficiently thin layer of porous material may be considered constant; while the associated air properties may be assumed constant for short time intervals. However, changes in specific material properties (i.e., temperature, moisture content) and air conditions (temperature and humidity) will occur as the airflow through the porous material dries the thin layer of interest. These changes may be described and evaluated according to several distinct equations (i.e., heat balance, mass balance and drying rate among others).

Diffusion has been considered a primary heat and moisture transfer mechanism in terms of many thin-layer drying models (Parry, 1985); although the complete description of convection-based heat and mass transfer requires a more thorough assessment of the momentum and energy transport. In fact, the effects of temperature gradients on moisture diffusion may only be considered significant under specific conduction-based processes. Thin-layer drying equations typically relate the material properties to the air conditions using a specific drying rate for the given process. One such relationship that generally holds for agricultural materials may be expressed in terms that are analogous to Newton's law of cooling as follows:

$$-\frac{\mathrm{dm}}{\mathrm{dt}} = k(\mathrm{m} - \mathrm{m_e}) \qquad [3.4.7]$$

where: m = moisture content (%); k = drying rate constant (s^{-1}); and the subscript e represents equilibrium conditions. The drying constant may be based on specific thin-layer drying parameters associated with the material properties and/or environmental conditions (Erbay and Icier, 2010).

However, practical agricultural applications typically contain deep beds of the porous media with the spatial and temporal variations in the material and air properties. Although, thin layer models alone are insufficient in describing deep bed transfer processes, they may provide some useful information for predicting the drying rates (Parry, 1985). Direct integration from thin layer experiments is possible in some cases, but algorithms for the full scale process are needed. Deep-bed models are generally categorized as logarithmic, heat and mass balance, or partial differential equation (PDE)

models (Morey et al., 1978); although classification is somewhat arbitrary due to the overlapping features of these model types.

A simple deep bed drying analysis was presented by Hukill (1954) under the assumption that the spatial temperature change was proportional to the drying rate as follows:

$$G_a c_a \frac{\delta T}{\delta x} = \rho_p h_{fg} \frac{\delta M}{\delta t} \quad [3.4.8]$$

where: G = flow rate (kg m^{-2}); c = specific heat (J kg^{-1} °C^{-1}); ρ = density of grain (kg m^{-3}); h_{fg} = latent heat of vaporization of water (J kg^{-1}); T = air temperature (°C); M = moisture content (%-db); and the subscripts a and p represent the characteristics of the air and grain, respectively. In this case, the sensible heating of the solid material may be neglected as only the latent heat of vaporization is accounted for. Although this type of model is computationally simple and straightforward, such models are typically limited to applications with low temperatures and/or airflow rates.

Boyce (1965) also presented a layer-by-layer model of temperature and moisture content for grain drying applications which accounted for sensible heating of the material. Simulations were performed for barley using an empirical expression of the heat transfer coefficient. Thompson et al. (1968) and Henderson and Henderson (1968) presented similar models, but incorporated several procedures for adjusting the predicted air temperature and relative humidity values. Ohm et al. (1971) also proposed a simplified mass and energy balance for hay stacks which indicated diminished drying rates downward in the stack. Although logarithmic and heat/mass balance models have provided insight and knowledge of the various processes involved in deep bed drying, both model types suffer limitations in terms of the accuracy and range of applicability due to the inherent assumptions associated with their respective derivations.

A one-dimensional model of moisture diffusion in bulk grain was presented by Thorpe (1982) using the sorption isotherm for wheat and a steady state temperature profile. Temperature models for packed beds have also been developed with and without an assumed equilibrium between gas and solid phases (Sole-Mauri et al., 2007; VanderGhenyst et al., 1997). Fanaei and Vaziri (2009) also developed a mathematical

model to describe temperature profiles in a simple packed bed reactor assuming thermal equilibrium between the gas and solid phases and negligible transport in the radial direction. Their distributive model included convective, evaporative and heat generation terms as follows:

$$\rho_b C_{pb}\left(\frac{\delta T}{\delta t}\right) = \rho_s(1-\varepsilon)Y_Q\frac{dX}{dt} - \rho_a c_{p,a} V_z\frac{\delta T}{\delta z} - \rho_a f\lambda V_z\frac{\delta T}{\delta z} + k_b\frac{\delta^2 T}{\delta z^2} \qquad [3.4.9]$$

where: ρ_b, ρ_s, ρ_a = density of the bed, substrate and moist air, respectively; c_{pb}, c_{pa} = heat capacity of the substrate bed and moist air, respectively; Y_Q = metabolic heat yield coefficient; ε = void fraction; V_Z = moist air velocity; Z = bed height; T = temperature; f = water carrying capacity; λ = latent heat of evaporation; and k_b = thermal conductivity.

Various computational techniques have further promoted accurate drying models in terms of the evaluation of partial differential equations (PDE). Van Arsdel (1955) and Klapp (1963) were among the first to present PDE models describing simultaneous heat and mass transfer in fixed beds of grain; which were later applied to pea beans (Ngoddy et al., 1966), onions (Huang and Gunkel, 1974) and other particulate solids (Laws and Parry, 1983). Numerical solutions of fixed bed models have been obtained by the center-difference approximation of the spatial derivatives (Bagnall et al., 1970; Spencer, 1969) and with explicit finite-difference techniques (Bakker-Arkema et al., 1974; Brooker et al., 1974); while assuming constant heat transfer and heat capacity for the general mathematical model given by:

$$\frac{\delta^2 T}{\delta X \delta t} = -\frac{\delta T}{\delta t} + \frac{\delta T}{\delta x} - \frac{h_{fg}}{h}m \qquad [3.4.10]$$

where: T = air temperature (°C); x = depth variable (-); h_{fg} = latent heat of vaporization of water (J kg^{-1}); h = volumetric heat transfer coefficient (J m^{-3} s^{-1} °C^{-1}); and m = net density of vapor formed per unit time (kg m^{-3} s^{-1}).

While thin-layer models may provide a framework for deep bed simulations, these integrated models rely on the complimentary assumptions associated with the basic model (i.e., the geometry, mass diffusivity and thermal conductivity of a typical particle);

thus requiring intensive computational processing. Bagnall et al. (1970) also found the diffusivity to be directionally-dependent with greater radial (cuticular layers) values indicating reduced moisture flow in the radial direction compared to the axial. However, many of these diffusion-based theories represent physically unrealistic conditions since the mass transfer is generally assumed to occur as a result of a single mechanism.

3.4.2.3 Empirical Modeling

In many deep bed applications, the heat and mass transfer occurring by diffusion have been considered negligible compared to the principles of convection. However, the derivation of a model describing the time evolution of evaporation or condensation may be performed through the coupling of Fick's first law of diffusion (spatial gradient) with a relevant mass balance equation. In fact, Ingram (1976) simulated the experimental results from a deep barley bed (Boyce, 1965) with a moisture diffusion model which resulted in better prediction accuracy than the empirical drying rate expression. Henderson and Pabis (1961) also presented an empirical drying rate model based on Fick's second law of diffusion and the Lewis (1921) model of moisture content in a porous, hygroscopic material assuming constant moisture diffusivity. This model has become widely used for grain drying models particularly in describing the falling rate period (Smith, 1990) as follows:

$$\frac{M-M_e}{M_0-M_e} = ae^{-k(t)} \qquad [3.4.11]$$

where: M = moisture content (%); k = drying rate constant (s^{-1}); a = 1 representing a geometric slab indication; and the subscripts e and 0 represent the equilibrium and initial conditions, respectively.

Empirical drying models of this form typically assume thin material, high air velocity, and/or constant drying conditions (i.e., temperature and relative humidity). It may also be noted that the error in neglecting the equilibrium moisture content term is typically minimal; particularly with those cases with an initial moisture content below 50 % (Mujumdar, 2004; Rotz and Chen, 1985). Therefore, assuming negligible equilibrium moisture content, a simplified model follows:

$$M = M_0 a e^{-(kt)} \quad [3.4.12]$$

Further modifications of the Lewis Newton model have also been developed with the inclusion of a dimensionless empirical constant (n) for shelled corn (Page, 1949) and soybeans (Overhults et. al, 1973; White et al., 1980) as follows:

$$\frac{M - M_e}{M_0 - M_e} = e^{(-kt^n)} \quad [3.4.13]$$

Sherwood (1931) also developed the hypotheses of Lewis (1921) using a one-dimensional diffusion equation; while McCready and McCabe (1933) later improved on this approach by considering vapor and free water diffusion through the solid structure. Capillary effects have also been noted according to the capillary potential (Buckingham, 1907) and Richards' equation (Richards, 1931); while King (1968) and Harmathy (1969) developed isotherm-based drying models assuming moisture movement by vapor diffusion only. However, Hougen et al. (1940) reported that moisture transfer strictly by liquid diffusion was physically unrealistic in the drying of porous solids. Thus, the exclusion of bound liquid movement limited many of these models to the second falling rate stage.

Hybrid Mixture Theory (HMT) has also been used in deriving various extensions to Darcy's, Fick's and Fourier's laws in porous media (Bennethum and Cushman, 1999; Cushman et al., 2002; Gray and Hassanizadeh, 1998; Sullivan, 2013; Weinstein, 2005). HMT involves the volume-averaging of pore-scale balance laws with the derivation of constitutive restrictions based on the second law of thermodynamics. Bennethum and Cushman (1999) specifically applied HMT to an extended DeVries model for heat transfer in saturated porous media using temperature gradients and the chemical potential in describing the thermal diffusion process and the secondary processes (i.e., advection), respectively.

Distributed models also consider simultaneous heat and mass transfer; thus providing more accurate predictions of temperature and moisture gradients by considering internal and external factors (Erbay and Icier, 2009). Many distributed

models are derived according to Fick's second law of diffusion (Luikov, 1975) with the expressions for the change in moisture, temperature and pressure given as follows:

$$\frac{\delta M}{\delta t} = \nabla^2 K_{11} M + \nabla^2 K_{12} T + \nabla^2 K_{13} P \quad [3.4.14]$$

$$\frac{\delta T}{\delta t} = \nabla^2 K_{21} M + \nabla^2 K_{22} T + \nabla^2 K_{23} P \quad [3.4.15]$$

$$\frac{\delta P}{\delta t} = \nabla^2 K_{31} M + \nabla^2 K_{32} T + \nabla^2 K_{33} P \quad [3.4.16]$$

where: M = moisture content; T = temperature; P = pressure, t = time; K_{11}, K_{22}, K_{33} = phenomenological coefficients; and K_{12}, K_{13}, K_{21}, K_{23}, K_{31}, K_{32} = coupling coefficients. Lumped parameter models further assume uniform temperature distributions that are equivalent to the drying air temperature; thus simplifying the relevant expressions as:

$$\frac{\delta M}{\delta t} = K_{11} \nabla^2 M \quad [3.4.17]$$

$$\frac{\delta T}{\delta t} = K_{22} \nabla^2 T \quad [3.4.18]$$

Here, the phenomenological coefficient K_{11} represents the effective moisture diffusivity (D_{eff}); while K_{22} represents the thermal diffusivity (α). The above equations may also be arranged as follows for constant values of moisture diffusivity and thermal diffusivity (Erbay and Icier, 2009):

$$\frac{\delta M}{\delta t} = D_{eff} \left[\frac{\delta^2 M}{\delta x^2} + \frac{a_1}{x} \frac{\delta M}{\delta x} \right] \quad [3.4.19]$$

$$\frac{\delta T}{\delta t} = \alpha \left[\frac{\delta^2 T}{\delta x^2} + \frac{a_1}{x} \frac{\delta T}{\delta x} \right] \quad [3.4.20]$$

where: a_1 = geometric indicator term (0-planar; 1-cylindrical; 2-spherical).

Theoretical thin-layer models (based on Fick's second law of diffusion) are typically limited in considering the internal resistance to moisture content. Hence, many of the associated theoretical model assumptions may result in substantial errors during calculations (Erbay & Icier, 2010). In contrast, empirical models are strongly dependent on experimental data while accounting for the external resistance to moisture transfer (Erbay & Icier, 2010). Semi-theoretical models (based on Fick's second law and Newton's law of cooling) are typically considered to be easier to implement; while requiring fewer assumptions (Erbay & Icier, 2010). Various models have been developed for simulating the environmental effects on drying alfalfa hay (Hill et al., 1977), timothy hay (Savoie & Mailhot, 1986) and cut ryegrass (Wright et al., 2001) using vapor pressure deficit among other environmental factors (Bartzanas et al., 2010).

3.4.2.4 Modeling Solutions

The modeling of a complex agricultural process often results in systems of nonlinear equations which require simultaneous solutions. Analytical and differential solutions may be computationally efficient, but these methods may become challenging; particularly with nonlinear models. The development of nonlinear models and inclusion of more variables has trended towards numerical solutions for many agricultural models (Higgins & Walker, 2001; Mujumdar, 2004; Sole-Mauri et al., 2007). The finite difference method (FDM) and finite element method (FEM) are two common numerical solution strategies. Both schemes require discretization of the differential equation; with the simultaneous solution of the algebraic equations providing approximate solutions to the governing equations. Discretization may be performed by direct approximation (derivatives are replaced by difference ratios), Taylor series (derivatives are expressed in terms of a Taylor series expansion), or by finite volume approach (control volume) which is particularly well-suited for discretization of conservation laws (e.g., mass conservation) (Patankar, 1980; Whitaker, 1986).

Numerical approximations may be easily implemented through finite differences; which is particularly useful when dependent parameters are unable to be described algebraically (Gardner et al., 1981). The finite difference method is generally considered for regular geometries (i.e., cases involving physical surfaces that coincide with constant

coordinate planes); while the finite element method is typically used with materials exhibiting variable properties and mixed boundary conditions. The finite difference method is expected to suffice for rectangular-baled switchgrass while avoiding the additional complexity associated with the FEM.

Model calibration may be performed in evaluating the ability of the model to describe the associated data. It may be noted that model calibration serves a distinct purpose during model development, as parameter values are determined to ensure optimal correspondence of data and model prediction. Model validation can then be performed as an assessment of model quality in terms of its intended use. A primary component for model validation involves the comparison of the model predictions with new data that is not associated with parameter estimation. Model validation can be further analyzed through a rigorous statistical framework such as root mean square error analysis (Erbay & Icier, 2010). Computational fluid dynamics (CFD) have also been applied in recent years for simulating agricultural drying operations (Amanlou and Zomorodian, 2010; Margaris and Ghiaus, 2006; Prukwarun et al., 2013; Román et al., 2012; Weigler et al., 2011).

3.4.2.5 Available Biomass Models

Many of the modeling theories discussed in this review involve assumptions which limit the applicability of their relevant theories. Some of these models have assumed constant coefficients (i.e., diffusion coefficients) with no dependence on the moisture content or temperature; while others implied continuous liquid paths; a condition which is only valid in the constant and first falling rate phase of drying. While many of these models involve a combination of transfer mechanisms, most of these theories excluded the possibility of bound liquid movement. Alternative models have also been proposed that allow for liquid movement (capillary flow), vapor movement (diffusion) and bound liquid movement while assuming constant diffusion coefficients, a linear sorption isotherm, and a moisture-independent void volume term (Chen and Pei, 1989; Krischer and Kast, 1963).

However, these theories become difficult to apply in practical situations as many of the terms appearing in the governing equations are difficult to determine

experimentally. Berger and Pei (1973) extended some of this previous work by replacing the sorption isotherm relation with the Clausius-Clapyron equation. However, the proposed numerical method would not converge for realistic values of the convection coefficients. Therefore, many of these early modeling approaches for porous media are highly idealized, represent limited applicability, and indicate a need for accurate models that are relevant to densified agricultural material.

Little to no attempts have been reported for heat and mass transfer modeling within baled biomass during storage and/or bioconversion. However, temperature and moisture content have been modeled for various agricultural products including grain, forage and composting materials throughout the available literature. In fact, grain storage and drying models have been widely investigated; generally, in terms of an empirical analyses. Deep bed predictions have been developed through the integration of experimental results for shallow grain beds. Likewise, hay drying models (field and densified) may involve superimposed thin layers; while woody biomass has been modeled according to natural convective drying processes. However, many models have neglected microbial activity and the subsequent heat development which could be rapid; thereby inhibiting the prediction accuracy.

On the other hand, mathematical models of the physical and biological laws governing compost processes (i.e., domestic solid waste, sanitary landfills, synthetic food waste, etc.) have also been presented with relevant mass and energy conservation equations coupled with simple dynamic models based on microbial kinetics. Aerobic biodegradation has received a great deal of attention for high-solids environments with the prevention of metabolic heat removal and limitation of oxygen availability. Storage of lignocellulosic biomass may also involve components of solid-state anaerobic digestion (i.e., municipal solid waste composting), although anaerobic models require extensive microbial assessment through coupling of respiration quotients with precise stoichiometry.

While anaerobic decomposition may occur in densified feedstocks, concerns may arise regarding the energy requirement necessary in supplying reaction temperatures. Anaerobic fermentation products may also oxidize and diffuse; thereby resulting in an overall aerobic stoichiometry (Richard, 2003). In fact, anaerobic cultures developing

within a few hours of an O_2-exhausted state, typically do not reach a size that quantitatively impacts bioconversion (Kaiser, 1996). Therefore, aerobic decomposition is expected to have a much greater influence in modeling a high-solids environment such as baled biomass due to the quick reaction rates.

Detailed analyses of porous media applications have also been developed in recent years as based on conductive, convective (natural and forced), radiative and various heat generation source terms. A brief review of these various models is provided here with particular attention paid to those principles and model components which are considered relative to the current application and modeling of temperature and moisture transfer within baled switchgrass.

3.4.3 Grain Models

3.4.3.1 Grain Storage Theory

The heat and mass transfer processes occurring within stored grain are driven by the differences in temperature and moisture content that arise from various physical, chemical and/or biological activities. The subsequent accumulation of heat and moisture may accelerate grain spoilage as temperature and vapor pressure gradients are known to cause localized areas of spoilage. Thus, grain quality must be protected from insect and microbial growth during storage; conditions that may be accomplished through the assessment of temperature and moisture content.

Grain temperature and moisture changes are known to occur in response to internal and external heat sources (Converse et al., 1973; Sinicio et al., 1995). Internal heat sources arise from the respiration of grain, microorganisms and insects; while external sources include ambient air temperature, solar radiation, storage structure, local wind velocity and air convection (natural and/or forced convection by aeration) among others. Specific driving forces for moisture transfer also include the temperature and moisture gradient (i.e., vapor pressure gradient) and the potential for condensation to form along the surface of the grain.

Accordingly, temperature, moisture content and gas composition are considered primary abiotic factors which influence grain storage quality (Longstaff and Banks, 1987;

Muir et al., 1980; Sun and Woods, 1997a, 1997b). The accumulation of heat in localized areas may accelerate grain degradation since both the thermal conductivity and air flow among the grain are generally minimal. Large differences between the grain and ambient air temperature may also promote natural convection currents (Abbouda, 1992) which drive the moisture movement (Sinha and Wallace, 1977). Thus, moisture migration generally occurs as a result of thermal gradients; which are dependent on many factors associated with grain quality, environmental conditions and storage configuration (i.e., ambient temperature and relative humidity). This regular moisture movement widens the insect and microbial distributions; thereby, expediting grain deterioration (Brooker et al., 1992; Converse et al., 1973; Jia, 1995; Muir et al., 1980).

Since respiration releases energy in the form of heat, localized regions may experience significantly greater temperature and moisture content. The respiration of grain, insects and/or microbial populations may also produce water vapor; thereby, affecting the overall moisture content. Another mechanism of moisture migration involves molecular diffusion resulting from vapor pressure gradients; predominately through the inter-granular spaces (Thorpe et al., 1991a, 1991b). However, changes in moisture content due to molecular diffusion are typically only significant over a few centimeters due to the hygroscopic nature of grain kernels and their much higher densities relative to air.

3.4.3.2 Grain Modeling Theory

Mathematical modeling and simulations are becoming more prevalent in a variety of grain applications (i.e., deep-bed drying, thin-layer and equilibrium moisture content models). Many heat, mass and momentum models have been used for grain storage applications; although much of the available research on this topic has involved the evaluation of heat conduction using the FDM for temperature prediction within grain bins (Chang et al., 1993; Obaldo et al., 1990; Sun and Woods, 1997a, 1997b).

Comparisons of the predicted and measured grain temperatures have been validated graphically (Jia et al., 2000; Khankari et al., 1995); with error quantifications and standard errors widely reported (Alagusundaram et al., 1990; Jian et al., 2005; Montross et al., 2002a, 2002b). Hence, these mathematical models enable the accurate

predictions of temperature within stored grain while promoting the identification of deteriorative conditions. These research efforts also promote the development of best management practices (BMP) for grain storage; particularly with the evaluation of comprehensive stored grain models (Montross et al., 2002a, 2002b).

3.4.3.3 Grain Models

Agricultural dryer performance has been simulated by O'Callaghan et al. (1971) based on thin-layer drying rates and relevant heat and mass balances. Sutherland (1971) also developed an analytical model with temperature and moisture equilibrium between the grain and surrounding air. The effects of the sorption hysteresis, diffusion, biochemical change and tortuosity were all considered negligible; while the porosity, inter-granular pressure, bulk density and air density were all assumed constant. The water and energy conservation was expressed for uniformly-moving air through a cylindrical bed of grain as follows:

$$\frac{\delta w}{\delta \theta} + \nu \frac{\delta w}{\delta x} + \mu \frac{\delta W}{\delta \theta} = 0 \qquad [3.4.21]$$

$$\frac{\delta h}{\delta \theta} + \nu \frac{\delta h}{\delta x} + \mu \frac{\delta H}{\delta \theta} = 0 \qquad [3.4.22]$$

where: w = moisture content of air (lb lb^{-1}); W = moisture content of grain (lb lb^{-1}); θ = time (min); x = distance in direction of flow (ft); h = enthalpy of moist air (Btu lb^{-1}); and H = enthalpy of moist grain (Btu lb^{-1}).

The temperature distribution of many grain storage applications have been modeled by conduction alone; with minimal effect of natural convection (Smith and Sokhansanj, 1989; Yaciuk et al., 1975). Alagusundaram et al. (1990) accordingly presented two components of a heat conduction model for grain storage bins; with one component based on the grain mass and the other based on the bin wall. A similar partial differential equation for transient heat transfer was given by Bathe (1982) for an anisotropic solid body:

$$\frac{\delta}{\delta x}\left(k_x \frac{\delta T}{\delta x}\right) + \frac{\delta}{\delta y}\left(k_y \frac{\delta T}{\delta y}\right) + \frac{\delta}{\delta z}\left(k_z \frac{\delta T}{\delta z}\right) + \dot{q} = \rho c \frac{\delta T}{\delta \tau} \qquad [3.4.23]$$

where: k = thermal conductivity (W m^{-1} K^{-1}); $\dot{q}$ = internal heat generation in an element (W m^{-3}); ρ = density of grain (kg m^{-3}); and c = specific heat of grain (J kg^{-1} K^{-1}). Simulated results were compared with a previous finite difference model (Muir et al., 1980) and validated with rapeseed (canola) and barley storage data.

Freer et al. (1990) used the method presented by Nguyen et al. (1987) to develop a two-dimensional model of temperature and moisture changes during the storage of rough rice. Inputs included the thermal properties of the grain and physical dimensions of the bunker. The governing equations were numerically solved and simulated for various grain temperatures and moisture contents; with results indicating increased spoilage and microbial activity at elevated temperatures and moisture contents at the peak of the bunker. Nguyen et al. (1987) and Beukema et al. (1983) also showed that air circulation within stored grain may occur in response to strong convection flows within the headspace. Montross et al. (2002a, 2002b) also developed a two-dimensional grain temperature model; while three-dimensional heat transfer models were later developed for similar grain storage applications (Andrade et al., 2002; Jian et al., 2005).

In fact, Thorpe et al. (1992) developed a three-dimensional model for free convection within hygroscopic porous media; while Singh et al. (1993a, 1993b) later developed a heat, mass and momentum transfer model for bulk grain with no boundary heat losses, impermeable boundaries, and negligible solar radiation heat flux. In this case, inter-granular airflow was assumed to be incompressible; while most physical properties were assumed to be constant. Casada and Young (1994a, 1994b) also predicted the heat and mass transfer within porous media in terms of the natural convection and diffusion effects with for application with shelled peanuts.

Khankari et al. (1994) model the simultaneous heat and mass transfer within stored grain with the integration of a sorption isotherm describing the moisture diffusion. Local thermodynamic equilibrium was assumed between the grain and the surrounding air; with stagnant inter-granular air and negligible convection. The resulting energy and moisture balance were expressed as:

$$(\rho C)_{bulk}\frac{\delta T}{\delta t} = \frac{\delta}{\delta x_j}\left(k_{bulk}\frac{\delta T}{\delta x_j}\right) + \rho_{bulk}h_{fg}\frac{\delta W_g}{\delta t} \quad [3.4.24]$$

$$\frac{\delta}{\delta t}\left[(\varepsilon\rho_{air}W_a) + (\rho_{bulk}W_g)\right] = \frac{\delta}{\delta x_j}\left[\frac{D_v\varepsilon}{\tau}\frac{\delta}{\delta x_j}(\rho_{air}W_a)\right] \quad [3.4.25]$$

where: ρ = density (kg m^{-3}); C = specific heat (J kg^{-1} °C^{-1}); k = thermal conductivity (W m^{-1} °C^{-1}); h_{fg} = heat of vaporization/condensation of grain moisture (J kg^{-1}); W = moisture content (kg kg^{-1}); D_v = diffusivity of water vapor in air (m^2 s^{-1}); ε = porosity (m^3 m^{-3}); the subscripts a and g represent the air and ground, respectively; and the subscripts air and bulk represent the properties of the dry air and bulk grain, respectively. In this case, the diffusion of grain moisture through direct contact was considered negligible (Stewart, 1975).

Internal heat generation has also been simulated in stored wheat using an electric heater (Jia et al., 2000); although subsequent mathematical models given by the theory of heat transfer within cylindrical bins neglected internal heat sources with the following heat transfer function (Jia et al., 2001):

$$\rho c\frac{\delta T}{\delta t} = k\left(\frac{\delta^2 T}{\delta z^2} + \frac{1}{r}\frac{\delta T}{\delta t} + \frac{\delta^2 T}{\delta r^2}\right) \quad [3.4.26]$$

where: ρ = density of grain (kg m^{-3}); c = specific heat of grain (J kg^{-1}); and k = thermal conductivity of grain (W m^{-1} °C^{-1}). The boundary conditions were assumed to experience a combination of solar radiation and ambient air convection as expressed by the general form:

$$-k\frac{\delta T}{\delta n} = h_s\left(T - T_{s_2}\right) - q_w - q_b \quad (t > 0) \quad [3.4.27]$$

where: k = thermal conductivity of grain (W m^{-1} °C^{-1}); h = convective heat transfer coefficient (W m^{-2} °C^{-1}); q = radiation (W m^{-2}); the subscript s represents the respective surface; and the subscripts w and b represent the wall and roof surfaces, respectively.

While many of these previous models neglected the complex internal sources of heat, Lawrence et al. (2013a, 2013b) developed a three-dimensional, transient heat, mass and momentum model for stored grain which included heat and moisture generation. Hourly weather data was used for the model input. The governing equations for three-dimensional heat and mass transfer were modified from the Khankari et al. (1995) model as follows:

$$(\rho C)_{bulk}\frac{\delta T}{\delta t} + (\rho C)_a u_j \frac{\delta T}{\delta x_j} = \frac{\delta}{\delta x_j}\left(k_{bulk}\frac{\delta T}{\delta x_j}\right) + \rho_{bulk} h_{fg}\frac{\delta M}{\delta t} + Q_h \qquad [3.4.28]$$

$$\rho_{bulk}\frac{\delta M}{\delta t} + \left(\frac{\sigma}{R_v T_{ab}}\right) u_j \frac{\delta M}{\delta x_j} = \frac{\delta}{\delta x_j}\left(D_M \frac{\delta M}{\delta x_j}\right) + \frac{\delta}{\delta x_j}\left(D_T \frac{\delta T}{\delta x_j}\right) - \left(\frac{\omega}{R_v T_{ab}}\right) u_j \frac{\delta T}{\delta x_j} + Q_m \qquad [3.4.29]$$

where: Q_h = internal heat generation (J m^{-3}); Q_m = internal moisture generation due to respiration (kg m^{-3}); u = velocity of species (m s^{-1}); D_M = diffusion of moisture (m^2 s^{-1}); D_T = diffusivity of water vapor (m^2 s^{-1}); and j =1, 2, and 3 represents the three dimensions. The momentum component of this comprehensive model was developed with both forced and natural convection components. In this case, uniform and non-uniform velocity fields were implemented during forced convection, as based on the procedure described by Garg (2005); while incompressible flow for natural convection was based on the relationship of vorticity and vector potential (Singh et al., 1993). The resulting mass balance, velocity loss (Darcy's law), velocity fields (vector potential), and momentum equation were expressed as follows:

$$\nabla \cdot v = 0 \qquad [3.4.30]$$

$$v = -\frac{K}{\mu}(\nabla p - \rho_f g) \qquad [3.4.31]$$

$$\nabla^2 \psi = -\frac{K}{\mu}\beta_t g \nabla T \qquad [3.4.32]$$

$$u_1 = \frac{\delta\psi_3}{\delta x_2} - \frac{\delta\psi_2}{\delta x_3}, \quad u_2 = \frac{\delta\psi_1}{\delta x_3} - \frac{\delta\psi_3}{\delta x_1}, \quad u_3 = \frac{\delta\psi_2}{\delta x_1} - \frac{\delta\psi_1}{\delta x_2} \qquad [3.4.33]$$

where: v = air velocity in the y-direction (m s^{-1}); K = intrinsic permeability of the air (m^2 s^{-1}); μ = dynamic viscosity of air (Pa s^{-1}); p = vapor pressure (Pa); ρ_f = density of air (kg m^{-3}); g = acceleration due to gravity (9.81 m s^{-2}); ψ = vector potential function; β_t = coefficient of thermal expansion (K^{-1}); and u = air velocity (m s^{-1}).

Internal heat generation of this model was based on the evolution of carbon dioxide as the carbohydrates were broken down according to the Steele formula (Thompson, 1972), ASABE Standard D535 (ASABE Standards, 2005) and the associated chemical reaction that details this process (Bhat, 2006). The moisture relationship between the grain and surrounding air was accounted for according to the modified Chung-Pfost equilibrium equation (Chung and Pfost, 1967); while structural and plenum conditions were modeled by Lawrence and Maier (2011). Predicted temperatures and humidities within the grain bin were used in evaluating the EMC, while providing the prescribed boundary conditions during non-aeration. The moisture content of the lower boundary was also evaluated in accordance with a thin-layer drying model (Montross et al., 2002a).

The surface of the grain was also assumed to be impermeable in large bins; while smaller bins employed a constant air infiltration according to the natural convection currents (Montross et al., 2002a, 2002b). Results indicated that internal heat generation did not improve the accuracy of the model, while natural convection had only minimal influence on temperature prediction. The pressure difference formed inside the storage bin also contributed to air infiltration and natural convection currents as was previously approximated by Montross et al. (2002b). Model predictions were validated with previous corn and wheat storage data with and without aeration (Reed and Pan, 2000).

3.4.3.4 Application in Current Study

Although various modeling approaches for grain are proposed in the available literature, many of these attempts are limited in their dimensionality. The main limitations associated with the one and two-dimensional models are the implementation of three-dimensional variations with the boundary conditions and locations of higher

temperature regions within the grain mass. Many of these models were also developed based on simple, unrealistic boundaries such as those considering only the convection effects of the mixed boundaries; while convection at the top or bottom surface has typically been neglected. Although these modeling limitations may restrict the usage in irregular boundary applications, the modification of a comprehensive heat, mass and momentum transfer model may be adapted for baled biomass applications.

3.4.4 Forage Models

3.4.4.1 Forage Modeling Theory

Although current modeling techniques for the temperature and moisture distribution within agricultural materials are rather limited, recent studies in hay drying have presented several methods for predicting the drying time for various agricultural forages. Much of the available research involves the assessment of field drying rates over a wide range of environmental conditions. However, exponential drying rates have also been approximated with functions based on the saturation vapor pressure deficit or latent evaporation (Agena, 1968; Kemp et al., 1972). Further research has been conducted in modeling the temperature and moisture distribution within densified forages. A brief summary of these efforts is provided here to highlight the relevant accomplishments in the field of heat and mass transfer in agricultural biomass.

3.4.4.2 Hay Drying Rate Models

Non-linear regression techniques have previously been used in developing empirical models which fit the experimental drying data of agricultural forages to exponential decay curves. These empirical models are typically presented as functions of relevant environmental factors (i.e., ambient temperature, solar insolation, etc.). A variety of different forage types have been considered in previous studies to dry according to the thin-layer drying relationship as follows (Hill, 1976; Rotz and Chen, 1985):

$$\mathrm{MR} = \frac{\mathrm{M}-\mathrm{M_e}}{\mathrm{M_0}-\mathrm{M_e}} = e^{-k\mathrm{t}} \qquad [3.4.34]$$

where: MR = moisture ratio (-); M = moisture content (%-db); the subscripts 0 and e represent the initial and equilibrium conditions, respectively; t = time (hr); and *k* = drying rate constant (hr^{-1}) which serves as a single parameter that integrates all factors influencing the drying rate.

In many cases, results have indicated that the equilibrium moisture generally has minimal influence on drying, thus simplifying the drying theory (Rotz and Chen, 1985):

$$M = M_0 e^{-k(t)} \quad [3.4.35]$$

The development and basic structure of many of these empirical drying models have considered this fundamental drying theory.

3.4.4.3 Heat and Mass Transfer Models

Sokhansanj (2003) developed a one-dimensional heat and moisture balance equations for alfalfa cubes based on thermal and vapor diffusion, as well as, natural convection. Moisture transfer within an alfalfa cube pile was specifically modeled with negligible convection mass transfer with the ambient air. The heat (conduction and convection) and moisture balance equations were expressed by:

$$\frac{\delta T}{\delta t} = k\frac{\delta^2 T}{\delta x^2} - \hat{u}\frac{\delta T}{\delta x} \quad [3.4.36]$$

$$D_m \frac{\delta^2 M}{\delta x^2} = \frac{\delta M}{\delta t} = \frac{\gamma \varepsilon D_v}{R(T)} \frac{\delta^2 P}{\delta x^2} \quad [3.4.37]$$

where: k = thermal conductivity ($W\ m^{-1}\ K^{-1}$); $\hat{u}$ = velocity component ($m\ s^{-1}$); D_m = moisture diffusion coefficient ($m^2\ s^{-1}$); M = moisture concentration ($kg\ m^{-3}$); γ = obstructive factor (tortuosity and constriction factors); ε = porosity of the bulk (-); D_v = water vapor diffusion coefficient ($m^2\ s^{-1}$); R = universal gas constant for water vapor ($J\ kg^{-1}\ K^{-1}$); T = temperature (K); P = partial pressure of interstitial water vapor (Pa).

The general format for heat transfer stipulated for the boundary conditions included convection and radiative terms as follows:

$$-k\frac{\delta T}{\delta x}\Big|_{x=0} = h(T_a - T_s) + \varepsilon\sigma[(T_c)^4 - (T_s)^4] \quad [3.4.38]$$

where: T = temperature (K); k = thermal conductivity (W m^{-1} K^{-1}); h = convection heat transfer coefficient (W m^{-2} K^{-1}); ε = net emissivity or absorptivity (-); σ = Stefan–Boltzman constant (W m^{-2} K^{-4}); and the subscripts a, c and s represent the air, ceiling and surface conditions, respectively.

Morissette and Savoie (2008) developed a multiple thin-layer approach for simulating the artificial drying of thick hay bales with the associated heat and mass transfer based on a previous model that was proposed by Sokhansanj and Wood (1991). In this case, several superimposed thin layers were considered with the heat balance of air and hay, as well as, the moisture balance of air and hay proposed as:

$$\frac{\delta T_a}{\delta x} = \frac{-h_c a(T_a - T_p) - \left(h_{fg} + c_v(T_a - T_p)\right)\rho_a v_a \frac{\delta H}{\delta x}}{\rho_a v_a (c_a + c_v H)} \quad [3.4.39]$$

$$\frac{\delta T_p}{\delta t} = \frac{h_c a + c_w \rho_a v_a \frac{\delta H}{\delta x}}{\rho_p (c_p + c_w M)} \left(T_a - T_p\right) \quad [3.4.40]$$

$$\frac{\delta H}{\delta x} = -\frac{\rho_p}{\rho_a v_a} \frac{\delta M}{\delta t} \quad [3.4.41]$$

$$\frac{\delta M}{\delta t} = -k(M - M_e) \quad [3.4.42]$$

where: T = temperature (°C); M = moisture content (g g^{-1}); $h_c a$ = volumetric convective heat transfer coefficient (J m^{-3} °C^{-1} s^{-1}); h_{fg} = water enthalpy (J kg^{-1}); ρ = density (kg m^{-3}); v = velocity (m s^{-1}); H = air moisture ratio (kg kg^{-1}); c = specific heat (J kg^{-1} °C^{-1}); *k* = drying constant (s^{-1}); and the subscripts a, e, p, v and w represent air, equilibrium, product, water vapor and water conditions, respectively.

The moisture transfer coefficient and the equilibrium moisture content were estimated with experimental data from lab drying of Timothy grass since the EMC of

baled hay remains widely unreported (ASABE, 2008). Hay density was found to be the primary characteristic affecting the heat and mass transfer rates; while model validation was performed with previous experimental data (Descoteaux et al., 2002; Morissette, 2006).

Román and Hensel (2014) simulated the air distribution and drying of round hay bales with computational fluid dynamics (CFD); while assuming cylindrical porous structures with soft cores and varying dry matter density. Although drying experiments were conducted with alfalfa hay, model simulations were performed for grass hay with the pressure drop through bales determined by experimental resistance coefficients (VanDuyne and Kjelgaard, 1964) as follows:

$$\Delta P = a\rho_{bd}^{2.31} v^{1.6} \quad [3.4.43]$$

where: P = pressure (Pa); ρ_{bd} = bulk dry matter density (kg m^{-3}); v = air velocity (m s^{-1}); and a = experimental parameter. It may also be noted here that the pressure drop through rectangular bales was found to depend on the directional airflow relative to the bale (i.e., cut edge or side of the bale).

This drying simulation specifically involved the coupling of the CFD model with an external drying model according to the moisture and heat source terms:

$$S_w = -\rho_{bd} \frac{dW}{dt} = \rho_{bd} k(W - W_e) \quad [3.4.44]$$

$$S_h = h_s \rho_{bd} \frac{dW}{dt} = -h_s S_w = -h_s \rho_{bd} k(W - W_e) \quad [3.4.45]$$

where: S_w = moisture source (kg m^{-3} s^{-1}); S_h = heat source (W m^{-3}); W = moisture content (kg kg^{-1}); h_s = heat of sorption (J kg^{-1}); *k* = drying constant (s^{-1}); and the subscript e represents equilibrium conditions.

Results indicated optimal drying conditions were achieved in those bales with central axial voids; thus permitting radial, outward movement of the drying front from the center of the bale. Although moisture content in the specified range was found to have no

effect on the airflow resistance, dry matter density had significant effects. In particular, those bales with deficient density profiles (DLG, 2007) indicated air distribution distortions which negatively affected the drying process.

3.4.4.4 Woody Biomass Models

The heat and mass transfer of convectional wood drying has also been modeled in several studies (Gigler et al., 2000, 2004; Thomas, 1980; Younsi, 2006); while Bedane et al. (2011) developed a two-dimensional model of natural convective drying of woody biomass piles. In this case, the mechanical deformation (due to shrinking/swelling) and internal heat generation were neglected. Capillary forces were assumed predominate as the model simulation was governed by diffusion. The temperature (governing heat balance) and moisture profile (Fick's diffusion) for the woody biomass were expressed as:

$$\rho c_p \frac{\delta T}{\delta t} = k_T \left[\frac{\delta^2 T}{\delta x^2} + \frac{\delta^2 T}{\delta y^2}\right] \quad [3.4.46]$$

$$\frac{\delta M}{\delta t} = D_{eff} \left[\frac{\delta^2 M}{\delta x^2} + \frac{\delta^2 M}{\delta y^2}\right] \quad [3.4.47]$$

where: ρ = density (kg m^{-3}); c_p = specific heat capacity (J kg^{-1} K^{-1}); k_T = thermal conductivity (W m^{-1} K^{-1}); D_{eff} = effective diffusivity of water in the wood (m^2 s^{-1}); T = temperature (°C); M = moisture content of wood (%); and x and y = the distance in the x- and y-directions, respectively.

The temperature and moisture transfer between the woody biomass and the surrounding air:

$$-k_T \frac{\delta T}{\delta n} = h(T - T_\infty) \quad [3.4.48]$$

$$-D_{eff} \frac{\delta M}{\delta n} = k(M - M_\infty) \quad [3.4.49]$$

Simulations were performed using constant drying air conditions with results indicating that the temperature of the biomass followed the same trend as the ambient air. However, the internal temperature development was neglected in this study.

3.4.4.5 Application in Current Study

The modification of these empirical and analytical equations may hold significant potential in developing a comprehensive model of the temperature and moisture content within baled biomass such as switchgrass. Predictive models could help to preserve the storage quality and enhance bioconversion efficiency; specifically through the development of a relevant heat and mass transfer model. However, many current models neglect the porous nature of the biomass; while ignoring the underlying biological activity that is known to occur in these environments.

3.4.5 Compost Models

3.4.5.1 Compost Defined

Composting involves the biological and microbial decomposition of organic substrates (e.g., plant matter) into stable humic products. Hence, composting is generally characterized as a solid-state fermentation (SSF) process involving environmental control to achieve efficient substrate degradation in aerobic environments. Compost is a porous system that consists of solid (feedstock), liquid (water film) and gas (air) components; with an overall nonhomogeneous structure. The solid phase includes biodegradable substrates, microbes and humic substances; while the gas phase consists of oxygen, nitrogen, carbon dioxide and water vapor.

The organic solid phase slowly dissolves in the surrounding liquid phase (water film) where the biomass activity occurs. Dissolved substrate and oxygen are consumed during microbial growth; thereby releasing water and heat as byproducts which are exchanged at the liquid-gas interface from convective transfer and the enthalpy associated with the phase change (Petric and Selimbašić, 2008). Not all of these phases, however, are necessarily represented in a model. Earlier studies modelled the gas phase (Stombaugh and Nokes, 1996) and the combined liquid and gas phases (Petric and

Selimbašić, 2008); while more elaborate models have implemented the solubilization of the solid phase (Sole-Mauri et al., 2007).

Degradation occurs in compost through the development of complex microbial communities consisting of various bacterial and fungal (including mold and yeast) colonies. Molds are strictly aerobic while yeast can switch to anaerobic behavior as the conditions require. Aerobic, mesophilic fungi are generally considered suitable for most composting systems, while yielding metabolic products including carbon dioxide and heat (Pandey, 1992). There are also numerous reports on thermophilic bacterial growth in SSF suggested for the removal of heat (Gervais and Molin, 2003; Pandey et al., 2000; Reddy et al., 1999).

Aerobic composting is generally faster and prevents the emission of noxious gases; while the inhibition of oxygen in SSF is known to induce anaerobic degradation (Tanaka et al., 1986). In early models, representation of only one strain of microorganism in the biomass was common (Ishii et al., 2007; Stombaugh and Nokes, 1996); although more recent models typically include the representation of multiple strains (Fazaeli et al., 2004; Sole-Mauri et al., 2007).

Composting generally involves a low-temperature heating process (microbial growth and respiration) and a high-temperature process (cellulosic oxidation) (Cassidy and Hudak, 2001; Rynk, 2000). The exothermic nature of these chemical and biological processes may be reinforced by simultaneous oxidation of the organic matter resulting in spontaneous combustion. During the initial stage of composting, temperatures quickly rise from ambient as the high-energy and easily-degradable compounds (e.g., sugar and protein) are metabolized (Diaz and Savage, 2007). A subsequent decrease in temperature may then occur toward more stable values (Herrero et al., 1998; Zanetti et al. 1997); with water content having the potential to dictate the biological stability (Gervais and Molin, 2003). From an engineering point of view, the aerobic metabolic processes may be improved by controlling the composting environment through the use of forced aeration to remove the sensible and latent heat.

3.4.5.2 Compost Modeling Theory

The basic approach for modeling the composting process involves the coupling of substrate degradation kinetics with the fundamental mass and energy balances. Most models describe internal composting processes in terms of specific environmental factors with relevant parameters typically attributed to the fundamental air, water and insulating properties; the raw material characteristics; and the substrate degradation rates (Mason, 2006). However, the actual number of parameters may widely vary between models with environmental state variables generally including temperature, moisture content, oxygen, biomass, porosity, particle size, airflow, and carbon-to-nitrogen ratio; among others (Haug, 1980; Mason, 2006; Mohee et al., 1998; Stombaugh & Nokes, 1996).

Other differences between various composting models are associated with the specific assumptions made regarding heat and mass transport and the particular system of model evaluation (i.e., lumped-parameter or distributed-parameter). Distributed parameter systems have been developed for compost models with bulk or conductive mechanisms coupled with the heat generation term (Keener et al., 1993; Stombaugh and Nokes, 1996; VanderGheynst, 1997), while lumped parameter models have been developed with energy balances based predominately on evaporative mechanisms (Haug, 1993; Ishii et al., 2004; Oppenheimer, 1997). Many of these studies are based on enthalpy balance; although more complex equations have been suggested by coupling heat and mass transfer with the matric potential (Bongochgetsakul and Ishida, 2008).

Most composting models are considered within a thermodynamic framework which requires an energy balance of the system. In this case, the heat transfer (conductive, convective and evaporative), mass diffusion, energy accumulation and microbial heat generation may be accounted for. Heat released from the biomass may lead to significant buoyancy forces and natural convection effects which are capable of renewing the oxygen supply within the porous matrix (Yu et al., 2005); although forced aeration may be necessary in some composting applications that require additional oxygen supply for sustained aerobic conditions (Bari et al., 2000). In essence, passive aeration can be considered an extreme case of forced aeration with a negligible forced component. There are a wide range of numerical modeling techniques for turbulent flow including phenomenological approaches, direct numerical simulation (DNS) of the

Navier–Stokes expressions, and variants of the lattice Boltzmann method (Choi and Lin, 2010).

The turbulence models generally balance the description of the mean flow physics with reasonable computational resources; which is particularly relevant with complex flow regimes that are coupled with heat and mass transfer. The κ–ε model introduced by Jones and Launder (1972, 1973) is the most widely used among these methods.

The inclusion of microbial activity is essential for deriving an accurate energy balance while providing a better understanding of the dynamic interactions occurring in the composting environment. Early models indirectly incorporated microbial growth kinetics using the rate of oxygen uptake (VanderGheynst et al., 1997), carbon dioxide evolution rate (Richard and Walker, 2006) and/or the biological volatile solids (Haug, 1993; Higgins and Walker, 2001). Later efforts explicitly incorporated microbial growth kinetics by considering microbial growth in terms of the logistic growth equation (Dalsenter et al., 2005), the exponential growth equation (Sangsurasak and Mitchell et al., 1998), Monod kinetics (Agamuthu, 2000; Hammerlers, 1993; Pommier et al., 2008; Sole-Mauri et al., 2007; Stombaugh and Nokes, 1996) or other empirical growth equations (Ikasari and Mitchell, 2000). The development and application of these kinetic growth equations is, however, complicated as microbial populations change spatially and temporally during substrate decomposition (Adney et al., 2008).

3.4.5.3 Compost Models

Halvadakis (1983) and El-Fadel et al. (1995) developed systems of equations describing microbial landfill dynamics with biokinetic models; while Mitchell et al. (1991) presented a semi-mechanistic model describing microbial growth within SSF of cassava starch. Georgiou and Shuler (1986) also presented a simple model for mold growth on a surface with cellular differentiation and spatial heterogeneity. However, these early SSF models generally neglected temperature effects on the physical, chemical and biological processes involved. Saucedo-Castañeda et al. (1990) also simulated the heat generation and transfer within a packed-bed, static bioreactor with a set of equations describing the relevant physiological processes and a pseudo-homogeneous, mono-dimensional dynamic energy balance. Although a mass balance was not considered in

this case, verification of the model was achieved by comparison with the experimental temperatures of inoculated cassava, with results indicating that the main heat transfer resistance through the fixed bed was conduction.

Aerobic composting models have also been reported in numerous studies (Hamoda et al., 1998; Haug, 1993; Keener et al., 1993; Person and Shayya, 1994); with some studies including biological components expressed at a particle level (Hamelers, 1993). Lindstrom (1992) also presented a one-dimensional mathematical model for a homogeneous porous medium that included modified Monod kinetics in describing the dynamic aerobic population. Likewise, Kaiser et al. (1995) coupled an organic composting conversion process with the mathematical model describing heat and mass transfer within a porous media context. A dynamic model for aerobic compost was also developed by Stombaugh and Nokes (1996) based on Monod growth kinetics expressed as functions of the concentration of the substrate and oxygen, as well as, the temperature and moisture content of the composting material. The movement of air between each layer was explicitly modeled, although fluid dynamics were not specified. Anaerobic digestion models have also been presented for the temperature evolution of landfills (Yoshida et al., 1997) and municipal solid waste in continuously-stirred tank reactors (Kiely et al., 1997) with results indicating significant temperature rise in the media.

Oppenheimer (1997) proposed a moisture transport balance with the assumption that water was only generated by metabolic activity, while water loss was reflected in the humidity ratio, as follows:

$$\frac{dM}{dt} = \frac{mH(T_r) - H(T_a) + \beta\frac{d(BVS)}{dt}}{\rho V} \qquad [3.4.50]$$

where: M = moisture content; m = mass flow rate of air, H = saturation humidity of air; T = air temperature; β = moisture yield coefficient, BVS = biological volatile solids; V = system volume; ρ = density of the dry bulk; and the subscripts r and a represent the reactor and ambient air conditions, respectively.

Lefebvre et al. (2000) also characterized the temperature field in municipal solid wastes; while Sidhu et al. (2007) later developed a two-dimensional, spatially dependent

model of landfilling which contains thermal energy generation from the exothermic microbial reactions (monotonic increasing/decreasing function) and cellulosic oxidation (Arrhenius kinetics). Results were validated with spatial and temporal data from a study of municipal solid waste which indicated microbial death and/or dormancy at high temperatures. Petric and Selimbašić (2008) later distinguished the water present in the gas phase from that present in the composting material. The resulting mass balance also accounted for the dissolved gases, water generation from organic matter degradation and the transfer rate of water between each phase according to the following equation:

$$\frac{dm_w}{dt} = -Y_w \frac{dm_{OM}}{dt} - k_L a_w (P_s - P_v) \qquad [3.4.51]$$

Xi et al. (2010) similarly modeled domestic solid waste composting based on the microbial process kinetics, mass conservation, energy conservation and water balance equations. A series of aerobic composting experiments with domestic solid waste were conducted to verify the model. Escudey (2011) also developed a transient heat and oxygen diffusion model for sewage sludge that includes heat generation from aerobic activity and cellulose oxidation.

Fontenelle (2011a, 2011b) combined empirically-derived microbial growth kinetics for bacteria, fungi and yeasts with the relevant heat and mass transfer phenomena occurring during aerobic composting of a switchgrass/dog food mixture. In this case, the substrate bed was considered to be a homogeneous mixture with thermal equilibrium assumed to exist between the solid phase and gas phase. Conduction and diffusion were considered minimal due to forced aeration; while the energy transfer rate was expressed as follows:

$$\frac{\delta T}{\delta t} = \frac{\frac{dQ_{bio}}{dt} - V\rho_a(T)\left(c_{p,a} + de^{mT}\right)V_z\frac{\delta T}{\delta z}}{V\left[\varepsilon\rho_a(T)\left(c_{p,a} + de^{mT}c_{p,v}\right) + (1-\varepsilon)\rho_s\left(c_{p,s} + c_{p,w}M_d\right)\right]} \qquad [3.4.52]$$

where: T = temperature (K), V = system volume (m^3), ρ_a and ρ_s = density of air and the dry bulk, respectively; ε = porosity of the substrate bed; $c_{p,a}$, $c_{p,s}$, $c_{p,w}$, $c_{p,v}$ = specific heat

at constant pressure (kJ kg^{-1} K^{-1}) of air, dry bulk, water and water vapor, respectively; V_z = superficial air velocity; and M_d = moisture content (%-db).

Zambra et al. (2011, 2012) developed a three-dimensional mathematical model for porous compost based on unsteady, turbulent flow field, energy transport, and self-heating from biological activity. In this case, the Navier–Stokes equation was used to describe the air flow over the compost pile, along with the *k–ε* turbulence model (Launder and Spalding, 1974) as follows:

$$\frac{\delta}{\delta t}(\rho u_i) + \frac{\delta}{\delta x_j}\left(\rho u_j u_i\right) = \frac{\delta p}{\delta x_i} + \frac{\delta \tau_{ij}}{\delta x_{ij}} - \rho g \delta_{i3} \quad [3.4.53]$$

$$\mu_t = \rho C_u \frac{\kappa^2}{\varepsilon} \quad [3.4.54]$$

where: u_i = velocity vector field (m s^{-1}); ρ = air density (kg m^{-3}); p = pressure (Pa); τ_{ij} = deviatoric stress tensor (N m^{-2}); μ_t = turbulent viscosity (N s m^{-2}); C_u = phenomenological constant (-); κ = turbulent kinetic energy (J kg^{-1}); and ε = rate of dissipation (J kg^{-1} s^{-1}). Here, the subscript 3 represents the directional orientation associated with the gravitational acceleration. The flow must also adhere to the principles of mass conservation as expressed by the following equation:

$$\frac{\delta \rho}{\delta t} + \frac{\delta}{\delta x_i}(\rho u_i) = 0 \quad [3.4.55]$$

In this case, the thermal energy for the air has been expressed as:

$$\frac{\delta}{\delta t}(\bar{\rho}\overline{T}) + \frac{\delta}{\delta x_j}(\bar{\rho}\bar{u}_i\overline{T}) = \frac{\delta}{\delta x_i}\left[\left(k + \frac{\mu_t}{\sigma_t}\right)\frac{\delta \overline{T}}{\delta x_j}\right] \quad [3.4.56]$$

where: σ_t = turbulent Prandtl number (-); and k = thermal conductivity of the air outside the pile (W m^{-2} K^{-1}). Here, the superscript bars represent the average values of the respective parameters.

Cellulosic oxidation and microbial activity were also included in a volumetric heat generation source term, assuming negligible depletion of cellulose, biomass and oxygen. Interphase temperature gradients have also been assumed to be negligible in several studies with a single temperature often describing the local conditions in accordance with the following for of the heat transfer equation (Escudey, 2011; Sidhu et al., 2007; Zambra et al., 2011, 2012):

$$\left(\rho C_p\right)_{eff}\frac{\delta T}{\delta t} = k_{eff}\nabla^2 T + Q_c(1-\varepsilon)A_c\rho_c C_{ox}\exp\left(\frac{-E_c}{RT}\right) + Q_b(1-\varepsilon)\rho_b\rho_c\left[\frac{A_1\exp\left(\frac{-E_1}{RT}\right)}{1+A_2\exp\left(\frac{-E_2}{RT}\right)}\right] \quad [3.4.57]$$

where: A_c = pre-exponential factor for the oxidation rate of cellulose; C_{ox} = oxygen concentration (kg m^{-3}); C_p = specific heat capacity (J kg^{-1} K^{-1}); T = temperature (K); Q_c = exothermicity from cellulose oxidation (J kg^{-1}); R = ideal gas constant (J K^{-1} mol^{-1}); E_c, E_1, E_2 = activation energies for the cellulose oxidation, biomass growth and inhibition of biomass growth, respectively; and the subscripts eff, 1 and 2 represent an effective property, biomass growth and biomass inhibition, respectively.

3.4.5.4 Application in Current Study

The complex bioprocesses occurring within these SSF environments involve numerous coupled physical and biological mechanisms which describe the heterogeneous substrate and diverse microbial activity. Therefore, these coupled mechanisms are generally difficult to empirically and theoretically and analyze. Specific modeling complications are typically associated with the geometrically complex nature and the non-homogeneous spatial distribution of SSF systems. Agricultural substrates may also be structurally and nutritionally heterogeneous; thereby preventing accurate determination of important process variables. Numerous challenges also exist with direct experimental measurements within the SSF environment; while average parameter values may inadequately reflect local conditions.

Despite understanding the general physical processes that occurring during composting operations, the underlying microbial mechanisms that drive these changes are

poorly understood and are often inadequately characterized. Hence, the modeling and simulation of these composting processes remain rather challenging; particularly due to the intricate complexities of the biotic and abiotic interactions occurring in the porous matrix. However, the modification and integration of relevant composting model components may contribute to the improved design, control and optimization of underlying heat and mass transfer mechanisms that occur within baled biomass.

3.4.6 Porous Models

3.4.6.1 Porous Modeling Theory

A porous medium is characterized by several parameters including the porosity and permeability of the material; with the latter term quantifying the ability to transmit fluid. Constrictivity is another important parameter which is expressed as the ratio of particle diameter to the pore size. Thus, constrictivity may be considered a scaling parameter characterizing lower diffusive flow at boundaries. Similarly, tortuosity is an evaluation of the complexity of the network of pores assessed by evaluating all the pathways from one side of the porous medium to the other. The tortuosity of each pathway is defined as the ratio between its total length and the direct distance between the starting and ending points.

The number of heat and mass transfer models for porous media continues to grow due to the wide array of applications across many fields of study. Early work performed by Philip and DeVries (1957) addressed heat and water (liquid and fluid phases) transport with porous media in response to the temperature and water content gradients. An enhancement factor was implemented to account for the inadequate description of Fickian diffusion in a porous media. One-dimensional heat and mass transfer within porous hygroscopic materials was described by (Luikov, 1966; Prigogine, 1961) with no free water considered to exist within the pores according to the principles of non-equilibrium thermodynamics as follows:

$$J_m = L_{mq}\frac{\delta T}{\delta x} + L_{mm}\frac{\delta M}{\delta x} \qquad [3.4.58]$$

$$J_q = L_{qq}\frac{\delta T}{\delta x} + L_{qm}\frac{\delta M}{\delta x} \quad [3.4.59]$$

where: J_m and J_q = moisture and heat fluxes, respectively; and L_{mq}, L_{mm}, L_{qq}, and L_{qm} are phenomenological coefficients.

The moisture conservation (without chemical reaction) (Siau, 1983) and energy balance conservation for a capillary porous medium (Luikov, 1966) were defined by:

$$\frac{\delta M}{\delta t} = D\left(\frac{\delta^2 M}{\delta x^2}\right) + \left(\frac{\delta D}{\delta M}\right)\left(\frac{\delta M}{\delta x}\right)^2 + \left(\frac{\delta \phi}{\delta M} + \frac{\delta D}{\delta T}\right)\left(\frac{\delta M}{\delta x}\right)\left(\frac{\delta T}{\delta x}\right) + \left(\frac{\delta \phi}{\delta T}\right)\left(\frac{\delta T}{\delta x}\right)^2 + \phi\left(\frac{\delta^2 M}{\delta x^2}\right) \quad [3.4.60]$$

$$\frac{\delta T}{\delta t} + \frac{1}{\rho C_T}\left(k_T\frac{\delta^2 T}{\delta x^2}\right) + \frac{E_b \lambda}{C_T}\left(\frac{\delta m}{\delta t}\right) \quad [3.4.61]$$

where: M = moisture content (%-db); D = transverse diffusion coefficient ($cm^2\ s^{-1}$); ϕ is a factor of L_{mq}; T = temperature (K); k_T = transverse thermal conductivity coefficient (cal $cm^{-1}\ K^{-1}\ s^{-3}$); m = fractional moisture content (g g^{-1}, db); C_T = specific heat of wood (cal $g^{-1}\ K^{-1}$); λ = ratio between the vapor diffusion coefficient and total moisture diffusion coefficient; and E_b = activation energy (cal mol^{-1}).

Vafai and Tien (1981) established steady-state equations describing a porous medium with the volume-averaging technique; while Darcy's equation has been used in several studies for modeling porous media flows (Durlofsky and Brady, 1987; Rajamani et al., 1995; Vasseur et al., 1990). Avramidis et al. (1992) also developed a conductive model for a hygroscopic porous material while considering the water chemical potential gradient to be the dominate diffusion force. In this case, the temperature gradient derivation was based on non-equilibrium thermodynamic principles, with the results indicating thermal-diffusion throughout the initial stages of desorption.

Experimental and numerical investigations have also been performed in accessing the heat transfer and fluid flow within porous enclosures. In fact, Chang and Liu (1994) studied various effects of the convective heat transfer in rectangular porous cavities. Numerical heat and mass transfer modeling has also been performed for various drying

processes; although self-heating has generally been excluded in many models (Bae et al., 2010; Bubnovich et al., 2008, 2009; Lamnatou et al., 2009; Lee et al., 2007).

3.4.6.2 Forced Convection

Forced convection flow in porous media has been widely investigated throughout the available literature (Bejan, 2004; Ingham and Pop, 2005; Leu et al., 2009; Nield and Bejan, 2006; Vadász, 2008; Vafai et al., 2005). Kaya et al. (2006) analyzed the heat and mass transfer processes associated with the drying of a two-dimensional, rectangular object exposed to forced laminar convection. In this case, the thermal and physical properties were considered to be constant with incompressible flow. The partial differential equations governing the drying fluid in two dimensions were given in terms of the mass (continuity), momentum (x- and y- directional) and energy conservation:

$$\frac{\delta u}{\delta x} + \frac{\delta v}{\delta y} = 0 \qquad [3.4.62]$$

$$\rho\left(u\frac{\delta u}{\delta x} + v\frac{\delta u}{\delta y}\right) = -\frac{\delta p}{\delta x} + \mu\left(\frac{\delta^2 u}{\delta x^2} + \frac{\delta^2 u}{\delta y^2}\right) \qquad [3.4.63]$$

$$\rho\left(u\frac{\delta v}{\delta x} + v\frac{\delta v}{\delta y}\right) = -\frac{\delta p}{\delta y} + \mu\left(\frac{\delta^2 v}{\delta x^2} + \frac{\delta^2 v}{\delta y^2}\right) \qquad [3.4.64]$$

$$u\frac{\delta T}{\delta x} + v\frac{\delta T}{\delta y} = \alpha\left(\frac{\delta^2 T}{\delta x^2} + \frac{\delta^2 T}{\delta y^2}\right) \qquad [3.4.65]$$

where: u and v = velocities in the x-and y- direction (m s^{-1}); ρ = density (kg m^{-3}); and p = pressure (Pa). Numerical procedures were also developed for diffusion-based heat and mass transfer assuming negligible material shrinkage/deformation, heat generation, and radiation effects. Under these assumptions, the two-dimensional model of the porous structure was expressed as:

$$u\frac{1}{\alpha}\frac{\delta T}{\delta t} = \frac{\delta^2 T}{\delta x^2} + \frac{\delta^2 T}{\delta y^2} \qquad [3.4.66]$$

$$\frac{1}{D}\frac{\delta M}{\delta t} = \frac{\delta^2 M}{\delta x^2} + \frac{\delta^2 M}{\delta y^2} \quad [3.4.67]$$

with the following boundary conditions:

$$-k\frac{\delta T}{\delta n} = h(T - T_{air}) \quad [3.4.68]$$

$$-D\frac{\delta M}{\delta n} = h_m(M - M_{air}) \quad [3.4.69]$$

where: n = directional coordinate normal to the surface; k = thermal conductivity (W m^{-1} K^{-1}); D = moisture diffusivity obtained from the Arrhenius equation (m^2 s^{-1}).

3.4.6.3 Natural Convection

Considerable attention has also been given to the effects of natural convection heat transfer within porous media (in terms of the internal heat generation) due to the growing number of research applications in recent years (Nield and Bejan, 2006).

A review of the early research involving natural convective heat transfer in porous media was conducted by Cheng (1978) while various models have been developed for heat generation and the associated natural convection within confined porous mediums (Acharya and Goldstein, 1985; Bejan, 1984; Beukema et al., 1983; El-Khatib and Prasad, 1987; Haajizadeh, 1984; Robillard, 1988). The dimensionless form of the governing equations have typically been expressed in accordance with Darcy's law (Darcy, 1830) and the Boussinesq approximation as follows:

$$\frac{\delta^2 \psi}{\delta x^2} + \frac{\delta^2 \psi}{\delta y^2} = -R\frac{\delta T}{\delta x} \quad [3.4.70]$$

$$u\frac{\delta T}{\delta x} + v\frac{\delta T}{\delta y} = \frac{\delta^2 T}{\delta x^2} + \frac{\delta^2 T}{\delta y^2} + 1 \quad [3.4.71]$$

$$u = \frac{\delta \psi}{\delta y} \quad v = \frac{\delta \psi}{\delta x} \quad [3.4.72]$$

where: ψ = stream function and R = Rayleigh number.

Numerical studies of free convection have also been performed for various arrangements porous layers in accordance with Darcy's law (Chen and Chen, 1988; Poulikakos et al., 1986). The Darcy flow model offers the advantage of linearizing the momentum equation; thereby simplifying the solutions of the governing equations (Haajizadeh, 1984; Prasad, 1987). However, the no-slip boundary condition cannot be accounted for by Darcy's law, which poses an issue for highly porous materials and fibrous media (Vasseur and Robillard, 1987). An evaluation of natural convection heat transfer within an enclosed porous media was also reported Chan et al. (1970) in accordance with the Brinkman-extended Darcy model. Tatsuo et al. (1986) and Sathe et al. (1988) also used the Brinkman-extended Darcy model (Brinkman, 1947) to describe natural convection within a porous layer while a non-Darcian model was developed by Beckermann and Viskanta (1988) for a rectangular enclosure that was considered to be partially filled with a saturated porous medium. In this case, the Brinkman and Forcheimer extensions for a high-permeability porous media were invoked.

Singh (1995) later described a comparative evaluation of the Darcy, Brinkman-extended Darcy and Brinkman-Forchheimer-extended Darcy models of natural convection within a porous layer with all three models yielding similar results for low Darcy numbers. However, the Brinkman Forchheimer- extended Darcy model was preferable at higher Darcy numbers as it accounted for the effects of inertia. The Darcy model applied with the B-J condition (Beavers and Joseph; 1967) resulted in a slip velocity condition at the interface, as well as, at the impermeable walls. On the other hand, the use of the Brinkman or Brinkman-Forchheimer models with the velocity continuity at the interface satisfied the no-slip criteria, as well as, the impermeable surface conditions.

Natural convection within homogeneous porous media subjected to discrete heat sources have been investigated for rectangular enclosures (Basak et al., 2011; Cheikh et al., 2007; Churbanov et al., 1994; Degan et al., 1995; Haghshenas et al., 2010; Lakhal et al., 1995; Lin, 1993; Mobedi et al., 2010; Ni and Beckermann, 1993; Nield et al., 1993; Sathiyamoorthy et al., 2007; Varol et al., 2009), inclined rectangular enclosures (Hsiao and Chen, 1994; Oztop, 2007), wavy rectangular enclosures (Sompong and

Witayangkurn, 2012), vertical cylinders (Chang and Hsiao, 1993), vertical cones (Kumari and Jayanthi, 2005; Kumari and Nath, 2009) and isothermal spheres (Ghodeswar, 2010); for both steady-state and transient conditions. These numerical models have involved localized isothermal heat sources (Aydin and Yang, 2000) and constant flux heat sources (Sharif and Mohammad, 2005). In most cases, the discrete heating sources were applied on distinct cavity walls with a constant heat flux; with all remaining walls considered adiabatic (Calcagni et al., 2005; Saeid and Pop, 2005).

The enclosures and porous media are typically assumed to be anisotropic; while the thermophysical fluid properties are generally considered to be constant. The viscous drag and inertia terms have also been neglected in many of these studies due to the sufficiently slow flow and the local thermodynamic equilibrium between the porous material and fluid. Based on these assumptions, the conservation of mass, momentum (axial and transverse), energy and concentration for unsteady flow within a two-dimensional porous medium have been expressed in the general form (Bejan, 1984; Jang and Ni, 1989) as follows:

$$\frac{\delta u}{\delta x} + \frac{\delta v}{\delta y} = 0 \qquad [3.4.73]$$

$$u = -\frac{\kappa}{\mu}\frac{\delta p}{\delta x} \qquad [3.4.74]$$

$$v = -\frac{\kappa}{\mu}\left(\frac{\delta p}{\delta y} + \rho g\right) \qquad [3.4.75]$$

$$\frac{\delta T}{\delta t} + u\frac{\delta T}{\delta x} + v\frac{\delta T}{\delta y} = \alpha\left(\frac{\delta^2 T}{\delta x^2} + \frac{\delta^2 T}{\delta y^2}\right) \qquad [3.4.76]$$

$$\varepsilon\frac{\delta c}{\delta t} + u\frac{\delta c}{\delta x} + v\frac{\delta c}{\delta y} = D\left(\frac{\delta^2 c}{\delta x^2} + \frac{\delta^2 c}{\delta y^2}\right) \qquad [3.4.77]$$

where: u and v = Darcy's velocity in the x- and y-directions; κ = permeability of the saturated porous media; μ = viscosity; D = equivalent thermal and mass diffusivities; σ = heat capacity ratio between the porous medium and fluid; and ε = porosity (-).

Zhang et al. (1993) investigated Benard convection in a cavity containing an anisotropic porous medium; while Zhao et al. (2008) numerically evaluated the convective flow within a porous enclosure subjected to localized heating. The Darcy-Brinkman model was used for the momentum conservation while satisfying the no-slip boundary condition. Mahapatra et al. (2011) evaluated the effects of natural convection and thermal radiation within a square cavity containing a porous medium. Results indicated that the Rayleigh number and porosity have considerable influence on heat transfer.

Alam (2011) and Kalaoka and Witayangkurn (2013) numerically evaluated natural convection within two-dimensional square enclosures filled with porous media with constant heating and cooling from the side walls. Convective fluid flow and heat flow were visualized with the stream function and heat function; respectively. All thermophysical properties of the media were assumed to be constant with isotropic effective thermal diffusivity and negligible internal radiation. The Brinkman extended non-Darcy model was implemented according to the conversation of mass, momentum (x- and y- directional) and energy as follows:

$$\frac{\delta u}{\delta x} + \frac{\delta v}{\delta y} = 0 \qquad [3.4.78]$$

$$u\frac{\delta u}{\delta x} + v\frac{\delta u}{\delta y} = -\frac{1}{\rho}\frac{\delta p}{\delta x} + \nu\left[\frac{\delta^2 u}{\delta x^2} + \frac{\delta^2 u}{\delta y^2}\right] - \frac{\nu}{\kappa}u \qquad [3.4.79]$$

$$u\frac{\delta v}{\delta x} + v\frac{\delta v}{\delta y} = -\frac{1}{\rho}\frac{\delta p}{\delta y} + \nu\left[\frac{\delta^2 v}{\delta x^2} + \frac{\delta^2 v}{\delta y^2}\right] - \frac{\nu}{\kappa}v + g\beta(T - T_0) \qquad [3.4.80]$$

$$u\frac{\delta T}{\delta x} + v\frac{\delta T}{\delta y} = \alpha\left[\frac{\delta^2 T}{\delta x^2} + \frac{\delta^2 T}{\delta y^2}\right] \qquad [3.4.81]$$

where: u and v = Darcy's velocity in the x- and y-directions; κ = permeability of the saturated porous media (m^2); ν = kinematic viscosity ($m^2\ s^{-1}$); ρ = density ($kg\ m^{-3}$); p = pressure (Pa); α = thermal diffusivity ($m^2\ s^{-1}$); and βT = volume expansion coefficient

(K^{-1}). In general, the streamlines were found to increase as Darcy and Grashof numbers increased; while heatlines typically decreased.

3.4.6.4 Mixed Convection

The numerical analysis of mixed (forced and natural) convection through variable porosity media has also been reported for horizontal layers with multiple isothermal heat sources (Lai and Kulacki, 1991; Lai et al., 1990), immersed spheres (Sano, 1996) and two-dimensional rectangular cavities (Nithiarasu et al., 1997). These generalized non-Darcian models account for the inertial and viscous forces within the fluid.

3.4.6.5 Hybrid Mixture Theory

The Hybrid Mixture Theory (HMT) has also been used to extend Darcy's, Fick's and Fourier's laws for porous media applications (Coleman and Noll, 1963; Cushman et al., 2002; Hassanizadeh and Gray, 1979). Studies involving HMT have used volume-averaged conservation laws to provide thermodynamically consistent equations for saturated (Bennethum and Cushman, 1999) and unsaturated (Kleinfelter et al., 2007) porous media. Extensions to Darcy's law have also indicated that the macroscale chemical potential can be applied in those applications involving diffusive velocity within saturated porous media (Schreyer-Bennethum, 2012; Weinstein, 2005). HMT correction terms in Richards' equation also suggest that the capillary pressure rate of change may impact the overall saturation dynamics (Beliaev and Hassanizadeh, 2001; Hassanizadeh et al., 2002).

Sullivan (2013) also applied HMT and the macroscale chemical potential for the case of unsaturated porous media (i.e., soil). In this study, the predominant physical processes were coupled with a single physical measurement (chemical potential). Grillo et al. (2012) also evaluated the mass transport within a saturated porous media that was characterized as a deformable internal structure. The dynamic interaction of the porous medium and saturating fluid were described on a coarse scale with the application of the Mixture Theory and Continuum Mechanics.

Recent studies involving natural convection through a saturated porous medium exposed to a uniform magnetic field have also been reported using the Brinkman model

(Alchaar et al., 1995; Barletta et al., 2008; Nield, 2008). Numerical investigations of laminar, two-dimensional magneto-hydrodynamic (MHD) convection in porous media have been performed with rectangular cavities assuming constant fluid properties except density with the buoyancy effects included through the Boussinesq approximation (Grosan et al., 2009; Khanafer and Chamkha, 1998). Pressure work, viscous dissipation, radiation and Joule heating effects were generally considered negligible; with the conservation of mass, momentum and energy transfer generally given as:

$$\frac{\delta u}{\delta x} + \frac{\delta v}{\delta y} = 0 \qquad [3.4.82]$$

$$\frac{\delta u}{\delta y} - \frac{\delta v}{\delta x} = -\frac{g\kappa\beta}{\nu}\frac{\delta T}{\delta x} + \frac{\sigma\kappa\beta_0^2}{\mu}\left(-\frac{\delta u}{\delta y}\sin^2\gamma + 2\frac{\delta v}{\delta y}\sin\gamma\cos\gamma + \frac{\delta v}{\delta x}\cos^2\gamma\right) \qquad [3.4.83]$$

$$u\frac{\delta T}{\delta x} + v\frac{\delta T}{\delta y} = \alpha_m\left(\frac{\delta^2 T}{\delta x^2} + \frac{\delta^2 T}{\delta y^2}\right) + \frac{q_0'''}{\rho c_p} \qquad [3.4.84]$$

where: u and v = the velocity components along the x- and y-directions (m s^{-1}), respectively; g = gravitational acceleration (m s^{-2}); κ = permeability of the porous medium (m^2); β = coefficient of thermal expansion (K^{-1}); μ = dynamic viscosity (kg m^{-1} s^{-1}); γ = angle of inclination to the horizontal of applied magnetic field (rad); σ = electrical conductivity (Ω^{-1} m^{-1}); ρ = fluid density (kg m^{-3}); c_p = specific heat at constant pressure (kJ kg^{-1} K^{-1}); α_m = effective thermal diffusivity (m^2 s^{-1}); and q_0''' = volumetric heat generation rate (W m^{-3}).

3.4.6.6 Application in Current Study

The relevant models reviewed here are expected to provide an adequate understanding of the relevant characteristics and mechanisms that are associated with the development of heat and mass transfer models for porous media such as baled biomass. While many of the studies reviewed here provide practical insight into the heat and mass transfer occurring within porous media, most of these models have not been validated with experimental data. Additionally, many of the current modeling efforts in porous media have focused on isotropic and homogeneous media; although agricultural products

such as baled biomass may exhibit nonisotropic and heterogeneous characteristics in most practical applications. Therefore, while some of the mechanisms discussed in this review are not applicable, the fundamental theories that underlie these porous models may provide a general framework for the current study. The effect of self-heating has also been neglected in most porous models which may require further modification for implementation in the current study.

3.4.7 Practical Application

The foregoing discussion illustrates the ongoing investigation of natural-convection fluid flow and heat transfer within densified biomass. While many of these models offer a representation of the relevant features of various biomass applications, no comprehensive model is currently available; particularly for the baled format. Furthermore, many of the previous diffusion-based models neglect fluid flow and are relatively unsophisticated compared with a complete diffusion-convection model; although requiring less computational effort. Many of these studies have also unrealistically assumed constant heat and mass transfer coefficients. Therefore, the motivation for the proposed work is based on the need for an accurate description of underlying mechanisms driving energy and mass transfer within rectangular bales of switchgrass. The development of an effective model should allow for the prediction of storage effects (i.e., temperature and moisture migration patterns resulting from diffusion); optimization of storage operations (minimization of storage losses); and the assessment of biomass quality.

As such, the key objective of the current study was to describe the underlying theories and mechanisms of heat transfer and moisture migration within the high-solids, porous media environment of switchgrass stored in the rectangular baled format. Hence the distribution of temperature and moisture within baled switchgrass is of particular interest as based upon the assumed and empirically-derived physical and thermal properties of the material. A specific objective of the current research was aimed at the development of a comprehensive, two-dimensional model describing the relevant heat and mass transfer mechanisms according to the fundamental theories of diffusion,

conduction and convection for hygroscopic porous environments such as baled switchgrass.

The resulting system of equations was to be numerically evaluated in accordance with the finite difference method while assessing the impact of the initial moisture content on model predictions. The ability to accurately describe process dynamics was also validated in terms of the experimental storage data that was collected under controlled environmental and constant drying air conditions (i.e., fixed temperature, relative humidity, etc.). Model accuracy was further assessed with the inclusion of microbial heat generation, liquid diffusion flow and a generalized framework for natural convective flow.

The proposed model was expected to be in close agreement with experimentally determined temperature and moisture data for baled switchgrass. Furthermore, the inclusion of heat generation (from plant respiration and/or microbial activity), liquid diffusion and natural convection modeling components was expected to improve model validation and prediction accuracy. The integration of empirically-derived, internal heat generation was only expected to contribute minimal heat gain at lower moisture levels; with the primary driving force attributed to the fundamental principles governing heat conduction and/or convection. Hence, temperature development within baled switchgrass was expected to exhibit the same general trend as ambient air temperature; with moisture content exhibiting a uniform decline throughout storage. The integration of natural convection flow and liquid diffusion through the porous material was expected to further improve the spatial and temporal simulation of temperature and moisture compared with the simple case of a one-dimensional assessment of pure heat conduction and mass diffusion.

Hence, the current model was based on a thermal conductivity approach although heat development within the bale by other physical and/or biological processes was also accounted for in order to achieve greater prediction accuracy which may be considered novel in terms of similar biomass models. The primary input parameters for the model were air temperature and relative humidity, as well as, specific characteristics of the feedstock. The primary output parameters associated with this model were the temperature and moisture content of the baled biomass as a function of time. The

boundary conditions were primarily governed by a derivation of the typical heat and moisture equations; while internal bale conditions were based primarily on Fick's moisture diffusion and the heat balance equation for temperature simulation. Specific consideration was also given to the extended forms of Darcy's equation of motion (with convective terms), while simultaneously solving the stream function and energy conservation in regards to the buoyancy-driven natural convection flow.

The analytical methods of Krischer and Kast (1963) and Berger and Pei (1973) describing the drying of a hygroscopic porous solid were adapted and expanded in the current study for a baled switchgrass with two distinct length scales. A generalized form of the equations governing phase change was also presented in the current study to allow diffusional coefficients to vary with both temperature and moisture content. An attempt was also made to preserve the generalities of the proposed model in order to maintain validity for any hydroscopic porous media. Hence, the current model was based on the fundamental principles which govern the thermophysical processes occurring within a porous media which can be easily modified for application in a wide variety of materials, bulk formats and environmental conditions.

CHAPTER 4:MODEL DEVELOPMENT

4.1 Physical Description

A mathematical model describing the heat and mass transfer within a rectangular bale of switchgrass was developed in the current study. The bale itself was conceptualized as a porous medium composed of individual porous elements (stems) which contain free liquid. This study specifically considers a storage application of the bale under controlled environmental conditions. In this case, the exposure of the bale to dry, heated air was considered at the exposed surfaces of the bale and throughout the porous structure as the air permeated into the material. Based on this proposed analysis, two regions or domains were defined in this problem with each addressing a disparate length scale. Figure 4.1 depicts a two-dimensional cross-section of a porous bale (corresponding to the same vertical orientation as that of a flake) with identification of an inner and outer domain.

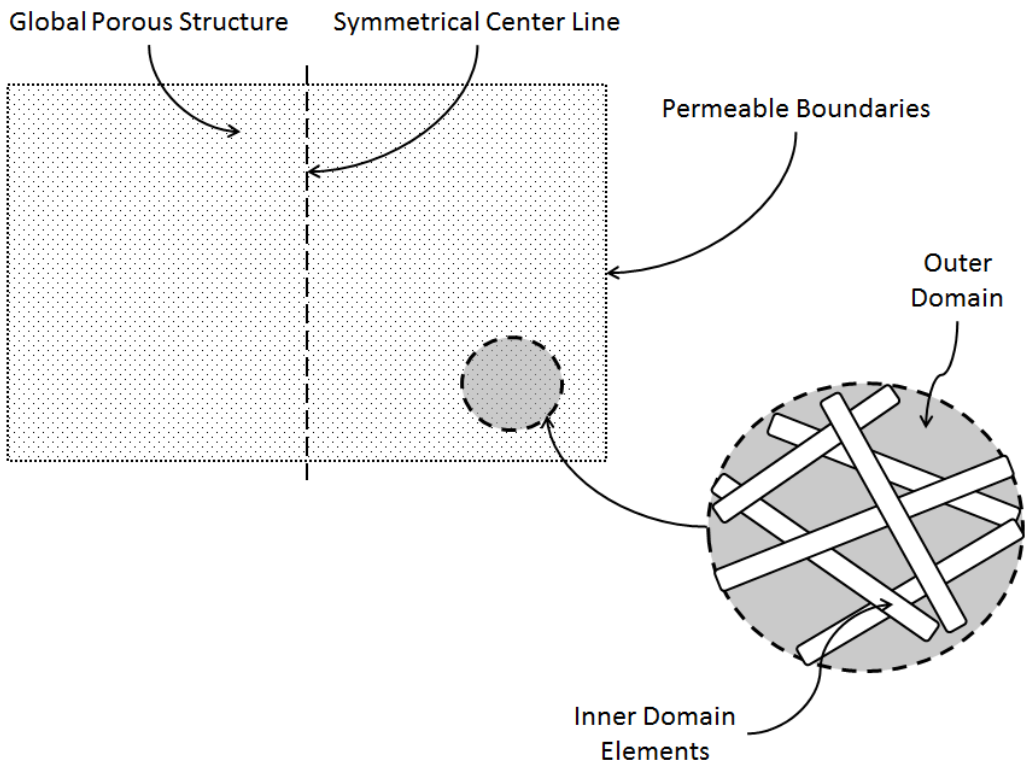

Figure 4.1 A two-dimensional cross-section of a rectangular bale of switchgrass identifying the outer domain (dry air and water vapor) and inner domain (solid stem material, liquid water, water vapor and dry air).

The ‘inner domain’ consists of the individual, cylindrical solid elements which represent the stems of switchgrass. These elements collectively form the global porous structure (bale). Moreover, the inner domain is itself considered a porous structure composed of a solid matrix, liquid water, water vapor and air. The free liquid contained within the elements of the inner domain was assumed to be removed during the storage conditions proposed for this study. The heat and mass transfer processes occurring within the inner domain were assumed to be one-dimensional since switchgrass stems have a waxy coating that is relatively resistant to mass transfer (Shinners and Porter, 2012).

The ‘outer domain’ is considered to be everything external to the inner domain, but internal to the overall structure of the bale. Hence, the outer domain represents the void space within the bale. In this case, water vapor and dry air were considered to be the only constituents existing within the outer domain. The global porous structure is composed of the outer domain along with many inner domain elements which are assumed to have random angular orientation within the vertical plane (flake) that is formed by the plunging action of the baling process. Thus, these angular stem orientations are aligned in parallel with the flake composition. The directionally-specific thermophysical properties are further discussed in section 5.3 with regards to the directional orientation of the stems.

The dynamic processes occurring during storage involve the simultaneous heat and mass transfer mechanisms of the inner domain coupled with those of the outer domain. These physical and thermophysical mechanisms proceed throughout storage as ambient air comes into contact with the inner domain elements; either flowing across the surface of the global structure or permeating into the outer domain. In the case of warmer ambient conditions, particularly in the absence of excess environmental moisture, this heat from the surrounding air will be convected to the inner domain elements. A portion of this energy may cause vaporization of the free liquid water which subsequently diffuses through the inner domain and is convected away at the interface between the inner and outer domain.

The rate of heat and mass transfer may be either convection-limited by the outer domain or conduction-limited by the inner domain depending on specific parameters discussed in this study. The limiting mechanism may also vary throughout different

regions of the porous structure, while modeling schemes which account for only one rate-limiting mechanism may not accurately represent the heat and mass transfer occurring over a wide range of conditions.

Based on this physical description of the problem, a mathematical model was developed to investigate the storage of rectangular bales of switchgrass under controlled environmental conditions. The heat and mass transfer formulation proposed here is based on previous porous media modeling theories (Kakaç et al., 2012; Nield and Bejan, 2006; Phillips, 1989); although natural convection and heat generation components are also incorporated. In this case, each domain was considered separately since the physical processes occurring in each domain are different. Relevant assumptions are highlighted throughout the discussion of this model development and are summarized in greater detail at the end of this chapter.

4.2 Inner Domain

4.2.1 Mass Conservation

The heat and mass transfer formulation proposed here for the inner domain is based on that of hygroscopic capillary porous solids (Berger and Pei, 1973; Krischer and Kast, 1963; Phillips, 1989). The dominant modes of mass transfer for the inner domain were assumed to include capillary liquid conduction, water vapor diffusion and bound liquid movement. The inner domain was assumed to be isotropic and homogeneous porous medium with the solid, liquid and vapor phases considered to be in thermodynamic equilibrium. Under these assumptions, the capillary flux was expressed as (Miller and Miller, 1955):

$$J_c = \dot{m}_c = -k_c \rho_s \nabla M = -k_c \rho_s \frac{\delta M}{\delta x} \qquad [4.1]$$

where: $J_c = \dot{m}_c$ = capillary mass flux (kg m^{-2} s^{-1}); ρ_s = solid phase density (kg m^{-3}); ∇ = gradient operator (m^{-1}); M = moisture content (kg^3 kg^{-3}); x = length coordinate (m); and k_c = capillary liquid conductivity (m^2 s^{-1}) which is a function of the temperature and moisture content.

Chen and Pei (1989) described bound liquid movement in terms of the bound liquid flux expressed as a function of the moisture content gradient:

$$J_b = \dot{m}_b = -k_b \rho_s \nabla M = -k_b \rho_s \frac{\delta M}{\delta x} \qquad [4.2]$$

where: $J_b = \dot{m}_b$ = mass flux of bound liquid (kg m^{-2} s^{-1}) and k_b = bound liquid conductivity (m^2 s^{-1}) which is also a function of the temperature and moisture content. Negligible temperature gradients were assumed in the derivation of this bound liquid expression. Thus, the inner domain elements were assumed to have negligible temperature gradients in the present study. This assumption does not, however, rule out the possibility of convective heat transfer from the outer domain to the inner domain or by conduction through an inner domain element.

It should be noted, that Equations 4.1 and 4.2 have limited applications as capillary conduction and bound water movement occur only in regions with continuous streams of free liquid and in regions with no free water, respectively (Chen and Pei, 1989). The dependence of both of these transfer mechanisms on the moisture content gradient suggests the formulation of a comprehensive liquid movement term of the form:

$$J_L = \dot{m}_L = -D_L \rho_s \nabla M = -D_L \rho_s \frac{\delta M}{\delta x} \qquad [4.3]$$

where: $J_L = \dot{m}_L$ = mass liquid flux (kg m^{-2} s^{-1}); and D_L = liquid conductivity (m^2 s^{-1}) which was assumed to be a function of the temperature and moisture content.

Although the liquid conductivity was expected to be of minimal practical value in the current study since the liquid was assumed to be initially bound, the assessment of this term was still given some consideration as will be discussed further in the application of this model (see Appendix B.1).

The vapor diffusive flux can be expressed in terms of either the vapor pressure or the vapor density as follows:

$$J_v = \dot{m}_v = -D_v \left(\varepsilon_I - \frac{\rho_s}{\rho_L} M\right) \nabla \left(\frac{P_v}{RT}\right) = -\frac{D_v}{RT} \left(\varepsilon_I - \frac{\rho_s}{\rho_L} M\right) \frac{\delta P_v}{\delta x} \qquad [4.4a]$$

$$J_v = \dot{m}_v = -D_v\left(\varepsilon_I - \frac{\rho_s}{\rho_L}M\right)\nabla\rho_{vI} = -D_v\left(\varepsilon_I - \frac{\rho_s}{\rho_L}M\right)\frac{\delta\rho_{vI}}{\delta x} \quad [4.4b]$$

with the assumption that the partial vapor pressure gradient is proportional to the vapor density gradient for small (negligible) temperature gradients:

$$\frac{1}{RT}\frac{\delta p_v}{\delta x} = \frac{\delta}{\delta x}\left[\frac{p_v}{R_v T}\right] = \frac{\delta\rho_v}{\delta x} \quad [4.5]$$

where: $J_v = \dot{m}_v$ = vapor diffusive flux (kg m^{-2} s^{-1}); D_v = vapor diffusivity (m^2 s^{-1}); ε_I = porosity of the inner domain (m^3 m^{-3}); ρ_L and ρ_{vI} = liquid and vapor density of the inner domain, respectively (kg m^{-3}); P = pressure (N m^{-2}); R_v = gas constant of the vapor (m^2 K^{-1}); T = temperature (K); and p_v = partial vapor pressure (kg m^{-1} s^{-3}).

A mass balance for a differential element of the inner domain was formulated in accordance with these mass flux terms. A general schematic of this differential element of the inner domain is shown in Figure 4.2. It should be noted, that this differential element must remain large enough to retain characteristic material properties (e.g., porosity) as opposed to an arbitrarily small volume (Bear, 1972). The mass balance with respect to this differential element is expressed in general terms as:

$$\begin{bmatrix}\text{Mass Flow}\\ \text{Rate In}\end{bmatrix} = \begin{bmatrix}\text{Mass Flow}\\ \text{Rate Out}\end{bmatrix} + \begin{bmatrix}\text{Rate of Change}\\ \text{of Mass Stored}\end{bmatrix} \quad [4.6]$$

or in mathematical terms:

$$J_L + J_v = \left(J_L + \frac{\delta J_L}{\delta x_I}dx_I\right) + \left(J_v + \frac{\delta J_v}{\delta x_I}dx_I\right) + \frac{\delta(\rho_s M)}{\delta t}dx_I + \frac{\delta}{\delta t}\left[\left(\varepsilon_I - \frac{\rho_s}{\rho_L}M\right)\rho_{vI}\right]dx_I \quad [4.7]$$

Rearrangement and simplification of this equation results in:

$$-\left(\frac{\delta J_L}{\delta x_I} + \frac{\delta J_v}{\delta x_I}\right) = \rho_s\frac{\delta M}{\delta t} + \frac{\delta}{\delta t}\left[\left(\varepsilon_I - \frac{\rho_s}{\rho_L}M\right)\rho_{vI}\right] \quad [4.8]$$

Substitution of the mass liquid flux (equation 4.3) and vapor diffusive flux (equation 4.4b) yields:

$$\frac{\delta}{\delta x_I}\left[D_L \rho_s \frac{\delta M}{\delta x_I}\right] + \frac{\delta}{\delta x_I}\left[D_v \left(\varepsilon_I - \frac{\rho_s}{\rho_L} M\right) \frac{\delta \rho_{vI}}{\delta x_I}\right] = \rho_s \frac{\delta M}{\delta t} + \frac{\delta}{\delta t}\left[\left(\varepsilon_I - \frac{\rho_s}{\rho_L} M\right) \rho_{vI}\right] \qquad [4.9]$$

which may be further simplified as:

$$\frac{\delta}{\delta x_I}\left[D_L \rho_s \frac{\delta M}{\delta x_I} + D_v \left(\varepsilon_I - \frac{\rho_s}{\rho_L} M\right) \frac{\delta \rho_{vI}}{\delta x_I}\right] = \rho_s \left(1 - \frac{\rho_{vI}}{\rho_L}\right) \frac{\delta M}{\delta t} + \left(\varepsilon_I - \frac{\rho_s}{\rho_L} M\right) \frac{\delta \rho_{vI}}{\delta t} \qquad [4.10]$$

The left-hand side of the equation represents the mass liquid flux and the diffusive flux effect of mass transfer; while the right-hand side represents the change of moisture content and vapor density. This derivation inherently assumes that porosity is not a function of time (rigid solid).

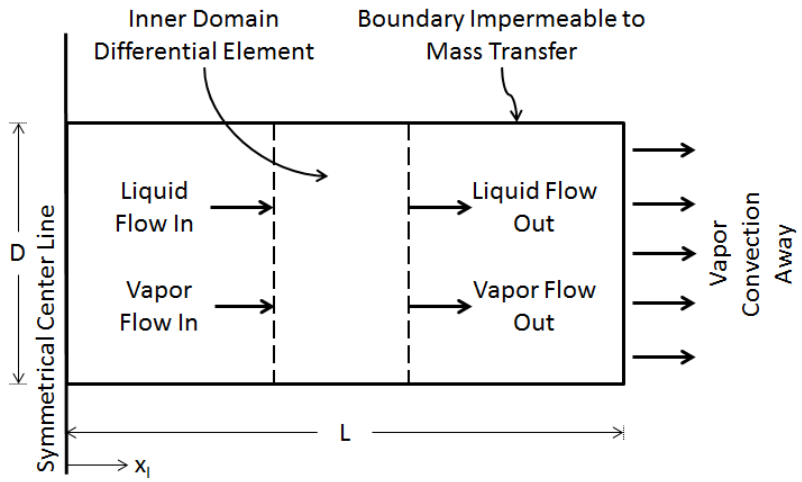

Figure 4.2 Mass balance for a differential element of the inner domain.

4.2.2 Energy Conservation

This study considers energy transfer by convection, liquid evaporation and heat conduction; while radiative heat transfer is considered negligible. Two distinct sources of conduction are specifically considered in this study including heat conduction through inner domain elements ('local') and through the global porous structure ('global'). The

global conduction term develops from the physical contact established between many inner domain elements. However, this global contribution to heat conduction is rather challenging in practical applications due to the geometric and mathematical complexity required in representing the actual points of contact between individual elements. Thus, a simplified treatment of this phenomenon is formulated in the current study by considering a succession of porous media.

At one limit, the global porous structure is considered to contain only a single inner domain element. In this case, there is no global (i.e., element-to-element) conduction. The addition of a second element; such that the two elements are in contact with each other (at least at one point), causes a global conduction phenomena in response to any temperature difference between the two elements. For a control volume surrounding only the first element, global conduction then appears to be an energy source (sink) at the point(s) of contact. As more elements are added, these energy sources (sinks) become distributed more closely along the length of the first element.

In the other limiting case, the energy sources (sinks) are distributed across the entire length of the element, with the global conduction term treated as an evenly distributed energy source along its entire length. The amount of heat conducted to the element from the neighboring elements can be assumed constant in this case. For many porous media applications, a large number of elements (and associated contact points) may indeed exist within a small volume of the porous media. In the current study, the global conduction term may, therefore, be modeled as an energy source (sink) of constant strength distributed along the entire length of an element.

A more detailed assessment of the conductive load may be necessary in strictly conductive heat transfer applications. However, the consideration of the convective contributions was expected to support this rather simplistic approximation of the conductive load. An energy balance was developed for a differential element of the inner domain (see Figure 4.3) based on these underlying principles. The general form of this energy balance follows:

$$\begin{bmatrix}\text{Rate at which}\\ \text{Energy Enters}\\ \text{the Element}\end{bmatrix} = \begin{bmatrix}\text{Rate at which}\\ \text{Energy Leaves}\\ \text{the Element}\end{bmatrix} + \begin{bmatrix}\text{Rate of Change}\\ \text{of Energy Stored}\\ \text{in the Element}\end{bmatrix} \qquad [4.11]$$

This expression of the energy balance can also be expanded to provide differentiation between the distinct modes of heat transfer as follows:

$$\begin{bmatrix}\text{Rate at which Energy}\\ \text{Enters the Element}\\ \text{from Respiration}\end{bmatrix}+\begin{bmatrix}\text{Rate at which}\\ \text{Energy is Conducted}\\ \text{into the Element}\end{bmatrix}+\begin{bmatrix}\text{Rate at which}\\ \text{Energy is Convected}\\ \text{to (from) the Element}\end{bmatrix}+$$

$$\begin{bmatrix}\text{Rate at which}\\ \text{Latent Heat is used}\\ \text{in the Element}\end{bmatrix}=\begin{bmatrix}\text{Rate at which}\\ \text{Energy is Conducted}\\ \text{out of the Element}\end{bmatrix}+\begin{bmatrix}\text{Rate of Change}\\ \text{of Energy Stored}\\ \text{in the Element}\end{bmatrix} \quad [4.12]$$

or in mathematical terms,

$$S_T A_x dx_I - k_s A_x \frac{\delta T_i}{\delta x_I} + h_c(T_a - T_I)P_x dx_I - \dot{m}_{ev} L_v A_x dx_I = \left[-k_s A_x \frac{\delta T_I}{\delta x_I} - \frac{\delta}{\delta x_i}\left(k_s A_x \frac{\delta T_I}{\delta x_I}\right) dx_I\right] + \rho_s Cp_s A_x \frac{\delta T_I}{\delta t} dx_I \quad [4.13]$$

Rearrangement and omission of opposing terms on either side of the equation yields:

$$S_T + h_c(T_a - T_I)\frac{P_x}{A_x} - \dot{m}_{ev} L_v = -\frac{\delta}{\delta x_I}\left(k_s \frac{\delta T_I}{\delta x_I}\right) + \rho_s Cp_s \frac{\delta T_I}{\delta t} \quad [4.14]$$

where: S_T = energy source (W m^{-3}); A_x = cross-sectional area of an inner domain element (m^2); k_s = thermal conductivity of the solid phase (W m^{-1} K^{-1}); T = temperature (K); h_c = convective heat transfer coefficient (W m^{-2} K^{-1}); P_x = length of distance around an inner domain element (m); $\dot{m}_{ev}$ = evaporative mass flow rate (kg m^{-3} s^{-1}); L_v = latent heat of vaporization (J kg^{-1}); Cp = specific heat (J kg^{-1} K^{-1}); and the subscripts s, a and I represent the solid phase, ambient and inner domain respectively.

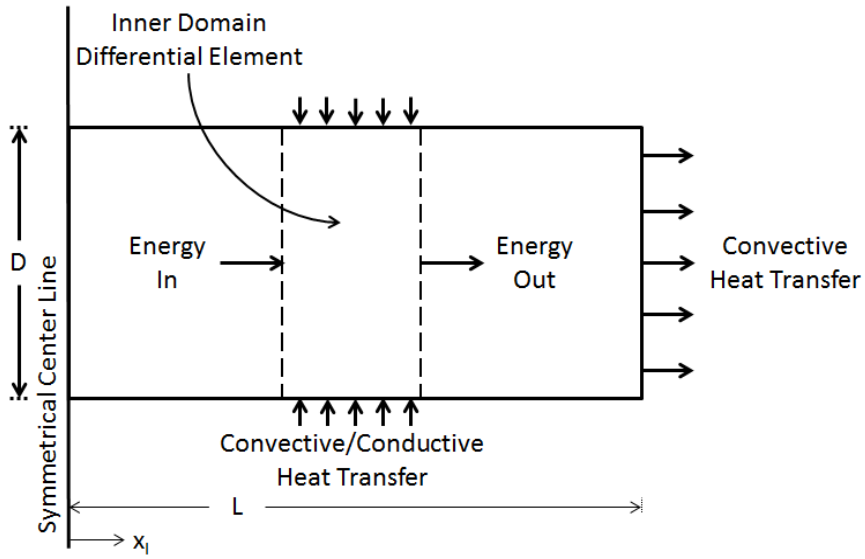

Figure 4.3 Energy balance on a differential element of the inner domain.

A mass balance was also performed for the vapor phase of the inner domain in order to obtain an expression of the evaporative mass flow rate ($\dot{m}_{ev}$). The general form of this mass vapor balance follows:

$$\begin{bmatrix}\text{Rate of Liquid}\\ \text{Evaporation}\\ \text{in the Element}\end{bmatrix}+\begin{bmatrix}\text{Mass Flow Rate}\\ \text{of Vapor into}\\ \text{the Element}\end{bmatrix}=\begin{bmatrix}\text{Mass Flow Rate}\\ \text{of Vapor out}\\ \text{of the Element}\end{bmatrix}+\begin{bmatrix}\text{Rate of Change of}\\ \text{the Mass of Vapor}\\ \text{Stored in Element}\end{bmatrix} \quad [4.15]$$

or in mathematical terms:

$$\dot{m}_{ev}A_x dx_I - D_v A_x\left(\varepsilon_I - \frac{\rho_s}{\rho_L}M\right)\frac{\delta\rho_{vI}}{\delta x_I} = \left\{-D_v A_x\left(\varepsilon_I - \frac{\rho_s}{\rho_L}M\right)\frac{\delta\rho_{vI}}{\delta x_I} - \frac{\delta}{\delta x_I}\left[D_v\left(\varepsilon_I - \frac{\rho_s}{\rho_L}M\right)\frac{\delta\rho_{vI}}{\delta x_I}\right]dx_I\right\} + \frac{\delta}{\delta t}\left[\left(\varepsilon_I - \frac{\rho_s}{\rho_L}M\right)\rho_{vI}\right]A_x dx_I \quad [4.16]$$

Rearrangement and omission of any opposing terms results in the following simplified expression for the evaporative mass flow rate:

$$\dot{m}_{ev} = -\frac{\delta}{\delta x}\left[D_v\left(\varepsilon_I - \frac{\rho_s}{\rho_L}M\right)\frac{\delta\rho_{vI}}{\delta x_I}\right] + \frac{\delta}{\delta t}\left[\left(\varepsilon_I - \frac{\rho_s}{\rho_L}M\right)\rho_{vI}\right] \quad [4.17]$$

Substitution of this evaporative mass flow rate into the energy balance equation (4.14) yields:

$$S_T + h_c(T_a - T_I)\frac{P_x}{A_x} + \left\{\frac{\delta}{\delta x_I}\left[D_v\left(\varepsilon_I - \frac{\rho_s}{\rho_L}M\right)\frac{\delta \rho_{vI}}{\delta x_I}\right] - \frac{\delta}{\delta t}\left[\left(\varepsilon_I - \frac{\rho_s}{\rho_L}M\right)\rho_{vI}\right]\right\}L_v + \frac{\delta}{\delta x_I}\left(k_s\frac{\delta T_I}{\delta x_I}\right) = \rho_s Cp_s\frac{\delta T_I}{\delta t} \quad [4.18]$$

This energy conservation equation can also be expressed in terms of the thermal diffusivity (α) as follows:

$$\frac{\delta T_I}{\delta t} = \frac{S_T}{\rho_s Cp_s} + \frac{h_c}{\rho_s Cp_s}\frac{P_x}{A_x}(T_a - T_I) + \left\{\frac{\delta}{\delta x_I}\left[D_v\left(\varepsilon_I - \frac{\rho_s}{\rho_L}M\right)\frac{\delta \rho_{vI}}{\delta x_I}\right] - \frac{\delta}{\delta t}\left[\left(\varepsilon_I - \frac{\rho_s}{\rho_L}M\right)\rho_{vI}\right]\right\}\frac{L_v}{\rho_s Cp_s} + \alpha_s\frac{\delta^2 T_I}{\delta x_I^2} \quad [4.19]$$

The left-hand side of this equation represents the energy that is stored within the specified control volume while the first term on the right-hand side represents the energy source. The derivation of this energy source term will be discussed later in this study (see Appendix B.7). The second term on the right-hand side represents the energy that is convected between the inner and outer domain. The third and fourth terms represent the mass of vapor flow and the vapor flow rate, respectively. The final term on the right-hand side of the equation represents the conduction within the inner domain.

4.2.3 Boundary Conditions

The boundary conditions for equations 4.10 (mass conservation) and 4.19 (energy conservation) are obtained by performing flux balances at the boundaries of the inner domain. Assuming that $x_I = 0$ is a plane of symmetry (see Figures 4.2 and 4.3); the liquid conduction, vapor diffusion and energy conduction at the axial boundary can be expressed as:

$$\rho_s D_L\frac{\delta M}{\delta x_I} = 0 \quad [4.20]$$

$$D_v\left(\varepsilon_I - \frac{\rho_s}{\rho_L}M\right)\frac{\delta\rho_{vI}}{\delta x_I} = 0 \quad [4.21]$$

$$k_s\frac{\delta T_I}{\delta x_I} = 0 \quad [4.22]$$

Likewise, the mass and energy balance at $x_I = L$ can be expressed as:

$$\rho_s D_L\frac{\delta M}{\delta x_I} + D_v\left(\varepsilon_I - \frac{\rho_s}{\rho_L}M\right)\frac{\delta\rho_{vI}}{\delta x_I} = h_m(\rho_{va} - \rho_{vI}) \quad [4.23]$$

$$k_s\frac{\delta T_I}{\delta x_I} - L_v\rho_s D_L\frac{\delta M}{\delta x_I} = h_c(T_a - T_I) \quad [4.24]$$

where: ρ_{va} = ambient vapor density (kg m^{-3}).

4.2.4 Initial Conditions

The initial conditions for the inner domain can be expressed as:

$$T_I = T_{I_0} \qquad 0 \le x_I \le L \quad [4.25]$$

$$M = M_0 \qquad 0 \le x_I \le L \quad [4.26]$$

$$\rho_{vI} = \rho_{vI_0} \qquad 0 \le x_I \le L \quad [4.27]$$

4.2.5 Thin-Layer Drying Model

Equations 4.10 (mass transfer) and 4.19 (energy transfer) form a system of two equations with three unknowns (T_I, M and ρ_{vI}); thus, requiring another relation to complete the mathematical model of the inner domain. A thin-layer drying model was implemented in this case to fulfill the requirement by evaluating the moisture content of the inner domain according to the general form of:

$$MR = \frac{M_t - M_e}{M_0 - M_e} = e^{-kt} \quad [4.28]$$

where: MR = moisture ratio (-); M = moisture content (%); k = drying rate constant (s^{-1}); t = time (s); and the subscripts 0, t and e represent the initial, time step and equilibrium values, respectively.

Previous models have reported negligible effects with the omission of the equilibrium moisture term (M_e) due to fluctuations in ambient relative humidity (Subahana et al., 2015); particularly in those cases in which the initial moisture content is below 50 % (Mujumdar, 2004; Rotz and Chen, 1985). However, this equilibrium moisture term was maintained in the current study as it was expected to improve model accuracy under the steady ambient conditions considered. A sorptional isotherm was used in this case to provide the necessary relationship for equilibrium moisture content as based on the modified GAB model (type II curve). The general form of this model follows:

$$M_e = \frac{A\left(\frac{C}{T}\right)(B \cdot RH_e)}{(1-B \cdot RH_e)\left[1-(B \cdot RH_e)+\left(\frac{C}{T}\right)B \cdot RH_e\right]} \quad [4.29]$$

where: M_e = equilibrium moisture content (%-db); RH_e = equilibrium relative humidity (dec.); T = temperature (°C); and A, B and C are model constants. The best fitting model for milled switchgrass was developed by Godbolt et al. (2013) with constant values of 12.91, 0.38, and 160.7 for A, B and C, respectively.

In this case, the moisture content was assumed to be in equilibrium with the relative humidity of the air within the inner domain. The validity of this assumption is supported by the relatively small scale of the inner domain in comparison to the global domain. In fact, the void space of within the inner domain is estimated to be roughly 1E6 times smaller than that of the global domain based on the respective porosities. Extended storage assessment intervals were also expected to allow for equilibrium conditions to be reached within these small volumes.

The drying rate constant (k) in this analysis was based on several previously reported models (Khanchi et al., 2013; Khanchi, 2015; Subahana et al., 2015) which follow the general form:

$$k = \exp(\mathrm{A} \cdot \mathrm{Rad} + \mathrm{B} \cdot \mathrm{VPD} - \mathrm{C} \cdot \mathrm{WS} - \mathrm{D} \cdot \mathrm{M} - \mathrm{E}) \quad [4.30]$$

where: Rad = average daily radiation (W m^{-2}); VPD = vapor pressure deficit (kPa); WS = wind speed (m s^{-1}); M = moisture content (dec., db); and the coefficients A, B, C, D and E are empirical constants.

The radiation term was considered negligible in the current study, while the natural convection velocity streams were used to simulate the wind speed. The empirical coefficients used in the current study were based on values reported for the seed-development and seed-shattered stages of switchgrass. Coefficient values for the seed-development stage were 3.39E-3, 5.281E-1, 1.511E-1, 7.635E-5 and 8.74856 for A, B, C, D and E, respectively; while those for the seed-shattered stage were 3.33E-3, 1.1141E-1, 1.4002E-1, 9.93E-3 and 6.64547 for A, B, C, D and E, respectively. The drying rate constants obtained from both stages were averaged together for use in the current study.

4.2.6 Inner Domain Summary

The complete description of heat and mass transfer within the inner domain is provided by the two governing equations (4.10, 4.19), the boundary conditions (equations 4.20 – 4.24), the initial conditions (equations 4.25 – 4.27) and the thin-layer drying model (equation 4.28). It will also be noted here, once more, that the liquid conductivity (D_L) and vapor diffusion (D_V) coefficients are dependent upon the characteristics of the porous media, may vary with the temperature and moisture content, and must be determined from empirical data. The consideration of these diffusional coefficients will be further discussed in the Appendix of this study (section B.1). It also becomes evident that the heat and mass transfer processes occurring within the inner domain are coupled to those occurring in the outer domain; thus, requiring a simultaneous solution of the governing equations for the outer domain. This interdependence between the inner and outer domain is discussed in further detail following the development of the outer domain equations.

4.3 Outer Domain

The global porous structure represents a rectangular cross-section of the bale aligned parallel to the lateral, flake orientation as indicated in Figure 4.4. The justification for the proposed geometry is based on the assumption that the distribution and angular orientation of the inner domain elements may vary within a layer (flake) of the bale. However, the axial orientation (z) of the bale, which corresponds to the direction of bale compression, has not been considered in the current study. This axial orientation represents a relatively long dimensional aspect with distinct rates of heat and mass transfer; particularly in terms of the thermophysical properties (see section 5.3).

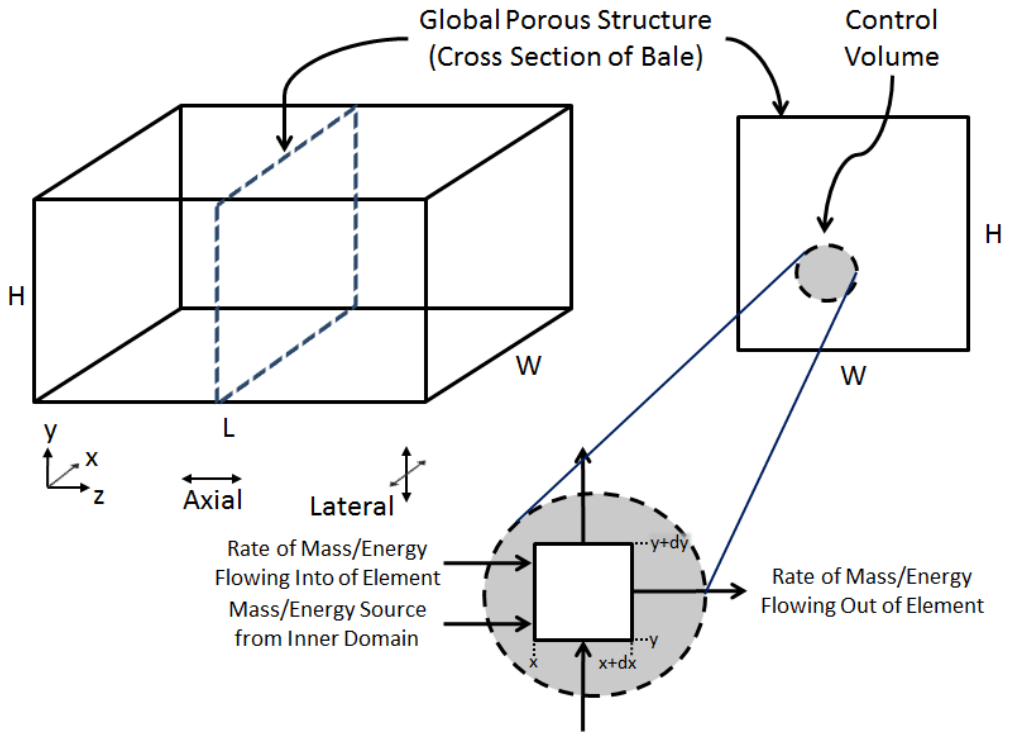

Figure 4.4 Mass and energy balance on a differential element of the outer domain.

The two-dimensional global porous structure was considered nonhomogeneous due to the spatial variance in material properties (i.e., porosity and permeability), but isotropic assuming no directional dependence due to the random distribution and angular orientation of inner domain elements. The solid structure is likewise considered rigid with negligible porosity variation with respect to time.

In the present application, water vapor was assumed to be removed from the inner domain by convection to the outer domain. The removal of this liquid was expected to occur over extended periods of time with a relatively small rate of change of water vapor mass within the outer domain. The volumetric flow rate of water vapor was also expected to have negligible effects on the air flow through the outer domain. A mathematical model for the outer domain was formulated based on similar agricultural models (Buckmaster, 1986; Phillips, 1989); although natural convection and heat generation compontents were also included. This model was developed in accordance with these underlying assumptions with respect to the differential element shown in Figure 4.4.

4.3.1 Mass Conservation

A mass balance was developed for a differential element in terms of the conservation of dry air and water vapor. Figure 4.5 depicts the two-dimensional control volume of the outer domain with flow rates indicated. It may be noted that the velocity field is considered unsteady in time due to the mass diffusion and natural convection effects.

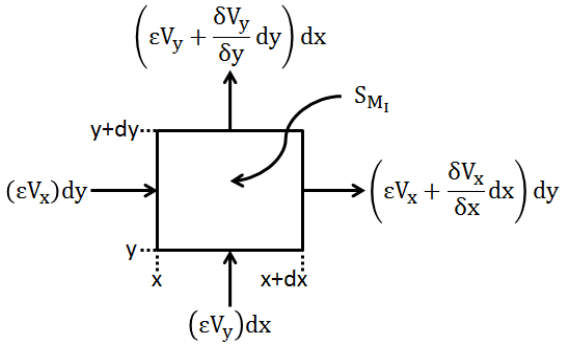

Figure 4.5 Differential element of the outer domain indicating flow through each surface.

The conservation of mass may be written in general terms as:

$$\begin{bmatrix}\text{Mass Flow}\\ \text{Rate In}\end{bmatrix} = \begin{bmatrix}\text{Mass Flow}\\ \text{Rate Out}\end{bmatrix} + \begin{bmatrix}\text{Rate of Change}\\ \text{of Mass Stored}\end{bmatrix} \qquad [4.31]$$

In accordance with this general mass balance, the mass transfer equation for dry air can be expressed in mathematical terms as:

$$\varepsilon V_x dy + \varepsilon V_y dx = \left(\varepsilon V_x + \frac{\delta \varepsilon V_x}{\delta x} dx\right) dy + \left(\varepsilon V_y + \frac{\delta \varepsilon V_y}{\delta y} dy\right) dx \quad [4.32]$$

where: ε = porosity of the outer domain ($m^3\ m^{-3}$); V = velocity ($m\ s^{-1}$); and the subscripts x and y indicate the horizontal and vertical directions, respectively. This expression may be simplified through the omission of opposing terms on either side of the equation as follows:

$$\frac{\delta}{\delta x}(\varepsilon V_x) + \frac{\delta}{\delta y}\left(\varepsilon V_y\right) = 0 \quad [4.33]$$

Air accumulation and diffusion-based gas transfer were assumed to be negligible in this case.

Mass conservation principles were also applied to the water vapor in the outer domain, with its density distribution directly influencing mass transfer from the inner domain. The resulting mass conservation equation of water vapor in the outer domain was expressed as:

$$\varepsilon \frac{\delta \rho_v}{\delta t} + \frac{\delta}{\delta x}(\varepsilon \rho_v V_x) + \frac{\delta}{\delta y}\left(\varepsilon \rho_v V_y\right) = S_{M_I} \quad [4.34]$$

where: S_{M_I} = volumetric mass source ($kg\ m^{-3}\ s^{-1}$) which represents the water vapor transfer from the inner domain to the outer domain. This source term may be defined as:

$$S_{M_I} = \frac{h_m(\rho_{vI} - \rho_v)NA_s}{V} \quad [4.35]$$

where: h_m = convection mass transfer coefficient ($m\ s^{-1}$); N = number of inner domain elements (-); A_s = surface area of an inner domain element (m^2); and V = outer domain control volume (m^3). A discussion and evaluation of the mass transfer coefficient (h_m) is provided later in this study (see Appendix B.6).

Substitution of this source term into equation 4.34 yields:

$$\varepsilon\frac{\delta\rho_v}{\delta t}+\frac{\delta}{\delta x}(\varepsilon\rho_v V_x)+\frac{\delta}{\delta y}(\varepsilon\rho_v V_y)=\frac{h_m(\rho_{vI}-\rho_v)NA_s}{V} \quad [4.36]$$

The first term on the left-hand side of the equation represents the accumulation of gas concentration over time. The remaining terms appearing on the left-hand side represent the convective gas transfer phenomena which accounts for the natural convection effect of mass transfer. Again, the right-hand side of this equation represents the mass source of vapor from the inner domain to the outer domain. The assumption that the water vapor and dry air are 'well-mixed' (i.e., have the same velocity at any point in the outer domain) is also implicit in this formulation.

The number of inner domain elements (N) can be estimated based on the proposed geometry of the porous material. In this case, the number of inner domain elements can be expressed as a ratio of the size of the outer domain to that of the inner domain as follows:

$$N=\frac{V}{2A_x L}(1-\varepsilon) \quad [4.37]$$

where: N = number of stems in the outer domain (-); A_x = cross-sectional area of an inner domain element (m^2); V = outer domain control volume (m^3); L = half-length of an inner domain element (m); and ε = porosity of the outer domain ($m^3\ m^{-3}$).

4.3.2 Momentum (Darcy's Law)

The thermally-conducting fluid was evaluated under the assumption of two-dimensional, unsteady, laminar, incompressible flow through the porous media. In this case, Darcy's law replaces Newton's Second Law with a proportional pressure drop and velocity across the porous medium. The Darcy model is essentially an empirical formula relating the pressure gradient, bulk viscous resistance and gravitational force. Although extensions to this model, such as the Brinkman (no-slip boundary conditions) and Forcheimer (drag force) terms may be necessary at high flow velocities and

permeabilities (Nield and Bajan, 2006), these conditions are not expected in the current application with slow fluid flow and low Reynolds numbers.

The present study was also conducted under the assumption of hydrodynamic and thermal isotropy with uniform porosity and permeability. The pressure work, viscous dissipation (turbulent flow), inertial effects and mass diffusive flux (binary mixture diffusion) were assumed negligible in this derivation. Darcy's law was considered to be valid under these assumptions; with the resulting momentum equation expressed in both principal length coordinates as:

$$-\frac{\delta P}{\delta x} = \frac{\mu}{\kappa} V_x \qquad [4.38a]$$

$$-\frac{\delta P}{\delta y} = \frac{\mu}{\kappa} V_y - \rho g \qquad [4.38b]$$

where: P = pressure (Pa); μ = dynamic viscosity (kg m^{-1} s^{-1}); V_x and V_y = velocity components in each respective direction (m s^{-1}); ρ = density (kg m^{-3}); g = gravitational acceleration (m s^{-2}); and κ = intrinsic permeability (m^2); the assessment of which will be further discussed in Appendix C.1.

Solving this form of Darcy's law in terms of each velocity component follows:

$$V_x = -\frac{\kappa}{\mu}\left(\frac{\delta P}{\delta x}\right) \qquad [4.39a]$$

$$V_y = -\frac{\kappa}{\mu}\left(\frac{\delta P}{\delta y} + \rho_a g\right) \qquad [4.39b]$$

Taking the derivative of each component with respect to its orthogonal length coordinate leads to:

$$\frac{\delta V_x}{\delta y} = -\frac{\kappa}{\mu}\left(\frac{\delta^2 P}{\delta x \delta y}\right) \qquad [4.40a]$$

$$\frac{\delta V_y}{\delta x} = -\frac{\kappa}{\mu}\left(\frac{\delta^2 P}{\delta x \delta y} + \frac{\delta \rho_a g}{\delta x}\right) \quad [4.40b]$$

Now, combining both terms into a single momentum expression yields:

$$\frac{\delta V_x}{\delta y} - \frac{\delta V_y}{\delta x} = \frac{\kappa g}{\mu}\frac{\delta \rho_a}{\delta x} \quad [4.41]$$

With the introduction of the stream function (Ψ) defined as:

$$V_x = \frac{\delta \Psi}{\delta y} \quad [4.42a]$$

$$V_y = -\frac{\delta \Psi}{\delta x} \quad [4.42b]$$

the momentum equation becomes:

$$\frac{\delta\left(\frac{\delta \Psi}{\delta x}\right)}{\delta x} + \frac{\delta\left(\frac{\delta \Psi}{\delta y}\right)}{\delta y} = \frac{\delta^2 \Psi}{\delta x^2} + \frac{\delta^2 \Psi}{\delta y^2} = \frac{\kappa g}{\mu}\frac{\delta \rho_a}{\delta x} \quad [4.43]$$

The change in density was assumed to be a linear function of the temperature variation according to the well-known Boussinesq approximation:

$$\rho = \rho_0[1 - \beta(T - T_0)] \quad [4.44a]$$

or,

$$\rho = \rho_0 - \rho_0 \beta T - \rho_0 \beta T_0 \quad [4.44b]$$

where the volumetric thermal expansion coefficient (K^{-1}) is given as:

$$\beta = \frac{1}{T} \quad [4.45]$$

assuming the ideal gas model applies with the air at standard atmospheric conditions.

Substitution of the Boussinesq approximation (4.44) into the momentum equation (4.43) yields:

$$\frac{\delta^2\Psi}{\delta x^2}+\frac{\delta^2\Psi}{\delta y^2}=\frac{\kappa g}{\mu}\left(\frac{\delta(\rho_0)}{\delta x}-\frac{\delta(\rho_0\beta T)}{\delta x}-\frac{\delta(\rho_0\beta T_0)}{\delta x}\right) \qquad [4.46]$$

which was further simplified by recognition of the negligible terms (derivative of the constants are zero). The resulting expression describing the potential flow in terms of the stream function follows:

$$\frac{\delta^2\Psi}{\delta x^2}+\frac{\delta^2\Psi}{\delta y^2}=-\frac{\kappa g\rho_0\beta}{\mu}\frac{\delta T}{\delta x} \qquad [4.47]$$

The mass conservation for dry air (equation 4.33), mass conservation of water vapor (equation 4.36) and Darcy's Law (equation 4.47) form a system of three equations with four unknowns (V_x, V_y, T and ρ_v). Hence, the solution of the velocity component of this model is interdependent on the solution to the temperature field.

4.3.3 Energy Conservation

An energy balance was developed for the outer domain based on a similar rectangular differential element (see Figure 4.5) according to the general expression:

$$\begin{bmatrix}\text{Rate at which Energy}\\ \text{Enters the Element}\\ \text{from 'Source' Terms}\end{bmatrix}+\begin{bmatrix}\text{Rate at which}\\ \text{Energy is Convected}\\ \text{into the Element}\end{bmatrix}+\begin{bmatrix}\text{Rate at which}\\ \text{Energy is Conducted}\\ \text{into the Element}\end{bmatrix}=$$
$$\begin{bmatrix}\text{Rate at which}\\ \text{Energy is Convected}\\ \text{out of the Element}\end{bmatrix}+\begin{bmatrix}\text{Rate at which}\\ \text{Energy is Conducted}\\ \text{out of the Element}\end{bmatrix}+\begin{bmatrix}\text{Rate of Change}\\ \text{of Energy Stored}\\ \text{in the Element}\end{bmatrix} \qquad [4.48]$$

or in mathematical terms:

$$S_{T_I}dxdy + \left[\rho_a Cp_a \varepsilon V_x T - k_a \varepsilon \frac{\delta T}{\delta x}\right] dy + \left[\rho_a Cp_a \varepsilon V_y T - k_a \varepsilon \frac{\delta T}{\delta y}\right] dx = \left[\rho_a Cp_a \varepsilon V_x T + \frac{\delta}{\delta x}(\rho_a Cp_a \varepsilon V_x T)dx - k_a \varepsilon \frac{\delta T}{\delta x} - \frac{\delta}{\delta x}\left(k_a \varepsilon \frac{\delta T}{\delta x}\right) dx\right] dy + \left[\rho_a Cp_a \varepsilon V_y T + \frac{\delta}{\delta y}\left(\rho_a Cp_a \varepsilon V_y T\right)dy - k_a \varepsilon \frac{\delta T}{\delta y} - \frac{\delta}{\delta y}\left(k_a \varepsilon \frac{\delta T}{\delta y}\right) dy\right] dx + \frac{\delta}{\delta t}(\rho_a Cp_a \varepsilon T)dxdy \quad [4.49]$$

Omission of those terms representing opposing energy flows into and out of the differential element yielded:

$$S_{T_I} + \frac{\delta}{\delta x}\left(k_a \varepsilon \frac{\delta T}{\delta x}\right) + \frac{\delta}{\delta y}\left(k_a \varepsilon \frac{\delta T}{\delta y}\right) = \frac{\delta}{\delta x}(\rho_a Cp_a \varepsilon V_x T) + \frac{\delta}{\delta y}\left(\rho_a Cp_a \varepsilon V_y T\right) + \frac{\delta}{\delta t}(\rho_a Cp_a \varepsilon T) \quad [4.50]$$

where: k = thermal conductivity (W m^{-1} K^{-1}); Cp = specific heat (J kg^{-1} K^{-1}); ρ = density (kg m^{-3}); the subscript a represents the respective moist air condition; and S_{T_I} = energy source term (W m^{-3}) which includes the energy transfer by convection to the inner domain.

This source term consequently accounts for any heat sources (sinks) considered within the inner domain such as evaporative effects and microbial heating from biological activity. This source term is defined as:

$$S_{T_I} = \frac{h_{cI} A_s (T_I - T) N}{V} \quad [4.51]$$

where: h_c = heat transfer coefficient (W m^{-2} K^{-1}) and A_s = surface area of an inner domain element (m^2). Substitution of this source term into the energy equation (4.50) yields:

$$\frac{h_{cI} A_s (T_I - T) N}{V} + \frac{\delta}{\delta x}\left(k_a \varepsilon \frac{\delta T}{\delta x}\right) + \frac{\delta}{\delta y}\left(k_a \varepsilon \frac{\delta T}{\delta y}\right) = \frac{\delta}{\delta x}(\rho_a Cp_a \varepsilon V_x T) + \frac{\delta}{\delta y}\left(\rho_a Cp_a \varepsilon V_y T\right) + \frac{\delta}{\delta t}(\rho_a Cp_a \varepsilon T) \quad [4.52]$$

Substituting thermal diffusivity into this energy equation yields:

$$\frac{h_{c_I} A_s (T_I - T) N}{\rho_a C p_a V} + \alpha_a \left[\frac{\delta}{\delta x} \left(\varepsilon \frac{\delta T}{\delta x} \right) + \frac{\delta}{\delta y} \left(\varepsilon \frac{\delta T}{\delta y} \right) \right] = \frac{\delta}{\delta x} (\varepsilon V_x T) + \frac{\delta}{\delta y} (\varepsilon V_y T) + \varepsilon \frac{\delta T}{\delta t} \quad [4.53]$$

The first term on the left-hand side represents the convective source term (volumetric energy source from the inner domain to the outer domain); while the second term represents conduction in accordance with Fourier's Law. The first two terms on the right-hand side of the equation represent convection to the inner domain in terms of the two lateral orientations (x and y); while the final term represents the energy stored (enthalpy change). The directional dependence of the thermophysical properties was assumed negligible in this derivation (see section 5.3).

Several parameters identified in this study of the outer domain are dependent on specific parameters appearing in the inner domain (in particular, h_c, h_m and T_i). Thus, it is evident that the convective mass and energy source terms couple the inner and outer domain models.

4.3.4 Boundary Conditions

The boundary conditions for the outer domain were expressed as:

$$T = T_a \qquad x = 0, x = W, y = 0, y = H \quad [4.54]$$

$$\rho_v = \rho_{v_a} \qquad x = 0, x = W, y = 0, y = H \quad [4.55]$$

$$\frac{\delta \Psi}{\delta x} = 0 \qquad x = 0, x = W \quad [4.56]$$

$$\frac{\delta \Psi}{\delta y} = 0 \qquad y = 0, y = H \quad [4.57]$$

In this case, all four boundaries of the global domain were assumed to be representative of the ambient air which permeates the outer domain at the global interface.

4.3.5 Initial Conditions

The initial conditions for the outer domain were described as:

$$T = T_0 \qquad 0 \leq x \leq W\,,\ 0 \leq y \leq H \qquad [4.58]$$

$$\rho_v = \rho_{v_0} \qquad 0 \leq x \leq W\,,\ 0 \leq y \leq H \qquad [4.59]$$

$$V_x = V_y = 0 \qquad 0 \leq x \leq W\,,\ 0 \leq y \leq H \qquad [4.60]$$

4.4 Analytical Summary

The model development presented in this chapter resulted in a set of seven governing equations including the conservation of mass (4.10), the conservation of energy (4.19), and thin-layer drying (4.28) for the inner domain; as well as, the conservation of mass for dry air (4.33), the conservation of mass for water vapor (4.36), the conservation of energy (4.53) and Darcy's Law (4.47) for the outer domain.

According to this discussion, there are seven unknowns (V_x, V_y, T, T_I, M, ρ_v, ρ_{vI}) along with an appropriate set of initial conditions for the inner domain (4.25-4.27) and outer domain (4.58-4.60); as well as, boundary conditions for the inner domain (4.20-4.24) and outer domain (4.54-4.57).

The overall solution to this model may be thought to consist of two essential components: one for the determination of the velocity field and another for the heat and mass transfer analyses. The velocity field is based upon the conservation of mass for dry air (4.33) and Darcy's Law (4.47) with respect to three unknowns (V_x, V_y, T). However, the dependence on the outer domain temperature (T) indicates that the solution to the velocity field is coupled with the remainder of the problem.

The other component of this model involves the coupled heat and mass transfer mechanisms occurring in both domains. Hence, the solution of this mass and energy component necessitates the simultaneous solution of the conservation of mass (4.10), conservation of energy (4.19), and thin-layer drying equation (4.28) for the inner domain; as well as, the conservation of mass (4.36) and conservation of energy (4.53) for the outer domain. There are five unknowns is this set of equations (T, T_I, M, ρ_v, ρ_{vI}), however, not

all the parameters appearing in these equations are independent. A discussion of some of these dependent parameters may be found in the appendices at the end of this study; including a discussion of the parameters appearing in the simple conduction model (Appendix A), the inner domain (Appendix B) and the outer domain (Appendix C).

4.5 Assumptions

The basic assumptions made in the formulation of this mathematical model are outlined in the following discussion.

4.5.1 Inner Domain

The inner domain (representing the physical structure of a switchgrass stem) was assumed to be a homogeneous porous media, with the interior of the stem considered to contain uniformly distributed material. Hence, this porous inner domain (containing liquid water, water vapor and dry air) was assumed to be isotropic and homogeneous. The liquid held within the inner domain was treated as pure water in terms of the energy required for vaporization; an assumption based on previous studies indicating minimal difference between liquid vaporization from a hay stalk and that of pure water (Bledsoe and Hitch, 1989).

The next assumption concerns the physical makeup of the global porous structure. In this case, the two-dimensional cross-section of the bale (see Figure 4.4) was assumed to consist of random angular orientations of the inner domain elements. It should be noted in this discussion, that distinct layers (flakes) of switchgrass are formed by the plunging effect of the rectangular baling process. During the baling process, a portion of the freshly harvested switchgrass is compressed onto the forming end of the bale. The result is an apparently random angular orientation of stems within each composite layer (flake). However, minimal change in flow may be assumed at the interface of these layers due to the significant compaction of the bale. Further elaboration on this point is provided in section 5.3 of this study.

Capillary liquid transfer, water vapor diffusion, and bound liquid movement were assumed to be the dominate mass transfer mechanisms occurring in the present application. While the typical pressure drop across a bale of switchgrass has been reported on the order of 0.1 psi (Román, 2014); the pressure gradient along the outside

(from end to end) of an inner domain element is assumed negligible in the current study. Any resulting liquid or vapor flow induced by an external pressure gradient was considered to be relatively small, while assuming negligible effusion flow and surface diffusion since this term is only relevant in the final stages of drying where the liquid content is very low.

Thermodynamic equilibrium was also assumed to exist between each phase of the inner domain (solid, liquid, vapor and dry air), with gradual temperature changes occurring throughout storage. The temperature gradient between inner domain elements was assumed negligible; although the convective heat transfer with the outer domain and the conductive heat transfer within the inner domain were both considered in this study. The temperature gradient along an individual stem was also expected to be relatively small; particularly considering the convective heat transfer occurring between the inner and outer domain. The solid component of the inner domain was also assumed to be rigid with negligible shrinkage and constant porosity with respect to time.

4.5.2 Outer Domain

The structure of the outer domain was considered to be isotropic since it was assumed to consist of random angular orientations of the inner domain elements within the lateral bale orientation. Current baling practice, however, may result in an uneven distribution of material within a rectangular bale, causing spatial variation of the dry matter density throughout the bale (Bledsoe et al., 1986). The porosity of the outer domain was likewise considered to be a function of the spatial position with the assumption of a nonhomogeneous porous media.

The axial direction of bale compression (z) was not considered in the current study due to the increased length scale and the slow heat and mass transfer mechanisms that were assumed to occur with respect to that direction. The addition of mass to the outer domain as water vapor was also expected to be slow over the storage conditions; particularly considering low temperature gradients and the presence of natural convective currents within the porous media.

CHAPTER 5:METHODS AND MATERIALS

5.1 Hydraulic Conductivity Analysis

5.1.1 Material Preparation

Switchgrass (*Panicum virgatum L.*) and miscanthus (*Miscanthus x giganteus*) were harvested at the University of Kentucky Spindletop Research Farm near Lexington, KY, USA (38˚8′ N, 84˚31′ W) in March 2013. Standard farm practices were carried out during cultivation of each feedstock type which were cut with a New Holland H6830 disc mower (with no conditioning rolls) at a height of approximately 15 cm (6 inches). Due to the time of year, the crop was dry and was immediately baled with a New Holland BC5070 baler (New Holland North America, Inc., New Holland, PA). Small rectangular bales (~102 x 46 x 36 cm^3) of each feedstock type were removed from the field within 24 h of production. The bales were transported to the University of Kentucky research farm in Woodford County (KY, USA) where they were stored for a minimum of 50 days in a single layer in a well-ventilated barn.

Following the storage period, the bales were transported to the Biosystems and Agricultural Engineering Department at the University of Kentucky in Lexington (KY, USA) and were stored indoors in an air conditioned laboratory. After storage, the bales were further compressed in the transverse direction using a custom built 20.68 MPa (3000 psi) hydraulic press as shown in Figure 5.1.1. Based on the bale weight and moisture content, bales were recompressed until the desired density was achieved. Nominal dry matter bulk density levels of 150, 175, 200 and 225 kg m^{-3} were targeted. These values are in the range typically reported for large square bales of switchgrass and similar types of biomass (Kemmerer and Liu, 2012; Sokhansanj et al., 2009).

Figure 5.1.1 Compression of bales in the transverse direction using a 20.68 MPa (3000 psi) hydraulic press.

Rough areas of each bale were trimmed to achieve relatively flat surfaces. Bale dimensions and weight were accessed after trimming using a platform scale (CKW30L, Ohaus Corp., Parsippany, NJ) and measuring tape (average of 12 individual bale measurements per rectangular dimension); respectively. Although the non-uniform packing of baled material may result in distinct layers of variable density throughout a bale, the 'apparent' bale density is reported in this study by considering the bulk homogeneous properties of each bale. The average initial moisture content of each feedstock type was determined by oven-drying at 103 ± 1 °C for 24 h, according to standard S358.2 (ASABE Standards, 2006).

5.1.2 Saturated Conditions

Saturated moisture content and leaching characteristics were first assessed by fully submerging 12 bales of each feedstock (3 reps per density level) in a water bath for approximately 15 minutes to ensure initial saturation. The target dry matter density levels were 150, 175, 200 and 225 kg m^{-3} as achieved with the hydraulic press. The fully saturated bales were then placed on a platform scale stored indoors to permit excess water to drain from the material. The weight of each bale was monitored for 36 hours which is

expected to be appropriate and sufficient for on-farm bioconversion. Three subsamples were then collected from each bale using a 2-inch-diameter bale probe and were stored at -9°C for several days. After thawing to room temperature, samples were weighed, placed in paper bags and oven-dried at 103 ± 1°C for 24 h. The initial and final mass of each sample was then measured by weighing scale and correlated to the saturated moisture content of each bale as a function of the bulk density and type of feedstock (switchgrass or miscanthus).

The saturated hydraulic conductivity was also determined for each feedstock type using a constant head technique with flow direction perpendicular to the consolidation direction (vertical hydraulic conductivity). Each bale was first fitted within a plywood frame leaving the top and bottom of the bale exposed. Spray insulation foam (Great Stuff, Dow Chemicals) was then applied between the wooden frame and the vertical surfaces of each bale to ensure a water-tight seal as shown in Figure 5.1.2. The insulation foam effectively prevented boundary flow and allowed for the assumption of one-dimensional flow through each bale from top to bottom. An aluminum box (with outlets at varying heights) was firmly secured to the wooden box with the bale using ratchet straps in order to provide a constant head.

Figure 5.1.2 Bale fitted in plywood frame with spray insulation foam preventing boundary flow.

Water was supplied to the experimental setup from a 1050 L (275 gal) polyethylene reservoir located above the aluminum head control box which was attached to the wooden bale frame as shown in Figure 5.1.3. Spacers in the bottom of the catch basin allowed restriction-free flow through the bale. Constant head was maintained by allowing excess water to drain from the head control box away from the catch basin. Thus, a fixed hydraulic gradient was established through the cross-sectional area of the bale. Steady-state flow conditions were confirmed by constant flow readings in order to ensure the bales were fully saturated.

Tests were conducted at three head levels for each bale (50.8 ± 2.3, 57.9 ± 2.5 and 68.3 ± 2.8 cm). The volume of water flowing through each bale was determined by collecting and weighing the runoff water from an outflow catchment over a specified time period, typically between 30 to 90 seconds depending on the rate of flow. Triplicate readings were taken to ensure constant flow within ± 50.0 g which corresponded to ± 50.0 ml based on the density of water. The saturated hydraulic conductivity of each bale was then determined by Darcy's law which describes the relationship between flow rate and head loss through a saturated porous medium as follows:

$$K_s = \frac{Q}{A}\frac{L}{H} \qquad [5.1.1]$$

where: K_s = saturated hydraulic conductivity (cm s^{-1}), Q = flow rate (cm^3 s^{-1}), A = cross-sectional area of the bale, perpendicular to the direction of flow (cm^2), and H/L = the potential gradient or head loss per unit length (cm cm^{-1}).

Darcy's Law assumes laminar flow through the material, while turbulent flow associated with higher flow rates results in nonlinear behavior. Each density level was assessed in triplicate for a total of 12 observations for each feedstock type (3 reps per density level). All data was analyzed by the GLM procedure of SAS (SAS Institute, Cary, NC) with bale density and feedstock type treated as fixed effects. The pairwise *t* test was used for means comparison with a 0.05 statistical significance.

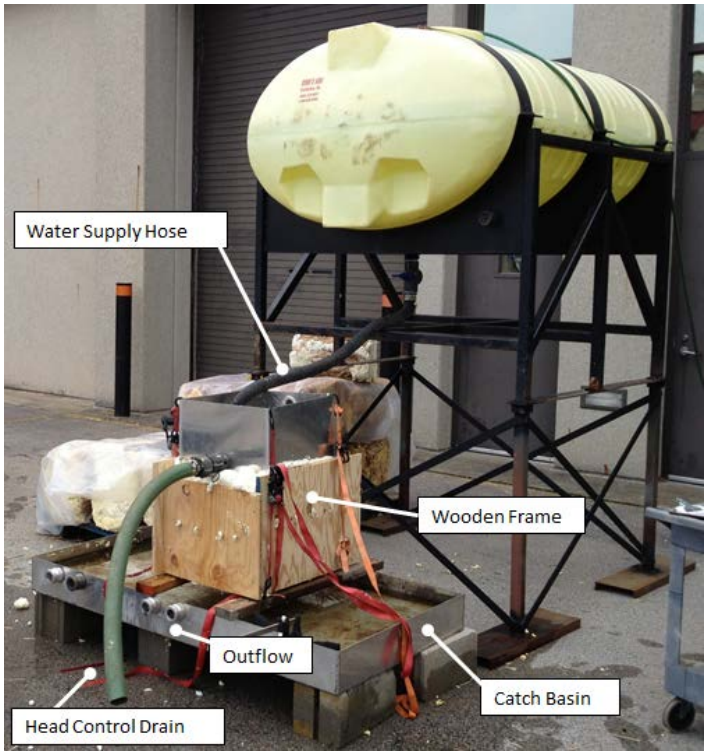

Figure 5.1.3 Constant head apparatus with reservoir supplying water to the constant head sleeve which is positioned on top of the framed bale.

5.1.3 Unsaturated Conditions

Water retention data within baled switchgrass was also determined by the filter paper method at three target dry matter density levels (175, 200 and 225 kg m^{-3}). This analysis was accomplished through the use of a water characteristic curve (WCC) according to the American Society for Testing and Materials standard D5298 for soil samples (ASTM, 1992). It should be noted that filter paper tests are highly sensitive suction measurements which generally require a high degree of controlled protocol in order to attain accurate results. Thus, care was exercised in performing these experiments which are assumed to provide sufficient estimates of the matric suction within baled biomass. Accordingly, bales were prepared at target moisture levels ranging from 10 to 40 %-wb with increments of 5 %-wb.

Individual filter papers (Whatman 42) were prepared by oven-drying overnight (16 h), cutting, and then sandwiching between two larger size (5.5 cm diameter) protective filter papers. The sandwiched filter papers were inserted into three locations between the flakes of each bale while ensuring good contact with the biomass material.

Hence, matric suction was measured since the flow of liquid water was expected to significantly contribute to the establishment of equilibrium conditions, particularly at higher moisture levels. The bales were wrapped in impermeable plastic to prevent water exchange with the environment and stored in the lab for 10 days. Thus, the filter paper was allowed to equilibrate with the porous material through liquid flow (matric suction) while held at a relative constant temperature in the lab (21.7 ± 0.4 °C). The filter papers were carefully extracted after equilibrium was established and the water content of each filter paper was then measured by standard gravimetric analysis.

The corresponding matric suction values were identified using a WCC (ASTM D 5298) and were subsequently plotted against the average moisture content of three replicate subsamples from the corresponding region within each bale. Inverse modeling of the van Genuchten model was then carried out with a computational solver (Seki, K., SWRC fit 2007) in order to provide optimized values of the water content - pressure head data using the least squares method. The van Genuchten equation is expressed as:

$$\theta_e = \frac{\theta-\theta_s}{\theta_s-\theta_r} = \left[\frac{1}{1+(\alpha h)^n}\right]^m \quad , \quad m=1-1/n \qquad [5.1.2]$$

where θ = the water content (%); θ_e = the effective water content (%); θ_s and θ_r = the saturation and residual moisture (%), respectively; α (m^{-1}), n (-) and m (-) are the empirical parameters; and h is the pressure head (cm).

Infiltration tests were then performed on baled switchgrass by modifying the experimental methods described by Hillel (1982). For each density level, a 3.1 cm-diameter infiltrometer (Mini Disk v9, Decagon Devices, Inc., Pullman, Wa) was used to infiltrate water into bales at a tension of -2 cm of water. The treatments consisted of three target dry matter densities (175, 200 and 225 kg m^{-3}) and four target moisture levels (10, 20, 30 and 40 %-wb). Replicate infiltration tests were performed at three locations on each bale, while each treatment was performed with triplicate bales for a total of 108 observations (12 treatments x 3 locations x 3 reps).

A 5.08 cm steel feedstock probe with a serrated tip was carefully drilled through each bale with minimal disturbance to the material as shown in Figure 5.1.4. A thin layer (5 mm) of fine silica sand was applied at each measurement location to smooth out

surface irregularities and to ensure good contact with the infiltrometer membrane. The volume of water (I) and infiltration time (t) were recorded at regular intervals (30 seconds) during infiltration. Philip's two-term equation (Philip, 1957) was then applied to the cumulative infiltration data as follows:

$$I = C_1 t + C_2 \sqrt{t} \qquad [5.1.3]$$

where I = the cumulative infiltration (ml), t = time (s); and C_1 ($m\,s^{-1}$) and C_2 ($m\,s^{-½}$) are the hydraulic conductivity and sorptivity coefficients, respectively. This model assumes steady-state water flow, constant water content within the transport volume, and minimum lateral mixing.

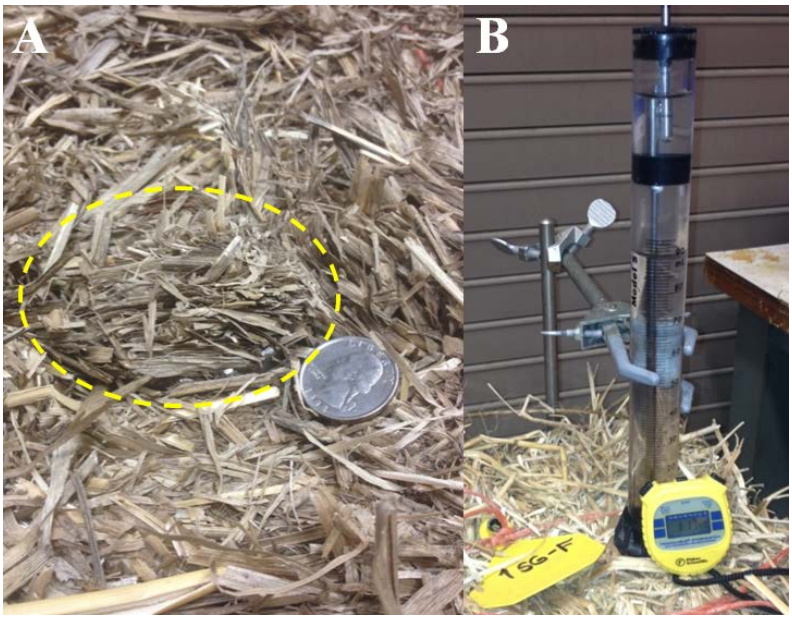

Figure 5.1.4 A) A 5.08 cm diameter probe inserted through baled switchgrass to limit lateral flow while exhibiting minimal disruption of the material; and B) the infiltrometer device positioned on the surface of the bale.

The Mualem hydraulic parameters, unsaturated hydraulic conductivity (K_u) and sorptivity (S), were then estimated for baled switchgrass at variable densities using the inverse modelling approach with the fitted values, C_1 and C_2 according to the following equations:

$$K_u(\theta, h) = \frac{C_1}{A_1} \quad [5.1.4]$$

$$S(\theta, h) = \frac{C_2}{A_2} \quad [5.1.5]$$

where A_1 and A_2 are dimensionless coefficients estimated as follows (Zhang, 1997):

$$A_1 = \frac{11.65(n^{0.1}-1)\exp[2.92(n-1.9)\alpha h_o]}{(\alpha r_o)^{0.91}}, n \geq 1.9 \quad [5.1.6]$$

$$A_1 = \frac{11.65(n^{0.1}-1)\exp[7.5(n-1.9)\alpha h_o]}{(\alpha r_o)^{0.91}}, n < 1.9 \quad [5.1.7]$$

$$A_2 = \frac{1.4b^{0.5}(\theta_o-\theta_i)^{0.25}\exp[3(n-1.9)\alpha h_o]}{(\alpha r_o)^{0.15}} \quad [5.1.8]$$

where n and α are the van Genuchten parameters which were calculated using the equations listed, r_o = the ring diameter (cm), b = 0.55 (Warrick and Broadbridge, 1992), h_o = the suction (tension with h<0) at the disk surface (-2 cm), and θ_o and θ_i = the water content (%) at h_o and h_i, respectively. The data were analyzed by the GLM procedure (SAS Institute, Cary, NC) with bale density treated as a fixed effect (α=0.05).

5.2 Moisture Measurement

5.2.1 Instrumentation

The calibration of a time domain reflectometry (TDR) moisture probe was first conducted by static and dynamic moisture measurements in a controlled lab setting. The electronic configuration consisted of a CS615 TDR sensor (Campbell Scientific®, Logan, Utah), a 12V lead-acid battery (Enercell, 12Vm/12Ah), and a CR10 data logger (Campbell Scientific®, Logan, Utah) for monitoring the output of the sensor. The specifications of these TDR soil moisture probes are summarized in Table 5.2.1. The output of the CS615 sensor ranged between 0V (dry material) to 4.97V (water) as was verified by a 2-point calibration between dry air and water (21.7 ± 1.2 °C).

Table 5.2.1 Specifications of the CS615 TDR soil moisture probe.

Property	**Value**	**Units**
Power Consumption	70	mA
Supply Voltage	9 to 18	VDC
Frequency Range	600 to1500	Hz
Period	0.7 to 1.6	ms
Output	± 2.5	VDC
Probe Length	30.0	cm

A CS615 sensor was then inserted into different compositions of switchgrass as outlined in the following discussion along with a Type-T thermocouple (24 AWG, Omega Engineering, Inc., Atlanta, GA) to ensure constant temperature during all experiments. Measurements were conducted by applying a 12 V excitation voltage to the sensors and recording the average of triplicate readings after 2 minutes in order to ensure full stabilization. The CR10 data logger was used to collect the signal output of each sensor with a PC used for programming and data retrieval according to the schematic shown in Figure 5.2.1.

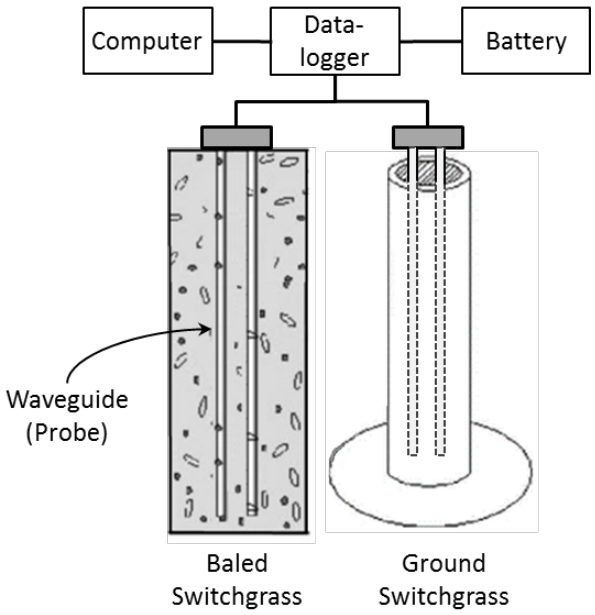

Figure 5.2.1 Experimental setup for measuring the moisture in baled and ground switchgrass using a CS615 TDR soil moisture probe.

5.2.2 Ground Switchgrass

Switchgrass was cut and baled in Lexington, KY in April 2013 before transporting and storing at the University of Kentucky Biosystems and Agricultural Engineering Department. After several months of storage indoors, preliminary trials were conducted with ground switchgrass since this physical format was assumed to resemble that of soil to a greater extent. Bales were ground through a 2mm screen using a knife grinder mill (Dietz-motoren GmbH & Co KG, D-7319) and prepared at a total of 12 consecutive moisture contents ranging from 8 %-wb to fully saturated. The appropriate amount of water was mixed with each ground sample of switchgrass and allowed to equilibrate in separate jars for 72 hours. The actual moisture levels were verified by gravimetric procedure at 103 °C for 24 hrs according to Standard S358.2 (ASABE Standards, 2006).

Each sample of ground switchgrass was then packed into a cylindrical PVC tube (H=12 in or 40.48 cm; D=4 in or 10.16 cm) at six dry bulk densities (75, 100, 125, 150, 175 and 200 kg m^{-3}). Hence, with 12 moisture levels and six density levels, there were a total of 72 treatment regimens of ground switchgrass that were each measured in triplicate (72 x 3 = 216 readings). The bulk density of each sample was reported on a dry basis according to:

$$\rho_b = m_{dry}/V_t \quad [5.2.1]$$

where V_t = total volume of bulk sample (m^3), m_{dry} = mass of the dry switchgrass (kg); and ρ_b = density of switchgrass (kg m^{-3}).

A CS615 sensor was then inserted into each sample of ground switchgrass along with a Type-T thermocouple (24 AWG, Omega Engineering, Inc., Atlanta, GA) to ensure constant temperature during all experiments. In this case, the stabilized temperature was approximately 23.9 °C. While numerous studies have indicated that TDR measurements are largely insensitive to temperature variations compared to other calibration errors (Da Silva et al., 1998; Dalton and van Genuchten, 1986; Davis and Chudobiak, 1975; Hook and Livingston, 1996; Ledieu et al., 1986; Starr et al., 1999; Topp et al., 1984), it has been noted that the temperature effects might impose an apparent change in the moisture reading when employing a single probe (Persson et al., 2000).

While these baseline measurements of ground switchgrass were conducted at the ambient temperature of the laboratory, additional measurements were performed at increased temperature levels. All measurements were repeated by first allowing the sealed jars containing each sample of ground switchgrass to equilibrate for approximately 30 minutes within a drying oven set at sequential temperatures of 32.2 and 40.6 °C. Thus, three temperature treatments were evaluated for ground switchgrass.

5.2.3 Baled Switchgrass

Measurements were also conducted with small rectangular bales at variable density and moisture levels under controlled lab conditions. Individual flakes of switchgrass were first cut into 4x4 in^2 sections on a table saw which was large enough to handle one flake at a time, while minimizing leaf shatter. The small flakes were manually packed into a bale chamber and hydraulically pressed in order to prepare miniature, rectangular bales (38 x 46 x 94 cm^3) according to a procedure documented by Coblentz et al. (1993). Figure 5.2.2 shows the compaction of the flakes in the newly fabricated bale chamber.

Figure 5.2.2. Flake compaction to form miniature bales (38 x 46 x 94 cm^3) using a newly fabricated bale chamber.

The variables considered in the evaluation of baled switchgrass were moisture content and bulk density; while the effect of temperature was dismissed based on the results obtained from the ground switchgrass samples (see section 6.3).

Density was controlled by maintaining a constant bale volume and varying the amount of plant material placed into the chamber. Nominal dry matter bulk density levels of 125, 150, 175 and 200 kg m^{-3} were targeted. Lower density levels were not evaluated in this study since the integrity of the miniature bales was poor at low densities due to the loose binding of the material. However, the density values evaluated in this study were within the range typically reported for large square bales of switchgrass and similar agricultural materials (Kemmerer and Liu, 2012; Sokhansanj et al., 2009). Five replicate bales were prepared for each density treatment with a total of 20 miniature bales prepared for this assessment of the moisture content via TDR measurements.

Each miniature bale was initially saturated by submerging in a water tank for 15 minutes and then individually sealed inside impermeable polyethylene bags. The sealed bales were stored within a controlled environmental chamber for approximately 24 hrs to permit relative temperature and moisture equilibrium to be achieved throughout each bale. Bale weights were measured before and after this short equilibrium storage period; with dry matter losses assumed to be negligible. An environmental temperature of 20.3 ± 0.3 °C was maintained within the environmental chamber, while the effect of ambient relative humidity was considered negligible with the bales sealed within impermeable plastic.

After this brief equilibrium storage period, CS615 sensors were inserted into 32 gauge (2.95 mm) pilot holes in each miniature bale along with a Type-T thermocouple to

ensure constant temperature during readings. As mentioned previously, a 2 minute stabilization period was maintained after the probes were inserted into the material to achieve relative equilibrium between the probes and material. Three replicate measurements were then recorded by the datalogger for each miniature bale. With three replicate bales prepared for each unique level of bulk density level, a total of 36 readings were taken at each moisture level.

The temperature and relative humidity within the environmental chamber were also monitored by Type E thermocouples (24 AWG, Omega Engineering, Inc., Atlanta, GA) and a CS-500L relative humidity probe (Campbell Scientific, Logan, UT); respectively. An AM416 thermistor (Campbell Scientific, Logan, UT) was used as a reference within the data acquisition box. The weight and temperature of each bale were recorded before each equilibrium storage period.

After all measurements were performed for a given moisture level, lower moisture was achieved by placing the miniature bales in a drying oven at 70 °C for approximately 30 minutes. Upon removal from the drying cabinet, the miniature bales were sealed once again inside plastic bags and held within the controlled environmental chamber for approximately 24 hrs to achieve relative temperature and moisture equilibrium. Measurements were taken at this subsequent moisture level; with bale weights taken before and after this brief storage. The experimental procedure was repeated in this manner until each miniature bale was completely dry (weights within ± 0.01 g); which required an average of 10 to 14 days to complete depending on the temperature-dependent rate of drying for each bale. The final moisture content of each miniature bale was verified by standard gravimetric analysis and was used to retrospectively determine moisture content at each interval.

This procedure was followed in the current study in order to minimize the actual number of bales that had to be produced, as well as, minimize the variation associated with the production of additional bales (i.e., bulk density variation and probe insertion inconsistencies). The method of saturating the newly formed miniature bales was also preferred in the current study since other methods of moisture conditioning could contribute to several issues. For example, the wetting and conditioning of loose switchgrass flakes prior to baling led to moisture inconsistencies between treatments. Pre-

wetted flakes also presented a challenge in terms of hydraulically pressing the material to desired density levels while leaching was observed when compressing higher moisture treatments. The oven-drying process was also implemented in this study to expedite the equilibration process while achieving target moisture levels.

5.2.4 Data Analysis

Although the water content in soils is often expressed in terms of the volumetric water content ($m^3\ m^{-3}$), the voltage output data in this study was correlated to the mass-based moisture content ($kg\ kg^{-1}$) of both the ground and baled formats of switchgrass on a wet basis. A set of moisture-voltage calibration curves were developed for both physical formats of the material since single prediction equations were unsuitable under all experimental conditions. These calibration curves were also developed with respect to the bulk density of the biomass using multivariate regression analysis (SAS 9.3). Thus, the impacts of moisture content and bulk density on the voltage output were assessed through analysis of variance (ANOVA).

5.2.5 Sensor Validation

Dynamic storage trials were also conducted in the lab to validate sensor accuracy with larger bale sizes where more variability was expected. Additional rectangular bales of switchgrass (~102 x 46 x 36 cm^3) that had not used in preparing the ground and miniature bales were used in this validation procedure. The bales were stored in a controlled environment chamber according to the experimental procedure described in section 5.4.5. In this case, the bales were stored on 91.44 cm (36 in) high, metal wire shelves arranged in three rows (replications) within the chamber for 60 days. The specific layout for this experiment is depicted in Figure 5.4.5.

The environmental chamber was initially maintained at approximately 22 °C and 51 % relative humidity for the first 36 hours to establish baseline storage conditions in line with the ambient laboratory conditions. After this initial storage period, the environmental conditions were adjusted and maintained for 60 days at 29.5 ± 0.6 °C with the driest relative humidity possible under the proposed conditions and within the limitations of the environmental chamber (23.2 ± 3.9 %). Bales were weighed upon

entering the environmental chamber and approximately every two weeks (day 14, 31, 45 and 60) throughout the storage period. A 5.08 cm forage probe with a serrated tip was used to collect three subsamples from each destructive bale replication on the same sampling interval according to the coring pattern presented by Smith et al., (2013). Three subsamples were also collected from each bale on day 60 of the storage experiment; including the R1-R3 bale replications (3 sampling locations x 3 bale replicates = 9 subsamples per interval). These subsamples were used in determining the moisture content at each sampling interval through gravimetric analysis.

Voltage output was measured with a CS615 TDR sensor at diagonal positions throughout each bale at lower (~5 inch above the bottom surface), central (centered with the height) and upper (~5 inch below the top surface) positions. The TDR sensors provided an averaged value across the length of the probe corresponding to a depth of 12 inches into the bale; while accounting for any potential variation which could occur in the three principle coordinates. Triplicate measurements of the voltage output from the TDR sensor were recorded at the same time interval of every two weeks (day 14, 31, 45 and 60). The resulting voltage data was converted to moisture content using the previously developed calibration curve for the TDR probe. This TDR-based moisture data was compared and validated with the corresponding moisture content that was determined from gravimetric analysis (oven-drying) of the subsamples.

5.3 Thermal Analysis

5.3.1 Probe Construction

The dual thermal probe employed in the current study for the evaluation of the thermophysical properties of baled switchgrass consisted of a thermal conductivity probe with a heating element and a secondary probe for the evaluating the thermal diffusivity. These two probes were spaced 7.27 mm (0.28 in) apart. Each probe was constructed from a 152.4 mm (6 in) long cylindrical Type 304 stainless steel tube with 2.38 mm (0.094 in) outer diameter and1.88 mm (0.074 in) inner diameter.

5.3.1.1 Thermal Conductivity Probe

For the construction of the thermal conductivity probe, a 0.254 mm (0.01 in) diameter constantan heating wire was coated with a high thermally conductive silicone paste (Thermalcote I, AAVID Thermalloy, LLC., Concord, NH) before being inserted into a four-hole, 1.575 mm (0.062 in) diameter ceramic tube (Scientific Instrument Services, Inc., Rigoes, NJ) with inner diameter holes of 0.406 mm (0.016 in). After passing through one hole of the ceramic tube, the constantan heating wire was looped back through a second hole; thereby, establishing a complete heating circuit as shown in the schematic of Figure 5.3.1 and the photograph of Figure 5.3.2. Constantan was used for the heating element due to its relatively low resistivity temperature coefficient (Lobo and Cohen, 1990).

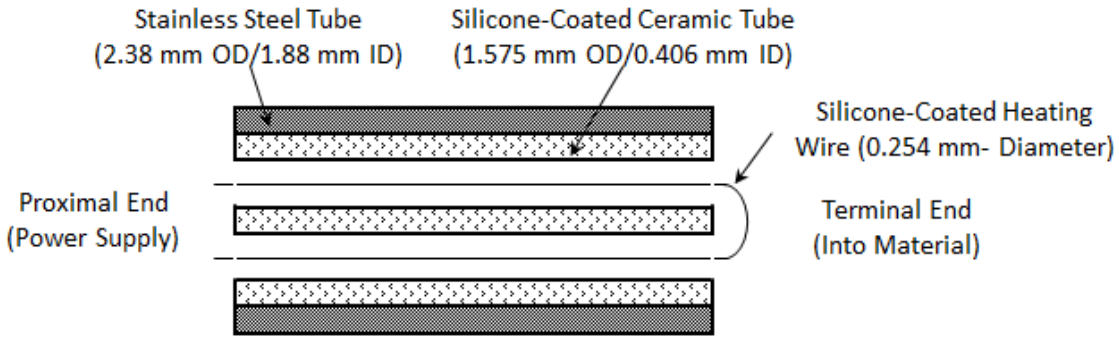

Figure 5.3.1 Schematic of the thermal conductivity probe shown as the longitudinal cross-section (not to scale).

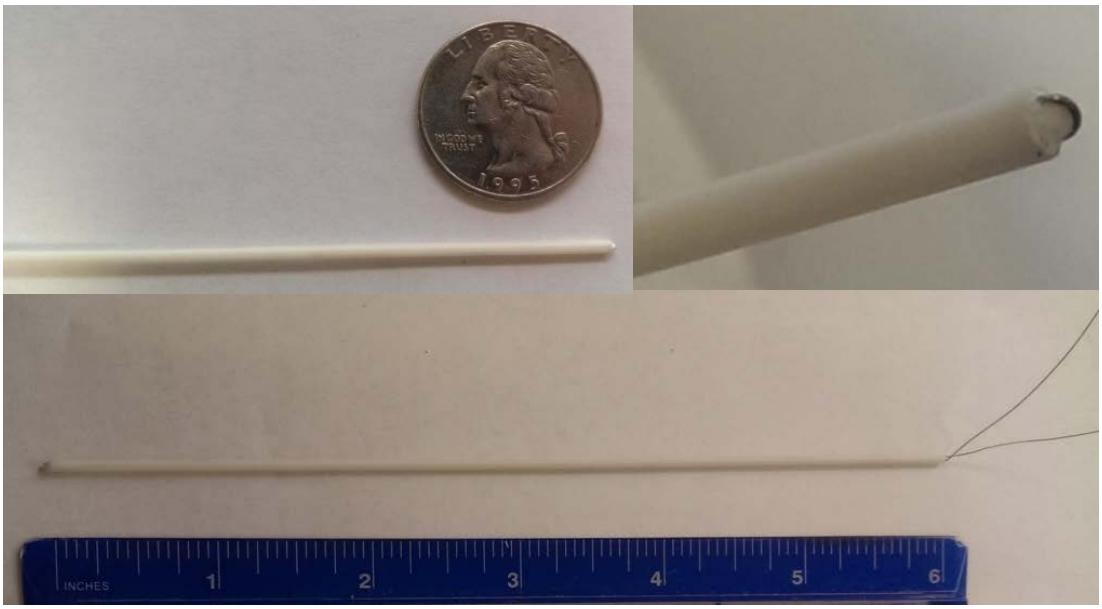

Figure 5.3.2 Heating wire coated with silicone paste and inserted through ceramic tube. Rubber silicone glue was applied at the terminal end of the probe to protect the heating wire loop.

Two separate sets of 0.051 mm (0.002 in), copper/constantan thermocouples (Omega Engineering, Inc., Springdale, CT) were also coated with silicone paste and inserted into the remaining two holes of the ceramic tube. These T-type thermocouples were selected for use in the current study as they provide a good deal of sensitivity in measuring small temperature changes (43 μV $°C^{-1}$). Each thermocouple was assumed to provide an average reading of the entire probe length since each set of wires was carefully twisted together to provide close contact between the copper and constantan components (essentially serving as a thermopile).

The ceramic tube was subsequently coated with silicone paste and inserted into one of the stainless steel tubes. The terminal end of the thermal conductivity probe was sealed with a drop of silicone rubber caulk which presumably resisted temperature transfer at the terminal end while providing the heating wire loop with at least some level of protection from potential physical damage. The thermal conductivity of the stainless steel and silicone rubber used is this study were approximately 16 and 0.2 W m^{-1} K^{-1}, respectively, within the temperature range that was considered.

5.3.1.2 Thermal Diffusivity Probe

The thermal diffusivity probe was assembled in a similar fashion; with two sets of constantan-copper thermocouples; separately twisted for good contact between the individual thermocouple components, coated with silicone paste, and inserted into two opposing holes of the secondary ceramic tube. This ceramic tube itself was, in turn, coated with silicone paste and inserted inside the second stainless steel tube. Silicone rubber caulk was also used to seal the terminal end of the thermal diffusivity probe.

5.3.1.3 Dual Thermal Probe

Both probes were inserted through plastic connectors and subsequently bonded with epoxy glue (J-B Weld, Sulphur Springs, TX) to maintain parallel orientation. Epoxy glue was also used to further seal the terminal ends of each probe, as well as, to protect and stabilize all the bare wires at the proximal end of each probe. The dual thermal probe described here is shown in Figure 5.3.3.

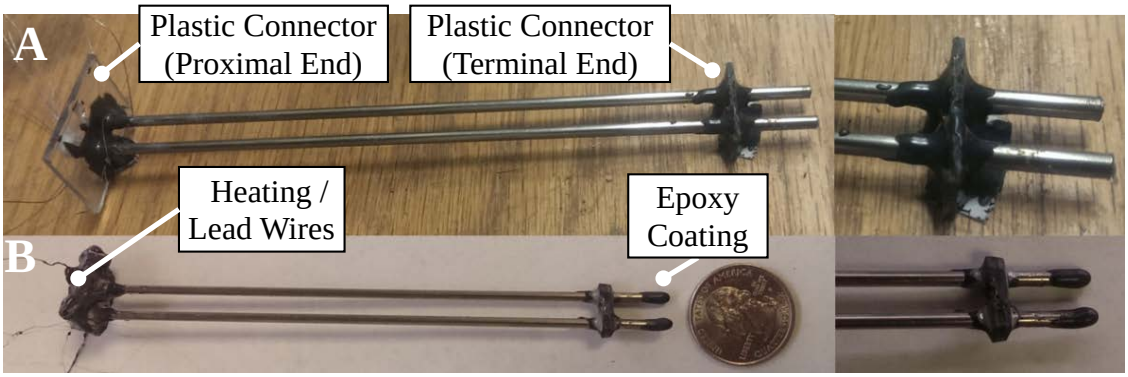

Figure 5.3.3 Dual thermal probes used to determine the thermal properties of baled switchgrass. (A) Placement of plastic connectors to maintain positioning; and (B) application of epoxy glue to the terminal and proximal ends for protection.

5.3.2 Material Preparation

Switchgrass (*Panicum virgatum L.*) was harvested at the University of Kentucky Spindletop Research Farm near Lexington, KY, USA (38˚8′ N, 84˚31′ W) in March 2013. Standard farm practices were carried out during cultivation using a New Holland H6830 disc mower (with no conditioning rolls) at a height of approximately 15 cm (6 inches). Due to the time of year, the crop was dry and was immediately baled with a New Holland BC5070 baler (New Holland North America, Inc., New Holland, PA). Small rectangular

bales (~102 x 46 x 36 cm^3) were removed from the field within 24 h of production. The bales were transported to the University of Kentucky research farm in Woodford County (KY, USA) where they were stored for a minimum of 50 days in a single layer in a well-ventilated barn.

The bales were transported to the Biosystems and Agricultural Engineering Department at the University of Kentucky in Lexington (KY, USA) and were stored indoors in an air conditioned laboratory. Random bales were then removed from storage in order to evaluate the thermophysical properties of the material (additional bales remained in storage for later use in validation tests as discussed further in section 5.3.9). The average initial moisture content of each bale was first determined by oven-drying three subsamples collected from each bale using a 2-inch-diameter bale probe. These subsamples were placed in paper bags, weighed and then oven-dried at 103 ± 1 °C for 24 h, according to standard S358.2 (ASABE Standards, 2006). The initial and final mass of each subsample was measured by weighing scale and used to calculate the average moisture content of the material which was found to be 10.1 %-wb.

5.3.3 Treatments

The variables assessed in this study included dry bulk density (150, 175, 200 and 225 kg m^{-3}), moisture content (10, 20, 30 and 40 %-wb), temperature (20, 30 and 40 °C), and direction of heat flow (parallel or perpendicular to the stem orientation). Individual flakes were separated from the source bales and were subsequently cut into 4x4 in^2 sections on a table saw which was large enough to handle one flake at a time, while minimizing leaf shatter. These small sections of flake were manually packed into a bale chamber and hydraulically pressed in order to prepare small, rectangular bales (38 x 46 x 94 cm^3) according to a procedure documented by Coblentz et al. (1993).

Density was controlled by maintaining a constant bale volume and varying the amount of plant material placed into the chamber. Nominal dry matter bulk density levels of 150, 175, 200 and 225 kg m^{-3} were targeted. These values are in the range typically reported for large square bales of switchgrass and other similar types of biomass (Kemmerer and Liu, 2012; Sokhansanj et al., 2009). Five replicate bales were prepared

for each density treatment with a total of 20 miniature bales prepared for this assessment of the thermophysical properties.

To achieve target moisture levels, each miniature bale was initially saturated by submerging in a water tank for approximately 15 minutes. The bales were then allowed to dry at approximately 70 °C in a drying oven until reaching specified weights (within ± 0.1 g) which were predetermined to correspond with the desired moisture content of each treatment (target moisture contents were 10, 20, 30 and 40 %-wb). After achieving one of the target moisture contents through this drying process, the miniature bales were removed from the drying oven and placed in a controlled environmental chamber for approximately 3 days to achieve temperature and moisture equilibrium. A summary to this measurement procedure is depicted in Figure 5.3.4.

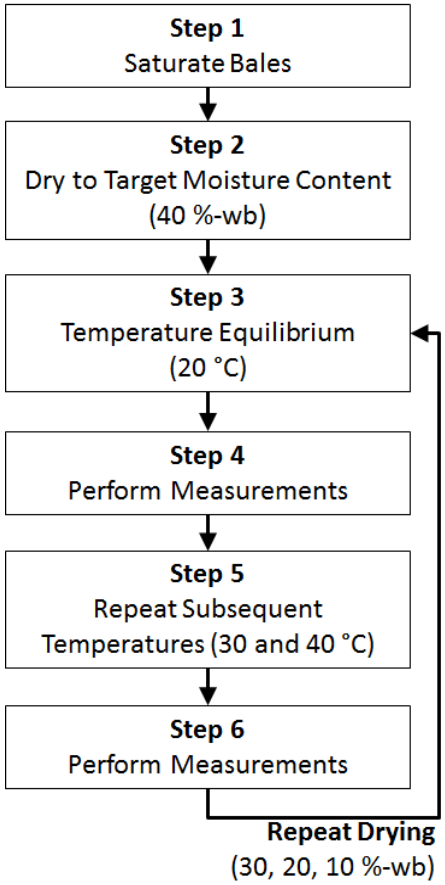

Figure 5.3.4 Flow chart of the material preparation and measurement procedure.

A constant temperature was maintained within the environmental chamber in accordance with the particular target treatment level; while relative humidity was maintained at corresponding equilibrium conditions based on the sorption isotherm of 8-mm milled switchgrass (Godbolt et al., 2013). It should be noted that the application of these sorption isotherms provided only a rough estimate of the desired equilibrium relative humidity as the bulk material considered in the current study represents a unique physical composition which holds water differently than the milled samples utilized in previous studies. In those cases exceeding the saturated air conditions and/or the operational limitations of the environmental chamber, the relative humidity was set at the maximum attainable level of approximately 90 %. This regulation of the relative humidity may be considered an additional level of control since the miniature bales were sealed within impermeable polyethylene.

Bale weights were also measured before and after this storage period to ensure minimal moisture exchange (wetting and/or drying processes) between the bales and the air within the environmental chamber. Based on this information, dry matter losses were assumed to be negligible during this short storage period. The final target moisture content (10 %-wb) was verified for each bale by standard gravimetric analysis. This data was also used to retrospectively validate the moisture content for each of the moisture replications that were performed in this experiment.

After all measurements were performed for a given treatment (a methodology discussed in section 5.3.4), the environmental chamber was adjusted and maintained at the next sequential target temperature (20, 30 and 40 °C) for each respective treatment; while the relative humidity was maintained at the corresponding equilibrium value based on the sorption isotherm. Again, in those cases exceeding the saturated air conditions and/or the operational limitations of the environmental chamber, the relative humidity was set at the maximum attainable level of approximately 90 %. After the measurements were performed for all of the target temperatures of interest, the miniature bales were placed into a drying oven to attain lower moisture content treatments as described earlier.

This storage and equilibration procedure was repeated until all specified density, moisture and temperature treatments were achieved. This specific procedure was followed in the current study in order to minimize the actual number of bales that had to

be produced; as well as, minimize the variation associated with the production of additional bales (i.e., bulk density variation and probe insertion inconsistencies). The method of saturating the newly formed miniature bales was also preferred in the current study since other methods of moisture conditioning could contribute to several issues. For example, the wetting and conditioning of loose switchgrass flakes prior to baling led to moisture inconsistencies between treatments. Pre-wetted flakes also presented a challenge in terms of hydraulically pressing the material to desired density levels while leaching was observed when compressing higher moisture treatments. The oven-drying process was also implemented in this study to expedite the equilibration process while achieving target moisture levels within a reasonable degree of accuracy.

5.3.4 Measurement Procedure

Pilot holes were formed in each miniature bale using a 2.38 mm (3/32 in) diameter solid brass rod (Model #163, K & S Precision Metals, Chicago, IL) which allowed easier insertion of the dual thermal probes. The probes themselves were inserted into the material until the plastic connector at the proximal end became flush with the bale surface. In this case, the plastic connector between the two rods was essentially thin enough to insert into the baled material. The probes were allowed to reach constant temperature equilibrium with the switchgrass for several minutes.

A constant voltage power supply (Model 382260, Extech Instruments Corporation, Nashua, NH) was connected to the heating wire in series with a standard resistor (10 Ω) and activated with 2.0 V. This relatively low voltage was employed in the current study to reduce any potential moisture diffusion to negligible levels. The current through the heating wire was verified by measuring the voltage across the resistor and applying Ohm's law. In this case, the resistance of the heater wire was measured as 0.405 $\Omega\ m^{-1}$ based on the constant current of 0.135 A that was supplied. Figure 5.3.5 shows a schematic of the experimental setup for this study.

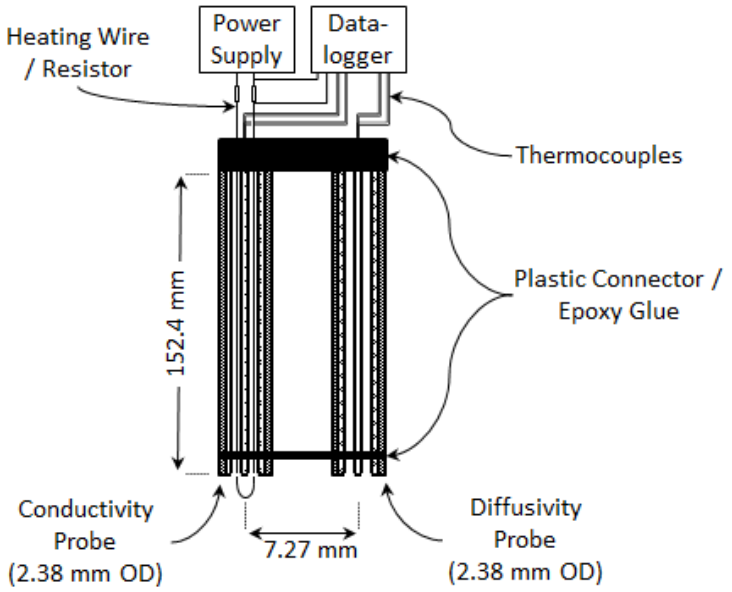

Figure 5.3.5 Instrumentation used in measuring thermophysical properties of baled switchgrass (not to scale).

Each test was allowed to run for three minutes while the temperature of each thermocouple, current through the heating wire, and voltage were all scanned and recorded using a datalogger (Model CR10, Campbell Scientific, Inc., Logan, UT) at one-second intervals. A period of approximately 5 min was maintained between each test to allow stable thermal equilibrium to be reached by the probe. The temperature and relative humidity of the environmental chamber were also monitored by several Type-E thermocouples (Omega Engineering, Inc., Atlanta, GA) and a relative humidity probe (CS500-L, Campbell Scientific, Logan, UT); respectively. Three replicate bales were measured at each combination of bulk density, mean environmental temperature, and moisture content (144 total readings).

It should also be noted that the thermal conductivity was measured with respect to the directional orientation of the probe within each bale. The bale orientation and the associated coordinates referenced in the current study are presented in Figure 5.3.6; with the lateral plane (formed by the x and y axes) parallel to the flake orientation. In contrast, the transverse direction (z-axis) represents the direction of bale compression which is perpendicular to the stem and flake orientation.

The current study only considers the thermal conductivity in relation to the two principal orientations (lateral and transverse). Under this general premise, both of the

lateral coordinates (x and y directions) are assumed to be equal to each other. The validity of this assumption is based on the apparently random angular orientation of stems within each layer (flake) of the bale. However, the transverse direction (z-axis) is assumed to represent a unique physical composition which is perpendicular to the stem orientation.

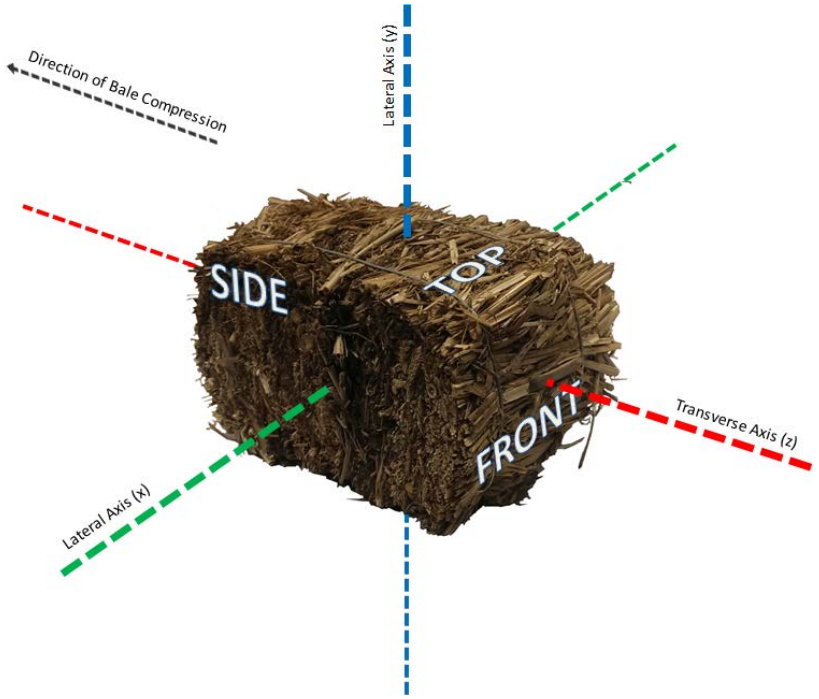

Figure 5.3.6 Directional components of switchgrass bales in line with the Cartesian coordinates.

The experimental setup of the dual thermal probe is shown in Fig 5.3.7. The thermal conductivity of the lateral orientation (x and y axes) was measured by inserting the dual thermal probe into the front surface of the bale. This measurement essentially accounts for the horizontal (x) and vertical (y) axes which are parallel to the stem orientation. Again, both lateral orientations are assumed to be equal to each other as similar heat transfer mechanisms are expected to occur in both of these directions. On the other hand, thermal conductivities perpendicular to the stems (z-direction) were indirectly evaluated by inserting the probe into the side surface of each bale. In this case, the measurements were impacted by a combination of the two distinct directional conductivities (y and z axes). As such, the evaluation of the transverse conductivities required a relationship between the two distinct directional conductivities and the measured combination.

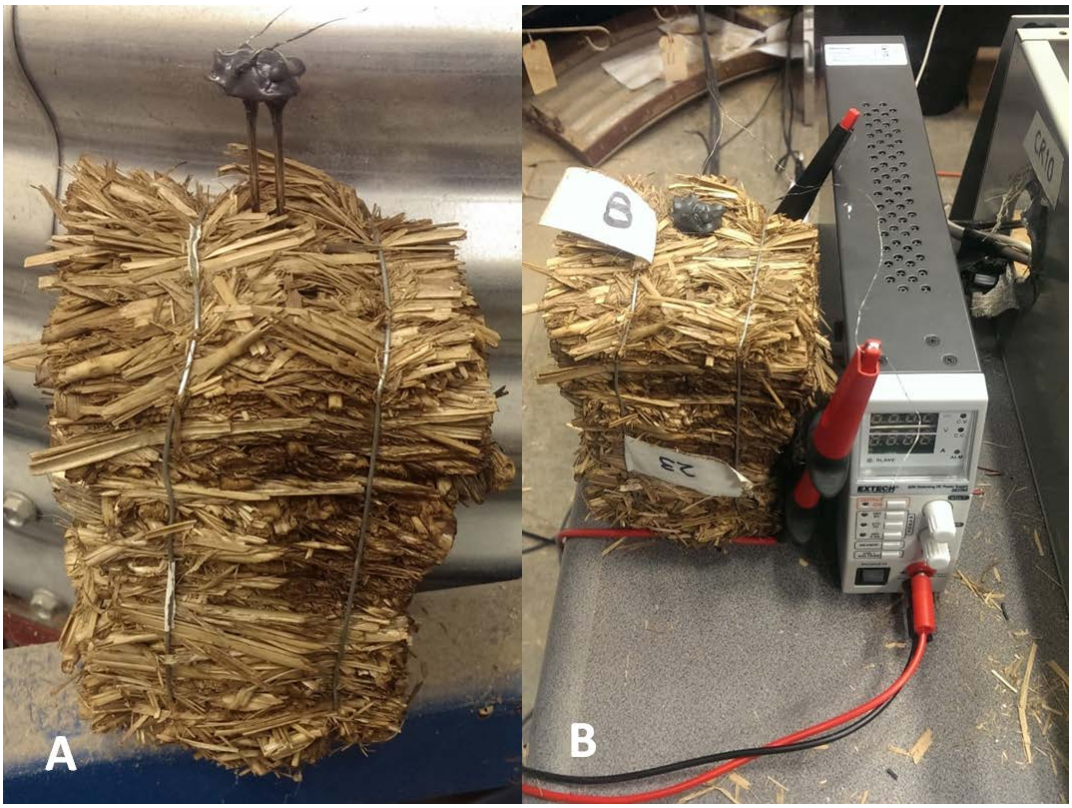

Figure 5.3.7 Experimental testing of the dual thermal probe in miniature bales of switchgrass. A) Insertion of the dual probe into a bale to measure the lateral direction; and B) connection of the voltage source to the heating wire.

5.3.5 Thermal Conductivity

Thermal conductivity was calculated from this data based on the line heat source method which considers the rate of heat conduction from an infinitely-long and infinitesimally-thin, cylindrical heating element (Lobo and Cohen, 1990). As such, this method is based on a long-time solution of the radial heat diffusion equation in accordance with Fourier's law. In this approach, a constant amount of heat (Q) is generated per unit length of the heating element over a relatively short time period. In this case, a linear relationship describes the temperature change (ΔT) in terms of the natural logarithm of the heating time (t) and the heat input (Q) is given as follows:

$$\Delta T = T_2 - T_1 = \frac{Q}{4\pi k} \ln\left(\frac{t_2}{t_1}\right) \qquad [5.3.1]$$

where: Q = heat input per length of the probe (W m^{-1}); k = thermal conductivity (W m^{-1} $°C^{-1}$); T = temperature (°C); t = time (s); and the subscripts 1 and 2 represent the initial and final state of the heating process, respectively.

The deviation of the current experimental setup from ideal conditions was also accounted for in the current study using a calibration constant. In this case, a probe calibration was performed through the evaluation of specific reference materials including distilled water with and without 1 % (w/b) agar at room temperature. A probe constant (C) was investigated according to this calibration procedure; with the actual value of the coefficient dependent on the characteristic properties of the reference material, as well as, those of the probe (Wang and Hayakawa, 1993). Modification of this fundamental relationship to incorporate the probe calibration yields (Lobo and Cohen, 1990):

$$\Delta T = T_2 - T_1 = \frac{CQ}{4\pi k} \ln\left(\frac{t_2}{t_1}\right) \quad [5.3.2]$$

This expression was rearranged and expressed in terms of the thermal conductivity as follows:

$$k = \frac{CQ}{4\pi(T_2 - T_1)} \ln\left(\frac{t_2}{t_1}\right) \quad [5.3.3a]$$

or by replacing $Q = I^2R$ according to Ohm's Law:

$$k = \frac{CI^2R}{4\pi(T_2 - T_1)} \ln\left(\frac{t_2}{t_1}\right) \quad [5.3.3b]$$

where: k = thermal conductivity (W m^{-1} $°C^{-1}$); C = probe calibration constant; I = current (A); and R = heater wire resistance (Ω m^{-1}).

Here, the calibration coefficient represents the relationship between the true (k_r) as measured (k_m) value of thermal conductivity of the reference material as follows:

$$k_r = Ck_m \quad [5.3.4]$$

In accordance with these calibration procedures, the thermal conductivity of distilled water with and without 1 % (w/v) agar were measured at several temperatures. The actual value of this calibration coefficient has been reported to depend on the characteristic properties of the probe with generally no temperature sensitivity (Lobo and Cohen, 1990). Measured values were compared with those previously reported in literature (Emami et al., 2007; Iroba, 2013; Singh and Heldman, 2009); while the percentage error was evaluated according to the following ratio (Fontana et al., 2001):

$$e_k = \frac{|k_r - k_m|}{k_r} \quad [5.3.5]$$

where: k = thermal conductivity (W m^{-1} °C^{-1}) for the reference value (r) and measured value (m) of the material, respectively.

The thermal conductivity of baled switchgrass was then measured and determined for each respective treatment using the calibrated formulation of the fundamental equation (5.3.3). The local slope (S) between the natural logarithm of time and the probe temperature was calculated from the collected data points of each treatment using linear regression analysis:

$$S = \frac{(T_2 - T_1)}{\ln(t_2/t_1)} \quad [5.3.6]$$

where: S = slope (°C) which was determined successively for each treatment. Substitution of the slope term into Equation 5.3.3 yields:

$$k = \frac{I^2 R}{4\pi S} = \frac{Q}{4\pi A} \quad [5.3.7]$$

Each measurement was performed for a total of 4 min (240 sec) with the probe temperature rise between 60 and 180 s considered in the least-squares best fit evaluation. The slope corresponding to the highest coefficient of determination (R^2) was used in

calculating the thermal conductivity while the maximum slope was used for those conductivity calculations involving the same R^2 values (Wang and Hayakawa, 1993).

The measured thermal conductivity (k_m) in either direction of a two-dimensional, anisotropic system can be expressed in terms of (Carslaw and Jaeger, 1959):

$$k_m = \frac{k_x + k_y}{k_y l^2 + k_x m^2} \quad [5.3.8]$$

where: l and m indicate the directional cosines in relation to the principal axes; while k_x and k_y represent the principal thermal conductivities. Integration of the measured thermal conductivity expression over one symmetric quadrant follows as:

$$k_r = \frac{2}{r}\int_0^{\pi/2} \frac{k_x + k_y}{k_y \cos^2\theta + k_x \sin^2\theta} d\theta \quad [5.3.9]$$

Integration of this expression results in the following:

$$k_r = \frac{2}{\pi}\sqrt{k_x k_y}\left[\tan^{-1}\left(\frac{k_x}{k_y}\tan\theta\right)\right]_0^{\pi/2} \quad [5.3.10]$$

Upon substitution of the limits of integration, the expression may be simplified as:

$$k_r = \sqrt{k_x k_y} \quad [5.3.11]$$

Thus, the perpendicular conductivity can be evaluated based on the known lateral (parallel) conductivity and the combined conductivity according to the following expression which was developed for orthogonal anisotropic materials (Takegoshi et al., 1982; Woodside, 1959) such as baled burley tobacco (Casada and Walton, 1989):

$$k_{per} = \frac{k_{comb}^2}{k_{par}} \quad [5.3.12]$$

where: k = thermal conductivity (W m^{-1} °C^{-1}); and the subscripts per, par and comb represent the perpendicular, parallel, and combination orientation. Hence, Equation 5.3.7 directly provided as assessment of the parallel conductivities, while Equation 5.3.12 was used to evaluate the perpendicular conductivities.

5.3.6 Thermal Diffusivity

Thermal diffusivity was determined according to the following expression (Nix et al., 1967):

$$\Delta T = \frac{I^2 R}{2\pi k}\left(-\frac{C_e}{2} - \ln\beta + \frac{\beta^2}{2*1!} - \frac{\beta^4}{4*2!} + \cdots\right) \quad [5.3.13]$$

where: ΔT = temperature rise measured at a specified distance from the heater probe (°C); C_e = Euler-Mascheroni constant (0.5772156649); and β = dimensionless coefficient defined as:

$$\beta = \frac{r}{2\sqrt{\alpha t}} \quad [5.3.14]$$

where: r = radial distance between the probes (m); t = heating time (s); and α = thermal diffusivity (m^2 s^{-1}).

The thermal diffusivity of each miniature bale treatment was evaluated using the data points that were obtained throughout the heating process (from approximately 60 to 180 sec) according to the aforementioned equation. The heating time was used to estimate the β coefficient at each data point based on an assumed value of the thermal diffusivity. This estimation of the β coefficient was then used to calculate the temperature rise at each data point. The differences between the measured and calculated values of the temperature rise were then summed for all data points. The results were subsequently analyzed using the Goal Seek Add-In (Microsoft Excel, Microsoft Corp., Redmond, WA). The thermal diffusivity of each particular treatment was evaluated according to the final summation.

5.3.7 Specific Heat

The specific heat of each miniature bales was also estimated according to the indirect method (Singh and Heldman, 2009; Yang et al., 2002) with the application of the fundamental thermophysical relationship:

$$C_p = \frac{k}{\rho\alpha} \qquad [5.3.15]$$

where: C_p = specific heat (J kg^{-1} °C^{-1}); k = thermal conductivity (W m^{-1} °C^{-1}); α = thermal diffusivity (m^2 s^{-1}); and ρ = density (kg m^{-3}).

Since the specific heat was calculated as a secondary quantity, the estimation uncertainty of this parameter was considered with regards to the uncertainties of the primary (measured) quantities including thermal conductivity, thermal diffusivity and bulk density. The uncertainty associated with the specific heat evaluation (ω_{C_p}) was calculated by (Huggins, 1983; Ma et al., 1998):

$$\omega_{C_p} = \sqrt{\left(\frac{\delta_{C_p}}{\delta_k}\omega_k\right)^2 + \left(\frac{\delta_{C_p}}{\delta_\alpha}\omega_\alpha\right)^2 + \left(\frac{\delta_{C_p}}{\delta_\rho}\omega_{\rho_b}\right)^2} \qquad [5.3.16]$$

where: ω_k, ω_α and ω_{ρ_b} = uncertainty of thermal conductivity, thermal diffusivity and bulk density, respectively. Each error term was first replaced according to the following thermophysical equalities:

$$\frac{\delta_{C_p}}{\delta_k}\omega_k = \frac{1}{\alpha\rho}\omega_k \qquad [5.3.17a]$$

$$\frac{\delta_{C_p}}{\delta_\alpha}\omega_\alpha = \frac{k}{\alpha^2\rho}\omega_\alpha \qquad [5.3.17b]$$

$$\frac{\delta_{C_p}}{\delta_\rho}\omega_\rho = \frac{k}{\alpha\rho^2}\omega_\rho \qquad [5.3.17c]$$

Substituting these equalities into the uncertainty equation (5.3.16) yields:

$$\omega_{C_p} = \sqrt{\left(\frac{1}{\alpha\rho}\omega_k\right)^2 + \left(\frac{k}{\alpha^2\rho}\omega_\alpha\right)^2 + \left(\frac{k}{\alpha\rho^2}\omega_\rho\right)^2} \quad [5.3.18]$$

In this case, the uncertainty of the specific heat (ω_{C_p}) was evaluated at three temperature levels (20, 30 and 40 °C), four bulk density levels (150, 175, 200, and 225 kg m^{-3}), and four moisture content levels (10, 20, 30 and 40 %-wb).

These indirect estimates of specific heat were also compared to previously reported values of dried, ground switchgrass (200 μm) obtained by differential scanning calorimeter techniques between 313 and 353 K (Dupont et al., 2014). These previously reported values were adjusted using the method of indirect mixtures (Rodriguez et al., 1995) which considers the influence of the moisture content with the inclusion of the specific heat of water (Cp_w) and air (Cp_a) in terms of the relative weight fractions of each constituent:

$$Cp = Cp_w X_w + Cp_a X_a + Cp_s(1 - X_w) \quad [5.3.19]$$

where: Cp = total specific heat (J kg^{-1} °C^{-1}); X = weight fraction (%-wb); as correlated to the porosity of each bale; and the subscripts w, s and a represent the properties of the water, dry switchgrass, and air respectively. Linear regression techniques were then applied to this adjusted data to obtain an overall expression of the specific heat of switchgrass as a function of the temperature, moisture content and density. The resulting model was then used to validate the values of specific heat that were estimated in the current study based on the dual probe method.

5.3.8 Statistical Analysis

The experimental data was analyzed using analysis of variance (ANOVA) at a 5 % significance level (SAS Version 9.3, Cary, NC). A multiple regression analysis was conducted in accordance with this assessment for each thermophysical parameter in terms of the initial temperature, moisture content, bulk density, and direction of heat flow

(lateral or transverse orientation) with three replications. Differences among means were determined according to Duncan's new multiple range test; while least-squares techniques were used to develop best fit regression equations.

5.3.9 Validation Tests

Additional bales were also removed from long-term storage and prepared for further storage-based experiments aimed at the validation of these thermophysical properties. A summary of the different storage evaluations conducted in this study are summarized in Figure 5.3.8 including this assessment of the thermophysical properties. The weight and physical dimensions of each small, rectangular bale (~102 x 46 x 36 cm) were measured; while the bulk density was determined as the mass to volume ratio of each bale. An estimate of the initial moisture content was also determined from three replicate bales from storage. Three subsamples were extracted from each of these replicate bales using a 5.08 cm steel feedstock probe with a serrated tip. All subsamples were oven-dried at 103 ± 1 °C for 24 h, according to standard S358.2 (ASABE Standards, 2006). The initial and final mass of each subsample was measured by weighing scale and used to calculate the average moisture content of the bales used in these validation experiments. The average initial moisture content of the switchgrass was determined to be 8.3 %-wb which was considered to be sufficiently low in terms of achieving minimal microbial growth and/or heat generation.

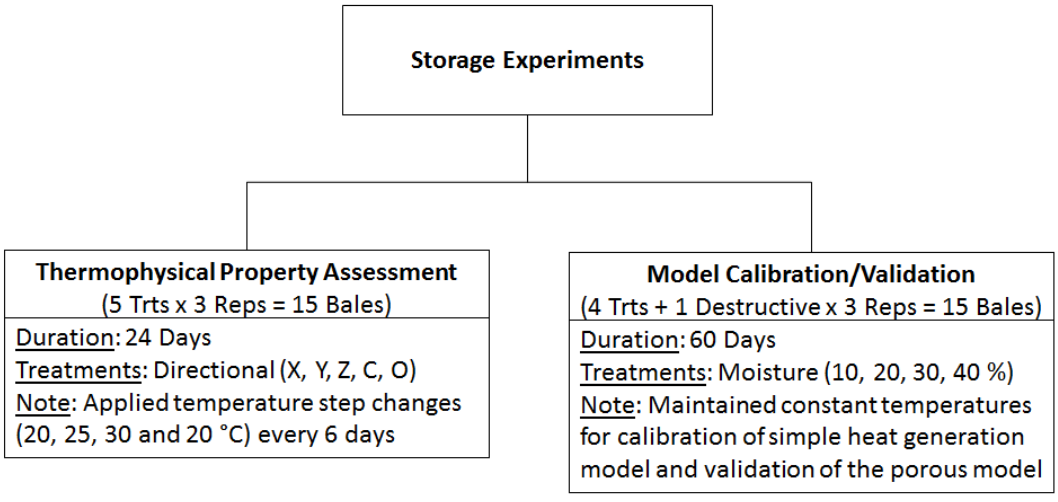

Figure 5.3.8 Summary of the different storage experiments that were performed in this study including the thermophysical property assessment and the model calibration/validation.

5.3.9.1 One-Dimensional Heat Transfer during Storage

The primary variable associated with this validation storage study was the direction of heat flow; which was either lateral (x and y axes) or transverse (z-axis) in relation to the stem/flake orientation (see Figure 5.3.6). One-directional heat transfer was achieved in respect to each of these directional orientations by applying two inches of low-pressure spray polyurethane foam (Handi-Foam Quick Cure, SPF-P10749, Fomo Products, Inc., Norton, OH) to specific surfaces of each bale. The application of this foam insulation was intended and assumed to effectively prevent the occurrence of heat and mass transfer on the covered surfaces of the bale, while allowing heat and mass transfer to occur on the exposed surfaces. This assumption was based on an assessment that 90 % heat resistance could be achieved with only 1.01 inches of foam under the experimental conditions considered in the current study.

All directional treatments were prepared according to the specific surface coverage necessary as shown in Figure 5.3.9. An additional treatment was also covered completely in foam on all surfaces (i.e., control) to effectively prevent heat and mass transfer with the surrounding environment. Another treatment was also left completely exposed to the environment with no spray foam application. In this case, heat and mass transfer were possible in all directions (x, y and z). Three replicate bales were prepared for each of these treatments; thereby, a total of 15 bales used in the storage validation experiments.

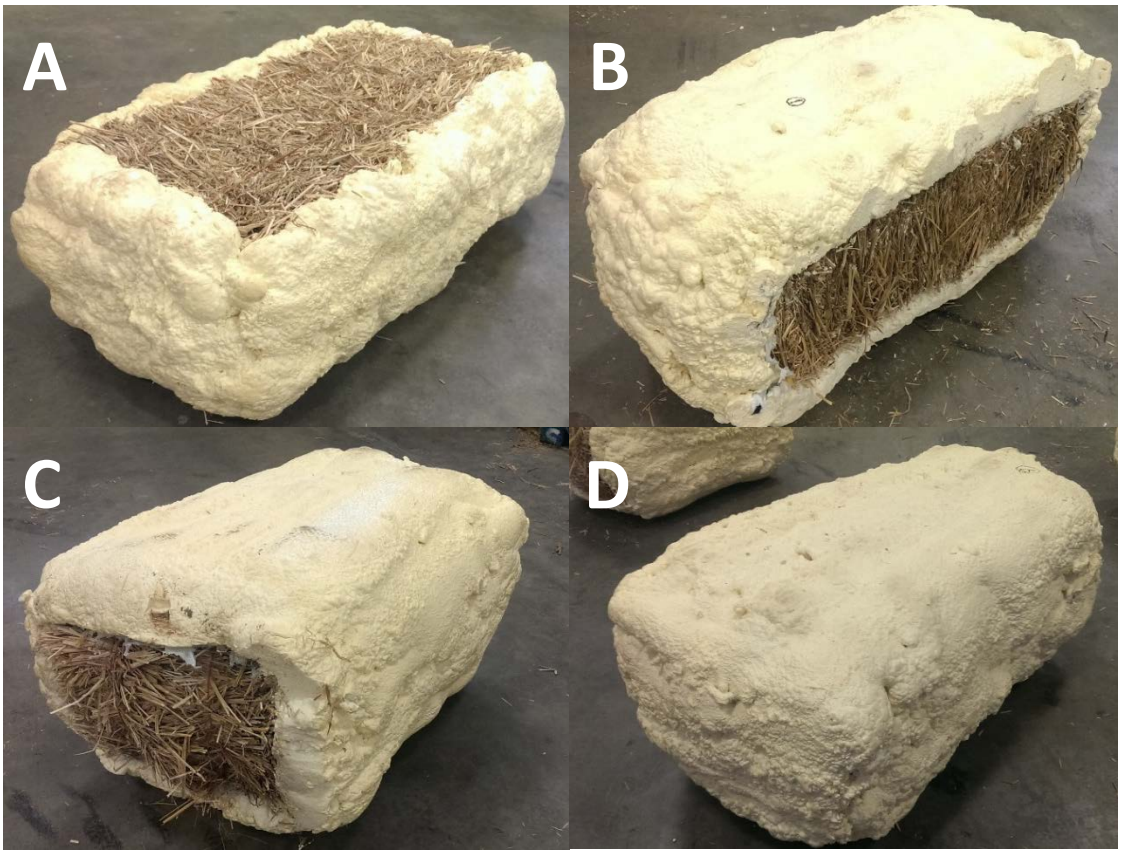

Figure 5.3.9 Spray foam application applied to prevent heat and mass transfer from respective surfaces of each bale treatment. (A) Treatment Y with the top and bottom surface exposed; (B) treatment X with the left and right surface exposed; (C) treatment Z with the front and back surface exposed; and (D) treatment C with no exposed surfaces.

5.3.9.2 Storage Layout

The bales were stored in a controlled environment chamber for 24 days on metal wire shelving arranged in three rows (replications) and elevated approximately 91 cm (36 inches) above the floor. The different treatments (directional orientations) were randomly assigned positions within their respective replication (row of bales) following a randomized block design. The bales within each row were generally spaced an average of 10.2 to 15.2 cm (4 to 6 in) apart; while each row of bales was spaced an average of 13.34 to 21.0 cm (5.25 To 8.25 in) apart. This specific storage layout is depicted in Figure 5.3.10; where the different treatments are denoted by X, Y, Z, C, and O for directional heat transfer in the x, y, and z axes, fully closed bale (spray foam on all sides), and fully open bale (no spray foam applied), respectively. Likewise, the R1-R3 denotations represent the three replications performed.

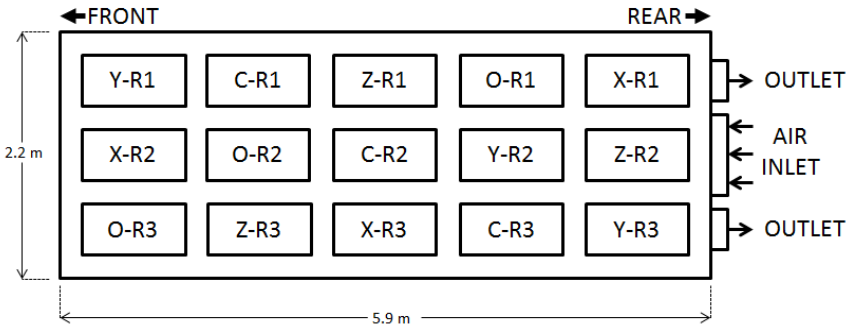

Figure 5.3.10 Storage layout for spray foam bales (treatments are heat transfer in X, Y, and Z directions, control (C), and open (O) with replicates noted as R1, R2, and R3).

A 30.5 cm (12 in) flexible air duct was extended through the lower central region of the environmental chamber at a height of 24.1 cm (9.5 in) above the floor; and with 7.6 cm (3 in) diameter outlets installed on both horizontal sides along its entire length to improve the uniform distribution of air throughout the chamber. These outlets were installed at intervals of approximately 91.4 cm (36 inches). It should also be noted that both of the 30.5 cm (12 in), square outlets for the environmental control chamber were positioned at the top rear of the room. The air inlet and outlet positions helped to ensure sufficient air circulation throughout the chamber as the incoming air was directed evenly through the central duct, before exhausting through the rear of the chamber.

5.3.9.3 Storage Procedure

The environmental chamber was initially maintained at a constant target temperature of 20 °C for 6 days; while the relative humidity was maintained at the corresponding equilibrium condition of 40.4 %, based on the sorption isotherm of 8-mm milled switchgrass (Godbolt et al., 2013). The moisture exchange between the bale and the surrounding air within the environmental chamber was assumed to be effectively prevented. A distinct series of step changes were then applied to the temperature and relative humidity of the chamber throughout the remainder of the 24 day storage period. In this manner, the temperature and relative humidity of the environmental chamber were adjusted every 6 days in order to attain progressive temperatures of 25, 30, and 20 °C along with the corresponding equilibrium relative humidity levels of 46.2, 51.3, and 40.4 %, respectively that limited moisture transfer.

5.3.9.4 Storage Measurements

Bales were weighed within several hours of foam application, as well as, on days 6, 12, 18 and 24 of the storage experiment. Three type-E thermocouples (24 AWG, Omega Engineering, Inc., Atlanta, GA) were inserted into each bale using rigid, 3.175 mm (1/8 in)-diameter, high-density polyethylene welding rods (Seelye Acquisitions, Inc., Ocoee, FL) which have improved tensile strength and the ability to continuously resist heat transfer up to temperatures of approximately 110 to 120 °C.

The thermocouples were positioned diagonally through each bale with a low (~13 cm above the bottom surface), central (centered with the height) and upper position (~13 cm below the top surface) for each treatment. The thermocouples were imbedded to three depths (~ 11, 23, and 34 cm) at three different distances on the side wall of each bale (~ 13, 51, and 89 cm) as shown in Figure 5.3.11. This measurement scheme allowed uniformity in measurement across the different treatments while accounting for any positional variation which could occur.

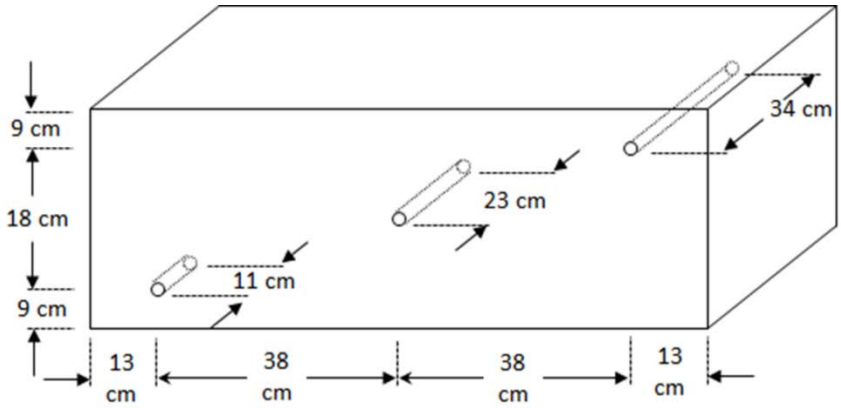

Figure 5.3.11 Thermocouple positioning schematic shown in all three perspectives.

Air temperature was also monitored at three vertical heights (low, middle, and high) and three horizontal positions (front, center, and rear) within the environmental chamber. These thermocouples were generally positioned 46 cm (18 in) from the walls of the environmental chamber for the relevant peripheral positions. Hence, this measurement scheme required a total of nine air temperature positions for each measurement interval. An additional relative humidity probe (CS500-L, Campbell Scientific, Logan, UT) was also positioned centrally within the chamber. Thermocouple

and relative humidity measurements were scanned and recorded to a datalogger (CR10, Campbell Scientific, Inc., Logan, UT) every 5 minutes.

The experimental data was averaged to provide a mean daily temperature for each treatment; further reducing the error caused by random variation. The resulting 60 data points represented the mean daily treatment temperatures recorded at each thermocouple location. This temperature data was subsequently used to determine the thermal diffusivity for each treatment based on a simple conduction model as presented in section 5.4.1. In this case, the heat generation (within the material) and the moisture transfer (between the environment and the material) were both considered negligible. The application of this simple conduction model was assumed to provide average (constant) approximate values of the thermal diffusivity in each directional orientation. These results were compared with those values determined by the dual thermal probe.

5.4 Numerical Analysis

An analytical solution to the heat and mass transfer model proposed in Chapter 4 was not feasible due to the complexity and interdependency of the characteristic variables. Therefore, a numerical solution was undertaken in the current study using the explicit finite difference method which is described here in terms of the baled, rectangular format of switchgrass; while accounting for the potential variation in material properties. Figure 5.4.1 represents the two-dimensional, rectangular cross-section of the switchgrass bale. The calculation domain was considered symmetric about the y axis so only half of the x domain was calculated; thereby, decreasing the number calculations needed for obtaining a solution.

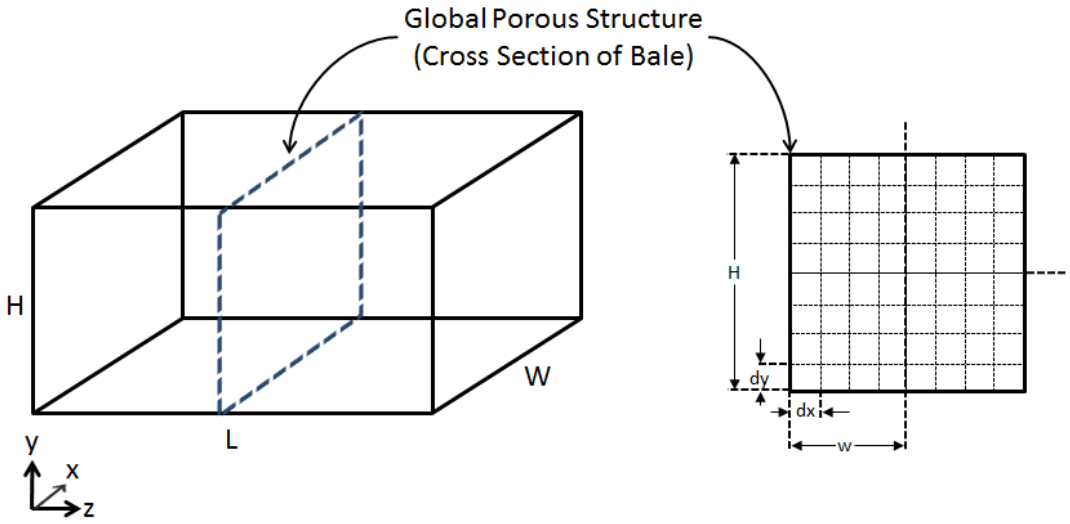

Figure 5.4.1 Finite difference model of an individual bale of switchgrass.

The surrounding air was assumed to have uniform temperature (T_a) and relative humidity (RH_a) which was in contact with the exposed porous boundaries on all three sides of the domain with the center line insulated. The convective heat transfer coefficient on all exposed sides was assumed to be equal. The resulting finite difference equation for each component of the proposed model (see Chapter 4) was developed by applying the principles of mass and energy conservation to small control volumes formed by the discretized domain. In the first analysis presented here, heat transfer within the bales was assumed to be entirely by conduction (section 5.4.1). This simple model provided a

baseline analysis and framework for ongoing model development. This conduction model also served as a validation of the thermophysical properties evaluated by the dual probe method (see section 5.3.9). The next case involves heat transfer occurring by the coupled mechanisms of conduction and convection (natural) as presented in Chapter 4 of this study.

5.4.1 Conduction Model

The first numerical analysis considered in this study involved heat transfer within baled switchgrass occurring entirely by conduction. For interior points of this baseline conductivity model, the source of heat was only by conductive transfer from neighboring control volumes; while points along the outside edge included an additional convection heat source (or sink) to the ambient air. In this case, natural convection boundary conditions were assumed at all exposed surfaces; while the center of the domain was considered insulated due to symmetry. The general form of the conductive model is:

$$\rho Cp\frac{\delta T}{\delta t} = k_x\frac{\delta^2 T}{\delta x^2} + k_y\frac{\delta^2 T}{\delta y^2} + \frac{h}{\delta n}(T_a - T) + G \qquad [5.4.1a]$$

or,

$$\frac{\delta T}{\delta t} = \alpha_x\frac{\delta^2 T}{\delta x^2} + \alpha_y\frac{\delta^2 T}{\delta y^2} + h\frac{\alpha_{x,y}}{k_{x,y}\delta n}(T_a - T) + G\frac{\alpha_{avg}}{k_{avg}} \qquad [5.4.1b]$$

where: Cp = specific heat (J kg^{-1} K^{-1}); k = thermal conductivity (W m^{-1} K^{-1}); T = temperature (K); ρ = density (kg m^{-3}); h = convective heat transfer coefficient (W m^{-2} K^{-1}); G = heat generation (W m^{-3}); α = thermal diffusivity (m^2 s^{-1}); and the subscripts a, n, x, y and avg represent those conditions related to the ambient, normal-to-surface, x-direction, y-direction and average of both directions, respectively. The heat transfer coefficient appearing in the convective term of this simple model depends on the surface of interest and the associated direction of heat transfer (see appendix A).

5.4.1.1 Finite Difference Method

Applying the principles of energy conservation to a two-dimensional control volume within the specified global domain led to the following explicit equations. Only the left half of the domain was considered in this analysis with symmetry assumed to exist along the axial center line. It may be also noted that at this point the convection term was omitted in the evaluation of the interior points.

- Interior points (x≠0; x≠w; y≠0; y≠H):

$$T_{i,j}^{n+1} = \left(\frac{\alpha_x^n \Delta t}{\Delta x^2}\right)\left(T_{i+1,j}^n + T_{i-1,j}^n - 2T_{i,j}^n\right) + \left(\frac{\alpha_y^n \Delta t}{\Delta y^2}\right)\left(T_{i,j+1}^n + T_{i,j-1}^n - 2T_{i,j}^n\right) + \left(\frac{\alpha_{avg}^n \Delta t}{k_{avg}^n}\right) G_{i,j}^n + T_{i,j}^n \quad [5.4.2a]$$

Similar expressions were also developed for those nodal positions along the symmetrical center line of the domain, as well as, the nodes along the external boundaries of the domain with the inclusion of heat convection as follows:

- Left edge points, external boundary (x=0; y≠0; y≠H):

$$T_{i,j}^{n+1} = 2\left(\frac{\alpha_x^n \Delta t}{\Delta x^2}\right)\left(T_{i+1,j}^n - T_{i,j}^n\right) + \left(\frac{\alpha_y^n \Delta t}{\Delta y^2}\right)\left(T_{i,j+1}^n + T_{i,j-1}^n - 2T_{i,j}^n\right) + \frac{\alpha_x^n \Delta t}{k_x^n \Delta x} h_{L_{i,j}}^n \left(T_a^n - T_{i,j}^n\right) + G_{i,j}^n \left(\frac{\alpha_{avg}^n \Delta t}{k_{avg}^n}\right) + T_{i,j}^n \quad [5.4.2b]$$

- Right edge points, symmetrical center line (x=w; y≠0; y≠H):

$$T_{i,j}^{n+1} = 2\left(\frac{\alpha_x^n \Delta t}{\Delta x^2}\right)\left(T_{i-1,j}^n - T_{i,j}^n\right) + \left(\frac{\alpha_y^n \Delta t}{\Delta y^2}\right)\left(T_{i,j+1}^n + T_{i,j-1}^n - 2T_{i,j}^n\right) + G_{i,j}^n \left(\frac{\alpha_{avg}^n \Delta t}{k_{avg}^n}\right) + T_{i,j}^n \quad [5.4.2c]$$

- Bottom edge points (x≠0; x≠w; y=0):

$$T_{i,j}^{n+1} = \left(\frac{\alpha_x^n \Delta t}{\Delta x^2}\right)\left(T_{i+1,j}^n + T_{i-1,j}^n - 2T_{i,j}^n\right) + 2\left(\frac{\alpha_y^n \Delta t}{\Delta y^2}\right)\left(T_{i,j+1}^n - T_{i,j}^n\right) + \frac{\alpha_y \Delta t}{k_y^n \Delta y} h_{B_{i,j}}^n \left(T_a^n - T_{i,j}^n\right) + G_{i,j}^n \left(\frac{\alpha_{avg}^n \Delta t}{k_{avg}^n}\right) + T_{i,j}^n \quad [5.4.2d]$$

- Top edge points (x≠0; x≠w; y=H):

$$T_{i,j}^{n+1} = \left(\frac{\alpha_x^n \Delta t}{\Delta x^2}\right)\left(T_{i+1,j}^n + T_{i-1,j}^n - 2T_{i,j}^n\right) + 2\left(\frac{\alpha_y^n \Delta t}{\Delta y^2}\right)\left(T_{i,j-1}^n - T_{i,j}^n\right) + \frac{\alpha_y \Delta t}{k_y^n \Delta y} h_{T_{i,j}}^{\ n}\left(T_a^n - T_{i,j}^n\right) + G_{i,j}^n \left(\frac{\alpha_{avg}^n \Delta t}{k_{avg}^n}\right) + T_{i,j}^n \quad [5.4.2e]$$

- Bottom left corner (x=0; y=0):

$$T_{i,j}^{n+1} = 2\left(\frac{\alpha_x^n \Delta t}{\Delta x^2}\right)\left(T_{i+1,j}^n - T_{i,j}^n\right) + 2\left(\frac{\alpha_y^n \Delta t}{\Delta y^2}\right)\left(T_{i,j+1}^n - T_{i,j}^n\right) + \frac{\alpha_x^n \Delta t}{k_x^n \Delta x} h_{L_{i,j}}^{\ n}\left(T_a^n - T_{i,j}^n\right) + \frac{\alpha_y^n \Delta t}{k_y^n \Delta x} h_{B_{i,j}}^{\ n}\left(T_a - T_{i,j}^n\right) + G_{i,j}^n \left(\frac{\alpha_{avg}^n \Delta t}{k_{avg}^n}\right) + T_{i,j}^n \quad [5.4.2f]$$

- Top left corner (x=0; y=H):

$$T_{i,j}^{n+1} = 2\left(\frac{\alpha_x^n \Delta t}{\Delta x^2}\right)\left(T_{i+1,j}^n - T_{i,j}^n\right) + 2\left(\frac{\alpha_y^n \Delta t}{\Delta y^2}\right)\left(T_{i,j-1}^n - T_{i,j}^n\right) + \frac{\alpha_x^n \Delta t}{k_x^n \Delta x} h_{L_{i,j}}^{\ n}\left(T_a^n - T_{i,j}^n\right) + \frac{\alpha_y^n \Delta t}{k_y^n \Delta x} h_{T_{i,j}}^{\ n}\left(T_a - T_{i,j}^n\right) + G_{i,j}^n \left(\frac{\alpha_{avg}^n \Delta t}{k_{avg}^n}\right) + T_{i,j}^n \quad [5.4.2g]$$

- Bottom right corner (x=w; y=0):

$$T_{i,j}^{n+1} = 2\left(\frac{\alpha_x^n \Delta t}{\Delta x^2}\right)\left(T_{i-1,j}^n - T_{i,j}^n\right) + 2\left(\frac{\alpha_y^n \Delta t}{\Delta y^2}\right)\left(T_{i,j+1}^n - T_{i,j}^n\right) + \frac{\alpha_x^n \Delta t}{k_x^n \Delta x} h_{R_{i,j}}^{\ n}\left(T_a^n - T_{i,j}^n\right) + \frac{\alpha_y^n \Delta t}{k_y^n \Delta x} h_{B_{i,j}}^{\ n}\left(T_a - T_{i,j}^n\right) + G_{i,j}^n \left(\frac{\alpha_{avg}^n \Delta t}{k_{avg}^n}\right) + T_{i,j}^n \quad [5.4.2h]$$

- Top right corner (x=w; y=H):

$$T_{i,j}^{n+1} = 2\left(\frac{\alpha_x^n \Delta t}{\Delta x^2}\right)\left(T_{i-1,j}^n - T_{i,j}^n\right) + 2\left(\frac{\alpha_y^n \Delta t}{\Delta y^2}\right)\left(T_{i,j-1}^n - T_{i,j}^n\right) + \frac{\alpha_x^n \Delta t}{k_x^n \Delta x} h_{R_{i,j}}^{\ n}\left(T_a^n - T_{i,j}^n\right) + \frac{\alpha_y^n \Delta t}{k_y^n \Delta x} h_{T_{i,j}}^{\ n}\left(T_a - T_{i,j}^n\right) + G_{i,j}^n \left(\frac{\alpha_{avg}^n \Delta t}{k_{avg}^n}\right) + T_{i,j}^n \quad [5.4.2i]$$

where: $T_{i,j}^n$ = temperature (K) at x node i, y node j, and time step of n; h = convective heat transfer coefficient (W m^{-2} K^{-1}); G = heat generation rate (W m^{-3}); T_a = ambient temperature (K); Δt = time increment (s); Δx and Δy = grid length increments (m); k = thermal conductivity (W m^{-1} K^{-1}); α = thermal diffusivity (m^2 s^{-1}); and the subscripts L,

R, T and B represent the conditions at the left, right, top and bottom surface of the domain, respectively.

Density variations were assumed to be caused solely by the loss in moisture. That is, dry matter density was assumed to remain constant; although this assumption may not be entirely correct as some dry matter losses and settling could occur (particularly in wetter treatments). However, the effects of settling and dry matter loss were generally expected to offset one another and was beyond the scope of this study.

5.4.1.2 Thin-Layer Drying Equation

The moisture content was assumed to change exponentially over time based on the thin-layer drying equation from Khanchi et al. (2013):

$$\mathrm{MR} = \frac{\mathrm{M_t} - \mathrm{M_e}}{\mathrm{M_0} - \mathrm{M_e}} = \mathrm{e}^{-kt} \qquad [4.28]$$

where: MR = moisture ratio (-); M = moisture content (%); k = drying rate constant (s^{-1}); t = time (s); and the subscripts 0, t and e represent the initial, moisture at time t and equilibrium values, respectively. In this case, the finite difference analysis yields:

$$\mathrm{M}_{\mathrm{i,j}}^{\mathrm{n+1}} = \left(\mathrm{M}_{\mathrm{i,j}}^{\mathrm{n}} - \mathrm{M}_{\mathrm{e}_{\mathrm{i,j}}}^{\mathrm{n}}\right) \mathrm{e}^{-k_{\mathrm{i,j}}\Delta \mathrm{t}} + \mathrm{M}_{\mathrm{e}_{\mathrm{i,j}}}^{\mathrm{n}} \qquad [5.4.3]$$

In the case of this simple conductive model, the value of the exponential constant for each treatment was determined based on the moisture content measured during the storage experiment (see section 5.4.5).

5.4.1.3 Model Parameters

Grid length increments for the x- and y-axes (dx and dy) were allowed to differ from each other to allow more flexibility in evaluating the distinct length scales in each principle direction. The Δx and Δy grid increments were set as 1.524 and 1.905 cm; respectively, since smaller grid sizes (Δx = 0.460 cm; Δy = 0.575 cm) only resulted in minimal changes in the predicted temperature profile. Increasing the grid increments above these values, however, was observed to cause significant differences in the

temperature profile. The time increment (Δt) was set at 0.5 hr, which provided a stable solution under the proposed conditions. The evaluation of the heat transfer coefficient for this conductive model is detailed in Appendix A.

The thermal conductivity and thermal diffusivity of the bulk material was evaluated based on the statistical analysis of experimental data collected from the dual thermal probe analysis (see sections 5.3 and 6.3). In the present case, both lateral orientations (x and y) were observed to have a similar structural composition. Hence, it was assumed that the thermal conductivity in both directions were equivalent ($k_x = k_y$). Although the transverse bale orientation (z) exhibited a statistical difference in terms of these thermophysical properties, this model was limited to the two lateral orientations based on the proposed two-dimensional domain. The implementation of the thermophysical properties involved a functional dependency on the temperature, moisture content and dry basis density based on the statistical analysis and corresponding empirical equations described in section 6.3.

5.4.1.4 Heat Generation Rate

The heat conduction equation (5.4.1) was solved in terms of the heat generation rate as follows:

$$G = \rho Cp \frac{\delta T}{\delta t} - k_x \frac{\delta^2 T}{\delta x^2} - k_y \frac{\delta^2 T}{\delta y^2} - \frac{h}{\delta n}(T_a - T) \qquad [5.4.4]$$

or, in terms of the finite difference method:

$$G_{i,j}^n = \left(\frac{k_{avg}^n}{\alpha_{avg}^n \Delta t}\right)\left(T_{i,j}^{n+1} - T_{i,j}^n\right) - \left(\frac{k_x^n \Delta t}{\Delta x^2}\right)\left(T_{i+1,j}^n + T_{i-1,j}^n - 2T_{i,j}^n\right) - \left(\frac{k_y^n \Delta t}{\Delta y^2}\right)\left(T_{i,j+1}^n + T_{i,j-1}^n - 2T_{i,j}^n\right) - \frac{h_{i,j}^n}{\Delta n}\left(T_a^n - T_{i,j}^n\right) \qquad [5.4.5]$$

where: G = heat generation rate (W m^{-3}); T = temperature (K); Δt = time increment (s); k = thermal conductivity (W m^{-1} K^1); α = thermal diffusivity (m^2 s^{-1}); the subscripts i and j represent the positional indexing for the x and y axes, respectively; the subscript n represents the normal-to-surface direction; and the superscripts n and n+1 represent the

current and ‘target’ conditions, respectively. The heat generation rate is the unknown variable in this analysis. Based on the target temperature (temperature measured at the next time step), the heat generation rate was calculated.

5.4.1.5 Solution Scheme

Figure 5.4.2 shows the numerical procedure that was used in this study for evaluating the heat generation rate which follows a similar procedure to that presented by Buckmaster (1986). According to this procedure, the heat generation rate was calculated at a given time using Equation 5.4.5, the immediate past temperatures ($T_{i,j}^{n}$, $T_{i-1,j}^{n}$, $T_{i+1,j}^{n}$, $T_{i,j-1}^{n}$, $T_{i,j+1}^{n}$) and the ‘target’ temperature ($T_{i,j}^{n+1}$) for the next time step. In this case, past temperatures were assessed in accordance with the finite difference model using the heat generation rates corresponding to the previous time step. The experimental data provided target temperatures for the following time step. Thus, the heat generation rate was used to calculate new temperatures throughout the bale while the target temperatures for the next time step were adopted from the experimental data until the total simulation time of 60 days was reached. It should be noted, however, that an initial estimate of the heat generation rate was necessary to initiate this procedure.

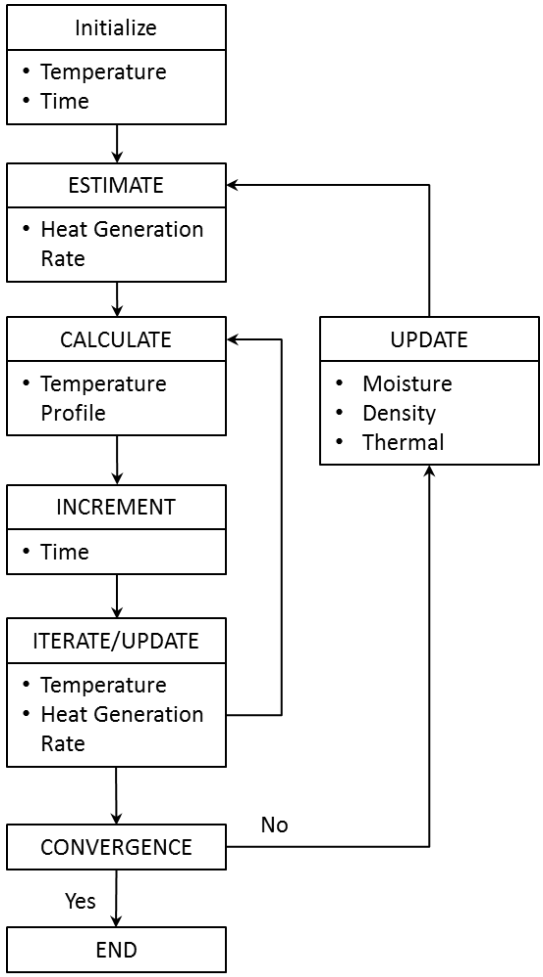

Figure 5.4.2 Procedural flowchart for estimating the heat generation rate (G) based on the simple conductive model over time.

More accurate methods of predicting unknown thermal characteristics (such as the heat generation rate) exist, but the curve form of how that specific property changes over time must be assumed from similar studies (Beck, 1977). Since the specific form of the heat generation curve was not known for the present case, the method described here was used. It was assumed that the error associated with this calculation procedure was relatively small compared to the variation in thermal properties within the bale. Parameter estimation also assumes that nodal conditions surrounding the 'target' node (i,j) remain constant over some time period.

5.4.1.6 Heat Generation Model

The sensible heat generation rate was also expressed as a function of the moisture content (%-wb) and storage time (days). This model was developed using 720 cases of temperature data (12 bales x 60 days) for varying moisture content and storage time. Nonlinear regression techniques were used in fitting an exponential model to this data with the heat generation rate serving as the dependent variable. The independent variables included moisture, storage time, interaction term (moisture*time), and the square and square root of each of these three terms. Although, temperature influenced the biological activity and subsequent heat generation, the temperature effect was excluded from the current model in order to simplify the estimation of mean heat generation under the proposed storage conditions.

5.4.2 Inner Domain

The analysis of the inner domain follows the model formulation presented in Chapter 4.

5.4.2.1 Mass Conservation

The general form of the mass conservation equation for the inner domain was given as:

$$\frac{\delta}{\delta x_I}\left[D_L \rho_s \frac{\delta M}{\delta x_I} + D_v\left(\varepsilon_I - \frac{\rho_s}{\rho_L} M\right)\frac{\delta \rho_{vI}}{\delta x_i}\right] = \rho_s\left(1 - \frac{\rho_{vI}}{\rho_L}\right)\frac{\delta M}{\delta t} + \left(\varepsilon_I - \frac{\rho_s}{\rho_L} M\right)\frac{\delta \rho_{vI}}{\delta t} \quad [4.10]$$

Solving this expression in terms of the change in vapor density with respect to time:

$$\frac{\delta \rho_{vI}}{\delta t} = \frac{\frac{\delta}{\delta x_I}\left[D_L \rho_s \frac{\delta M}{\delta x_I} + D_v\left(\varepsilon_I - \frac{\rho_s}{\rho_L} M\right)\frac{\delta \rho_{vI}}{\delta x_i}\right] - \rho_s\left(1 - \frac{\rho_{vI}}{\rho_L}\right)\frac{\delta M}{\delta t}}{\left(\varepsilon_I - \frac{\rho_s}{\rho_L} M\right)} \quad [5.4.6]$$

while the finite difference method yields the following components constituting this overall mass balance equation:

- Mass Liquid Flux:

$$MF = \frac{\rho_s}{\Delta x_I^2}\left[(MD_L)_{i+1}^n + (MD_L)_{i-1}^n - 2(MD_L)_i^n\right] \quad [5.4.7a]$$

- Diffusive Flux:

$$DF = \frac{\varepsilon_I}{\Delta x_I^2}\left[(\rho_{vI}D_v)_{i+1}^n + (\rho_{vI}D_v)_{i-1}^n - 2(\rho_{vI}D_v)_i^n\right] - \frac{\rho_s}{\rho_L \Delta x_I^2}\left[(\rho_{vI}D_v M)_{i+1}^n + (\rho_{vI}D_v M)_{i-1}^n - 2(\rho_{vI}D_v M)_i^n\right] \quad [5.4.7b]$$

- Moisture Content Change:

$$MC = \frac{\rho_s}{\rho_L \Delta t}\left[(\rho_{vI}M)_i^{n+1} - (\rho_{vI}M)_i^n\right] - \frac{\rho_s}{\Delta t}\left[M_i^{n+1} - M_i^n\right] \quad [5.4.7c]$$

The solution to the vapor density was then obtained by combining all of these different components into a single expression as follows:

$${\rho_{vI}}_i^{n+1} = \frac{(MF+DF+MC)\Delta t}{\left(\varepsilon_I - \frac{\rho_s}{\rho_L}M^{n+1}\right)} + \frac{\left(\varepsilon_I - \frac{\rho_s}{\rho_L}M^n\right)}{\left(\varepsilon_I - \frac{\rho_s}{\rho_L}M^{n+1}\right)}{\rho_{vI}}_i^n \quad [5.4.7d]$$

where: D_L = liquid conductivity ($m^2\ s^{-1}$); D_v = diffusion coefficient of water vapor in air ($m^2\ s^{-1}$); ε = porosity ($m^3\ m^{-3}$); M = moisture content, dm ($kg\ kg^{-1}$); ρ = density ($kg\ m^{-3}$); P = pressure ($N\ m^{-2}$); p = partial vapor pressure ($kg\ m^{-1}\ s^{-3}$); Δt = time increment (s); and Δx = grid length increment (m). The subscript I represents the inner domain characteristics; and the subscripts s, L and v represent the solid, liquid and vapor phase characteristics, respectively. A knowledge of the vapor pressure in the inner domain also allows for an analysis of the air properties within the inner domain based on relevant psychrometric relationships. Potential variations in the material properties were considered in this case.

5.4.2.2 Energy Conservation

The general form of the energy equation for the inner domain was given as:

$$\frac{\delta T_I}{\delta t} = \frac{S_T}{\rho_s Cp_s} + \frac{h_c}{\rho_s Cp_s}\frac{P_x}{A_x}(T_a - T_I) + \left\{\frac{\delta}{\delta x_I}\left[D_v\left(\varepsilon_I - \frac{\rho_s}{\rho_L}M\right)\frac{\delta \rho_{vI}}{\delta x_I}\right] - \frac{\delta}{\delta t}\left[\left(\varepsilon_I - \frac{\rho_s}{\rho_L}M\right)\rho_{vI}\right]\right\}\frac{L_v}{\rho_s Cp_s} + \alpha_s \frac{\delta^2 T_I}{\delta x_I^2} \quad [4.19]$$

while the finite difference method yields:

$$T_{I_i}^{n+1} = \frac{S_{T_i}^{n}\Delta t}{\rho_s Cp_{s_i}^{n}} + \frac{h_{c_i}^{n}\Delta t}{\rho_s Cp_{s_i}^{n}}\frac{P_x}{A_x}\left(T_a - T_{I_i}^{n}\right) + \frac{L_v D_v}{\rho_s Cp_{s_i}^{n}}\left(\varepsilon_I - \frac{\rho_s}{\rho_L}M\right)\left(\frac{1}{\Delta x_I^2}\right)\left(\rho_{vI_{i+1}}^{n} + \rho_{vI_{i-1}}^{n} - 2\rho_{vI_i}^{n}\right) + \frac{L_v}{\rho_s Cp_{s_i}^{n}}\left(\varepsilon_I - \frac{\rho_s}{\rho_L}M\right)\left(\frac{1}{\Delta t}\right)\left(\rho_{vI_i}^{n+1} - \rho_{vI_i}^{n}\right) + \frac{\alpha_s}{\Delta x_I^2}\left(T_{I_{i+1}}^{n} + T_{I_{i-1}}^{n} - 2T_{I_i}^{n}\right) + T_{I_i}^{n} \quad [5.4.8]$$

where: T = temperature (K); S_T = energy source (W m^{-3}); h_c = convective heat transfer coefficient (W m^{-2} K^{-1}); P_x = length of distance around an inner domain element (m); A_x = cross-sectional area of an inner domain element (m^2); L_v = latent heat of vaporization (J kg^{-1}); D_v = diffusion coefficient of water vapor in air (m^2 s^{-1}); ε = porosity (-); M = moisture content, dm (kg kg^{-1}); ρ = density (kg m^{-3}); α = thermal diffusivity (m^2 s^{-1}); Cp = specific heat (J kg^{-1} K^{-1}); Δt = time increment (s); and Δx = grid length increment (m).

The subscripts i and j represent the x and y node, respectively; the subscript I represents a characteristic of the inner domain; the superscript n represents the current time step; the subscripts a, v and s represent the characteristics of the ambient air, water vapor and solid phase, respectively. Again, the variation in material properties was considered in this formulation. The source term (S_T) for the inner domain was based on the aerobic respiration rate for switchgrass as discussed in the derivation of this source term are included in Appendix B.

5.4.2.3 Thin Layer Drying

The general form of the thin-layer drying model was given as:

$$MR = \frac{M_t - M_e}{M_0 - M_e} = e^{-kt} \quad [4.28]$$

while the finite difference method yields:

$$M_{i,j}^{n+1} = \left(M_{i,j}^{n} - M_{e_{i,j}}^{n}\right)e^{-k_{i,j}\Delta t} + M_{e_{i,j}}^{n} \quad [5.4.9]$$

where: MR = moisture ratio (-); M = moisture content (%); k = drying rate constant (s^{-1}); t = time (s); and the subscripts 0, t and e represent the initial, time step and equilibrium values, respectively. In this case, the equilibrium moisture content (M_e) was evaluated using the sorption isotherm of milled switchgrass (see section 4.2.5).

Further details regarding the implementation of this thin-layer drying model were outlined in section 4.2.5. Here, the drying coefficient (k) was expressed as a function of radiation, vapor pressure deficit, wind speed and moisture content according to the empirical equation (4.30) proposed by Khanchi et al. (2013). In this case, the radiation effect was considered negligible, the vapor pressure deficit was based on psychrometric relationships, wind speed was assumed as the average of the velocity components, and moisture content was applied directly.

5.4.2.4 Model Parameters

The density of the solid phase (ρ_s), density of the liquid phase (ρ_L), length of distance around an inner domain element (P_x), cross-sectional area of an inner domain element (A_x), inner domain porosity (ε_I), and grid length increment (Δx_I) were all assumed to be constant physical properties of the inner domain. The density of the solid phase was estimated as 437 kg m^{-3} based on the average particle density of switchgrass reported by Lam et al. (2007, 2008). The density of the liquid phase (water) was also assumed to be constant within the given temperature range with a value of 991.48 kg m^{-3}. The cross sectional area and distance around the inner domain element was based on the average stem diameter of switchgrass reported by Lam et al. (2007, 2008) as 2.698 mm, while the porosity of the inner domain was also assessed as:

$$\varepsilon_I = 1 - \frac{\rho_b}{\rho_s} \qquad [5.4.10]$$

where: ρ_b = bulk particle density which was taken as the average value reported by Lam et al. (2007, 2008) of 203 kg m^{-3}. In this case, the porosity of the inner domain was 0.535.

The grid length increment of the inner domain was approximately 2.1 mm. Likewise, the time increment (Δt) was set at a constant value of 0.5 hr as discussed and

implemented in the conduction model (see section 5.4.1.3). The derivation of the heat transfer coefficient for the inner domain is discussed in Appendix B; along with the other parameters appearing in this model of the inner domain.

5.4.3 Outer Domain

5.4.3.1 Mass Conservation (Dry Air)

The mass conservation of dry air for the outer domain was given as:

$$\frac{\delta}{\delta x}(\varepsilon V_x) + \frac{\delta}{\delta y}(\varepsilon V_y) = 0 \qquad [4.33]$$

Application of the finite difference method yields:

$$\frac{\left[(\varepsilon V_x)^n_{i+1,j} - (\varepsilon V_x)^n_{i-1,j}\right]}{2\Delta x} + \frac{\left[(\varepsilon V_y)^n_{i,j+1} - (\varepsilon V_y)^n_{i,j-1}\right]}{2\Delta y} = 0 \qquad [5.4.11]$$

where: ε = porosity (-); V = velocity (m s^{-1}); Δx and Δy = grid length increments (m); and Δt = time increment (s). The subscripts i and j represent the x and y node, respectively; and the superscript n represents the current time step. The central difference method was used in developing this discretized formulation.

5.4.3.2 Mass Conservation (Vapor)

The mass conservation of water vapor for the outer domain was given as:

$$\varepsilon\frac{\delta \rho_v}{\delta t} + \frac{\delta}{\delta x}(\varepsilon \rho_v V_x) + \frac{\delta}{\delta y}(\varepsilon \rho_v V_y) = \frac{h_m(\rho_{vI} - \rho_v)NA_s}{V} \qquad [5.4.12]$$

Substituting the geometric identity describing the number of inner domain elements (Equation 4.37) and solving for the vapor density of the outer domain with respect to time yields:

$$\varepsilon\frac{\delta \rho_v}{\delta t} = \frac{h_m A_s(\rho_{vi} - \rho_v)(1-\varepsilon)}{A_s L} - \frac{\delta}{\delta x}(\varepsilon \rho_v V_x) - \frac{\delta}{\delta y}(\varepsilon \rho_v V_y) \qquad [5.4.13]$$

Application of the finite difference method yields:

$$\rho_{v_{i,j}}^{n+1} = \frac{A_s \Delta t}{A_x L} \frac{h_{m_{i,j}}^{n}}{\varepsilon_{i,j}^{n+1}} \left(1 - \varepsilon_{i,j}^{n}\right) \left(\rho_{vI_{i,j}}^{n} - \rho_{v_{i,j}}^{n}\right) - \frac{\Delta t}{2\Delta x \varepsilon_{i,j}^{n+1}} \left((\varepsilon V_x \rho_v)_{i+1,j}^{n} - (\varepsilon V_x \rho_v)_{i-1,j}^{n}\right) -$$

$$\frac{\Delta t}{2\Delta y \varepsilon_{i,j}^{n+1}} \left(\left(\varepsilon V_y \rho_v\right)_{i,j+1}^{n} - \left(\varepsilon V_y \rho_v\right)_{i,j-1}^{n}\right) + \left(\frac{\varepsilon_{i,j}^{n}}{\varepsilon_{i,j}^{n+1}}\right) \rho_{v_{i,j}}^{n} \qquad [5.4.14]$$

where: ρ_v = vapor density (kg m^{-3}); ε = porosity (-); h_m = mas transfer coefficient (m s^{-1}); A_s = surface area of an inner domain element (m^2); A_x = cross-sectional area of an inner domain element (m^2); V = velocity (m s^{-1}); Δx and Δy = grid length increments (m); and Δt = time increment (s). The subscripts i and j represent the x and y node, respectively; the subscript I represents a characteristic of the inner domain; the superscript n represents the current time step; the subscript v represent the characteristics of the water vapor.

The central difference method was used in deriving the discretized form of the convective gas transfer terms. The average values of those terms representing the characteristics of the inner domain (h_m and ρ_{vI}) were applied in the formulation of this outer domain equation. In this case, the average values of these inner domain properties were taken at each outer domain grid point. The variation in material properties was considered in this formulation.

5.4.3.3 Energy Conservation

The energy equation for the outer domain was given as:

$$\frac{h_{cI} A_s (T_I - T) N}{\rho_a C p_a V} + \alpha_a \left[\frac{\delta}{\delta x}\left(\varepsilon \frac{\delta T}{\delta x}\right) + \frac{\delta}{\delta y}\left(\varepsilon \frac{\delta T}{\delta y}\right)\right] = \frac{\delta}{\delta x}(\varepsilon V_x T) + \frac{\delta}{\delta y}(\varepsilon V_y T) + \varepsilon \frac{\delta T}{\delta t} \qquad [4.53]$$

Substituting the basic thermophysical relationship ($k=\alpha\rho Cp$) and the geometric identity describing the number of inner domain elements (Equation 4.37); while solving for the temperature change with respect to time yields:

$$\varepsilon \frac{\delta T}{\delta t} = \frac{h_{cI} A_s \alpha_a (T_I - T)(1-\varepsilon)}{k_a A_x L} + \alpha_a \left[\frac{\delta}{\delta x}\left(\varepsilon \frac{\delta T}{\delta x}\right) + \frac{\delta}{\delta y}\left(\varepsilon \frac{\delta T}{\delta y}\right)\right] - \frac{\delta}{\delta x}(\varepsilon V_x T) - \frac{\delta}{\delta y}(\varepsilon V_y T)$$

[5.4.15]

The finite difference method was applied to each of the terms appearing in this equation. The resulting discretized form of each component forming this energy balance is:

- Convective Source Term:

$$ST = \frac{A_s}{A_x L}\frac{\alpha_{a_{i,j}}^{n}}{k_{a_{i,j}}^{n}} h_{cI_{i,j}}^{n}\left(1-\varepsilon_{i,j}^{n}\right)\left(T_{I_{i,j}}^{n}-T_{i,j}^{n}\right) \quad [5.4.16a]$$

- Conductive Heat Transfer:

$$COND = \frac{\alpha_{a_{i,j}}^{n}}{(\Delta x)^2}\left((\varepsilon T)_{i+1,j}^{n}+(\varepsilon T)_{i-1,j}^{n}-2(\varepsilon T)_{i,j}^{n}\right)+\frac{\alpha_{a_{i,j}}^{n}}{(\Delta y)^2}\left((\varepsilon T)_{i,j+1}^{n}+(\varepsilon T)_{i,j-1}^{n}-2(\varepsilon T)_{i,j}^{n}\right) \quad [5.4.16b]$$

- Convective Heat Transfer:

$$CONV = \frac{\left[(\varepsilon V_x T)_{i+1,j}^{n}-(\varepsilon V_x T)_{i-1,j}^{n}\right]}{2\Delta x}+\frac{\left[(\varepsilon V_y T)_{i,j+1}^{n}-(\varepsilon V_y T)_{i,j-1}^{n}\right]}{2\Delta y} \quad [5.4.16c]$$

The central difference method was used in deriving the convective heat transfer term here. The solution to the vapor density was then obtained by combining all of these different components into a single expression as follows:

$$T_{i,j}^{n+1} = \frac{\Delta t}{\varepsilon_{i,j}^{n+1}}(ST+COND-CONV)+\left(\frac{\varepsilon_{i,j}^{n}}{\varepsilon_{i,j}^{n+1}}\right)T_{i,j}^{n} \quad [5.4.16d]$$

where: T = temperature (K); h_{cI} = convective heat transfer coefficient for the inner domain (W m^{-2} K^{-1}); ε = porosity (-); A_s = surface area of an inner domain element (m^2); A_x = cross-sectional area of an inner domain element (m^2); L = length of inner domain element (m); α = thermal diffusivity (m^2 s^{-1}); k = thermal conductivity (W m^{-1} K^{-1}); V = velocity (m s^{-1}); Δx and Δy = grid length increments (m); and Δt = time increment (s). The subscripts i and j represent the x and y node, respectively; the subscript I represents a

characteristic of the inner domain; the superscript n represents the current time step; the subscripts a, v and s represent the characteristics of the ambient air, water vapor and solid phase, respectively.

It should be noted that the variation of material properties was considered in this formulation of the outer domain model. The average values of those terms representing inner domain characteristics (h_{cI}, ρ_{vI}, and T_I) were also applied here to the each outer domain grid point.

5.4.3.4 Momentum Equation (Darcy's Law)

The momentum equation for the outer domain was given as:

$$\frac{\delta^2\Psi}{\delta x^2}+\frac{\delta^2\Psi}{\delta y^2}=-\frac{\kappa g\rho_0\beta}{\mu}\frac{\delta T}{\delta x} \qquad [4.47]$$

Application of the finite difference method yields:

$$\frac{1}{(\Delta x)^2}\left(\Psi^n_{i+1,j}+\Psi^n_{i-1,j}-2\Psi^n_{i,j}\right)+\frac{1}{(\Delta y)^2}\left(\Psi^n_{i,j+1}+\Psi^n_{i,j-1}-2\Psi^n_{i,j}\right)=-\frac{\kappa g\rho_0\beta}{\mu}\frac{\left(T^n_{i+1,j}-T^n_{i-1,j}\right)}{2\Delta x} \qquad [5.4.17]$$

in which case the central difference method was applied. Solving for the target nodal position yields:

$$2\Psi^n_{i,j}\left(\frac{1}{(\Delta x)^2}+\frac{1}{(\Delta y)^2}\right)=\frac{1}{(\Delta x)^2}\left(\Psi^n_{i+1,j}+\Psi^n_{i-1,j}\right)+\frac{1}{(\Delta y)^2}\left(\Psi^n_{i,j+1}+\Psi^n_{i,j-1}\right)+\frac{\kappa g\rho_0\beta}{\mu}\frac{\left(T^n_{i+1,j}-T^n_{i-1,j}\right)}{2\Delta x} \qquad [5.4.18]$$

Multiplying both sides of the equation by Δx and substituting kinematic viscosity ($\nu = \mu/\rho$) yields:

$$2\Psi^n_{i,j}\left(1+\frac{(\Delta x)^2}{(\Delta y)^2}\right)=\left(\Psi^n_{i+1,j}+\Psi^n_{i-1,j}\right)+\frac{(\Delta x)^2}{(\Delta y)^2}\left(\Psi^n_{i,j+1}+\Psi^n_{i,j-1}\right)+\frac{\kappa g\beta\Delta x}{2\nu}\left(T^n_{i+1,j}-T^n_{i-1,j}\right) \qquad [5.4.19]$$

To simplify this expression, a geometric ratio was defined as:

$$r = \frac{(\Delta x)^2}{(\Delta y)^2} \qquad [5.4.20]$$

Substituting this geometric ratio into the momentum equation yields:

$$2\Psi^n_{i,j}(1+r) = \left(\Psi^n_{i+1,j} + \Psi^n_{i-1,j}\right) + r\left(\Psi^n_{i,j+1} + \Psi^n_{i,j-1}\right) + \frac{\kappa g \beta \Delta x}{2\nu}\left(T^n_{i+1,j} - T^n_{i-1,j}\right) \qquad [5.4.21]$$

Further simplification of the momentum conservation yields:

$$\Psi^n_{i,j} = \frac{\left(\Psi^n_{i+1,j}+\Psi^n_{i-1,j}\right)+r\left(\Psi^n_{i,j+1}+\Psi^n_{i,j-1}\right)}{2(1+r)} + \frac{\kappa g \beta \Delta x\left(T^n_{i+1,j}-T^n_{i-1,j}\right)}{4(1+r)\nu} \qquad [5.4.22]$$

where: ψ = stream function ($m^2\ s^{-1}$); g = gravitational acceleration (9.81 m s^{-2}); Δx and Δy = grid length increments (m); V_x and V_y = velocity components in each respective direction (m s^{-1}); β = volumetric thermal expansion coefficient (K^{-1}); ν = kinematic viscosity ($m^2\ s^{-1}$); and κ = intrinsic permeability (m^2); the assessment of which will be further discussed in Appendix C.

This formulation of the momentum equation requires an iterative solution for the stream line function (see section 5.4.4) which is subsequently translated back into the velocity components (V_x and V_y) using Equation 4.39.

5.4.3.5 Model Parameters

The solution variables within the outer domain include the vapor density (ρ_v and ρ_{vI}), temperature (T and T_I), stream function (ψ), and velocity field (V_x and V_y). As discussed in Chapter 4, the interdependency of the inner and outer domain becomes evident with the coupled terms appearing in the outer domain model. The length of the inner domain element (L), cross-sectional area of an inner domain element (A_x), surface

area of an inner domain element (A_s), and grid length increments (Δx and Δy) were all assumed to be constant physical properties of the inner domain.

The cross sectional area and distance around the inner domain element were based on the average stem diameter of switchgrass of 2.698 mm as reported by Lam et al. (2007, 2008). Although a length of 41.9 cm was assumed for the inner domain elements, this value is somewhat arbitrary in the current formulation since the surface area of the inner domain is calculated using this same length. In this case, the length terms are canceled out by the geometry of the problem.

Grid length increments for the x and y axes (dx and dy) were allowed to differ from each other to allow more flexibility in evaluating the distinct length scales in each principle direction. The Δx and Δy grid increments were specifically set as 1.524 and 1.905 cm; respectively, since smaller grid sizes (Δx = 0.460 cm; Δy = 0.575 cm) only resulted in minimal variation. Increasing the grid increments above these values, however, was observed to cause significant error. The time increment (Δt) was set at 0.5 hr, which provided a stable solution under the proposed conditions. The spatial and temporal discretization specified here represented the same conditions proposed for the conduction model (see section 5.4.1).

The kinematic viscosity (ν) and thermophysical properties of the air (k_a and α_a) were based on empirical functions of the air temperature; while the thermal expansion coefficient ($\beta=1/T_f$) was estimated according to the ideal gas model and assuming the air was at standard atmospheric conditions. The derivation of the heat and mass transfer coefficients for the inner domain (h_{cI} and h_{mI}) are discussed in Appendix B; while the other dependent parameters appearing in the outer domain model (ε and κ) are discussed in Appendix C.

5.4.4 Solution Scheme

The evaluation of this set of discretized equations specifically involves the solution of the heat and mass transfer component (equation 5.4.7 - 5.4.9, 5.4.14, 5.4.16) in terms of the temperature (T, T_I), vapor density (ρ_v, ρ_{vI}) and moisture (M) fields; as well as, the velocity component (equation 5.4.11, 5.4.22) in terms of the stream function (ψ) and velocity field (V_x, V_y). The heat and mass transfer component of this model further

involves two distinct sets of equations: one set for the outer domain, and a second set for the inner domain. Each set of equations requires a distinct solution algorithm which will be outlined in the following discussion.

The first step of this solution procedure is to establish the computational grid for the inner and outer domain according to the parameters specified in section 5.4.2 and section 5.4.3; respectively. In this case, the inner domain is considered to represent a single element of the overall porous structure. As such, the inner domain represents a physically distinct structure requiring a unique discretized grid. It may also be noted, that each outer domain control volume contains a number of inner domain elements that must be specified.

Now, the vapor density (ρ_v) and temperature (T) of the air flowing through the outer domain directly influence the amount of mass and energy transferred between the inner and outer domain. Therefore, a solution to the inner domain equations was necessary at each outer domain grid point. Specific terms that were representative of the inner domain (h_{cI}, h_m and T_I) were each averaged to provide single representative values of each variable at each outer domain grid point.

The next step was to evaluate the various solution fields in terms of each component of the overall model. Evaluation of the outer domain involved the solution of the outer domain equations governing mass conservation (5.4.14) and energy conservation (5.4.16) in terms of the vapor density (ρ_v) and temperature fields (T), respectively. The solution then proceeded with the evaluation of the inner domain in terms of the moisture content (M) according to the thin layer drying model (equation 5.4.9). The application of this thin-layer drying model inherently assumes that equilibrium conditions are achieved within an inner domain element based on the discussion provided in Section 4.2.5.

Without this relationship between the temperature and moisture content of the inner domain, the solution of the inner domain would necessarily become an iterative process requiring the simultaneous solution of the mass and energy conservation equations for the inner domain. If that were the case, any two of solution fields would need to be evaluated through this iterative process since the inner domain vapor density (ρ_{vI}), moisture content (M) and temperature (T_I) are interdependent. Implementation of

this thin-layer drying model, however, provides some simplification of the inner domain model assuming equilibrium conditions within the inner domain over the specified time increment. The solution procedure then continues with the assessment of the inner domain equations governing mass conservation (5.4.7) and energy conservation (5.4.8) in terms of the vapor density (ρ_{vI}) and temperature fields (T_I); respectively.

The velocity field (V_x and V_y) was then solved in accordance with the heat and mass transfer component of the porous model. The assessment of the momentum equation (5.4.22) over the entire outer domain grid specifically required an iterative solution since the stream function could not be solved analytically. The model solution, therefore proceeded in an iterative manner until no significant change was found to exist between the predicted streamline results and those obtained from the previous iteration. In this case, a tolerance or threshold of 1E-9 $m^2\ s^{-1}$ was specified for the stream function.

The full solution algorithm is summarized in terms of following steps which are depicted in the flowchart shown in Figure 5.4.3:

1. All solution variables (T, T_I, M, ρ_v, ρ_{vI}, V_x, V_y) were initialized in accordance with the initial conditions for the inner domain (4.25-4.27) and initial conditions for the outer domain (4.58-4.60).
2. The mass conservation of water vapor for the outer domain (5.4.14) was solved at each outer domain grid point. The 'new' vapor pressure density field (ρ_v^{n+1}) for the outer domain was determined in this step. These updated values of vapor density were then set equal to the values at the 'current' time step ($\rho_v^n = \rho_v^{n+1}$).
3. The energy conservation equation for the outer domain (5.4.16) was solved at each outer domain grid point. The 'new' temperature field (T^{n+1}) for the outer domain was determined in this step. These updated values of temperature were then set equal to the values at the 'current' time step ($T_v^n = T_v^{n+1}$).
4. The thin-layer drying model (5.4.9) was solved for the inner domain at each outer domain grid point. The 'new' moisture content field (M^{n+1}) of the inner domain was determined in this step. These updated values of vapor density were then set equal to the values at the 'current' time step ($M^n = M^{n+1}$).

5. The mass conservation equation for the inner domain (5.4.7) was solved for the inner domain elements at each outer domain grid point. This procedure accounted for the amount of mass transferred from an inner domain element in each outer domain control volume. The 'new' vapor pressure density field (ρ_{vI}^{n+1}) for the inner domain was determined in this step. These updated values of vapor density were then set equal to the values at the 'current' time step ($\rho_{vI}^{n} = \rho_{vI}^{n+1}$).
6. The energy conservation equation for the inner domain (5.4.8) was solved for the inner domain elements at each outer domain grid point. This procedure accounted for the amount of energy transferred from an inner domain element in each outer domain control volume. The 'new' temperature field (T_I^{n+1}) for the inner domain was determined in this step. These updated values of temperature were then set equal to the values at the 'current' time step ($T_I^{n} = T_I^{n+1}$).
7. The momentum conservation equation for the outer domain (5.4.22) was solved in terms of the stream function (ψ) in accordance with the heat and mass transfer components of the model. Convergence was then evaluated in terms of the specified tolerance or threshold given for the stream function. Iterative changes at any grid point within the outer domain exceeding this threshold indicated that convergence had not been achieved. Consequently, this step was repeated until convergence was achieved. The updated values of the stream function were then set equal to the values at the 'current' time step ($\psi^{n} = \psi^{n+1}$).
8. The 'new' velocity field (V_x^{n+1} and V_y^{n+1}) was determined based on the updated solution of the stream function. These resulting velocity values were substituted into the continuity equation (5.4.11) to check for convergence; otherwise, an apparent 'mass source' could arise. The updated values of the velocity components were then set equal to the values at the 'current' time step ($V_x^{n} = V_x^{n+1}$ and $V_y^{n} = V_y^{n+1}$).
9. The time step was incremented each interval and steps 2 – 8 were repeated until the total simulation time (60 days) had been reached.
10. At the termination of the calculation routine, the solution fields were output.

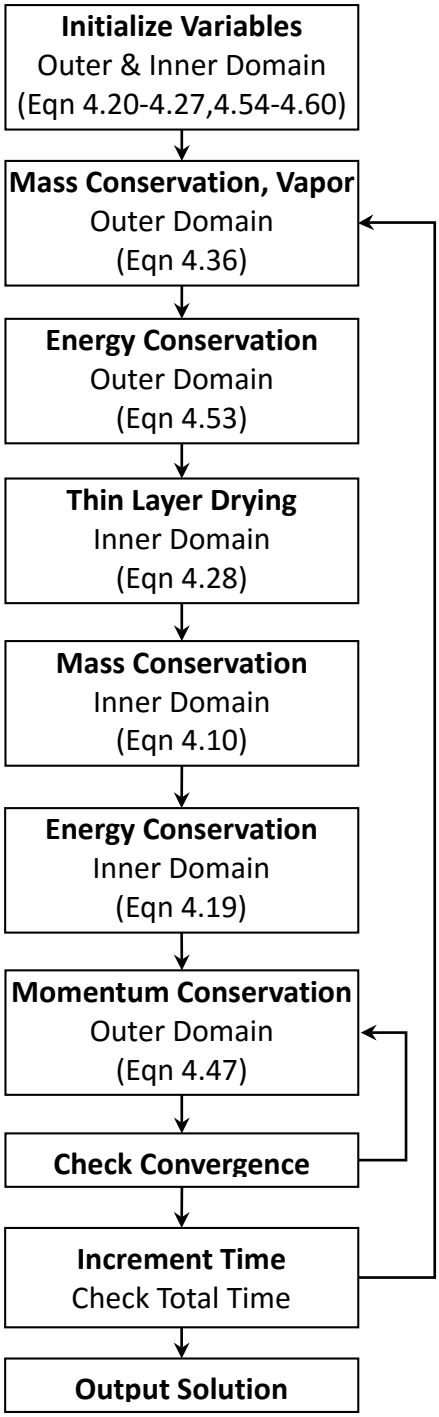

Figure 5.4.3 Overview of the solution algorithm for the porous media model.

More specific details of this solution procedure are shown in Figure 5.4.4 which depicts a flowchart of the calculation routine implemented in this study. The specific variables associated with each step in this process are indicated along with the respective discretized equations where relevant.

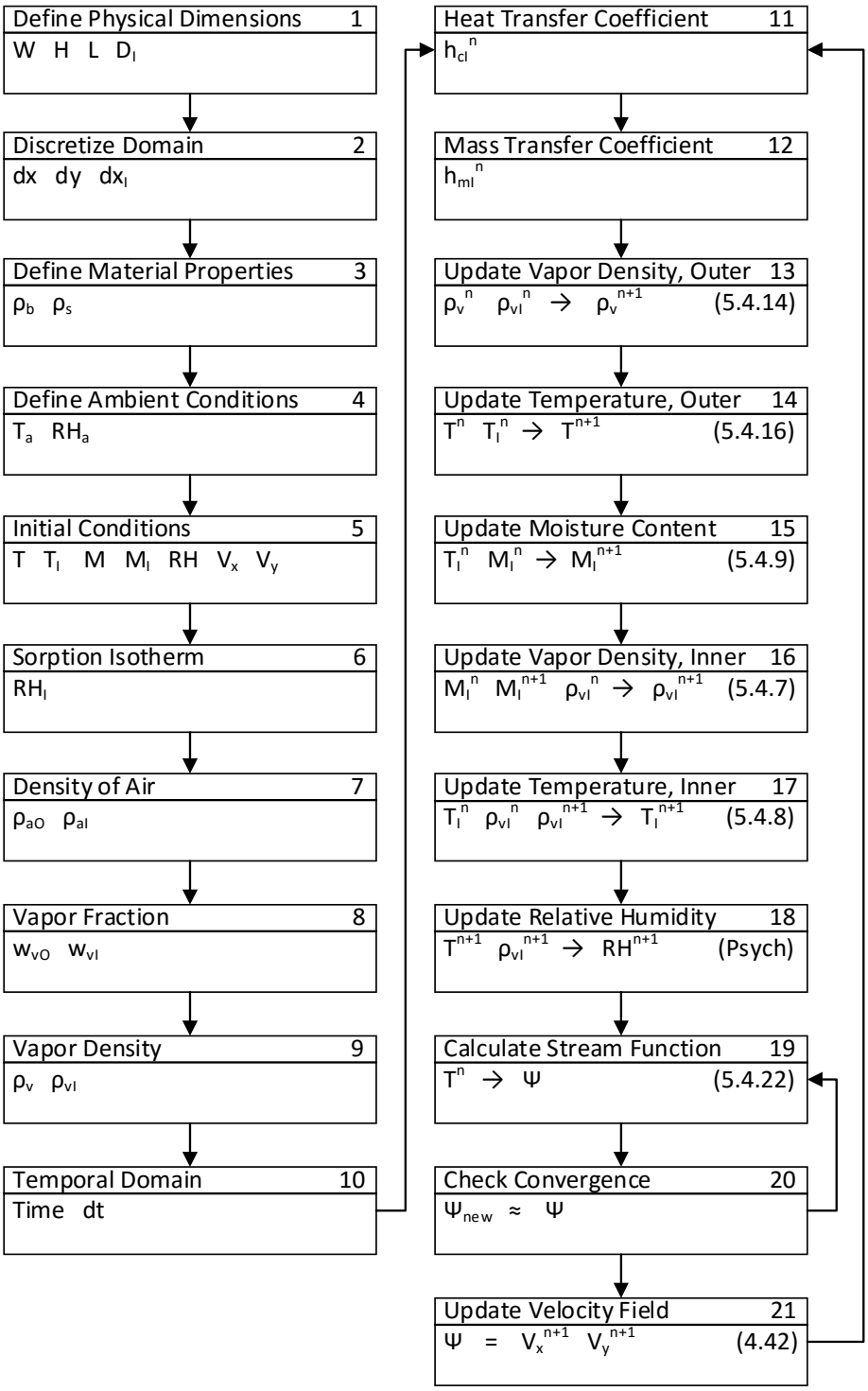

Figure 5.4.4 Detailed solution procedure of the porous media model in terms of the heat, mass and momentum conservation components described in this study.

.

Modeling and simulation of the current study was performed using the MATLAB program (MATLAB R2013b, MathWorks, Inc., Natick, MA) with LiveLink (COMSOL Multiphysics, Palo Alto, CA). The simulation domain was first generated and a finite numerical scheme was used to solve all of the governing equations and relevant parameters. The system was treated as a quasi-steady process over the specified time step with the simulation results of the previous time step set as the next time step's initial conditions.

In step 5, a moisture content (M) was defined for outer domain even though the outer domain contains no solid phase which would be represented by this term. In this case, the moisture content of the outer domain simply represents the average value of the moisture content of the inner domain (M_I) at each outer domain grid point. The initial relative humidity of the outer domain (RH) was assumed to be equivalent to the relative humidity of the ambient air (RH_a). The relative humidity of the inner domain (RH_I) was initialized in step 6 using the sorption isotherm of milled switchgrass (Godbolt et al., 2013) based on the temperature (T_I) and moisture content (M_I) of the inner domain.

This evaluation is based on the assumption that the moisture content of the inner domain is in equilibrium with the relative humidity of the inner domain since the inner domain (stem) represents a much smaller volume relative to the global domain (bale cross-section). In fact, the void space of the inner domain is roughly 1E6 times smaller than the void space of the global domain. A large time step also allows sufficient time for equilibrium conditions to be reached within the relatively small volume of the inner domain. The relative humidity was simply set at 100 % in those cases exceeding the saturated state.

The density of the air in the inner domain (ρ_{aI}) and outer domain (ρ_{aO}) were evaluated in step 7 based on empirical functions of their respective temperature terms. The distinct phases composing the inner domain (solid, vapor, liquid and dry air) were assumed to be in local thermodynamic equilibrium with each other. Hence, the density of the air in the inner domain was based on the temperature of the inner domain (T_I). The density of the air in the outer domain was evaluated similarly.

The vapor fraction or humidity ratio of the inner domain (w_{vI}) and outer domain (w_{vO}) were evaluated in step 8 based on psychrometric relationships in terms of the dry

bulb temperature and relative humidity of each domain. These psychrometric calculations were primarily derived from ASHRAE Fundamentals (2011). The vapor density of the inner domain (ρ_{vI}) and outer domain (ρ_v) are then determined in step 9 as a product of the relative air density and vapor fraction.

The heat transfer coefficient for the inner domain (h_{cI}) is evaluated in step 11 according to the boundary layer theory and packed bed formulation described in Appendix B. The mass transfer coefficient for the inner domain (h_{mI}) is evaluated in step 12 based on the Chilton-Colburn factor which relates to the heat transfer coefficient (Carlton and Oxley, 1967; Kandula, 2011; Lees, 2012; Rao, 2015). A detailed description of the derivation of the mass transfer coefficient is also discussed in the Appendix B.

The vapor density of the outer domain (ρ_v) is updated for the next time interval (n+1) in step 13 based on mass conservation of water vapor (equation 5.4.14). The temperature of the outer domain (T) is updated for the next time interval in step 14 based on the energy conservation of the outer domain (equation 5.4.16). The moisture content of the inner domain (M_I) is updated for the next time interval in step 15 based on the thin-layer drying model (equation 5.4.9). The vapor density of the inner domain (ρ_{VI}) is updated for the next time interval in step 16 based on the mass conservation of the inner domain (equation 5.4.7). The temperature of the inner domain (T_I) is updated for the next time interval in step 17 based on the energy conservation of the inner domain (equation 5.4.8). The relative humidity of the outer domain (RH) is updated for the next time interval in step 18 based on the relevant psychrometric relationships.

The stream function (ψ) is updated for the next time interval in step 19 based on the momentum conservation of the outer domain (5.4.22). An iterative procedure is initiated in step 20 to achieve convergence within a specified threshold or tolerance. Steps 19 and 20 will continue until the solution of the stream function converges. The velocity field (V_x and V_y) is updated for the next time interval in step 21 based on the definition of the stream function (equation 4.42). The time step is incremented while steps 11-21 are repeated until the total simulation time is reached.

5.4.5 Model Validation

Model validation was performed with baled switchgrass stored in the same controlled environment chamber as was discussed in section 5.2.5 using the following experimental procedure.

5.4.5.1 Material Preparation

Switchgrass (*Panicum virgatum L.*) was harvested at the University of Kentucky Spindletop Research Farm near Lexington, KY, USA (38˚8′ N, 84˚31′ W) in March 2013. Standard farm practices were carried out during cultivation using a New Holland H6830 disc mower (with no conditioning rolls) at a height of approximately 15 cm (6 inches). Due to the time of year, the crop was dry and was immediately baled with a New Holland BC5070 baler (New Holland North America, Inc., New Holland, PA). Small rectangular bales (~102 x 46 x 36 cm^3) were removed from the field within 24 h of production and transported to the University of Kentucky research farm in Woodford County (KY, USA) where they were stored for a minimum of 50 days in a single layer in a well-ventilated barn. The bales were then transported to the Biosystems and Agricultural Engineering Department at the University of Kentucky in Lexington (KY, USA) and were stored indoors in an air conditioned laboratory for several days.

The average initial moisture content of the bales was determined by extracting three subsamples from three replicate bales (3 x 3 = 9 subsamples) using a 5.08 cm steel hay sampling probe with a serrated tip. All subsamples were oven-dried at 103 ± 1 °C for 24 h according to standard S358.2 (ASABE Standards, 2006). The initial and final mass of each subsample was measured by weighing scale and used to calculate the average initial moisture content of the bales used in the storage validation experiments. In accordance with this assessment, the average initial moisture content of the switchgrass was estimated to be 10.1 %-wb which was considered to be sufficiently low in terms of achieving minimal microbial growth and/or heat generation.

5.4.5.2 Storage Treatments

The primary variable associated with this storage validation test was moisture content; which was assessed at four target levels including 10, 20, 30 and 40 %-wb. To

achieve these moisture levels, the bales were cut open and spread into four separate windrows on an asphalt surface. Each windrow was conditioned with a different amount of water based on the mass-based ratio of water to dry matter corresponding to the targeted moisture content. The conditioning or rewetting process has previously been shown to provide material that behaves similarly to naturally wet material (Abbasi, et al., 2009; Baker et al., 2008; Turner, 2014). The windrows were conditioned with the use of a 4 gallon garden sprayer with manual hand pump; while windrows were frequently turned by hand during the rewetting process. It should be noted here, that no water was added to the target treatment of 10 %-wb under the assumption that the initial moisture content of the material was sufficiently close to this target moisture level.

Each windrow was immediately re-baled (using the same baler as was used in the field operations) to form small rectangular bales (~102 x 46 x 36 cm) that were stored overnight (~12 hr) in an air conditioned laboratory. The weight and physical dimensions of each experimental bale were measured; while the bulk density was assessed as the mass-to-volume ratio. The initial moisture content of each treatment was also determined from six subsamples (~350 g) collected from each windrow at the time of baling. In accordance with this assessment, the average initial moisture content for each bale treatment was 10.7 ± 0.1, 22.6 ± 1.0, 31.6 ± 2.0, and 41.8 ± 2.1 %-wb.

5.4.5.3 Storage Layout

The bales were stored on 91.4 cm (36 in) high, metal wire shelves arranged in three rows (replications) within a controlled environmental chamber for 60 days. Each replicate bale treatment (moisture content) was randomized within its respective row. The bales within each row were spaced an average of 13 cm (5 in) apart; while each row was spaced 21.0 cm (8.25 in) apart as depicted schematically in Figure 5.4.5 and shown in the photograph of the actual experimental setup in Figure 5.4.6. It was assumed that sufficient distance was maintained between each treatment with uniform temperature and relative humidity throughout the environmental chamber. The different treatments are denoted by M10, M20, M30, and M40 for the target moisture content levels of 10, 20, 30, and 40 %-wb, respectively. Likewise, the R1-R3 denotations represent the three

replications performed; while D represents the bales used for destructive sampling at specific intervals during the storage period.

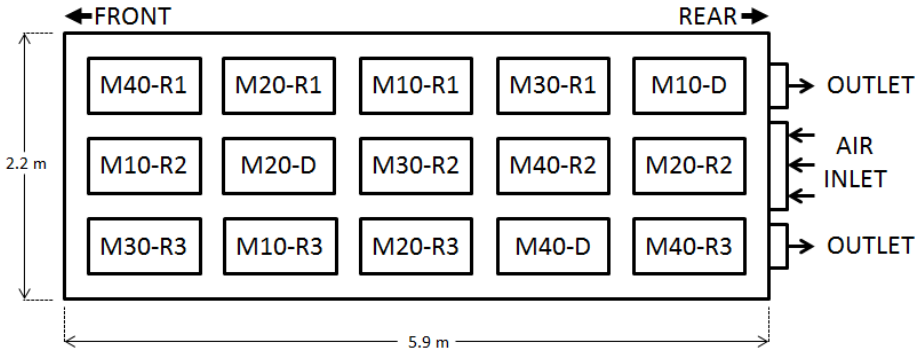

Figure 5.4.5 Storage layout for moist bales in environmental chamber. M10, M20, M30, and M40 represent the target moisture content levels of 10, 20, 30, and 40 %-wb, respectively, R1-R3 are replicates, and D represents destructively sampled bales.

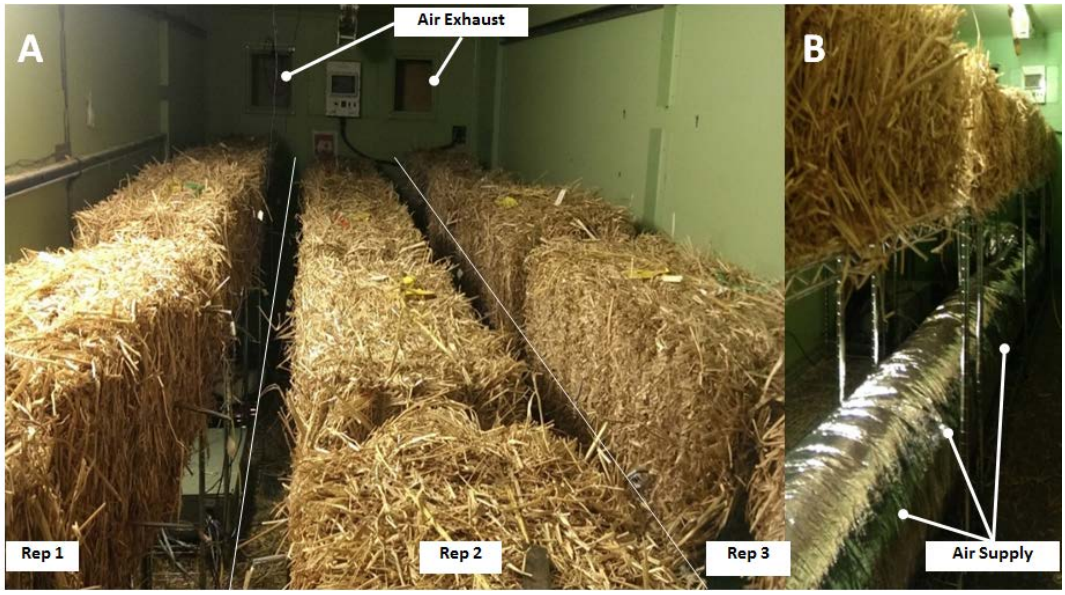

Figure 5.4.6 Photograph of experimental storage setup. A) Two air exhaust openings in the rear of the environmental chamber and three replications of each moisture treatment. B) Supply duct for air distribution within the environmental chamber with airflow ports installed along its length.

A 30.5 cm (12 in) flexible air duct was extended through the lower central region of the environmental chamber at a height of 24.1 cm (9.5 in) above the floor; and with 7.6 cm (3 in) diameter outlets installed on both horizontal sides along its entire length to improve the uniform distribution of air throughout the chamber. These outlets were installed at intervals of approximately 91.4 cm (36 inches). It should also be noted that

both of the 30.5 cm (12 in), square outlets for the environmental control chamber were positioned at the top rear of the room. The air inlet and outlet positions helped to ensure sufficient air circulation throughout the chamber as the incoming air was directed forward through the central duct, before exhausting through the rear of the chamber.

5.4.5.4 Storage Procedure

The environmental chamber was maintained at approximately 22 °C and 51 % relative humidity for the first 36 hours to establish baseline storage conditions in line with the ambient laboratory conditions. After this initial storage period, the environmental chamber was adjusted to a target storage temperature of 30 °C and the lowest achievable relative humidity under the given conditions for 60 days. The actual conditions recorded during storage were 29.5 ± 0.6 °C and 23.2 ± 3.9 %. These particular conditions were selected for the current study in order to expedite the natural heating and drying processes that were expected to occur in storage; while avoiding more severe conditions which could result in rapid dry matter loss and/or spontaneous combustion.

5.4.5.5 Storage Measurements

Bales were weighed upon entering the environmental chamber and approximately every two weeks (day 14, 31, 45 and 60) throughout storage. A 5.1 cm forage sampling probe with a serrated tip was used to collect subsamples from the destructive bale replications at these same time intervals according to the coring pattern presented by Smith et al., (2013). Three subsamples were also collected from each bale after 60 days of storage; including the R1-R3 replications. Type-E thermocouples (24 AWG, Omega Engineering, Inc., Atlanta, GA) were inserted into the bales using rigid, 3.175 mm (1/8 in)-diameter, high-density polyethylene welding rods (Seelye Acquisitions, Inc., Ocoee, FL) which have improved tensile strength and the ability to continuously resist heat transfer up to temperatures of approximately 110 to 120 °C.

Three thermocouples were positioned diagonally through each bale with a low (~13 cm (~5 inch) above the bottom surface), central (centered with the height) and upper position (~13 cm (~5 inch) below the top surface) for each treatment. The thermocouples were imbedded to three depths (~ 11, 23, and 34 cm (~ 4.5, 9.0, and 13.5 in)) at three

different distances on the side wall of each bale (~ 13, 51, 89 cm (5, 20, and 35 in)).This particular measurement scheme allowed for uniform measurements across all treatments while accounting for any potential variation which could occur in one or more of the principle coordinates. This measurement scheme is depicted in Figure 5.4.7. Thus, experimental time/temperature data were collected at three locations within each bale with three replications per treatment (moisture content level).

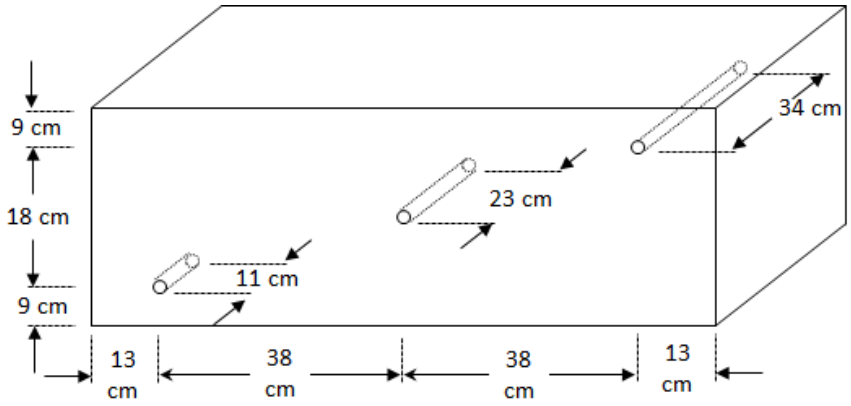

Figure 5.4.7 Thermocouple positioning schematic shown in all three Cartesian coordinates.

Air temperature was monitored at three vertical heights (low, middle and high) and three horizontal positions (front, center and rear) within the environmental chamber. The thermocouples were generally positioned 46 cm (18 in) from the walls of the environmental chamber for the peripheral positions. Hence, this measurement scheme required a total of nine air temperature positions for each measurement interval. An additional relative humidity probe (CS500-L, Campbell Scientific, Logan, UT) was also positioned centrally within the chamber. Thermocouple and relative humidity measurements were scanned and recorded to a datalogger (CR10, Campbell Scientific, Inc., Logan, UT) every 5 minutes.

The experimental data was averaged to provide a mean daily temperature for each treatment; further reducing the error caused by random variation. The resulting 60 data points for each treatment were assumed to represent the mean daily treatment temperatures recorded at each thermocouple location. The null hypotheses for testing model validity were that the intercept and slope of the predicted temperature versus measured temperature were different from 0.0 and 1.0, respectively.

CHAPTER 6:RESULTS AND DISCUSSION

6.1 Fluid Analysis

6.1.1 Material Preparation

The average moisture content was 10.9 ± 0.3 %-wb and 9.6 ± 0.3 %-wb for switchgrass and miscanthus, respectively. The levels were low and uniform due to extended storage within a climate controlled laboratory.

6.1.2 Saturated Results

The average saturated moisture content of both feedstock types was plotted in Figure 6.1.1 as a function of the dry bale density. Based on preliminary tests, accurate measurements were unattainable at bale densities below 150 kg m^{-3} (db) due to rapid leaching. However, the elevated density levels presented here are assumed to be desirable since they would be ideal in terms of minimizing transportation costs. The average saturated moisture content ranged between 55.9 and 71.9 %-wb for switchgrass and between 60.5 and 73.9 %-wb for miscanthus bales, depending on the density. Linear models were applied to both feedstock types in order to describe the inverse correlation between saturated moisture content and bale density as follows:

$$M_S = 175.9 - 0.501\rho_b \quad [6.1.1]$$

$$M_M = 101.6 - 0.203\rho_b \quad [6.1.2]$$

where: ρ_b = dry bale density (kg m^{-3}) and M_S and M_M = saturated moisture content (%-wb) for switchgrass and miscanthus, respectively.

The corresponding R^2 regression coefficients were 0.99 for both feedstocks. This inverse correlation between saturated moisture content and bale density ($p < 0.01$) was attributed primarily to the water entrapment in the void spaces. The larger and more extensive void spaces associated with lower density bales allowed increased water storage. Likewise, the miscanthus bales offered increased void space for water to fill, thereby increasing the saturated moisture content at all density levels.

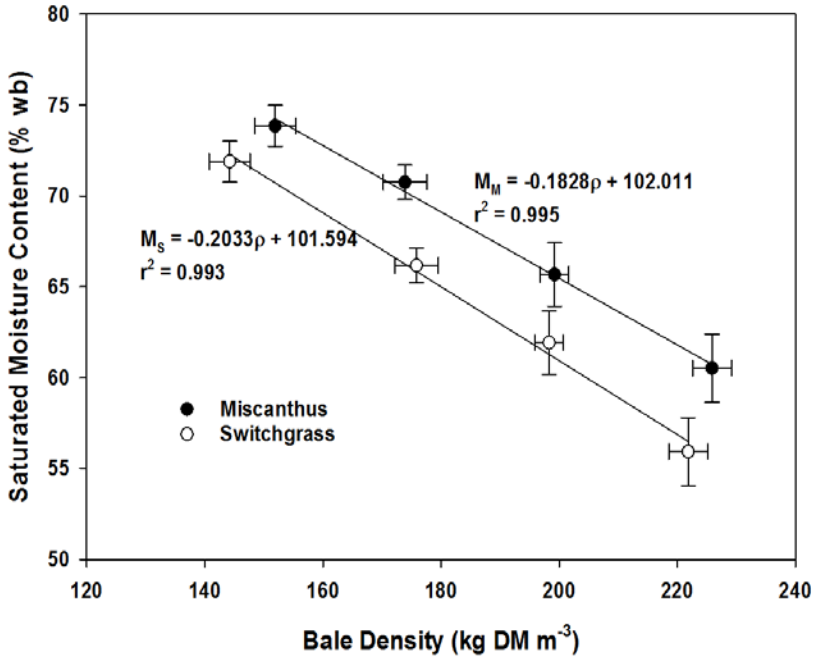

Figure 6.1.1 Saturated moisture content (M) of baled switchgrass and miscanthus as a function of the dry bale density with linear regression coefficients (R^2) of 0.99 for both feedstocks.

The average leaching behavior of saturated bales is shown in Figure 6.1.2 for the first five hours. Each curve represents the average of three replicate bales. Rapid leaching of water was observed within the first three hours with average reductions in moisture content of 9.8 and 10.3 percentage points (wb) for switchgrass and miscanthus, respectively. Leaching then continued at steady-state for the remaining time (analysis concluded at 62 hours) with further reductions of 1.9 and 2.1 percentage points (wb) for switchgrass and miscanthus, respectively. Based on these results, the density and feedstock-type interactions were both significant at $\alpha = 0.05$ ($p < 0.01$).

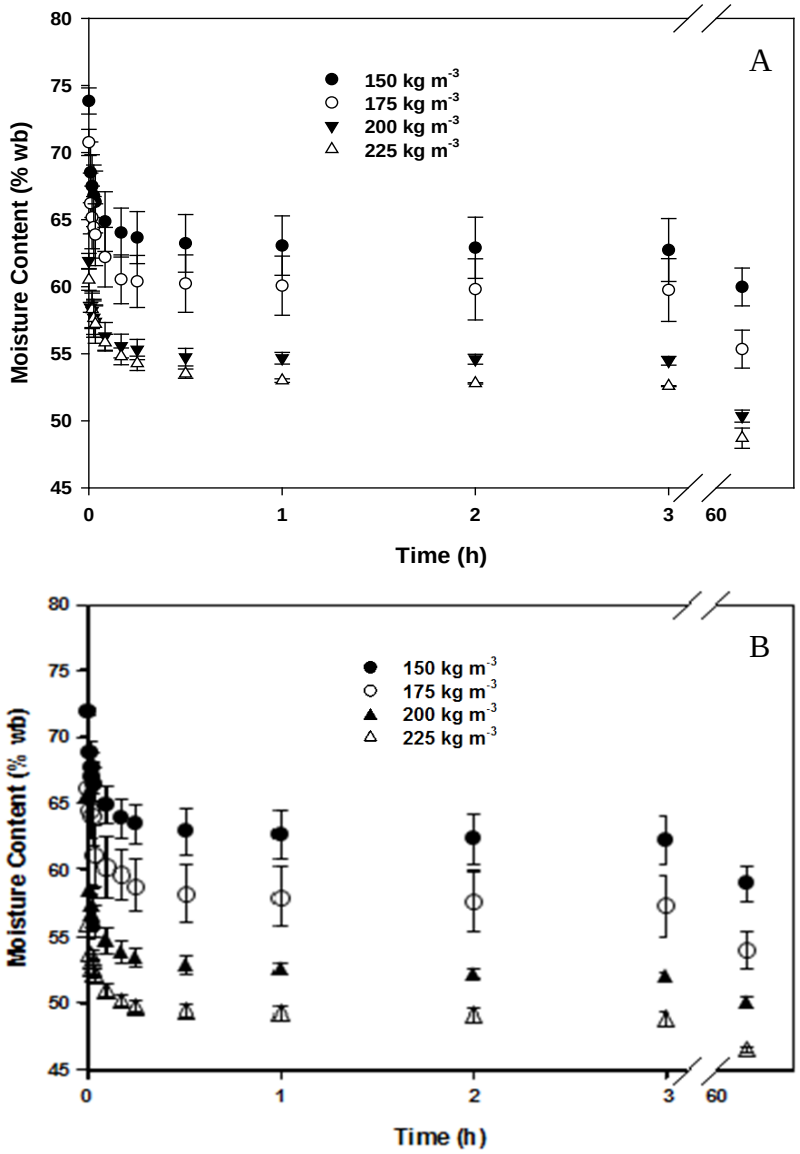

Figure 6.1.2 Leaching curves for fully saturated miscanthus (A) and switchgrass (B) bales at four target dry matter densities (150, 175, 200 and 225 kg m^{-3}).

The hydraulic flux (Q/A) was plotted as a function of the hydraulic gradient (H/L) for both feedstock types as shown in Figure 6.1.3 with respect to the density level. Preliminary trials indicated that density levels below 150 kg m^{-3} (db) resulted in turbulent flow which violated the assumption of Darcy's Law. Thus, the effect of bale density for values below 150 kg m^{-3} (db) could not be accurately determined due to rapid flow rates. However, each data set presented here represents the average of three replicate observations (bales) for both feedstock types assessed at three hydraulic gradients.

Saturated hydraulic conductivity was then determined for each data set by linear regression to determine the associated slopes (saturated hydraulic conductivity) which were fit to the experimental data (forced through zero).

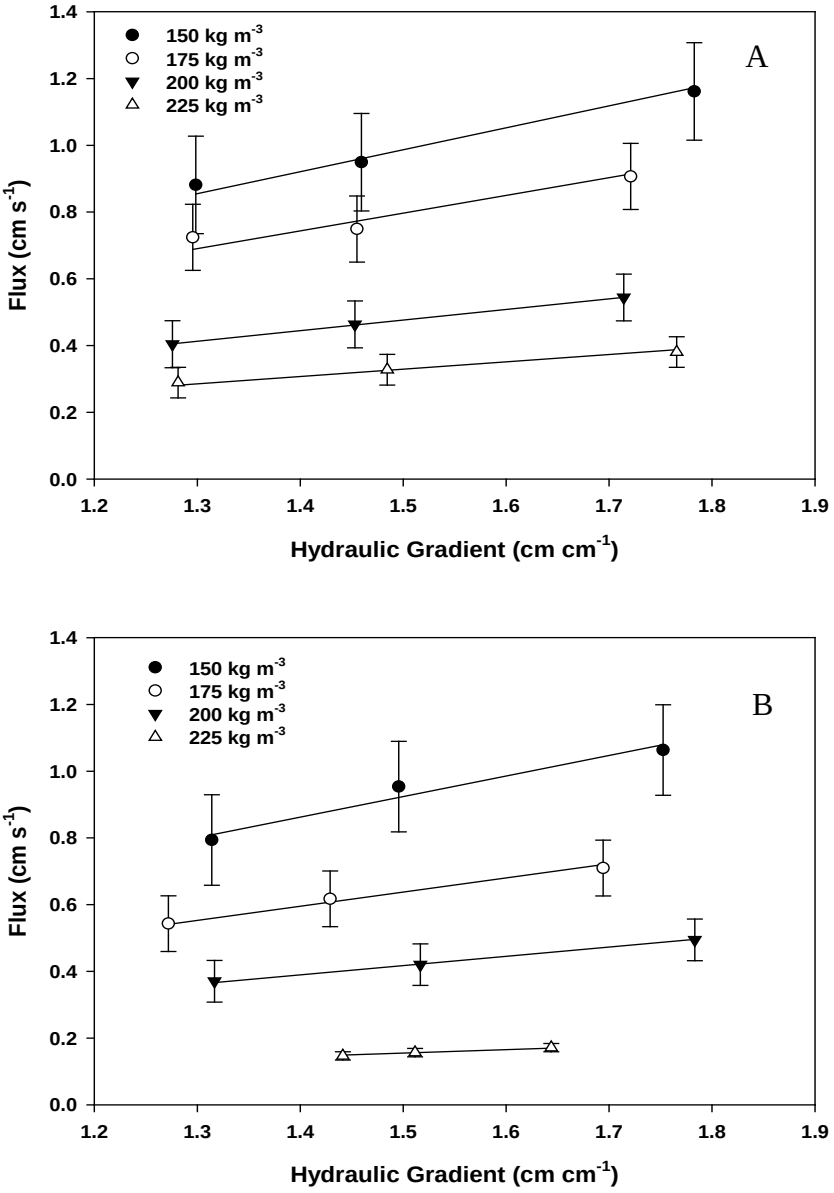

Figure 6.1.3 Water flux and standard deviation versus hydraulic gradient of baled miscanthus (A) and switchgrass (B) at target densities of 150, 175, 200 and 225 kg DM m-3 with linear regression lines.

The estimates of hydraulic conductivity are summarized in Table 6.1.1 based on the results of linear regression models of both feedstock types. The average saturated

hydraulic conductivity ranged between 0.103 and 0.616 cm s^{-1} for baled switchgrass and between 0.219 and 0.658 cm s^{-1} for baled miscanthus, depending on the dry bale density. As expected, these results are slightly lower than values reported for various wood media which ranged between 2.4 ± 2.0 and 11.01 ± 3.0 cm s^{-1} (Chun et. al, 2009; Robertson et al., 2005; Van Driel et al., 2006), but are elevated compared with that of alfalfa silage (Yao and Jofriet, 1992), chopped sorghum (Custer et. al, 1990) and fill media (Christianson et. al, 2010). These differences are attributed to the inherent material properties of the bales and the variable density levels.

Table 6.1.1 Mean values of saturated hydraulic conductivity (K_s) for switchgrass and miscanthus at four apparent dry matter bale densities; with the linear regression coefficient and standard error.

		Switchgrass			***Miscanthus***		
Density (kg m^{-3})	**S_e** (kg m^{-3})	**K_s** (cm s^{-1})	**S_e** (cm s^{-1})	**R^2** (-)	**K_s** (cm s^{-1})	**S_e** (cm s^{-1})	**R^2** (-)
144.2	6.7	0.616	0.136	0.96	0.658	0.146	0.98
173.0	4.4	0.425	0.084	0.98	0.531	0.099	0.90
201.8	3.8	0.278	0.062	0.99	0.318	0.070	0.99
225.9	3.4	0.103	0.012	0.98	0.219	0.046	0.97

The saturated hydraulic conductivity of both feedstock types was plotted versus the apparent density in Figure 6.1.4. Results indicated that the saturated hydraulic conductivity was strongly influenced by the apparent bale density ($p < 0.02$). In fact, the K_s values at the lowest target dry matter density (150 kg m^{-3}) were only 16.7 and 33.3 % of the values recorded at the highest target dry matter density (225 kg m^{-3}) for switchgrass and miscanthus, respectively. Furthermore, the feedstock type effects were found to be minimal particularly at the lower bale densities; while a significant feedstock type effect ($p < 0.0001$) was observed at the highest target dry matter density (225 kg m^{-3}). Linear models were fitted to the conductivity data which was inversely related to bale density; a scenario which was valid for most soils (Lambe and Whitman, 1979). The two best-fit models are:

$$K_{S(S)} = 1.5728 - 0.0066\rho_b \quad [6.1.3]$$

$$K_{S(M)} = 1.5898 - 0.0062\rho_b \quad [6.1.4]$$

where: $K_{S(S)}$ and $K_{S(M)}$ are the saturated hydraulic conductivities for switchgrass and miscanthus (cm s^{-1}), respectively, while ρ_b is the apparent dry bale density (kg m^{-3}).

These prediction equations for density-dependent hydraulic conductivity were found to fit the data very well with R^2 values of 0.99 and 0.97 for switchgrass and miscanthus, respectively. The standard deviations of the two feedstock types were observed to overlap, although the hydraulic conductivity for switchgrass was statistically lower ($p < 0.01$) than miscanthus bales at the highest target dry matter density (225 kg m^{-3}).

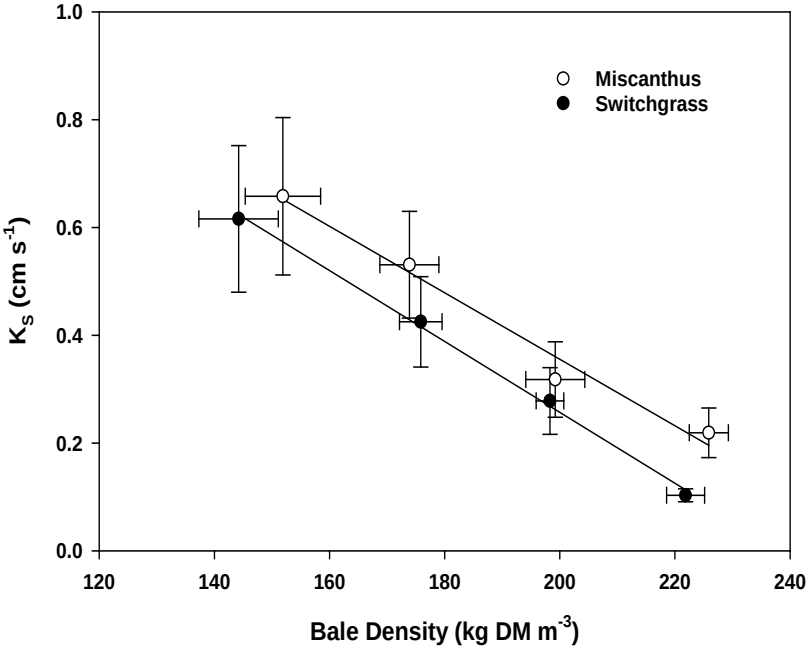

Figure 6.1.4 Saturated hydraulic conductivity (K_s) of baled switchgrass and miscanthus, and regression lines as a function of the dry bale density with R^2 values of 0.99 and 0.97; respectively.

6.1.3 Unsaturated Results

The matric suction of baled switchgrass resulting from the filter paper tests is plotted versus volumetric water content in Figure 6.1.5; along with the water retention curve developed by inverse modeling of van Genuchten. Results showed a satisfactory agreement between the van Genuchten model and experimental data at each density.

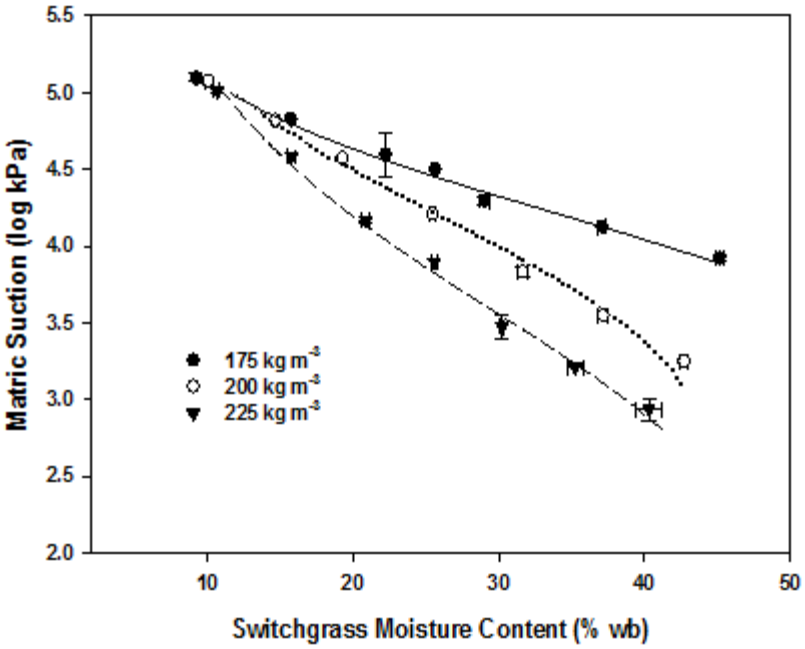

Figure 6.1.5 Measured matric suction values versus volumetric water content for baled switchgrass at target densities of 175, 200 and 225 kg m^{-3} (db). Lines are the water retention curve developed by inverse modeling of van Genuchten parameters.

The van Genuchtan parameters, α and n, were both plotted as functions of the bale density in Figure 6.1.6. Each data set represents the average of three replicate observations (bales) which have been described by linear trendlines with regression coefficients of 0.93 and 0.99 for α and n, respectively. These results indicate a significant correlation with the bulk density ($p<0.05$). Table 6.1.2 also presents the fitted van Genuchten parameters along with the standard errors.

Table 6.1.2 Average values of the van Genuchten parameters, α and n, for baled switchgrass at three target dry matter densities; with standard error.

Density (kg m^{-3})	**α** (m^{-1})	**SE** 10^{-3} (m^{-1})	**n** (-)	**SE** (-)
175	0.270	9.600	10.345	1.647
200	0.245	9.987	7.913	1.260
225	0.235	11.024	5.415	1.965

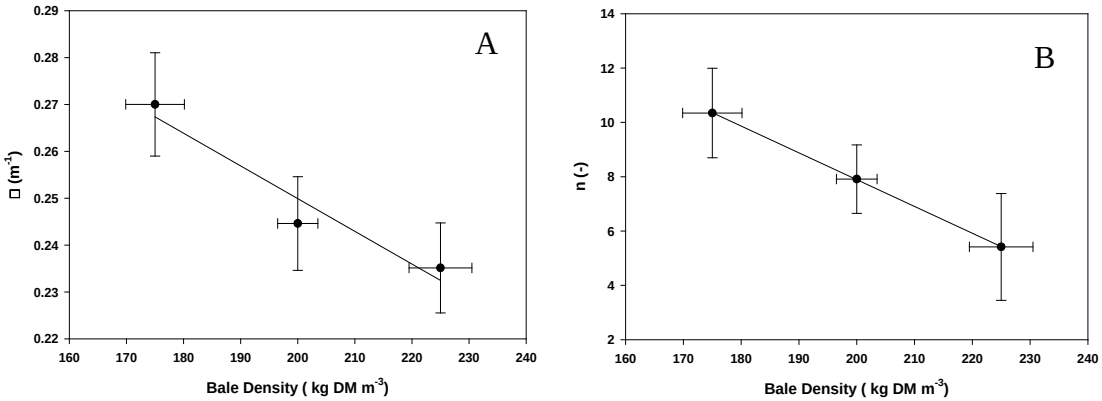

Figure 6.1.6 The van Genuchten parameters, α (A) and n (B), of baled switchgrass plotted as functions of dry matter density.

Figure 6.1.7 presents the average values of the hydraulic parameters, C_1 and C_2, as functions of the bale density. Each curve represents the average of three replicate bales, as determined from the cumulative infiltration data. The average value of C_1 ranged between 0.086 and 0.779 cm s^{-1} and between 0.200 and 5.805 cm $s^{-½}$ for C_2 depending on the bale density and moisture content. In fact, bale moisture ($p<0.01$) and density ($p<0.02$) were both observed to have a significant impact on these hydraulic parameters according to the two-way analysis of variance. The average hydraulic parameter values are also summarized in Table 6.1.3. These results are greater than those reported for soil (Zhang, 1997) which was expected due to the larger pore space within baled switchgrass.

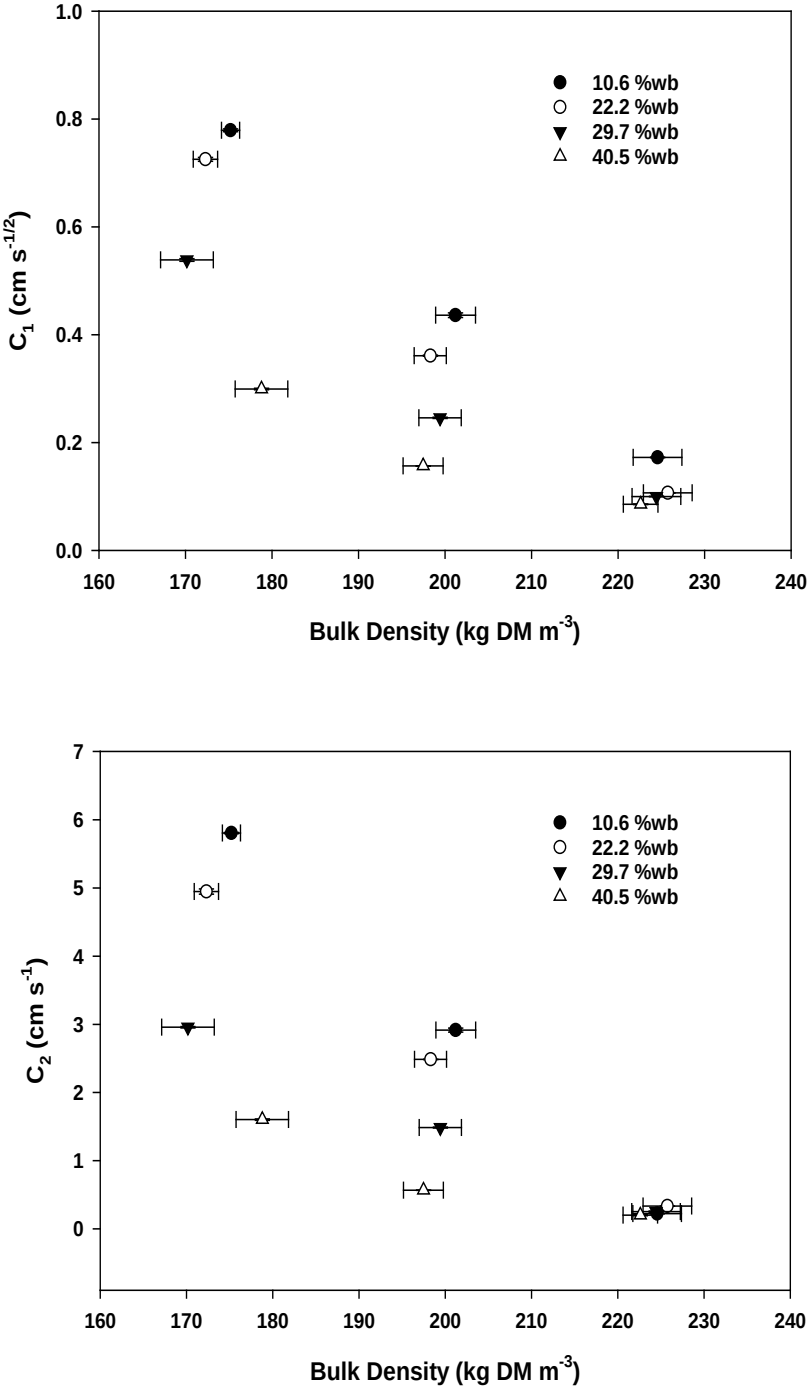

Figure 6.1.7 Curve fitting parameters, C_1 and C_2, of Philip's two-term equation for baled switchgrass as functions of dry matter density at four moisture levels (10.6, 22.2, 29.7 and 40.5 %-wb). Standard errors of C_1 and C_2 are minimal with averages of only ± 0.5% and ± 1.0% of the reported values, respectively.

The hydraulic conductivity and sorptivity of baled switchgrass, as estimated from the cumulative infiltration data are shown in Figure 6.1.8 and Figure 6.1.9; respectively. The average unsaturated K_u value ranged between 0.019 and 0.272 cm s^{-1} depending on the bale density and moisture content. The calculated K_u values resulted in a good description of the infiltration data and are in agreement with literature values for other materials such as soil, with typical K_u values between 3.32 x10^{-6} and 6.79 x10^{-6} m s^{-1} (Zhang, 1997). As expected, the K_u values for baled switchgrass were higher than those reported for soil, likely due to the increased pore space and corresponding higher water flow rate through the material. Likewise, these results are consistent with the saturated values reported earlier in this study, which were higher due to the fully-saturated, steady-state flow conditions. Thus, the unsaturated K_u values developed for baled switchgrass may be considered appropriate for use in unsaturated flow calculations. The estimates of unsaturated hydraulic conductivity and sorptivity are also summarized in Table 6.1.3.

Table 6.1.3 Hydraulic parameters (C_1 and C_2), unsaturated hydraulic conductivity (K_u) and sorptivity (S) values calculated from the cumulative infiltration data in baled switchgrass at -0.2 cm of tension and variable moisture contents (M) and dry matter densities.

	174.1 (± 3.2) kg m^{-3}				**199.1** (± 1.4) kg m^{-3}				**224.3** (± 1.1) kg m^{-3}			
M (%-wb)	**C_1** x10^{-6} (cm s^{-1})	**K_u** (cm s^{-1})	**C_2** x10^{-6} (cm $s^{-½}$)	**S** (cm $s^{-½}$)	**C_1** x10^{-6} (cm s^{-1})	**K_u** (cm s^{-1})	**C_2** x10^{-6} (cm $s^{-½}$)	**S** (cm $s^{-½}$)	**C_1** x10^{-6} (cm s^{-1})	**K_u** (cm s^{-1})	**C_2** x10^{-6} (cm $s^{-½}$)	**S** (cm $s^{-½}$)
10.6	0.779	0.272	5.805	2.103	0.437	0.126	2.916	1.219	0.172	0.024	0.223	0.539
22.2	0.726	0.184	4.948	1.276	0.361	0.103	2.485	0.939	0.107	0.028	0.333	0.465
29.7	0.539	0.145	2.958	0.990	0.246	0.084	1.485	0.465	0.100	0.011	0.252	0.168
40.5	0.299	0.073	1.601	0.677	0.157	0.061	0.567	0.155	0.086	0.019	0.200	0.048

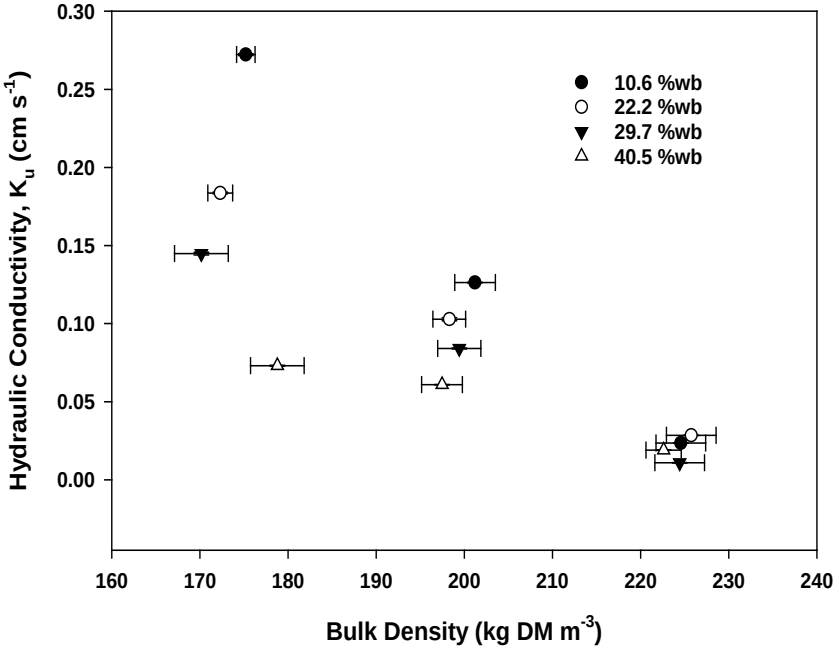

Figure 6.1.8 Unsaturated hydraulic conductivity (K_u) of baled switchgrass as a function of dry bale density at four moisture content levels (10.6 ± 1.2, 22.2 ± 1.6 29.7 ± 2.2 and 40.5 ± 1.6 %-wb).

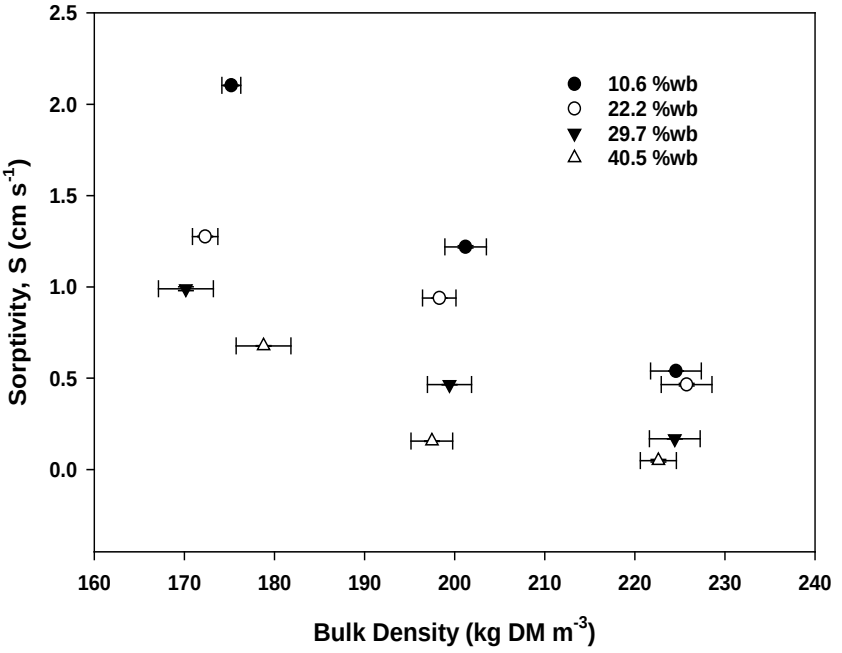

Figure 6.1.9 Sorptivity (S) of baled switchgrass as a function of dry bale density at four moisture content levels (10.6 ± 1.2, 22.2 ± 1.6 29.7 ± 2.2 and 40.5 ± 1.6 %-wb).

Bale density ($p<0.01$) and moisture content ($p<0.02$) were both found to significantly affect the unsaturated hydraulic conductivity and sorptivity according to a two-way analysis of variance. The inverse relationship between hydraulic parameters and bale density is associated with the void and inter-particle space in which fluid flow occurs. Accordingly, the higher density bales have less inter-particle space thereby inhibiting fluid flow. This effect is reversed in lower-density bales as the large void space permits greater fluid flow through the bales. Initially, the moisture content was observed to inhibit the flow of water through the material, thereby resulting in lower K_u values. This is expected to be a result of various adhesive forces between the water and surfaces of the switchgrass. Additional fluid must either be redirected into new pore channels or overcome these surface forces. This effect is at least minimized in saturated conditions in which steady-state flow is established through all pore channels. For most cases, the standard errors were within 1 %, while the maximum standard error was 1.6 %. In general, the computation of K_u is more sensitive to the moisture content, and less sensitive to density, than that of S.

6.2 Moisture Measurement

6.2.1 Calibration

The relationship between moisture content and the voltage output from the TDR probe is graphically presented in Figure 6.2.1 for ground switchgrass and Figure 6.2.2 for miniature baled switchgrass. Both physical formats (ground and baled) are shown in the respective figure with each density treatment fitted with a quartic calibration curve. Some density levels were unattainable in the course of this evaluation due to the physical limitations associated with the packing ability and the saturated state (amount of moisture capable of being held within the material); a factor that becomes particularly relevant at the lower density treatments which hold less water at saturation. It should also be noted that the data presented for ground switchgrass is averaged over all three temperatures evaluated in this study (23.3, 32.2 and 40.6 °C) since no statistical difference ($p = 0.24$) was observed with the temperature effect.

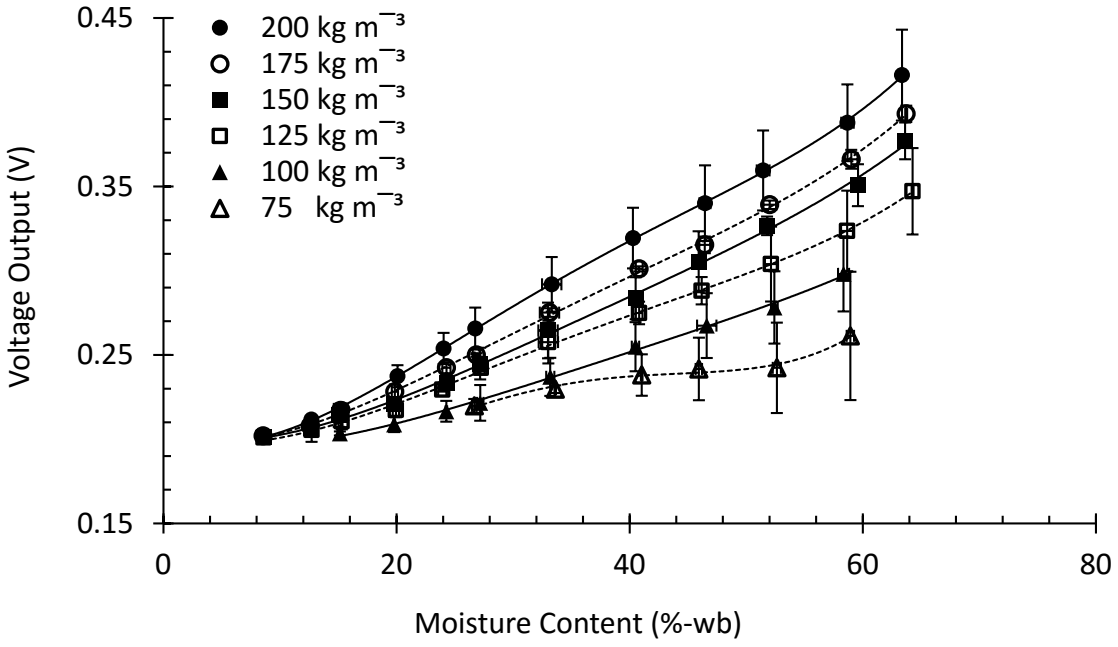

Figure 6.2.1 Calibration curves describing the relationship between moisture content and the voltage output from a CS615 TDR probe for 2-mm ground switchgrass at variable bulk densities.

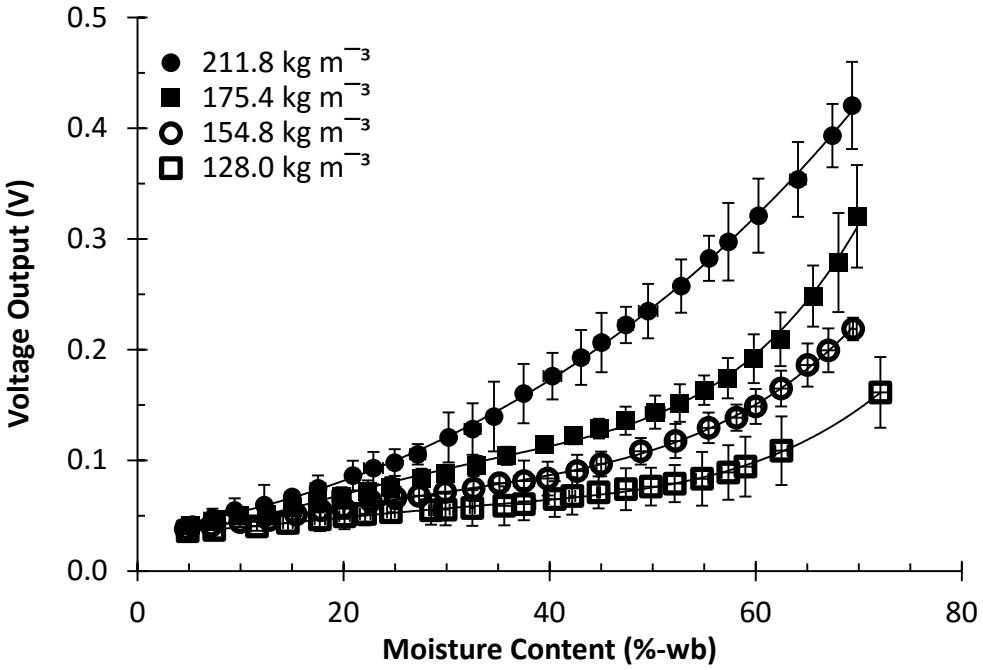

Figure 6.2.2 Calibration curves describing the relationship between moisture content and the voltage output from a CS615 TDR probe for miniature baled switchgrass at variable bulk densities.

All sensors appeared to perform well within the whole range of moisture contents assessed in this study. The inverse relationship with density indicates the importance of good contact between the sensor and the material, which is difficult to achieve with loose packing. As such, a single prediction equation was not suitable to estimate the moisture content under all experimental conditions. Measurement error may also have been introduced by the shrink-swell nature of the material as well as the development of air gaps as the probes were repeatedly inserted and removed from the material. A summary of the quartic polynomial curve parameters are given in Table 6.2.1 for each density level of both physical formats of switchgrass.

Table 6.2.1 Forth-order polynomial coefficients fitted to the voltage-moisture content data obtained from the TDR readings for ground and miniature baled switchgrass.

	Density (kg m^{-3})	Intercept (mV)	Linear Coefficient	Squared Coefficient	Cubic Coefficient	Quartic Coefficient	R^2 (-)
Ground	75	0.2015	-5.7488E-3	4.8190E-4	-1.1411E-5	8.7862E-8	0.9859
	100	0.2015	-1.7354E-3	1.5190E-4	-2.6179E-6	1.7226E-8	0.9978
	125	0.2015	-1.7595E-3	2.0803E-4	-4.1549E-6	2.9433E-8	0.9989
	150	0.2015	-1.4044E-3	1.8166E-4	-3.2621E-6	2.2420E-8	0.9984
	175	0.2015	-1.6770E-3	2.3063E-4	-4.5266E-6	3.2305E-8	0.9994
	200	0.2015	-2.2834E-3	3.1337E-4	-6.4009E-6	4.5210E-8	0.9998
Baled	128.0	0.0348	1.1030E-5	6.1796E-5	-1.8132E-6	1.7872E-8	0.9982
	154.8	0.0355	4.1599E-4	6.4259E-5	-1.8919E-6	2.0626E-8	0.9993
	175.4	0.0356	-3.6484E-4	1.8640E-4	-5.1600E-6	4.8290E-8	0.9974
	211.8	0.0366	1.1030E-3	6.0437E-5	-2.2885E-7	3.8171E-9	0.9995

Significant correlation was observed between the voltage output and the moisture content ($p < 0.0001$) and bulk density ($p < 0.0001$) for both physical formats of the switchgrass. However, the measurement accuracy was somewhat compromised at the lower levels of bulk density as indicated by a greater standard error.

6.2.2 Validation

The moisture content of full sized baled switchgrass at the highest initial moisture treatment (initial target of 40 %-wb) over the 60 day storage evaluation is shown in Figure 6.2.3. The two data sets represent the gravimetrically determined moisture content and the moisture content determined from the empirical TDR calibration. In this case, the gravimetric evaluation was based on the moisture content determined from triplicate subsamples cored from each bale that were destructively sampled on a two-week interval (day 14, 31, 45 and 60). Although the initial moisture profile of each bale was spatially variable with slightly higher moisture content in the base and below the major axis of each bale, the average moisture content for each bale is presented here in order to limit the apparent variation in the data. Hence, the gravimetric line represents the average of three subsamples from three replicate bales at each interval (3 subsamples x 3 replicate bales = 9 readings per interval). The initial moisture content was based on samples collected from the windrow at the time of baling.

On the other hand, TDR measurements were performed within a single bale replicate (3 positions x 1 replicate bale x 1 treatment = 3 total measurements) due to the limited number of TDR probes available in the current study. In this case, three measurements were recorded at each sampling interval according to the positional arrangement discussed in section 5.2.5. Measurements were taken at all three locations on a 10 minute sampling interval. Daily average values were obtained from the voltage output data and subsequently used in determining the moisture content according to the appropriate TDR calibration curve.

Although periodic measurements were also taken for each bale replication of the other moisture treatments (on days 14, 31, 45 and 60), the data presented here pertains only to a single bale prepared at the highest initial moisture treatment (initial target of 40 %-wb). While the use of additional TDR sensors could have provided more frequent assessments of the other moisture treatments, no further measurements were pursued in this study due to the poor fit of the data observed in the preliminary results. It will also be noted here that the average air temperature within the environmental chamber during the monitoring period was 29.5 ± 0.6 °C.

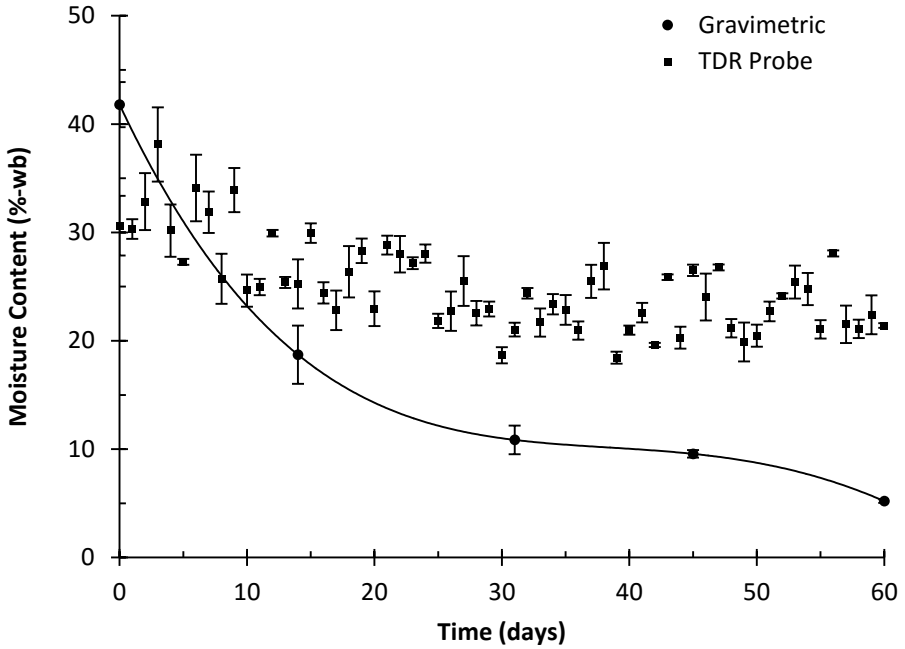

Figure 6.2.3 Moisture content of baled switchgrass at the highest moisture treatment (initial target of 40 %-wb) measured gravimetrically and with TDR probe (CS615) over the 60 day storage evaluation.

The drying curves obtained from the gravimetric method and the TDR calibration were significantly different based on these results. In this case, the values determined by the gravimetric method provided reliable moisture data; indicating a gradual reduction in the moisture content over the storage period (41.8 to 5.2 %-wb). However, the TDR-based approximation of the moisture content indicated an average decline of only 16.7 %-wb over the storage period. The moisture data obtained from the TDR calibration evidently resulted in overvalued approximations of the moisture content with significant standard error.

This deviation from the true moisture content was attributed to the high degree of inherent variability with the larger bale size which significantly affected the TDR readings. While a separate calibration of the TDR sensor could be performed with this larger bale size, the high degree of error would still be a limiting factor in the application of this technology. Although a validation of the TDR method was unable to be achieved with the larger bale size in this study, these results at least indicated a high degree of sensitivity to the material properties which must be tightly controlled in order to obtain reasonable estimates of the moisture content. This level of control was only attainable in the calibration procedure with the smaller sample sizes.

6.3 Thermal Property Analysis

6.3.1 Calibration

The average thermal conductivity (k) values determined for each calibration medium (distilled water and distilled water containing 1 % w/v agar) are shown in Table 6.3.1. The measured (k_m) and reference (k_r) values of thermal conductivity were both observed to increase as the temperature increased. The calibration coefficient (C) and percentage error (e_k) were calculated using equations 5.3.4 and 5.3.5; respectively, for each medium and temperature level evaluated in this study.

Table 6.3.1 Thermal conductivity (k) of distilled water with and without 1 % (w/v) agar at various temperatures.

	Temp (°C)	Measured, k_m (W m^{-1} $°C^{-1}$)	Reference, k_r * (W m^{-1} $°C^{-1}$)	Error † e_k (%)	Calibration ‡ C (-)
Water	20	0.607 (0.003)	0.597 (0.0045)	1.66	0.984
	25	0.621 (0.004)	0.606 (0.0067)	2.49	0.976
	90	0.744 (0.019)	0.678 (0.0155)	9.75	0.911
Water & Agar	4	0.582 (0.004)	0.572 (0.0038)	1.75	0.983
	22	0.615 (0.005)	0.603 (0.0055)	2.13	0.979
	40	0.657 (0.005)	0.625 (0.0077)	5.09	0.952

§ Values in parenthesis represent standard error, n = 3
* Reference: Rahman (1995); Singh and Heldman (2009)
† Error values (e_k) calculated from equation 5.3.5
‡ Calibration coefficient (C) calculated from equation 5.3.4.

The average thermal diffusivity (α) values determined for distilled water are shown in Table 6.3.2. The measured (α_m) and reference (α_r) values of thermal diffusivity were also observed to increase as the temperature increased. The percentage error (e_α) at each temperature level was calculated using an analogous expression to equation 5.3.5.

Table 6.3.2 Thermal diffusivity (α) of distilled water at different temperatures based on the temperature-dependent specific heat, density and reference thermal conductivity.

Temp (°C)	Measured, α_m 10^{-7} (m^2 s^{-1})	Reference α_r * 10^{-7} (m^2 s^{-1})	Error e_α (%)
22	1.485 (0.003)	1.430 (0.0108)	3.85
25	1.515 (0.007)	1.454 (0.0161)	4.20
90	1.797 (0.019)	1.670 (0.0382)	7.63

§ Values in parenthesis represent standard error, n = 3
* Reference: Emami et al. (2007); Singh and Heldman (2009)
† Error values (e_α) calculated from an analogous expression to equation 5.3.5

The calibration coefficient ranged between 0.911 and 0.984 for both mediums; indicating that the dual probes were suitable for measuring thermal conductivity and diffusivity. The average calibration coefficient was implemented in the current study with a value of 0.964. The error and variability observed in this study may be attributed to imprecise construction of the probe or natural convection currents which could affect the measurements of the diffusivity probe.

Following the calibration procedure, three replicate bales were measured at each combination of dry bulk density (157.2, 172.4, 197.2 and 230.1 kg m^{-3}), mean environmental temperature (20.3, 30.2 and 40.1 ºC) and moisture content (11.4, 20.8, 29.0 and 42.3 %-wb) for a total of 144 readings. Measurements were performed in both the lateral plane (parallel to the flake orientation) and the transverse orientation (axial direction of bale compression) in order to determine the relevant thermal properties in relation to both directional orientations.

A typical measurement of the temperature rise in both probes is shown in Figure 6.3.1. The temperature rise data for the thermal conductivity probe typically exhibited linearity after 80 s. This linear trend continued until approximately 240 s when the tests were concluded. Based on this analysis, the linear portions (approximately 80 to 200 s) of all data sets were used for determining the thermal properties. The R^2 values for all tests were at least 0.9994; indicating sufficient temperature predictions were achieved with the mathematical model (equation 5.3.2).

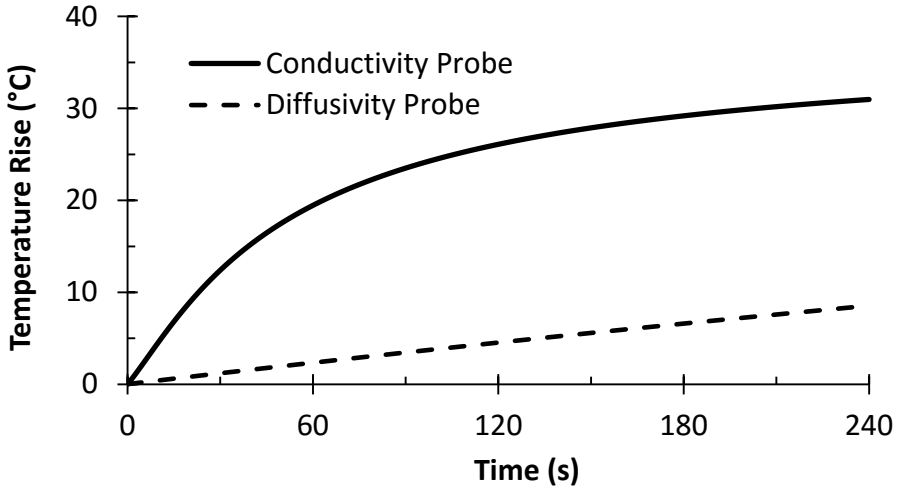

Figure 6.3.1 Typical temperature measurements within baled switchgrass as were measured with the dual thermal probe.

6.3.2 Thermal Conductivity

6.3.2.1 Overview

The average values and variation of the thermal conductivity are discussed here with respect to each independent variable assessed in this study; including the dry bulk density, moisture content, temperature and bale orientation (lateral or transverse). A summary of the average thermal conductivity values obtained for all three replicate bales is given in Table 6.3.3 with respect to each of these independent variables. The thermal conductivity ranged from 2.73E-2 to 6.10E-2 W m^{-1} °C^{-1} for the lateral orientation; and from 1.04E-2 to 5.96E-2 W m^{-1} °C^{-1} for the transverse orientation.

Table 6.3.3 Thermal conductivity (k) of baled switchgrass in the lateral and transverse orientations at variable temperature, moisture content and dry bulk density levels.

Temp (°C)	Moisture Content (%wb)	Effective Thermal Conductivity, k (W m^{-1} °C^{-1})							
		at 157 kg m^{-3}		at 172 kg m^{-3}		at 197 kg m^{-3}		at 230 kg m^{-3}	
		Lat	Tran	Lat	Tran	Lat	Tran	Lat	Tran
20.3	11.4	0.027	0.010	0.032	0.021	0.034	0.033	0.037	0.036
30.2	11.4	0.032	0.024	0.034	0.015	0.036	2.31	0.040	0.024
40.1	11.4	0.039	0.032	0.046	0.032	0.045	0.042	0.051	0.034
20.3	20.8	0.029	0.026	0.033	0.030	0.034	0.032	0.039	0.038
30.2	20.8	0.034	0.032	0.039	0.038	0.040	0.033	0.042	0.036
40.1	20.8	0.044	0.040	0.044	0.043	0.051	0.045	0.052	0.050
20.3	29.0	0.031	0.026	0.037	0.035	0.033	0.030	0.037	0.036
30.2	29.0	0.036	0.035	0.042	0.040	0.040	0.039	0.044	0.043
40.1	29.0	0.047	0.047	0.047	0.043	0.054	0.051	0.055	0.053
20.3	42.3	0.030	0.028	0.033	0.032	0.037	0.035	0.039	0.037
30.2	42.3	0.039	0.038	0.040	0.038	0.042	0.040	0.045	0.045
40.1	42.3	0.049	0.048	0.048	0.041	0.047	0.045	0.061	0.060

† Each thermal conductivity value represents the average measurement of 3 replicate bales.

Similar values of thermal conductivity have been reported in the range of 0.028 to 0.061 W m^{-1} °C^{-1} for baled timothy hay (Opoku et al., 2004) and between 0.045 to 0.076 W m^{-1} °C^{-1} for baled tobacco (Casada and Walton, 1989). It may also be noted that these values are lower than those for ground barley straw reported in the range of 0.641 to 0.845 W m^{-1} °C^{-1} (Iroba et al., 2013) since the inherently tighter compaction of ground material promotes heat transfer by conduction to a greater extent.

6.3.2.2 Density Effect

Figure 6.3.2 shows the thermal conductivity in both directional orientations as a function of the square root of dry bulk density. This particular analysis considers the averaged values of thermal conductivity across all moisture content and temperature levels. In this case, the lower bulk density levels exhibited lower thermal conductivity at all moisture and temperature treatments. This positive correlation between bulk density and thermal conductivity was attributed to the improved level of heat conduction that is established by greater amounts of solid material that become available for conductive heat transfer at higher densities. On the other hand, lower bulk densities treatments exhibited lower values of thermal conductivity as a consequence of the increased porosity.

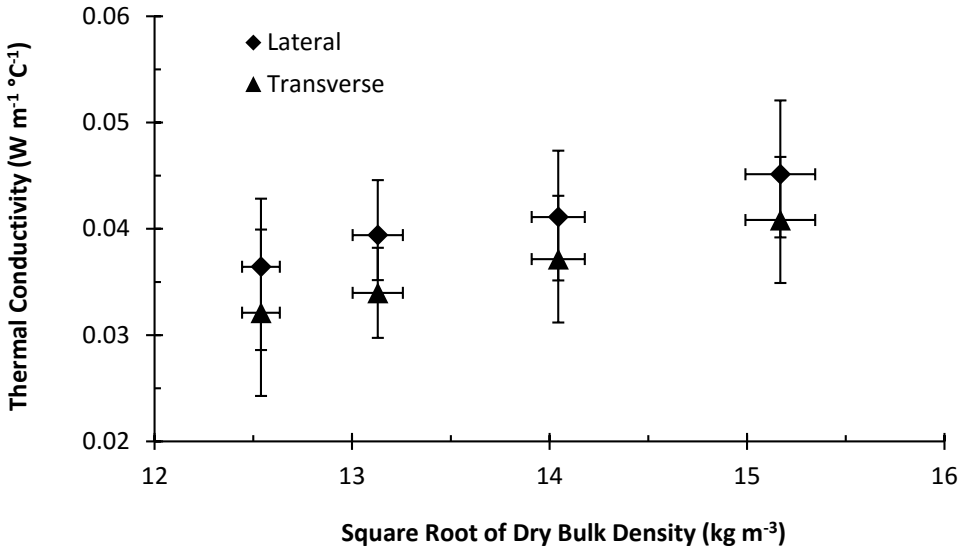

Figure 6.3.2 Thermal conductivity (k) of baled switchgrass as a function of the dry bulk density in both directional orientations (lateral and transverse) averaged across all temperature and moisture content levels.

These results also indicated a nearly linear dependence on the square root of dry bulk density with the regression lines for the lateral and transverse orientations having R^2 values of 0.977 and 0.999, respectively. The slope of the least-squares best fit line was greater for the lateral plane (parallel to the flake orientation) compared to the slope for the transverse direction (perpendicular to the flake orientation) since the heat transfer mechanisms were different with respect to each directional orientation.

6.3.2.3 Moisture Effect

Figure 6.3.3 shows the average thermal conductivity across all temperature and bulk density levels in both directional orientations as a function of the moisture content. In this case, the lower moisture content levels exhibited lower thermal conductivity for all temperature and bulk density treatments.

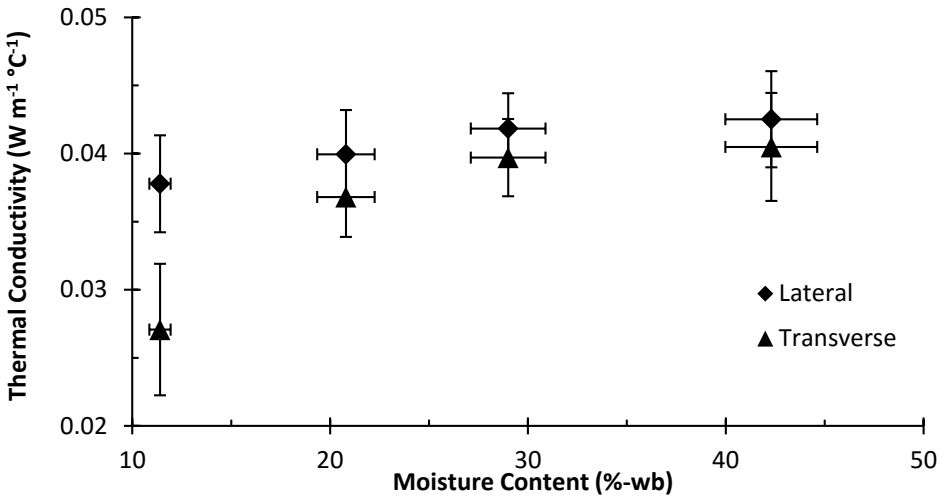

Figure 6.3.3 Thermal conductivity (k) of baled switchgrass as a function of moisture content in the lateral and transverse bale orientation averaged across all temperature and bulk density levels.

These results also indicate a curvilinear dependence on the moisture content with less difference between the lateral and transverse orientations observed at the higher moisture contents. The seemingly convergent nature of the trendlines indicates that the thermal conductivity at high levels of moisture content is influenced to a greater extent by the water contained within the material. The second-order polynomial regression for the lateral and transverse orientations had R^2 values of 0.9920 and 0.9916, respectively.

6.3.2.4 Temperature Effect

Figure 6.3.4 shows the thermal conductivity in both directional orientations (lateral and transverse) as a function of the temperature averaged across all levels of moisture content and bulk density. Results indicated a slightly positive correlation between thermal conductivity and temperature over the given range (20.3 to 40.1 °C) which is a typical trend for a narrow temperature range (Carslaw and Jaeger, 1959). This

trend occurs as the elevated temperatures contribute to increased atomic motion within the biomass; thus, promoting heat transfer within the material.

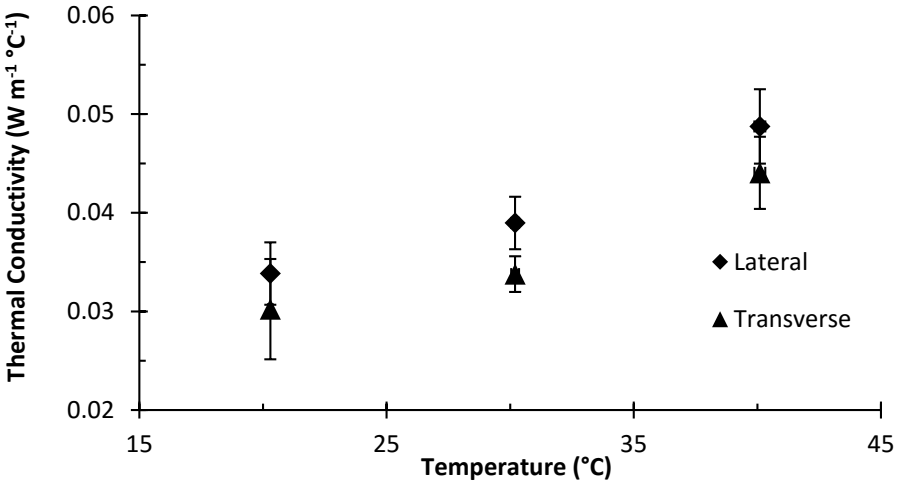

Figure 6.3.4 Thermal conductivity (k) of baled switchgrass as a function of temperature in the lateral and transverse orientations averaged across all moisture content and bulk density levels.

Casada and Walton (1989b) reported a positive linear correlation between the temperature and thermal conductivity of burley tobacco leaf with values ranging from 0.0554 to 0.0704 W m^{-1} °C^{-1} depending on the moisture content (17.0 to 24.0 %-wb) and the dry bulk density (values not given). Positive correlations between temperature and thermal conductivity were also reported for apple (Ramaswamy and Tung, 1981); chickpea flour (Emami et al., 2007), granular starch (Drouzas and Saravacos, 1988; Lan et al., 2000); rhizomes (Izadifar and Baik, 2007), sucrose gel (Renaud et al., 1992), sugarbeet roots (Tabil et al., 2003) and tomato paste (Drusas and Saravacos, 1985). In the present case, the second-order polynomial regression for the lateral and transverse orientations had R^2 values of 0.999 and 0.999, respectively.

6.3.2.5 Statistics

The analysis of variance indicated that dry bulk density, moisture content and temperature all had significant effects ($P < 0.0001$) on thermal conductivity at a 0.05 significance level; except for some levels of the moisture content with the lateral orientation. The analysis of variance further indicated a significant directional effect

(lateral or transverse) at the 0.05 level. The average thermal conductivity values across all temperature, moisture content and bulk density treatments were 0.041 and 0.036 W m^{-1} $°C^{-1}$ for the lateral and transverse orientations, respectively. Based on this analysis, the thermal conductivity in both directional orientations was modeled as a function of the dry bulk density, moisture content and temperature as follows:

$$k_L = -1.155(10^{-2}) - 7.1158(10^{-4})T + 2.435(10^{-5})T^2 + 4.2222(10^{-4})M - 4.94(10^{-6})M^2 + 3.12(10^{-3})\rho_b^{0.5} \quad [6.3.1a]$$

$$k_T = -2.618(10^{-2}) - 1.41(10^{-3})T + 3.502(10^{-5})T^2 + 1.70(10^{-3})M - 2.385(10^{-5})M^2 + 3.33(10^{-3})\rho_b^{0.5} \quad [6.3.1b]$$

where: k_L and k_T = lateral and transverse thermal conductivity (W m^{-1} $°C^{-1}$), respectively; ρ_b = dry bulk density (kg m^{-3}); M = moisture content (%-wb); and T = temperature (°C).

6.3.3 Thermal Diffusivity

6.3.3.1 Overview

The thermal diffusivity of the baled switchgrass was also evaluated using the data collected from the diffusivity probe at the same temperatures (20.3, 30.2 and 40.1 °C), moisture contents (11.4, 20.8, 29.0 and 42.3 %-wb) and dry bulk density levels (157, 172, 197 and 230 kg m^{-3}) as discussed earlier. Table 6.3.4 shows the resulting values of the thermal diffusivity in relation to these independent variables. The thermal diffusivity ranged from 1.443E-7 to 2.031E-7 m^2 s^{-1} for the lateral orientation; and from 0.863E-7 to 2.284E-7 m^2 s^{-1} for the transverse orientation.

Table 6.3.4 Thermal diffusivity (α) of baled switchgrass in the lateral and transverse orientations at variable temperature, moisture content and dry bulk density levels.

Temp (°C)	Moisture Content (%wb)	Thermal Diffusivity, α ($m^2 s^{-1}$) x 10^{-7}							
		at 157 kg m^{-3}		at 172 kg m^{-3}		at 197 kg m^{-3}		at 230 kg m^{-3}	
		Lat	Tran	Lat	Tran	Lat	Tran	Lat	Tran
20.3	11.4	1.723	1.650	1.724	1.045	1.881	2.284	1.531	1.233
30.2	11.4	1.583	0.863	1.554	1.505	1.443	1.473	1.597	1.419
40.1	11.4	1.684	1.468	1.695	1.553	1.673	1.288	1.703	1.550
20.3	20.8	1.802	1.685	1.758	1.379	1.599	1.536	1.634	1.714
30.2	20.8	1.706	1.308	1.767	1.721	1.597	1.186	1.781	1.410
40.1	20.8	1.752	1.905	1.851	1.267	1.657	0.995	1.476	1.550
20.3	29.0	1.830	1.628	1.628	1.469	1.807	1.340	1.566	1.296
30.2	29.0	1.843	1.520	1.885	1.863	1.581	1.675	1.565	1.478
40.1	29.0	1.682	1.574	1.713	0.998	1.749	1.634	1.813	1.257
20.3	42.3	1.705	1.471	1.784	1.599	1.748	1.165	1.655	1.152
30.2	42.3	2.031	1.451	1.807	1.464	1.650	1.650	1.592	1.452
40.1	42.3	1.959	1.755	1.769	1.839	1.730	1.560	1.748	1.486

† Each thermal diffusivity value represents the average measurement of 3 replicate bales.

Similar values of thermal diffusivity have been reported for baled timothy hay in the range of 1.042E-7 to 3.031E-7 $m^2 s^{-1}$ (Opoku et al., 2004) and single alfalfa stems between 0.789E-7 and 1.076E-7 $m^2 s^{-1}$ as assessed at variable temperatures (20 to 50 °C) and moisture contents (46.75 to 58.54 %-wb) (Ford and Bilanski, 1969). The thermal diffusivity values reported in the current study for baled switchgrass are somewhat lower than those for ground barley straw which have been reported in the range of 3.511E-3 to 1.8714E-4 $m^2 s^{-1}$ (Iroba et al., 2013), this was expected since ground material reacts to changes in temperature more readily.

6.3.3.2 Density Effect

Figure 6.3.5 shows the average thermal diffusivity across all levels of moisture content and temperature in both directional orientations as a function of the dry bulk density.

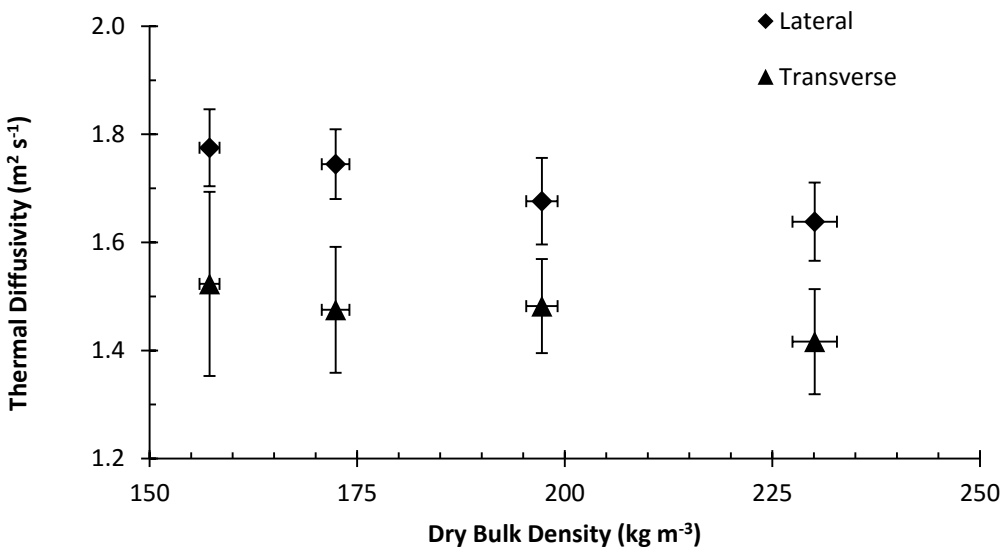

Figure 6.3.5 Thermal diffusivity (α) of baled switchgrass as a function of the dry bulk density in both directional orientations (lateral and transverse) averaged across all temperature and moisture content levels.

In this case, the lower bulk density levels exhibited slightly greater values of thermal diffusivity. In fact, the thermal diffusivity of many biological materials is influenced by the local variation in the physical structure (Kostaropoulos and Saravacos, 1997). For instance, Emami et al. (2007) reported an inverse correlation between the thermal diffusivity and bulk density of chickpea flour (416.49 to 504.12 kg m^{-3}), isolated starch (346.68 to 427.10 kg m^{-3}) and isolated protein (335.06 to 414.98 kg m^{-3}). The thermal diffusivity for baled switchgrass followed a similar trend in this study.

The linear regression lines for the lateral and transverse orientations in baled switchgrass had R^2 values of 0.9661 and 0.8547, respectively. However, minimal influence was observed in the transverse orientation due to the inherently unique physical composition of the material within the axial direction of bale compression. This particular response to the bulk density may be attributed to the variation in porosity and material heterogeneity in the transverse orientation. For instance, the existence of discontinuous porous cavities in the transverse orientation could result in a slower response to temperature change. While higher densities could potentially indicate a strong correlation to bulk density in the transverse orientation.

6.3.3.3 Moisture Effect

Figure 6.3.6 shows the average thermal diffusivity across all temperature and bulk density levels in both directional orientations as a function of the moisture content. The thermal diffusivity generally showed minimal correlation with the moisture content over the range evaluated in this study (11.4 to 42.3 %-wb). Linear regression lines for the lateral and transverse orientations had R^2 values of 0.9819 and 0.9682, respectively.

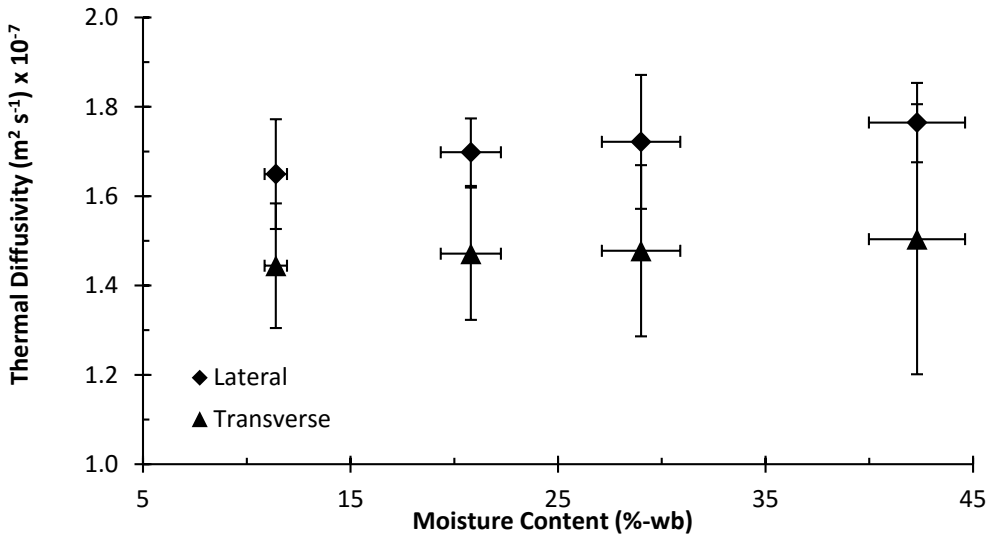

Figure 6.3.6 Thermal diffusivity (α) of baled switchgrass as a function of the moisture content in both directional orientations (lateral and transverse) averaged across all temperature and bulk density levels.

6.3.3.4 Temperature Effect

Figure 6.3.7 shows the thermal diffusivity in both directional orientations as a function of temperature averaged across all levels of moisture content and bulk density. In general, the thermal diffusivity showed no correlation with the temperature over the range evaluated in this study (20.3 to 40.1 °C).

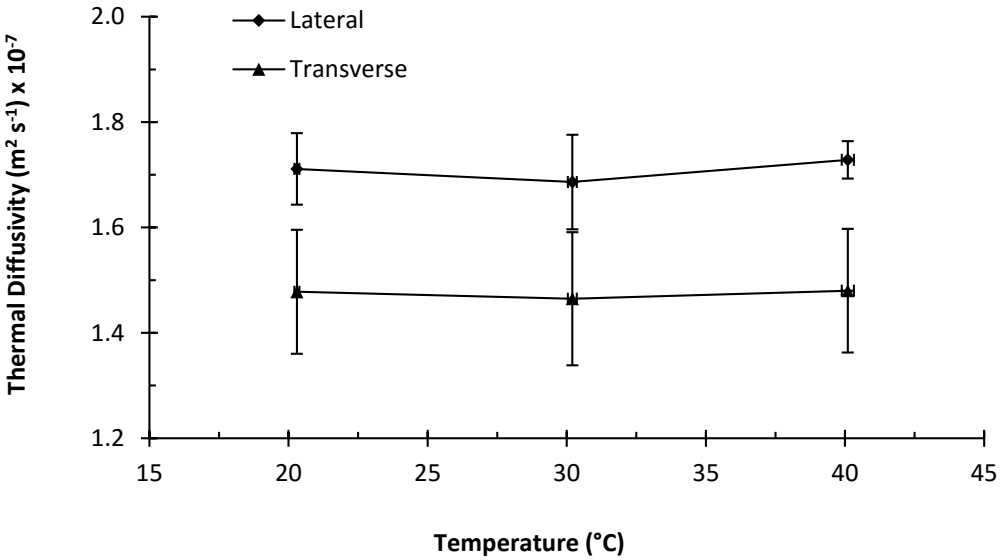

Figure 6.3.7 Thermal diffusivity (α) of baled switchgrass as a function of temperature in the lateral and transverse orientations averaged across all moisture content and bulk density levels.

Random correlations between thermal diffusivity and temperature have been reported in the literature for various biological materials (Emami et al., 2007; Lan et al., 2000). Average values of thermal diffusivity may be considered adequate in such cases; particularly with small effects relative to the moisture and density effects. Moreover, random variation in the data could make the consideration of the small temperature effect superfluous.

6.3.3.5 Statistics

The analysis of variance generally indicated that there were significant moisture and density effects (P = 0.0002) on the thermal diffusivity of baled switchgrass in the lateral orientation at a significance level of 0.05. However, the transverse orientation indicated no significant correlation between the independent parameters. In this case, measurement variation was attributed to the physical and biological variation of the material within the bale, as well as, limitations in the probe construction. Based on this analysis, the thermal diffusivity in the lateral orientation was modeled as function of the moisture content and dry bulk density as follows:

$$\alpha_L = 2.34974 + 3.63(10^{-3})M - 5.362(10^{-2})\rho_b^{0.5} \quad [6.3.2]$$

where: α_L = lateral thermal diffusivity (10^{-7} m^2 s^{-1}); M = moisture content (%-wb) and ρ_b = dry bulk density (kg m^{-3}). Since no significant correlation was observed for the transverse orientation, the average value of 1.474 x 10^{-7} m^2 s^{-1} in this directional treatment was assumed sufficient for this study. Similar results have been reported for the thermal diffusivity of haylage with the moisture content and bulk density having a significant effect at a 1 % level according to a nonlinear relationship (Jiang et al., 1986).

6.3.4 Specific Heat

6.3.4.1 Overview

The specific heat of baled switchgrass was estimated from the experimentally-determined values of thermal conductivity and thermal diffusivity according to the fundamental thermophysical relationship ($k=\alpha\rho C$). The resulting values of specific heat are shown in Table 6.3.5 for the various levels of temperature, moisture content and dry bulk density evaluated in this study. The specific heat varied from 0.92 to 1.79 kJ kg^{-1} $°C^{-1}$ for the lateral orientation and from 0.40 to 2.51 J kg^{-1} $°C^{-1}$ for the transverse orientation depending on the particular values of the independent parameters that were assessed in this study. The lateral and transverse orientations are presented separately to maintain a consistent analysis; although no significant differences were observed between these two principal orientations.

Table 6.3.5 Specific heat (Cp) of baled switchgrass in the lateral and transverse orientations calculated from experimentally-determined values of thermal conductivity and thermal diffusivity at variable temperature, moisture content and bulk density levels.

Temp (°C)	Moisture Content (%wb)	Specific Heat, Cp (kJ kg^{-1} °C^{-1})							
		at 157 kg m^{-3}		at 172 kg m^{-3}		at 197 kg m^{-3}		at 230 kg m^{-3}	
		Lat	Tran	Lat	Tran	Lat	Tran	Lat	Tran
20.3	11.4	1.008	0.40	1.071	1.191	0.926	0.731	1.056	1.252
30.2	11.4	1.266	1.733	1.280	0.583	1.277	0.796	1.076	0.729
40.1	11.4	1.480	1.365	1.578	1.190	1.359	1.636	1.310	0.965
20.3	20.8	1.006	0.974	1.075	1.257	1.070	1.064	1.032	0.951
30.2	20.8	1.276	1.570	1.280	1.270	1.278	1.400	1.023	1.113
40.1	20.8	1.590	1.349	1.379	1.964	1.575	2.286	1.517	1.394
20.3	29.0	1.081	1.016	1.318	1.373	0.924	1.129	1.033	1.201
30.2	29.0	1.236	1.460	1.280	1.261	1.275	1.167	1.231	1.256
40.1	29.0	1.789	1.892	1.579	2.510	1.573	1.569	1.310	1.840
20.3	42.3	1.123	1.210	1.072	1.171	1.072	1.503	1.033	1.404
30.2	42.3	1.231	1.644	1.278	1.502	1.277	1.228	1.230	1.333
40.1	42.3	1.591	1.747	1.581	1.296	1.391	1.477	1.518	1.744

† Each specific heat value represents the average measurement of 3 replicate bales.

Similar results have been reported for the specific heat of tobacco with values ranging from 2.1143 to 2.4493 kJ kg^{-1} °C^{-1} at a temperature of 23.3 °C and variable moisture content (7.4 and 16.7 %-wb) (Brock and Samfield, 1958). Likewise, the specific heat of baled timothy hay has been reported in the range 2.31 and 5.17 kJ kg^{-1} °C^{-1} (Opoku et al., 2004); while the specific heat of baled alfalfa has been estimated as 2.105 to 2.402 kJ kg^{-1} °C^{-1} (Buckmaster, 1986).

Some of these materials that have previously been investigated have slightly higher values of specific heat due to the tighter compaction of the material compared to that which was achieved with switchgrass in the current study. In this case, the porosity of the baled switchgrass was expected to be somewhat larger due to the nature of the material which generally had larger stem sizes. The increased porosity within baled switchgrass indicates that greater amounts of air are present within the bulk material. Hence, the relatively low value of the specific heat of air contributed to relatively low values of specific heat for the baled switchgrass.

The specific heat of ground barley straw has also been reported in the range 0.821 to 2.856 kJ kg^{-1} °C^{-1} (Iroba et al., 2013), between 1.370 to 1.536 kJ kg^{-1} °C^{-1} for ground switchgrass (Dupont et al., 2014), and from 1.431 to 2.598 kJ kg-1 °C-1 for tobacco

(Chakrabarti and Johnson, 1972). In general, the specific heat increased with increasing temperature and moisture content, but decreased with increasing dry bulk density. Similar correlations with the moisture content and bulk density have been reported for the specific heat of haylage (Jiang et al., 1986).

6.3.4.2 Density Effect

Figure 6.3.8 shows the specific heat of the baled switchgrass in both directional orientations as a function of the dry bulk density. This particular analysis was based on experimental values of thermal conductivity and thermal diffusivity averaged across all moisture content and temperature levels. Since baled switchgrass is a compound rather than a pure substance, the specific heat may vary with the density of the material. In this case, greater values of specific heat were observed at the lower bulk density levels. In this case, the decrease of specific heat with increase in density may be explained by the change of bound water into free water and the change of inner structure at higher densities. This inverse correlation between bulk density and specific heat has also been reported for baled timothy hay (Opoku et al., 2004) and haylage (Jiang et al., 1986).

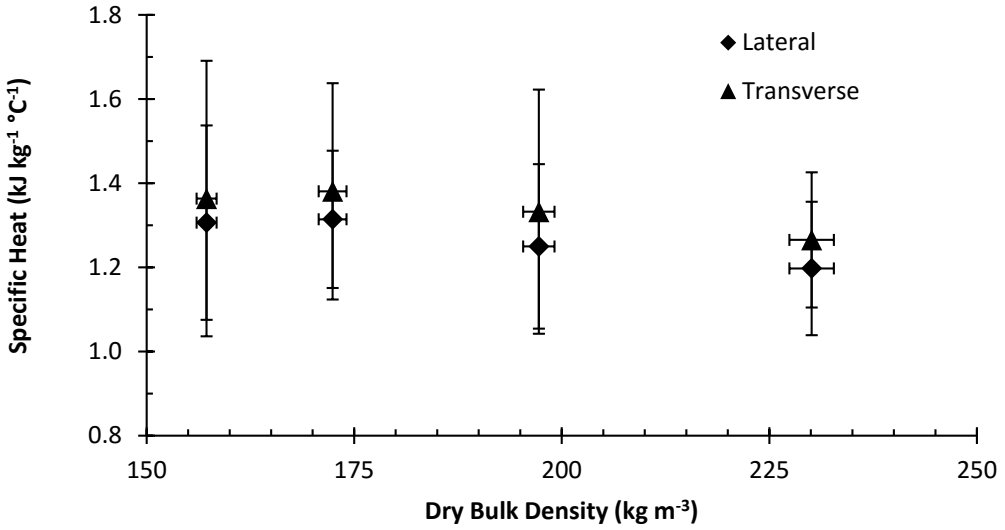

Figure 6.3.8 Specific heat (Cp) of baled switchgrass in the lateral and transverse orientations for each temperature treatment averaged across all moisture content levels.

Table 6.3.6 also summarizes the average specific heat for the baled switchgrass across all temperatures and moisture contents with respect to the dry bulk density of the

material. The standard error and uncertainty error are also provided at each level of dry bulk density evaluated in this study.

Table 6.3.6 Specific heat (Cp) of baled switchgrass at different dry bulk density levels averaged across all temperatures and moisture contents.

Dry Bulk Density ($kg\ m^{-3}$)	Lateral			Transverse		
	Cp ($kJ\ kg^{-1}\ s^{-1}$)	SE ($kJ\ kg^{-1}\ s^{-1}$)	ω_{Cp} x 10^{-3} ($kJ\ kg^{-1}\ s^{-1}$)	Cp ($kJ\ kg^{-1}\ s^{-1}$)	SE ($kJ\ kg^{-1}\ s^{-1}$)	ω_{Cp} x 10^{-3} ($kJ\ kg^{-1}\ s^{-1}$)
157.2	1.279	0.246	1.217	1.228	0.213	1.444
172.4	1.338	0.186	2.016	1.120	0.149	0.606
197.2	1.263	0.239	0.400	0.979	0.153	0.318
230.1	1.227	0.170	0.362	0.839	0.127	0.244

ω_{Cp} = the error of measurement or uncertainty of specific heat
SE = standard error, n = 3

6.3.4.3 Moisture Effect

Figure 6.3.9 shows the specific heat in both directional orientations as a function of the moisture content averaged across all other explanatory variables. A positive correlation was generally observed between the specific heat and moisture content with the lower levels of moisture content exhibiting lower values of specific heat for all temperature and bulk density treatments. In fact, the increase of biomass moisture is generally found to lead to a linear increase of heat capacity (Aviara and Haque, 2001; Bitra et al., 2010; Guo et al., 2013; Izadifar and Baik, 2007). Thus, in some cases, the measurement of dry biomass has been considered sufficient for the prediction of the heat capacity for moist biomass with water content below 60 % (Njie et al., 1998).

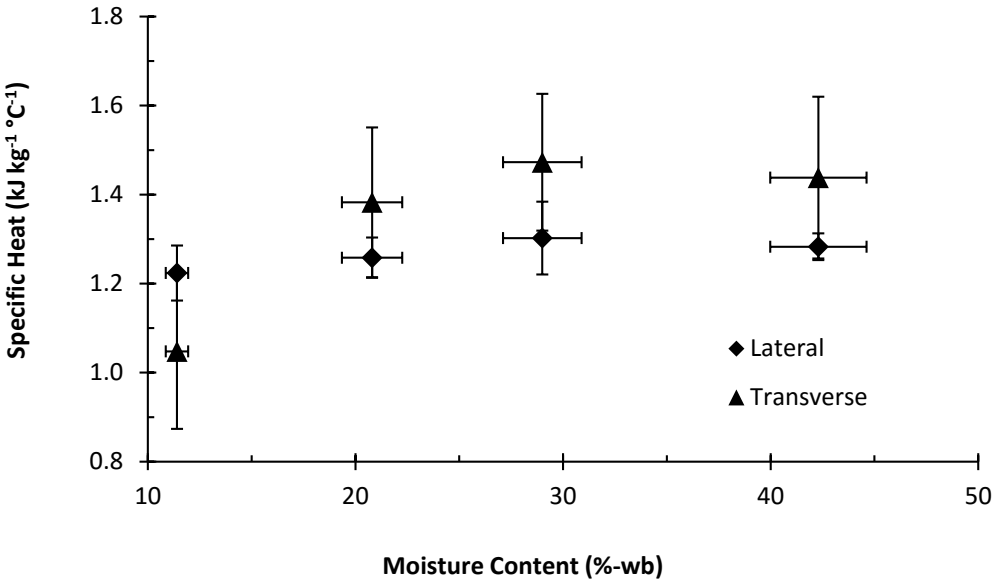

Figure 6.3.9 Specific heat (Cp) of baled switchgrass as a function of moisture content in the lateral and transverse orientations averaged across all temperature and bulk density levels.

Table 6.3.7 also summarizes the specific heat values of the baled switchgrass as a function of the moisture content averaged across all levels of temperature and dry bulk density. The standard error and uncertainty error are also provided at each level of moisture content evaluated in this study.

Table 6.3.7 Specific heat (Cp) of baled switchgrass at different moisture contents averaged across all temperatures and dry bulk densities.

Moisture Content (%-wb)	Lateral			Transverse		
	Cp (kJ kg^{-1} s^{-1})	SE (kJ kg^{-1} s^{-1})	ω_{Cp} x 10^{-3} (kJ kg^{-1} s^{-1})	Cp (kJ kg^{-1} s^{-1})	SE (kJ kg^{-1} s^{-1})	ω_{Cp} x 10^{-3} (kJ kg^{-1} s^{-1})
11.4	1.230	0.047	2.885	0.839	0.118	1.018
20.8	1.284	0.022	0.875	0.935	0.132	0.913
29.0	1.281	0.063	0.608	1.093	0.154	1.832
42.3	1.312	0.063	1.464	1.301	0.183	0.779

ω_α = the error of measurement or uncertainty of thermal diffusivity
SE = standard error (10^{-3}), n = 3

6.3.4.4 Temperature Effect

Figure 6.3.10 shows the average specific heat in both directional orientations as a function of the temperature averaged across all levels of moisture content and bulk

density. Results indicated a positive correlation between the specific heat and temperature over the specified range (20.3 to 40.1 °C). Previous studies have reported similar trends with flax fiber-HDPE biocomposites (Li et al., 2008), rhizome particle beds (Izadifar and Baik, 2007) and chickpea flour (Emami et al., 2007).

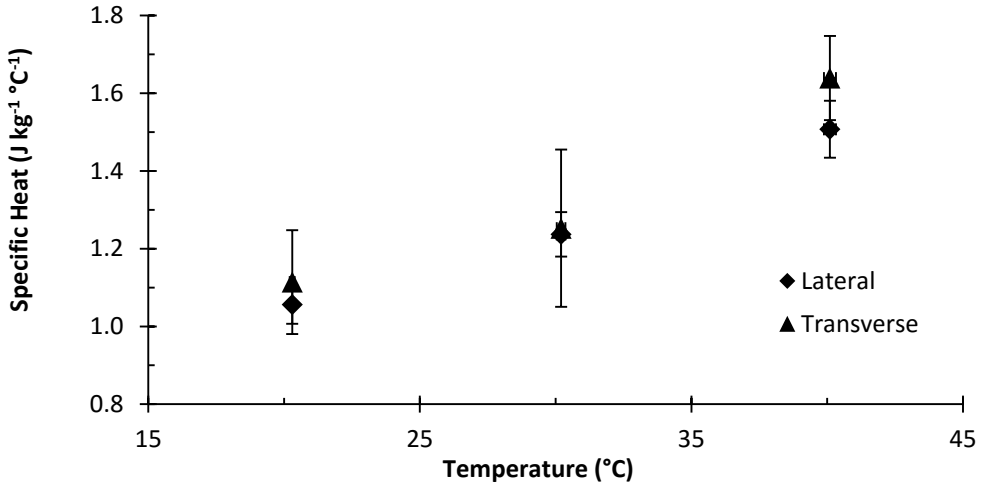

Figure 6.3.10 Specific heat (Cp) of baled switchgrass as a function of temperature in the lateral and transverse orientations averaged across all levels of moisture content and bulk density.

Table 6.3.8 also summarizes the average specific heat for the baled switchgrass across all moisture content and dry bulk density levels with respect to temperature. The standard error and uncertainty error are also provided at each level of moisture content evaluated in this study.

Table 6.3.8 Average specific heat (Cp) of baled switchgrass at different temperatures for all moisture contents and dry bulk densities.

Temperature (°C)	**Lateral**			**Transverse**		
	Cp (kJ kg^{-1} s^{-1})	SE (kJ kg^{-1} s^{-1})	ω_{Cp} x 10^{-3} (kJ kg^{-1} s^{-1})	Cp (kJ kg^{-1} s^{-1})	SE (kJ kg^{-1} s^{-1})	ω_{Cp} x 10^{-3} (kJ kg^{-1} s^{-1})
20.3	1.035	0.030	2.163	0.822	0.116	1.271
30.2	1.245	0.032	1.266	1.117	0.157	1.934
40.1	1.550	0.094	1.465	1.187	0.167	2.039

ω_α = the error of measurement or uncertainty of thermal diffusivity
SE = standard error (10^{-3}), n = 3

6.3.4.5 Statistics

The analysis of variance indicated that dry bulk density, moisture content and temperature all had a significant effects ($P < 0.0001$) on the specific heat at a significance level of 0.05; except for some treatment levels. This statistical analysis also indicated that the directional orientation had a significant effect ($P < 0.05$); although not all treatment levels exhibited this trend. Multiple regression models of the specific heat were developed as follows:

$$Cp_L = 1.15581 + 3.8064(10^{-4})T^2 + 2.02(10^{-3})M - 1.65(10^{-3})\rho_b \quad [6.3.3a]$$

$$Cp_T = 2.204 + 4.4899(10^{-4})T^2 + 6.295(10^{-2})M - 9.4372(10^{-4})M^2 \quad [6.3.3b]$$

where: Cp_L and Cp_T = lateral and transverse specific heat (kJ kg^{-1} $°C^{-1}$), respectively; M = moisture content (%-wb); T = temperature (°C); and ρ_b = dry bulk density (kg m^{-3}).

6.3.5 Application of Heat Conduction Model Validation

The initial model validation was performed using only one-dimensional heat conduction. However, the tests were designed so that one dimensional heat transfer models could be evaluated in the lateral (x and y direction) and transverse orientation (z-direction). This simple modeling step was performed to evaluate the measured thermophysical parameters and evaluate the anisotropic behavior within the bale.

Temperature data collected during the storage experiment from Section **Error! Reference source not found.** is shown in Figure 6.3.11 with each line representing the mean daily temperature evaluated for each directional treatment. In this case, random variation in the temperature data was minimized by averaging all thermocouple positions (n = 3) and treatment replications (n = 3). The results indicated a slower response to the temperature change in the transverse orientation (z-direction); while the lateral orientations (x and y directions) responded somewhat quicker. This difference was attributed to the greater values of thermal conductivity that were measured in the lateral orientation, as well as, the promotion of convective heat transfer through the continuous pore channels formed within the lateral orientation. The similar response time for both of

the lateral components (x and y directions) also indicated that the thermophysical properties are relatively similar within the plane parallel to the flake orientation.

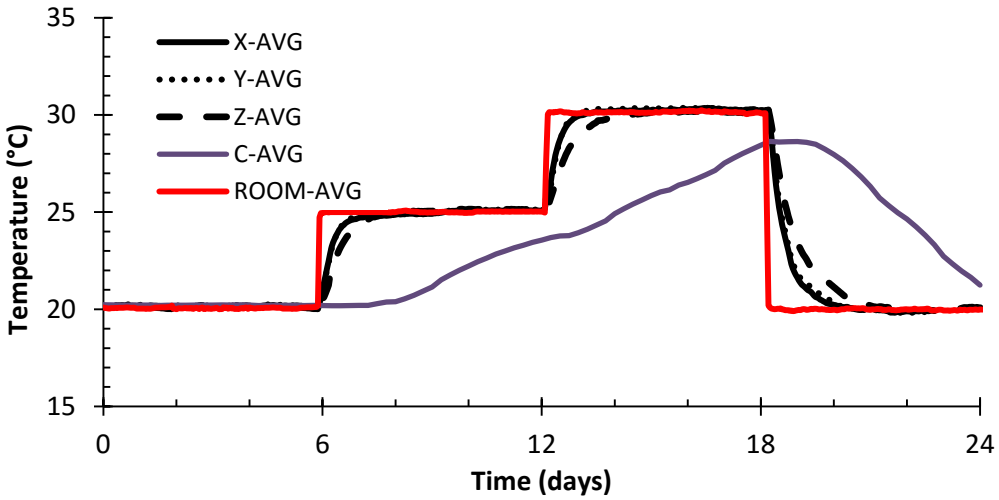

Figure 6.3.11 Temperatures recorded in the storage evaluation of baled switchgrass with respect to the three directional treatments (x, y and z); as well as the average room temperature.

The resulting temperature data for each directional treatment was implemented in the simple conduction model presented in section 5.4.1 in order to generate the daily average thermal diffusivity for each respective treatment (x, y and z). In this case, the heat generation (within the material) and the moisture transfer (between the environment and the material) were both considered negligible. The validity of this assumption was substantiated by the fact that no weight change was observed for any treatment over the storage period. It was also evident that the temperature changes observed in each treatment were in direct response to changes in the environmental temperature rather than other sources such as microbial activity.

The resulting values of thermal diffusivity according to the conduction model (α_m) are shown in Figure 6.3.12, along with the results obtained from the dual probe method (α_p).

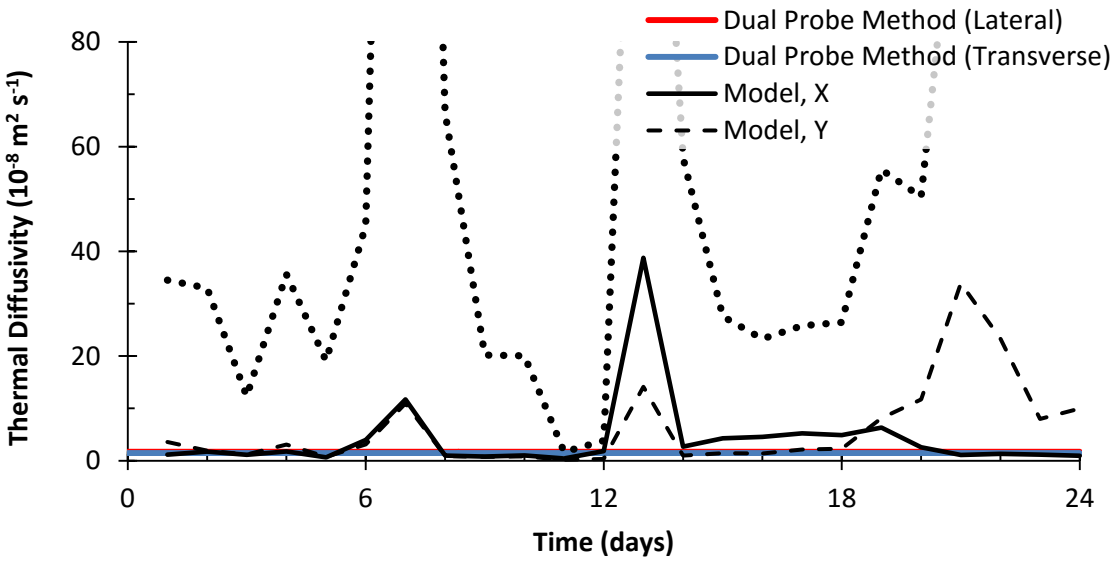

Figure 6.3.12 The thermal diffusivity of baled switchgrass determined from the statistical analysis of the dual thermal probe method (α_p) and those values determined from a simple conduction model (α_m). Values are referenced at the center position of each bale.

In this case, the dual probe method provided constant thermal diffusivity values in both directional orientations since there were no significant correlations observed with respect to temperature. The daily average thermal diffusivity values for both lateral components (α_x and α_y) determined from the conduction model were generally similar to the statistical results, but only during the periods of relative temperature stability. In fact, the model estimated values of thermal diffusivity were generally within ± 30 % during the constant temperature periods. However, more significant errors resulted in the conduction model during the transitional periods (day 6, 12, and 18).

The failure of the conduction model during each transitional period is largely attributed to the limited number of thermocouple positions that were used to measure the temperature during this storage experiment. Further refinement of the spatial discretization could be achieved with additional instrumentation; thereby, improving the model predictions. The thermal diffusivities of both components of the lateral orientation were also slightly underpredicted compared with the statistical model during those periods of stable temperature. While these low calculations of thermal diffusivity according to the simple conduction model may be attributed in part to the limited grid

refinement, the oversimplification of this conduction model was also considered to impact these results.

It may also be noted that the solution of this simple conduction model in terms of the thermal diffusivity of the transverse orientation (α_z) resulted in much greater error. In this case, the results obtained for the periods of temperature stability were greatly overvalued; while the transitional temperature periods experienced more significant error. Thus, conclusive validation of the thermal diffusivity was not obtained from this analysis; particularly in regards to the transverse orientation. However, there was a clear indication that different heat transfer mechanisms are involved in the transverse orientation. Hence, the results of this modeling study further demonstrated the anisotropic nature of the miniature bales of switchgrass with regards to the lateral and transverse orientations. These results also indicate the involvement of other heat transfer mechanisms since the thermal diffusivity was generally undervalued in both lateral orientations during the constant temperature periods.

6.4 Heat and Mass Transfer Model

6.4.1 Experimental Data

Experiments were performed with baled switchgrass stored inside a controlled environment chamber for 60 days according to the procedure outlined in section 5.4.5. Three replicate bales were prepared at each initial moisture treatment with the average value of each treatment measured as 10.7 (± 0.1), 22.6 (± 1.0), 31.6 (± 2.0) and 41.8 (± 2.8) %-wb. These initial moisture content values were relatively close to the target levels; particularly considering the potential for significant material variation during the conditioning and baling processes. The average densities for these unique treatments were approximately 100.2 (± 3.3), 123.5 (± 4.6), 152.1 (± 4.2), and 172.3 (± 9.2) kg m^{-3} on a dry basis as achieved by the rectangular baler.

6.4.1.1 Temperature

The temperature within each bale was monitored at 10 minute intervals for 60 days according to the procedure described in section 5.4.3. Average daily temperatures were obtained from this data to minimize random variation. The air temperature within the environmental chamber was also monitored in this storage assessment following a similar procedure. It should be noted here that the peripheral thermocouple positions within each bale were not employed in this analysis due to an apparent random variation in the measured temperatures at those positions. This random temperature variation may be attributed to a significant variation of the characteristic physical properties of the material along the edges of each bale. In this case, the baling process was believed to cause significant variation in the bulk density and porosity, among other factors, at the peripheral surfaces of the bale. In addition, the inaccurate/inconsistent placement and material disturbance due to the thermocouples could have led to random temperature variations. These conditions were expected to affect the heat and mass transfer within the material and were therefore omitted from the current analysis. However, the center temperatures were expected to provide more reliable temperature data as the bulk properties were more consistent within the interior of each bale.

The average daily temperatures for each moisture treatment are shown in Figure 6.4.1 along with the average daily air temperature within the environmental chamber. A more detailed view is also depicted in Figure 6.4.2 for the first 48 hours of the storage evaluation. Each line presented in this set of figures represents the average temperatures recorded at the center position of all three bale replications. The line representing room temperature was also averaged for all nine thermocouple positions within the environmental chamber. It may be noted here that a minimal temperature difference was observed between the different thermocouple positions within the environmental chamber. In fact, the average temperature difference between the front and back of the environmental chamber was only 0.8 °C throughout the storage evaluation. The effects of this small temperature difference were further minimized through random distribution of the bale treatments within the environmental chamber. The average room temperature was maintained at approximately 29.5 (± 0.6) °C throughout the storage evaluation.

The initial bale temperature for all treatments was approximately 23 °C in accordance with the environmental conditions at the time of baling. The average temperature of each bale treatment was then observed to increase for at least 40 days before reaching a relative temperature equilibrium with the ambient air. This equilibrium process was believed to be expedited with the relatively small bale size that was used in the current study. These daily average temperatures for each moisture treatment, as well as, those temperatures measured at the central position of each bale, were specifically used for model validation

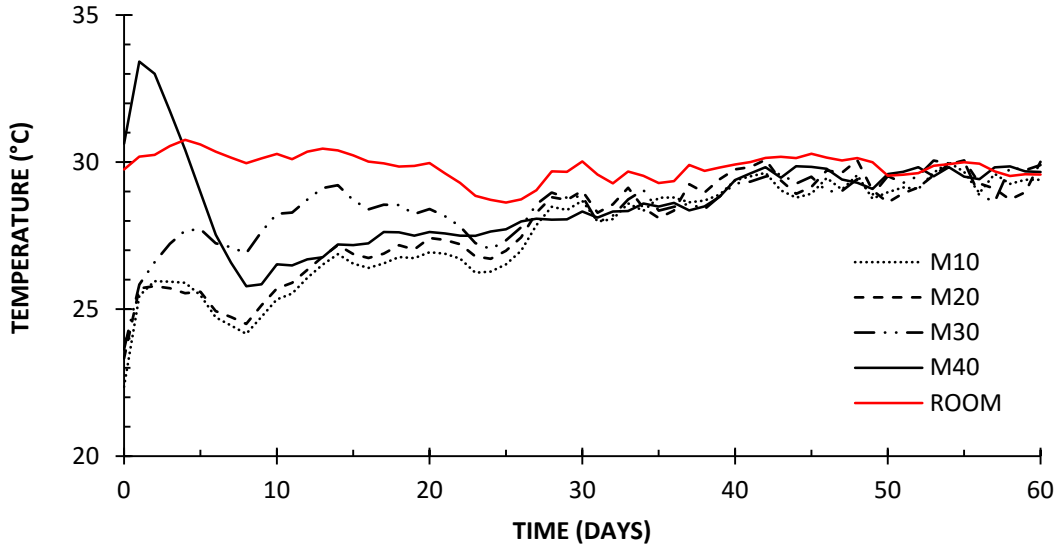

Figure 6.4.1 Average daily temperature at the center of baled switchgrass stored for 60 days in a controlled environmental chamber that was maintained at 29.5 ± 0.6 °C and relative humidity of 23.2 ± 3.9 %. Each line represents the average of three replicate bales prepared for each target moisture treatment (M10=10%, M20=20%, M30=30%, and M40=40%-wb).

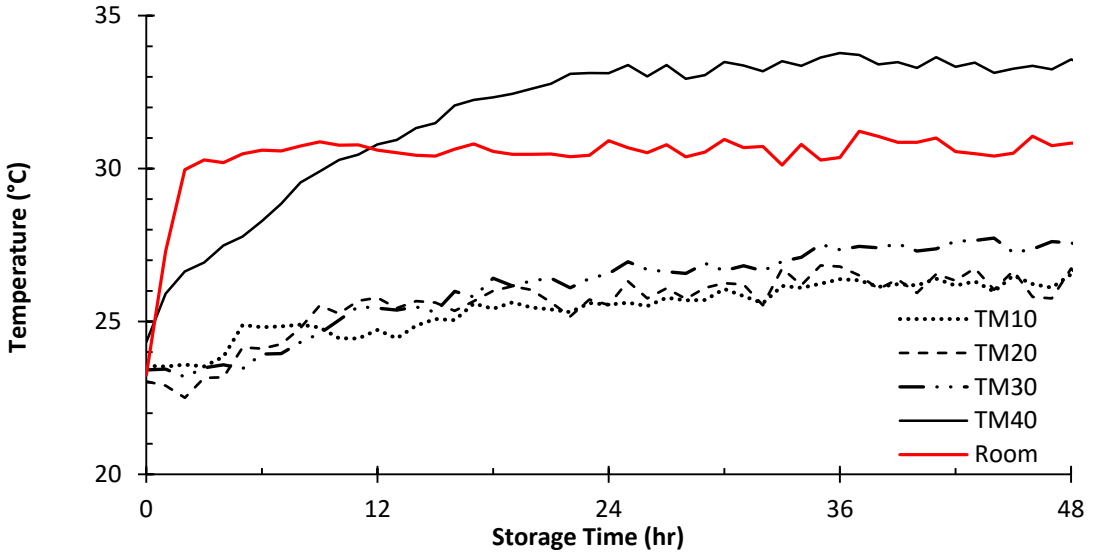

Figure 6.4.2 Average hourly temperature at the center of baled switchgrass for the first 48 hours in a controlled environmental chamber that was maintained at 29.5 ± 0.6 °C and relative humidity of 23.2 ± 3.9 %. Each line represents the average of three replicate bales prepared for each target moisture treatment (M10=10%, M20=20%, M30=30%, and M40=40%-wb).

Two distinct trends were observed in the temperature data. The first trend involves a temperature rise occurring in the initial storage period up to approximately 10 days. This initial temperature rise was believed to be strongly influenced by the microbial (mesophilic) heat generation occurring within the higher moisture material. The varying extent of this initial temperature rise for each respective treatment indicates a strong influence and correlation with the moisture content which has been previously documented in baled hay (Farm and Ranch Extension, 2012).

As discussed earlier in this report, moist environments (such as the rewetted bales of switchgrass) are more conducive to microbial growth and respiration. As a result, considerable amounts of heat are generated in moist material with the consumption of dry matter occurring through various biological processes. Since microbial activity and respiration contribute to dry matter losses, a positive correlation can be made between the moisture content, rise in temperature and the amount of dry matter loss.

The maximum temperatures achieved in this initial stage of the storage evaluation were approximately 25.9, 25.8, 27.7 and 33.4 °C for the target moisture treatments of 10, 20, 30 and 40 %-wb, respectively. The high moisture treatment experienced the greatest temperature change during this period. The maximum temperature is an important parameter for many storage and bioconversion applications since it indicates the effective (i.e., nutrient retention) and safe (i.e., no combustion) storability of the biomass.

Further analysis indicated that an increase in the moisture content at the time of baling increased the maximum temperature observed in storage ($r = 0.743$). In fact, results of a one-way analysis of variance indicated significant effects of the moisture treatment on the maximum temperature ($p = 0.05$). A subsequent drop in temperature was then observed for each treatment between days 4 to 8; which has commonly been attributed to diminished microbial activity within stored bales (Buckmaster, 1986).

The next phase of temperature development observed during this storage evaluation indicated a gradual heating towards the constant temperature of the air within the environmental chamber; hereafter referred to as room temperature. Minimal heat generation was assumed to occur in this secondary heating period; particularly beyond the first 20 days of storage. This assumption was substantiated by an apparent reduction in the moisture content for each initial moisture treatment. Average bale temperatures

during this phase were also higher in the wetter treatments; further supporting the idea that higher respiration rates and increased microbial activity are promoted in wetter biomass.

6.4.1.2 Moisture Content

Moisture content was also evaluated gravimetrically every two weeks (day 14, 31, 45 and 60) by removing subsamples from each destructive bale replicate according to the procedure discussed in section 5.4.3. Three subsamples were also collected from every replicate bale on day 60 for gravimetric analysis. The average moisture content between these three sampling locations is shown in Figure 6.4.2 for each of the target moisture treatments prepared in this study. In this case, each line represents the average moisture content measured between the three sampling locations within the bale. It may also be noted, that the initial moisture content was based on subsamples taken from the windrow at the time of baling.

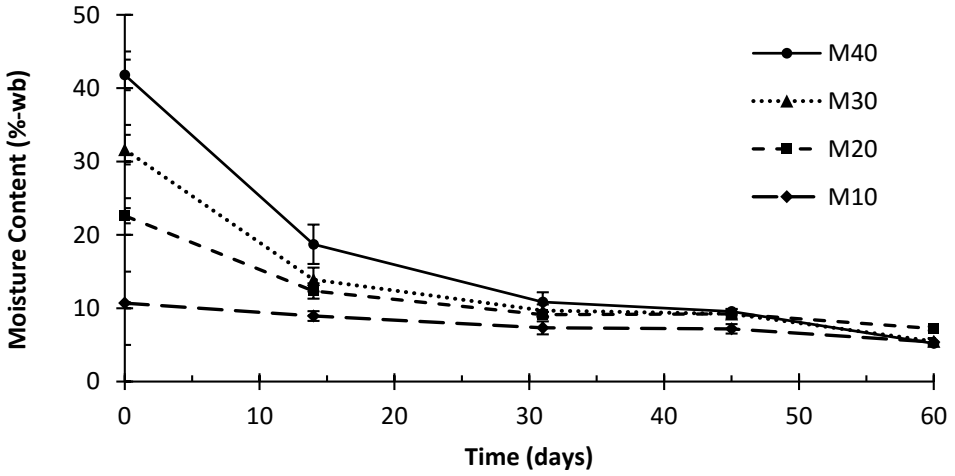

Figure 6.4.3 Average moisture content based on triplicate subsamples cored from each bale. Each line represents the average of three replicate bales with the associated SE indicated with vertical bars (data includes peripheral sampling). The initial moisture content (time zero) and SE were based on hand samples from the windrow prior to baling.

The gravimetrically-determined values of moisture content for each treatment were found to be in good agreement with the average values that were determined in accordance with the change in bale weights (assessed at the same sampling interval). In

this case, there were generally no significant differences between the values of moisture content determined from gravimetric analysis and those values determined from bale weights at a significance level of 0.05. The minimal differences that were observed between these two methods of measurement were attributed to the material loss that occurred from the physical handling of the bales. The overall agreeance of these two methods of measurement supported the use of the gravimetrically-determined values of moisture content from the destructive bale replicates.

In general, minimal variation in the moisture content was observed throughout each bale; particularly at the lower moisture treatments. This observation was attributed to the relatively small bale size used in this study. However, the moisture was generally found to be the highest in the center of the bale; a condition that was more pronounced at the highest moisture level. This moisture data was also used to calculate a simple drying coefficient according to the standard form of the drying equation:

$$\mathrm{M} = \mathrm{M}_0 \mathrm{e}^{-k\mathrm{t}} \qquad [6.4.1]$$

where: M = moisture content (%-wb); k = drying coefficient (s^{-1}); t = time (s) and the subscript 0 represents the initial value. In this case, the average value of the drying coefficient was 5.711E-8, 3.953E-7, 1.879E-7 and 2.099E-7 s^{-1} for the target moisture treatments of 10, 20, 30 and 40 %-wb, respectively. Hence, larger drying constants were observed in the wetter bales.

These values of the drying coefficient were also compared with the more sophisticated model described in Chapter 4 of this study (equation 4.30). The radiation term was considered negligible in this evaluation; with an assumed wind speed of 1 m s^{-1} which was considered to be a reasonable estimate of the flow rate of air moving through the environmental chamber. In this case, the resulting values of the drying coefficient ranged from 1.082E-3 to 1.085E-3 s^{-1} which was somewhat higher than the rates that were determined according to the periodic assessments made in the storage evaluation. This difference was attributed to the much higher levels of density for the baled format of switchgrass which was expected to slow the rate of drying.

6.4.1.3 Dry Matter Loss

The average dry matter loss (DML) for each treatment was also determined based on the difference between the initial and final mass of the solid content assessed on day 60. The mass of the solid content for each treatment was evaluated using the bale weights and the corresponding moisture content for each respective bale replication. A moisture content of 18 %-wb is generally considered to be the upper limit of the acceptable level for baled switchgrass in order to effectively prevent quality changes or excessive DML from occurring. On the other hand, baling above 20 % moisture may lead to significant quality changes.

The relatively short duration of this storage evaluation, and the promotion of a relatively dry environment, resulted in minimal DML even at the highest moisture treatments with values of only 0.73 (± 0.5), 0.51 (± 0.11), 1.82 (± 0.20) and 2.68 (± 0.45) % for the target moisture treatments of 10, 20, 30 and 40 %-wb, respectively. In this case, DML consistently increased with an increase in the initial moisture content. It may also be noted that no moisture treatments resulted in a DML value of zero, even with the lowest moisture treatment. Of course, it should also be noted that some of the observed losses were associated with the physical handling of the material. Regardless, a higher DML was observed in the wetter bale treatments.

Results of one-way analyses of variance indicated a significant treatment effect of the moisture content on DML ($p = 0.05$). Based on these results, the moisture content was considered to be an important factor affecting DML. Two-way analysis of variance further suggested that DML had a significant positive correlation with the initial moisture content ($r=0.92$) and the maximum temperature ($r=0.96$). In this case, the increased microbial activity occurring at high moisture levels contributed to elevated levels of temperature and DML. On the other hand, lower levels of temperature and moisture content indicate that DML will be reduced since it is correlated to temperatures and heating.

6.4.2 Heat Generation Calibration

The simple conduction heat transfer model developed in this study (see section 5.4.1) was applied to this experimental data for empirical calibration of the heat

generation rate. This heat generation model was evaluated with respect to the four unique moisture treatments that were assessed in this storage evaluation. All bales were considered to be in thermal equilibrium with the air temperature of 23 °C at the onset of storage. The ambient temperature within the environmental chamber was subsequently maintained at a constant 29.5 °C throughout the simulation of this storage evaluation, which eliminated any potential discrepancies that could otherwise be introduced with a dynamic environmental temperature. Likewise, the moisture content of each treatment was initialized as 10.7, 20.6, 31.6, and 41.8 %-wb in accordance with the experimental data.

The heat generation rates determined from the simple conductive model were averaged for each day; with the resulting heat generation rate plotted over time as shown in Figure 6.4.3 for each respective moisture treatment. Only the first 30 days of storage are presented in this figure since the heat generation values remained fairly constant beyond that time period. This plot illustrates the important effect of time and moisture content on heating. It may also be noted that the heat generation rate was not monotonic with an initial linear increase in the heat generation rate for several days and subsequent linear decrease thereafter. In this case, the maximum heat generation rates were observed at approximately 3 to 4 days into the storage evaluation.

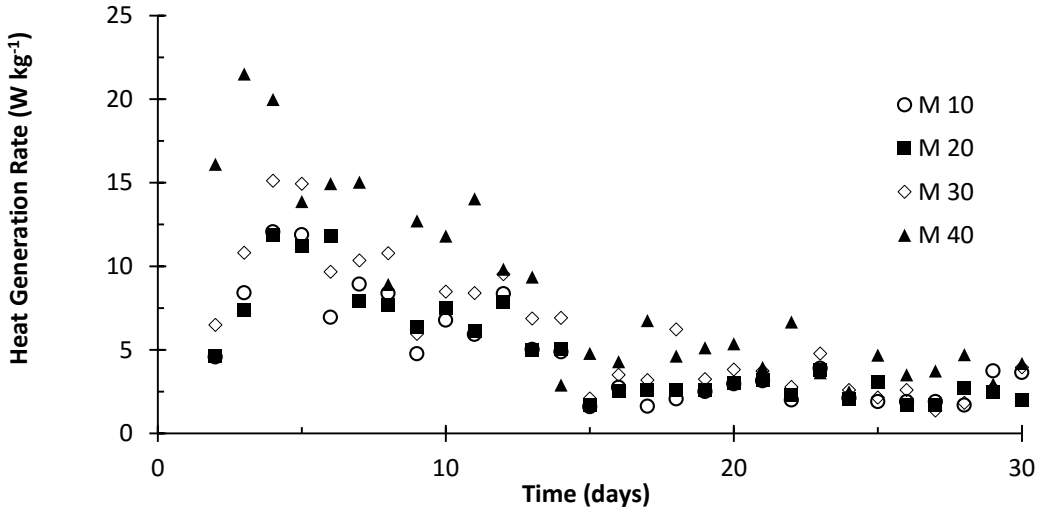

Figure 6.4.4 Heat generation rates of the baled switchgrass over time for the first 30 days of storage.

The heat generation rate calculated for day 14, 31, 45 and 60 are also summarized in Table 6.4.1 along with those values that were calculated according to the formulation presented in Appendix B (see section B.7) for aerobic respiration. In this case, the aerobic respiration rate was expressed as a function (equation B.15) of the temperature and moisture contents that were evaluated on those same days.

Table 6.4.1 Heat generation rates of baled switchgrass on the specified days during the storage evaluation with respect to each initial moisture treatment.

DAY	M10		M20		M30		M40	
	Y_T * (W kg^{-1})	G † (W kg^{-1})	Y_T * (W kg^{-1})	G † (W kg^{-1})	Y_T * (W kg^{-1})	G † (W kg^{-1})	Y_T * (W kg^{-1})	G † (W kg^{-1})
2	3.79	4.58	11.67	4.65	10.19	6.49	5.49	16.10
14	3.99	4.88	9.27	5.07	12.70	6.91	3.44	2.89
31	2.12	2.70	8.67	1.68	12.57	3.07	3.54	2.71
45	2.18	1.77	3.67	2.49	4.46	2.68	5.89	3.78
60	1.69	2.01	5.62	2.41	3.88	1.81	4.42	1.70

* Evaluation according to the aerobic respiration formulation (see section B.7)
† Evaluation according to the simple conduction model (see section 5.4.1)

The heat generation rates determined from both methods were generally similar, while the average heat generation rates over the entire 60-day storage period were determined (in accordance with the conductive model) to be 3.65, 3.88, 4.47 and 5.66 W kg^{-1} for the target moisture treatments of 10, 20, 30 and 40 %-wb, indicating that both methods resulted in a strong positive correlation with the moisture content. It may also be noted that the values presented here for baled switchgrass were lower than those reported for paper mill sludge with broiler litter at 28.18 W kg^{-1} (Ekinci et al., 2006), straw and poultry manure composting at 32.30 W kg^{-1} (Harper et al., 1992) and municipal waste composting at 69.44 W kg^{-1} (Irvine et al., 2010).

The heat generation rate data (12 bales x 60 days each = 720 data points) were analyzed for statistical significance using analysis of variance. In this case, the sensible heat generation rate was expressed as a function of both the moisture content and storage time by means of nonlinear (stepwise) regression analysis. It may be noted, however, that the heat generation rate could not be expressed in terms of a single independent moisture variable, nor could the storage time be expressed in terms of a constant power, since the overall trend was not monotonic. Therefore, two distinct sets of data were considered

with the first set corresponding to the increasing trend ($t \leq 4$ days) and the other set corresponding to the decreasing trend ($t \geq 4$ days). Data from day 4 of the storage evaluation was used in both equations to provide continuity.

This stepwise regression was specifically developed with an assessment of the following independent variables: moisture content, bulk density, an interaction term (moisture content times bulk density), the square and square root of each of these terms, and storage time. The resulting best fit equations ($p = 0.05$) predicting the sensible heat generation rate of baled switchgrass as a function of the significant independent variables were determined according to the following expressions:

$$G = C_0 + C_1 t + C_2 M + C_3 \rho^2 + C_4 M\rho \quad (t \leq 4) \qquad [6.4.2a]$$

$$G = \Gamma_0 + \Gamma_1 t + \Gamma_2 M - \Gamma_3 \rho + \Gamma_4 M^2 - \Gamma_5 (M\rho)^2 + \Gamma_6 (M\rho)^{0.5} \quad (t \geq 4) \qquad [6.4.2b]$$

where: G = heat generation rate (W kg^{-1}); M = moisture content (dec. wb); ρ = density (kg m^{-3}); t = storage time (days) and the subscript i represents the initial conditions. The coefficients C_0 to C_4 are given as 14.11368, 3.615, -1.511, -1.68E-3 and 1.535E-2, respectively; while the coefficients Γ_0 to Γ_6 were given as 4.68691, -0.10778, -10.91246, -0.51698, 0.17547, -3.18E-6 and 4.69077, respectively. The R^2 values were 0.78 and 0.55 for equations 6.4.2a and 6.4.2b, respectively. Both portions of this model generally indicated a positive correlation between the moisture content and heat generation rate.

The total heat generated within baled switchgrass was also determined by integrating this set of equations over the specified storage time (60 days), yielding:

$$Q = \beta_0 + \beta_1 M + \beta_2 \rho + \beta_3 M^2 + \beta_4 \rho^2 + \beta_5 M\rho + \beta_6 (M\rho)^2 + \beta_7 (M\rho)^{0.5} \qquad [6.4.3]$$

where: Q = total sensible heat generated (kJ kg^{-1}) and the coefficients β_0 to β_7 are given as 128.926, -614.121, -28.951, 9.826, -0.003, 0.031, -1.781E-4 and 262.683, respectively.

The accuracy of the heat transfer model directly affects the accuracy of this heat generation model with the application of the relevant thermophysical property (expressed in terms of either the thermal conductivity or thermal diffusivity) expected to cause the largest source of error in this finite difference model. Hence, the sensitivity of this simple heat generation model was assessed by changing the value of thermal diffusivity by 10% and observing the change in estimated heat generation rate. On average, a 10% increase in thermal diffusivity yielded an increase of 5.2 % in estimated heat generation rate; while a 10 % decrease in thermal diffusivity led to a 7.2 % decrease in the estimated heat generation rate.

6.4.3 Model Simulation

The two-dimensional finite difference model describing heat and mass transfer within a porous bale (see Chapter 4) was also validated with the storage data obtained in this study. The model was specifically used in predicting the temperature and moisture content within baled switchgrass with respect to each unique moisture treatment considered in the storage evaluation. As such, the moisture content of each treatment was initialized as 10.7, 20.6, 31.6, and 41.8 %-wb in accordance with the experimental data. All bales were considered to be in thermal equilibrium with the air temperature of 23 °C (296.15 K) at the onset of the storage simulation.

The model simulation was then performed with the ambient air set at a temperature of 29.5 °C and a relative humidity of 23.2 % in accordance with the experimental conditions maintained within the environmental chamber throughout the storage evaluation. The simulated temperature and moisture distribution for each target treatment is shown in Figure 6.4.4 and Figure 6.4.5, respectively. In this case, data is presented at the same two-week interval (day 14, 31, 45 and 60) in which measurements and subsampling were performed during the storage evaluation.

Higher temperatures were initially observed in the central region of each domain due to the increased levels of microbial heating; particularly with the higher moisture treatments. This prominent trend indicated that the effects of microbial heating were rather significant during the initial storage period ($t \leq 4$ days). However, these microbial heating effects appeared to diminish over the course of this model simulation as drying

progressed within each treatment. Hence, the effects of microbial heating became somewhat negligible throughout much of the simulation with the overall material observed to be rather dry (< 18 %) in most treatments by approximately two weeks. The resulting temperature variation observed in the wetter treatments on day 14, indicated the residual effects of the microbial contributions to heat development within the material.

Higher temperatures were also observed at the peripheral surfaces of each domain in response to the elevated temperature of the ambient air. This trend was maintained throughout the course of the storage simulation with a gradual temperature flux moving inwards toward the center of each domain. This heating flux further progressed as the moisture was removed from each treatment. It may also be noted that the central region of each domain responded relatively slowly to the imposed temperature flux compared with the response of the surrounding material. This trend may indicate a dominant effect of conductive heat transfer, while a more even distribution would have indicated significant convective effects. The heated air would more readily permeate throughout the material under dominant convective forces.

The remaining moisture within each domain generally accumulated within those regions with large temperature gradients. High moisture levels were typically observed in the center region of each bale with a relatively slow diffusion of moisture away from the center of the domain. Higher concentrations of moisture were also observed below the central axis of each domain during the first several days of the simulation; particularly in the higher moisture treatments. The moisture in these regions slowly diffused as the simulation time progressed. Although the average temperatures within each time iteration were generally higher than the calculated dewpoint temperature, the moisture content may have been underestimated in some cases in which condensation could occur.

The dryer initial moisture treatments (10 and 20 %-wb) generally exhibited a uniform distribution of heat flux throughout the simulation. However, the wetter initial moisture treatments (30 and 40 %-wb) exhibited a somewhat uneven heat distribution with an apparent vertical temperature gradient; particularly in the latter stages of the simulation. This uneven temperature distribution in the wetter treatments may be attributed to the higher moisture regions that are observed in the upper portions of each domain towards the completion of the storage evaluation on day 60.

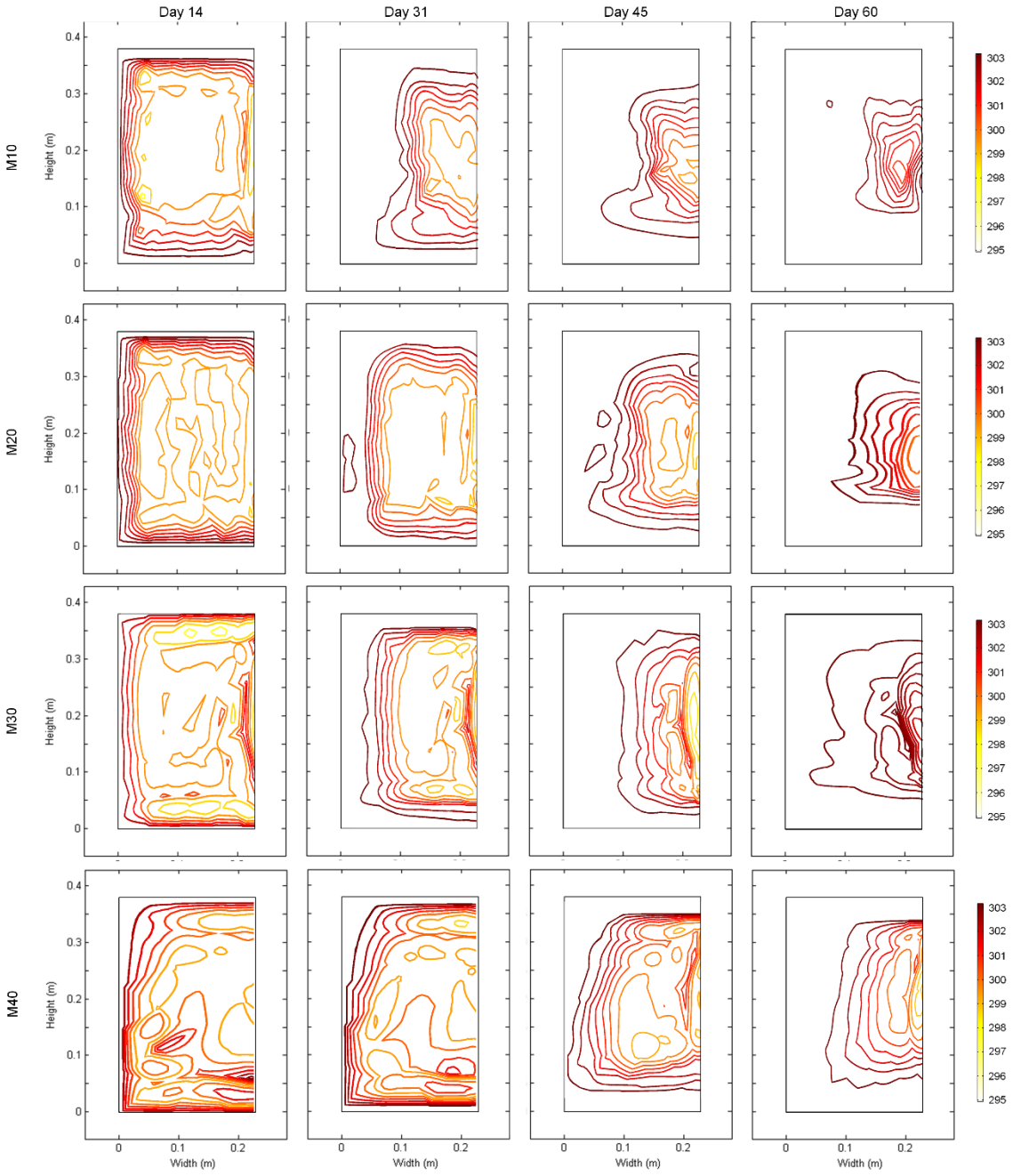

Figure 6.4.5 Simulated temperature distributions (K) for each initial moisture treatment (10, 20, 30 and 40%-wb target) at two-week intervals (day 14, 31, 45 and 60). The box in each contour plot represents half the domain with the right side treated as the symmetrical center line.

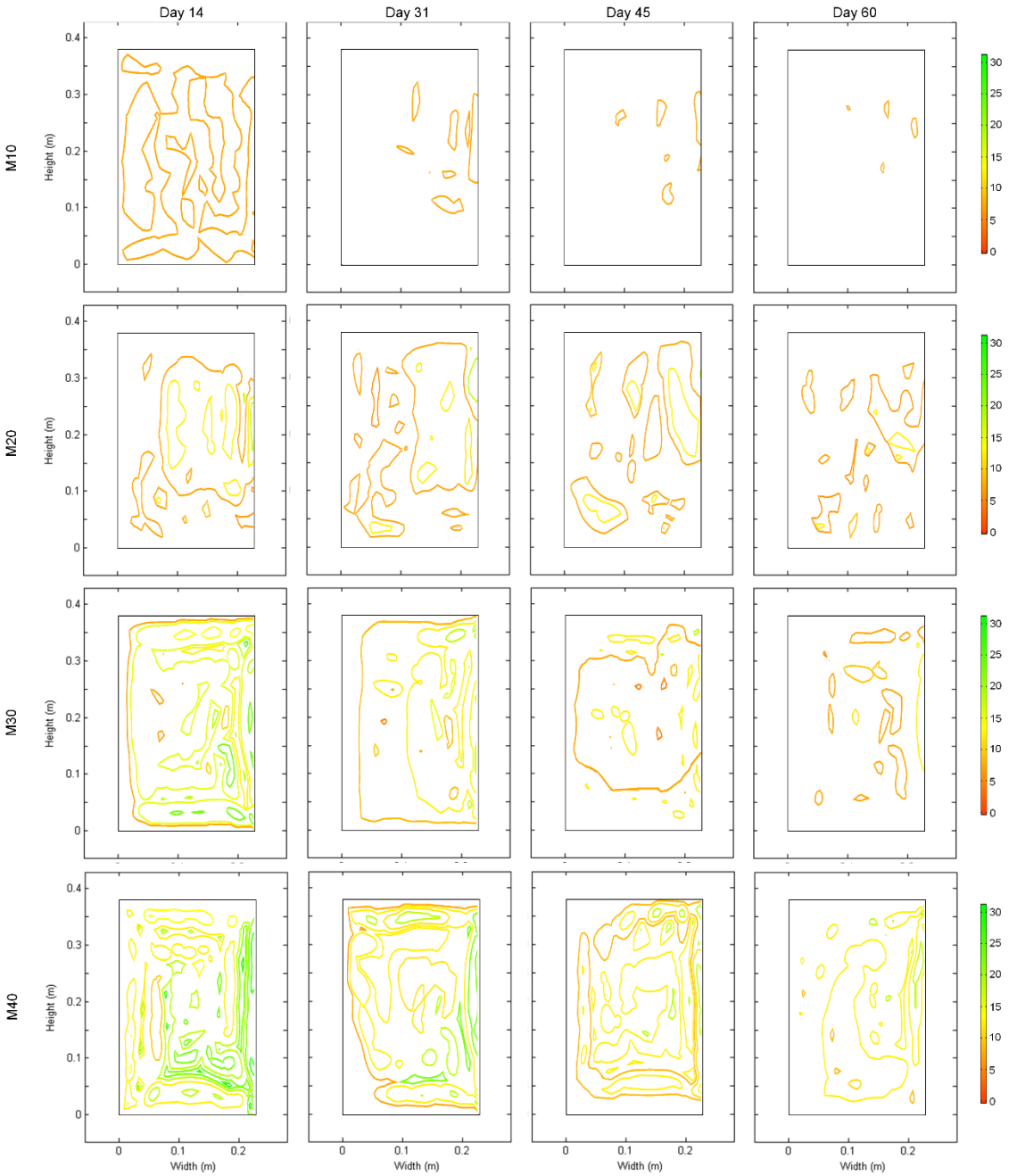

Figure 6.4.6 Simulated moisture content distributions (%-wb) for each initial moisture treatment (10, 20, 30 and 40%-wb target) at two-week intervals (day 14, 31, 45 and 60). The box in each contour plot represents half the domain with the right side treated as the symmetrical center line.

A comparison of the DML rates and the accumulated DML for each moisture treatment is also presented in Figure 6.4.6. In this case, the accumulated DML (%) for each moisture treatment was evaluated according to the following equation:

$$DML_T = \sum_{n=0}^{t} \overline{DML} = \sum_{n=0}^{t} Y_{DML} \frac{\Delta V}{V} \Delta t \qquad [6.4.4]$$

where: DML_T = accumulated dry matter loss (%); $\overline{DML}$ = average dry matter loss rate for each respective day (%); Y_{DML} = dry matter loss rate due to respiration (% day^{-1}); t = storage time (day); Δt = time step (day); ΔV = control volume (m^3); and V = total volume (m^3).

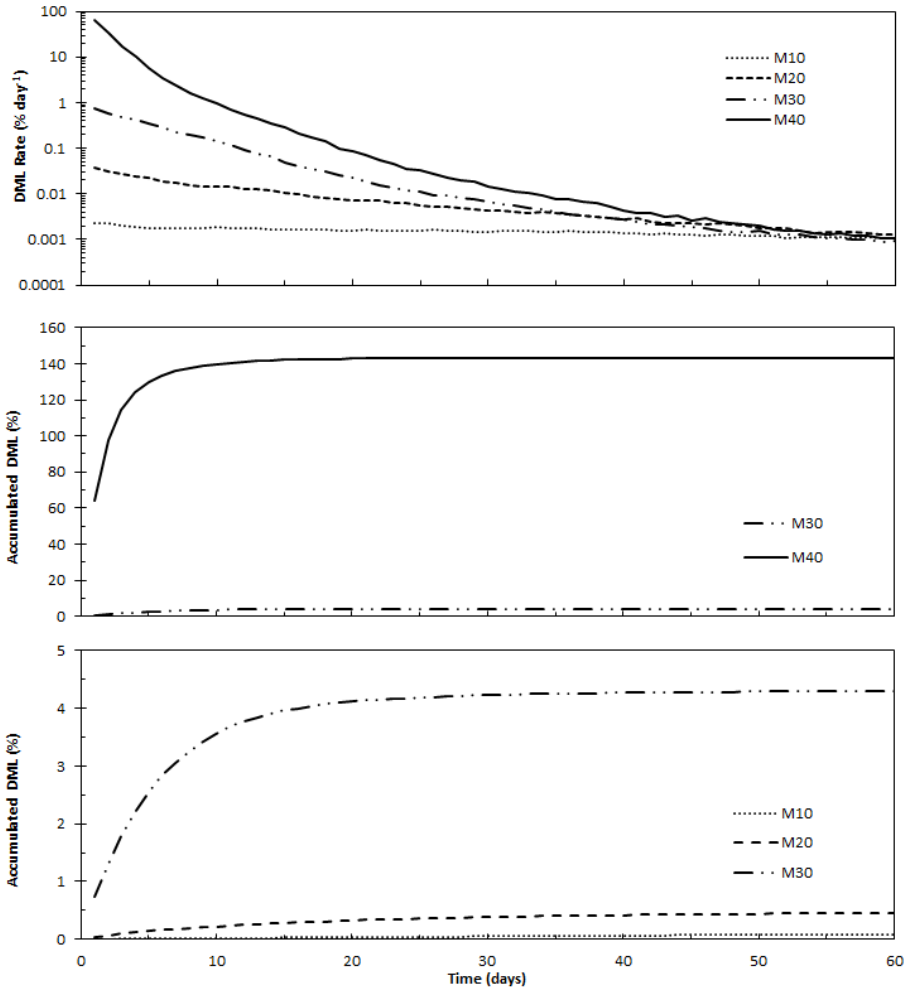

Figure 6.4.7 Comparison of dry matter loss (DML) rates and accumulated dry matter loss (DML_T) for each moisture treatment (10, 20, 30 and 40 %-wb target) of the 60 day storage evaluation.

Based on this analysis, larger DML rates were generally observed in the higher moisture treatments due to an increased level of microbial activity within the wetter biomass. Although the accumulated DML at the surface of each bale was generally similar, higher DML was specifically predicted within the central regions of each domain in accordance with the temperature and moisture content distributions. In fact, the DML-rates typically followed the simulated moisture content due to the strong correlation that was attributed to microbial activity; particularly at the higher moisture treatments.

The accumulated DML values after 60 days was determined to be 0.09, 0.46, 4.30 and 143.22 % for the 10, 20, 30 and 40 %-wb moisture treatments, respectively. Obviously a dry matter loss greater than 100% was not realistic. The DML model utilized in this study was based on aerobic respiration of glucose to carbon dioxide, heat, and water. The moisture content and density of the 40 %-wb treatment could have been conducive to degradation by processes other than the aerobic respiration of glucose. Savoie et al. (2006) alternatively reported a diminishing rate of dry matter loss approaching an asymptotic maximum in corn silage. A moisture content of 40 % is known to be aerobically unstable and would lead to storage problems (Miller et al., 1967; Nehrir et al., 1978; Nelson, 1968; Rohweder et al., 1978). Hence, the overall accumulated DML for the highest moisture treatment was over 1000 times higher than for the lowest moisture treatment (10 %-wb); while the accumulated DML for the 30 %-wb treatment was approximately 47 times greater. It may be noted, however, that the overall DML for each treatment may have been underpredicted since condensation was largely ignored in this simulation. Despite the potential underestimation of the moisture content, these results may still predict reasonable estimates of the likely magnitudes of DML within the lower moisture treatments.

6.4.4 Model Validation

6.4.4.1 Temperature

The simulated temperatures were also compared to the measured temperatures for each initial moisture treatment. In this case, the measured daily temperature at the center

of each bale was averaged between the three replicate bales prepared for each respective moisture treatment. The resulting data for the center position of each bale treatment is shown in Figure 6.4.7 for the respective moisture treatments. The simulated temperatures were generally in good agreement with the measured temperatures at the lower moisture treatments (10 and 20 %-wb), but considerable deviation was observed in the higher moisture treatments (30 and 40 %-wb).

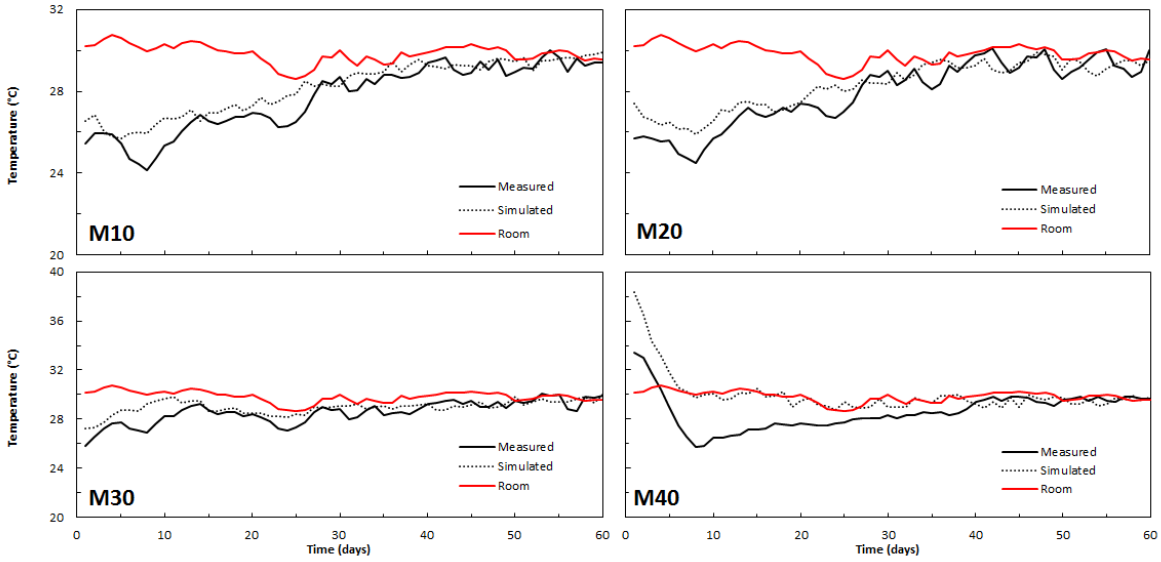

Figure 6.4.8 Temperature data at the center position of the bale from thermocouple measurements and model simulations at each treatment level.

The average daily temperatures that were measured at the central position within each bale were also plotted against the model-predicted values in Figure 6.4.8 for each moisture treatment. In this analysis, the temperature measured at each thermocouple position was averaged between the three replicate bales that were prepared for each treatment. The ideal case for model validation would provide an intercept and slope of 0.0 and 1.0, respectively.

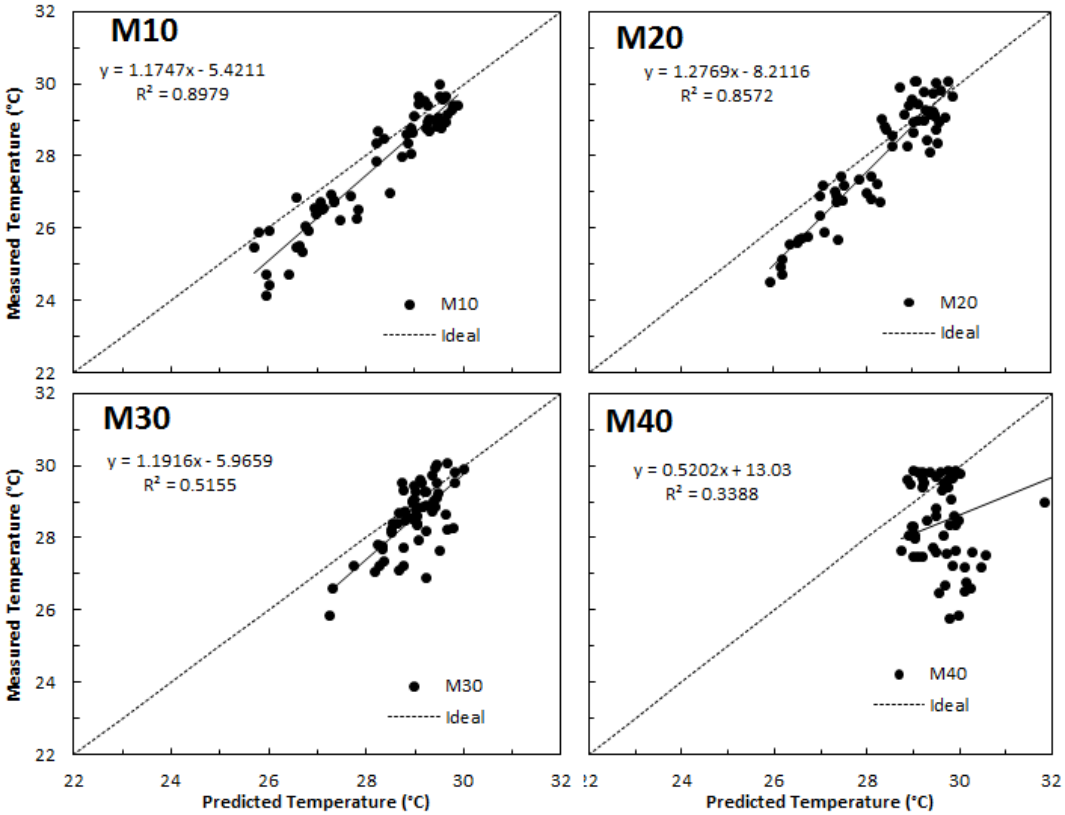

Figure 6.4.9 Measured vs simulated daily temperatures for baled switchgrass (means of three replicate bales) for each respective moisture treatment. The dashed lines represent the ideal case for model validation with an intercept and slope of 0.0 and 1.0, respectively. The solid lines represent the actual regression between the measured and predicted temperatures.

In general, these results indicated that the simulated predictions of temperature were considerably more accurate at the lower moisture treatments (10 and 20 %-wb), moderately accurate at the intermediate moisture treatment (30 %-wb) and much less accurate at the highest moisture treatment (40 %-wb). Model validity was specifically investigated for each of these moisture treatments according to the linear regression performed between the measured and predicted temperature data. The regression results for each treatment are summarized in Table 6.4.1 along with the coefficients of determination (R^2) and the associated standard errors (SE).

Table 6.4.2 Model validation by regression of predicted daily temperatures vs. measured daily temperatures for each moisture treatment during the 60 day storage evaluation.

Linear Regression Results	10 %-wb Target	20 %-wb Target	30 %-wb Target	40 %-wb Target
Slope †	1.1747	1.2769	1.1916	0.5202 *
Slope S.E.	0.0520	0.0684	0.1517	0.0954
Intercept †	-5.4211	-8.2116	-5.9659 *	13.0302 *
Intercept S.E.	1.4684	1.9377	4.3955	2.8669
R^2	0.8979	0.8572	0.5155	0.3388
Standard Error (°C)	0.5220	0.6069	0.6504	1.2270

*Slope was different from unity ($p < 0.05$) or intercept was different from zero ($p < 0.05$)
† Values represent the average measurement of 3 replicate bales
·S.E. = standard error; R^2 = coefficient of determination

The null hypotheses used in evaluating the validity of the model were that the intercept and slope were different from 0.0 and 1.0 respectively. The null hypotheses were rejected at the lowest moisture levels (10 and 20 %-wb) using the student's t-test with n-2 degrees of freedom. In accordance with this assessment, the model was considered valid for temperature prediction at these low levels of moisture content. However, the null hypotheses were not rejected at the intermediate (30 %-wb) and highest (40 %-wb) moisture treatments; indicating invalid temperature predictions at those elevated levels.

The residuals between measured and predicted temperatures (as shown in Figure 6.4.10) further indicated that the most significant error occurred within the initial stage of the storage evaluation ($t \leq 4$ days). The error arising in this period may be attributed to an overestimation of the heat generation within the biomass and/or the neglecting liquid water movement which could exist in the global domain at these moisture levels.

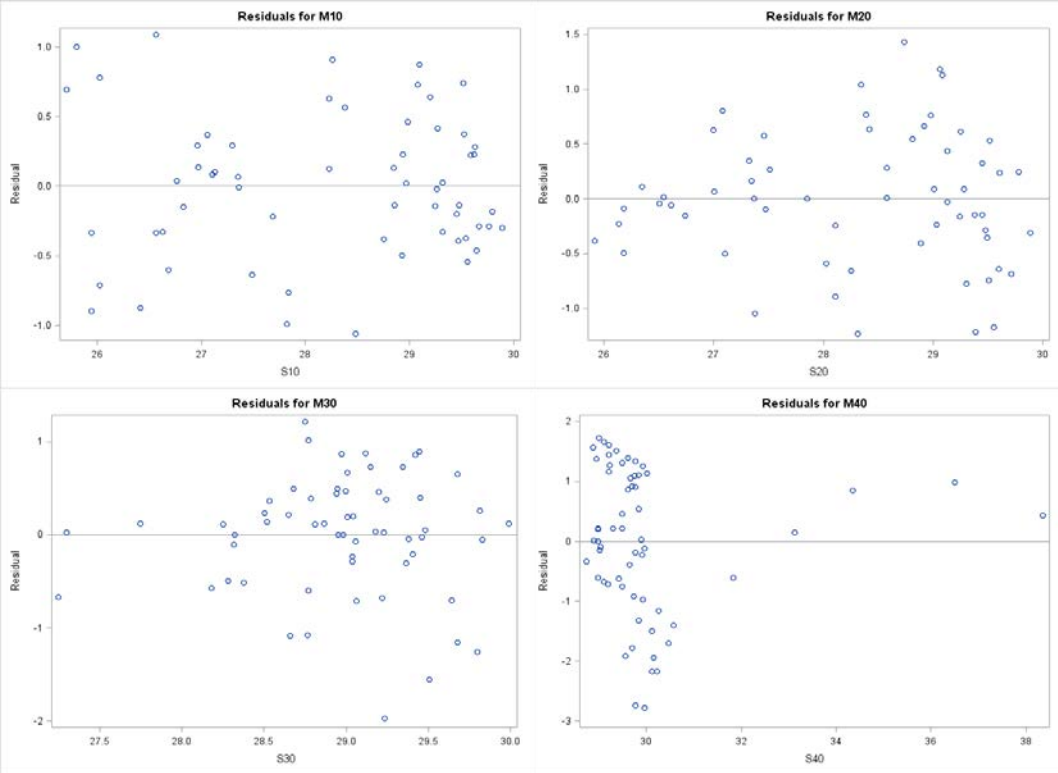

Figure 6.4.10 Residuals between the measured and predicted temperatures for each respective moisture treatment.

Based on these results, the temperature trends of the lowest moisture treatments (10 and 20 %-wb) were considered to be predicted to a reasonable extent, with rather high values of coefficients of determination for each treatment. The slope and intercept test generally resulted in a valid model with an explanation of 90 and 86 % of all temperature variation for the 10 and 20 %-wb treatment, respectively. Although the comparison of the measured and predicted temperature data at these low moisture levels indicated some error in the model, the deviations were generally on the same order as the deviations observed within the validation data. The 95 % confidence interval for each moisture treatment is shown in Figure 6.4.11. These results further indicate the good agreement between the simulated and measured temperatures of the lower moisture treatments given the errors in measurement.

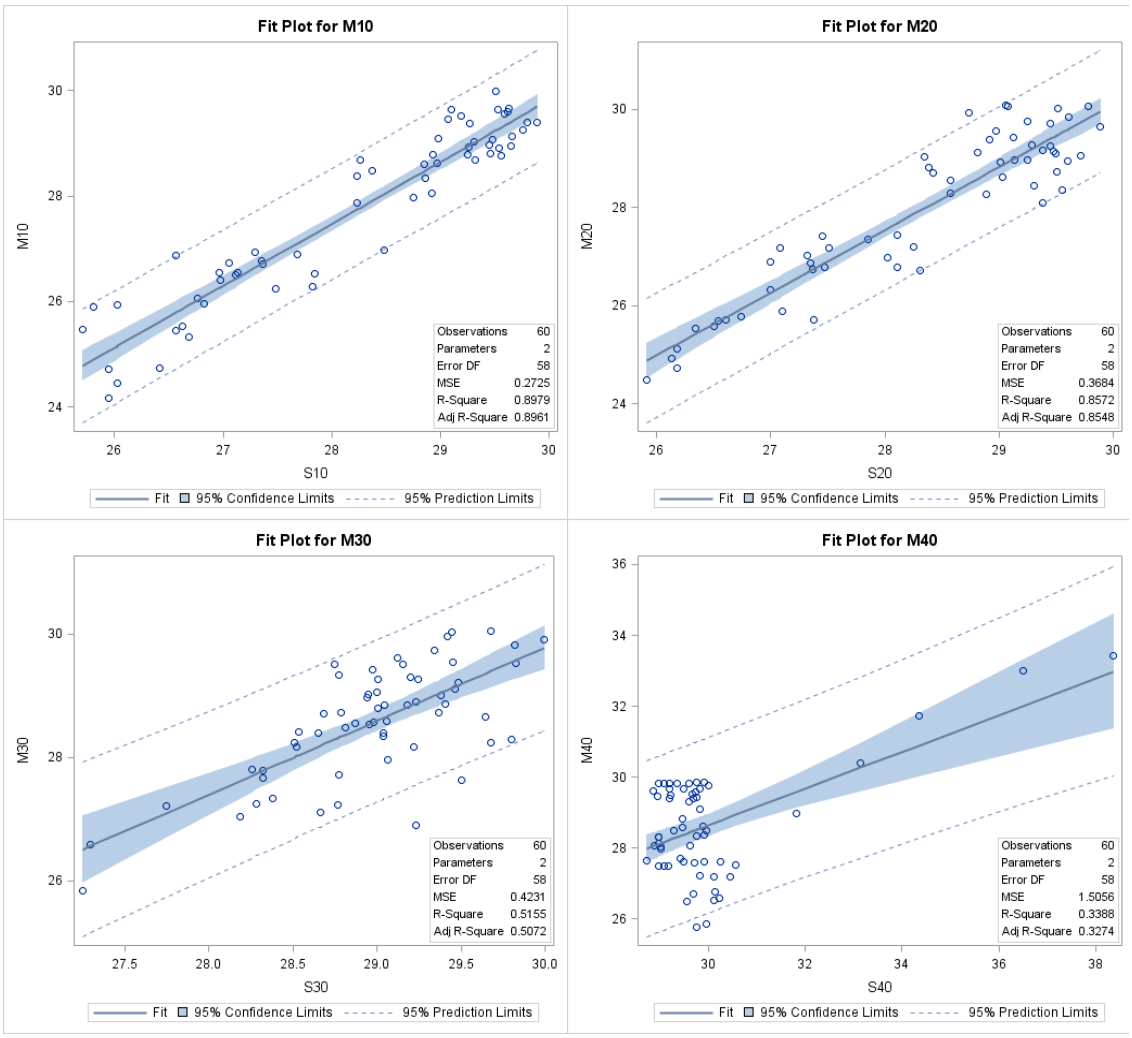

Figure 6.4.11 Confidence intervals (95 %) for measured and predicted temperatures for each respective moisture treatment.

While the model predicted the temperature trends of the intermediate moisture treatment (30 %-wb) to a reasonable extent, the coefficient of determination was relatively low with a value of approximately 0.52. Regardless of the indication that this model was invalid at the 30 %-wb level, an explanation of 52 % of all temperature variation was considered reasonable in the current study; particularly in light of the general complexity of the porous structure as the associated model. Hence, this model was generally considered to be sufficient for temperature estimation within baled switchgrass; particularly at the lower levels of moisture content. Of course, further developments are expected to improve the temperature predictions.

6.4.4.2 Moisture Content

The simulated moisture content data was also compared to the moisture contents that were measured during the storage evaluation. In this case, the moisture content determined at each particular sampling position within a bale (sampling positions are discussed in section 5.4.5.5) was averaged between three replicate bales. The measured and simulated moisture content for the center position of each moisture treatment is shown in Figure 6.4.11. In this case, each line represents a unique moisture treatment with the average moisture content measured in three replicate bales and the simulated moisture content according to the model results.

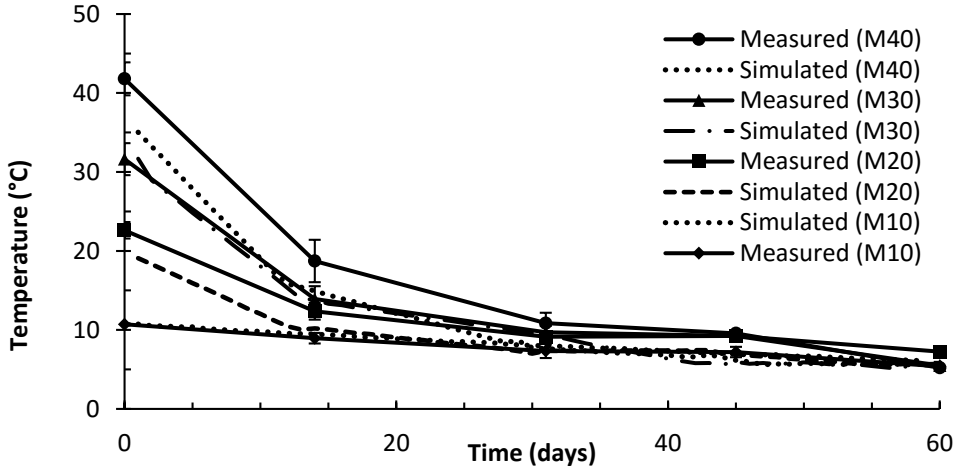

Figure 6.4.12 Simulated and measured moisture content data for the center position of each bale moisture treatment.

Simulated moisture content was generally in good agreement with the measured values at the lower (10 and 20 %-wb) and intermediate (30 %-wb) moisture content levels throughout the model simulation. It may be noted, however, that the predicted values of moisture content were generally lower than the measured values. Despite these minor discrepancies between the measured and predicted values of moisture content, the model simulation and analyses presented in this study are expected to provide a sufficient framework for the assessment of a variety of storage conditions for baled switchgrass within the range of the lower moisture contents. On the other hand, the simulated moisture content at the highest moisture treatment (40 %-wb) was significantly

undervalued compared with the measured values. This indicates that the actual rate of drying for the high moisture treatment occurred more slowly.

The variation in moisture content at the conclusion of the storage evaluation (day 60) has also been summarized in Table 6.4.2 for each initial moisture treatment. Based on the three distinct sampling locations within each bale, the mean moisture contents were found to be 5.5, 5.6, 5.7 and 5.6 % for each respective moisture treatment. These values were not significantly different from each other, even considering the differing drying rates associated with each treatment. These results indicated that the material represented in each moisture treatment dried to the same extent, while the overall results indicated that the model could predict moisture changes fairly well in the lower moisture treatments since the measured and simulated temperatures were similar.

Table 6.4.3 Variation in the moisture content (%-wb) of baled switchgrass after 60 days of storage in a controlled environmental chamber at 29.5 °C and 23.2 % RH.

Sampling Location*	10 %-wb Target		20 %-wb Target		30 %-wb Target		40 %-wb Target	
	Predict	Observe †	Predict	Observe †	Predict	Observe †	Predict	Observe †
1	5.3	5.5	6.0	5.8	5.5	5.4	5.1	5.1
2	5.3	5.5	5.3	6.0	6.2	5.6	6.3	5.3
3	5.8	5.1	5.4	5.7	5.5	5.5	5.4	5.2
Mean	5.5	5.4	5.6	5.8	5.7	5.5	5.6	5.2

† Values represent the average measurement of 4 total bales

* Sampling locations are depicted in Figure 5.4.7

6.4.4.3 Dry Matter Loss

The simulated DML data was also compared to the average measurements recorded during the storage evaluation. In general, the simulated DML data was in reasonable agreement with the average measurements recorded for the lower moisture treatments. However, more significant discrepancies were observed for the highest moisture treatment (40 %-wb). In fact, the total simulated DML at the end of the storage evaluation (day 60) was observed to be 0.09, 0.46, 4.30 and 143.22 %; while the measured values were 0.51, 0.73, 1.82 and 2.68 % for each respective moisture treatment. In this case of the highest moisture treatment, the total predicted DML was significantly greater than the average measured value; although a dry matter loss greater than 100% was obviously not realistic.

Despite these apparent discrepancies between measured and predicted DML values, the simulated data was still able to predict correct trends; particularly at the lower moisture levels. Moreover, the total predicted DML of was generally on the same order of magnitude as previously reported for baled switchgrass stored indoors (Sanderson et al., 1997). For these reasons, the model simulation is expected to provide a sufficient framework for the assessment of a variety of storage conditions including the DML for baled switchgrass.

CHAPTER 7:CONCLUSION

This dissertation addresses the analysis of liquid flow through baled biomass (section 1); the measurement of moisture content with TDR sensors (section 2); the assessment of thermophysical properties within baled switchgrass (section 3); and the evaluation of heat and mass transfer within the porous bale (section 4). Together, these sections support and demonstrate the practical evaluation of storage conditions on the temperature and moisture content within baled switchgrass. As such, these analyses could lead to the identification and improvement of the best management practices for biomass storage in order to minimize nutrient degradation and prevent hazardous conditions (i.e., combustion) without the need for extensive field tests.

7.1 Fluid Analysis

7.1.1 Saturated

A methodology was proposed in this study for estimating the hydraulic properties within baled feedstocks. The saturated moisture content and leaching ability of switchgrass and miscanthus were accessed by allowing fully saturated bales to drain excess water for 36 hrs. The average saturated moisture content ranged between 55.9 and 71.9 %-wb for switchgrass and between 60.5 and 73.9 %-wb for miscanthus depending on the bale density. The R^2 regression coefficients for the linear models describing this inverse relationship were 0.99 for both feedstocks. This trend between saturated moisture content and bale density was primarily due to water entrapment within the void spaces of each bale.

Based on leaching analysis, the baled miscanthus typically had increased void space, thus permitting higher flow rates. In fact, the miscanthus bales had higher saturated moisture contents due to the increased pore space, but leaching generally occurred more quickly as a result. The feedstock-type effect became less pronounced at higher density levels since the pore space was significantly diminished in both feedstocks. Regardless, rapid leaching occurred within the first five hours with average reductions in moisture content of 9.8 and 10.3 %-wb for switchgrass and miscanthus, respectively. These results indicated that significant amounts of water were shed from the

large pore channels within the bales of each feedstock type during this initial leaching period. Leaching then continued at a steady rate until the experiment was terminated at 36 hours. During this steady-state leaching period, switchgrass and miscanthus dropped an additional 1.9 and 2.1 %-wb, respectively.

Saturated hydraulic conductivity tests were also carried out on 12 bales each of switchgrass and miscanthus with a constant head system. Bale density was found to have significant effects on the saturated hydraulic conductivity. In fact, the saturated hydraulic conductivity at the lowest target dry matter density (150 kg m^{-3}) was only 16.7 and 33.3 % of the value recorded at the highest dry bale density (225 kg m^{-3}) for switchgrass and miscanthus bales, respectively. The best-fit models describing the density-dependent hydraulic conductivity were found to fit the data very well with R^2 values of 0.99 and 0.97 for switchgrass and miscanthus, respectively. The inverse relationship between hydraulic conductivity and bale density is associated with the void and inter-particle space in which fluid flow occurs. The higher density bales have less inter-particle space thereby inhibiting fluid flow.

This effect is reversed in lower-density bales as the large void space permits greater fluid flow through the bales. These factors all contribute to the development of unique pore connectivity within the bales. Furthermore, significant feedstock type effects were observed particularly at the highest dry bale density (225 kg m^{-3}). Thus, higher flow rates were attained in miscanthus bales due to the greater void space and increased pore connectivity. These results indicated a strong correlation between the saturated hydraulic conductivity of the bales and other intrinsic properties such as surface roughness, size, geometry and stratification of the material.

7.1.2 Unsaturated

The matric suction of unsaturated switchgrass was also assessed at varying bale densities and moisture contents using the contact filter paper method. Hence, this study explored the validity of a semi-empirical approach to obtain estimates of the unsaturated hydraulic conductivity and sorptivity from disk infiltrometer data with baled switchgrass. Accordingly, the van Genuchten parameters (α, n, θ_s, θ_r) were first determined for baled switchgrass at variable densities. The van Genuchtan parameters ranged between 0.235

and 0.270 m^{-1} for α; and between 5.415 and 10.345 for n, depending on the density. In fact, the results indicated a strong correlation between the bale density of switchgrass and van Genuchten's parameters. Infiltration tests were also carried out on 36 bales of switchgrass with a minidisk infiltrometer. Three replicates per bale density were evaluated at each target moisture level (10, 20, 30 and 40 %-wb). The curve-fitting parameters of Philip's two-term equation ranged between 0.086 and 0.0779 cm s^{-1} for C_1, and between 0.200 and 5.805 cm $s^{-½}$ for C_2, depending on the density and moisture content. Likewise, the unsaturated hydraulic conductivity ranged between 0.019 and 0.272 cm s^{-1}, while sorptivity ranged between 0.048 and 2.103 cm $s^{-½}$, depending on the density ($p<0.01$) and moisture content ($p<0.02$).

These results may be used to estimate the unsaturated hydraulic conductivity and sorptivity at intermediate densities and moisture contents. These results indicated the presence of certain adhesive forces between the water and switchgrass material. In the case of saturated experiments, these forces appear to have been overcome by higher flow rates indicated by the increased values of saturated hydraulic conductivity. In general, these results showed that flow was permitted through high-density bales and verifies the feasibility of removing the end-products of biomass conversion. Hence, this analysis allows for the prediction of water runoff and water retention within bales resulting from rainfall and/or water percolation during storage or bioconversion, respectively.

These hydraulic parameters are also expected to offer significant contributions to the ongoing investigation and development of heat and mass transfer modeling within baled biomass; while ultimately enabling a better understanding of the quality of baled biomass during on-farm storage and/or high-solids biomass conversion. Although this study provides a good measure of the initial hydraulic conductivity, further research is recommended to address the hydraulic properties over time as the material breaks down. An assessment of different flow directions may also be of interest in the future, with higher flow rates expected through the horizontal orientation of a bale. A rain simulator could also be used to evaluate infiltration into the material, while further validation could be performed using larger bale sizes.

7.2 Moisture Measurement

7.2.1 Calibration

Preliminary results have been presented in this study which document the calibration of real time, TDR monitoring for biomass feedstocks. The purpose of this study was to specifically characterize a CS615 TDR sensor (Campbell Scientific, Logan Utah) for measuring the moisture content of densified switchgrass. Measurements were performed at variable levels of bulk density and moisture content for both physical formats of the material (ground and miniature bales). The density levels ranged from 75 to 200 kg m^{-3} for ground switchgrass and from approximately 128 to 212 kg m^{-3} for the miniature bales. The moisture content ranged between dry (~ 8 %) to fully saturated (67 to 73 %) depending on the achievable moisture level for each sample. Three temperature levels (23.3, 32.2 and 40.6 °C) were also assessed for the ground samples.

A significant correlation was generally observed between the voltage output and the moisture content ($p < 0.001$), as well as, the bulk density ($p < 0.001$) of the material. The physical format of the material (ground or miniature bale) was also found to have a significant effect ($p < 0.01$) on the voltage output which was expected due to the inherent differences in the physical composition of each bulk format. However, the temperature effect was found to be negligible ($p = 0.24$) within the range assessed in this study.

Quartic regression models were developed for the voltage-moisture data of both physical formats based on these dependencies following the approach of Topp et al. (1980). Calibration data for both physical formats were well described by their respective quartic fits. Although both physical formats resulted in similar calibration curves, the ground switchgrass model generally provided a better fit of the experimental data with slightly greater coefficients of determination (R^2) at corresponding density levels. The unique calibration curves for each density level were also indicative of the significant bulk density effect.

A sensitivity of 5.1E-1 mV (kg m^{-3})$^{-1}$ was verified for ground switchgrass, while baled switchgrass was approximately 3.5 E-3 mV (kg m^{-3})$^{-1}$. This variation of the output voltage (by the order of hundreds of millivolts) was considered adequate for assessing moisture content; particularly when accounting for the repeatability of the sensor. Hence,

these preliminary results demonstrated the effective calibration of a TDR probe for ground and miniature bales of switchgrass.

7.2.2 Validation

Dynamic validation tests were also performed with larger bales prepared at four unique moisture contents (10.7, 20.6, 31.6 and 41.8 %-wb) and stored in a controlled environment for 60 days while measurements were performed using CS615 TDR probes. The resulting voltage data was converted to moisture content using the previously developed calibration curve for baled switchgrass and compared with corresponding gravimetric results. The moisture contents reported for these larger bales were generally overestimated by an average of 16.7 % which may be attributed to the significant variation in the material properties throughout each bale. In fact, the variations in the bulk density, porosity and conductivity were all expected to contribute to this overestimation.

Although the validation tests were generally unsuccessful, the accuracy of the TDR measurements may be improved at higher density levels where more uniform bulk properties (i.e., porosity) are expected. While this development has yet to be investigated, it is possible that more accurate and precise results could be obtained at the higher density levels which are more consistent with the target densities of biomass feedstocks. As such, this TDR application could represent a potential approach for the dynamic measurement of moisture content in densified perennial grasses based on the strong correlations that were observed in the calibration data. Hence, the continued investigation of TDR technology at elevated density levels may provide more promising developments for biomass research and management in terms of moisture measurements.

7.3 Thermal Analysis

The thermophysical properties of baled switchgrass were characterized in this study using a dual thermal probe. The thermal conductivity, thermal diffusivity and specific heat were specifically evaluated in this analysis. Measurements were performed at variable levels of bulk density (157.2, 172.4, 197.2 and 230.1 kg m^{-3}), moisture content (11.4, 20.8, 29.0 and 42.3 %-wb) and temperature (20.3, 30.2, 40.1 °C). These thermophysical properties were also investigated with respect to the directional orientation (lateral or transverse) within each bale. The following conclusions were developed based on the experimental results.

7.3.1 Thermal Conductivity

The thermal conductivity of baled switchgrass ranged from 2.73E-2 to 6.10E-2 W m^{-1} $°C^{-1}$ for the lateral orientation; and from 1.04E-2 to 5.96E-2 for the transverse orientation. The thermal conductivity was generally higher in the lateral orientation (parallel to flake orientation) than for the transverse orientation (direction of bale compression) at similar treatment levels due to the different mechanisms of heat transfer associated with each direction. The lateral orientation involved heat conduction through continuous solid stem material; while the transverse orientation involved heat transfer through successive air spaces. Hence, the thermal conductivity in the lateral orientation was expected to match more closely to the thermal conductivity of the solid material; an idea that may be substantiated through further investigation of the thermophysical properties of individual stems of switchgrass.

It was also noted that the initial temperature, moisture content, and dry bulk density had significant effects on the thermal conductivity of the material. In fact, the thermal conductivity had a positive correlation with each independent parameter over the associated ranges evaluated in this study. In this case, higher temperatures promoted heat transfer within the material indicated by increased values of thermal conductivity in both orientations. Increasing levels of moisture content also increased the thermal conductivity with the water contained in the bale imposing a greater influence on the measurements at the highest moisture treatment. The positive correlation between dry bulk density and thermal conductivity was attributed to the improved level of heat conduction that was

established by greater amounts of solid material that became available for conductive heat transfer at higher densities. On the other hand, lower bulk densities resulted in lower thermal conductivity due to the increased porosity of the material. Based on this analysis, the thermal conductivity in both directional orientations was modeled as a function of the temperature, moisture content and dry bulk density.

7.3.2 Thermal Diffusivity

The mean thermal diffusivity of the baled switchgrass ranged from 1.443 x 10^{-7} to 2.031 x 10^{-7} m^2 s^{-1} for the lateral orientation; and from 0.863 x 10^{-7} to 2.284 x 10^{-7} m^2 s^{-1} for the transverse orientation. The thermal diffusivity generally exhibited nonlinear relationships with the moisture content and bulk density; while showing little to no correlation with temperature. Hence, it was concluded that the average thermal diffusivity over the entire temperature range evaluated in this study could be adopted for many applications considering the negligible effect of temperature relative to the effects of the other independent parameters. Furthermore, random variation in the data could make the consideration of the small temperature effect superfluous. In this case, measurement variation was attributed to the physical and biological variation of the material within the bale, as well as, limitations in the probe construction such as the uncertainty in measuring the radial distance to the thermocouple.

The thermal diffusivity followed a slightly positive linear trend across the range of moisture contents evaluated in this study while the lower bulk density levels exhibited somewhat greater values of thermal diffusivity due to the local variation in the physical structure. However, minimal influence of the bulk density was typically observed in the transverse orientation due to the inherently unique physical composition of the material with respect to the axial direction of bale compression. This particular response to the bulk density was attributed to the variation in porosity and material heterogeneity in the transverse orientation (i.e., discontinuous porous cavities). While higher densities could potentially indicate a strong correlation to bulk density in the transverse orientation, such conditions would exceed the target density range for biomass feedstocks.

Statistical analysis supported these conclusions while further indicating that there were no significant correlations for any of the independent parameters in the transverse

orientation. Since no significant correlation was observed for the transverse orientation, the average value of 1.4742 $m^2 s^{-1}$ for this directional treatment was considered sufficient for this study. However, the moisture content and dry bulk density were both found to have significant effects on the thermal diffusivity of the material in the lateral orientation at a significance level of 0.05. Based on this analysis, the thermal diffusivity in the lateral orientation was modeled as function of the moisture content and dry bulk density.

7.3.3 Specific Heat

Specific heat was estimated from the measured values of thermal conductivity and thermal diffusivity with values ranging from 0.92 to 1.79 kJ kg^{-1} °C^{-1} for the lateral orientation; and from 0.40 to 2.51 kJ kg^{-1} °C^{-1} for the transverse orientation depending on the values of the independent parameters. In general, the specific heat increased with increasing temperature and moisture content, but decreased with increasing dry bulk density. Specific heat was observed to vary with the density of the material since baled switchgrass is a compound rather than a pure substance. As such, the inverse correlation with bulk density was explained by the change of bound water into free water and the change of inner structure at higher densities. Hence, the dry bulk density, moisture content, temperature and directional orientation were found to have significant effects on the specific heat for most treatment levels. Based on this analysis, the specific heat for both directional orientations was modeled as function of the temperature, moisture content and dry bulk density. Continued efforts in this area may involve the measurement of specific heat with a calorimeter.

7.3.4 Validation

The resulting values of thermal diffusivity were also validated using a simple heat conduction model which was applied using the temperature data collected from a separate storage evaluation. The directional orientation was also accounted for in this validation procedure. Temperature data collected from the storage evaluation indicated that both lateral orientations responded to temperature changes similarly; while a slower response was observed in the transverse orientation. The similar response time for both lateral

components indicated that the thermophysical properties were relatively similar within the cross-sectional plane that is parallel to the flake orientation.

The model-estimated values of thermal diffusivity were generally within ± 30 % of the values determined by the dual probe method. In fact, the thermal diffusivities for both lateral orientations were typically underpredicted during those periods exhibiting relatively stable temperatures; while more significant errors were observed during temperature transitions. The low evaluation of thermal diffusivity according to the simple conduction model was attributed to the limited grid refinement and the oversimplification of the conduction model. Further refinement of the spatial discretization could be achieved with additional instrumentation in order to provide some improvement of the model predicted values of thermal diffusivity.

It may also be noted, that the model-predicted values of thermal diffusivity in the transverse orientation resulted in much greater error. In this case, the thermal diffusivity was greatly overvalued; with the most significant errors observed during transitional temperature periods. While conclusive validation of the thermal diffusivity was not specifically obtained from this analysis, the results did provide some indication of anisotropic behavior of baled switchgrass. Although the model predicted similar values of thermal diffusivity for both lateral orientations, the model predicted much greater values of thermal diffusivity in the transverse orientation. This anisotropic behavior observed between the lateral and transverse orientations further demonstrates that different heat transfer mechanisms may be involved in the transverse orientation. Continued efforts in this area may also involve the measurement of the thermophysical properties of individual stems of switchgrass. The thermophysical assessment of larger bales is also necessary for the further evaluation of the anisotropic nature of the baled material.

7.4 Heat and Mass Transfer

7.4.1 Solid Model (Conduction)

A simple conduction heat transfer model was developed in this study considering baled switchgrass to be a solid material. The resulting finite difference model was applied to temperature data collected from a storage evaluation in order to fit an empirical calibration of the heat generation rate with respect to four unique moisture treatments (10, 20, 30 and 40 %-wb). Results indicated a monotonic time course with the heat generation rate increasing during the first several days of storage ($t \leq 4$ days) and decreasing thereafter as the material dried ($t \geq 4$ days). Hence, the maximum heat generation rate for each moisture treatment was observed at approximately 3 to 4 days into the storage evaluation, while values beyond 30 days remained low and fairly constant.

The heat generation rates determined from this conduction model were generally similar to those values determined from the formulation presented for aerobic respiration (see section B.7). The average heat generation rates over the entire 60-day storage period were determined (in accordance with the conductive model) to be in the range of 3.65 to 5.66 W kg^{-1} while indicating a positive correlation with the moisture content.

Analysis of the bale temperatures in accordance with this conductive model also indicated that the sensible heat generation rate was significantly correlated with the moisture content and bulk density of the material. A set of empirical models was developed for the heat generation rate based on these results. The data was specifically split into two distinct sets corresponding to the increasing and decreasing monotonic trends. The resulting model was integrated over the specified storage time (60 days) to obtain an equation which predicts the sensible heat generation as a function of the initial moisture content and bulk density.

The accuracy of the resulting heat generation model was also investigated in terms of the thermal diffusivity applied in the heat conduction model. A 10 % increase in thermal diffusivity yielded an increase of 5.2 % in estimated heat generation rate; while a 10 % decrease in thermal diffusivity led to a 7.2 % decrease in the estimated heat generation rate. While these empirical relationships apply to the specific conditions that were evaluated in the current study, the results indicate general trends that may be

expected under similar conditions; while further demonstrating the ability to calibrate heat generation models for baled biomass.

7.4.2 Porous Model

A two-dimensional mathematical model describing heat and mass transfer within rectangular bales of switchgrass was also developed in this study to evaluate the storage conditions within a controlled environment. Two disparate length scales were considered in the model formulation with one domain characterizing the overall bale structure (global domain) and the other representative of the individual stems of switchgrass (local domain). Each of these domains was considered to involve different physical processes; while the overall model also accounted for the effect of internal heat generation and temperature-induced free convection within the material in order to improve prediction accuracy which is considered novel in terms of similar biomass models. As such, the model allowed for the prediction of the temperature and moisture content distributions throughout a two-dimensional, rectangular cross-section of a bale.

Model validity was assessed with baled switchgrass prepared at four initial moisture contents (10, 20, 30 and 40 %) and stored within a controlled environmental chamber for 60 days. The initial stage of the storage evaluation ($t \leq 10$ days) was largely governed by the microbial heat generation occurring within the material with maximum temperatures ranging between 25.8 and 33.4 °C depending on the initial moisture content. A significant positive correlation was observed between the moisture content and the maximum temperature. Subsequent temperature development within each bale was considered to be driven primarily by the environmental temperature with gradual heating observed until temperature equilibrium was achieved with respect to the ambient air.

Moisture content was generally found to be the highest in the center of each bale; a condition that was more pronounced at the highest moisture level. A simple drying coefficient was calculated based on the resulting moisture data with average values ranging between 5.7E-8 and 3.9E-7 s^{-1} which were somewhat lower than those rates estimated according to empirical thin-layer drying models of switchgrass. These differences were attributed to the greater density of baled switchgrass which slowed the drying rate. Minimal amounts of DML were observed with values ranging from 0.51 to

2.68 % depending on the moisture content. A significant positive correlation was observed between the moisture content, rise in temperature and the amount of DML.

The temperature and moisture content were simulated using the explicit two-dimensional finite difference model and compared with the results of the storage evaluation. Simulated temperatures generally appeared to be in good agreement with the measured temperatures at the lower moisture treatments (10 and 20 %-wb), moderately accurate at the intermediate moisture treatment (30 %-wb) and much less accurate at the highest moisture treatment (40 %-wb). The model validity was specifically investigated according to the linear regression of measured temperature data versus predicted temperature data. In this case, the null hypotheses for testing model validity were that the intercept and slope were different from 0.0 and 1.0 respectively.

Results led to the rejection of the null hypotheses at the lowest moisture levels with the slope and intercept test indicating a valid model with an explanation of 90 and 86 % of all temperature variation for the 10 and 20 %-wb treatment, respectively. Although the comparison of the measured and predicted temperature data at these low moisture levels indicated some error in the model, the deviations were generally on the same order as the deviations observed within the validation data. Hence, the model was considered reasonably valid for temperature prediction at these low levels of moisture content.

However, the null hypotheses were not rejected at the intermediate (30 %-wb) and highest (40 %-wb) moisture treatments; indicating an invalid model for temperature prediction at those elevated moisture levels. While the model predicted the temperature trends of the intermediate moisture treatment (30 %-wb) to a reasonable extent, the coefficient of determination was relatively low with a value of approximately 0.52. Regardless of the indication that this model was invalid at the 30 %-wb level, an explanation of 52 % of all temperature variation was considered practical and relevant in the current study considering the complexity of the problem. It was also noted that the most significant error occurred within the initial stage of the storage evaluation ($t \leq 4$ days) which was attributed to an overestimation of the heat generation within the biomass and/or the negligence of liquid content which could exist in the global domain at these elevated moisture levels.

The simulated moisture content data were also compared to the moisture contents that were measured during the storage evaluation. In this case, the simulated moisture content was generally in good agreement with the measured values at the lower (10 and 20 %-wb) and intermediate (30 %-wb) moisture content levels although the values were generally underpredicted. However, the simulated moisture content at the highest moisture level (40 %-wb) was significantly undervalued; indicating that the actual drying rate of the material was much slower. The variation in moisture content at the end of the storage simulation (day 60) ranged from 5.46 to 5.74 %, while the measured moisture content ranged from 5.20 to 5.84 % depending on the moisture treatment. These values were not significantly different from each other, even considering the differences that were observed in the average drying rates. These results indicated that the model could predict moisture changes fairly well in the dryer moisture treatments since the measured and simulated temperatures were significantly similar.

The simulated DML data was also compared to the average measurements recorded during the storage evaluation with a reasonable agreement generally observed at the lower moisture treatments. However, more significant discrepancies were observed for the highest moisture treatment (40 %-wb). As such, the total simulated DML at the end of the storage evaluation (day 60) was observed to be 0.09, 0.46, 4.30 and 143.22 %; while the measured values were 0.51, 0.73, 1.82 and 2.68 % for each respective moisture treatment. In this case of the highest moisture treatment, the total predicted DML was significantly greater than the average measured value; although a dry matter loss greater than 100% was obviously not realistic.

Despite these apparent discrepancies between the measured and predicted values of DML, the simulated data was still able to predict correct trends; particularly at the lower moisture levels. In this regard, the DML was found to be significantly correlated to the initial moisture content, with the simulated values of total DML found to be on the same order as previously reported in the literature for baled switchgrass stored indoors.

The model formulation, simulation and analyses presented in this study have provided a sufficient framework for the ongoing assessment of a variety of storage conditions for baled switchgrass; particularly within the range of the lower moisture

contents that were assessed in this study. Of course, further developments and validation procedures are expected to provide significant improvements of the model predictions.

Model accuracy is expected to improve through revision of several key assumptions including the evaluation of moisture exchange with the environment. Although the average temperatures within each time iteration were generally higher than the calculated dewpoint temperature, the moisture content may have been underestimated in some cases in which moisture would not evaporate as easily and/or condensation could occur; particularly at the higher moisture treatments. Hence, the incorporation of these effects may improve model accuracy since moisture content influences temperature and drives the respiration and associated DML rates. Further storage experiments could also be conducted with naturally-wetted material, as well as, switchgrass with higher concentrations of bound water.

A more detailed representation of the porous structure could also be obtained with better approximations of the particle sizes, geometry and orientation through image acquisition techniques (i.e., MRI). A detailed parametric study could also be performed in order to determine the relative contributions and effects of the significant parameters appearing in this model. This could involve an assessment of the intrinsic permeability, as well as, an investigation of the Biot number to provide an indication of the relative importance of the conductive and convective effects. The thermophysical properties of the inner domain could also be better defined through experimental measurements. A more extensive investigation of the respiration and microbial activity occurring within the material may further improve the model accuracy with consideration given to gas compositions (i.e., carbon dioxide and oxygen) and a mass source of water from microbial processes.

Model validation can also be performed with larger bales under typical storage conditions which may involve imposed wind currents that increase heat transfer from the bale to the environment. An assessment of the flow resistance through the material may become necessary under those conditions. Analysis of larger bale sizes would also provide unique results since they have less global surface area per unit volume; thereby reducing the effective heat dissipation from the material. Consequently, heat generation in

larger bales may be more influential. Such developments, may allow for the simulation of temperature and moisture contents within bales of any size.

7.5 Future Efforts

Further developments and validation procedures are expected to provide significant improvements in terms of the evaluated parameters and model predictions through the revision of several key assumptions including the evaluation of moisture exchange with the environment. In fact, the incorporation of condensation effects may improve model accuracy since moisture content influences temperature and drives the respiration and associated DML rates. Further storage experiments could also be conducted with naturally-wetted material, as well as, switchgrass with higher concentrations of bound water. The accuracy and precision of the TDR measurements in such storage evaluations may be improved by using higher density levels where more uniform bulk properties (i.e., porosity) are expected. As such, higher density levels may be considered to be more consistent with the target densities of biomass feedstocks.

A more detailed representation of the porous structure could also be obtained with better approximations of the particle sizes, geometry and orientation through image acquisition techniques (i.e., MRI). The development of a three-dimensional mathematical model could also improve model accuracy with a more realistic physical assessment of the porous structure. Further assessment of the hydraulic properties may also be conducted with an evaluation conducted over time as the material biodegrades, as well as, an evaluation of different flow directions through the material. As such, higher flow rates are expected through the horizontal orientation of a bale. A rain simulator may also be used to evaluate infiltration into the material, while further validation could be performed using larger bale sizes.

Continued efforts may also involve the measurement of specific heat with a calorimeter, as well as, the measurement of the thermophysical properties of individual stems of switchgrass. The thermophysical assessment of larger bales is also necessary for evaluating the anisotropic nature of the baled material. Further refinement of the spatial discretization could also be achieved with additional instrumentation in order to provide some improvement of the model predicted values of thermal diffusivity according to the simple conduction model. A more extensive investigation of the respiration and microbial

activity occurring within the material may further improve the model accuracy with consideration given to gas compositions (i.e., carbon dioxide and oxygen) and a mass source of water from microbial processes.

A detailed parametric study could also be performed in order to determine the relative contributions and effects of the significant parameters appearing in this model. This could involve an assessment of the intrinsic permeability, as well as, an investigation of the Biot number to provide an indication of the relative importance of the conductive and convective effects. Model validation may also be performed with larger bales under typical storage conditions which may involve imposed wind currents that increase heat transfer from the bale to the environment. An assessment of the flow resistance through the material may become necessary under such conditions. Analysis of larger bale sizes would also provide unique results since they have less global surface area per unit volume; thereby reducing the effective heat dissipation from the material. Consequently, heat generation in larger bales may be more influential. Such developments, may allow for the simulation of temperature and moisture contents within bales of any size.

APPENDICES

Appendix A. Conduction Model Parameters

A.1 Heat Transfer Coefficient (Global Domain)

The heat transfer coefficient at each surface of the two-dimensional global domain was evaluated in accordance with the boundary layer theory. In this case, the Grashof (Gr) and Rayleigh (Ra) numbers were determined according to:

$$\mathrm{Gr} = \frac{L_c^3 g \rho^2 \beta (T_{surf} - T_a)}{\mu^2} = \frac{L_c^3 g \beta (T_{surf} - T_a)}{\nu^2} \quad [A.1]$$

$$\mathrm{Ra} = \mathrm{Gr} \cdot \mathrm{Pr} \quad [A.2]$$

where: L_c = characteristic length (m); g = gravitational acceleration ($m^3\ s^{-1}$); ρ = fluid density ($kg\ m^{-3}$); β = coefficient of thermal expansion (K^{-1}); T_{surf} and T_a = surface and ambient temperature (K), respectively; μ = dynamic viscosity ($kg\ m^{-1}\ s^{-1}$); ν = kinematic viscosity ($m^2\ s^{-1}$).

In this case, the characteristic lengths for the horizontal and vertical surfaces of the two-dimensional rectangular domain were defined as dx and dy; respectively (Kozanoglu and Rubio, 2014; Remsburg, 2011; Thirumaleshwar, 2009). Film temperature (T_f) was considered to be the average between the surface temperature and the ambient temperature; while the thermal expansion coefficient ($\beta=1/T_f$) was estimated according to the ideal gas model and assuming the air was at standard atmospheric conditions. The Prandtl number, thermal conductivity and kinematic viscosity of the air at each surface of the domain were all estimated based on appropriate empirical relationships which were evaluated as functions of the film temperature. The absolute value of the temperature difference was also implemented in this assessment in order to avoid complex numbers in determining the heat transfer coefficient.

Assuming laminar flow, with a Rayleigh number less than 1E9 under the proposed conditions, the generalized form of the Nusselt number for the horizontal surfaces (top and bottom) was described as (Bejan, 2004; Çengel and Ghajar, 2011) :

$$\mathrm{Nu} = \mathrm{C} \cdot (\mathrm{Ra})^{0.25} \qquad [A.3]$$

where: C is an empirical coefficient which has been defined as a function of the geometry and the Rayleigh number. This coefficient takes a value of 0.54 for those cases involving the upper surface of a heated horizontal plate or the lower surface of a colder horizontal plate. Alternatively, this coefficient takes a value of 0.27 for the lower surface of a heated plate or upper surface of a cold horizontal plate. Hence, the solution of the Nusselt number for the horizontal surfaces depends on the relative temperature at the surface. This expression for the Nusselt number was used in evaluating the heat transfer coefficient at the top (h_T) and bottom (h_B) surfaces of the global domain.

The Nusselt number for the vertical surfaces (left and right) was described in terms of the following relationship (Bejan, 2004; Çengel and Ghajar, 2011):

$$\mathrm{Nu} = \left\{0.825 + \frac{0.387(\mathrm{Ra})^{1/6}}{\left[1+(0.492/\mathrm{Pr})^{9/16}\right]^{8/27}}\right\}^2 \qquad [A.4]$$

which is evidently dependent on both the Rayleigh Number (Ra) and Prandtl number (Pr) correlations. This expression for the Nusselt number of the vertical surfaces was used in evaluating the heat transfer coefficient of the left (h_L) and right (h_R) surfaces of the domain of interest.

The heat transfer coefficient was subsequently determined based on the general relationship with the Nusselt number as follows:

$$\mathrm{h_c} = \frac{\mathrm{Nu \cdot k_a}}{\mathrm{L_c}} \qquad [A.5]$$

where: k_a = thermal conductivity of air (W m^{-1} K^{-1}). Heat transfer coefficient for gases in free convection is typically on the order of 5 to 37 W m^{-2} K^{-1}.

Appendix B. Inner Domain Parameters

B.1 Diffusion

The movement of bound water can play an important role in moisture transfer in the sorption region. While the effect of condensate flow in fine capillaries may also be regarded as bound water in sorptive porous materials (Okazaki, 1985), a challenge exists in distinguishing whether the water in fine capillaries comes from condensation or from connected fine capillaries. In this case, the solution field for the model proposed in Chapter 4 was observed to have minimal sensitivity to the liquid conductivity (D_L) due to the relative magnitude of the moisture content gradient. Nevertheless, this parameter was evaluated as a function of the temperature and moisture content as detailed in many previous studies (Achariyaviriya and Puttakarn, 2003; Becker, 1959; Chen et al., 2012a, 2012b; Coradi et al., 2014; Erbay and Icier, 2010; Gaston et al., 2003; Górnicki and Kaleta, 2011; Lu and Siebenmorgen, 1992; Sobukola and Dairo, 2007; Taheri-Garvavand et al., 2011). In this case, the following relationship describing bound liquid conductivity was employed (Chen and Pei, 1989):

$$D_L = D_0 \left(\frac{M - M_e}{M_{ms} - M_e}\right)^3 \exp\left(\frac{-E_a}{RT_I}\right) \quad [B.1]$$

where: D_L = liquid conductivity or moisture diffusivity ($m^2\ s^{-1}$); D_0 = pre-exponential Arrhenius-type factor for mass diffusivity ($m^2\ s^{-1}$); M = moisture content, dm ($kg\ kg^{-1}$); E_a = activation energy of moisture diffusion ($kJ\ mol^{-1}$); R = universal or ideal gas constant (8.3145E-3 $kJ\ mol^{-1}\ K^{-1}$); T_I = inner domain temperature (K); and the subscripts e and ms represent the equilibrium and maximum sorptional conditions, respectively. The sorption isotherm of milled switchgrass (Godbolt et al., 2013; Karunanithy et al., 2013) was used in determining the relevant moisture parameters of this model.

Representative values for the pre-exponential constant, D_0, are presented in Table B.1 for various materials. An intermediate value of 1.0E-3 $m^2\ s^{-1}$ was considered in the present study since no data was available for switchgrass. However, this estimated value was assumed to have minimal influence on the solution field as mentioned previously.

Table B.1 Pre-Exponential Arrhenius Factor for various materials.

Type	Material	Pre-Exponential Arrhenius Factor D_0 (m^2 s^{-1})	Source
Assorted	Brick	9.80E-2	Chen and Pei, 1989
	Wool	6.20E-2	Chen and Pei, 1989
Grain	Wheat Kernel	7.68E-3	Becker, 1959
	Rice	3.30E-4	Lu and Siebenmorgen, 1992
Leaves	Lemon Grass	3.17E-5	Coradi et al., 2014
Fruits	Tomato	1.77E-4	Taheri-Garavand et al., 2011
	Lychee	8.90E-6	Achariyaviriya and Puttakarn, 2003

The activation energy described here is different from the vaporization heat of free water as the sorption characteristics of the material influence the liquid movement (Bramhall, 1979; Chirife, 1983). This activation energy, E_a, essentially represents the energy required to vaporize the bound water. Table B.2 contains a summary of the activation energies reported for various biological and agricultural materials. Based on the previously reported data for these materials, an intermediate value within the typical range of non-wood fibers was selected for switchgrass in the present study with a value of 16.22 kJ mol^{-1}.

The vapor diffusion coefficient (D_v) was determined according to a common empirical relationship for the diffusion of water vapor in air (Çengel and Ghajar, 2011; Fair and Lerner, 1956; Marrero and Mason, 1972):

$$D_v = 1.87 \times 10^{-10} \frac{T^{2.072}}{P} \quad [B.2]$$

where: D_v = vapor diffusion coefficient (m^2 s^{-1}); T = temperature (K); and P = total pressure (atm).

Table B.2 Activation energy (E_a) for various biological materials.

Type	Material	Activation Energy E_a (kJ mol^{-1})	Source
Leaves	Barley	81.64	Montanuci et al., 2013
	Fever	80.78	Sobukola and Dairo, 2007
	Lemon Grass	62.84	Coradi et al., 2014
Fruits / Vegetables	Tomato	38.28	Taheri-Garavand et al., 2011
	Wheat Parboiled	37.01	Mohapatra and Rao, 2005
	Kale	36.12	Mwithiga and Olwal, 2005
	Aspen	32.20	He et al., 2012
	Lychee	29.11	Achariyaviriya and Puttakarn, 2003
Grains / Legumes	Wheat Kernel	28.71	Becker, 1959; Gaston et al., 2003
	Mung Beans	23.28	Li and Kobayashi, 2005
	Parboiled Paddy	22.89	Rao et al., 2007
	Olive Husk	21.30	Celma et al., 2007
	Powdered Peanut Shell	21.20	Chen et al., 2012a
	Rice (Rough)	19.77	Iguaz et al., 2003; Lu and Siebenmorgen, 1992
Non-wood Fibers	Bagasse	19.47	Vijayaraj et al., 2007
	Cotton Stalk	15.10	Chen et al., 2011
	Wheat Straw	14.10	Cai and Chen, 2008
Assorted	Olive-Waste Cake	12.34	Vega-Galvez et al., 2010
	Poplar Sawdust	12.30	Chen et al., 2012b

B.2 Latent Heat

The latent heat of vaporization (L_v) for water was approximated as a function of temperature using the common empirical relationship as follows (ASHRAE, 2011; Rogers and Yau, 1989):

$$L_v = 2500.8 - 2.36T + 0.0016T^2 - 0.00006T^3 \quad [B.3]$$

where: Lv = latent heat of vaporization of water (kJ kg^{-1}) and T = temperature (°C).

B.3 Thermophysical

The thermal diffusivity of the inner domain (α_s) was based on the thermophysical properties evaluated in the dual thermal probe analysis (see section 5.3). In this case, the

thermal conductivity of the baled switchgrass was expressed as a function of the three distinct components within the global domain (solid phase, dry air and water) as follows:

$$k_B = \frac{1}{\frac{X_s}{k_s}+\frac{X_a}{k_a}+\frac{X_w}{k_w}} \quad [B.4]$$

where: k = thermal conductivity (W m^{-1} K^{-1}); X = volumetric ratio (m^3 m^{-3}); and the subscripts B, s, a and w represent the overall bale, solid phase, dry air and water, respectively.

Now, considering a dry bale of switchgrass ($X_w = 0$), this expression may be simplified as:

$$k_{dB} = \frac{1}{\frac{X_s}{k_s}+\frac{X_a}{k_a}} \quad [B.5]$$

where: the subscript dB indicates as assessment of the bale under dry conditions. This expression is further simplified by recognizing that the sum of both fractional components must equal one ($X_s + X_a = 1$):

$$k_{dB} = \frac{k_a k_s}{k_a(1-X_a)+k_s X_a} \quad [B.6]$$

Now, solving in terms of the thermal conductivity of the solid phase (k_s) yields:

$$k_s = \frac{k_{dB} k_a (1-X_a)}{k_a - k_{dB} X_a} \quad [B.7]$$

It should also be noted here, that the volumetric ratio of dry air was assumed to be synonymous with the porosity of the outer domain ($X_a = \varepsilon$), thus, yielding:

$$k_s = \frac{k_{dB} k_a (1-\varepsilon)}{k_a - k_{dB} \varepsilon} \quad [B.8]$$

In this formulation, the thermal conductivity of the air (k_a) was based on a polynomial function of air temperature. This expression for the thermal conductivity of the solid phase (k_s) was then used as the basis for the evaluation of the thermophysical properties of the inner domain with the thermal conductivity of the inner domain (k_I) expressed as a function of the moisture content (Anderson, 1950; Buckmaster, 1989; Stroshine, 2004):

$$k_I = Mk_w + (1 - M)k_s \quad [B.9]$$

where: M = moisture content (kg kg^{-1}) and the subscript I represents an evaluation of the inner domain.

The thermal diffusivity of the inner domain (α_I) was then based on the thermophysical relationship:

$$\alpha_I = \frac{k_I}{\rho Cp} \quad [B.10]$$

where: α = thermal diffusivity (m^2 s^{-1}); k = thermal conductivity (W m^{-1} K^{-1}); ρ_s = density (kg m^{-3}); and Cp_s = specific heat (kJ kg^{-1} K^{-1}). The density of the inner domain was estimated as 437 kg m^{-3} based on the average particle density of switchgrass reported by Lam et al. (2007, 2008). In this formulation, the specific heat of switchgrass was estimated based on a polynomial curve fit of the data presented by Dupont et al. (2013) as a function of the inner domain temperature.

B.4 Heat Transfer Coefficient

The heat transfer coefficient of the inner domain (h_{cI}) was evaluated based on the boundary layer theory and the packed bed formulation which was expected to provide a better approximation of the heat transfer compared with the application of the cylindrical geometric expression. The empirical correlations discussed in this formulation describe natural convection heat transfer through packed beds (Bird et al., 2007; Cussler, 1997). In deriving this parameter for the current study, the general form of the Chilton-Colburn relationship was first described as:

$$j_H = St_H(Pr)^{2/3} = \frac{h_c}{\rho_a Cp_a}(Pr)^{2/3} \quad [B.11]$$

where: j_H = Chilton-Colburn Factor (-); St_H = Stanton number for heat transfer (-); h_c = heat transfer coefficient (W m^{-2} K^{-1}); ρ_a = air density (kg m^{-3}); Cp_a = specific heat of air (J kg^{-1} K^{-1}); and Pr = Prandtl Number (-).

The formulation of the Nusselt number for this application then proceeded according to the following heat transfer definitions for the Prandtl (Pr), Grashof (Gr) and Rayleigh (Ra) numbers according to:

$$Pr = \frac{\nu}{\alpha} \quad [B.12]$$

$$Gr = \frac{L_c^3 g \rho^2 \beta (T_{surf} - T)}{\mu^2} = \frac{L_c^3 g \beta (T_{surf} - T)}{\nu^2} \quad [B.13]$$

$$Ra = Gr \cdot Pr \quad [B.14]$$

where: ν = kinematic viscosity (m^2 s^{-1}); α = thermal diffusivity (m^2 s^{-1}); L_c = characteristic length (m); g = gravitational acceleration (m^3 s^{-1}); ρ = fluid density (kg m^{-3}); β = coefficient of thermal expansion (K^{-1}); T = temperature (K); μ = dynamic viscosity (kg m^{-1} s^{-1}); and the subscript surf represents the conditions at the surface of the inner domain. In this case, it should be noted that the outer domain temperature (T) was considered to be the temperature of the ambient environment surrounding the inner domain.

The characteristic length for the inner domain was defined as the average diameter of switchgrass as 2.698 mm (Lam et al., 2007, 2008). Film temperature (T_f) was considered to be the average between the surface temperature and the outer domain temperature; while the thermal expansion coefficient ($\beta=1/T_f$) was estimated according to the ideal gas model and assuming the air was at standard atmospheric conditions. The Prandtl number, thermal conductivity and kinematic viscosity of the air at each surface of the domain were all estimated based on appropriate empirical relationships which were evaluated as functions of the film temperature. The absolute value of the temperature

difference was also implemented in this assessment in order to avoid complex numbers in determining the heat transfer coefficient.

Assuming laminar flow, the generalized form of the Nusselt number was described as:

$$\mathrm{Nu} = \mathrm{C} \cdot (\mathrm{Ra})^{0.25} \quad [B.15]$$

where: C = shape factor which has been defined as a function of the geometry and the Rayleigh number. It follows, that this shape factor can be expressed in terms of its two distinct constituents as follows:

$$\mathrm{C} = \mathrm{C}_1(\mathrm{shape}) \cdot \mathrm{C}_2(\mathrm{Pr}) \quad [B.16]$$

with the shape function, $C_1 = 0.772$ for horizontal cylinders; and the Prandtl number function, C_2, defined by Churchill and Usagi (1972) as follows:

$$\mathrm{C}_2 = \frac{0.671}{\left[1+(0.492/\mathrm{Pr})^{9/16}\right]^{4/9}} \quad [B.17]$$

The heat transfer coefficient was determined based on the solution of the Nusselt number as follows:

$$\mathrm{h_c} = \frac{\mathrm{Nu} \cdot \mathrm{k_a}}{\mathrm{L_c}} \quad [B.18]$$

where: k_a = thermal conductivity of air (W m^{-1} K^{-1}). The heat transfer coefficient for gases in free convection is typically on the order of 5 to 37 W m^{-2} K^{-1}.

B.6 Mass Transfer Coefficient

The convective mass transfer coefficient (h_m) using the previously determined heat transfer coefficient according to the Chilton-Colburn analogy (Bird et al., 2007;

Carlton and Oxley, 1967; Çengel and Ghajar, 2011; Kandula, 2011; Lees, 2012; Marrero and Mason, 1972; Rao, 2015) with:

$$j_M = St_M(Sc)^{2/3} = \frac{h_m M_a}{M_v}(Sc)^{2/3} \quad [B.19]$$

where: j_M = Chilton-Colburn Factor for mass transfer (-); St_M = Stanton number for mass transfer (-); h_m = mass transfer coefficient (m s^{-1}); M = molecular weight (g mol^{-1}); Sc = Schmidt number (-); and the subscripts a and v denote air and water vapor, respectively.

The Schmidt number is defined as the ratio between momentum and mass diffusivity as follows:

$$Sc = \frac{\nu}{D} = \frac{\mu}{\rho D} \quad [B.20]$$

where: D = mass diffusivity (m^2 s^{-1}).

Setting the aforementioned definitions of j_H and j_M equal to each other in accordance with the Chilton-Colburn analogy yields:

$$\frac{h_c}{\rho_a Cp_a}(Pr)^{2/3} = \frac{h_m M_a}{M_v}(Sc)^{2/3} \quad [B.21]$$

Solving for the mass transfer coefficient (h_m) yields:

$$h_m = \frac{M_v h_c}{M_a \rho_a Cp_a}\left(\frac{Pr}{Sc}\right)^{2/3} \quad [B.22]$$

where ρ_a and Cp_a are based on the moist air conditions.

Applications involving higher surface moisture contents may require changes to these functional dependencies in order to account for the influence of surface moisture content (Chen and Pei, 1989). However, the present application was considered to initiate within the sorption region with relatively low surface moisture content.

B.7 Source Term

The source term for the inner domain (S_T) was based on the aerobic respiration rate for switchgrass according to the following respiration equation (Fontenelle et al., 2011a, 2011b):

$$C_6H_{12}O_6\ (s) + 6{\cdot}O_2\ (g) \rightarrow 6{\cdot}CO_2\ (g) + 6{\cdot}H_20\ (g) + HEAT\ (2557\text{-}2870\ kJ\ mol^{-1})$$

The respiration rate of biological materials is largely dependent on the moisture content and ambient air temperature (McDonald, 1981). Hence, the respiration rate of switchgrass (a term considered synonymous to the generation rate of carbon dioxide), was estimated according to an empirical model described by Emery (2013) as follows:

$$Y_{CO_2} = (28 - 3.9T - 160M + 0.034T^2 + 22T \cdot M)/90 \qquad [B.23]$$

where: Y_{CO_2} = generation rate of carbon dioxide ($g_{CO_2}\ kg_{dm}^{-1}\ day^{-1}$); T= temperature (°C); and M = moisture content (dec-wb).

Respiration was the only biochemical process considered in this study; disregarding any other potential sources of carbon dioxide (e.g., respiration from fungal and insect growth). The generation rate of carbon dioxide was subsequently used in determining the heat generation rate:

$$Y_T = \frac{2.87E6\ (J) \times Y_{CO_2}\left(\frac{g}{kg\ day}\right)}{6\left(\frac{mol}{mol}\right)} \qquad [B.24]$$

where: Y_T = heat generation rate ($J\ kg^{-1}\ day^{-1}$); 2.87E6 represents the amount of heat generation from the oxidation of glucose ($J\ mol^{-1}$); and 6 refers to the molar ratio of carbon dioxide.

These particular rate equations were used to derive the source term appearing in the energy conservation equation of the inner domain:

$$S_T = \rho_{BD} \cdot Y_T \quad [B.25]$$

where: S_T = source term (W m^{-3}) and ρ_{BD} = dry matter density (kg m^{-3}).

B.7 Dry Matter Loss

The dry matter loss rate was also determined according to the aerobic respiration equation as a function of the generation rate of carbon dioxide as follows:

$$Y_{DML} = \frac{1\left(\frac{mol}{mol}\right) \times Y_{CO_2}\left(\frac{g}{kg\ day}\right)}{6\left(\frac{mol}{mol}\right)} \quad [B.26]$$

where: Y_{DML} = dry matter loss rate (mg kg^{-1} day^{-1}); Y_{CO_2} = generation rate of carbon dioxide (g_{CO_2} kg_{dm}^{-1} day^{-1}); and 6 refers to the molar ratio of carbon dioxide.

B.8 Porosity

The porosity of the inner domain (ε_I) was assumed to be constant with respect to time; and was evaluated according to the following expression:

$$\varepsilon_I = 1 - \frac{\rho_b}{\rho_s} \quad [B.27]$$

where: ε_I = porosity of the inner domain (-) and ρ_b and ρ_s = the bulk density and solid density (kg m^{-3}), respectively. In this case, the density of the switchgrass was assumed to be constant with no DML. The average solid particle density and bulk density reported by Lam et al. (2007, 2008) were applied in this evaluation with values of 437 and 203 kg m^{-3}, respectively.

Appendix C. Outer Domain Parameters

C.1 Permeability

The permeability (κ) of the baled switchgrass was estimated as a function of the hydraulic conductivity according to the procedure documented by Zhang (2004). The hydraulic conductivity represents both the properties of the porous medium, as well as, the properties of the fluid flowing through the porous medium. To separate the properties of the porous medium from the properties of the fluid, the intrinsic permeability term may be introduced to represent the size and interconnectedness of the pores within the porous medium. The intrinsic permeability can be expressed in terms of the hydraulic conductivity as follows:

$$\kappa = K\left(\frac{\mu}{\rho g}\right) \qquad [C.1]$$

where: κ = intrinsic permeability (cm^2); K = hydraulic conductivity ($cm\ s^{-1}$); μ = dynamic viscosity ($kg\ m^{-1}\ s^{-1}$); ρ = density ($kg\ m^{-3}$); and g = gravitational acceleration ($9.81\ m\ s^{-2}$).

In this case, the kinematic viscosity and density of the fluid phase are based on empirical functions of the water temperature. For reference, the intrinsic permeability of certain types of well-sorted gravel is typically reported to be in the range of 9.87E-12 to 9.87E-10 m^2. The hydraulic conductivity was based on the results of the constant head test performed in this study (see sections 5.1 and 6.1).

C.2 Porosity

Although the porosity of the inner domain (ε_I) was regarded as a constant value in this study, the porosity of the outer domain (ε) was assessed as a function of the moisture as:

$$\varepsilon = 1 - \left(\frac{\rho_{bd}}{\rho_s} + \frac{\rho_{b0} M_0}{\rho_w}\right) \qquad [C.2]$$

where: ρ = density (kg m^{-3}); M = moisture content (dec. wb); and the subscripts b, s, d, w and 0 represent the bulk, solid phase, dry matter, water and initial conditions, respectively.

In this case, the density of the solid phase (ρ_s) was estimated as 437 kg m^{-3} based on the average particle density of switchgrass reported by Lam et al. (2007, 2008). The density of the water (ρ_w) was assumed to be a constant 991.48 kg m^{-3} with a negligible effect of temperature. The initial bulk density of the bales (ρ_{b0}) was determined by dividing the bale weight with its volume, both of which were measured directly after baling. Using the initial moisture content of the bales (M_0) the dry matter density was estimated according to:

$$\rho_{bd} = \rho_{b0}(1 - M_0) \qquad [C.3]$$

The bulk density on a dry basis (ρ_{bd}) was assumed to be constant for each treatment analyzed in this study; the value of which was dependent on the initial bulk density and moisture level for the treatment. This formulation was also considered under the assumption of negligible shrinkage throughout storage.

BIBLIOGRAPHY

References (Chapter 1)

Agblevor, F. A., Evans, R. J., & Johnson, K. D. (1994). Molecular-beam mass-spectrometric analysis of lignocellulosic materials: I. Herbaceous biomass. *Journal of Analytical and Applied Pyrolysis*, 30(2), 125-144.

Agblevor, F. A., Rejai, B., Evans, R. J., & Johnson, K. D. (1993). Pyrolytic analysis and catalytic upgrading of lignocellulosic materials by molecular beam mass spectrometry. *Energy from Biomass and Wastes*, 16, 767-767.

Albert, R. A., Huebner, B., & Davis, L. W. (1989). Role of water activity in the spoilage of alfalfa hay. *Journal of Dairy Science*, 72(10), 2573-2581.

Atchison, J. E., & Hettenhaus, J. R. (2003). Innovative Methods for Corn Stover Collecting. *Handling, Storing and Transporting*, Mar, 24-25.

Barnes, R. F., Nelson, C. J., Moore, K. J., Collins, M. (2007). Forages: The science of grassland agriculture: 6(11), Blackwell Publishing.

Baron, V. S., Dick, A. C., & Young, D. G. (1991). Laboratory system for evaluation of hay preservatives. *Agronomy Journal*, 83(4), 659-663.

Barr, A. G., Smith, D. M., & Brown, D. M. (1995). Estimating forage yield and quality changes during field drying for hay 1. Model of dry-matter and quality losses. *Agricultural and Forest Meteorology*, 76(2), 83-105.

Bergman, R. P., Reed, D. L., Taylor, A. M., Harper, D. P., & Hodges, D. G. (2015). Cradle-to-gate life cycle assessment of switchgrass fuel pellets manufactured in the Southeastern United States. *Wood and Fiber Science* 47(2): 1-13.

Bransby, D. I., Smith, H. A., Taylor, C. R., & Duffy, P. A. (2005). Switchgrass budget model: an interactive budget model for producing & delivering switchgrass to a bioprocessing plant. *Industrial Biotechnology*, 1(2), 122-125.

Buckmaster, D. R., & Rotz, C. A. (1986). A model of hay storage. ASAE Paper 86-1036. *Proc. Mtg. Am. Soc. Agric. Eng.*, San Luis Obispo, CA.

Buckmaster, D. R., Rotz, C. A., & Martens, D. R. (1989). A model of alfalfa hay storage. *Transactions of the ASAE*, 32(1), 30-0036.

Cundiff, J. S. & Marsh, L. S. (1995). Effects of ambient environment on the storage of switchgrass for biomass to ethanol and thermochemical fuels. *National Renewable Energy Laboratory*, Golden.

Cusi, D. S. (1979). Nonwood Plant Fiber Pulping Progress Report No. 10. *TAPPI: Atlanta, GA*, 33.

Chen, S. F., Mowery, R. A., Sevcik, R. S., Scarlata, C. J., & Chambliss, C. K. (2010). Compositional analysis of water-soluble materials in switchgrass. *Journal of Agricultural and Food Chemistry*, 58(6), 3251-3258.

Chico-Santamarta, L., Humphries, A. C., Chaney, K., White, D. R., Magan, N., &

Godwin, R. J. (2011). Microbial changes during the on-farm storage of canola (oilseed rape) straw bales and pellets. *Biomass and Bioenergy*, 35(7), 2939-2949.

Chico-Santamarta, L., Humphries, A. C., White, D., Chaney, K., Godwin, R. J., Smith, L. & Weightman, R. (2010). The use of oilseed rape (Brassica napus) straw for combustion purposes: a review of the advantages and disadvantages. *Aspects of Applied Biology*, (101), 63-69.

Coble, C. G., & Egg, R. (1987). Dry matter losses during hay production and storage of sweet sorghum used for methane production. *Biomass*, 14(3), 209-217.

Coble, C. G., Egg, R. P., & Salge, M. D. (1985). Harvesting sorghum for grain and biomass.

Coblentz, W. K. (2009). Effects of wrapping method and soil contact on hay stored in large round bales in central Wisconsin. *Applied Engineering in Agriculture*, 25(6), 835-850.

Coblentz, W. K., & Hoffman, P. C. (2009). Effects of spontaneous heating on fiber composition, fiber digestibility, and in situ disappearance kinetics of neutral detergent fiber for alfalfa-orchardgrass hays. *Journal of dairy science*, 92(6), 2875-2895.

Coblentz, W. K., Fritz, J. O. & Bolsen, K. K. (1993a). Baling system for making laboratory-scale hay bales. *Agronomy Journal*, 85(4), 962-965.

Coblentz, W. K., Fritz, J. O. & Bolsen, K. K. (1993b). Comparison of conventional and laboratory-scale alfalfa hay bales in small haystacks.

Coblentz, W. K., Fritz, J. O., & Bolsen, K. K. (1994). Performance comparisons of conventional and laboratory-scale alfalfa hay bales in isolated environments. Agronomy Journal, 86(5), 811-819.

Coblentz, W. K., Fritz, J. O., Bolsen, K. K., & Cochran, R. C. (1996). Quality changes in alfalfa hay during storage in bales. *Journal of dairy science*, 79(5), 873-885.

Coblentz, W. K., Turner, J. E., Scarbrough, D. A., Lesmeister, K. E., Johnson, Z. B., Kellogg, D. W., Coffey, K. P., McBeth, L. J. & Weyers, J. S. (2000). Storage characteristics and nutritive value changes in bermudagrass hay as affected by moisture content and density of rectangular bales. *Crop Science*, 40(5), 1375-1383.

Collins, M., Ditsch, D., Henning, J. C., Turner, L. W., Isaacs, S., & Lacefield, G. D. (1997). Round bale hay storage in Kentucky. *University of Kentucky College of Agriculture, Lexington, and Kentucky State University, Frankfort. Copyright*.

Collins, M., Owens VN. (2003). Preservation of forage as hay and silage. In: *Barnes RF, et al., editors. Forages: An Introduction to Grassland Agriculture*. Iowa State Press, Ames, IA, USA 6(1): 443–471.

Collins, M., Paulson, W. H., Finner, M. F., Jorgensen, N. A., & Keuler, C. R. (1987). Moisture and storage effects on dry matter and quality losses of alfalfa in round bales. *Transactions of the ASAE*, 30(4), 913-0917.

Collins, M., Swetnam, L. D., Turner, G. M., Hancock, J. N., & Shearer, S. A. (1995). Storage method effects on dry matter and quality losses of tall fescue round bales.

Journal of production agriculture, 8(4), 507-514.

Cundiff, J. S. & Marsh, L. S. (1995). Effects of ambient environment on the storage of switchgrass for biomass to ethanol and thermochemical fuels. *National Renewable Energy Laboratory*, Golden.

Cusi, D. S. (1979). Nonwood Plant Fiber Pulping Progress Report No. 10. *TAPPI: Atlanta, GA*, 33.

Darr, M. J., & Shah, A. (2012). Biomass storage: an update on industrial solutions for baled biomass feedstocks. *Biofuels*, 3(3), 321-332.

Davies, O. D., & Nicholson, R. J. (1999, July). Effluent production from grass ensiled in round big bale wrapped with 4 layers of plastic film. In *Proc. Int. Silage Conf., 12th, Uppsala, Sweden* (pp. 5-7).

Dehority, B. A. (1993). Microbial ecology of cell wall fermentation in: Forage cell wall structure and digestibility (Ed HG Jung, DR Buxton, RD Hatfield and J. Ralph). *American society of Agronomy. Inc. Madison W*, 1, 425-453.

Dewar, W. A., McDonald, P., & Whittenbury, R. (1963). The hydrolysis of grass hemicelluloses during ensilage. *Journal of the Science of Food and Agriculture*, 14(6), 411-417.

Dien, B. S., Jung, H. J. G., Vogel, K. P., Casler, M. D., Lamb, J. F., Iten, L., Mitchell, R. B. & Sarath, G. (2006). Chemical composition and response to dilute-acid pretreatment and enzymatic saccharification of alfalfa, reed canarygrass, and switchgrass. *Biomass and Bioenergy*, 30(10), 880-891.

Digman, M. F., Shinners, K. J., Muck, R. E. & Dien, B. S. (2010a). Full-scale on-farm pretreatment of perennial grasses with dilute acid for fuel ethanol production. *Bioenergy Research* 3: 335-341.

Digman, M. F., Shinners, K. J., Muck, R. E. & Dien, B. S. (2010b). Pilot-scale on-farm pretreatment of perennial grasses with dilute acid and alkali for fuel ethanol production. *Transactions of the ASABE* 53: 1007-1014.

Duffy, M. (2007). Estimated costs for production, storage and transportation of switchgrass. PM 2042. Iowa State University Extension, Ames: A1-22.

Festenstein, G. N. (1971). Carbohydrates in hay on self-heating to ignition. *Journal of the Science of Food and Agriculture*, 22(5), 231-234.

Festenstein, G. N., Lacey, J., Skinner, F. A., Jenkins, P. A., Pepys, J., & Lacey, J. (1965). Self-heating of hay and grain in Dewar flasks and the development of farmer's lung antigens. *Microbiology*, 41(3), 389-407.

FPL (2004) Fuel value calculator. Techline. USDA Forest Service, Forest Products Laboratory, Madison, WI. 3 pp. http:// www.fpl.fs.fed.us/documnts/techline/fuel-value-calculator.pdf (19 May 2015).

Goering, H. K., & Van Soest, P. J. (1970). Forage fiber analyses (apparatus, reagents, procedures, and some applications). *USDA Agricultural Handbook*.

Goering, H. K., Van Soest, P. J., & Hemken, R. W. (1973). Relative susceptibility of

forages to heat damage as affected by moisture, temperature, and pH. *Journal of Dairy Science*, 56(1), 137-143.

Goldstein, N. (2006). Woody biomass as a renewable energy resource. *Biocycle* 47(11): 29-31.

Gordon, C. H., Derbyshire, J. C., Wiseman, H. G., Kane, E. A., & Melin, C. G. (1961). Preservation and feeding value of alfalfa stored as hay, haylage, and direct-cut silage. *Journal of Dairy Science*, 44(7), 1299-1311.

Gordon, C. H., Kane, E. A., Derbyshire, J. C., Jacobson, W. C., Melin, C. G., & McCalmont, J. R. (1959). Nutrient losses, quality, and feeding values of wilted and direct-cut orchardgrass stored in bunker and tower silos. *Journal of Dairy Science*, 42(10), 1703-1711.

Greenlees, W. J., Hanna, H. M., Shinners, K. J., Marley, S. J., & Bailey, T. B. (2000). A comparison of four mower conditioners on drying rate and leaf loss in alfalfa and grass. *Applied Engineering in Agriculture*, 16(1), 1.

Groothuis, M. D., Womac, A. R., Braswell, G., & Bitra, V. S. (2011). Compaction experiences with bulk-format switchgrass in commercial transfer systems. In *2011 Louisville, Kentucky, August 7-10, 2011* (p. 1). American Society of Agricultural and Biological Engineers.

Gupta, M. L., McMahon, T. A., Macmillan, R. H., & Bennett, D. W. (1990). Simulation of hay-making systems: Part 1—development of the model. *Agricultural systems*, 34(4), 277-299.

Haghighi, A., Medero, G. M., Marinho, F. A. M, Mercier, B. & Woodward, P. K. (2012). Temperature effects on suction measurement using the filter paper technique. *Geotech. Test Journal* 35(1): 83-90.

Haghighi, K. (1990). Finite element simulation of the thermo-hydro stresses in a viscoelastic sphere during drying. *Drying Technology*, 8(3), 465-498.

Han, K. J., Collins, M., Vanzant, E. S., & Dougherty, C. T. (2004). Bale density and moisture effects on alfalfa round bale silage. *Crop science*, 44(3), 914-919.

Harrigan, T. M., & Rotz, C. A. (1994). Net, plastic, and twine-wrapped large round bale storage loss. *Applied Engineering in Agriculture*, 10(2), 189-194.

Hathaway, J. E., Koegel, R. G., & Straub, R. J. (1984). Requirements for ammonia preservation of high moisture forages. *Paper-American Society of Agricultural Engineers* (USA).

Henriksen, T. M., & Breland, T. A. (1999). Nitrogen availability effects on carbon mineralization, fungal and bacterial growth, and enzyme activities during decomposition of wheat straw in soil. *Soil Biology and Biochemistry*, 31(8), 1121-1134.

Hess, J. R., Kenney, K. L., Ovard, L. P., Searcy, E. M. & Wright, C. T. (2009). Uniform-format bioenergy, annual corn and uncultivated systems in southern Quebec. *Agriculture, Ecosystems and Environment* 86: 135-144.

Hess, J. R., Wright, C. T. & Kenney, K. L. (2007). Cellulosic biomass and logistics for ethanol production. *Biofuels, Bioproducts and Biorefining* 1: 181-190.

Hess, J. R., Wright, C. T., Kenney, K. L., & Searcy, E. M. (2009). *Uniform-Format Solid Feedstock Supply System: A Commodity-Scale Design to Produce an Infrastructure-Compatible Bulk Solid from Lignocellulosic Biomass--Executive Summary* (No. INL/EXT-09-15423). Idaho National Laboratory (INL).

Huhnke, R. L. (1988). Large round bale alfalfa hay storage. *Applied Engineering in Agriculture*, 4(4), 316-323.

Huhnke, R. L. (1990a). Round bale bermudagrass hay storage losses. *Applied Engineering in Agriculture*, 6(4), 396-400.

Huhnke, R. L. (1990b). Round bale wheat hay storage losses. *Applied Engineering in Agriculture*, 6(5), 569-574.

Huhnke, R. L. (2003). Round bale hay storage. Division of Agricultural Sciences and Natural Resources, Oklahoma State University.

Huhnke, R. L., Muck, R. E., & Payton, M. E. (1997). Round bale silage storage losses of ryegrass and legume-grass forages. *Applied Engineering in Agriculture*, 13(4), 451-457.

Inman, D., Nagle, N., Jacobson, J., Searcy, E., & Ray, A. E. (2010). Feedstock handling and processing effects on biochemical conversion to biofuels. *Biofuels, Bioproducts and Biorefining*, 4(5), 562-573.

Jirjis, R. (2005). Effects of particle size and pile height on storage and fuel quality of comminuted Salix viminalis. *Biomass and Bioenergy*, 28(2), 193-201.

Jirjis, R., & Theander, O. (1990). The effect of seasonal storage on the chemical composition of forest residue chips. *Scandinavian Journal of Forest Research*, 5(1-4), 437-448.

Johnson, K. D., Cherney, J. H., Greene, D. K., & Valence, I. J. (1991). Evaluation of switchgrass and sorghum biomass potential. *Oak Ridge National Laboratory, Oak Ridge*.

Johnson, T. R., Thomas, J. W., Rotz, C. A., & Tesar, M. B. (1984). Drying rate of cut forages after spray treatments to hasten drying. *Journal of Dairy Science*, 67(8), 1745-1751.

Jung, H. G., & Deetz, D. A. (1993). Cell wall lignification and degradability. *Forage cell wall structure and digestibility*, (foragecellwalls), 315-346.

Jung, H. J. G., & Lamb, J. F. (2004). Prediction of cell wall polysaccharide and lignin concentrations of alfalfa stems from detergent fiber analysis. *Biomass and Bioenergy*, 27(4), 365-373.

Khanchi, A., Jones, C. L., & Sharma, B. (2009). Characteristics and compositional variation in round and square sorghum bales under different storage conditions. In *2009 Reno, Nevada, June 21-June 24, 2009* (p. 1). American Society of Agricultural and Biological Engineers.

Kubler, H. (1987). Growth stresses in trees and related wood properties. In *For. Prod. Abst*racts: 10 (pp. 61-119).

Kumar, A., & Sokhansanj, S. (2007). Switchgrass (Panicum vigratum, L.) delivery to a biorefinery using integrated biomass supply analysis and logistics (IBSAL) model. *Bioresource Technology*, 98(5), 1033-1044.

Lacey, J., & Lord, K. A. (1977). Methods for testing chemical additives to prevent molding of hay. *Annals of Applied Biology*, 87(3), 327-335.

Lacey, J., & Magan, N. (1991). Fungi in cereal grains: their occurrence and water and temperature relationships. *Developments in Food Science (Netherlands)*.

Larson, J. A., Mooney, D. F., English, B. C., & Tyler, D. D. (2010, February). Cost analysis of alternative harvest and storage methods for switchgrass in the Southeastern US. In *2010 Annual Meeting of Southern Agricultural Economics Association* (pp. 6-9).

Lazarus, W. F., & Selley, R. (2002). *Farm machinery economic cost estimates for 2002*. University of Minnesota Extension Service, College of Agricultural, Food and Environmental Sciences.

Leong, E. C., He, L., & Rahardjo, H. (2002). Factors Affecting the Filter Paper Method for Total and Matric Suction Measurements, *Geotech. Test*, 1(25), 3.

Magan, N. (1988). Fungal colonization and decomposition of cereal straw. *International Biodeterioration*, 24(4), 435-443.

Martin, N. P. (1980). Harvesting and storage of quality hay. In *Proceedings of the. Forage and Grassland Conference*.

Martinson, K., Coblentz, W. & Sheaffer, C. (2011). The effect of harvest moisture and bale wrapping on forage quality, temperature, and mold in orchardgrass hay. *Journal of Equine Veterinary Science*, 31(12), 711-716.

McDonald, P., Henderson, A. R., & Heron, S. (1991). JE The biochemistry of silage. *Marlow, UK: Chalcombe Publications*.

Miller, H. (1947). Dry matter loss in haymaking due to bacterial action. *Agricultural Engineering*, 28, 243-244.

Miller, L. G., Clanton, D. C., Nelson, L. F., & Hoehne, O. E. (1967). Nutritive value of hay baled at various moisture contents. *Journal of Animal Science*, 26(6), 1369-1373.

Mitchell, R., & Schmer, M. (2012). Switchgrass harvest and storage. In *Switchgrass* (pp. 113-127). Springer London.

Mitchell, R., Vogel, K. P., & Sarath, G. (2008). Managing and enhancing switchgrass as a bioenergy feedstock. *Biofuels, Bioproducts and Biorefining*, 2(6), 530-539.

Monti, A., Fazio, S., & Venturi, G. (2009). The discrepancy between plot and field yields: Harvest and storage losses of switchgrass. *Biomass and bioenergy*, 33(5), 841-847.

Mooney, D. F., Larson, J. A., English, B. C., & Tyler, D. D. (2012). Effect of dry matter loss on profitability of outdoor storage of switchgrass. *Biomass and Bioenergy*, 44, 33-41.

Moore, K. J., Lechtenberg, V. L., Lemenager, R. P., Patterson, J. A., & Hendrix, K. S. (1985). In vitro digestion, chemical composition, and fermentation of ammoniated grass and grass-legume silage. *Agronomy Journal*, 77(5), 758-763.

Moore, K.J. & Peterson, M.A. (1995). *Post-harvest physiology and preservation of forages. American Society of Agronomy*, Crop Science Society of America, Madison, Wisconsin. CSSA Special Publication: 39-66.

Moore, L. A., & Thomas, J. W. (1960). The acceptability of grass/legume silage by dairy cattle. *Proc. 8th Intl Grassland Cong*. 1960.

Moser, L. E. (1980). Quality of forage as affected by post-harvest storage and processing. *Crop quality, storage, and utilization*, (cropqualitystor), 227-260.

Muck, R. E., & Holmes, B. J. (2000). Factors affecting bunker silo densities. *Applied Engineering in Agriculture*, 16(6), 613.

Muck, R. E., & Shinners, K. J. (2001, February). Conserved forage (silage and hay): progress and priorities. In *International Grassland Congress* (Vol. 19, pp. 753-762). São Pedro: SBZ.

Mwithiga, G., Mazwiduma, P. J., & Tsopito, C. M. (2012). Alternative methods of harvesting and storage of grass biomass in a semi-arid region. *African journal of agricultural research*, 7(14), 2166-2173.

Nehrir, H., Kjelgaard, W. L., Anderson, P. M., Long, T. A., Hoffman, L. D., Washko, J. B., Wilson, J. P. & Mueller, J. P. (1978). Chemical additives and hay attributes. *Transactions of the ASAE*, 21(2), 217-221.

Nelson, L. F. (1968). Spontaneous heating, gross energy retention and nutrient retention of high-density alfalfa hay bales. *Transactions of the ASAE*, 11(5), 595-600.

Nelson, L. F. (1972). Storage characteristics and nutritive value of high-density native hay bales. *Transactions of the ASAE*, 15(2), 201-0205.

Perlack, R. D., Wright, L. L., Turhollow, A. F., Graham, R. L., Stokes, B. J., & Erbach, D. C. (2005). *Biomass as feedstock for a bioenergy and bioproducts industry: the technical feasibility of a billion-ton annual supply*. Oak Ridge National Lab TN.

Petit, H. V., & Tremblay, G. F. (1992). In situ degradability of fresh grass conserved under different harvesting methods. *Journal of dairy science*, *75*(3), 774-781.

Philipp, D., Moore, K. J., Pedersen, J. F., Grant, R. J., Redfearn, D. D., & Mitchell, R. B. (2007). Ensilage performance of sorghum hybrids varying in extractable sugars. *Biomass and Bioenergy*, 31(7), 492-496.

Ream, H. W., Jorgensen, N. A., Koegel, R. G., & Bruhn, H. D. (1983). On-farm forage harvesting: plant juice protein production system in a humid temperate climate. *Ref*, 4, 467-489.

Rhein, R. T., Coblentz, W. K., Rosenkrans Jr, C. F., Sauer, T. J., & Kellogg, D. W. (1985). Aerobic Stability of Wheat and Orchardgrass Round-Bale Silage. *Research Series*, (522), 30.

Richard, T. L. (2010). Challenges in scaling up biofuels infrastructure. *Science (Washington)*, 329(5993), 793-796.

Rider, A. R., Batchelder, D., & McMurphy, W. (1979). Effects of long term outside storage on round bales. *American Society of Agricultural Engineering, St. Joseph, MI, ASAE Paper*, (79-1538), 5.

Rinehart, L. (2006). Switchgrass as a bioenergy crop. A Web Publication of ATTRA–National Sustainability Agriculture Information Service. 12 pp. https://attra.ncat.org/publication.html (19 May 2015).

Roberts, C. A. (1995). Microbiology of stored forages. *Post-harvest physiology and preservation of forages*, (postharvestphys), 21-38.

Rohweder, D. A., Barnes, R. F., & Jorgensen, N. (1978). Proposed hay grading standards based on laboratory analyses for evaluating quality. *Journal of Animal Science*, 47(3), 747-759.

Rotz, C. A. (2003). How to maintain forage quality during harvest and storage. *Advanced Dairy Technology*, 15, 227-239.

Rotz, C., Muck, R., Fahey JR, G. C., Moser, L., & Mertens, D. (1994). National conference on forage quality, evaluation, and utilization. In *National conference on forage quality, evaluation, and utilization*. Madison: University of Nebraska.

Russell, J. R., & Buxton, D. R. (1985). Storage of large round bales of hay harvested at different moisture concentrations and treated with sodium diacetate and/or covered with plastic. *Animal Feed Science and Technology*, 13(1), 69-81.

Russell, J., Yoder, S. J., & Marley, S. J. (1990). The effects of bale density, type of binding and storage surface on the chemical composition, nutrient recovery and digestibility of large round hay bales. *Animal Feed Science and Technology*, 29(1), 131-145.

Sanderson, M. A., Adler, P. R., Boateng, A. A., Casler, M. D., & Sarath, G. (2006). Switchgrass as a biofuels feedstock in the USA. *Canadian Journal of Plant Science*, 86(Special Issue), 1315-1325.

Sanderson, M. A., Egg, R. P., & Wiselogel, A. E. (1997). Biomass losses during harvest and storage of switchgrass. *Biomass and Bioenergy*, 12(2), 107-114.

Savoie, P., D'Amours, L., Amyot, A., & Theriault, R. (2006). Effect of Density, cover, depth, and storage time on dry matter loss of corn silage. In *2006 ASAE Annual Meeting* (p. 1). American Society of Agricultural and Biological Engineers.

Savoie, P., Rotz, C. A., Bucholtz, H. F., & Brook, R. C. (1982). Hay harvesting system losses and drying rates. *Transactions of the ASAE*, 25(3), 581-0585.

Schmer, M. R., Vogel, K. P., Mitchell, R. B., & Perrin, R. K. (2008). Net energy of cellulosic ethanol from switchgrass. *Proceedings of the National Academy of Sciences*, 105(2), 464-469.

Scudamore, K. A., & Livesey, C. T. (1998). Occurrence and significance of mycotoxins in forage crops and silage: a review. *Journal of the Science of Food and Agriculture*, 77(1), 1-17.

Shah, A., Darr, M. J., Webster, K., & Hoffman, C. (2011). Outdoor storage characteristics of single-pass large square corn stover bales in Iowa. *Energies*, 4(10), 1687-1695.

Shinners, K. J. (2000). Evaluation of methods to improve storage characteristics of large square bales in a humid climate. *Applied Engineering in Agriculture*, *16*(4), 341.

Shinners, K. J., Binversie, B. N., Muck, R. E., & Weimer, P. J. (2007). Comparison of wet and dry corn stover harvest and storage. *Biomass and Bioenergy*, 31(4), 211-221.

Shinners, K. J., Boettcher, G. C., Muck, R. E., Weimer, P. J., & Casler, M. D. (2006). Drying, harvesting and storage characteristics of perennial grasses as biomass feedstocks. In *2006 ASAE Annual Meeting* (p. 1). American Society of Agricultural and Biological Engineers.

Shinners, K. J., Boettcher, G. C., Muck, R. E., Weimer, P. J., & Casler, M. D. (2010). Harvest and storage of two perennial grasses as biomass feedstocks. *Transactions of the ASABE*, 53(2), 359-370.

Shinners, K. J., Huenink, B. M., Muck, R. E., & Albrecht, K. A. (2009a). Storage characteristics of large round and square alfalfa bales: Low-moisture wrapped bales. *Transactions of the ASABE*, 52(2), 401-407.

Shinners, K. J., Huenink, B. M., Muck, R. E., & Albrecht, K. A. (2009b). Storage characteristics of large round alfalfa bales: Dry hay. *Transactions of the ASABE*, 52(2), 409-418.

Shinners, K. J., Wepner, A. D., Muck, R. E., & Weimer, P. J. (2011). Aerobic and anaerobic storage of single-pass, chopped corn stover. *BioEnergy Research*, 4(1), 61-75.

Smith, W. A., Bonner, I. J., Kenney, K. L. & Wendt, L. M. (2013). Practical considerations of moisture in baled biomass feedstocks. *Biofuels*, 4(1), 95-110.

Sokhansanj, S., & Turhollow, A. F. (2004). Biomass densification-cubing operations and costs for corn stover. *Applied Engineering in Agriculture*, 20(4), 495-502.

Sokhansanj, S., Mani, S., Turhollow, A., Kumar, A., Bransby, D., Lynd, L., & Laser, M. (2009). Large-scale production, harvest and logistics of switchgrass (Panicum virgatum L.)–current technology and envisioning a mature technology. *Biofuels, Bioproducts and Biorefining*, 3(2), 124-141.

Summers, M. D., Blunk, S. L., & Jenkins, B. M. (2003). How straw decomposes: Implications for straw bale construction. *Ecological Building Network*, San Rafael, CA, USA.

Tabacco, E., Piano, S., Cavallarin, L., Bernardes, T. F., & Borreani, G. (2009). Clostridia spore formation during aerobic deterioration of maize and sorghum silages as influenced by Lactobacillus buchneri and Lactobacillus plantarum inoculants. *Journal of applied microbiology*, 107(5), 1632-1641.

Taylor, R. K., Blasi, D. A., & Dhuyvetter, K. C. (1995). Large round bale hay storage. Cooperative Extension Service, Kansas State University.

Taylor, R. K., Blasi, D. A., & Shroyer, J. P. (1994). Storage losses in net-wrapped, large round bales of alfalfa. *Applied Engineering in Agriculture*, 10(3), 317-320.

Turhollow, A., Downing, M. & Butler, J. (1998). Forage harvests and transportation costs. *Oak Ridge National Laboratory, Oak Ridge*.

Vogel, K. P., Sarath, G., Saathoff, A. & Mitchell, R. (2011). Switchgrass. In: *Halford N, Karp A (eds) Energy Crops*. The Royal Society of Chemistry, Cambridge.

Waldo, D. R., & Jorgensen, N. A. (1981). Forages for high animal production: nutritional factors and effects of conservation. *Journal of Dairy Science*, 64(6), 1207-1229.

Weeks, S. A., Owen, F. G., & Petersen, G. M. (1975). Storage characteristics and feeding value of mechanically stacked loose hay. *Transactions of the ASAE*, 18(6), 1065-1069.

Wiselogel, A. E., Agblevor, F. A., Johnson, D. K., Deutch, S., Fennell, J. A., & Sanderson, M. A. (1996). Compositional changes during storage of large round switchgrass bales. *Bioresource Technology*, 56(1), 103-109.

Wolfrum, E. J., & Lorenz, A. J. (2009). Correlating detergent fiber analysis and dietary fiber analysis data for corn stover collected by NIRS. *Cellulose*, 16(4), 577-585.

Woolford, M. K., & Tetlow, R. M. (1984). The effect of anhydrous ammonia and moisture content on the preservation and chemical composition of perennial ryegrass hay. *Animal Feed Science and Technology*, 11(3), 159-166.

Yu, Y. (1977). Effect of heating of forages on quantitative changes of acid-detergent insoluble nitrogen. *Journal of Dairy Science*, 60(11), 1813-1815.

Zhu, Z., Sun, D. A., Zhou, A., & Qiu, Z. (2016). Calibration of two filter papers at different temperatures and its application to GMZ bentonite. *Environmental Earth Sciences*, 75(6), 1-11.

References (Chapter 3)

References (Section 3.1)

Al-Khafaf, S., & Hanks, R. J. (1974). Evaluation of the filter paper method for estimating soil water potential. *Soil Science*, 117(4), 194-199.

Anne-Marie, W., Sandra, L. H., & William, N. H. (1994). Laboratory filter paper suction measurements.

ASTM Standards. (1992). D 5298-92. Standard test method for measurement of soil potential (suction) using filter paper. Philadelphia, Pa.: ASTM.

Balat, M., & Balat, H. (2009). Recent trends in global production and utilization of bio-ethanol fuel. *Applied Energy*, 86(11), 2273-2282.

Berry, P. L., & Vickers, B. (1975). Consolidation of fibrous peat. *Journal of the Geotechnical Engineering Division*, 101(8), 741-753.

Bhave, S., & Sreeja, P. (2013). Influence of initial soil condition on infiltration characteristics determined using a disk infiltrometer. *ISH Journal of Hydraulic Engineering*, 19(3), 291-296.

Bicalho, K. V., Cupertino, K. F. & Bertolde, A. I. (2011). Evaluation of suction-water content calibrations of filter paper. In *2011 Pan-Am CGS Geotechnical Conference on Soil Mechanics and Geotechnical Engineering (PCSMGE)*, Toronto, Canada.

Burdine, N. (1953). Relative permeability calculations from pore size distribution data. *Journal of Petroleum Technology*, 5(03), 71-78.

Chandler, R. J., Harwood, A. H., & Skinner, P. J. (1992). Sample disturbance in London clay. *Geotechnique*, 42(4), 577-585.

Chandler, R. J., & Gutierrez, C. I. (1986). The filter-paper method of suction measurement. *Géotechnique*, 36(2), 265-268.

Christianson, L., Castelló, A., Christianson, R., Helmers, M., & Bhandari, A. (2010). Technical note: Hydraulic property determination of denitrifying bioreactor fill media. *Applied Engineering in Agriculture*, 26(5), 849-854.

Chun, J. A., Cooke, R. A., Eheart, J. W., & Kang, M. S. (2009). Estimation of flow and transport parameters for woodchip-based bioreactors: I. laboratory-scale bioreactor. *Biosystems Engineering*, 104(3), 384-395.

Custer, M. H., Sweeten, J. M., Reddell, D. L., & Egg, R. (1986). The hydraulic conductivity of chopped sorghum. *Paper, American Society of Agricultural Engineers*, (86-6580).

Custer, M. H., Sweeten, J. M., Reddell, D. L., & Egg, R. P. (1990). Hydraulic conductivity of chopped sorghum. *Transactions of the ASAE*, 33(4), 1275-1280.

Delage, P., & Lefebvre, G. (1984). Study of the structure of a sensitive Champlain clay and of its evolution during consolidation. *Canadian Geotechnical Journal*, 21(1), 21-35.

Fasinmirin, J. T., & Olorunfemi, I. E. (2013). Soil moisture content variation and mechanical resistance of Nigerian Alfisol under different tillage systems. *Journal of Agricultural Engineering and Technology*, 21(2), 11-20.

Fawcett, R. G., & Collis-George, N. (1967). A filter-paper method for determining the moisture characteristics of soil. *Animal Production Science*, 7(25), 162-167.

Fernando, A. M., & Orlando, M. O. (2006). The filter paper method revisited.

Fonnesbeck, P. V., De Hernandez, M. G., Kaykay, J. M., & Saiady, M. Y. (1986). Estimating yield and nutrient losses due to rainfall on field-drying alfalfa hay. *Animal Feed Science and Technology*, 16(1), 7-15.

Fredlund, D. G., Vanapalli, S. K., Xing, A., & Pufahl, D. E. (1995, September). Predicting the shear strength function for unsaturated soils using the soil-water characteristic curve. In *First International Conference on Unsaturated Soils, Paris, France* (pp. 6-8).

Fredlund, D. G., & Rahardjo, H. (1993, March). The role of unsaturated soil behaviour in geotechnical engineering practice. In *Proceedings of the 11th Southeast Asian Geotechnical Conference, Singapore* (pp. 37-49).

Gardner, R. (1937). A Method of measuring the capillary tension of soil moisture over a wide moisture range. *Soil Science*, 43(4), 277-284.

Goldstein, N. (2006). Woody Biomass as renewable energy source. *Biocycle*, 47(11), 29-31.

Gonzalez-Sosa, E., Braud, I., Dehotin, J., Lassabatère, L., Angulo-Jaramillo, R., Lagouy, M., Branger, F., Jacqueminet, C., Kermadi, S. & Michel, K. (2010). Impact of land use on the hydraulic properties of the topsoil in a small French catchment. *Hydrological processes*, 24(17), 2382-2399.

Greacen, E. L., Walker, G. R., & Cook, P. G. (1989). *Procedure for filter paper method of measuring soil water suction*. CSIRO.

Guber, A., Pachepsky, Y. A., Shein, E., & Rawls, W. J. (2004). Soil aggregates and water retention. *Dev Soil Sci*, 30, 143-151.

Hamblin, A. P. (1981). Filter-paper method for routine measurement of field water potential. *Journal of Hydrology*, 53(3), 355-360.

Hillel, D. (1998). *Environmental Soil Physics: Fundamentals, applications, and environmental considerations*. San Diego, Calif.: Academic Press.

Lau, Y. L. (1983). Suspended sediment effect on flow resistance. *Journal of Hydraulic Engineering*, 109(5), 757-763.

Lee, H. C., & Wray, W. K. (1995). Techniques to evaluate soil suction-a vital unsaturated soil water variable. In *Proceedings of the First International Conferences on Unsaturated Soils/Unsat'5, Paris, France*, 6-8 September 15. Volume 2.

Likos, W. J., & Lu, N. (2002). Water vapor sorption behavior of smectite-kaolinite mixtures. *Clays and Clay Minerals*, 50(5), 553-561.

Likos, W. J., & Lu, N. (2004). Hysteresis of capillary stress in unsaturated granular soil. *Journal of Engineering Mechanics*, 130(6), 646-655.

Marinho, F. A. M. (1994, November). Suction measurement using filter paper method. In *Proceedings of the X Brazilian National Conference on Soil Mechanics and Geotechnical Engineering, Foz do Iguaç, Brazil* (pp. 5-7).

Martin, N. P. (1980). Harvesting and storage of quality hay. *In Proceedings of the Forage and Grassland Conference*.

McKeen, R. G. (1980, June). Field studies of airport pavements on expansive clay. In *Expansive Soils* (pp. 242-261). ASCE.

McQueen, I. S., & Miller, R. F. (1968). Determination of Soil Moisture Potential. *Water in the Unsaturated Zone*, (82), 147-155.

Miller, L. G., Clanton, D. C., Nelson, L. F., & Hoehne, O. E. (1967). Nutritive value of hay baled at various moisture contents. *Journal of Animal Science*, 26(6), 1369-1373.

Moody, D. R., Schlossberg, M. J., Archibald, D. D., McNitt, A. S., & Fidanza, M. A. (2009). Soil water repellency development in amended sand rootzones. *Crop Science*, 49(5), 1885-1892.

Moore, K.J., Peterson, M.A. (1995). Post-harvest physiology and preservation of forages. *American Society of Agronomy, Crop Science Society of America, Madison*, Wisconsin. CSSA Special Publication pp. 39-66.

Moser, L. E. (1980). Quality of forage as affected by post-harvest storage and processing. *Crop quality, storage, and utilization*, (cropqualitystor), 227-260.

Mualem, Y. (1976). A new model for predicting the hydraulic conductivity of unsaturated porous media. *Water Resources Research*, 12(3), 513-522.

Muck, R. E., & Shinners, K. J. (2001, February). Conserved forage (silage and hay): progress and priorities. In *International Grassland Congress* (Vol. 19, pp. 753-762). São Pedro: SBZ.

Nehrir, H., Kjelgaard, W. L., Anderson, P. M., Long, T. A., Hoffman, L. D., Washko, J. B., Wilson, L. L. & Mueller, J. P. (1978). Chemical additives and hay attributes. *Transactions of the ASAE*, 21(2), 217-0221.

Nelson, L. F. (1968). Spontaneous heating, gross energy retention and nutrient retention of high-density alfalfa hay bales. *Transactions of the ASAE*, 11(5), 595-0600.

Nelson, L. F. (1972). Storage characteristics and nutritive value of high-density native hay bales. *Transactions of the ASAE*, 15(2), 201-0205.

Ohm, A., Vogtländer, J. G., & Kossen, N. W. F. (1971). Heat-and Mass Transfer in Barn Hay-Drying Systems. *Journal of Agricultural Engineering Research*, 16(3), 254-268.

Parker, B. F., White, G. M., Lindley, M. R., Gates, R. S., Collins, M., Lowry, S., & Bridges, T. C. (1992). Forced-air drying of baled alfalfa hay. *Transactions of the ASAE*, 35(2), 607-615.

Perkins, K. S. (2011). *Measurement and modeling of unsaturated hydraulic conductivity* (pp. 419-434). INTECH Open Access Publisher.

Richards, L. A. (1931). Capillary conduction of liquids through porous mediums. *Journal of Applied Physic*s, 1(5), 318-333.

Ridley, A. M., & Burland, J. B. (1993). A new instrument for the measurement of soil moisture suction. *Géotechnique*, 43(2), 321-4.

Ridley, A. M., & Wray, W. K. (1996). Suction measurement: a review of current theory and practices. In *Proceedings of the First International Conference on Unsaturated Soils/Unsat'95, Paris, France 6-8 September 1995*. Volume 3.

Román, F. D., & Hensel, O. (2014). Numerical simulations and experimental measurements on the distribution of air and drying of round hay bales. *Biosystems Engineering*, 122, 1-15.

Ronayne, M. J., Houghton, T. B., & Stednick, J. D. (2012). Field characterization of hydraulic conductivity in a heterogeneous alpine glacial till. *Journal of Hydrology*, 458, 103-109.

Sanderson, M. A., Martin, N. P., & Adler, P. (2007). Biomass, energy, and industrial uses of forages. Forages. *The science of grassland agriculture*, 2, 635-647.

Schmer, M. R., Vogel, K. P., Mitchell, R. B., & Perrin, R. K. (2008). Net energy of cellulosic ethanol from switchgrass. *Proceedings of the National Academy of Sciences*, 105(2), 464-469.

Schmid, P., & Luthin, J. (1964). The drainage of sloping lands. *Journal of Geophysical Research*, 69(8), 1525-1529.

Soil Survey Technical Note. (2004). Saturated hydraulic conductivity: water movement concepts and class history. *National Leader for Soil Classification and Standards, National Soil Survey Center*, Lincoln, NE.

Tang, J., & Jofriet, J. C. (1991). Hydraulic conductivity of whole plant corn silage. *Canadian Agri. Eng*, 33(1), 161-167.

Van Driel, P. W., Robertson, W. D., & Merkley, L. C. (2006). Denitrification of agricultural drainage using wood-based reactors. *Transactions of the ASABE*, 49(2), 565-573.

Van Genuchten, M. T. (1980). A closed-form equation for predicting the hydraulic conductivity of unsaturated soils. *Soil Science Society of America Journal*, 44(5), 892-898.

Varvel, G. E., Vogel, K. P., Mitchell, R. B., Follett, R. F., & Kimble, J. M. (2008). Comparison of corn and switchgrass on marginal soils for bioenergy. *Biomass and bioenergy*, 32(1), 18-21.

Wallach, R., Da Silva, F. F., & Chen, Y. (1992). Unsaturated hydraulic characteristics of agricultural wastes, tuff, and their mixtures. *Soil Science*, 153(6), 434-441.

Wiselogel, A. E., Agblevor, F. A., Johnson, D. K., Deutch, S., Fennell, J. A., & Sanderson, M. A. (1996). Compositional changes during storage of large round switchgrass bales. *Bioresource technology*, 56(1), 103-109.

Yao, Z., & Jofriet, J. C. (1992). Hydraulic Conductivity of Alfalfa Silage. *Transactions of the ASAE*, 35(4), 1291-1296.

Zhao, Y., Wu, P., Zhao, S., & Feng, H. (2013). Variation of soil infiltrability across a 79-year chronosequence of naturally restored grassland on the Loess Plateau, China. *Journal of Hydrology*, 504, 94-103.

References (Section 3.2)

Birchak, J. R., Gardner, C. G., Hipp, J. E., & Victor, J. M. (1974). High dielectric constant microwave probes for sensing soil moisture. *Proceedings of the IEEE*, 62(1), 93-98.

Bockris, J. M., Devanathan, M. A. V., & Muller, K. (1963, June). On the structure of charged interfaces. In *Proceedings of the Royal Society of London A: Mathematical, Physical and Engineering Sciences* (Vol. 274, No. 1356, pp. 55-79). The Royal Society.

Cai, L., Chen, T. B., Gao, D., Liu, H. T., Chen, J., & Zheng, G. D. (2013). Time domain reflectometry measured moisture content of sewage sludge compost across temperatures. *Waste Management*, 33(1), 12-17.

Cai, L., Gao, D., Chen, T. B., Liu, H. T., Zheng, G. D., & Yang, Q. W. (2012). Moisture variation associated with water input and evaporation during sewage sludge bio-drying. *Bioresource Technology*, 117, 13-19.

Campbell, J. E. (1990). Dielectric properties and influence of conductivity in soils at one to fifty megahertz. *Soil Science Society of America Journal*, 54(2), 332-341.

Chan, C. Y., & Knight, R. J. (1999). Determining water content and saturation from dielectric measurements in layered materials. *Water Resources Research*, 35(1), 85-93.

Chen, J., Chen, T. B., Gao, D., Lei, M., Zheng, G. D., Liu, H. T. & Cai, L. (2011). Reducing H 2 S production by O 2 feedback control during large-scale sewage sludge composting. *Waste Management*, 31(1), 65-70.

Chico-Santamarta, L., Humphries, A. C., Chaney, K., White, D. R., Magan, N., & Godwin, R. J. (2011). Microbial changes during the on-farm storage of canola (oilseed rape) straw bales and pellets. *Biomass and Bioenergy*, 35(7), 2939-2949. Cormier et al. 2007

Hallikainen, M. T., Ulaby, F. T., Dobson, M. C., El-Rayes, M. A., & Wu, L. K. (1985). Microwave dielectric behavior of wet soil-part 1: empirical models and experimental observations. *Geoscience and Remote Sensing, IEEE Transactions*, (1), 25-34.

Ferre, P. A., Redman, J. D., Rudolph, D. L., & Kachanoski, R. G. (1998). The dependence of the electrical conductivity measured by time domain reflectometry on the water content of a sand. *Water Resources Research*, 34(5), 1207-1213.

Friedman, S. P., & Seaton, N. A. (1998). Critical path analysis of the relationship between permeability and electrical conductivity of three-dimensional pore networks. *Water Resources Research*, 34(7), 1703-1710.

Heimovaara, T. J. (1994). Frequency domain analysis of time domain reflectometry waveforms: 1. Measurement of the complex dielectric permittivity of soils. *Water Resources Research*, 30(2), 189-199.

Jones, S. B., Wraith, J. M., & Or, D. (2002). Time domain reflectometry measurement principles and applications. *Hydrological Processes*, 16(1), 141-153.

Jones, S. B., & Or, D. (2001, September). Frequency-domain methods for extending TDR measurement range in saline soils. In *Proceedings of the Second International Symposium and Workshops on Time Domain Reflectometry for Innovative Geotechnical Applications, Northwestern University, Evanston, Illinois* (pp. 5-7).

Jones, S. B., & Or, D. (2003). Modeled effects on permittivity measurements of water content in high surface area porous media. *Physica B: Condensed Matter*, 338(1), 284-290.

Martinson, K., Coblentz, W., & Sheaffer, C. (2011). The effect of harvest moisture and bale wrapping on forage quality, temperature, and mold in orchardgrass hay. *Journal of Equine Veterinary Science*, 31(12), 711-716.

McIsaac, G. (2010). Time domain reflectometry measurement of water content and electrical conductivity using a polyolefin coated TDR probe.

Mojid, M. A., Wyseure, G. C., & Rose, D. A. (1998). The use of insulated time-domain reflectometry sensors to measure water content in highly saline soils. *Irrigation Science*, 18(2), 55-61.

Moret-Fernández, D., Lera, F., Arrúe, J. L., & López, M. V. (2009). Measurement of soil bulk electrical conductivity using partially coated TDR probes. *Vadose Zone Journal*, 8(3), 594-600.

Noborio, K. (2001). Measurement of soil water content and electrical conductivity by time domain reflectometry: a review. *Computers and Electronics in Agriculture*, 31(3), 213-237.

Opoku, A., Tabil, L. G., Crerar, B., & Shaw, M. D. (2004). Thermal properties of timothy hay. In *2004 ASAE Annual Meeting* (p. 1). American Society of Agricultural and Biological Engineers.

Opoku, A., Tabil, L. G., Crerar, B., & Shaw, M. D. (2006). Thermal conductivity and thermal diffusivity of timothy hay. *Canadian Biosystems Engineering*, 48, 3.

Or, D., & Wraith, J. M. (1999). Temperature effects on soil bulk dielectric permittivity measured by time domain reflectometry: A physical model. *Water Resources Research*, 35(2), 371-383.

Pepin, S., Livingston, N. J., & Hook, W. R. (1995). Temperature-dependent measurement errors in time domain reflectometry determinations of soil water. *Soil Science Society of America Journal*, 59(1), 38-43.

Persson, M., & Berndtsson, R. (1998). Texture and electrical conductivity effects on temperature dependency in time domain reflectometry. Soil Science Society of America Journal, 62(4), 887-893.Plaut, 2013

Persson, M., Berndtsson, R., Nasri, S., Albergel, J., Zante, P., & Yumegaki, Y. (2000). Solute transport and water content measurements in clay soils using time domain reflectometry. *Hydrological Sciences Journal*, 45(6), 833-847.

Robinson, D. A., Schaap, M., Jones, S. B., Friedman, S. P., & Gardner, C. M. K. (2003). Considerations for improving the accuracy of permittivity measurement using TDR: Air/water calibration, effects of cable length. *Soil Sci. Soc. Am. J.*, (67), 62.

Roth, K., Flühler, H., & Attinger, W. (1990). Transport of a conservative tracer under field conditions: Qualitative modelling with random walk in a double porous medium. In *Field-Scale Water and Solute flux in Soils* (pp. 239-249). Birkhäuser Basel.

Sanderson, M. A., Egg, R. P., & Wiselogel, A. E. (1997). Biomass losses during harvest and storage of switchgrass. *Biomass and Bioenergy*, 12(2), 107-114.

Savoie, P., Cormier, E., & Morissette, R. (2011). Continuous monitoring of moisture content in compacted hay during drying. *Applied Engineering in Agriculture*, 27(1), 127-132.

Schwartz, R., Evett, S., & Bell, J. (2009). A Complex Permittivity Model for Field Estimation of Soil Water Contents Using Time Domain Reflectometry. In *ASA-CSSA-SSSA Annual Meeting Abstracts*.

Shinners, K. J., Boettcher, G. C., Muck, R. E., Weimer, P. J., & Casler, M. D. (2010). Harvest and storage of two perennial grasses as biomass feedstocks. *Transactions of the ASABE*, 53(2), 359-370.

Spaans, E. J., & Baker, J. M. (1993). Simple baluns in parallel probes for time domain reflectometry. *Soil Science Society of America Journal*, 57(3), 668-673.

Starr, G. C., Lowery, B., Cooley, E. T., & Hart, G. L. (1999). Development of a resonant length technique for soil water content measurement. *Soil Science Society of America Journal*, 63(2), 278-285.

Sun, Z. J., & Young, G. D. (2001, September). A cost effective soil moisture instrument based on time-domain transmission measurement. In *Int. Symp. and Worksh. on Time Domain Reflectometry for Innovative Geotechnical Applications, 2nd, Evanston, IL* (pp. 5-7).

Shewmaker, G. E., & Thaemert, R. (2004, December). Measuring moisture in hay. In *Proc. National Alfalfa Symposium* (pp. 13-15).

Thorp, J. M. (1959). The dielectric behaviour of vapours adsorbed on porous solids. *Transactions of the Faraday Society*, 55, 442-454.

Topp, G. C., Davis, J. L., & Annan, A. P. (1980). Electromagnetic determination of soil water content: measurements in coaxial transmission lines. *Water Resources Research*, 16(3), 574-582.

White, I., & Zegelin, S. J. (1995). Electric and dielectric methods for monitoring soil-water content. *Handbook of Vadose Zone Characterization and Monitoring*, 343-385.

Wiselogel, A. E., Agblevor, F. A., Johnson, D. K., Deutch, S., Fennell, J. A., & Sanderson, M. A. (1996). Compositional changes during storage of large round switchgrass bales. Bioresource technology, 56(1), 103-109.

Wraith, J. M., & Or, D. (1999). Temperature effects on soil bulk dielectric permittivity measured by time domain reflectometry: Experimental evidence and hypothesis development. *Water Resources Research*, 35(2), 361-369.

Yue, B., Chen, T. B., Gao, D., Zheng, G. D., Liu, B., & Lee, D. J. (2008). Pile settlement and volume reduction measurement during forced-aeration static composting. *Bioresource Technology*, 99(16), 7450-7457.

Zahiroddini, H., Baah, J., Absalom, W., & McAllister, T. A. (2004). Effect of an inoculant and hydrolytic enzymes on fermentation and nutritive value of whole crop barley silage. *Animal Feed Science and Technology*, 117(3), 317-330.

References (Section 3.3)

Alagusundaram, K., Jayas, D. S., Muir, W. E., & White, N. D. G. (1991). Thermal conductivity of bulk barley, lentils, and peas. *Transactions of the ASAE*, 34(4), 1784-1788.

Alam, A., & Shove, G. C. (1973). Hygroscopicity and thermal properties of soybeans. *Transactions of the ASAE*, 16(4), 707-0709.

Andersland, O., & Anderson, D. (1978). *Geotechnical engineering for cold regions*.

Andersland, O. B., & Ladanyi, B. (1994). Physical and thermal properties. In *An Introduction to Frozen Ground Engineering* (pp. 23-63). Springer US.

Anderson, S. A. (1950). Automatic Refrigeration. MacLaren and Son Ltd. For Donfoss. Norborg, Denmark.

Asher, G. B., Sloan, E. D., & Graboski, M. S. (1986). A computer-controlled transient needle-probe thermal conductivity instrument for liquids. *International Journal of Thermophysics*, 7(2), 285-294.

ASHRAE. (1989). Thermal Properties of Foods. ASHRAE Handbook. Atlanta, Ga.

Babbitt, J. D. (1945). The thermal properties of wheat in bulk. *Canadian Journal of Research*, 23(6), 388-401.

Baik, O. D., & Mittal, G. S. (2003). Determination and modeling of thermal properties of tofu. *International Journal of Food Properties*, 6(1), 9-24.

Bakke, A. L., & Stiles, H. (1935). Thermal conductivity of stored oats with different moisture content. *Plant Physiology*, 10(3), 521.Becker et al., 1992

Bern, C. J. (1964). The specific heat of alfalfa. *M.Sc Thesis. University of Nebraska, Lincoln, Nebraska*.

Bilanski, W. K., & Fisher, D. R. (1976). Thermal conductivity of rapeseed. *Transactions of the ASAE*, 19(4), 788-0791.

Bush, R. A., Black, W. Z., & Martin Jr, M. A. (1979, April). Soil thermal properties and their effect on thermal stability and the rating of underground power cables. In *Transmission and Distribution Conference and Exposition, 1979. 7 IEEE/PES* (pp. 275-280). IEEE.

Blackwell, J. H. (1956). The axial-flow error in the thermal-conductivity probe. *Canadian Journal of Physics*, 34(4), 412-417.

Bristow, K. L., Campbell, G. S., & Calissendorff, K. (1993). Test of a heat-pulse probe for measuring changes in soil water content. *Soil Science Society of America Journal*, 57(4), 930-934.

Bristow, K. L., Kluitenberg, G. J., & Horton, R. (1994). Measurement of soil thermal properties with a dual-probe heat-pulse technique. *Soil Science Society of America Journal*, 58(5), 1288-1294.

Samfield, M., & Brock, B. A. (1958). The bulk thermal conductivity of tobacco. *Tobacco Science*, 2, 49-50.

Brooker, D. B., Bakker-Arkema, F. W., & Hall, C. W. (1992). Drying and storage of grains and oilseeds. *Springer Science & Business Media*.

Butts, C. L., Mishoe, J. W., & Chau, K. V. (1990). Measuring thermal diffusivity of soil. *Transactions of the ASAE*, 33(1), 179-0184.

Campbell, G. S., Calissendorff, C., & Williams, J. H. (1991). Probe for measuring soil specific heat using a heat-pulse method. *Soil Science Society of America Journal*, 55(1), 291-293.

Carslaw, H. S., & Jaeger, J. C. (1959). Conduction of heat in solids. *Oxford: Clarendon Press, 1959*, 2nd ed.

Casada, M. E., & Walton, L. R. (1989a). New model for determining thermal diffusivity with the thermal probe. *Transactions of the ASAE*, 32(3), 973-0976.

Casada, M. E., & Walton, L. R. (1989b). Thermal conductivity of baled burley tobacco. *Transactions of the ASAE*, 32(3), 977-0982.

Chandra, S., & Muir, W. E. (1971). Thermal conductivity of spring wheat at low temperatures. *Transactions of the ASAE*, 14(4), 644-0646.

Chang, C. S. (1986). Thermal conductivity of wheat, corn, and grain sorghum as affected by bulk density and moisture content. *Transactions of the ASAE*, 29(5), 1447-1450.

Chang, C. S., Lai, F. S., & Miller, B. S. (1980). Thermal conductivity and specific heat of grain dust. *Transactions of the ASAE*, 23(5), 1303-1306.

Childs, D. P., Fletcher, L. W., Beard, J. T., & Iachetta, F. A. (1983). Cooling tobacco in warehouses during the winter to kill cigarette beetles, Part I: Relevant physical properties of stored tobacco. *Tobacco Science*, 27, 116-124.

Choi, Y., & Okos, M. R. (1983). The thermal properties of tomato juice concentrates. *Transactions of the ASAE*, 26(1), 305-0311.

Choi, Y., & Okos, M. R. (1986). Thermal properties of liquid foods: review.

Costa, V. A. F. (2006). Thermodynamic analysis of building heating or cooling using the soil as heat reservoir. *International Journal of Heat and Mass Transfer*, 49(21), 4152-4160.

De Vries, D. A. (1963). Thermal properties of soils. *Physics of plant environment*.

De Vries, D. A., & Afgan, N. H. (1975). Heat and mass transfer in the biosphere. 1. Transfer processes in the plant environment. *Scripta Book Co*.

De Vries, D. A., & Peck, A. J. (1958). On the cylindrical probe method of measuring thermal conductivity with special reference to soils. I. Extension of theory and discussion of probe characteristics. *Australian Journal of Physics*, 11(2), 255-271.

Dickerson, R. W. (1965). An apparatus for the measurement of thermal diffusivity of foods. *Food Technology*, 19(5), 198-204.

Disney, R. W. (1954). The specific heat of some cereal grains. *Cereal Chemistry*, 31(3), 229-239.

Drouzas, A. E., & Saravacos, G. D. (1988). Effective thermal conductivity of granular starch materials. *Journal of Food Science*, 53(6), 1795-1799.

Dua, K., & Ojha, T. P. (1969). Measurement of thermal conductivity of paddy grains and its by-products. *Journal of Agricultural Engineering Research*, 14(1), 11-17.

Duncan, G. A., Bunn, J. M., & Henson, W. H. (1966). Thermal conductivity of burley tobacco during the cure. *Transactions of the ASAE*, 9(1), 36-0038.

Dutta, S. K., Nema, V. K., & Bhardwaj, R. K. (1988). Thermal properties of gram. *Journal of Agricultural Engineering Research*, 39(4), 269-275.

Emami, S., Tabil, L. G., & Tyler, R. T. (2007). Technical Note: Thermal Properties of Chickpea Flour, Isolated Chickpea Starch, and Isolated Chickpea Protein. *Transactions of the ASABE*, 50(2), 597-604.

Farouki, O. T. (1981). Thermal properties of soils (No. CRREL-MONO-81-1). *Cold Regions Research and Engineering Lab*, Hanover, NH.

Fontana, A. J., Wacker, B., Campbell, C. S., & Campbell, G. S. (1998). Simultaneous thermal conductivity, thermal resistivity, and thermal diffusivity measurement of selected foods and soil. In *2001 ASAE Annual Meeting* (p. 1). American Society of Agricultural and Biological Engineers.

Ford, R. M., & Bilanski, W. K. (1969). Thermal diffusivity of alfalfa stems. *Transactions of the ASAE*, 12(2), 249-0251.

Goodrich, L. E. (1986). Field measurements of soil thermal conductivity. *Canadian Geotechnical Journal*, 23(1), 51-59.

Hanson, J. L., Edil, T. B., & Yesiller, N. (2000). Thermal properties of high water content materials. In *Geotechnics of High Water Content Materials*. ASTM International.

Haswell, G. A. (1954). A note on the specific heat of rice, oats, and their products. *Cereal chemistry*, 31(4), 341-342.

Hearmon, R. F. S. (1957). Some applications of physics to wood. *British journal of applied physics*, 8(2), 49.

Hearmon, R. F. S., & Burcham, J. N. (1955). Specific heat and heat of wetting of wood.

Henry, P. S. H. (1939). Diffusion in absorbing media. In *Proceedings of the Royal Society of London A: Mathematical, Physical and Engineering Sciences* (Vol. 171, No. 945, pp. 215-241). The Royal Society.

Hiraiwa, Y., & Kasubuchi, T. (2000). Temperature dependence of thermal conductivity of soil over a wide range of temperature (5–75 C). *European Journal of Soil Science*, 51(2), 211-218.

Hooper, F. C., & Lepper, F. R. (1950). Transient heat flow apparatus for the determination of thermal conductivities. *National Emergency Training Center*.

Hwang, M. P., & Hayakawa, K. I. (1979). A specific heat calorimeter for foods. *Journal of Food Science*, 44(2), 435-448.

Ingersioll, L., Zobel, O. J., & Ingersoll, A. C. (1954). Heat Conduction: With Engineering Geological And Other Applications.

Iroba, K. L., Tabil, L. G., Venkatesh, M., & Oon-Doo, B. (2013). Thermal properties of lignocellulosic biomass barley straw. In *2013 Kansas City, Missouri, July 21-July 24, 2013* (p. 1). American Society of Agricultural and Biological Engineers.

Iroba, K. L., & Tabil, L. G. (2013). Lignocellulosic Biomass: Feedstock Characteristics, Pretreatment Methods and Pre-Processing for Biofuel and Bioproduct Applications, US and Canadian Perspective. *Biomass Processing, Conversion and Biorefinery, New York: Nova Science Publishers, Inc.*, 61-98.

Iwabuchi, K., Kimura, T., & Otten, L. (1999). Effect of volumetric water content on thermal properties of dairy cattle feces mixed with sawdust. *Bioresource Technology*, 70(3), 293-297.

Izadifar, M., & Baik, O. D. (2007). Determination of thermal properties of the rhizome of Podophyllum peltatum for drying and ethanol extraction. *Biosystems engineering*, 97(3), 357-370.

Jackson, R. D., & Taylor, S. A. (1986). Thermal conductivity and diffusivity. Methods of Soil Analysis: Part 1—Physical and Mineralogical Methods, (methodsofsoilan1), 945-956.

Jasansky, A., & Bilanski, W. K. (1973). Thermal conductivity of whole and ground soybeans. *Transactions of the ASAE*, 16(1), 100-0103.

Jiang, S., Jofriet, J. C., & Mittal, G. S. (1986). Thermal properties of haylage. *Transactions of the ASAE*, 29(2), 601-0606.

Kazarian, E. A., & Hall, C. W. (1965). Thermal properties of grain. *Transactions of the ASAE*, 8(1), 33-0037.

Kluitenberg, G. J., Ham, J. M., & Bristow, K. L. (1993). Error analysis of the heat pulse method for measuring soil volumetric heat capacity. *Soil Science Society of America Journal*, 57(6), 1444-1451.

Kluitenberg, G. J., Das, B. S., & Bristow, K. L. (1995). Error analysis of heat pulse method for measuring soil heat capacity, diffusivity, and conductivity. *Soil Science Society of America Journal*, 59(3), 719-726.

Kobari, M., Shimizu, Y., Endo, M., & Inazumi, H. (1985). Contact drying of fibrous sheet material. *Industrial & Engineering Chemistry Process Design and Development*, 24(1), 188-194.

Larson, T. H. (1988). Thermal measurement of soils using a multineedle probe with a pulsed-point source. *Geophysics*, 53(2), 266-270.

Lawrence, A. S., & William, D. K. (1983). The use of property tests to determine the thermal properties of soils.

Lobo, H. and C. Cohen. (1990). Measurement of thermal conductivity of polymer melts by the line-source method. *Polymer Engineering and Science*, 30(2): 65-70.

Locklair, E. E., Galloway, W. D., & Samfield, M. (1957). The thermal diffusivity of tobacco. *Tobacco Science*, 1, 28-32.

MacLean, J. D. (1941). Thermal conductivity of wood. *Heating, piping, and air Conditioning*, 101(6).

Marousis, S. N., Karathanos, V. T., & Saravacos, G. D. (1991). Effect of physical structure of starch materials on water diffusivity. *Journal of Food Processing and Preservation*, 15(3), 183-195.

Martens, T. (1980). Mathematical model of heat processing in flat containers. *Ph.D. Thesis*. Katholeike University., Leuven, Belgium.

Mitchell, J. K., & Kao, T. C. (1978). Measurement of soil thermal resistivity. *Journal of Geotechnical and Geoenvironmental Engineering*, 104(ASCE 14080 Proc Paper).

Mohsenin, N. N. (1980). Thermal properties of foods and agricultural materials. New York. USA.

Moore, G. A., & Bilanski, W. K. (1992). Thermal properties of high moisture content alfalfa. *Applied Engineering in Agriculture*, 8(1), 61-64.

Moote, I. (1953). The effect of moisture on the thermal properties of wheat. *Canadian Journal of Technology*, 31(2/3), 57.

Moysey, E. B., Shaw, J. T., & Lampman, W. P. (1977). The effect of temperature and moisture on the thermal properties of rapeseed. *Transactions of the ASAE*, 20(3), 461-0464.

Muck, R., R. Leibensperger, H. & Pitt, R. W. (1983). Mathematical simulation of silage fermentation. *ASAE Paper No. 83-1530, St. Joseph, MI 49085-9659 Nevada*.

Murakami, E. G., & Okos, M. R. (1986). *Predicting the thermal conductivity of dry porous foods* (No. 86-6538). ASAE Paper.

Nix, G. H., Lowery, G. W., Vachon, R. I., & Tanger, G. E. (1967). Direct determination of thermal diffusivity and conductivity with a refined line-source technique. Progress in aeronautics and astronautics: *Thermophysics of spacecraft and planetary bodies*, 20, 865-878.

Nix, G. H., Vachon, R. I., Lowery, G. W., & McCurry, T. A. (1969). The line source method: procedure and iteration scheme for combined determination of conductivity and diffusivity. In Proceedings of 8th Conference on Thermal Conductivity, Plenum Press, NY.

Nusier, O., & Abu-Hamdeh, N. (2003). Laboratory techniques to evaluate thermal conductivity for some soils. *Heat and Mass Transfer*, 39(2), 119-123.

Ojha, T. P., Farrall, A. W., Dhanak, A. M., & Stine, C. M. (1967). A method of determining heat transfer through powdered food products. *Transactions of the ASAE*, 10(4), 543-0545.

Opoku, A., Tabil, L. G., Crerar, B., & Shaw, M. D. (2004). Thermal properties of timothy hay. In *2004 ASAE Annual Meeting* (p. 1). American Society of Agricultural and Biological Engineers.

Opoku, A., Tabil, L. G., Crerar, B., & Shaw, M. D. (2006). Thermal conductivity and thermal diffusivity of timothy hay. *Canadian Biosystems Engineering*, 48, 3.

Ott, L. E. (1964). *Thermal diffusivity of compressed alfalfa hay* (Doctoral dissertation, University of Nebraska (Lincoln campus)--1964.). Oxley (1944

Rodriguez, R. P., M. E. Rodrigo and P. Kelly. (1995). A calorimetric method to determine specific heats of prepared foods. *Journal of Food Engineering*, 26(1): 81-96.

Pfalzner, P. M. (1951). The specific heat of wheat. *Canadian Journal of Technology*, 29(6), 261-268.

Philip, J. R., & De Vries, D. A. (1957). Moisture movement in porous materials under temperature gradients. Eos, *Transactions American Geophysical Union*, 38(2), 222-232.

Ramaswamy, H. S., & Tung, M. A. (1981). Thermophysical properties of apples in relation to freezing. *Journal of Food Science*, 46(3), 724-728. Reece, 1996

Abu-Hamdeh, N. H., & Reeder, R. C. (2000). Soil thermal conductivity effects of density, moisture, salt concentration, and organic matter. *Soil science society of America Journal*, 64(4), 1285-1290.

Reid, D. (2005). Guarded hot plate apparatus design and construction for thermal conductivity measurements. *Master's, Ryerson University, Toronto*.

Reidy, G. A., & Rippen, A. L. (1971). Methods for determining thermal conductivity in foods. *Transactions of the ASAE*, 14(2), 248-0254.

Rice, P., Selman, J. D., & ABDUL-REZZAK, R. K. (1988). Effect of temperature on thermal properties of 'Record' potatoes. *International Journal of Food Science & Technology*, 23(3), 281-286.

Rowley, F. B. (1933). The heat conductivity of wood at climatic temperature differences. *Heating, Piping, and Air Conditioning*, 5, 313-323.

Salmon, D. (2001). Thermal conductivity of insulations using guarded hot plates, including recent developments and sources of reference materials. *Measurement Science and Technology*, 12(12), R89.

Salomone, L. A., Kovacs, W. D., & Kusuda, T. (1984). Thermal performance of fine-grained soils. *Journal of Geotechnical Engineering*, 110(3), 359-374.

Samfield, M., & Brock, B. A. (1958). The bulk thermal conductivity of tobacco. *Tobacco Science*, 2, 49-50.

Scermely, J. (1975). Heat-technical examination of green fodder storing towers. *Farm Mach. Res. Inst., Hungary*, 42.

Sepaskhah, A. R., & Boersma, L. (1979). Thermal conductivity of soils as a function of temperature and water content. *Soil Science Society of America Journal*, 43(3), 439-444.

Sharma, D. K., & Thompson, T. L. (1973). Specific heat and thermal conductivity of sorghum. *Transactions of the ASAE*, 16(1), 114-0117.

Singh, R. P., & Heldman, D. R. (2009). Introduction to food engineering. (No. TP370. S4518 2009).

Skaggs, R. W., & Smith, E. M. (1968). Apparent thermal conductivity of soil as related to soil porosity. *Transactions of the ASAE*, 11(4), 504-0507.

Slusarchuk, W. A., & Foulger, P. H. (1973). Development and calibration of a thermal conductivity probe apparatus for use in the field and laboratory.

Spells, K. E. (1960). The thermal conductivities of some biological fluids. *Physics in Medicine and Biology*, 5(2), 139.

Spells, K. E. (1960). The thermal conductivities of some biological fluids. *Physics in Medicine and Biology*, 5(2), 139.

Steinmanis, J. E. (1982). Thermal property measurements using a thermal probe. *Underground cable thermal backfill*, 72-85.

Sturtevant, J. M. (1949). Calorimetry. In *Weissberger, A., Technique of Organic Chemistry, 2(1) 731, Interscience Publishers Inc., New York.*

Suter, D. A., Agrawal, K. K., & Clary, B. L. (1975). Thermal properties of peanut pods, hulls and kernels. *Transactions of the ASAE*, 18(2), 370-0375.

Sweat, V. (1976). A miniature thermal conductivity probe for foods. *ASME paper*, (76-HT), 60.

Sweat, V. E., & Haugh, C. G. (1974). A thermal conductivity probe for small food samples. *Transactions of the ASAE*, 17(1), 56-0058.

Sykes, L. M., & Johnson, W. H. (1973). Bulk thermal conductivity of cured bright tobacco shreds during freeze drying. *Tobacco* New York.

Tabil, L. G., Eliason, M. V., & Qi, H. (2003). Thermal properties of sugarbeet roots. *Journal of sugar beet research*, 40(4), 209-228.

Tang, J., Sokhansanj, S., Yannacopoulos, S., & Kasap, S. O. (1991). Specific heat capacity of lentil seeds by differential scanning calorimetry. *Transactions of the ASAE*, 34(2), 517-0522.

Timbers, G. E. (1975). Thermal diffusivity and specific heat of rapeseed. *Can. Agric. Eng*, 17, 81-84.

Tollner, E. W., & Verma, B. P. (1984). Modified cone penetrometer for measuring soil mechanical impedance. *Transactions of the ASAE*, 27(2), 331-0336.

Tollner, E. W., & Verma, B. P. (1987). Apparent thermal conductivity of organic potting mixes. *Transactions of the ASAE*, 30(2), 509-0513.

Wallapapan, K., & Sweat, V. E. (1982). Thermal conductivity of defatted soy flour. *Transactions of the ASAE*, 25(5), 1440-1444.

Wang, J., & Hayakawa, K. I. (1993). Maximum slope method for evaluating thermal conductivity probe data. *Journal of Food Science*, 58(6), 1340-1345.

Wangaard, F. F. (1940). Transverse heat conductivity of wood. *Heating, Piping, & Air Conditioning, (July)*, 459-64.

Ward, R. J. (1960). A dynamic method for determining specific heat and thermal conductivity of wood base materials as a function of temperature.

Ward, R., & Skaar, C. (1963). Specific heat and conductivity of particleboard as a function of temperature. *For. Prod. J*, 13(1), 32.

Weld, L. D. (1948). *A Textbook of Heat: For Upperclassmen*. Macmillan.

White, W. P. (1928). The modern calorimetry.

Woodside, W. (1958). Probe for thermal conductivity measurement of dry and moist materials. *Heating, Piping, Air Conditioning*, 30, 1-10.

Woodside, W. (1959). Probe for thermal conductivity measurement of dry and moist materials. Transactions of the ASHVE, 65: 291-310.

Yang, W., Sokhansanj, S., Tang, J., & Winter, P. (2002). Determination of thermal conductivity, specific heat and thermal diffusivity of borage seeds. *Biosystems Engineering*, 82, 169-176.

Yang, W., Sokhansanj, S., Tabil, L., Tang, J., & Yannacopoulos, S. (1997). Measurement of heat capacity for borage seeds by differential scanning calorimetry. *Journal of Food Processing and Preservation*, 21(5), 395-407.

References (Section 3.4)

Abbouda, S. K., Chung, D. S., Seib, P. A., & Song, A. (1992). Heat and Mass Transfer in Stored Milo. Part I. Heat Transfer Model. Transactions of the ASAE, 35(5), 1569-1573.

Acharya, S., & Goldstein, R. J. (1985). Natural convection in an externally heated vertical or inclined square box containing internal energy sources. Journal of heat transfer, 107(4), 855-866.

Adney, W. S., Taylor, L. E., Johnson, D., Park, S., Knoshaug, E. P., Nimlos, M. R. & Himmel, M. E. (2008). Deconstruction of Biomass: Understanding Enzyme/Substrate Interactions. National Renewable Energy Laboratory (NREL), Golden, CO.

Agamuthu, P., Choong, L. C., Hasan, S., & Praven, V. V. (2000). Kinetic evaluation of composting of agricultural wastes. Environmental Technology, 21(2), 185-192.

Agena, M. (1968). Harvesting, storing and feeding of hay. *LandTecknik*, 23(22), 762.

Alagusundaram, K., Jayas, D. S., White, N. D. G., & Muir, W. E. (1990). Three-dimensional, finite element, heat transfer model of temperature distribution in grain storage bins. *Transactions of the ASAE,* 33(2), 577-0584.

Alam, P., Ansari, S. R., & Kumar, R. (2011). Numerical study on natural convection in a porous cavity due to partial heating and cooling at vertical walls. Int. J. of Appl. Math and Mech, 7(18), 1-21.

Alchaar, S., Vasseur, P., & Bilgen, E. (1995). Natural convection heat transfer in a rectangular enclosure with a transverse magnetic field. Journal of Heat Transfer, 117(3), 668-673.

Amanlou, Y., & Zomorodian, A. (2010). Applying CFD for designing a new fruit cabinet dryer. Journal of food engineering, 101(1), 8-15.

Andrade, E. T., Couto, S. M., Queiroz, D. M., Faroni, L. R., & de Sousa Damasceno, G. (2002). Three-dimensional simulation of the temperature variation in corn stored in metallic bin. In *2002 ASAE Annual Meeting* (p. 1). American Society of Agricultural and Biological Engineers.

Arinze, E. A., Sakhansanj, S., Schoenau, G. J., & Trauttmansdorff, F. G. (1994). Design, evaluation and optimization of a heated-air batch hay dryer operated with automatic bale wagon. In *American Society of Agricultural Engineers. Meeting (USA).*

ASABE Standards. (2005). D535: Shelled corn storage time for 0.5% dry matter loss. St. Joseph, Mich.: ASABE.

ASABE. (2008). Moisture relationships of plant-based agricultural products. ASABE Standards, D245.5. In ASABE Standards 2008, 55th edition: 1-35. St. Joseph, MI: ASABE.

Avramidis, S., & Siau, J. F. (1987). Experiments in nonisothermal diffusion of moisture in wood. *Wood science and technology*, *21*(4), 329-334.

Avramidis, S., Englezos, P., & Papathanasiou, T. (1992). Dynamic nonisothermal transport in hygroscopic porous media: moisture diffusion in wood. *AIChE journal*, *38*(8), 1279-1287.

Aydin, O., & Yang, W. J. (2000). Natural convection in enclosures with localized heating from below and symmetrical cooling from sides. *International Journal of Numerical Methods for Heat & Fluid Flow*, *10*(5), 518-529.

Bae, S. H., Nam, J. H., Song, C. S., & Kim, C. J. (2010). A numerical model for freeze drying processes with infrared radiation heating. *Numerical Heat Transfer, Part A: Applications*, *58*(5), 333-355.

Bagnall, L. O., Millier, W. F., & Scott, N. R. (1970). Drying the alfalfa stem. *Transactions of the ASAE*, *13*(2), 232-0236.

Bakker-Arkema, F. W. (1974). Grain dryer simulation.

Bakker-Arkema, F. W., Haight, J., Roth, M. G., & Brooker, D. B. (1976). Required weather data for simulation of solar grain drying. *Am. Soc. agric. Engrs, Paper*, (76-3020).

Bari, Q. H., Koenig, A., & Guihe, T. (2000). Kinetic analysis of forced aeration composting–I. Reaction rates and temperature. *Waste Management and Research*, *18*(4), 303-312.

Barletta, A., Lazzari, S., Magyari, E., & Pop, I. (2008). Mixed convection with heating effects in a vertical porous annulus with a radially varying magnetic field. *International Journal of Heat and Mass Transfer*, *51*(25), 5777-5784.

Bartzanas, T., Bochtis, D. D., Sørensen, C. G., Sapounas, A. A., & Green, O. (2010). A numerical modelling approach for biomass field drying. *Biosystems Engineering*, *106*(4), 458-469.

Basak, T., Kaluri, R. S., & Balakrishnan, A. R. (2011). Effects of thermal boundary conditions on entropy generation during natural convection. *Numerical Heat Transfer, Part A: Applications*, *59*(5), 372-402.

Bathe, K. J. (1982). Finite element procedures in engineering analysis (Book). *Englewood Cliffs, NJ, Prentice-Hall, Inc., 1982. 746 p*.

Beavers, G. S., & Joseph, D. D. (1967). Boundary conditions at a naturally permeable wall. *Journal of fluid mechanics*, *30*(01), 197-207.

Beckermann, C., & Viskanta, R. (1988). Natural convection solid/liquid phase change in porous media. *International journal of heat and mass transfer*, *31*(1), 35-46.

Beckermann, C., Viskanta, R., & Ramadhyani, S. (1986). A numerical study of non-Darcian natural convection in a vertical enclosure filled with a porous medium. *Numerical Heat Transfer*, *10*(6), 557-570.

Bedane, A. H., Afzal, M. T., & Sokhansanj, S. (2011). Simulation of temperature and moisture changes during storage of woody biomass owing to weather variability. *Biomass and Bioenergy*, *35*(7), 3147-3151.

Bejan, A. (2004). Designed porous media: maximal heat transfer density at decreasing length scales. *International Journal of Heat and Mass Transfer*, *47*(14), 3073-3083.

Bejan, A. (1984). Principles of Convection through Porous Media. *Convection Heat Transfer*, *10*, 343-387.

Beliaev, A. Y., & Hassanizadeh, S. M. (2001). A theoretical model of hysteresis and dynamic effects in the capillary relation for two-phase flow in porous media. *Transport in Porous media*, *43*(3), 487-510.

Bellon-Maurel, V., Orliac, O., & Christen, P. (2003). Sensors and measurements in solid state fermentation: a review. *Process Biochemistry*, *38*(6), 881-896.

Bender, E. A. (1978). *An Introduction to Mathematical Modelling*. Wiley.

Bennethum, L. S., & Cushman, J. H. (1999). Coupled solvent and heat transport of a mixture of swelling porous particles and fluids: single time-scale problem. *Transport in Porous Media*, *36*(2), 211-244.

Berger, D., & Pei, D. C. T. (1973). Drying of hygroscopic capillary porous solids—a theoretical approach. *International Journal of Heat and Mass Transfer*, *16*(2), 293-302.

Bergholz, R. F. (1980). Natural convection of a heat generating fluid in a closed cavity. *Journal of Heat Transfer*, *102*(2), 242-247.

Beukema, K. J., Bruin, S., & Schenk, J. (1983). Three-dimensional natural convection in a confined porous medium with internal heat generation. *International Journal of Heat and Mass Transfer*, *26*(3), 451-458.

Bhat, C. (2006). Early detection of grain spoilage and prediction of movement of low levels of CO_2 in a storage tank. *MS thesis*. West Lafayette, Ind.: Purdue University.

Bongochgetsakul, N., & Ishida, T. (2008). A new analytical approach to optimizing the design of large-scale composting systems. *Bioresource technology*, *99*(6), 1630-1641.

Borreani, G., & Tabacco, E. (1998). Effects of crop properties, weather conditions and mechanical treatments on the wilting rate of diploid and tetraploid Italian ryegrass for silage. *Grass and forage science*, *53*(2), 179-188.

Boyce, D. S., & Davies, J. K. (1965). Air distribution from a lateral duct with different escape areas in barley. *Journal of Agricultural Engineering Research*, *10*(3), 230-234.

Brinkman, H. C. (1947). A calculation of the viscosity and the sedimentation constant for solutions of large chain molecules taking into account the hampered flow of the solvent through these molecules. *Physica*, *13*(8), 447-448.

Brooker, D. B., Bakker-Arkema, F. W., & Hall, C. W. (1974). *Drying cereal grains* (No. SB189. B76 1974.). AVI Publishing Company.

Brooker, D. B., Bakker-Arkema, F. W., & Hall, C. W. (1992). *Drying and storage of grains and oilseeds*. Springer Science & Business Media.

Brunauer, S., Emmett, P. H., & Teller, E. (1938). Adsorption of gases in multimolecular layers. *Journal of the American chemical society*, *60*(2), 309-319.

Brunauer, S., Deming, L. S., & DEMING TELLER, W. S. (1940). Types of adsorption isotherms. *J. Am. Chem. Soc*, *62*, 1723.

Bubnovich, V., Quijada, E., & Reyes, A. (2009). Computer simulation of atmospheric freeze drying of carrot slices in a fluidized bed. *Numerical Heat Transfer, Part A: Applications*, *56*(2), 170-191.

Bubnovich, V., Villarreal, C., & Reyes, A. (2008). Computer simulation of the drying of seeds and vegetables in a discontinuous fluidized bed. *Numerical Heat Transfer, Part A: Applications*, *54*(3), 255-278.

Buckingham, E. (1907). Studies on the movement of soil moisture: II The capillary potential.

Ceaglske, N. H., & Hougen, O. A. (1937). Drying granular solids. *Industrial & Engineering Chemistry*, *29*(7), 805-813.

Calcagni, B., Marsili, F., & Paroncini, M. (2005). Natural convective heat transfer in square enclosures heated from below. *Applied Thermal Engineering*, *25*(16), 2522-2531.

Casada, M. E., & Young, J. H. (1994a). Model for heat and moisture transfer in arbitrarily shaped two-dimensional porous media. *Transactions of the ASAE, 37*(6), 1-1938.

Casada, M. E., & Young, J. H. (1994b). Heat and moisture transfer during transportation of shelled peanuts. *Transactions of the ASAE, 37*(6), 1939-1946.

Cass, A., G. S.*Campbell*, and Jones, T. L. (1984). Enhancement of thermal water vapor diffusion in soil. *Soil Sci. Soc. Am. J.*, 48*(*1*)*, 25–32.

Cassidy, D. P., & Hudak, A. J. (2001). Microorganism selection and biosurfactant production in a continuously and periodically operated bioslurry reactor. *Journal of hazardous materials*, *84*(2), 253-264.

Chan, B. K. C., Ivey, C. M., & Barry, J. M. (1970). Natural convection in enclosed porous media with rectangular boundaries. *Journal of heat transfer*, *92*(1), 21-27.

Chandra, R. P., Bura, R., Mabee, W. E., Berlin, D. A., Pan, X., & Saddler, J. N. (2007). Substrate pretreatment: The key to effective enzymatic hydrolysis of lignocellulosics. In *Biofuels* (pp. 67-93). Springer Berlin Heidelberg.

Chang, S. Y., Liu, L., & Asher, S. A. (1994). Creation of templated complex topological morphologies in colloidal silica. *Journal of the American Chemical Society*, *116*(15), 6745-6747.

Chang, C. S., Converse, H. H., & Steele, J. L. (1993). Modeling of temperature of grain during storage with aeration. *Transactions of the ASAE, 36*(2), 509-519.

Cheikh, N. B., Beya, B. B., & Lili, T. (2007). Influence of thermal boundary conditions on natural convection in a square enclosure partially heated from below. *International communications in heat and mass transfer*, *34*(3), 369-379.

Chen, F., & Chen, C. F. (1988). Onset of finger convection in a horizontal porous layer underlying a fluid layer. *Journal of heat transfer*, *110*(2), 403-409.

Chen, C. S., & Johnson, W. H. (1969). Kinetics of moisture movement in hygroscopic materials (I. Theoretical considerations of drying phenomena). *Transactions of the ASAE, 12*(1), 109-0113.

Chen, P. & Pei, D. C. (1989). A mathematical model of drying processes. *International Journal of heat and mass transfer*, *32*(2), 297-310.

Cheng, P. (1978). Convective heat transfer in porous layers by integral methods. *Letters in Heat and Mass Transfer*, *5*(5), 243-252.

Choi, S. K., & Lin, C. L. (2010). A simple finite-volume formulation of the lattice Boltzmann method for laminar and turbulent flows. *Numerical Heat Transfer, Part B: Fundamentals*, *58*(4), 242-261.

Chung, D. S., & Pfost, H. B. (1967). Adsorption and desorption of water vapor by cereal grains and their products Part I: Heat and free energy changes of adsorption and desorption. *Transactions of the ASAE, 10*(4), 549-0551.

Churbanov, A. G., Vabishchevich, P. N., Chudanov, V. V., & Strizhov, V. F. (1994). A numerical study on natural convection of a heat-generating fluid in rectangular enclosures. *International journal of heat and mass transfer*, *37*(18), 2969-2984.

Coleman, B. D., & Noll, W. (1963). The thermodynamics of elastic materials with heat conduction and viscosity. *Archive for Rational Mechanics and Analysis*, *13*(1), 167-178.

Converse, H. H., Graves, A. H., & Chung, D. S. (1973). Transient heat transfer within wheat stored in a cylindrical bin. *Transactions of the ASAE*, *16*(1), 129-0133.

Coumans, W. J. (1987). *Power law diffusion in drying processes*. Technische Universiteit Eindhoven.

Coumans, W. J. (2000). Models for drying kinetics based on drying curves of slabs. *Chemical Engineering and Processing: Process Intensification*, *39*(1), 53-68.

Cushman, J. H., Bennethum, L. S., & Hu, B. X. (2002). A primer on upscaling tools for porous media. *Advances in Water Resources*, *25*(8), 1043-1067.

Cussler, E. (1997). Diffusion: Mass transfer in fluid systems: Cambridge Univ Pr. *View Article PubMed/NCBI Google Scholar*.

Dalsenter, F. D. H., Viccini, G., Barga, M. C., Mitchell, D. A., & Krieger, N. (2005). A mathematical model describing the effect of temperature variations on the kinetics of microbial growth in solid-state culture. *Process Biochemistry*, *40*(2), 801-807.

Degan, G., Vasseur, P., & Bilgen, E. (1995). Convective heat transfer in a vertical anisotropic porous layer. *International journal of heat and mass transfer*, *38*(11), 1975-1987.

Derjani, G., Taim, M. E., & Narusawa, U. (1986). Effect of boundary conditions on thermal instability of superposed porous and fluid layer. *Natural Convection in Enclosures*, 83-89.

Descôteaux, S., & Savoie, P. (2003). Artificial drying of big square bale hay. In *International conference on crop harvesting and processing* (p. 21). American Society of Agricultural and Biological Engineers.

Descôteaux, S., Tremblay, Y., & Savoie, P. (2002). Drying characteristics of high density hay bales. In *2002 ASAE Annual Meeting* (p. 1). American Society of Agricultural and Biological Engineers.

DeVries, D. A. (1958). Simultaneous heat and mass transfer in porous media. *Eos Trans. AGU*, *39*(5), 909-916.

Diaz, L. F., & Savage, G. M. (2007). Factors that affect the process. *Compost Science and Technology*, *1*.

DLG. (2007). *Rundballenpresse Fendt 2900 VS – Durchsatz und Pressdichte* (pp. 1–8). Retrieved from http://www.dlg-test.de/pbdocs/5717F.pdf.

Droin, A., Taverdet, J. L., & Vergnaud, J. M. (1988). Modeling the kinetics of moisture adsorption by wood. *Wood Science and Technology*, *22*(1), 11-20.

Durlofsky, L., & Brady, J. F. (1987). Analysis of the Brinkman equation as a model for flow in porous media. *Physics of Fluids*, *30*(11), 3329-3341.

Eckert, E. R. G., & Faghri, M. (1980). A general analysis of moisture migration caused by temperature differences in an unsaturated porous medium. *International Journal of Heat and Mass Transfer*, *23*(12), 1613-1623.

El-Fadel, M., Findikakis, A., & Leckie, J. (1995). Landfill simulation models.

El-Khatib, G., & Prasad, V. (1987). Effects of stratification on thermal convection in horizontal porous layers with localized heating from below. *Journal of heat transfer*, *109*(3), 683-687.

Epstein, N. (1989). On tortuosity and the tortuosity factor in flow and diffusion through porous media. *Chemical Engineering Science*, *44*(3), 777-779.

Erbay, Z., & Icier, F. (2009). Optimization of hot air drying of olive leaves using response surface methodology. *Journal of Food Engineering*, *91*(4), 533-541.

Erbay, Z., & Icier, F. (2010). A review of thin layer drying of foods: theory, modeling, and experimental results. *Critical reviews in food science and nutrition*, *50*(5), 441-464.

Escudey, M., Zambra, C., Antilén, M., & Moraga, N. (2011). *Sewage Sludge Disposal and Applications: Self-heating and Spontaneous Combustion of Compost Piles-Trace Metals Leaching in Volcanic Soils After Sewage Sludge Disposal*. INTECH Open Access Publisher.

Fanaei, M. A., & Vaziri, B. M. (2009). Modeling of temperature gradients in packed-bed solid-state bioreactors. *Chemical Engineering and Processing: Process Intensification*, *48*(1), 446-451.

Fontenelle, L. (2011a). Solid state fermentation of switchgrass mixtures: Experimentation, modeling and analysis.

Fontenelle, L. T., Corgié, S. C., & Walker, L. P. (2011b). Integrating mixed microbial population dynamics into modeling energy transport during the initial stages of the aerobic composting of a switchgrass mixture. *Bioresource technology*, 102(8), 5162-5168.

Fortes, M., & Okos, M. R. (1980). Drying theories: their bases and limitations as applied to foods and grains. *Advances in drying*, *1*, 119-154.

Freer, M. W., Siebenmorgen, T. J., Couvillion, R. J., & Loewer, O. J. (1990). Modeling temperature and moisture content changes in bunker-stored rice. *Transactions of the ASAE*, *33*(1), 211-0220.

Gajalakshmi, S., & Abbasi, S. A. (2008). Solid waste management by composting: state of the art. *Critical Reviews in Environmental Science and Technology*, *38*(5), 311-400.

Gardner, R. H. & O'Neill, R. V. & Carney, J. H. (1981). Spatial patterning and error propagation in a stream ecosystem model. In *Proceedings, Summer Computer Simulation Conference*, pp. 3910395. La Jolla, Calif.: Simulation Councils.

Garg, 2005. Modeling non-uniform airflow and its application for partial chilled aeration using PHAST-FEM. *MS thesis*. West Lafayette, Ind.: Purdue University.

Georgiou, G., & Shuler, M. L. (1986). A computer model for the growth and differentiation of a fungal colony on solid substrate. *Biotechnology and bioengineering*, *28*(3), 405-416.

Gervais, P., & Molin, P. (2003). The role of water in solid-state fermentation. *Biochemical Engineering Journal*, *13*(2), 85-101.

Ghodeswar, K. (2010). *Natural Convection in a Porous Medium Saturated by Nanofluid* (Doctoral dissertation, Cleveland State University).

Gigler, J. K., Van Loon, W. K. P., Vissers, M. M., & Bot, G. P. A. (2000). Forced convective drying of willow chips. *Biomass and bioenergy*, *19*(4), 259-270.

Gigler, J. K., van Loon, W. K., & Sonneveld, C. (2004). Experiment and modelling of parameters influencing natural wind drying of willow chunks. *Biomass and Bioenergy*, *26*(6), 507-514.

Grathwohl, P. (1998). Diffusion in natural porous media, topics in environmental fluid mechanics.

Gray, W. G., & Hassanizadeh, S. M. (1998). Macroscale continuum mechanics for multiphase porous-media flow including phases, interfaces, common lines and common points. *Advances in Water Resources*, *21*(4), 261-281.

Griffiths, H. J. (1964). *Bulk storage of grain: A summary of factors governing control of deterioration*. CSIRO.

Grillo, A., Lampe, M., Logashenko, D., Stichel, S., & Wittum, G. (2012). Simulation of salinity-and thermohaline-driven flow in fractured porous media. *Journal of Porous Media*, *15*(5).

Grosan, T., Revnic, C., Pop, I., & Ingham, D. B. (2009). Magnetic field and internal heat generation effects on the free convection in a rectangular cavity filled with a porous medium. *International Journal of Heat and Mass Transfer*, *52*(5), 1525-1533.

Gurr, C. G., Marshall, T. J., & Hutton, J. T. (1952). Movement of water in soil due to a temperature gradient. *Soil Science*, *74*(5), 335-346.

Haajizadeh, M., & Tien, C. L. (1984). Combined natural and forced convection in a horizontal porous channel. *International journal of heat and mass transfer*, *27*(6), 799-813.

Haghighi, K., Irudayaraj, J., & Stroshine, R. L. (1990). Grain kernel drying simulation using the finite element method. *Transactions of the ASAE*, *33*(6), 1957-1965.

Haghshenas, A., Nasr, M. R., & Rahimian, M. H. (2010). Numerical simulation of natural convection in an open-ended square cavity filled with porous medium by lattice Boltzmann method. *International Communications in Heat and Mass Transfer*, *37*(10), 1513-1519.

Halvadakis, C. P. (1983). Methanogenesis in solid-waste landfill bioreactors.

Hamelers, H. V. M. (1993). A theoretical model of composting kinetics.

Hamelers, H. V. M. (2004). Modeling composting kinetics: A review of approaches. *Reviews in Environmental Science and Bio/Technology*, *3*(4), 331-342.

Hamoda, M. F., Qdais, H. A., & Newham, J. (1998). Evaluation of municipal solid waste composting kinetics. *Resources, conservation and recycling*, *23*(4), 209-223.

Harmathy, T. Z. (1969). Simultaneous moisture and heat transfer in porous systems with particular reference to drying. *Industrial & Engineering Chemistry Fundamentals*, *8*(1), 92-103.

Hassanizadeh, M., & Gray, W. G. (1979). General conservation equations for multi-phase systems: 1. Averaging procedure. *Advances in Water Resources*, *2*, 131-144.

Hassanizadeh, S. M., Celia, M. A., & Dahle, H. K. (2002). Dynamic effect in the capillary pressure–saturation relationship and its impacts on unsaturated flow. *Vadose Zone Journal*, *1*(1), 38-57.

Jang, J. Y., & Ni, J. R. (1989). Transient free convection with mass transfer from an isothermal vertical flat plate embedded in a porous medium. *International Journal of Heat and Fluid Flow*, 10(1), 59-65.

Joekar-Niasar, V., Hassanizadeh, S. M., & Leijnse, A. (2008). Insights into the relationships among capillary pressure, saturation, interfacial area and relative permeability using pore-network modeling. *Transport in Porous Media*, *74*(2), 201-219.

Joekar-Niasar, V., & Hassanizadeh, S. M. (2012). Uniqueness of specific interfacial area–capillary pressure–saturation relationship under non-equilibrium conditions in two-phase porous media flow. *Transport in Porous Media*, *94*(2), 465-486.

Haug, R. T. (1980). *Compost engineering; principles and practice* (No. 631.875 H371). Technomic Publishing.

Haug, R. T. (1993). The principal handbook of compost engineering.

Henderson, J. M., & Henderson, S. M. (1968). A computational procedure for deep-bed drying analysis. *Journal of Agricultural Engineering Research*, *13*(2), 87-95.

Henderson, S. M., & Pabis, S. (1961). Grain drying theory I. Temperature effect on drying coefficient. *Journal of Agricultural Engineering Research*, *6*(3), 169-174.

Henry, P. S. H. (1939, May). Diffusion in absorbing media. In *Proceedings of the Royal Society of London A: Mathematical, Physical and Engineering Sciences* (Vol. 171, No. 945, pp. 215-241). The Royal Society.

Higgins, C. W., & Walker, L. P. (2001). Validation of a new model for aerobic organic solids decomposition: simulations with substrate specific kinetics. *Process Biochemistry*, *36*(8), 875-884.

Hill, R. R. (1976). Response to inbreeding in alfalfa populations derived from single clones. *Crop Science*, *16*(2), 237-241.

Hill, J. D., Ross, I. J., & Barfield, B. J. (1977). The use of vapor pressure deficit to predict drying time for alfalfa hay. *Transactions of the ASAE*, *20*(2), 372-0374.

Hougen, O. A., McCauley, H. J., & Marshall, W. R. (1940). Limitations of diffusion equations in drying. *Trans. AIChE*, *36*, 183-210.

Hsiao, S. W., & Chen, C. K. (1994). Natural convection heat transfer from a corrugated plate embedded in an enclosed porous medium. *Numerical Heat Transfer*, *25*(3), 331-345.

Huang, T. G., & Gunkel, W. W. (1974). Theoretical and experimental studies of the heating front in a deep bed hygroscopic product. *Transactions of the ASAE*, *17*(2), 346-0354.

Hukill, W. V. (1954). Grain drying with unheated air. *Agric. Eng*, *35*(6), 393-395.

Ikasari, L., & Mitchell, D. A. (2000). Two-phase model of the kinetics of growth of Rhizopus oligosporus in membrane culture. *Biotechnology and bioengineering*, *68*(6), 619-627.

Ingham, D. B., & Pop, I. (Eds.). (2005). *Transport phenomena in porous media III* (Vol. 3). Elsevier.

Ingram, G. W. (1976). Deep bed drier simulation with intra-particle moisture diffusion. *Journal of Agricultural Engineering Research*, *21*(3), 263-272.

Jang, J. Y., & Ni, J. R. (1989). Transient free convection with mass transfer from an isothermal vertical flat plate embedded in a porous medium. *International journal of heat and fluid flow*, *10*(1), 59-65.

Jia, D., Afzal, M. T., Gongc, M., & Bedane, A. H. (2010). Modeling of moisture diffusion and heat transfer during softening in wood densification. *Int. J. Eng*, *4*, 191-200.

Jia, C. C. (1995). Study of heat and mass transfer inside grain kernel and temperature pattern in grain storage bin. *PhD Thesis*.

Jia, C. C., Sun, D. W., & Cao, C. W. (2000). Mathematical simulation of temperature and moisture fields within a grain kernel during drying. *Drying Technology*, *18*(6), 1305-1325.

Jia, C. C., Sun, D. W., & Cao, C. (2001). Computer simulation of temperature changes in a wheat storage bin. *Journal of Stored Products Research*, *37*(2), 165-177.

Jian, F., Jayas, D. S., & White, N. D. (2005). Movement and distribution of adult Cryptolestes ferrugineus (Coleoptera: Laemophloeidae) in stored wheat in response to temperature gradients, dockage, and moisture differences. *Journal of Stored Products Research*, *41*(4), 401-422.

Joekar-Niasar, V., Hassanizadeh, M., Pyrak-Nolte, L., Berentsen, C., & Leijnse, A. (2007, December). Quasi-Static Pore-Scale Network Models for Studying Pc-Sw-anw Relationship in Drainage and Imbibition. In *AGU Fall Meeting Abstracts* (Vol. 1, p. 03).

Jones, W. P., & Launder, B. E. (1972). Some properties of sink-flow turbulent boundary layers. *Journal of Fluid Mechanics*, *56*(02), 337-351.

Jones, W. P., & Launder, B. (1973). The calculation of low-Reynolds-number phenomena with a two-equation model of turbulence. *International Journal of Heat and Mass Transfer, 16*(6), 1119-1130.

Kaiser, J. P., Neff, A., & Raschle, P. (1995). Biological Transformation (Composting) of Organic Materials. *Recovery, Recycling, and Reintegration*.

Kaiser, J. (1996). Modelling composting as a microbial ecosystem: a simulation approach. *Ecological Modelling*, *91*(1), 25-37.

Kalaoka, W., & Witayangkurn, S. (2013). Natural convection in porous square cavities with discrete heat sources on bottom and side walls. *Thai Journal of Mathematics*, *12*(1), 207-221.

Kaya, A., Aydın, O., & Dincer, I. (2006). Numerical modeling of heat and mass transfer during forced convection drying of rectangular moist objects. *International journal of heat and mass transfer*, *49*(17), 3094-3103.

Keener, H. M., Hansen, R. C., & Marugg, C. (1992). *Optimizing the efficiency of the composting process*.

Keey, R. B. (1991). *Drying of loose and particulate materials*. CRC Press.

Keey, R. B., Langrish, T. A., & Walker, J. C. (2000). Moisture Diffusion. In *Kiln-Drying of Lumber* (pp. 85-115). Springer Berlin Heidelberg.

Kemp, J. G., Misener, G. C., & Roach, W. S. (1972). Development of empirical formulae for drying of hay. *Transactions of the ASAE, 15*(4), 723-0725.

Khanafer, K. M., & Chamkha, A. J. (1998). Hydromagnetic natural convection from an inclined porous square enclosure with heat generation. *Numerical Heat Transfer, Part A Applications*, *33*(8), 891-910.

Khankari, K. K., Morey, R. V., & Patankar, S. V. (1994). Mathematical model for moisture diffusion in stored grain due to temperature gradients. *Transactions of the ASAE, 37*(5), 1591-1604.

Khankari, K. K., Patankar, S. V., & Morey, R. V. (1995). A mathematical model for natural convection moisture migration in stored grain. *Transactions of the ASAE, 38*(6), 1777-1787.

Kiely, G., Tayfur, G., Dolan, C., & Tanji, K. (1997). Physical and mathematical modelling of anaerobic digestion of organic wastes. *Water Research, 31*(3), 534-540.

Lee, S., Baek, S. W., Kim, M. Y., & Sohn, Y. M. (2007). Numerical investigation of the combustion characteristics and nitric oxide formation in a municipal waste incinerator. *Numerical Heat Transfer, Part A: Applications*, *52*(8), 713-735.

King, C. J. (1968). Rates of moisture sorption and desorption in porous dried foodstuffs. *Food Technology*, *22*(4), 509.

Klapp, E. (1963). Mathematical analysis of simultaneous heat and mass transfer processes in granular materials through which passes a gas. *Translation*, *254*, 360-372.

Kleinfelter, N., Park, M., & Cushman, J. H. (2007). Mixture theory and unsaturated flow in swelling soils. *Transport in porous media*, *68*(1), 69-89.

Krischer, O., & Kast, W. (1963). Scientific Fundamentals of Drying Technology.

Kumari, M., & Jayanthi, S. (2005). Uniform lateral mass flux on natural-convection flow over a vertical cone embedded in a porous medium saturated with a non-Newtonian fluid. *Journal of Porous Media*, *8*(1).

Kumari, M., & Nath, G. (2009). Analytical solution of unsteady three-dimensional MHD boundary layer flow and heat transfer due to impulsively stretched plane surface. *Communications in Nonlinear Science and Numerical Simulation*, *14*(8), 3339-3350.

Nield, D. A., Manole, D. M., & Lage, J. L. (1993). Convection induced by inclined thermal and solutal gradients in a shallow horizontal layer of a porous medium. *Journal of Fluid mechanics*, *257*, 559-574.

Lai, F. C., & Kulacki, F. A. (1990). The effect of variable viscosity on convective heat transfer along a vertical surface in a saturated porous medium. *International Journal of Heat and Mass Transfer*, *33*(5), 1028-1031.

Lai, F. C., & Kulacki, F. A. (1991). Coupled heat and mass transfer by natural convection from vertical surfaces in porous media. *International Journal of Heat and Mass Transfer*, *34*(4), 1189-1194.

Lakhal, E. K., Hasnaoui, M., Vasseur, P., & Bilgen, E. (1995). Natural convection in a square enclosure heated periodically from part of the bottom wall. *Numerical Heat Transfer, Part A: Applications*, *27*(3), 319-333.

Lamnatou, C., Papanicolaou, E., Belessiotis, V., & Kyriakis, N. (2009). Conjugate heat and mass transfer from a drying rectangular cylinder in confined air flow. *Numerical Heat Transfer, Part A: Applications*, *56*(5), 379-405.

Herrero, E. V., Mitchell, J. P., Campiglia, E., Lanini, W. T., Temple, S., & Miyao, G. (1998). Use of Cover Crop Mulches in a Processing Tomato Production System. *Horticultural Science*, *33*(3), 476-476.

Launder, B. E., & Spalding, D. B. (1974). The numerical computation of turbulent flows. *Computer methods in applied mechanics and engineering*, *3*(2), 269-289.

Lawrence, J., Maier, D. E., & Stroshine, R. L. (2013a). Three-dimensional transient heat, mass, momentum, and species transfer in the stored grain ecosystem: Part I. Model development and evaluation. *Transactions of the ASABE*, *56*(1), 179-188.

Lawrence, J., Maier, D. E., & Stroshine, R. L. (2013b). Three-Dimensional Transient Heat, Mass, Momentum, and Species Transfer in the Stored Grain Ecosystem: Part II. Model Validation. *Transactions of the ASABE*, *56*(1), 189-201.

Lawrence, J., & Maier, D. E. (2011). Three-dimensional airflow distribution in a maize silo with peaked, levelled and cored grain mass configurations. *Biosystems engineering*, *110*(3), 321-329.

Laws, N., & Parry, J. L. (1983, January). Mathematical modelling of heat and mass transfer in agricultural grain drying. In *Proceedings of the Royal Society of London A:*

Mathematical, Physical and Engineering Sciences (Vol. 385, No. 1788, pp. 169-187). The Royal Society.

Lefebvre, X., Lanini, S., & Houi, D. (2000). The role of aerobic activity on refuse temperature rise, I. Landfill experimental study. *Waste Management and Research, 18*(5), 444-452.

Leu, J. S., Jang, J. Y., & Chou, W. C. (2009). Convection heat and mass transfer along a vertical heated plate with film evaporation in a non-Darcian porous medium. *International Journal of Heat and Mass Transfer*, *52*(23), 5447-5450.

Lewis, W. K. (1921). The rate of drying of solid materials. *The Journal of Industrial and Engineering Chemistry*: 13(5), 42-432.

Fazaeli, H., Mahmodzadeh, H., Azizi, A., Jelan, Z. A., Liang, J. B., Rouzbehan, Y., & Osman, A. (2004). Nutritive value of wheat straw treated with Pleurotus fungi. *Asian Australasian Journal of Animal Sciences*, *17*(12), 1681-1688.

Lievense, L. C., Verbeek, M. A. M., Meerdink, G., & Van't Riet, K. (1990). Inactivation of Lactobacillus plantarum during drying. I. Measurement and modeling of the drying process. *Bioseparation*, *1*, 149-160.

Lin, D. K. (1993). Unsteady natural convection heat and mass transfer in a saturated porous enclosure. *Wärme-und Stoffübertragung*, *28*(1-2), 49-56.

Lindstrom, F. T. (1992). A mathematical model for the one-dimensional transport and fate of oxygen and substrate in a water-saturated sorbing homogeneous porous medium. *Water resources research*, *28*(9), 2499-2511.

Liu, A. J., Durian, D. J., Herbolzheimer, E., & Safran, S. A. (1990). Wetting transitions in a cylindrical pore. *Physical review letters*, *65*(15), 1897.

Ljung, L., & Glad, T. (1994). *Modeling of dynamic systems*. Englewood Cliffs: PTR Prentice Hall.

Longstaff, R. A., & Banks, H. J. (1987). Simulation of temperature fluctuations near the surface of grain bulks. *Journal of stored products research*, *23*(1), 21-30.

Luikov, A. V. (1966). Application of irreversible thermodynamics methods to investigation of heat and mass transfer. *International Journal of Heat and Mass Transfer*, *9*(2), 139-152.

Luikov, A. V. (1975). Systems of differential equations of heat and mass transfer in capillary-porous bodies (review). *International Journal of Heat and mass transfer*, *18*(1), 1-14.

Mahapatra, T. R., Pal, D., & Mondal, S. (2011). Natural convection in a lid-driven square cavity filled with Darcy-Forchheimer porous medium in the presence of thermal radiation. *International Journal of Nonlinear Science*, *11*(3), 366-379.

Margaris, D. P., & Ghiaus, A. G. (2006). Dried product quality improvement by air flow manipulation in tray dryers. *Journal of Food Engineering*, *75*(4), 542-550.

Mason, I. G. (2006). Mathematical modelling of the composting process: a review. *Waste Management*, *26*(1), 3-21.

Masuoka, T. (1974). Convective currents in a horizontal layer divided by a permeable wall. *Bulletin of JSME*, *17*(104), 225-232.

McCready, D. W., & McCabe, W. L. (1933). *The adiabatic air drying of hygroscopic solids*. University of Michigan.

Miller, F. C. (1989). Matric water potential as an ecological determinant in compost, a substrate dense system. *Microbial Ecology*, *18*(1), 59-71.

Mitchell, R., & Schmer, M. (2012). Switchgrass harvest and storage. In *Switchgrass* (pp. 113-127). Springer London.

Mitchell, D. A., Do, D. D., Greenfield, P. F., & Doelle, H. W. (1991). A semimechanistic mathematical model for growth of Rhizopus oligosporus in a model solid-state fermentation system. *Biotechnology and bioengineering*, *38*(4), 353-362.

Mitchell, D. A., Krieger, N., Stuart, D. M., & Pandey, A. (2000). New developments in solid-state fermentation: II. Rational approaches to the design, operation and scale-up of bioreactors. *Process Biochemistry*, *35*(10), 1211-1225.

Mobedi, M., Cekmer, O., & Pop, I. (2010). Forced convection heat transfer inside an anisotropic porous channel with oblique principal axes: Effect of viscous dissipation. *International Journal of Thermal Sciences*, *49*(10), 1984-1993.

Mohee, R., White, R. K., & Das, K. C. (1998). Simulation model for composting cellulosic (bagasse) substrates. *Compost Science & Utilization*, *6*(2), 82-92.

Montross, M. D., Maier, D. E., & Haghighi, K. (2002b). Development of a finite–element stored grain ecosystem model. *Transactions of the ASAE*, *45*(5), 1455.

Montross, M. D., Maier, D. E., & Haghighi, K. (2002b). Validation of a finite–element stored grain ecosystem model. *Transactions of the ASAE*, *45*(5), 1465.

Moore, K. J., & Peterson, M. A. (1995). *Post-harvest physiology and preservation of forages: proceedings of a symposium sponsored by C-6 of the Crop Science Society of America*. Crop Science Society of America.

Morey, R. V., Cloud, H. A., & Lueschen, W. E. (1976). Practices for the efficient utilization of energy for drying corn. *Transactions of the ASAE*, *19*(1), 151-0155.

Morissette, R., & Savoie, P. (2008). Simulation of baled hay drying with airflow inversion and exhaust air recirculation. *Canadian Biosystems Engineering*, *50*, 3-9.

Muck, R. E., & Shinners, K. J. (2001, February). Conserved forage (silage and hay): progress and priorities. In *International Grassland Congress* (Vol. 19, pp. 753-762). São Pedro: SBZ.

Muir, W. E., Fraser, B. M., & Sinha, R. N. (1980). Simulation model of two-dimensional heat transfer in controlled-atmosphere grain bins. *Controlled Atmosphere Storage of Grains*, 385-398.

Mujumdar, A. S. (2004). Research and development in drying: Recent trends and future prospects. *Drying Technology*, *22*(1-2), 1-26.

Ishii, N., Robert, M., Nakayama, Y., Kanai, A., & Tomita, M. (2004). Toward large-scale modeling of the microbial cell for computer simulation. *Journal of Biotechnology, 113*(1), 281-294.

Neale, G., & Nader, W. (1974). Practical significance of Brinkman's extension of Darcy's law: coupled parallel flows within a channel and a bounding porous medium. *The Canadian Journal of Chemical Engineering, 52*(4), 475-478.

Ngoddy, P. O., & Bakker-Arkema, F. W. (1970). A generalized theory of sorption phenomena in biological materials (Part I. The isotherm equation). *Transactions of the ASAE, 13*(5), 612-0617.

Ngoddy, P. O., Bakker-Arkema, F. W., & Bickert, W. G. (1966). Heat transfer in a deep bed of pea beans. *Michigan State University Agri. Eng. Sta., Bui*, *49*(2), 132.

Nguyen, H., Goto, K., & Yamashita, R. (1987). Study on separating of shape by using test rice grader, 4: Separating characteristics of rough rice and brown rice by indented cylinder separator. *Journal of the Japanese Society of Agricultural Machinery (Japan)*.

Ni, J., & Beckermann, C. (1993). Modeling of globulitic alloy solidification with convection. *Journal of Materials Processing and Manufacturing Science, 2*, 217-231.

Nield, D. A., & Bejan, A. (2006). *Convection in porous media*. Springer Science & Business Media.

Nield, D. A. (1983). The boundary correction for the Rayleigh-Darcy problem: limitations of the Brinkman equation. *Journal of Fluid Mechanics, 128*, 37-46.

Nield, D. A. (2008). Impracticality of MHD convection in a porous medium. *Transport in Porous Media*, *73*(3), 379-380.

Tatsuo, N., Toru, T., Mitsuhiro, S., Yuji, K., & Hiroyuki, O. (1986). Numerical analysis of natural convection in a rectangular enclosure horizontally divided into fluid and porous regions. *International journal of heat and mass transfer*, *29*(6), 889-898.

Nithiarasu, P., Seetharamu, K. N., & Sundararajan, T. (1997). Natural convective heat transfer in a fluid saturated variable porosity medium. *International Journal of Heat and Mass Transfer*, *40*(16), 3955-3967.

O'Callaghan, J. R., Menzies, D. J., & Bailey, P. H. (1971). Digital simulation of agricultural drier performance. *Journal of Agricultural Engineering Research*, *16*(3), 223-244.

Obaldo, L. G., Harner, J. P., & Converse, H. H. (1990). Predicting temperature changes in stored corn. *Paper-American Society of Agricultural Engineers (USA)*.

Ohm, A., Vogtländer, J. G., & Kossen, N. W. F. (1971). Heat-and Mass Transfer in Barn Hay-Drying Systems. *Journal of Agricultural Engineering Research*, 16(3), 254-268.

Oppenheimer, J. R. (1997). *Compost process model development, validation, and simulation to assess moisture and energy management*.

Overhults, D. G., White, G. M., Hamilton, H. E., & Ross, I. J. (1973). Drying soybeans with heated air. *Transactions of the ASAE, 16*(1), 112-0113.

Oztop, H. F. (2007). Natural convection in partially cooled and inclined porous rectangular enclosures. *International Journal of Thermal Sciences*, *46*(2), 149-156.

Pandey, A., Soccol, C. R., Nigam, P., & Soccol, V. T. (2000). Biotechnological potential of agro-industrial residues. I: sugarcane bagasse. *Bioresource technology*, *74*(1), 69-80.

Pandey, A. (1992). Recent process developments in solid-state fermentation. *Process Biochemistry*, *27*(2), 109-117.

Pandey, A. (2003). Solid-state fermentation. *Biochemical Engineering Journal*, *13*(2), 81-84.

Parker, B. F., White, G. M., Lindley, M. R., Gates, R. S., Collins, M., Lowry, S., & Bridges, T. C. (1992). Forced-air drying of baled alfalfa hay. *Transactions of the ASAE*, 35(2), 607-615.

Parr, L. F., Gardner, W. R. & Elliot, L. F. (1981). Water potential relations in soil microbiology. *SSSA Special Publication Number 9, Soil Science Society of America, Madison, WI.*

Parry, J. L. (1985). Mathematical modelling and computer simulation of heat and mass transfer in agricultural grain drying: a review. *Journal of Agricultural Engineering Research*, *32*(1), 1-29.

Patankar, S. V. (1980). Numerical heat transfer and fluid flow: Computational methods in mechanics and thermal science.

Pérez-Guerra, N., Torrado-Agrasar, A., López-Macias, C., & Pastrana, L. (2003). Main characteristics and applications of solid substrate fermentation. *Electronic Journal of Environmental, Agricultural and Food Chemistry*, *2*(3).

Person, H. L., & Shayya, W. H. (1994). Composting process design computer model. *Applied Engineering in Agriculture*, *10*(2), 277-284.

Petric, I., & Selimbašić, V. (2008). Development and validation of mathematical model for aerobic composting process. *Chemical Engineering Journal*, *139*(2), 304-317.

Philip, J. R., & De Vries, D. A. (1957). Moisture movement in porous materials under temperature gradients. Eos, *Transactions American Geophysical Union*, 38(2), 222-232.

Pommier, S., Chenu, D., Quintard, M., & Lefebvre, X. (2008). Modelling of moisture-dependent aerobic degradation of solid waste. *Waste Management*, *28*(7), 1188-1200.

Poulikakos, D. (1986). Double diffusive convection in a horizontal sparsely packed porous layer. *International communications in heat and mass transfer*, *13*(5), 587-598.

Poulsen, T. G., & Moldrup, P. (2007). Air permeability of compost as related to bulk density and volumetric air content. *Waste management & research*, *25*(4), 343-351.

Prasad, V., & Kulacki, F. A. (1987). Natural convection in horizontal porous layers with localized heating from below. *Journal of heat transfer*, *109*(3), 795-798.

Prigogine, I. (1961). Thermodynamics of Irreversible Processes, 2nd Wiley Interscience. *New York.*

Prukwarun, W., Khumchoo, W., Seancotr, W., & Phupaichitkun, S. (2013). CFD simulation of fixed bed dryer by using porous media concepts: Unpeeled longan case. *International Journal of Agricultural and Biological Engineering*, *6*(1), 100-110.

Raghavarao, K. S. M. S., Ranganathan, T. V., & Karanth, N. G. (2003). Some engineering aspects of solid-state fermentation. *Biochemical Engineering Journal*, *13*(2), 127-135.

Raimbault, M. (1998). General and microbiological aspects of solid substrate fermentation. *Electronic Journal of Biotechnology*, *1*(3), 26-27.

Rajamani R., Srinivasa, C., Nithiarasu, P., Seetharamu, K. N. (1995). Convective heat transfer in axisymmetric porous bodies. *International Journal of Numerical Methods in Heat and Fluid Flow*: 5, 829-837.

Reddy, K. R., White, J. R., Wright, A., & Chua, T. (1999). Influence of phosphorus loading on microbial processes in the soil and water column of wetlands. *Phosphorus biogeochemistry in subtropical ecosystems. Lewis Publishers, New York, NY*, 249-273.

Reddy, A. P., Allgaier, M., Singer, S. W., Hazen, T. C., Simmons, B. A., Hugenholtz, P., & VanderGheynst, J. S. (2011). Bioenergy feedstock-specific enrichment of microbial populations during high-solids thermophilic deconstruction. *Biotechnology and Bioengineering*, 108(9), 2088-2098.

Reed, C., & Pan, H. (2000). Loss of phosphine from unsealed bins of wheat at six combinations of grain temperature and grain moisture content. *Journal of stored products research*, *36*(3), 263-279.

Richard, T. L., Walker, L. P., & Gossett, J. M. (2006). Effects of Oxygen on Aerobic Solid-State Biodegradation Kinetics. *Biotechnology progress*, *22*(1), 60-69.

Richard, P. (2003). The rhythm of yeast. *FEMS Microbial Rev* 27: 547-557.

Richards, L. A. (1931). Capillary conduction of liquids through porous mediums. *Journal of Applied Physics*, *1*(5), 318-333.

Robillard, L., Wang, C. H., & Vasseur, P. (1988). Multiple steady states in a confined porous medium with localized heating from below. *Numerical heat transfer*, *13*(1), 91-110.

Robinzon, R., Kimmel, E., & Avnimelech, Y. (2000). Energy and mass balances of windrow composting system. *Transactions of the ASAE*, *43*(5), 1253.

Román, F., Strahl-Schäfer, V., & Hensel, O. (2012). Improvement of air distribution in a fixed-bed dryer using computational fluid dynamics. *Biosystems engineering*, *112*(4), 359-369.

Román, F. D., & Hensel, O. (2014). Numerical simulations and experimental measurements on the distribution of air and drying of round hay bales. *Biosystems Engineering*, 122, 1-15.

Rotz, C. A., & Chen, Y. (1985). Alfalfa drying model for the field environment. *Transactions of the ASAE*, *28*(5), 1686-1691.

Rudraiah, N., & Srimani, P. K. (1980, November). Finite-amplitude cellular convection in a fluid-saturated porous layer. In *Proceedings of the Royal Society of London A: Mathematical, Physical and Engineering Sciences* (Vol. 373, No. 1753, pp. 199-222). The Royal Society.

Rynk, R. (2000). Monitoring moisture in composting systems. *Biocycle*, *41*(10), 53-57.

Saeid, N. H., & Pop, I. (2005). Natural convection from a discrete heater in a square cavity filled with a porous medium. *Journal of Porous Media*, *8*(1).

Sangsurasak, P., & Mitchell, D. A. (1998). Validation of a model describing two-dimensional heat transfer during solid-state fermentation in packed bed bioreactors. *Biotechnology and bioengineering*, *60*(6), 739-749.

Sano, T. (1996). Unsteady forced and natural convection around a sphere immersed in a porous medium. *Journal of engineering mathematics*, *30*(5), 515-525.

Sathe, S. B., Lin, W. Q., & Tong, T. W. (1988). Natural convection in enclosures containing an insulation with a permeable fluid-porous interface. *International journal of heat and fluid flow*, *9*(4), 389-395.

Sathiyamoorthy, M., Basak, T., Roy, S., & Pop, I. (2007). Steady natural convection flow in a square cavity filled with a porous medium for linearly heated side wall (s). *International Journal of Heat and Mass Transfer*, *50*(9), 1892-1901.

Saucedo-Castañeda, G., Gutiérrez-Rojas, M., Bacquet, G., Raimbault, M., & Viniegra-González, G. (1990). Heat transfer simulation in solid substrate fermentation. *Biotechnology and bioengineering*, *35*(8), 802-808.

Savoie, P., & Mailhot, A. (1986). Influence of eight factors on the drying rate of timothy hay. *Canadian Agricultural Engineering*, *28*(2), 145-148.

Schreyer-Bennethum, L. (2012). Macroscopic flow potentials in swelling porous media. *Transport in porous media*, *94*(1), 47-68.

Seki, H. (2000). Stochastic modeling of composting processes with batch operation by the Fokker-Planck equation. *Transactions of the ASAE*, *43*(1), 169.

Sharif, M. A., & Mohammad, T. R. (2005). Natural convection in cavities with constant flux heating at the bottom wall and isothermal cooling from the sidewalls. *International Journal of Thermal Sciences*, *44*(9), 865-878.

Sherwood, T. K. (1931). Application of the theoretical diffusion equations to the drying of solids. *Trans. Am. Inst. Chem. Engrs*, *27*, 190-202.

Sherwood, T. K. (1929). The drying of solids—I. *Industrial & Engineering Chemistry*, *21*(1), 12-16.

Singh, A. K., & Thorpe, G. R. (1995). Natural convection in a confined fluid overlying a porous layer-A comparison study of different models. *Indian Journal of Pure and Applied Mathematics*, *26*, 81-95.

Shinners, K. J., Straub, R. J., Huhnke, R. L., & Undersander, D. J. (1996). Harvest and storage losses associated with mid-size rectangular bales. *Applied Engineering in Agriculture*, *12*(2), 167-173.

Siau, J. F. (1983). Chemical potential as a driving force for nonisothermal moisture movement in wood. *Wood Science and Technology*, *17*(2), 101-105.

Sidhu, H. S., Nelson, M. I., Luangwilai, T., & Chen, X. D. (2007). Mathematical modelling of the self-heating process in compost piles. *Chemical Product and Process Modeling*, *2*(2).

Singh, A. K., Leonardi, E., & Thorpe, G. R. (1993a). A solution procedure for the equations that govern three-dimensional free convection in bulk stored grains. *Transactions of the ASAE*, *36*(4), 1159-1173.

Singh, A. K., Leonardi, E., & Thorpe, G. R. (1993b). Three-dimensional natural convection in a confined fluid overlying a porous layer. *Journal of heat transfer*, *115*(3), 631-638.

Sinha, R. N., & Wallace, H. A. H. (1977). Storage stability of farm-stored rapeseed and barley. *Canadian Journal of Plant Science*, *57*(2), 351-365.

Sinicio, R., Muir, W. E., Jayas, D. S., & Cenkowski, S. (1995). Thin-layer drying and wetting of wheat. *Postharvest Biology and Technology*, *5*(3), 261-275.

Smith, E. A., & Sokhansanj, S. (1989). Heat and mass transfer in grain bulks induced by buoyancy forces. *Paper-American Society of Agricultural Engineers (USA)*.

Smith, E. A., Duncan, E. J., McGechan, M. B., & Haughey, D. P. (1988). A model for the field drying of grass in windrows. *Journal of Agricultural Engineering Research*, *41*(4), 251-274.

Smith, D. M., Davis, P. J., & Brinker, C. J. (1990). In-situ pore structure analysis during aging and drying of gels. In *MRS Proceedings* (Vol. 180, p. 235). Cambridge University Press.

Sokhansanj, S., Khoshtaghaza, H., Schoenau, G. J., Arinze, E. A., & Tabil, L. G. (2003). Heat and moisture transfer and quality changes in containerized alfalfa cubes during transport. *Transactions of the ASAE*, *46*(2), 423.

Sokhansanj, S., & Wood, H. C. (1991). Simulation of thermal and disinfestation characteristics of a forage dryer. *Drying Technology*, *9*(3), 643-656.

Sole-Mauri, F., Illa, J., Magrí, A., Prenafeta-Boldú, F. X., & Flotats, X. (2007). An integrated biochemical and physical model for the composting process. *Bioresource technology*, *98*(17), 3278-3293.

Sompong, P., & Witayangkurn, S. (2012). Simulation of natural convection in a complicated enclosure with two wavy vertical walls. *Applied Mathematical Sciences*, *6*(57-60), 2833-2842.

Spencer, H. B. (1969). A mathematical simulation of grain drying. *Journal of Agricultural Engineering Research*, *14*(3), 226-235.

Steger, K., Eklind, Y., Olsson, J., & Sundh, I. (2005). Microbial community growth and utilization of carbon constituents during thermophilic composting at different oxygen levels. *Microbial ecology*, *50*(2), 163-171.

Stewart, J. I., Misra, R. D., Pruitt, W. O., & Hagan, R. M. (1975). Irrigating corn and grain sorghum with a deficient water supply. *Transactions of the ASAE*, *18*(2), 270-0280.

Stombaugh, D. P., & Nokes, S. E. (1996). Development of a biologically based aerobic composting simulation model. *Transactions of the ASAE*, *39*(1), 239-250.

Sullivan, E. (2013). Heat and Moisture Transport in Unsaturated Porous Media--A Coupled Model in Terms of Chemical Potential. *arXiv preprint arXiv*: 1305-2373.

Sun, D. W., & Woods, J. L. (1997a). Simulation of the heat and moisture transfer process during drying in deep grain beds. *Drying Technology*, *15*(10), 2479-2492.

Sun, D. W., & Woods, J. L. (1997b). Deep-bed simulation of the cooling of stored grain with ambient air: a test bed for ventilation control strategies. *Journal of Stored Products Research*, *33*(4), 299-312.

Sutherland, J. W., Banks, P. J., & Griffiths, H. J. (1971). Equilibrium heat and moisture transfer in air flow through grain. *Journal of Agricultural Engineering Research*, *16*(4), 368-386.

Tanaka, H., Kurosawa, H., & Murakami, H. (1986). Ethanol production from starch by a co-immobilized mixed culture system of Aspergillus awamori and Zymomonas mobilis. *Biotechnology and bioengineering*, *28*(12), 1761-1768.

Thomas, H. R., Lewis, R. W., & Morgan, K. (1980). An application of the finite element method to the drying of timber. *Wood and Fiber*.

Thompson, T. L., Peart, R. M., & Foster, G. H. (1968). Mathematical simulation of corn drying—a new model. *Transactions of the ASAE*, *11*(4), 582-0586.

Thompson, T. L. (1972). Temporary storage of high-moisture shelled corn using continuous aeration. *Transactions of the ASAE*, *15*(2), 333-0337.

Thorpe, G. R. (1982). Moisture diffusion through bulk grain subjected to a temperature gradient. *Journal of Stored Products Research*, *18*(1), 9-12.

Thorpe, G. R., Tapia, J. A. O., & Whitaker, S. (1991a). The diffusion of moisture in food grains—I. The development of a mass transport equation. *Journal of Stored Products Research*, *27*(1), 1-9.

Thorpe, G. R., Tapia, J. A. O., & Whitaker, S. (1991b). The diffusion of moisture in food grains—II. Estimation of the effective diffusivity. *Journal of Stored Products Research*, *27*(1), 11-30.

Thorpe, G. R., & Whitaker, S. (1992). Local mass and thermal equilibria in ventilated grain bulks. Part I: The development of heat and mass conservation equations. *Journal of stored products research*, *28*(1), 15-27.

Tilman, D., Socolow, R., Foley, J. A., Hill, J., Larson, E., Lynd, L. & Williams, R. (2009). Beneficial biofuels—the food, energy, and environment trilemma. *Science*, *325*(5938), 270-271.

Tiquia, S. M., Wan, H. C., & Tam, N. F. (2002). Microbial population dynamics and enzyme activities during composting. *Compost science & utilization*, *10*(2), 150-161.

Vadász, P. (2008). Nanofluid suspensions and bi-composite media as derivatives of interface heat transfer modeling in porous media. In *Emerging Topics in Heat and Mass Transfer in Porous Media* (pp. 283-326). Springer Netherlands.

Vafai, K., & Tien, C. L. (1981). Boundary and inertia effects on flow and heat transfer in porous media. *International Journal of Heat and Mass Transfer*, *24*(2), 195-203.

Vafai, K., Khanafer, K., Minkowycz, W. J., & Bejan, A. (2005). Synthesis of models for turbulent transport through porous media. *Handbook of Numerical Heat Transfer, Wiley, New York, USA*.

Valentas, K. J., Rotstein, E., & Singh, R. P. (1997). *Handbook of food engineering practice*. CRC Press.

Van Arsdel, W. B. (1947). Approximate diffusion calculations for the falling-rate phase of drying.

Van Arsdel, W. B. (1955). Simultaneous heat and mass transfer in a nonisothermal system: through-flow drying in the low-moisture range. *American Institute of Chemical Engineering*, 47-58.

Van Genuchten, M. T. (1980). A closed-form equation for predicting the hydraulic conductivity of unsaturated soils. *Soil science society of America journal*, *44*(5), 892-898.

Van Ginkel, J. T., Van Haneghem, I. A., & Raats, P. A. C. (2002). SE–Structures and Environment: Physical Properties of Composting Material: Gas Permeability, Oxygen Diffusion Coefficient and Thermal Conductivity. *Biosystems Engineering*, *81*(1), 113-125.

VanderGheynst, J. S. (1997). *Experimentation, modeling and analysis of a high-solids aerobic decomposition process*. Cornell University, January.

VanderGheynst, J. S., Gossett, J. M., & Walker, L. P. (1997). High-solids aerobic decomposition: pilot-scale reactor development and experimentation. *Process Biochemistry*, *32*(5), 361-375.

VanDuyne, D. A., & Kjelgaard, W. L. (1964). Air-flow resistance of baled alfalfa and clover hay. *Transactions of the ASAE*, *7*(3), 267-0270.

Varol, Y., Oztop, H. F., & Pop, I. (2009). Natural convection in right-angle porous trapezoidal enclosure partially cooled from inclined wall. *International Communications in Heat and Mass Transfer*, *36*(1), 6-15.

Vasseur, P., Satish, M. G., & Robillard, L. (1987). Natural convection in a thin, inclined, porous layer exposed to a constant heat flux. *International Journal of Heat and Mass Transfer*, *30*(3), 537-549.

Vasseur, P., Wang, C. H., & Sen, M. (1990). Natural convection in an inclined rectangular porous slot: the Brinkman-extended Darcy model. *Journal of heat transfer, 112*(2), 507-511.

Vergnaud, J. M. (1991). *Liquid transport processes in polymeric materials: modeling and industrial applications*. Prentice Hall.

Vlyssides, A., Mai, S., & Barampouti, E. M. (2009). An integrated mathematical model for co-composting of agricultural solid wastes with industrial wastewater. *Bioresource Technology*, *100*(20), 4797-4806.

von Meien, O. F., & Mitchell, D. A. (2002). A two-phase model for water and heat transfer within an intermittently-mixed solid-state fermentation bioreactor with forced aeration. *Biotechnology and bioengineering*, *79*(4), 416-428.

Walker, J. C. F. (1993). The drying of timber. In *Primary Wood Processing* (pp. 247-284). Springer Netherlands.

Weigler, F., Scaar, H., & Mellmann, J. (2011). Investigation of grain and air flows in a mixed-flow dryer. 7th Asia-Pacific Drying Conference (ADC 2011). *Tianjin, China*, 18-20.

Weinstein, T. F. (2005). *Three-phase hybrid mixture theory for swelling drug delivery systems* (Doctoral dissertation, University of Colorado at Denver).

Wen-Jeng, C., & Chi-Feng, H. (1993). Natural convection in a vertical cylinder filled with anisotropic porous media. *International journal of heat and mass transfer, 36*(13), 3361-3367.

Whitaker, S. (1986). Flow in porous media I: A theoretical derivation of Darcy's law. *Transport in porous media*, *1*(1), 3-25.

White, G. M., Bridges, T. C., Loewer, O. J., & Ross, I. J. (1980). Seed coat damage in thin-layer drying of soybeans. *Transactions of the ASAE, 23*(1), 224-0227.

Wirleitner, G. (2010). Hay quality with energy efficient technology. In *Bericht. 36. Viehwirtschaftliche Fachtagung. Physiologie und Verdauung, Mineralstoffversorgung, Milchproduktion, Gesundheitsmonitoring Rind, Rindfleischproduktion, Heumilch, 13-14 April 2010, Raumberg-Gumpenstein, Austria.* (pp. 71-80). Lehr-und Forschungszentrum für Landwirtschaft Raumberg-Gumpenstein.

Womac, A. R., Igathinathane, C., Sokhansanj, S., & Pordesimo, L. O. (2005). Biomass moisture relations of an agricultural field residue: corn stover. *Transactions of the ASAE*, *48*(6), 2073-2083.

Wright, D. A., Frost, J. P., Patterson, D. C., & Kilpatrick, D. J. (2001). PA—Precision Agriculture: Development of a Model to predict Drying Rates of Cut Ryegrass. *Journal of agricultural engineering research*, *79*(1), 23-35.

Wright, D. A., Frost, J. P., & Kilpatrick, D. J. (2000). The influence of weather factors on the drying rate of cut perennial ryegrass herbage under controlled conditions. *Grass and Forage Science*, *55*(4), 331-342.

Wu, L., Bai, S., & Sun, Y. (2003). Development of Rigid Bidisperse Porous Microspheres for High-Speed Protein Chromatography. *Biotechnology progress*, *19*(4), 1300-1306.

Wyman, C. E., Dale, B. E., Elander, R. T., Holtzapple, M., Ladisch, M. R., & Lee, Y. Y. (2005). Comparative sugar recovery data from laboratory scale application of leading pretreatment technologies to corn stover. *Bioresource technology*, *96*(18), 2026-2032.

Xi, B., Wei, Z., & Liu, H. (2010). Dynamic simulation for domestic solid waste composting processes. *Academia Arena*, 76.

Xia, L., & Cen, P. (1999). Cellulase production by solid state fermentation on lignocellulosic waste from the xylose industry. *Process Biochemistry*, *34*(9), 909-912.

Yaciuk, G., Muir, W. E., & Sinha, R. N. (1975). A simulation model of temperatures in stored grain. *Journal of Agricultural Engineering Research*, *20*(3), 245-258.

Yoshida, H., Tanaka, N., & Hozumi, H. (1997, October). Theoretical study on heat transport phenomena in a sanitary landfill. In *Proc., 6th Int. Landfill Symp* (Vol. 1, pp. 110-119).

Younsi, R., Kocaefe, D., & Kocaefe, Y. (2006). Three-dimensional simulation of heat and moisture transfer in wood. *Applied Thermal Engineering*, *26*(11), 1274-1285.

Yu, A., Liang, Z., & Caruso, F. (2005). Enzyme multilayer-modified porous membranes as biocatalysts. *Chemistry of materials*, *17*(1), 171-175.

Yu, H., Zeng, G., Huang, H., Xi, X., Wang, R., Huang, D. & Li, J. (2007). Microbial community succession and lignocellulose degradation during agricultural waste composting. *Biodegradation*, *18*(6), 793-802.

Zambra, C. E., Moraga, N. O., & Escudey, M. (2011). Heat and mass transfer in unsaturated porous media: Moisture effects in compost piles self-heating. *International Journal of Heat and Mass Transfer*, *54*(13), 2801-2810.

Zambra, C. E., Moraga, N. O., Rosales, C., & Lictevout, E. (2012). Unsteady 3D heat and mass transfer diffusion coupled with turbulent forced convection for compost piles with chemical and biological reactions. *International Journal of Heat and Mass Transfer*, *55*(23), 6695-6704.

Zanetti, M. C., Marchese, F., & Genon, G. (1997). Investigation on quality of landfilled MSW. *Landfill Processes and Waste Pretreatment*, 155-162.

Zhang, X., Hung, N. T., & Kahawita, R. (1993). Convective flow and heat transfer in an anisotropic porous layer with principal axes non-coincident with the gravity vector. *ASME-Publications-HTD*, 264, 79-79.

Zhao, F. Y., Liu, D., & Tang, G. F. (2008). Natural convection in a porous enclosure with a partial heating and salting element. *International Journal of Thermal Sciences*, *47*(5), 569-583.

References (Chapter 4)

Bear, J. (1972). Dynamics of fluids in porous media. *American Elsevier, New York*.

Berger, D., & Pei, D. C. T. (1973). Drying of hygroscopic capillary porous solids—a theoretical approach. *International Journal of Heat and Mass Transfer*, *16*(2), 293-302.

Bird, R. B., Lightfoot, E. N., & Stewart, E. W. (2007). *Transport phenomenon*. Wiley.

Bledsoe, B. L. & Hitch, W. (1989). University of Tennessee. *Agricultural Engineering Report*.

Bledsoe, B. L., Hitch, J. W., Maples, J. E., & Shoulders, S. (1985). *Rapid solar-heated forced-air drying of large round hay bales: design and operating considerations* (No. CONF-851271-). American Society of Agricultural Engineers, St. Joseph, MI.

Chen, P. & Pei, D. C. (1989). A mathematical model of drying processes. International *Journal of heat and mass transfer*, 32(2), 297-310.

Cussler, E. L. (1997). Values of diffusion coefficients. *Diffusion Mass Transfer in Fluid Systems, Cambridge University Press, Cambridge, UK*, 117-126.

Fontenelle, L. (2011a). *Solid state fermentation of switchgrass mixtures: Experimentation, modeling and analysis* (Doctoral dissertation). Retrieved from Cornell University Library. (Accession No. 3484866)

Fontenelle, L. T., Corgié, S. C., & Walker, L. P. (2011b). Integrating mixed microbial population dynamics into modeling energy transport during the initial stages of the aerobic composting of a switchgrass mixture. *Bioresource technology*, 102(8), 5162-5168.

Godbolt, C., M. G. C. Danao and S. R. Eckoff. (2013). Modeling of the equilibrium moisture content (EMC) of switchgrass. *Transactions of the ASABE*, 56(4), 1495-1501.

Kakaç, S., Kilkis, B., Kulacki, F. A., & Annç, F. (Eds.). (2012). *Convective heat and mass transfer in porous media* (Vol. 196). Springer Science & Business Media.

Khanchi, A., C. L. Jones, B. Sharma, R. L. Huhnke, P. Weckler and N. O. Maness. (2013). An empirical model to predict infield thin layer drying rate of cut switchgrass. *Biomass and Bioenergy*, 58, 128-135.

Khanchi, A., & Birrell, S. (2015). Influence of weather and swath density on drying characteristics of corn stover and switchgrass. In *2015 ASABE Annual International Meeting* (p. 1). American Society of Agricultural and Biological Engineers.

Krischer, O., & Kast, W. (1963). Scientific Fundamentals of Drying Technology.

Miller, E. E., & Miller, R. D. (1955). Theory of capillary flow: I. Practical implications. *Soil Science Society of America Journal*, 19(3), 267-271.

Mujumdar, A. S. (2004). Research and development in drying: Recent trends and future prospects. *Drying Technology*, *22*(1-2), 1-26.

Nield, D. A., & Bejan, A. (2006). *Convection in porous media*. Springer Science & Business Media.

Phillips, T. J. (1989). *An investigation of the combined heat and mass transfer processes in the drying of hygroscopic porous media with two disparate length scales* (Doctoral dissertation). Retrieved from Trace, University of Tennessee – Knoxville.

Román, F. D., & Hensel, O. (2014). Numerical simulations and experimental measurements on the distribution of air and drying of round hay bales. *Biosystems Engineering*, 122, 1-15.

Rotz, C. A., & Chen, Y. (1985). Alfalfa drying model for the field environment. *Transactions of the ASAE*, *28*(5), 1686-1691.

Shinners, K. & Porter, P. (2012). Optimizing harvest logistics of perennial grasses used for biofuel. *Iowa State University, Extension and Outreach*, Ames, Iowa.

Subahana, K. R., Mathew, M., Awasthi, A., Muralidharan, N. G., & Natarajan, R. (2015). Experimental investigation of convective drying kinetics of switchgrass leaf in open sun and in a forced convection solar dryer. *International Journal of ChemTech Research*, *7*(5), 2399-2407.

References (Chapter 5)

References (Section 5.1)

ASABE Standards. (2006). S358.2: Moisture measurement—Forages. St. Joseph, Mich.: ASABE.

ASTM Standards. (1992). D 5298-92. Standard test method for measurement of soil potential (suction) using filter paper. Philadelphia, Pa.: ASTM.

Hillel, D. (1998). *Environmental Soil Physics: Fundamentals, applications, and environmental considerations*. San Diego, Calif.: Academic Press.

Kemmerer, B. and J. Liu. (2012). Effect of harvesting time and moisture content on energy consumption of compressing switchgrass. *American Journal of Plant Sciences*, 5(21): 3241-3249.

Philip, J. R. and D. A. De Vries. (1957). Moisture movement in porous materials under temperature gradients. *Eos, Transactions American Geophysical Union*, 38(2): 222-232.

Seki, K. (2007). SWRC fit – a nonlinear fitting program with a water retention curve for soils having unimodal and bimodal pore structure. *Hydrology Earth System Sciences Discussions*, 4(1): 407-437.

Sokhansanj, S., S. Mani, A. Turhollow, A. Kumar, D. Bransby, L. Lynd, and M. Laser. (2009). Large-scale production, harvest and logistics of switchgrass (*Panicum virgatum L.*) – current technology and envisioning a mature technology. *Biofuels, Bioproducts and Biorefining*, 3(2): 124-141.

Warrick, A. W. and P. Broadbridge. (1992). Sorptivity and macroscopic capillary length relationships. *Water Resource Research*, 28: 429-431.

Zhang, R. (1997). Determination of soil sorptivity and hydraulic conductivity from the disk infiltrometer. *Soil Science Society of America Journal*. 61: 1024-1030.

References (Section 5.2)

ASABE Standards. (2006). S358.2: Moisture measurement—Forages. St. Joseph, Mich.: ASABE.

Coblentz, W. K., J. O. Fritz, and K. K. Bolsen. (1993). Baling System for making laboratory-scale hay bales. *Agronomy Journal*, 85(4): 962-965.

Da Silva, F. F., Wallach, R., Polak, A., & Chen, Y. (1998). Measuring water content of soil substitutes with time-domain reflectometry (TDR). *Journal of the American Society for Horticultural Science*, 123(4), 734-737.

Dalton, F. N., & Van Genuchten, M. T. (1986). The time-domain reflectometry method for measuring soil water content and salinity. *Geoderma*, 38(1), 237-250.

Davis, J. L., & Chudobiak, W. J. (1975). In situ meter for measuring relative permittivity of soils. *Geol. Surv. Can. Pap*, 75(1A), 75-79.

Hook, W. R., & Livingston, N. J. (1996). Errors in converting time domain reflectometry measurements of propagation velocity to estimates of soil water content. *Soil Science Society of America Journal*, 60(1), 35-41.

Kemmerer, B. and J. Liu. (2012). Effect of harvesting time and moisture content on energy consumption of compressing switchgrass. *American Journal of Plant Sciences,* 5(21): 3241-3249.

Ledieu, J., De Ridder, P., De Clerck, P., & Dautrebande, S. (1986). A method of measuring soil moisture by time-domain reflectometry. *Journal of Hydrology*, 88(3), 319-328.

Persson, M., Berndtsson, R., Nasri, S., Albergel, J., Zante, P., & Yumegaki, Y. (2000). Solute transport and water content measurements in clay soils using time domain reflectometry. *Hydrological Sciences Journal*, 45(6), 833-847.

Smith, W. A., Bonner, I. J., Kenney, K. L., & Wendt, L. M. (2013). Practical considerations of moisture in baled biomass feedstocks. *Biofuels*, 4(1), 95-110.

Sokhansanj, S., S. Mani, A. Turhollow, A. Kumar, D. Bransby, L. Lynd, and M. Laser. (2009). Large-scale production, harvest and logistics of switchgrass (Panicum virgatum L.) – current technology and envisioning a mature technology. *Biofuels, Bioproducts and Biorefining*, 3(2): 124-141.

Starr, G. C., Lowery, B., Cooley, E. T., & Hart, G. L. (1999). Development of a resonant length technique for soil water content measurement. *Soil Science Society of America Journal*, 63(2), 278-285.

Topp, G. C., Zebchuk, W. D., Davis, J. L., & Bailey, W. G. (1984). The measurement of soil water content using a portable TDR hand probe. *Canadian Journal of Soil Science*, 64(3), 313-321

References (Section 5.3)

ASABE Standards. (2006). S358.2: Moisture measurement—Forages. St. Joseph, Mich.: ASABE.

Carslaw, H. S. and J. C. Jaeger. (1959). Conduction of heat in solids. *Oxford: Clarendon*

Press, 1959, 2nd ed.

Casada, M. E. and L. R. Walton. (1989). Thermal conductivity of baled burley tobacco. *Transactions of the ASAE*, 32(3), 977-982.

Coblentz, W. K., Fritz, J. O. & Bolsen, K. K. (1993a). Baling system for making laboratory-scale hay bales. *Agronomy Journal*, 85(4), 962-965.

Coblentz, W. K., Fritz, J. O. & Bolsen, K. K. (1993b). Comparison of conventional and laboratory-scale alfalfa hay bales in small haystacks.

Dupont, C., R. Chiriac, G. Gauthier, and F. Toche. (2014). Heat capacity measurements of various biomass types and pyrolysis residues. *Fuel*, 115: 644-651.

Emami, S., Tabil, L. G., & Tyler, R. T. (2007). Technical Note: Thermal Properties of Chickpea Flour, Isolated Chickpea Starch, and Isolated Chickpea Protein. *Transactions of the ASABE*, 50(2), 597-604.

Fontana, A. J., B. Wacker, C. S. Campbell and G. S. Campbell. (1998). Simultaneous thermal conductivity, thermal resistivity, and thermal diffusivity measurement of selected foods and soils. In *2001 ASAE Annual Meeting* (p. 016101). American Society of Agricultural and Biological Engineers.

Godbolt, C., M. G. C. Danao and S. R. Eckoff. (2013). Modeling of the equilibrium moisture content (EMC) of switchgrass. Transactions of the ASABE, 56(4), 1495-1501.

Huggins, L. F. (1983). Analysis and Interpretation. In *Instrumentation and Measurement for Environmental Sciences* (pp. 02-15). American Society of Agricultural Engineers (ASAE) St. Joseph.

Iroba, K. L., Tabil, L. G., Venkatesh, M., & Oon-Doo, B. (2013). Thermal properties of lignocellulosic biomass barley straw. In *2013 Kansas City, Missouri, July 21-July 24, 2013* (p. 1). American Society of Agricultural and Biological Engineers.

Kemmerer, B. and J. Liu. (2014). Effect of harvesting time and moisture content on energy consumption of compressing switchgrass. *American Journal of Plant Sciences*, 5(21): 3241-3249.

Lobo, H. and C. Cohen. (1990). Measurement of thermal conductivity of polymer melts by the line-source method. *Polymer Engineering and Science*, 30(2): 65-70.

Ma, L., D. C. Davis, L. G. Obaldo and G. V. Barbosa-Cánovas. (1998). *Engineering Properties of Food and other Materials: a laboratory manual*. American Society of Agricultural Engineers (ASAE) St Joseph.

Nix, G. H., G. W. Lowry, R. I. Vachon and G. E. Tanger. (1967). Direct determination of thermal diffusivity and conductivity with a refined line-source technique. *Progress in Aeronautics and Astronautics: Thermophysics of Spacecraft and Planetary Bodies*, 20: 865-878.

Rodriguez, R. P., M. E. Rodrigo and P. Kelly. (1995). A calorimetric method to determine specific heats of prepared foods. Journal of Food Engineering, 26(1): 81-96.

Singh R. P. and D. R. Heldman. (2009). *Introduction of Food Engineering*, 4th ed. San Diego, CA: Academic Press.

Sokhansanj, S., S. Mani, A. Turhollow, A. Kumar, D. Bransby, L. Lynd, and M. Laser. (2009). Large-scale production, harvest and logistics of switchgrass (*Panicum virgatum* L.) – current technology and envisioning a mature technology. *Biofuels, Bioproducts and Biorefining*, 3(2): 124-141.

Takegoshi, E., S. Imura and Y. Hirasawa. (1982). A method of measuring the thermal conductivity of orthogonal anisotropic materials by a transient hot wire method. *Heat Transfer*: *Japanese Research*, 11(3): 75-89.

Wang, J. and K. Hayakawa. (1993). Maximum slope method for evaluating thermal conductivity probe data. *Journal of Food Science*, 58(6): 1340-1345.

Woodside, W. (1959). Probe for thermal conductivity measurement of dry and moist materials. Transactions of the ASHVE, 65: 291-310.

Yang, W., S. Sokhansanj, J. Tang and P. Winter. (2002). Determination of thermal conductivity, specific heat, and thermal diffusivity of Borage seeds. *Biosystems Engineering*, 82(2): 169-176

References (Section 5.4)

Abbasi, A. A. F., Zahedi Far, M., Mansuri, H., Yunesi Alamuti, M., Teymur Nezhad, N., & Tokasi, M. V. (2009). A comparison between nutritive value of enriched straw by two different methods (routine and mechanical method).

ASABE Standards. (2006). S358.2: Moisture measurement—Forages. St. Joseph, Mich.: ASABE.

ASHRAE. (2011). HVAC applications. *ASHRAE Handbook*, 29.1–29.13.

Baker, K. D., Hughs, E., & Chun, D. T. W. (2008). Use of a Rotor Spray System for Moisture Addition to Cotton Lint. *Applied Engineering in Agriculture*, 24(4), 491-495.

Beck, J. V. (1977). Sequential estimation of thermal parameters. *Journal of Heat Transfer*, 99(2), 314-321.

Buckmaster, D. R. (1986). *Heat generation and dry matter loss during storage of rectangularly baled alfalfa hay*. (Master's thesis). Retrieved from Michigan State University.

Carlton, H. E. and J. H. Oxley. (1967). Forced and natural convective mass transfer in multicomponent gaseous mixtures. *AlChE Journal*, 13(3), 571-577.

Kandula, M. (2011). Frost growth and densification in laminar flow over flat surfaces. *International Journal of Heat and Mass Transfer*, 54(15), 3719-3731.

Khanchi, A., C. L. Jones, B. Sharma, R. L. Huhnke, P. Weckler and N. O. Maness. (2013). An empirical model to predict infield thin layer drying rate of cut switchgrass. *Biomass and Bioenergy*, 58, 128-135.

Lam, P. S., S. Sokhansanj, X. Bi, C. J. Lim, and S. Mani. (2007). Physical characterization of wet and dry wheat straw and switchgrass–bulk and specific density. In *2007 ASAE Annual Meeting* (p. 1-22). American Society of Agricultural and Biological Engineers.

Lam, P. S., S. Sokhansanj, X. Bi, C. J. Lim, L. J. Naimi, M. Hoque, S. Mani, A. R. Womac, S. Narayan, and X. P. Ye. (2008). Bulk density of wet and dry wheat straw and switchgrass particles. *Applied Engineering in Agriculture*, 24(3), 351-358.

Lees, F. (2012). *Lees' Loss prevention in the process industries: Hazard identification, assessment and control*. Butterworth-Heinemann.

Rao, A. (2015). *Sustainable Energy Conversion for Electricity and Coproducts: Principles, Technologies, and Equipment*. John Wiley & Sons.

Smith, W. A., Bonner, I. J., Kenney, K. L., & Wendt, L. M. (2013). Practical considerations of moisture in baled biomass feedstocks. *Biofuels*, 4(1), 95-110.

Turner, A. P. (2014). Laboratory scale concept validation and evaluation of compromising plant nodal integrity as a means to increase bale density.

References (Chapter 6)

References (Section 6.1)

Christianson, L., Castelló, A., Christianson, R., Helmers, M., & Bhandari, A. (2010). Technical note: Hydraulic property determination of denitrifying bioreactor fill media. *Applied Engineering in Agriculture*, *26*(5), 849-854.

Chun, J. A., Cooke, R. A., Eheart, J. W., & Kang, M. S. (2009). Estimation of flow and transport parameters for woodchip-based bioreactors: I. laboratory-scale bioreactor. *Biosystems Engineering*, *104*(3), 384-395.

Custer, M. H., Sweeten, J. M., Reddell, D. L., & Egg, R. P. (1990). Hydraulic conductivity of chopped sorghum. *Transactions of the ASAE*, *33*(4), 1275-1280.

Lambe, T. W., & Whitman, R. V. (1979). Soil Mechanics, SI Version, J.

Robertson, W. D., Yeung, N., VanDriel, P. W., & Lombardo, P. S. (2005). High-Permeability Layers for Remediation of Ground Water; Go Wide, Not Deep. *Ground water*, *43*(4), 574-581.

Van Driel, P. W., Robertson, W. D., & Merkley, L. C. (2006). Denitrification of agricultural drainage using wood-based reactors. *Transactions of the ASABE*, 49(2), 565-573.

Yao, Z., & Jofriet, J. C. (1992). Hydraulic Conductivity of Alfalfa Silage. *Transactions of the ASAE*, *35*(4), 1291-1296.

Zhang, R. (1997). Determination of soil sorptivity and hydraulic conductivity from the disk infiltrometer. *Soil Science Society of America Journal*, *61*(4), 1024-1030.

References (Section 6.3)

Aviara, N. A., & Haque, M. A. (2001). Moisture dependence of thermal properties of peanut kernel. *Journal of food engineering*, 47(2), 109-113.

Bitra, V. S., Banu, S., Ramakrishna, P., Narender, G., & Womac, A. R. (2010). Moisture dependent thermal properties of peanut pods, kernels, and shells. *Biosystems engineering*, 106(4), 503-512.

Brock, B. A., & Samfield, M. (1958). The heat capacity of tobacco—Part I. *Tobacco Science II*, 41-44.

Carslaw, H. S., & Jaeger, J. C. (1959). Conduction of heat in solids. *Oxford: Clarendon Press*, 1959, 2nd ed.

Casada, M. E., & Walton, L. R. (1989a). New model for determining thermal diffusivity with the thermal probe. *Transactions of the ASAE*, 32(3), 973-0976.

Casada, M. E., & Walton, L. R. (1989b). Thermal conductivity of baled burley tobacco. *Transactions of the ASAE*, *32*(3), 977-0982.

Chakrabarti, S. M., & Johnson, W. H. (1972). Specific heat of flue cured tobacco by differential scanning calorimetry. *Transactions of the ASAE*, 15(5), 928-0931.

Drouzas, A. E., & Saravacos, G. D. (1988). Effective thermal conductivity of granular starch materials. *Journal of Food Science*, 53(6), 1795-1799.

Drusas, A. E., & Saravacos, G. D. (1985). Thermal conductivity of tomato paste. *Journal of Food engineering*, 4(3), 157-168.

Dupont, C., Chiriac, R., Gauthier, G., & Toche, F. (2014). Heat capacity measurements of various biomass types and pyrolysis residues. *Fuel*, 115, 644-651.

Emami, S., & Tabil, L. G. (2006). Thermal Conductivity of Chickpea Flour and Isolated Starch and Protein. In *2006 ASAE Annual Meeting* (p. 1). American Society of Agricultural and Biological Engineers.

Emami, S., Tabil, L. G., & Tyler, R. T. (2007). Technical Note: Thermal Properties of Chickpea Flour, Isolated Chickpea Starch, and Isolated Chickpea Protein. *Transactions of the ASABE*, 50(2), 597-604.

Ford, R. M., & Bilanski, W. K. (1969). Thermal diffusivity of alfalfa stems. *Transactions of the ASAE*, *12*(2), 249-0251.

Guo, W., Lim, C. J., Bi, X., Sokhansanj, S., & Melin, S. (2013). Determination of effective thermal conductivity and specific heat capacity of wood pellets. *Fuel*, 103, 347-355.

Iroba, K. L., Tabil, L. G., Venkatesh, M., & Oon-Doo, B. (2013). Thermal properties of lignocellulosic biomass barley straw. In *2013 Kansas City, Missouri, July 21-July 24, 2013* (p. 1). American Society of Agricultural and Biological Engineers.

Izadifar, M., & Baik, O. D. (2007). Determination of thermal properties of the rhizome of Podophyllum peltatum for drying and ethanol extraction. *Biosystems engineering*, 97(3), 357-370.

Jiang, S., Jofriet, J. C., & Mittal, G. S. (1986). Thermal properties of haylage. *Transactions of the ASAE*, 29(2), 601-0606.

Kostaropoulos, A. E., & Saravacos, G. D. (1997). Thermal diffusivity of granular and porous foods at low moisture content. *Journal of food engineering*, 33(1), 101-109.

Lan, Y., Fang, Q., Kocher, M. F., & Hanna, M. A. (2000). Thermal properties of tapioca starch. *International Journal of Food Properties*, 3(1), 105-116.

Li, X., Tabil, L. G., Oguocha, I. N., & Panigrahi, S. (2008). Thermal diffusivity, thermal conductivity, and specific heat of flax fiber–HDPE biocomposites at processing temperatures. *Composites Science and Technology*, 68(7), 1753-1758.

Nix, G. H., Lowery, G. W., Vachon, R. I., & Tanger, G. E. (1967). Direct determination of thermal diffusivity and conductivity with a refined line-source technique. Progress in aeronautics and astronautics: *Thermophysics of spacecraft and planetary bodies*, 20, 865-878.

Njie, D. N., Rumsey, T. R., & Singh, R. P. (1998). Thermal properties of cassava, yam and plantain. *Journal of Food Engineering*, 37(1), 63-76.

Opoku, A., Tabil, L. G., Crerar, B., & Shaw, M. D. (2004). Thermal properties of timothy hay. In *2004 ASAE Annual Meeting* (p. 1). American Society of Agricultural and Biological Engineers.

Opoku, A., Tabil, L. G., Crerar, B., & Shaw, M. D. (2006). Thermal conductivity and thermal diffusivity of timothy hay. *Canadian Biosystems Engineering*, 48, 3.

Rahman, M. S. (1995). Handbook of Food Properties.

Ramaswamy, H. S., & Tung, M. A. (1981). Thermophysical properties of apples in relation to freezing. *Journal of Food Science*, 46(3), 724-728.

Renaud, T., Briery, P., Andrieu, J., & Laurent, M. (1992). Thermal properties of model foods in the frozen state. *Journal of Food Engineering*, 15(2), 83-97.

Rodriguez, R. P., M. E. Rodrigo and P. Kelly. (1995). A calorimetric method to determine specific heats of prepared foods. *Journal of Food Engineering*, 26(1): 81-96.

Singh, R. P., & Heldman, D. R. (2001). Introduction to Food Engineering. San Diego. Cal.: *Academic Press*.

Tabil, L. G., Eliason, M. V., & Qi, H. (2003). Thermal properties of sugarbeet roots. *Journal of sugar beet research*, 40(4), 209-228.

Woodside, W. (1958). Probe for thermal conductivity measurement of dry and moist materials. *Heating, Piping, Air Conditioning*, 30, 1-10.

References (Section 6.4)

Buckmaster, D. R., Rotz, C. A., & Muck, R. E. (1989). A comprehensive model of forage changes in the silo. *Transactions of the ASAE*, 32(4), 1143-1152.

Ekinci, K., Keener, H. M., & Akbolat, D. (2006). Effects of feedstock, airflow rate, and recirculation ratio on performance of composting systems with air recirculation. *Bioresource Technology*, 97(7), 922-932.

Farm and Ranch Extension in Safety and Health (FRESH). (2012). Community of Practice Preventing fires in baled hay and straw. Retrieved from http://www.extension.org/pages/66577/preventing-fires-in-baled-hay-and-straw.

Harper, E., Miller, F. C., & Macauley, B. J. (1992). Physical management and interpretation of an environmentally controlled composting ecosystem. *Animal Production Science*, 32(5), 657-667.

Irvine, G., Lamont, E. R., & Antizar-Ladislao, B. (2010). Energy from waste: reuse of compost heat as a source of renewable energy. *International Journal of Chemical Engineering*, 2010.

Miller, L. G., Clanton, D. C., Nelson, L. F., & Hoehne, O. E. (1967). Nutritive value of hay baled at various moisture contents. *Journal of Animal Science*, 26(6), 1369-1373.

Nehrir, H., Kjelgaard, W. L., Anderson, P. M., Long, T. A., Hoffman, L. D., Washko, J. B., Wilson, J. P. & Mueller, J. P. (1978). Chemical additives and hay attributes. *Transactions of the ASAE*, 21(2), 217-0221.

Nelson, Leon F. 1968. Spontaneous heating, gross energy retention and nutrient retention of high-density alfalfa hay bales. Transactions of the ASAE 11(5):575-600, 607.

Rohweder, D. A., Barnes, R. F., & Jorgensen, N. (1978). Proposed hay grading standards based on laboratory analyses for evaluating quality. *Journal of Animal Science*, 47(3), 747-759.

Sanderson, M. A., Egg, R. P., & Wiselogel, A. E. (1997). Biomass losses during harvest and storage of switchgrass. *Biomass and Bioenergy*, 12(2), 107-11.

References (Chapter 7)

Topp, G. C., Zebchuk, W. D., Davis, J. L., & Bailey, W. G. (1984). The measurement of soil water content using a portable TDR hand probe. *Canadian Journal of Soil Science*, 64(3), 313-321.

References (Appendices)

References (Appendix A)

Bejan, A. 2004. *Convection Heat Transfer*, 3rd Edition. John Wiley & Sons.

Çengel, Y. A. and A. J. Ghajar. (2011). Heat and Mass Transfer: *Fundamentals and Applications: 4th Edition in SI Units*.

Kozanoglu, B. and F. Rubio. (2014). The characteristic length on natural convection from a horizontal heated plate facing downwards. *Thermal Science*, 18(2), 555-561.

Remsburg, R. (2011). *Advanced thermal design of electronic equipment*. Spring Science & Business Media.

Thirumaleshwar, M. (2009). *Fundamentals of heat and mass transfer*. Pearson Education

References (Appendix B)

Achariyaviriya, S., & Puttakarn, B. (2003). A mathematical model of effective moisture diffusivity for lychee drying. In International Conference on Crop Harvesting and Processing (p. 12). American Society of Agricultural and Biological Engineers.

Anderson, S. A. (1950). Automatic Refrigeration. MacLaren and Son Ltd. For Donfoss. Norborg, Denmark.

ASHRAE. (2011). HVAC applications. ASHRAE Handbook, 29.1–29.13.

Becker, H. A. (1959). A study of diffusion in solids of arbitrary shape, with application to the drying of the wheat kernel. *Journal of Applied Polymer Science*, 1(2), 212-226.

Bird, R. B., Lightfoot, E. N., & Stewart, E. W. (2007). *Transport phenomenon*. Wiley.

Blake, G. R. and J. B. Page. (1949). Direct measurement of gaseous diffusion in soils. *Soil Science Society of America Journal*, 13(C), 37-42.

Bramhall, G. (1979) Sorption diffusion in wood. *Wood Science*, 12, 3-13.

Buckmaster, D. R., Rotz, C. A., & Muck, R. E. (1989). A comprehensive model of forage changes in the silo. *Transactions of the ASAE*, 32(4), 1143-1152.

Cai, J., & Chen, S. (2008). Determination of drying kinetics for biomass by thermogravimetric analysis under nonisothermal condition. *Drying Technology*, 26(12), 1464-1468.

Carlton, H. E., & Oxley, J. H. (1967). Forced and natural convective mass transfer in multicomponent gaseous mixtures. *AIChE Journal*, 13(3), 571-577.

Celma, A. R., Rojas, S., & Lopez-Rodriguez, F. (2008). Mathematical modelling of thin-layer infrared drying of wet olive husk. *Chemical Engineering and Processing: Process Intensification*, 47(9), 1810-1818.

Çengel, Y. A. and A. J. Ghajar. (2011). Heat and Mass Transfer: Fundamentals and Applications: 4th Edition in SI Units.

Chen, D., Li, K., & Zhu, X. (2012a). Determination of effective moisture diffusivity and activation energy for drying of powdered peanut shell under isothermal conditions. *BioResources*, 7(3), 3670-3678.

Chen, D., Zheng, Y., & Zhu, X. (2012b). Determination of effective moisture diffusivity and drying kinetics for poplar sawdust by thermogravimetric analysis under isothermal condition. *Bioresource Technology*, 107, 451-455.

Chen, D. Y., Zhang, D., & Zhu, X. F. (2011). Heat/mass transfer characteristics and nonisothermal drying kinetics at the first stage of biomass pyrolysis. *Journal of Thermal Analysis and Calorimetry*, 109(2), 847-854.

Chen, P. and D. C. Pei. (1989). A mathematical model of drying processes. *International Journal of Heat and Mass Transfer*, 32(2), 297-310.

Chirife, J. (1983). Fundamentals of the drying mechanism during air dehydration of foods. *Advances in Drying*, 2, 73-102.

Churchill, S. W., & Usagi, R. (1972). A general expression for the correlation of rates of transfer and other phenomena. *AIChE Journal*, 18(6), 1121-1128.

Coradi, P. C., de Castro Melo, E., & da Rocha, R. P. (2014). Mathematical modeling of the drying kinetics of the leaves of lemon grass (Cymbopogon citratus Stapf) and its effects on quality. *IDESIA (Chile)*, 32(4), 43-56.

Cussler, E. (1997). Diffusion: Mass transfer in fluid systems: Cambridge Univ Pr. *View Article PubMed/NCBI Google Scholar*.

Dupont, C., Chiriac, R., Gauthier, G., & Toche, F. (2014). Heat capacity measurements of various biomass types and pyrolysis residues. *Fuel*, 115, 644-651.

Emery, I. R. (2013). Direct and indirect greenhouse gas emissions from biomass storage: Implications for life cycle assessment of biofuels.

Erbay, Z., & Icier, F. (2010). A review of thin layer drying of foods: theory, modeling, and experimental results. *Critical Reviews in Food Science and Nutrition*, 50(5), 441-464.

Fair, J. R. and B. J. Lerner. (1956). A generalized correlation of diffusion coefficients. *AlChE Journal*, 2(1), 13-17.

Fontenelle, L. (2011a). Solid state fermentation of switchgrass mixtures: Experimentation, modeling and analysis.

Fontenelle, L. T., Corgié, S. C., & Walker, L. P. (2011b). Integrating mixed microbial population dynamics into modeling energy transport during the initial stages of the aerobic composting of a switchgrass mixture. *Bioresource technology*, 102(8), 5162-5168.

Gaston, A. L., Abalone, R. M., Giner, S. A., & Bruce, D. M. (2003). Geometry effect on water diffusivity estimation in PROINTA-Isla Verde and broom wheat cultivars. *Latin American Applied Research*, 33(3), 327-331.

Godbolt, C., M. G. C. Danao and S. R. Eckoff. (2013). Modeling of the equilibrium moisture content (EMC) of switchgrass. *Transactions of the ASABE*, 56(4), 1495-1501.

Górnicki, K., & Kaleta, A. (2011). Some Problems Related to Mathematical Modelling of Mass Transfer Exemplified of Convection Drying of Biological Materials. INTECH Open Access Publisher.

He, X., Lau, A. K., Sokhansanj, S., Lim, C. J., Bi, X. T., Melin, S., & Keddy, T. (2013). Moisture sorption isotherms and drying characteristics of aspen (Populus tremuloides). *Biomass and Bioenergy*, 57, 161-167.

Iguaz, A., San Martin, M. B., Mate, J. I., Fernandez, T., & Virseda, P. (2003). Modelling effective moisture diffusivity of rough rice (Lido cultivar) at low drying temperatures. *Journal of Food Engineering*, 59(2), 253-258.

Kandula, M. (2011). Frost growth and densification in laminar flow over flat surfaces. *International Journal of Heat and Mass Transfer*, 54(15), 3719-3731.

Karunanithy, C., K. Muthukumarappan and A. Donepudi. (2013). Moisture sorption

characteristics of switchgrass and prairie cord grass. *Fuel*, 103, 171-178.

Lam, P. S., S. Sokhansanj, X. Bi, C. J. Lim, and S. Mani. (2007). Physical characterization of wet and dry wheat straw and switchgrass–bulk and specific density. In *2007 ASAE Annual Meeting* (p. 1-22). American Society of Agricultural and Biological Engineers.

Lam, P. S., S. Sokhansanj, X. Bi, C. J. Lim, L. J. Naimi, M. Hoque, S. Mani, A. R. Womac, S. Narayan, and X. P. Ye. (2008). Bulk density of wet and dry wheat straw and switchgrass particles. *Applied Engineering in Agriculture*, 24(3), 351-358.

Lees, F. (2012). *Lees' Loss prevention in the process industries: Hazard identification, assessment and control*. Butterworth-Heinemann.

Li, Z., & Kobayashi, N. (2005). Determination of moisture diffusivity by thermo-gravimetric analysis under non-isothermal condition. *Drying technology*, 23(6), 1331-1342.

Lu, R., & Siebenmorgen, T. J. (1992). Moisture diffusivity of long-grain rice components. *Transactions of the ASAE*, 35(6), 1955-1961.

Marrero, T. R., & Mason, E. A. (1972). Gaseous diffusion coefficients. *Journal of Physical and Chemical Reference Data*, 1(1), 3-118.

McDonald, P. (1981). *The biochemistry of silage*. John Wiley & Sons, Ltd.

Mohapatra, D., & Rao, P. S. (2005). A thin layer drying model of parboiled wheat. *Journal of Food Engineering*, 66(4), 513-518.

Montanuci, F. D., Jorge, L. M. D. M., & Jorge, R. M. M. (2013). Kinetic, thermodynamic properties, and optimization of barley hydration. *Food Science and Technology (Campinas)*, 33(4), 690-698.

Mwithiga, G., & Olwal, J. O. (2005). The drying kinetics of kale (Brassica oleracea) in a convective hot air dryer. *Journal of Food engineering*, 71(4), 373-378.

Okazaki, M. (1985). Heat and mass transport properties of heterogeneous materials. In *Drying'85* (pp. 84-96). Springer Berlin Heidelberg.

Parti, M. and I. Dugmanics. (1990). Diffusion coefficient for corn drying. *Transactions of the ASAE*, 33(5), 1652-1656.

Rao, A. (2015). *Sustainable Energy Conversion for Electricity and Coproducts: Principles, Technologies, and Equipment*. John Wiley & Sons.

Rao, P. S., Bal, S., & Goswami, T. K. (2007). Modelling and optimization of drying variables in thin layer drying of parboiled paddy. *Journal of Food Engineering*, 78(2), 480-487.

Rogers, R. R., & Yau, M. K. (1989). *A short course in cloud physics, International series in natural philosophy*.

Sobukola, O. P., Dairo, O. U., & Odunewu, A. V. (2008). Convective hot air drying of blanched yam slices. *International journal of food science & technology*, 43(7), 1233-1238.

Stroshine, R. L. (2004). *Physical properties of agricultural materials and food products*. R. Stroshine.

Taheri-Garavand, A., Rafiee, S., & Keyhani, A. (2011). Effective moisture diffusivity and activation energy of tomato in thin layer dryer during hot air drying. International Transaction *Journal of Engineering, Management, & Applied Sciences & Technologies*, 2(2), 239-248.

Vega-Gálvez, A., Miranda, M., Díaz, L. P., Lopez, L., Rodriguez, K., & Di Scala, K. (2010). Effective moisture diffusivity determination and mathematical modelling of the drying curves of the olive-waste cake. *Bioresource Technology*, 101(19), 7265-7270.

Vijayaraj, B., Saravanan, R., & Renganarayanan, S. (2007). Studies on thin layer drying of bagasse. *International Journal of Energy Research*, 31(4), 422-437.

References (Appendix C)

Lam, P. S., S. Sokhansanj, X. Bi, C. J. Lim, and S. Mani. (2007). Physical characterization of wet and dry wheat straw and switchgrass–bulk and specific density. In *2007 ASAE Annual Meeting* (p. 1-22). American Society of Agricultural and Biological Engineers.

Lam, P. S., S. Sokhansanj, X. Bi, C. J. Lim, L. J. Naimi, M. Hoque, S. Mani, A. R. Womac, S. Narayan, and X. P. Ye. (2008). Bulk density of wet and dry wheat straw and switchgrass particles. *Applied Engineering in Agriculture*, 24(3), 351-358.

Zhang, P. (2004). Darcy's law and hydraulic conductivity [PDF document]. Retrieved from Lecture Notes Online Web Site: http://mail.sci.ccny.cuny.edu/~pzhang

VITA

Drew Frank Schiavone

EDUCATION

M.S. in Agricultural and Biological Engineering. University of Florida, Gainesville, FL. Completion Date: December 2011. Thesis Topic: Development and Evaluation of a Natural-Convection Solar Dryer for Mango in Rural Haitian Communities.

B.S. in Agricultural and Biological Engineering. University of Florida, Gainesville, FL. Completion Date: May 2008. Biomechanics Minor.

EXPERIENCE

Graduate Research Assistant: University of Kentucky, Biosystems and Agricultural Engineering Department, Lexington, Kentucky (2012-2016).

Lab Technician: University of Florida, Horticultural Sciences Department, Gainesville, Florida (2011-2012).

Lab Technician: Interdisciplinary Center for Biotechnology Research, Gainesville, Florida (2010-2011).

REFEREED PAPERS

Schiavone, **D.**, A. Teixeira, R. Bucklin, S. Sargent. 2013. *Design and Performance Evaluation of a Solar Convection Dryer for Tropical Fruit*. Applied Engineering in Agric. 29(3): 391-401.

HONORS AND AWARDS

Alpha Epsilon: Honor Society of Agricultural and Biological Engineers, University of Kentucky (2016).

Gamma Sigma Delta: Honor Society of Agriculture, University of Kentucky (2005).

Superior Paper Award: American Society of Agricultural and Biological Engineers (2014).

COMPETITIVE GRANTS (NOT FUNDED)

Schiavone, **D.**, M. Montross. 2012. Village scale cassava processing for food, feed and bioenergy. *USAID Feed the Future, Reduced Post-Harvest Losses*.

Schiavone, **D.**, M. Montross, R. Bucklin. 2012. Dry matter loss and gas production from stored biomass. *USDA-NIFA Sun Grant: Agriculture Systems and Technology*.

TECHNICAL PRESENTATIONS / ABSTRACTS

Schiavone, D., M. Montross. *Biomass Moisture Measurement via Time-Domain Reflectometry*. Paper Number 2179771, 2015 ASABE Annual Meeting.

Schiavone, D., M. Montross. *Heat and Mass Transfer Modeling of Baled Biomass.* Paper Number 2189014, 2015 ASABE Annual Meeting.

Sargent, S., **D. Schiavone**, A. Berry. *Development of an Integrated System to Rinse, Sanitize and Cool Fresh-Market Strawberries*. Number HP-12, 2014 Proc. Fla. State Hort. Society.

Schiavone, D., M. Montross. *Bale Moisture Measurement via Time-Domain Reflectometry*. Paper Number 232-43, 2014 ASABE Annual Meeting.

Turner, A., **D. Schiavone**, C. Rodrigues, J. Jackson, M. Montross, S. McNeill. *Field Measurement of Grain Packing*. Paper Number 131620198, 2013 ASABE Annual Meeting.

Schiavone, D., M. Montross, W. Adams. *Hydraulic Conductivity of Baled Biomass*. Paper Number 31619433, 2013 ASABE Annual Meeting.